ARISTOTLE UNIVERSITY OF THESSALONIKI
SCHOOL OF GEOLOGY
LAB OF ENGINEERING GEOLOGY AND HYDROGEOLOGY

POSTGRADUATE MASTER OF SCIENCE PROGRAM

'Applied and Environmental Geology'
Specialization: 'Environmental Hydrogeology'

VOULANAS ANTONIOU DIMITRIOS
Graduate Geologist A.U.Th

'Groundwater flow simulation using the FeFLOW software, for the alluvial aquifer of Kastoria'

MASTER THESIS

THESSALONIKI
2019

ΑΡΙΣΤΟΤΕΛΕΙΟ ΠΑΝΕΠΙΣΤΗΜΙΟ ΘΕΣΣΑΛΟΝΙΚΗΣ
ΤΜΗΜΑ ΓΕΩΛΟΓΙΑΣ
ΕΡΓΑΣΤΗΡΙΟ ΤΕΧΝΙΚΗΣ ΓΕΩΛΟΓΙΑΣ ΚΑΙ ΥΔΡΟΓΕΩΛΟΓΙΑΣ

ΠΡΟΓΡΑΜΜΑ ΜΕΤΑΠΤΥΧΙΑΚΩΝ ΣΠΟΥΔΩΝ Α' ΚΥΚΛΟΥ

'Εφαρμοσμένη και Περιβαλλοντική Γεωλογία'
Κατεύθυνση: 'Περιβαλλοντική Υδρογεωλογία'

ΤΟΥ ΤΜΗΜΑΤΟΣ ΓΕΩΛΟΓΙΑΣ

ΒΟΥΛΑΝΑΣ ΑΝΤΩΝΙΟΥ ΔΗΜΗΤΡΙΟΣ
ΠΤΥΧΙΟΥΧΟΣ ΓΕΩΛΟΓΟΣ Α.Π.Θ

«Προσομοίωση της υπόγειας ροής του αλλουβιακού υδροφορέα της Καστοριάς με τη χρήση του κώδικα FeFLOW»

ΜΕΤΑΠΤΥΧΙΑΚΗ ΔΙΑΤΡΙΒΗ ΕΙΔΙΚΕΥΣΗΣ

ΘΕΣΣΑΛΟΝΙΚΗ
2019

VOULANAS A. DIMITRIOS
Graduate Geologist A.U.Th

'GROUNDWATER FLOW SIMULATION USING THE FEFLOW SOFTWARE, FOR THE ALLUVIAL AQUIFER OF KASTORIA'

Submitted at School of Geology as part of the Postgraduate Program 'Applied and Environmental Geology', 'Environmental Hydrogeology'

Oral Examination: 6/9/2019

Three-member Examination Committee
Prof. Konstantinos Voudouris (supervisor)
Prof. Nicolaos Theodosiou
Dr. Christos Mattas, Laboratory Teaching Staff

‘GROUNDWATER FLOW SIMULATION USING THE FEFLOW SOFTWARE, FOR THE ALLUVIAL AQUIFER OF KASTORIA’

…dedicated to all of my good teachers...

Table of Contents

Acknowledgements ... 1
Abstract ... 2
Περίληψη ... 3
CHAPTER 1. Introduction ... 4
1.1 The study area ... 4
1.2 Aim of the Research ... 5
1.3 Structure of the Thesis ... 5
CHAPTER 2. Water Resources Management ... 7
2.1 EU Legal Framework ... 7
2.1.1 Directive 2000/60/E.C ... 7
2.1.2 Adoption of Directive 2000/60/E.C by Greece ... 8
2.2 Water Resources Management in Greece ... 9
2.3 Brief Information about Climate change and future climate projections ... 10
2.4 Modern examples of RCM-driven Water Resources Management ... 12
2.4.1 Single-RCM investigations ... 12
2.4.2 RCM-Ensembles approach ... 12
CHAPTER 3. Kastoria Basin, Western Macedonia ... 13
3.1 Geomorphology ... 13
3.1.1 Relief of crystalline and plutonic rocks ... 14
3.1.2 Relief of carbonate rocks ... 14
3.1.3 Relief of Generally Flat Relief ... 14
3.2 Geology of Kastoria Basin ... 17
3.2.1 Geologic succession of the broader research area ... 17
3.3 Tectonic Setting of Kastoria Basin ... 20
3.4 Climate of Kastoria Basin ... 22
3.4.1 Temperature and Evaporation patterns ... 23
3.4.2 Rainfall ... 29
3.4.3 Evapotranspiration ... 33
3.4.4 Climate Classification Assessment ... 38
3.4.5 Future Climate Projections ... 39
3.4.6 Future Climate Classification Assessment ... 62
3.5 Surface Hydrology of Kastoria Basin ... 63
3.5.1 Surface Runoff ... 64
3.5.2 Lake Orestiada ... 64
3.6 Hydrogeology – Groundwater Hydrology of Kastoria Basin ... 66
3.6.1 Hydrogeological units ... 66

3.6.2 Springs of Kastoria Basin 69
3.6.3 Granular aquifer sub-system of Kastoria 72
3.6.4 Hydraulic Parameters 80
3.6.5 Piezometry 82
3.6.6 Torrent-aquifer interaction 88
3.6.7 Water balance 92
3.7.1 Future Climate Change Impact at Korissos karst system 97
CHAPTER 4. Groundwater flow modelling 100
4.1 Model design 101
4.2 Simulation area 102
4.3 Selection of software 102
4.4 Mesh design 102
4.5 Boundary conditions 104
4.5.1 Specified heads 105
4.5.2 Head dependent flow 105
4.5.3 Assigned boundary conditions 105
4.5.4 Hydraulic parameters 107
4.5.5 Applied stresses 110
4.6 Calibration-verification of model 113
4.6.1 Calibration stages 113
4.6.2 Calibration criteria 114
4.6.3 Starting conditions 117
4.6.4 Single layer model design – 2D horizontal 117
4.7 Future groundwater management 121
4.7.1 Summarized Results 124
4.7.2 Calculation of Projected Water Balance of Kastoria Lake 129
CHAPTER 5. CONCLUSIONS AND PROPOSALS 142
5.1 Summary 142
5.2 Conceptual model 143
5.3 Proposals for future work 143
APPENDIX A. Western Macedonia Water District (GR 09) 146
A.1 Lithology of WD GR 09 147
A.1.1. Silting and fluvio-torrential deposits of the Quaternary 148
A.1.2. Neogene Lacustrine deposits 148
A.1.3 Quaternary sediments 148
A.1.4 Neogene sediments of the Mid-Hellenic Trench 148
A.1.5 Molassic sediments of the Mid-Hellenic Trench 149

A.1.6 Flysch ... 149
A.1.7 Heterochonous limestones and carbonate conglomerates of Mount Vermio ... 149
A.1.8. Cretaceous limestones of pelagic, sub-seminal and belt Axios ... 149
A.1.9. Ophiolithic complex ... 149
A.1.10 Triassic-Jurassic limestones ... 150
A.1.11 Crystalline bedrock of pre-Alpine age ... 150
A.2 General Morphology of Water District GR 09 ... 152
A.3 Hydrology of W.D GR 09 ... 152
A.3.1 Climate of W.D GR 09 ... 152
A.3.2 General Precipitation Characteristics of W.D GR 09 ... 153
A.4.1 General Percolation Characteristics ... 154
A.5.1 General Runoff Characteristics ... 154
A.4 General Hydrogeological setting of W.D GR 09 ... 154
A.4.1 Granular of alluvial aquifers of Quaternary sediments ... 155
A.4.2 Karst aquifers of limestone and marble rocks ... 155
A.4.3 Fractured aquifer of the ophiolithic and crystalline rocks ... 156
A.5 General Tectonic Setting of W.D GR 09 ... 157
A.6 Geology of W.D GR 09 ... 158
A.6.1 Pelagonian Zone ... 158
A.6.2 Meta-Alpine formations ... 159
A.7 Water Resources of W.D EL 09 ... 161
A.7.1 Granular or Alluvial Aquifers ... 161
A.7.2 Karst Aquifers ... 161
A.7.3 Fractured Aquifers ... 161
A.7.4 Aquifer Systems of W.D EL 09 ... 162
APPENDIX B. Theoretical Background (to be added at a later date) ... 164
APPENDIX C. Supplemental Figures ... 165
APPENDIX D. Supplemental Tables ... 200
References ... 219
Table of Figures (Figures) ... 231
Table of Figures (Tables) ... 234

Acknowledgements

The present thesis is required to complete the postgraduate program of the School of Geology of the Aristotle University of Thessaloniki (A.U.Th.) titled “Applied and Environmental Geology”, under the specialization of “Environmental Hydrogeology”. The area of interest is Kastoria basin, where an under exploitation alluvial aquifer resides.

Supervisor of this thesis is Professor K. Voudouris, Hydrogeologist PhD, School of Geology, A.U.Th. For the elaboration of this thesis, there was a close cooperation with Hellenic Agricultural Organisation “DEMETER" and especially with the Land Reclamation Department – Soil & Water Resources Institute, Sindos (Thessaloniki) and namely with Vaggelis Hatzigiannakis, Agronomist PhD, Reseacher B’ Grade, who scientifically hosted this M.Sc thesis. His advice was instrumental to complete this thesis. For the completion of this thesis, I would like to thank Prof. Voudouris for his guidance and for letting me choose the subject and design this thesis on my own. I would like to thank Prof. N. Theodosiou, Civil Engineer PhD, School of Civil Engineering, along with Christos Mattas, Laboratory Teaching Staff, School of Geology, A.U.Th for their scientific support, encouragement and guidance, which were very important for the completion of the present Master Thesis. The fourth person who greatly assisted with his comments, is Stratos Atsalos, B.Sc. Geology A.U.Th; I deeply thank him. Also, I would like to thank DHI-WASY for providing the FEFLOW program free of charge, FEFLOW tech support for their useful advice on FEFLOW related questions, IGME Kozanis namely fellow geologist A. Stamos, the Municipality of Kastoria namely the Department of the Environment and Water Resources as well as TOEVs Korissou-Lithias and Vasiliadas for their useful advice regarding the study area.

Thessaloniki, 31/5/2019
Voulanas A. Dimitrios (536)

Abstract

This thesis deals with the groundwater resources management of Kastoria basin of Western Macedonia, Greece though the use of FeFLOW v.7.2 groundwater flow modelling package in conjunction with ARCGIS v.10.6 and MATLAB, which were used to manage all the data used in this thesis and also to prepare the input data in the structure and format required by FeFLOW. Kastoria basin houses an extensive alluvial aquifer system, which is of fluvio-torrential origin and consists of alternating layers of coarse and fine-grained layers of small spatial and vertical extent. Precipitation is the main recharge element of the aquifer, where a representative annual value for the former is 770 mm. The modelled area consisted of the main body of the alluvial aquifer as a 100 m thick layer. Such an environment provides an inherit uncertainty regarding to the hydraulic properties, to alleviate a part of this uncertainty a stochastic approach used through PEST. The groundwater flow model was successfully calibrated first manually and then finally by PEST in all aspects, yielding RMSE=0.758 for the entire transient simulation. The water balance elements produced resemble those presented by previous studies. To further assess the evolution of the groundwater resources at Kastoria basin precipitation and temperature data of regional climate models were extracted from the EURO-CORDEX project, which provides the needed high spatial resolution (EUR-11) to spatially represent the future climate condition at the study area, for three 20 year long sub-periods between 2019-2078. After bias-correction of the 53 extracted EUR-11 region climate models, ten of those were selected and used further. Bias-correction was performed with the linear scaling method and monthly observed data of the 1986-2005 period. This showed improvements at the bias-corrected RCM data in comparison to raw data in representing observed patterns. The analysis presented that, as mean annual values, precipitation will reduce by 6% while temperature will increase by 2.5°C throughout the projected period. Based on the selected RCM data, ten groundwater scenarios were simulated by feeding the bias-corrected RCM data to the calibrated groundwater flow model. In summary of the results of the former, the groundwater level will practically remain the same. Kastoria lake water level will drop, if left unchecked, due to higher evaporation, reduced precipitation and lower lateral flow from Kastoria alluvial aquifer reduction while surface runoff will slightly increase. This will lead to the reduction of the total runoff or discharge through the Gkioli stream by a mean annual value of 4.82×10^6 m^3 or 9.2%. Finally, options to counter this change at the water balance of the basin were also proposed.

Keywords: FeFLOW, PEST, MATLAB, Groundwater Resources Management, EUROCORDEX, Regional Climate Models, RCM, ArcMAP, Kastoria basin, Water District GR 09, Alluvial Aquifer, Water Balanc, Groundwater Flow Simulation

Περίληψη

Η παρούσα διπλωματική εργασία ασχολείται με τη διαχείριση των υπόγειων υδάτων στη λεκάνη της Καστοριάς της Δυτικής Μακεδονίας με την χρήση του πακέτου προσομοίωσης ροής υπογείων υδάτων FeFLOW v.7.2 σε συνδυασμό με το ARCGIS v.10.6 και το MATLAB, τα οποία χρησιμοποιήθηκαν για τη διαχείριση όλων των δεδομένων που χρησιμοποιήθηκαν σε αυτή τη διατριβή και επίσης στο να προετοιμαστούν τα δεδομένα εισόδου στη δομή και τη μορφή που απαιτεί το FeFLOW. Η βροχόπτωση είναι το κύριο στοιχείο εμπλουτισμού της λεκάνης, όπου μία αντιπροσωπευτική ετήσια τιμή για την πρώτη είναι ίση με 770 mm. Στη λεκάνη της Καστοριάς βρίσκεται ένα εκτεταμένο προσχωσιγενές σύστημα υδροφόρου, το οποίο έχει χειμμαρική προέλευση και τα πρώτα 100 μέτρα αποτελούνται από εναλλασσόμενα στρώματα από χονδρόκοκκα και λεπτόκοκκα ιζήματα μικρής χωρικής έκτασης. Η περιοχή προσομοίωσης αποτελείται από το κύριο σώμα του προσχωσιγενή υδροφορέα ως στρώμα πάχους 100 μέτρων. Ένα τέτοιο περιβάλλον παρέχει μια αβεβαιότητα σχετικά με τις υδραυλικές παραμέτρους, για να απαληφεί ένα μέρος αυτής της αβεβαιότητας χρησιμοποιήθηκε μια στοχαστική προσέγγιση με βάση το PEST. Το μοντέλο ροής των υπόγειων υδάτων ρυθμίστηκε με επιτυχία πρώτα με δοκιμασία προσπάθειας-λάθους και τελικά με το PEST, αποδίδοντας RMSE = 0,758 για ολόκληρη την προσομοίωση. Τα στοιχεία υδατικού ισοζυγίου που παράχτηκαν από την προσομοίωση είναι παρόμοια με εκείνα που παρουσιάστηκαν από προηγούμενες μελέτες. Για να αξιολογηθεί περαιτέρω η εξέλιξη του ισοζυγίου των υπογείων υδάτων στη λεκάνη της Καστοριάς, χρησιμοποιήθηκαν δεδομένα, τριών υποπεριόδων 20 ετών για την περίοδο 2019-2078, των περιφερειακών κλιματικών μοντέλων του έργου EURO-CORDEX project, το οποίο παρέχει την απαιτούμενη υψηλή χωρική ανάλυση για τη χωρική αναπαράσταση της μελλοντικής κλιματικής κατάστασης στην περιοχή μελέτης. Μετά από τη διόρθωση των εξαγόμενων 53 κλιματικών μοντέλων, δέκα από αυτά επιλέχθηκαν και χρησιμοποιήθηκαν περαιτέρω. Η διόρθωση των bias των κλιματικών μοντέλων έγινε με τη μέθοδο linear scaling και τα μηνιαία ιστορικά δεδομένα της περιόδου 1986-2005. Η διόρθωση παρουσίασε βελτιώσεις στα δεδομένα των κλιματικών μοντέλων σε σύγκριση με τα μη διορθωμένα δεδομένα. Το αποτέλεσμα της ανάλυσης είναι ότι η βροχόπτωση θα μειωθεί κατά μέσο όρο 6% ενώ η θερμοκρασία θα αυξηθεί κατά 2,5°C, καθ 'όλη την προβλεπόμενη περίοδο. Με βάση τα επιλεγμένα δεδομένα, προτάθηκαν δέκα σενάρια εξέλιξης των υπόγειων υδάτων του αλλουβιακού υδροφορέα της Καστοριάς. Συνοπτικά τα αποτελέσματα αυτών παρουσιάσαν ότι το επίπεδο των υπόγειων υδάτων θα παραμείνει ως επί το πλείστον το ίδιο. Η στάθμη του νερού της λίμνης της Καστοριάς θα ελλαττωθεί, εάν αφεθεί ανεξέλεγκτη, λόγω της υψηλότερης εξάτμισης, της μειωμένης βροχόπτωσης και της χαμηλότερης πλευρικής εισροής από τον αλλουβιακό υδροφορέα της Καστοριάς παρόλου που η επιφανειακή απορροή θα αυξηθεί ελαφρά. Αυτό θα οδηγήσει σε μείωση της συνολικής απορροής ή εκφόρτισης μέσω του ρέμματος Γκιόλι κατά μέσο ετήσιο όρο των 4.82 x 10^6 m^3 or 9.2%. Τέλος, προτάθηκαν λύσεις για την αντιμετώπιση αυτής της αλλαγής στο υδάτινο ισοζύγιο της υπό μέλετης λεκάνης απορροής.

Λέξεις-κλειδιά: FeFLOW, PEST, MATLAB, Διαχείριση Υδατικών Πόρων, EUROCORDEX, Regional Climate Models, RCM, ArcMAP, Λεκάνη της Καστοριάς, Water District GR 09, Αλλουβιακός Υδροφορέας, Υδατικό Ισοζύγιο, Προσομοίωση της υπόγειας ροής

CHAPTER 1. Introduction

Water is of vital importance to continuous development of human society. For many years, humanity has been actively interfering in the environment and its resources, including water resources. Greek water resources organizations drained several lakes in 1930s, to create agricultural land for crop development so the Greece could sustain its ever-growing population. During the period 1960-1990 agriculture grew rapidly in combination with systematic irrigation of crops mainly through pumping wells, initially of low depth and then of greater depth to meet the irrigation demands and along with the construction of collective irrigation networks. This leap in agriculture development put huge constrains to water resources. This in combination with climate change, resulted in the early 1990s to have significant and irreversible effects on surface and groundwater bodies, which if left unattended could create severe water shortages. Due to such concerns about the well-being of current and newer generations, EU government bodies began to study and formulate new laws about the quantitative and qualitative characteristics of water resources. Thus, to answer those concerns the Water Framework Directive (2000/60/E.C) was created to regulate management of water resources via rational decision-making made possible through various tools such as simulation software. Simulation software that could bear certain mathematical models that can represent the underground water flow dynamically. They are an internationally accepted tool that provides significant support to studies carried out and especially in the management of water resources of one region. These codes can provide remarkable results with the condition that quality data are used as input (Wang & Anderson, 1982; Doherty, 2015). The lack of such data in Greece results in a more basic characterization of an aquifer system, which make the use of these models problematic (personal communication 2018, H.A.O. “DEMETER”).

In the context of Greece's compliance with the European Union's requirements and the new environmental standards, Directive 2000/60/E.C had to be implemented to assess the quality of the country's water and to propose management plans that would improve this situation. These plans where proposed and carried out in 2010 by the Special Secretariat for Water, which is part of ministry of environment and energy of Greece, and have since be revised in 2017.

This M.Sc. thesis deals with the quantitative status of the water resources of the basin of Kastoria through the use of groundwater simulation software to propose future management plans and the use of the programs ARCGIS and MATLAB for the generation and management of the input data of FEFLOW in an automated fashion.

In the study area, Kastoria basin, agriculture is the largest consumer of water. Droughts that our country has experienced over the last few years and the inappropriate use of water, we have been confronted with the quantitative (over-exploitation aquifers) and water quality (hydration, nitrate pollution, etc.). It is therefore of outmost importance to manage water resources in order to avoid more serious problems in the future. This management problem can be solved with the application of water resources management software, integrated hydrological modelling system i.e. MIKE-SHE and groundwater modelling software i.e. FeFLOW program. All primary data used in this thesis (water balance, climatic data, hydraulic parameters, river flows, water table levels, etc.) were obtained from various sources such as I.G.M.E, National Meteorological Service, the Municipality of Kastoria, which, after appropriate preparation with MATLAB, were used for the FeFLOW simulation. Finally, some hypothetical scenarios based on bias-corrected RCM results of EUROCORDEX project on the probable evolution of the basin's water potential were developed in tandem with a FeFLOW simulation in order to propose plans for the sustainable development and management of water in Kastoria basin.

1.1 The study area

The basin of Kastoria is situated in Western Macedonia, Water District GR 09 and it’s found between the Grammos Mountain in the west and the Vitsi Mountain in the east. The alluvial aquifer of Kastoria constitutes the central and eastern part of Kastoria basin, directly across the city of

Kastoria, and contains important quantities of groundwater, which cover almost all of the irrigation needs of the basin. It is bounded from all sides, except from the southernmost part, by rugged mountains consisting of the crystalline bedrock of the basin and the Korissos karst system. The average topographic elevation is 750 m a.m.s.l with gentle slopes of 1 – 3 degrees for Kastoria plains, while a considerable slope of 30-35 degrees is calculated for the surrounding mountainous region. The region of interest has a spatial extent of about 315 km^2. The extensive aquifer system developed within the alluvial deposits has a strong hydraulic interaction with the Korrisos karst system. The population of the region is about 15,000 inhabitants, most of whom live in the major city of Kastoria while the rest live at smaller and villages (Vafeiadis, 1983, Drougka, 2006).

Agricultural activities are based upon irrigation water drawn predominantly from boreholes. Agriculture is the main occupation of the basin's population. The use of irrigation water is regulated by local land reclamation organizations (TOEV) that operate under the supervision of the State's Land Reclamation Services. Two such organizations exist in the study area: TOEV Korissos-Lithias and TOEV Vasileiadas. TOEV Korissos-Lithias supply most of the irrigation demand by groundwater abstractions from boreholes. Groundwater is distributed to the fields via a pressurized network at the fields of the former TOEV. In contrast farmers, whose fields belong to the jurisdiction of TOEV Vasileiadas, their irrigation demand is covered by private and municipal boreholes because this TOEV's extent is too small and remote to have support its own collective irrigation network. Domestic water is supplied by groundwater for villages that exist on a higher altitude whilst those settlements that are located near karst systems i.e Korissos, Askepos or near the lake receive the water from springs and the lake of Kastoria respectively. Systematic exploitation of the groundwater resources of the alluvial aquifer system was initiated in the early 1970's (personal communication with the Department of Water resources and Environment of Kastoria).

Greek economy, in the mainland is mainly based upon agriculture, whose water demands during the dry months of the year use irrigation water derived from groundwater. Most of agricultural activities are taking place in the Quaternary alluvial basins of Greece. Excessive groundwater level decline has been of significant impact on the groundwater resources, both due to the socio-economic development of the country and with the changes in climatic conditions since the late 1980's. Consequently, concern has been raised nationally regarding the future sustainability of much of the readily groundwater resources.

1.2 Aim of the Research

This research study aims at determining the quantitative status of groundwater resources of the alluvial basin of Kastoria through the use of groundwater simulation software package FeFLOW v. 7.2 and also the proposal of RCM-driven water resources management scenarios. In doing so, the objective implies that the organization of typically limited and non-standardized data from the alluvial aquifer of Kastoria, that has been operated for irrigation over a long period of time, into a viable database, and to use this data base to develop a conceptual understanding of the hydrogeology of that system so that the system can be analyzed accurately. Also, the algorithms written in this thesis to process the RCM data, prepare maps and FeFLOW input data can be developed into a fully-fledged software suite. However, this goes beyond this thesis and will be developed at a later date. Conceptualization is a simplified description of the physical components and interaction of the surface and groundwater systems. These data and the conceptual model could be used in development of a numerical model that dynamically links surface water and groundwater. Then, the model could be used by decision makers to manage water resources within the basin. The research is focused on the Kastoria alluvial aquifer, which is a relatively small aquifer.

1.3 Structure of the Thesis

The work presented in this thesis is structured in the following way:

In Chapter 1, an introduction of the subject, the purpose and the structure of this thesis are presented.

In Chapter 2, the importance of water resources and their management, the relevant legislative framework applicable in Greece and the European Union. Also, brief information is given about climate change and future climate projections along with some modern examples

In Chapter 3, the characteristics of the study region are presented and examined in conjunction with previous studies, the results discussed and compared the results of IGME's study for the entire Water District of Western Macedonia submitted at APPENDIX A, when applicable. Specifically:

- The geology and its lithological characteristics are presented along with the geomorphology and tectonic setting of the basin.
- The climate of the area is discussed and the main climatological parameters are analyzed and their patterns presented. Also, future climate projections are made based on the bias corrected results of selected Regional Climate Models of EURO-CORDEX.
- The surface hydrology of Kastoria basin, the characteristics of Kastoria lake and its water balance.
- The hydrogeological setup of the study area is examined based on the data from previous studies by Vafeiadis, 1983, Gianneli, 2009, IGME, 2010, Hellenic Ministry for the environment, Energy and Climate Change – Special Secretariat for Water, 2014 and Hellenic Ministry of Agriculture, 2013.
- The geometry of the alluvial aquifer is described and its hydrogeological characteristics defined. The hydraulic properties of the alluvial aquifer system are also defined and their spatial distribution is studied.
- The piezometric data are processed and analyzed, with conclusions being drawn regarding the hydraulic interaction between the alluvial aquifer and karst aquifer. The extent of the hydraulic interaction between the aquifer and torrent Xiropotamos, is also examined using the estimated river bed transmission losses.
- Based on the conclusions drawn from the aforementioned study, the main groundwater flow mechanisms of the system are identified and the water balance of the studied system is calculated.

In Chapter 4, the mathematical groundwater flow modelling application is discussed. The steps followed in the design and the calibration procedure adopted are analyzed and their importance in the creation of a comprehensive model is demonstrated. Its ability to accurately simulate the main flow mechanisms of the studied system is tested in order to ensure credibility of the predictive simulations. A number of alternative future groundwater management scenarios are examined in terms of sustainability of the water resources and an optimal option is proposed based on these scenarios. The theoretical background of this Chapter will be presented at APPENDIX B.

In Chapter 5, the conclusions drawn from this research study are presented and discussed in terms of their contribution to the hydrogeological knowledge of the examined system and in terms of the advantages from their use to the future development of the region. Furthermore, the significance of the derived methodology as an effective and viable groundwater management tool. Finally, proposals are presented for the continuation of the current study.

CHAPTER 2. Water Resources Management

"Water is the most important natural resource. It covers about 70% of the Earth's surface but almost 97% of the world's water volume is saline and is located at planet's oceans. The rest 3% is 'freshwater', as it contains less than 1000 mg/l of dissolved solids, mainly salt" (Chahine, M. T., 1992). Nowadays, the status of freshwater, meaning both quantity and quality, is under stress, because water is in constant interaction with human activities. This interaction must be regulated if humans are to secure the harmonious continuation of human-environment coexistence for future generations. Water resources management is such a way to achieve this, due to its scientific approach. It's not one action but a whole set of actions, which include project development, regulations, agreements, etc. that all aim to achieve the aforementioned harmonious relationship between water resources and human-made environment, both in present and in future while having sustainable development in mind.

Sustainable Development is achieved with the harmonious relationship between availability of water resources, demand for water resources and environment and by proposing the necessary measures - projects and scenarios.

Water Management must be set to become:

- a gentle exploitation of water resources
- be guided by projects with minimal environmental and social costs
- enforce protection laws of water resources and the environment
- involve all stakeholders / reaching the maximum possible consensus

To achieve this rational management of water, stakeholders and governing bodies must avoid sectoral solutions and mono-critical approaches; and the starting point of each decision must take into account implicitly the environment with its limitations and capabilities (Tsakiris, 2008).

2.1 EU Legal Framework

2.1.1 Directive 2000/60/E.C

The management of water resources has been used by the International Community for quite some time. The dangers of pollution and contamination of the environment was recognized by the United Nations (UN). who in 1975, at within the framework of its UNEP (United nations Environment) Program, established the Global Logistics System (GEMS). National actions in its field environment were strengthened and united under its GEMS supervision. Many international organizations i.e. UNEP, the World Health Organization (WHO), the World Meteorological Organization (WMO), the Food and Agriculture Organization (FAO), the United Nations Nations Educational, Scientific and Cultural Organiztion (UNESCO) and other international and intergovernmental organizations have implemented such control programs. Since the problems in quality and quantity of water resources were detected both by the competent bodies in state level as well as the international community. The latter began to establish one a series of laws and directives which propose measures for the management of water resources to avoid further degradation of ecosystems or even improve wherever it is feasible. Taking all the above into account the European Community on 23 of October, 2000 adopted Directive 2000/60 of the European Parliament, to create a basic framework for water policy within and between communities.

The Water Framework Directive (2000/60/EC) created a new status for water management resources. Its predominant characteristics are, but not limited to, the management of water resources at watershed level, the achievement of specific qualitative objectives associated with the ecological status of surface waters, as well as maintaining or achieving "good status" of groundwater bodies. It introduces in a clear way the concept of "ecological importance" of water by defining series of necessary actions, such as the provision of environmental cost of use and the introduction of quality

objectives, with fixed deadlines for their implementation. The main objective of the Water Framework Directive (WFD) is to prevent further deterioration of all water types i.e. surface, transitional, underground and coastal waters and the ecosystems that exists within them.

The basic principles of this Directive are:

- Water is a non-commercial product but a heritage and must be protected
- Its primary objective is to improve the quality of water resources and, secondly, the quantity
- Renewable natural resources, after being estimated, are imposed to long-term design of their protection projects
- Sustainable water resource management is done within a single river basin
- Other sectors of community, i.e. energy, transport, agriculture, are incorporated in the protection and conservation of water resources
- The reduction of each observable upward trend of pollutants
- The situation is monitored on a comparable basis
- The ‘polluter pays’ principle is established along with the principles of 'Proportionality' and 'prevention'
- Systematic information and public participation shall be ensured in the decisions
- Emphasis is being placed on tackling floods and drought

Summarizing, the goal of the WFD is to expand and enforce the protection of all water and thus; ensuring that there shall be no further degradation of freshwater ecosystem resources.

2.1.2 Adoption of Directive 2000/60/E.C by Greece

Before the adoption of the Water Framework Directive, the national legislation was based on Law No 1739/87 on the management of water resources. Law No 1739/87 is now replaced by Law 3199/2003 that introduced a modern concept for dealing with water related matters like research, administration and everyday practice by establishing the procedures and governing bodies that allow water resources management both at national and regional level. Some of the most important procedures provided by this law are:

- Development of water resource development programs
- Determination of surface and groundwater resources
- Determination of the required quantities of water to maintain an aquatic ecosystem
- Establishment of a central governing body for water resources

These procedures are described by legislation at national level. In addition to the protection and the restoration of the national’s water resources, Directive 2006/118/EC further contributes groundwater status classification. This is an addition for Directive 2000/60/EC on groundwater resources. This Directive defines and enforces the adoption of several measures to prevent or restrict the introduction of pollutants therein (Directive 2000/60/E.C).

National Law of Greece complied with Directive 2000/60/EC, when the Parliament of Greece drafted Law 3199/2003, which provides for the establishment of the following governing bodies, each one with its own duties:

- The National Water Committee
- The National Water Council
- The Central Water Authority
- The Regional Water Council
- The Advisory Committee on Water at regional level
- The Water District Directorate

Some of their duties are:

- Preparation of management plans
- Establishment of programs of measures and monitoring of water status
- Establishment of anti-pollution programs
- Establishment of general rules for the use of water
- Recovery of costs for water services
- Establishing and enforcing administrative and criminal penalties on polluters of water resources

According to Law 1739/87, Greece is divided into 14 main water districts based on hydrological and hydrogeological characteristics, which is one of the necessary steps for the implementation of the Directive, such as these have been determined by the Decision of the National Water Committee of 16.07.2010. Some of those districts are further divided into smaller parts as shown in Fig. This division corresponds to administrative areas, based on drainage basins. The water districts of Greece are: 1) Western Peloponnese, 2) North Peloponnese, 3) Eastern Peloponnese, 4) Western & Central Greece, 5) Epirus, 6) Attica, 7) Eastern Central Greece & Evvoia, 8) Thessaly, 9) Western Macedonia, 10) Central Macedonia, 11) Eastern Macedonia, 12) Thrace, 13) Crete, 14) Aegean Islands. Every water district is defined by its own unique code i.e. GR 09 for the Water District of Western Macedonia.

Following the first implementation of the Directive, at 2015, the Management Plans will be revised and will be updated every six years (2021, 2027 etc.) taking into account the results of the previous program, as imposed by the National Water Monitoring Network. Any activity directly or indirectly related to the use of water resources is considered to be compatible with the objectives of the Directive and more specifically it is approved for each Water Management Plan.

2.2 Water Resources Management in Greece

Law 1739/87 was issued as an elaboration of management plans for water resources management. This has been a major concern for those involved and many studies have been carried out, since then, at different levels. The most important of such studies are:

- Management of water resources Louros and Arachthos (Ministry of Rural Development and Food/1991)
- Water resources management of the Aegean Water Department (Y.AN/1993)
- Draft plan for the management of the country's water resources (Ministry of Defense/1996 update 2003)
- Management of water resources of Kifissos, Voiteia (YPEXODE 2000)
- Water resources management of the Cyclades islands (N.A. KYKLAD/2001)
- Integrated Water Resources Management of Crete (Region Crete/2002)

The project titled "Management plans of water resources" is one of the most comprehensive study on the subject, and with specifications that meet national and international requirements. It was conducted with the framework of the Operational Competitiveness Program of the Ministry of Development. This project includes 29 subprojects, of which 4 are the main, took place simultaneously and covered the whole country, except for Crete, whose corresponding specifications study was completed in 2002.

The 4 main subprojects are:

- Development of water resource management systems and tools for the water districts of Attica, Eastern Sterea Greece, Western Sterea Greece and Thessaly

- Development of water resource management systems and tools for the water districts of the West, North and East Peloponnese
- Development of water resource management systems and tools for the water districts of Western Macedonia, Central Macedonia, East Macedonia and Thrace
- Development of water resource management systems and tools for the water districts of the Aegean Island

The beginning of the four main sub-projects took place in September 2003, and their completion in 2007. These studies-activities had as their main objective the production of a flexible, dynamic and efficient management tool. This integrated Decision Support System will allow authorities, responsible for the management of water resources, to evaluate and to compare alternative strategies and possible interventions scenarios for rational exploitation and sustainable management of aquatic water resources of their responsibility. The Decision Support System consists of databases and specialized simulation software with support of Geographical Information System, that will pipe data to management proposals dedicated in future scenarios that will include the possible conditions of supplying and demanding water. It therefore becomes clear that there is a need for integrated management water resources, which is not a simple process. A lot of data needs to be collected, then sorted and categorized, along with defining of large number of parameters so they can be fed all together into the specialized software, that will assist in any decision-making process. In this case, that software is the mathematical models of groundwater flow.

Mathematical models are mostly easy to use nowadays. Their step by step setup inside an integrated environment can be ferreted out and they can also analyze any possible relationships between any number of variables and problems, thus enabling full insight into the system that is being studied. However, a model's reliability is heavily dependent on the quality of the data fed. The GIGO (Garbage In Garbage Out) principle, describes the aforementioned analysis as reliable only if the data entered are reliable (Anderson & Woessner, 1992). If the assumptions for the model are fair in terms of representing reality as astutely as possible and the data entered are reliable, then the model should produce fair results that are close at representing the possible mechanics of reality in any particular case.

2.3 Brief Information about Climate change and future climate projections

Changes in the properties of the climate system, which persist for an extended period of time, typically decade or more, are characterized as Climate change. Climate change may occur due to natural phenomena or by human activities. Natural phenomena can be internal processes such as changes in solar radiation and volcanism that occur naturally and alter the composition of the atmosphere. In contrast, external influences are caused by human activities, that also contribute to the natural variability of the climate in a similar way. For the past three decades, it is widely recognized that the production of greenhouse emissions is responsible for such climatic changes in the natural environment. The most investigated properties of the climate system are the potential increase of global and local temperatures and the induced modification of rainfall distribution in space and time that follows. These effects could heavily affect the environment and the society, both directly and indirectly. The Special Reports of the Intergovernmental Panel summarized such effects, e.g. changes in water resources, increased desertification, loss of biodiversity, sea-level rise, and changes in agricultural productivity (IPCC, 1995a–c, 1997, 2007). Such alterations, natural or man-made, require studies to assess the impact they have on the climate system, and consequently on the human society, its growth and the feasible development of management plans (Piao et al., 2010).

Climate impact studies aim to improve environmental and economic benefits. These improvements must be feasibly in certain future period of time, thus; they require future climate estimations. These future climate projections are the projected changes in atmospheric variables under the climate change scenarios defined by the Intergovernmental Panel for Climate Change (IPCC, 2007). One way of tackling the impact that climate change has in hydrological processes is through

the use of methods and tools, such as the analysis of paleo-climate analogues, and that of proxy and historical data and support decision support systems (DSSs) and decision support tools (DSTs), respectively (Al-jawad et al., 2019). An alternative approach is the development of basin scale hydrological simulations using meteorological data as inputs derived from global climate models (GCMs), which are based on climate change scenarios (Burlando & Rosso, 2002). However, GSMs provide data of a coarse spatial scale, which have resolutions in the ranges of hundreds of kilometers. This can be a problem in representing future climate of a specific region, e.g. a medium-small basin, because they fail to adequately describe the local climate variability (Kim et al., 1984; Gates, 1985; Robinson & Finkelstein, 1989; Smith & Tirpak, 1989; Cohen, 1990). Moreover, most of such models use rough representations to describe hydrologic processes (Koster & Suarez, 1994; Blyth et al., 1999). These reasons impose a serious restriction in the use of GCM-based scenarios for investigating the possible impacts of climate change in large scale.

Regional climate models (RCMs) could be as fine as some tens of kilometers as opposed to GCMs. Local climate scenarios require data of larger scale for impact analysis; therefore, this imposes the use of RCMs. Many impact assessments require climate observations due to the fact that they are highly sensitive to fine-scale climate variations. This is especially true for regions of complex topography, coastal or island locations, and in regions of highly heterogeneous land-cover. RCMs are the better choice of such regions, which is the relevant scale for water resource management and mitigation strategies.

RCMs are derived from GCMs, which are downscaled GCMs results in order to produce the required spatial resolution. These derivations can be done with two possible approaches, which are the most common, statistical or dynamical, the latter is the simulations of RCMs for small regions, e.g. runoff basins, with initial and lateral boundary conditions based on results of GCM simulations while the former is based on the statistical relationships between large-scale climate information and regional variables (Hewitson & Crane, 1996; Wilby et al., 2004). Also, RCMs can be produced with a myriad of different techniques in terms of discretizing equations and representing sub-grid effects (Deque et al., 2007). Thus, every different RCMs is expected to give a variety of different, so-called ensemble predictions. The pros and cons of these two fundamental downscaling approaches have been widely discussed (Murphy, 1998, 2000; Wilby & Wigley, 1997) as well as their impacts on the resulting simulations (Hellstrom et al., 2001; Haylock et al., 2006; Schmidli et al., 2006). Xu et al. (2005) and Fowler et al. (2007), reviewed climate data downscaling methods and techniques, including combination of them, for hydrological modeling, concluding that there is generally no clear evidence to propose a specific downscaling technique or method (dynamic or statistical) as better for use in hydrological and water resources management studies but the combination of both downscaling methodologies is suggested for climate change impact studies (Turco et al., 2011) while Teutschbein & Seibert, 2010 suggest that ensembles approach should perform better than using the single RCM approach.

Several ensembles of RCMs outputs, such as ENSEMBLES (Van der Linden, & Mitchell, 2009), EURO-CORDEX (Gobiet & Jacob, 2011) and MEDCORDEX (Ruti et al., 2016), have been developed to provide model outputs for basin-scale studies. However, their outputs are often affected by a strong systematic bias. Bias correction is usually needed as climate models often provide biased representations of observed times series due to systematic model errors caused by imperfect conceptualization, discretization, regional averaging within grid cells and those inherited from GCMs. Typical examples of biases are the occurrence of too many wet days to those observed with low-intensity rain or incorrect estimation of extreme temperature in RCM simulations (Ines & Hansen, 2006). Such biases in RCM-simulated variables can result to, for example, unrealistic hydrological simulations of river runoff, which is highly sensitive parameter (Bergstrom et al. 2001). Thus, necessitating bias-correction of their outputs to remove the systematic bias (Wilby et al. 2000). This can be done via several methods, i.e Precipitation threshold, Scaling approach, Power transformation, Distribution transfer, Precipitation model, Empirical correction, Linear transformation, each one with their own advantages and drawbacks (Teutschbein & Seibert, 2010). In the

next Section, several examples of water resources management are given that use two common approaches: Single-RCM investigations and RCM-Ensembles approach.

2.4 Modern examples of RCM-driven Water Resources Management

2.4.1 Single-RCM investigations

The simple approach of using data derived from RCMs is the application of one RCM to simulate local hydrology. The modeling chain in these cases is usually very simple: (i) small number of greenhouse gas (GHG) emission scenarios, (ii) one to two GCMs, (iii) only one RCM and (iv) a small number of hydrological models (Teutschbein & Seibert, 2010). This approach is often used in very large watersheds, e.g. the Yangtze River basin, in which the severe flood case over East Asia during the 1998 summer was simulated using SNURCM RCM with 60 km horizontal resolution (Lee et al., 2004), the Upper Mississippi River basin, in which the impact of climate change on streamflow in the Upper Mississippi River Basin was evaluated by use of RegCM2 (Giorgi et al., 1993) coupled with a hydrologic model, Soil and Water Assessment Tool, SWAT (Jha et al., 2004), the Columbia River basin, in which the potential effects of climate change on the hydrology and water resources of the Columbia River Basin were evaluated using simulations from the U.S. Department of Energy and National Center for Atmospheric Research Parallel Climate Mode (Payne et al., 2004) and the Rhine River basin, in which a model chain was described and evaluated for studying streamflow responses to climate variations and anthropogenic climate change using CHRM (Kleinn et al. 2005).

2.4.2 RCM-Ensembles approach

This approach, ensemble, uses bias-corrected data and includes the parameter variability presented by each model used. This can be achieved by using more than one RCM and often also a range of emission scenarios, GCMs and/or hydrological models. Booij (2005), used one emission scenario and combined three GCMs (CGCM1, HadCM3, CSIR09) with two RCMs (HadRM2, HIRHAM4) to simulate future precipitation in the Meuse River basin. Leander et al. (2007, 2008) analyzed flood quantiles of the river Meuse by making RCM–GCM combinations. Those were setup by combining two global models (HadAM3H and ECHAM4⁄OPYC3) with two regional models (RACMO and RCAO) based on the A2 emission scenario. Block et al. (2009), created ten runs with the NCEP RSM–ECHAM4.5 AGCM system using observed sea-surface temperatures before simulating stream flow with two hydrological models. Pisinaras, 2016 used an ensembles SWAT-MODFLOW coupled approach to assess the potential impact of climate change in an aquifer in Northeastern Greece for the period 2041-2070. This study used three RCMs (HI-AR, Huagen & Haakensatd, 2005), RA-EC (Van Meijgaard et al., 2008) and RE-EC (Jacob, 2001) under the SRES A1B socio-economic scenario. These RCMs were bias corrected with the Cumulative Distribution Function. Arampatzis et al., 2018 assessed the future impact of climate change has on the quantitative status of the Pinios river basin, Thessaly, Greece water resources for the period 2021-2100. Data from four RCMs were extracted and bias-corrected with the linear scaling method. Panagopoulos et al., 2016 assessed the potential impacts of climate change in the water balance of Pinios river basin by applying an area-differentiated model for total run-off estimation bases on the GROWA model. This was applied with monthly bias-corrected precipitation and temperature data, via the linear scaling approach, using four RCMs for period 2020-2080. Foughali et al., 2015, used four regional climate models (DMI, ARP, SMH and ICT) from the European program ENSEMBLES, forced by two global climate models (GCM): ECHAM and ARPEGE to evaluate the performance of a hydrological balance model in a watershed located in northern Tunisia. The water balance components were simulated with a modified version (MBBH) of the lumped and single layer surface model BBH (Bucket with Bottom Hole model).

CHAPTER 3. Kastoria Basin, Western Macedonia

3.1 Geomorphology

Lake Orestiada is surrounded by a rocky mountainous and hilly areas. It is divided by the "Koritsa" peninsula in two parts, as follows: the northern or upper part with an area of 15.13 km^2 and the southern or lower part with an area of 11.47 km^2. The lakeside flat section is of relatively small extend: it appears only in the north, east and south part of the basin. The lake area shows a progressive shrinkage for over 50 years in terms of spatial extent, average depth and water volume of the lake (Tolikas & Mylopoulos, 2000; Pavlopoulos et al., 2010).

Table 1 presents the area of elevation classes and the percentage of a certain class to the total area of the basin. Also, 51.6% of its surface has altitude above 800 m. Consequently, the catchment area of Lake Kastoria is of mountainous type with a relatively high altitude. Also, as next two figures i.e the higher inclination at banks along the second part of Gkioli stream and the knick-point that separates the two parts of Gkioli stream, show that Kastoria basin has a different base level, that is defined by the Kastoria lake, than the rest of Aliakmonas catchment (Fig. 2).

Table 1 - Area and Percentage Share of Area of Elevation Classes

Elevation (m)	Area (km^2)	Percentage Share (%)
600-700	113.96	36.18
700-800	38.48	12.22
800-900	32.02	10.17
900-1000	30.89	9.81
1000-1100	29.98	9.52
1100-1200	25.11	7.97
1200-1300	21.17	6.72
1300-1400	12.34	3.92
1400-1500	4.10	1.30
1500-1600	2.91	0.92
1600-1700	2.87	0.91
1700-1800	0.88	0.28
1800-1900	0.23	0.07
1900-2000	0.02	0.01
Summary	314.94	100.00

The morphology of the study area is affected by the combination of the geological structure, recent tectonic development and erosion processes, with the latter causing a progressive smoothing of the relief. The eroded materials are transported and deposited in the lowest regions of the basin, which is the Lake Kastoria. Based on the geological structure and the composition of the rocks, there are three distinguished zones of the basin's relief (Vafeiadis, 1983; Drougka, 2006; Kastoria Lake Management Plan, 2015):

- Relief of crystalline and pluton rocks zone (granite-gneiss rocks): This zone consisted of the rocky, crystalline rocks and a part of the plutonic mass of Mount Verno, which stretches down to lake Kastoria. Also, this area has a profound effect in depth corrosion.
- Relief of karst zone (carbonate rocks): The carbonate rocks of the Mesozoic nappe that extends from the Korissos and Pyrgos to Askyos Mountains to Mount Triklarios at the northwest consist the second zone. These rocks are generally embossed advanced karstification and more specifically cracks, micro caves, dolines and leveling surfaces as mentioned in a previous chapter.
- Relief of generally flat zone: The third zone coincides with the lakeside plain, the south of the lake semi-enclosed area that ends before the valley of the River Aliakmonas and the eastern-

northeastern low inclination topographic area as shown at Fig. 1. It includes sediments of the Mid-Hellenic Trench, the Pleistocene deposits and finally from Holocene deposits.

3.1.1 Relief of crystalline and plutonic rocks

The relief of these rocks shows a large vertical displacement. Also, at this figure an altitude difference of 1,5 Km at a horizontal distance of 12 Km can be observed at this rocky relief zone. This area is dominated gneiss granite, which have a relatively intense topography with rocky outcrops while the relief of the soil part of the area is way gentler, due to the easier erosion of the shale rocks that can be found there.

3.1.2 Relief of carbonate rocks

The carbonate rocks of Korrisos, Pyrgos, Sarakinas present structures of advance karstification e.g. dolines. Also, there are some flat surfaces on the carbonate rocks of Korrisos. One of those can be found at the altitude 1,000 to 1,120 m, this is limited to the east by the hills of Mikris and Megalis Sarakinas, while in the west the limestones present a steep relief where the elevation of the surface's slope plummets at the altitude of 700 m and below the Quaternary and Tertiary sediments of the Ampelokoipi area. The surface drainage system of this limestone mass is very sparse and presents no flow.

The limestone ridge "Koritsa" (height 890 m), which has the form of a peninsula exists in lake of Kastoria, there are many and developed karst structures. This limestone mass, which is in hydraulic communication with lake Orestiada houses caves, both above the water level of the lake and below it.

3.1.3 Relief of Generally Flat Relief

The fan-like deposits of the torrents, the scree deposits, the old river terraces and the alluvial plain area belong to this category. Alluvial cones and fans are formed at the outlets of the torrents toward the plains area. When the relatively large slope of the torrent's bed decreases downstream to some extent that the carrying capacity is reduced capacity of flowing water; thus, deposition of the suspended materials occurs place and therefore the formation of alluvial cones and fans.

The surface of the alluvial cones and fans has large inclination, up to 15°. Such cones and fans can be observed at Aposkepos settlement, at the outlets of torrents Lakkos, Tichio, Metamorphosis, Melissotopos, Vassiliadas, etc. Those formations are characterized by the fan shape, their cross-section, the relative greater slope compared to that of the plains and the radial layout of the drainage network that can be found on them. In the area of Fotini-Stavropotamos, the alluvial fans of neighboring torrents are joined sideways and created composite fans. That zone extents a bit below the main plain area of Xiropotamos. Similar fans exist, about 5 Km in length, along of the western slopes of Korissos karst system. However, these have been formed partly from fans and scree deposits of limestone composition. The old river deposits that develop south of Dispilio, between the Aliakmon River and the Gkioli stream, give the area a hilly topographic relief. Also, the dense drainage network reflects their impermeability.

Finally, the lakeside plain area is characterized by almost flat relief, horizontal sediment horizons and the existence of deltaic deposits. Such deltaic deposits exist between Polykarpi and Mavrochori.

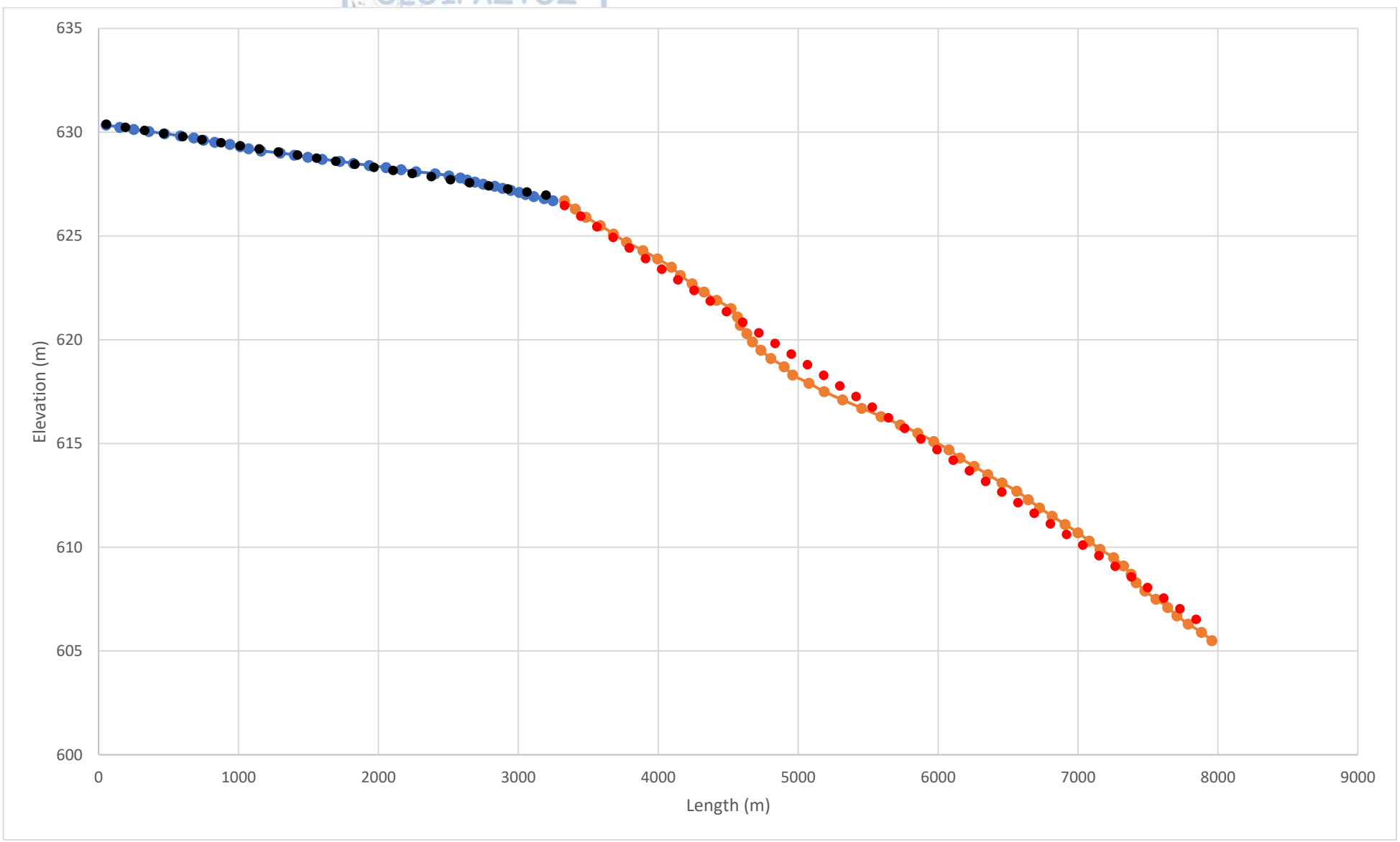

Figure 1 - Elevation along Gkioli stream

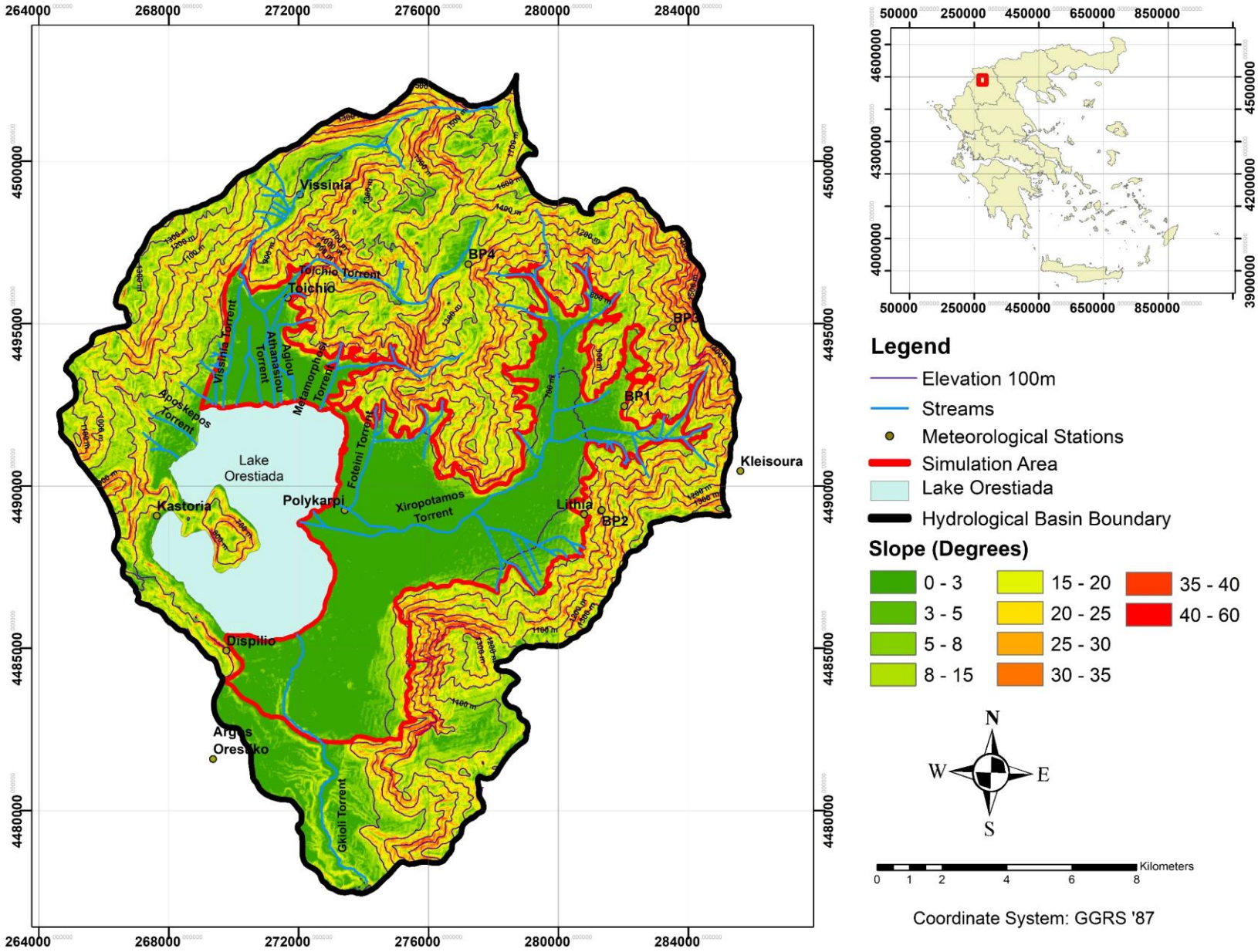

Figure 2 - Slope map of Kastoria Basin

3.2 Geology of Kastoria Basin

3.2.1 Geologic succession of the broader research area

The largest part of the Kastoria basin belongs to the Pelagonian zone while its western side represents part of the Sub-Pelagonian zone and the Mid-Hellenic trench. In general terms, the area consists of karst formations, alpine orogenesis metamorphosed plutonic rocks, molassic sediments of the Mid-Hellenic trench and in the uppermost strata loose quaternary formations with underlying Pleiocene sediments are found, which constitutes most of the formation types that are found in W.D GR 09. The metamorphic and plutonic rocks of the Pelagonian Zone exist in the north-eastern part of the area while the molassic sediments exist in the southwestern part. These geological formations have an orientation of NW-SE, as shown by the general tectonic movement of Greek formations (Brunn, 1956, 1959, 1961; IGME: Savoyat et al., 1971; Mountrakis, 1979, 1982b; Kilias, 1980; Mountrakis, 2010).

The main formations present in the study area are illustrated in Figures 2 and 3 are described below in chronological order of deposition, from older to younger.

Metamorphic bedrock. The crystalline bedrock of the Pelagonian zone is not homogeneous but consists of several rock strata that form an imbricate zone. Those rocks are considered to be parallel crystalline sequences of a common and uniform paleo-bedrock with similar lithological origin of Paleozoic or Pre-Cambrian age (Brunn, 1956, Maratos, 1972, Mountrakis, 1983). The metamorphosis of the crystalline bedrock is of greenschistolithic to amphibolitic phase and its metamorphosis took place in the Paleozoic before the Late Carboniferous (Mountrakis, 2010). The rocks that form the bedrock are mainly metamorphic and semi-metamorphic rocks (gneiss, amphibolites, amphibolitic and mica shale), with some appearances of plutonic rocks, i.e. gneiss granites. The gneiss of the crystalline bedrock is presented in segments with very good splitting, while in several positions they are deformed. Crystalline rock formations are all folded, due to the number of tectonic phases that have influenced the area. The general inclination of the foliation of gneisses and shales is NE to NW and almost always have small slopes i.e 15 – 25 degrees, while southwest slopes are also present at their body. In the broader area of this research, two series of the crystalline bedrock of the Pelagonian zone are found (Gianneli, 2009):

a) The Vitsio-Nympheo lower series, characterized by whitish or ashy colored gneisses, amphibolites and slates. This series is dominated by the presence of white colored gneisses, which are folded along with the other metamorphic rocks. The dense zones of mylonization, are an important feature of this series, which in some places are very characteristic of the intense tectonism that have occurred in the past as mentioned earlier.
b) The Kleisoura upper series, which consists mainly of amphibolites, epidote-amphibolite shale, two-mica shale, garnet-mica rich schists and gneisses. There are also several felsic magmatic intrusions in the rocks of this series. In some places serpentinites appearances are observed folded along with the rest of the series. The two series of Vitsi-Nymphaion and Kleisoura include shale appearances, that are found in both series, but differ in that the former is the lowest horizons with a usually normal transition to the upper horizons of the second series. Both series, however, form the undivided crystalline background of the Pelagonian zone.

The gneissed pluton of Kastoria. It is located in the lake of Kastoria, occupies the central mass of the Vitsi mountain range and extends to the northwest, where it merges with the granite of Florina and continues up in Yugoslavia (Mountrakis, 2010). These are magmatic penetrations of Upper Carboniferous age within the crystalline bedrock. This pluton basically is gneiss granite. Its feature is the light green color. It is folded along with the surrounding rocks during the alpine deformations during which alternations of rocks were position along several reverse faulting events.

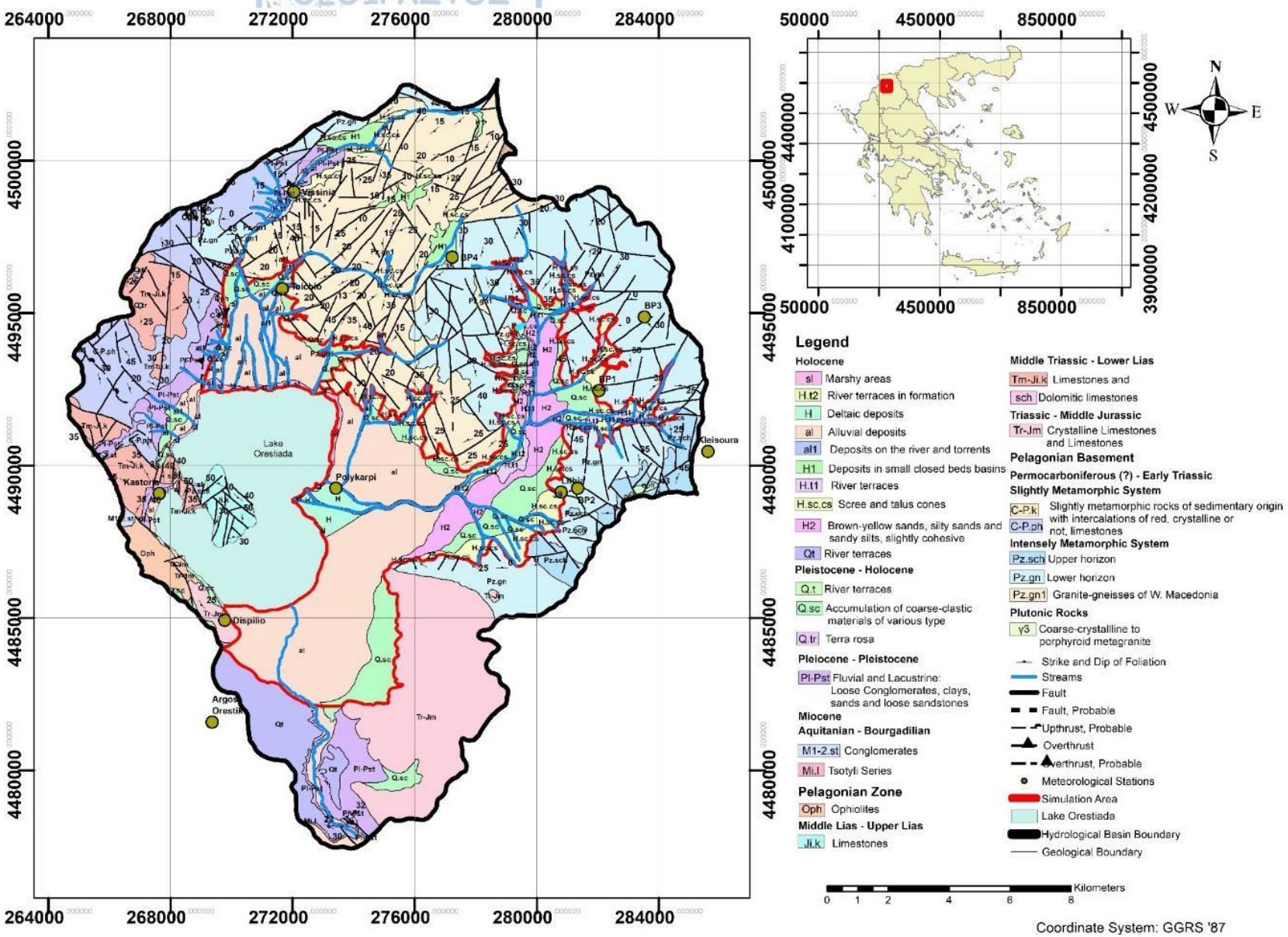

Figure 3 - Geological Map of Kastoria Basin (based on IGME sheets Kastoria, Argos Orestiko, Koristsa-Mesopotamia with modifications)

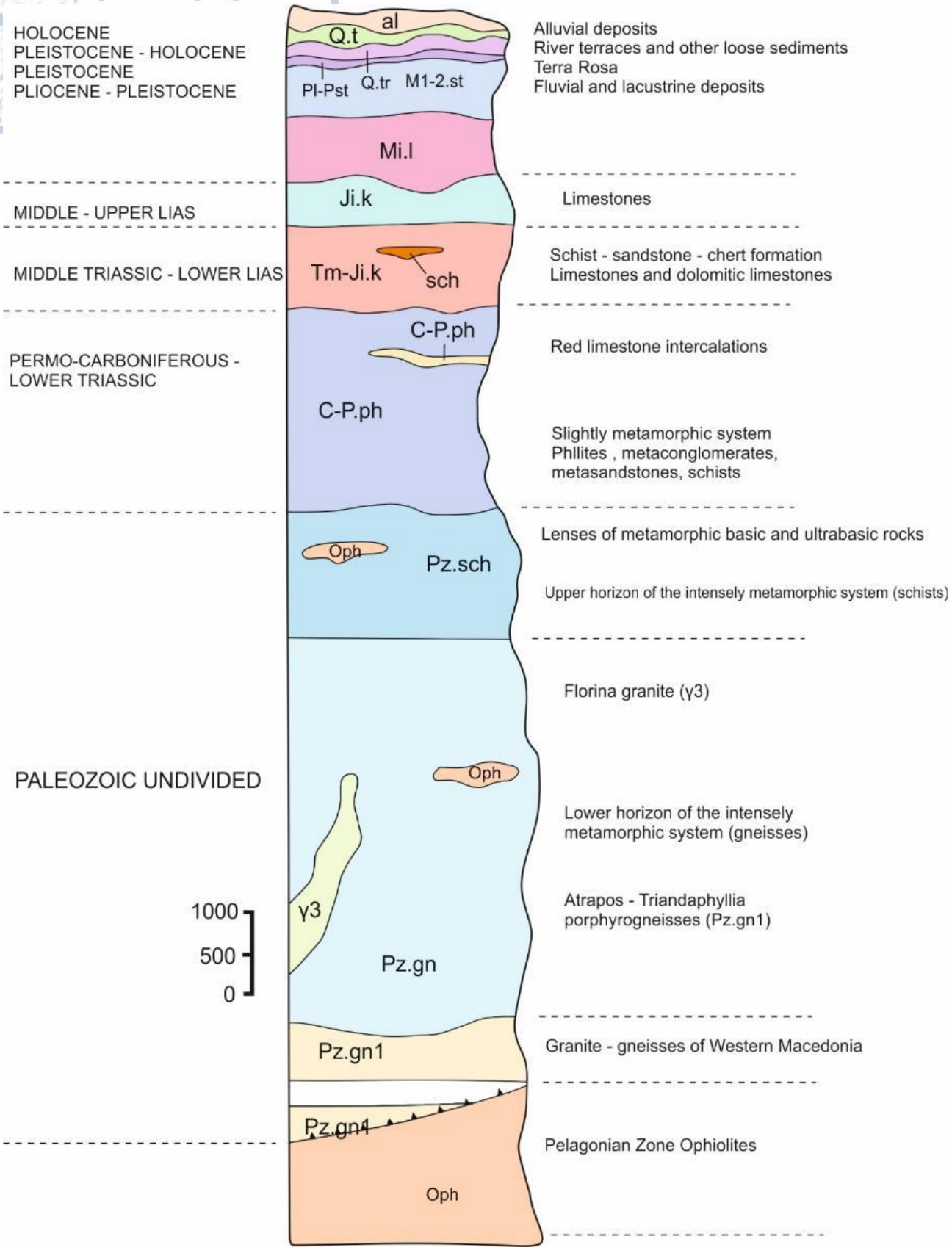

Figure 4 - Synthetic Stratigraphic Column of the main formations of Kastoria basin (adapted from IGME, 1981)

Permo-Triassic meta-clastic sequences. They exist on the western margin of Pelagonian zone and represent the old sedimentation of a continental slope developed during the continental fracturing, which led to the development of the ocean area west of the Pelagonian zone. The clastic sediments deposited there were metamorphosed during the Late Jurassic - Early Cretaceous in conditions of

the lower greenschist phase. The rocks that make up the meta-clastic sequences are phyllites, meta-arkoses, shales, quartzites, etc. (Vafeiadis, 1983).

Carbonate rocks. They consist of crystalline limestones, limestones and dolomite limestones. The limestone occurrences, based on paleontological findings found both in the broader research area and in adjacent areas, is of Triadic-Jurassic age (Brunn, 1956; IGME: Savoyat et al., 1971; Mountrakis, 1979, 2010). These rocks are highly fractured. Their most significant appearance is at the southeast of Lake Kastoria and south of Korissos. The occurrences of carbonate rocks are of particular hydrogeological interest to the wider region because they are associated with the appearance of significant karst springs, some of their occurrences greatly regulate the water balance of Lake Kastoria and finally discharge laterally into the granular aquifers of the lakeside plain (Vafeiadis, 1983).

Ophiolites. The Pelagonian ophiolithic mass is allochthonous. It originates from the two oceanic regions of the Axios and Sub-Pelagonian zones and were placed on the Triassic-Jurassic carbonate nappes on the two margins of each corresponding zones (Mountrakis, 2010). Those ophiolithic appearances that exist in Kastoria region, which is also the wider area of this research, are of small extent and isolated. The appearance of the most significant size is that at the south-west of the city of Kastoria, between the lake and the settlement Maniakoi (Vafeiadis, 1983).

Tertiary deposits. Tertiary formations are found mainly in the south-western part of the wider area, outside the boundaries of Kastoria basin. They are mostly composed of molassic sediments of the Mid-Hellenic trench (conglomerate, marls, sandstones) and, to a lesser extent, Pleio-Pleistocene fluvial deposits (conglomerate, cyan-green marls, loose sandstones, red clay). The Pleiocene sediments, found at the south part of the basin, were deposited after the emergence from below the sea of the molassic sediments and the formation of small lakes in the late Miocene - Pleiocene with the tectonic uplifting phase that followed (Vafeiadis, 1983).

Loose quaternary deposits. In the wider region, the quaternary formations exist around the homonymous lake of Kastoria. These quaternary deposits include: modern land deposits in the form of loose alluvia at valleys, river terraces, fluvio-torrential cones, alluvial fans and screes. The screes exist on the base of steep slopes at the edges of sub-hilly lands. The alluvial fans, which are deposited where the streams discharge on lower land and consist of moderately rounded pebbles and edgy pebbles. Among those deposits there is sand, sandy silt or brown-reddish clay. The thickness of those varies. Generally, those are less thick on the edges, while the fans themselves become thicker further downstream. Finally, the alluvial deposits of the main plain area consist of alternating layers of coarse and fine-grained deposits (gravel, sand pebbles, sandy clay, clay etc.). Their thickness is quite large i.e. up to 120m at the north and east, more than 300 m at the southern part of the basin (Vafeiadis, 1983).

3.3 Tectonic Setting of Kastoria Basin

As mentioned in a previous chapter the study area, belongs mainly to the Pelagonian Zone and at its southern part formations of the Mid-Hellenic Trench are found.

The Paleozoic basement of the Pelagonian zone, as shown by its age and tectonic processes deduced from its current structure, was influenced both by the Calidonian and Erkinian tectonic events as well as the Alpine orogenesis. These two former events (P1, P2) are also found in Kastoria basin, as in the rest of W.D GR 09 as mentioned in a previous chapter, where the crystalline rock formations are folded. The foliation of these folded rocks inclines generally towards the northeast, except from those found at the area of Lithia-Korissos where they incline towards the southwest. The carbonate rocks of Triassic – Jurassic age found at the Kastoria basin were brittly deformed by the P2 tectonic phase but they are also linked the upward movements that have occurred in the wider northern Hellenic and Balkan region during Neocene - Pleistocene (Mountrakis, 2010). Also,

the Miocene marine sediments currently located at altitudes of 600-700 meters a.m.s.l, give a measure of the uplifting tectonic process that followed after Middle Miocene, which was caused by the Neo-Alpine tectonics. Also, the flattened limestone surfaces on the Korissos and Kazani heights, which probably are part of a paleo coast, suggests that the upwards movement of the rock mass due to tectonic events (Vafeiadis, 1983).

During the Alpine folding event, a slip proportional to the gravity were created and can now be found on the schistokeratolithic with ophiolite rock complex. Considered as a phenomenon of this slip are the limestone and shale fragments encased in the Paleozoic diabasic schist at Kastoria-Dispilio area, the tectonic wedges of the shales and limestones in the ophiolites, the small ophiolithic appearances in the shale of the area of Kefalari, the presence of the gneissed granite of Kastoria on top of the area's ophiolites and finally the observed faults with clastite in their fracture zone at Kastoria basin, which are found at the limestones of Triassic-Jurassic age and the thrusted ophiolites on top of the limestones (Vafeiadis, 1983).

After the Alpine Orogenesis, the basement reacted as a brittle mass that gave faults at the general direction of the pre-existing folds and allowed the meta-alpine sediments to be deposited uncomfomibly on it during the meta-Alpine relaxation. Also, there were plutonic intrusion and volcanic activity, whose products are the basic rocks involved in the petrographic composition of PermioCarboniferous phyllites (Diabasic Shale of Kastoria-Dispilio).

Finally, the meta-Alpine tectonic relaxation is associated with vertical fractures of the Quaternary, which created the present geomorphology of the area.

3.4 Climate of Kastoria Basin

In the present thesis, data from twelve meteorological stations were used, which are found in the broader study area (Fig. 5), Those stations operate under the supervision of different organizations. Info data for these stations is summarized in Table 2. All the stations are equipped with rain and snow gauges and thermometers, while one is also equipped with evaporation pan. Snowfall has been converted to equivalent rainfall height automatically by the meteorological instruments of each station. Temperature data were available from seven stations; four within the study region and one outside of it. Evaporation was available only from the meteorological station of Dispilio so are not of an adequate spatial resolution to give any more insight for the wider study area. However, these data can give a reliable estimation about the plains of Kastoria basin, where the aforementioned station resides.

Table 2 - Meteorological Station Info used in this thesis

ID	Name	Latitude	Longitude	Elevation (m)	Owner/Operator	Rain	Temperature	Evaporation
1	Kleisoura	40.537144°	21.468548°	1180	DEH/meteo.gr	2000-2018	2010-2018	N/A
2	Argos Orestiko	40.452946°	21.280223°	661	NMS	2000-2018	2000-2018	N/A
3	Kastoria	40.519904°	21.257043°	630	M.E.D.C.C/meteo.gr	2000-2018	2010-2018	N/A
4	Dispilio	40.483109°	21.283854°	630	DEH	2008-2018	2000-2012	1999-2010
5	Tichio	40.581426°	21.302127°	663	RWM	2009-2018	2009-2018	N/A
6	Polykarpi	40.523023°	21.325206°	630	RWM	2009-2018	2009-2018	N/A
7	Vissinia	40.610178°	21.305468°	885	DEH	2000-2018	N/A	N/A
8	Lithia	40.523911°	21.412274°	940	RWM	2008-2018	2009-2018	N/A
9	BP1	40.5542°	21.4257°	760	Gianelli, 2009	2004-2007	N/A	N/A
10	BP2	40.5252°	21.4186°	940	Gianelli, 2009	2004-2007	N/A	N/A
11	BP3	40.5763°	21.4425°	1170	Gianelli, 2009	2004-2007	N/A	N/A
12	BP4	40.5923°	21.3675°	1250	Gianelli, 2009	2004-2007	N/A	N/A

POE (DEH = Dhmosia Epicheirish Hlektrikou Reumatos "Δημόσια Επιχείρηση Ηλεκτρικού Ρεύματος") = Public Organization of Electricity, RWM = Region of Western Macedonia, NMS = National Meteorological Service. Altitude is in m above mean sea level. N/A = Not available

Use of data from stations widely spread over the area offers the means to develop an understanding of the rainfall, temperature and evaporation pattern in the study area.

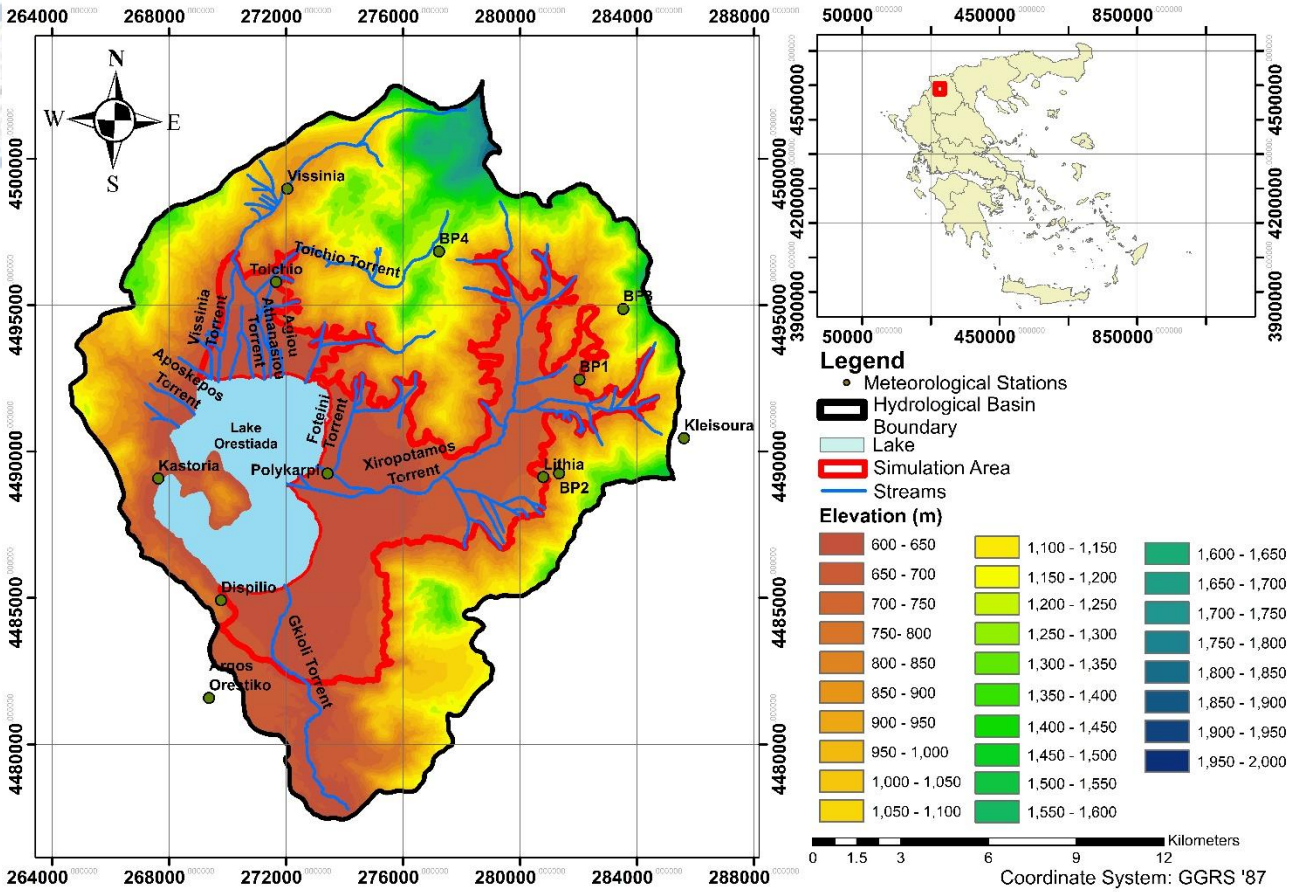

Figure 5 - Elevation map and positions of meteorological stations used in this thesis

3.4.1 Temperature and Evaporation patterns

Temperature measurements were available from the meteorological station of the National Meteorological Service of Greece, at Kastoria Airport, Argos Orestiko, the meteorological stations of Municipality of Kastoria located at Tichio, Polykarpi, Lithia and those of meteo.gr at Kastoria and Kleisoura. The stations are located within the study area, excluding the Argos Orestiko and Kleisoura station, the topography of which is gentle for its largest part, and within which the meteorological parameters do not vary significantly. Temperature data were available for the periods shown at Table 2.

3.4.1.1 Temperature

The mean annual temperature for Kastoria basin, for the period 2000-2018, was calculated to be 12.13°C. As expected in such a climate, maximum temperatures occur during the dry summer months, whereas the lowest are in the cold winter months. During the winter season, the mean monthly temperature can reach values of 3.45°C, whilst in the summer season it was 21.3°C. This displays a rather cold air temperature regime. A considerable annual variability in temperature exists in the region. Sometimes the temperature drops below 0°C while rarely exceeds 35°C. Such variabilities commonly have serious implications for agriculture. However, due to the low temperatures during the winter crops cannot be cultivated; thus, crops are cultivated only during spring, summer and the earliest part of autumn. Figure 6 displays the monthly temporal variations of mean, max and min temperatures while Fig. 7 displays the monthly means. Also, Table 3 summarizes annual statistics of all three type of temperatures while Table 4 presents monthly means for average temperature only. Finally, mean monthly, max mean monthly and min mean monthly temperature figures for the entire Kastoria basin along with a mean temperature figure for the W.D GR 09 are passed at APPENDIX C.

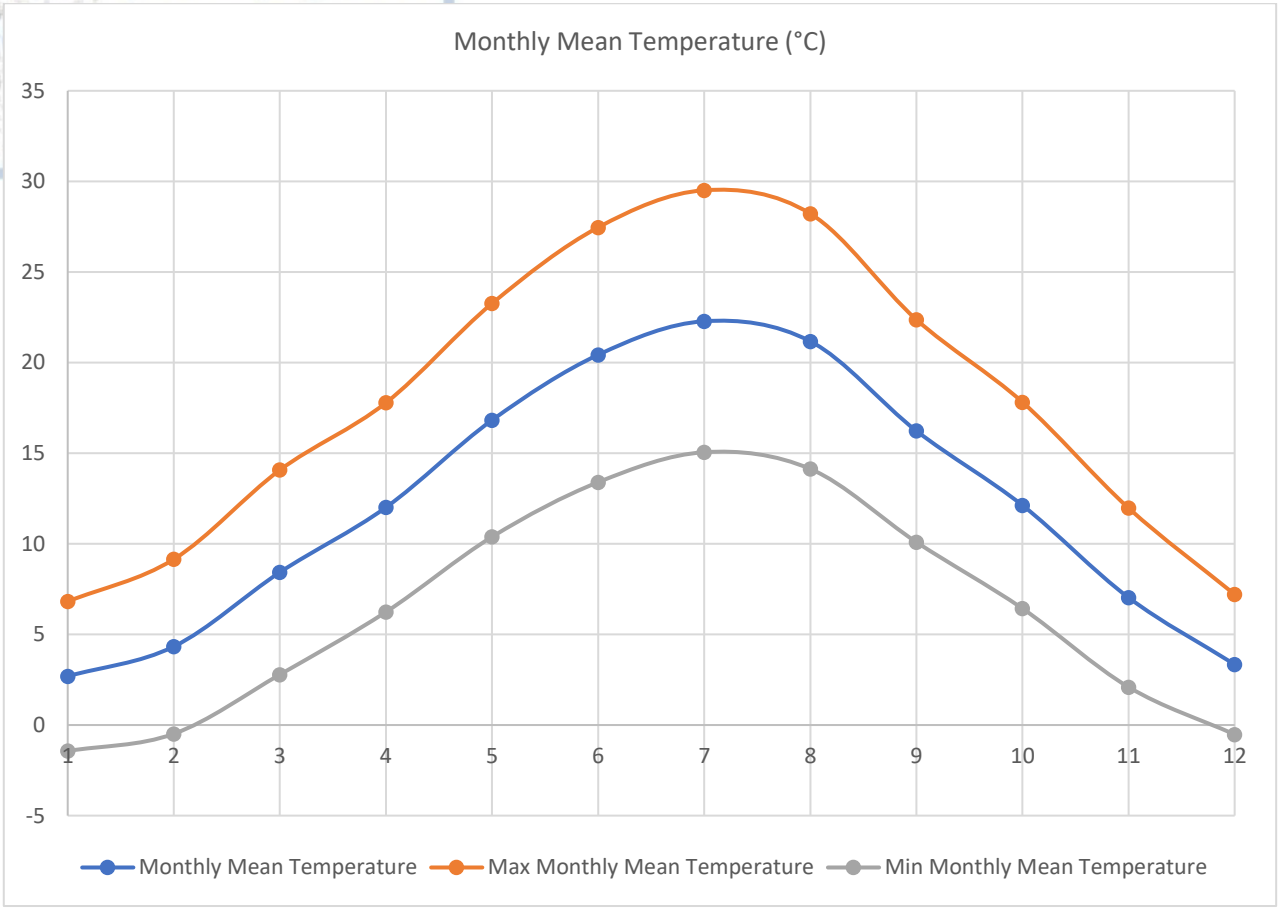

Figure 6 – Mean, Max and Min Monthly Temperature for period 2000-2018 at Kastoria Basin

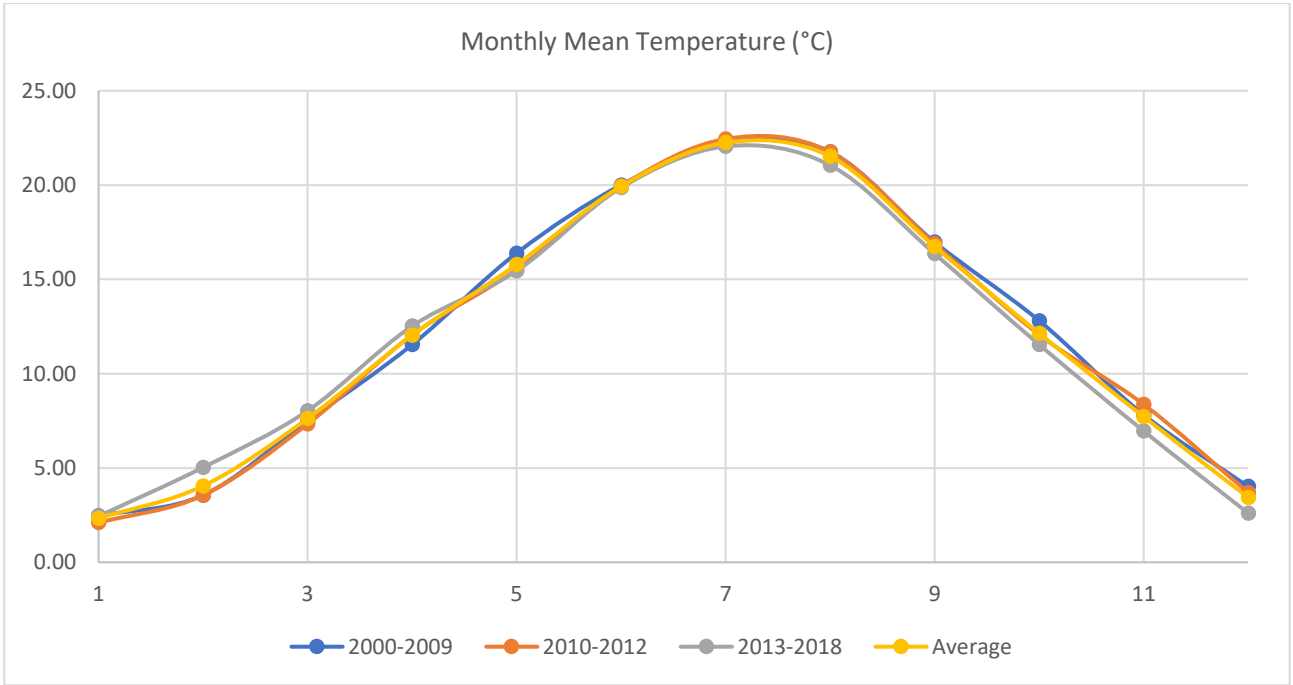

Figure 7 - Monthly Mean Temperature for period 2000-2018 at Kastoria Basin

Table 3 – Annual Temperature Statistics for period 2000-2018 at Kastoria Basin

Years	Temperature (°C)		
	Maximum	Minimum	Average
2000	22.31	-2.00	12.08
2001	23.97	0.90	12.91
2002	22.65	2.67	12.26
2003	22.84	-0.12	12.14
2004	22.12	1.24	11.99
2005	22.64	0.79	11.77
2006	22.07	-0.08	11.56
2007	23.56	3.44	13.06
2008	23.02	3.10	12.61
2009	22.76	3.07	12.76
2010	22.10	3.28	12.22
2011	23.13	1.15	11.85
2012	25.17	0.06	12.82
2013	15.14	3.01	9.80
2014	23.13	1.77	12.48
2015	23.34	0.25	12.72
2016	22.47	0.75	12.32
2017	23.17	3.48	12.54
2018	22.03	2.80	12.73
Mean	22.51	1.56	12.24

Table 4 - Monthly Means for 2000-2018 at Kastoria Basin

Month	Monthly Mean Temperature (°C)			
	2000-2009	2010-2012	2013-2018	Average
Jan	2.35	1.74	3.37	2.49
Feb	3.53	3.28	5.49	4.10
Mar	7.70	7.74	8.75	8.06
Apr	11.40	11.76	13.06	12.07
May	16.59	16.03	16.96	16.53
Jun	20.31	20.40	20.40	20.37
Jul	22.37	22.94	22.45	22.59
Aug	21.98	21.94	20.84	21.59
Sep	17.00	17.03	15.96	16.66
Oct	13.04	10.76	11.29	11.69
Nov	7.97	6.13	6.51	6.87
Dec	3.60	2.74	2.68	3.01
Average	12.32	11.87	12.31	12.17

For the spatial distribution of the mean, maximum and minimum temperature five stations were used. They are located at Argos Orestiko, Kleisoura, Toichio, Lithia and Polykarpi. As observed at Fig. 8, 9 & 10 the higher values are found at the west side of the basin while the minimum values are found at the east side, which is of higher elevation.

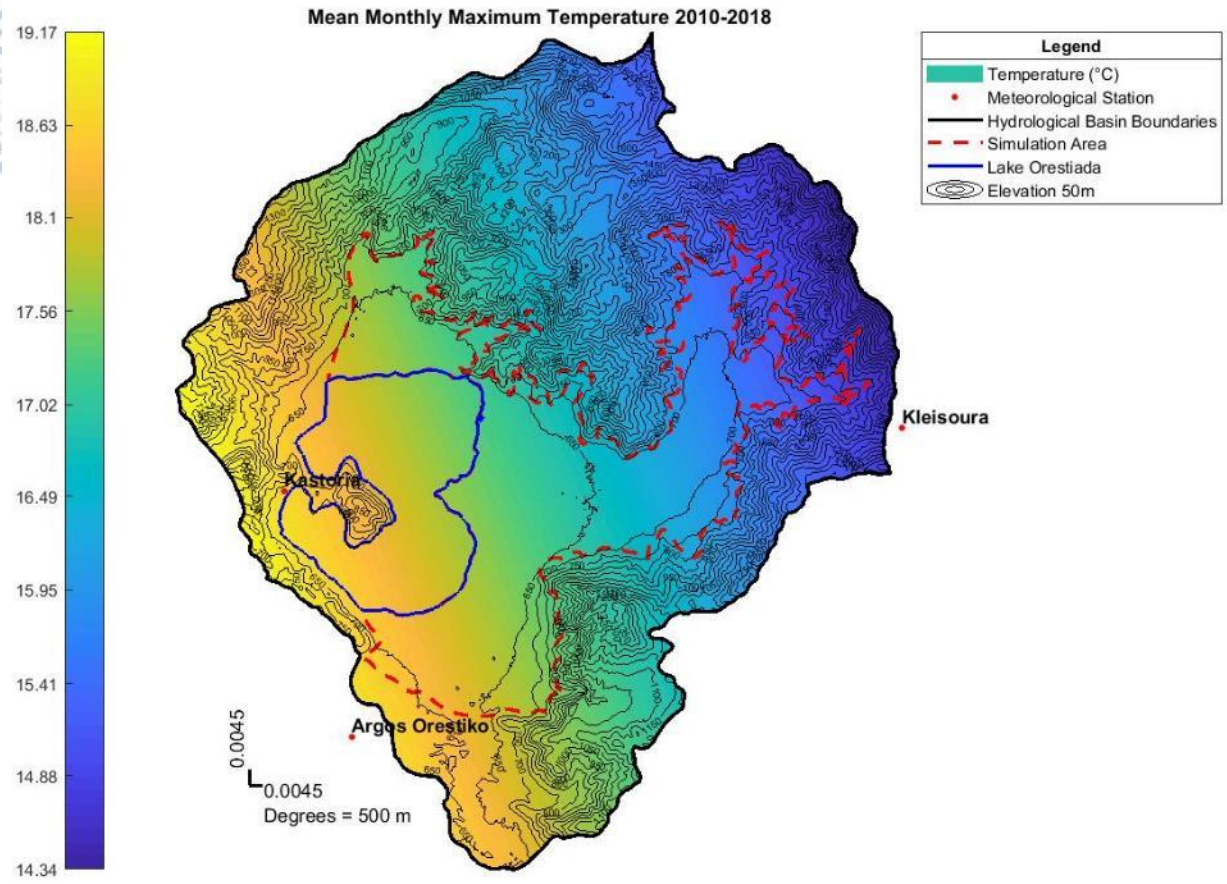

Figure 8 - Mean Monthly Maximum Temperature for period 2010-2018 at Kastoria basin

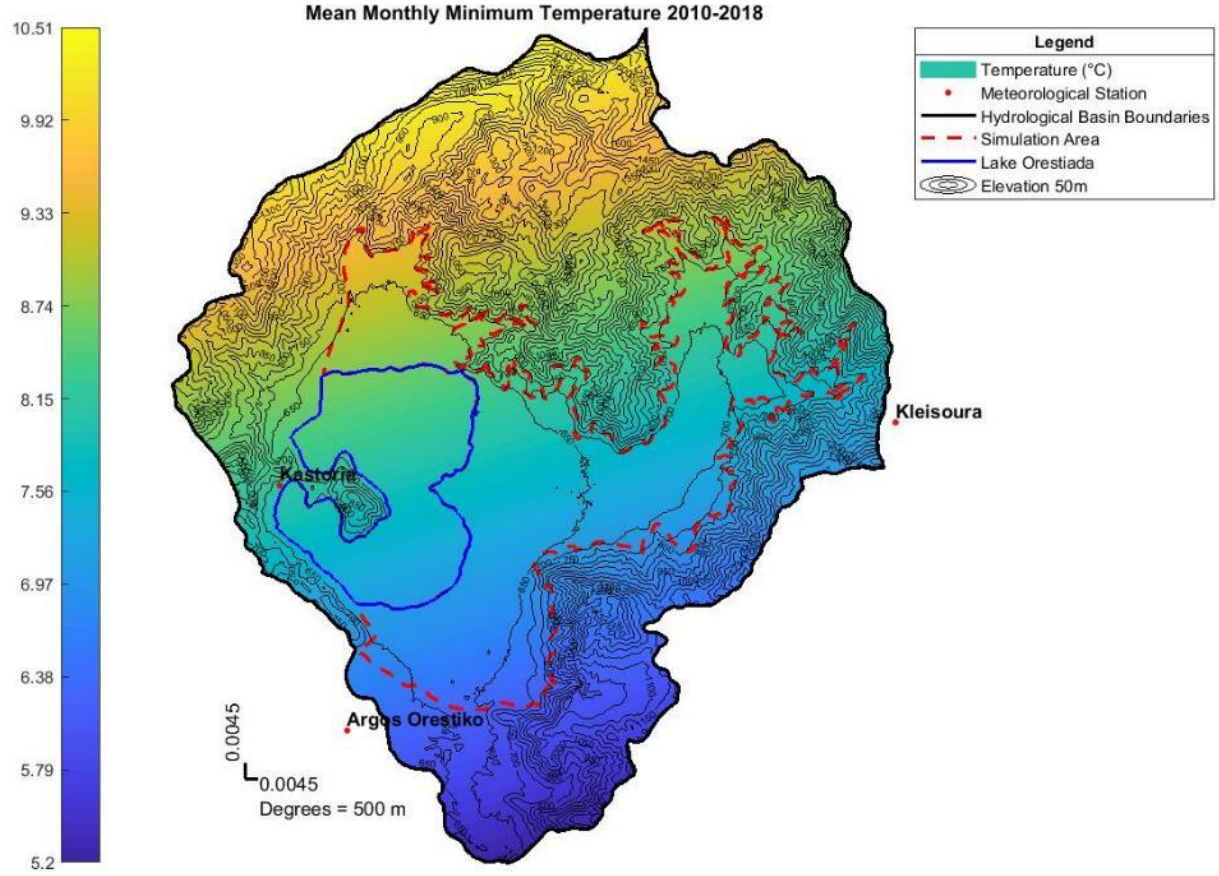

Figure 9 - Mean Monthly Minimum Temperature for period 2010-2018 at Kastoria basin

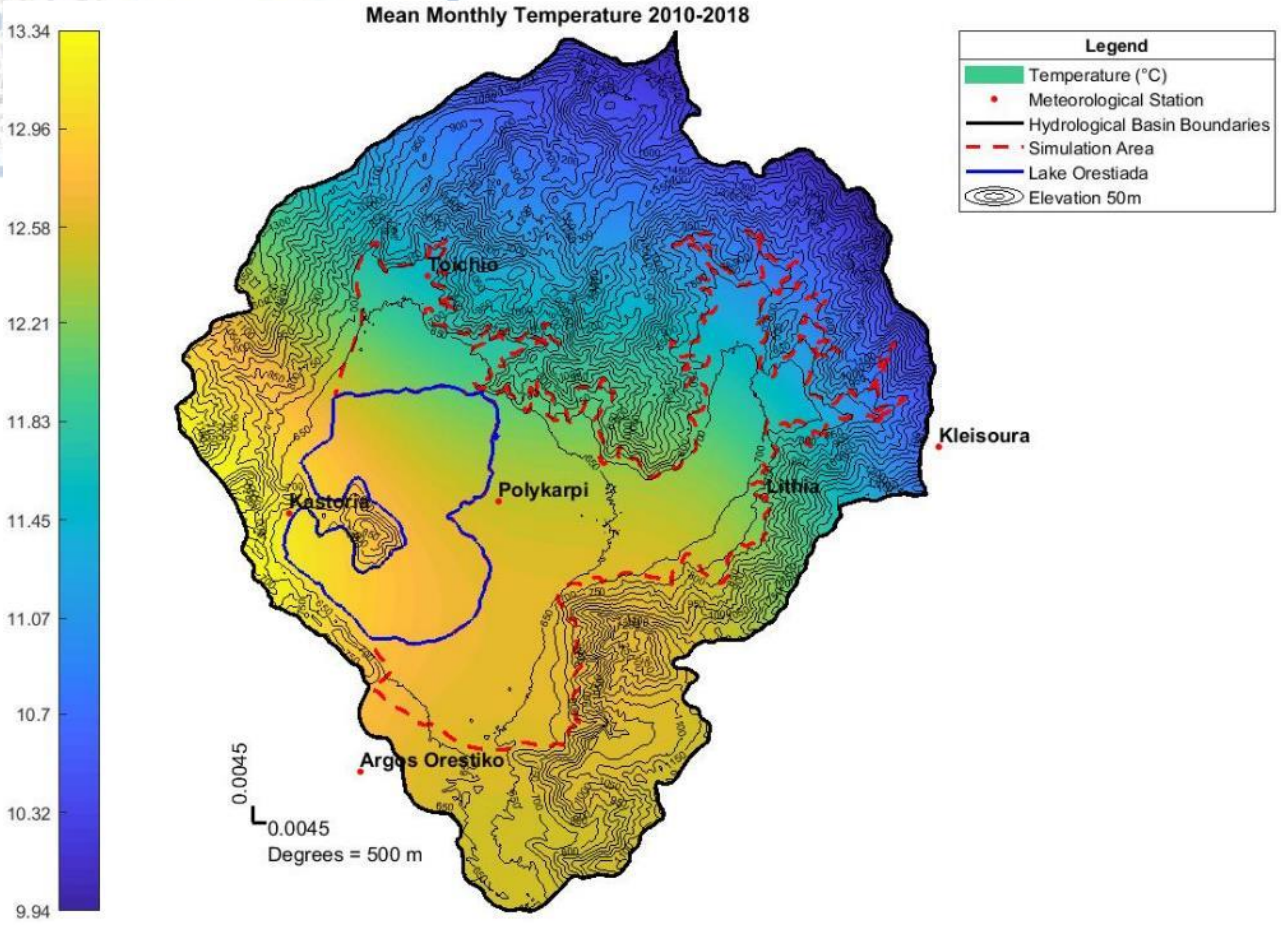

Figure 10 - Mean Monthly Temperature for period 2010-2018 at Kastoria Basin

3.4.1.2 Evaporation

Evaporation is one of the parts of the hydrological cycle, being so vital to assess the hydrologic regime of any region, and is affected by a number of factors. Seven in total and listed as such: 1. Latent heat required for changing the phase from liquid to gaseous. 2. Temperature of the liquid and the surrounding air. 3. Vapor capacity of the air. 4. Wind speed. 5. Weather pattern (pressure). 6. Nature of evaporating surface. 7. Soil moisture content (Ven Te Chow, 1964).

Measurements obtained from a pan evaporimeter at the Dispilio station were used for the assessment of the evaporation over the study region. Data for the rest of EL 09 were not available and given its size the data from Dispilio station cannot produce a meaningful conclusion for the rest of Kastoria basin. Analysis of the available data (1999-2010), in the form of total monthly evaporation values, shows that actual evaporation varies considerably over the year, reaching its highest values in the late Spring-dry summer months-early autumn and its lowest by mid-Autumn and Winter (Fig. 13). During the 12 years of available records the minimum monthly evaporation recorded was 6 mm in Jan 2001 while the highest recorded in August 1999 was 221.1 mm. Annual values vary from 759.89 mm to 1267.40 mm with an average of 972.33 mm. Annual statistical data are summarized to Table 5 while mean monthly statistical data are summarized to Table 6.

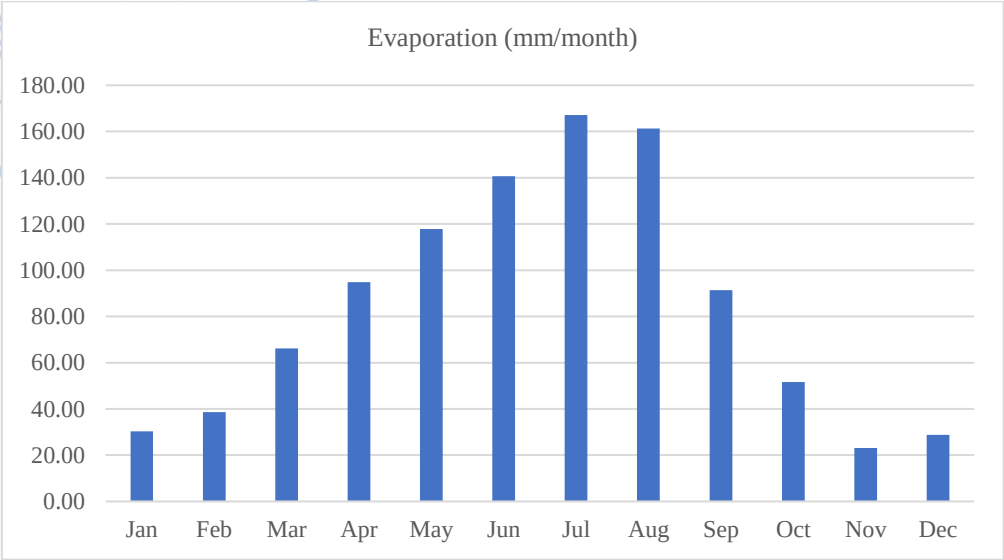

Figure 11 - Mean Monthly Evaporation for period 1999-2010 at Dispilio station

Table 5 - Monthly Evaporation Statistics for period 1999-2010 at Dispilio station

Month	Evaporation (mm/month)		
	Mean	Max	Min
Jan	30.33	61.70	6.00
Feb	38.66	71.50	16.40
Mar	66.15	88.60	26.00
Apr	94.87	205.30	50.00
May	117.88	173.00	43.50
Jun	140.74	169.90	79.50
Jul	167.15	202.90	117.00
Aug	161.33	221.10	123.40
Sep	91.41	120.00	57.00
Oct	51.63	102.90	21.10
Nov	23.07	46.10	9.69
Dec	28.86	65.00	9.60
Sum	1012.08	-	-

Table 6 - Annual Evaporation Statistics for period 1999-2010 at Dispilio station

Years	Evaporation (mm)			
	Mean	Max	Min	Sum
1999	63.32	221.10	9.69	759.89
2000	99.36	186.60	9.60	1192.32
2001	87.29	168.50	6.00	1047.47
2002	92.11	146.80	22.20	1105.32
2003	84.78	156.50	12.60	1017.36
2004	85.82	158.90	14.20	1029.84
2005	83.61	149.60	16.76	1003.26
2006	93.97	165.00	21.86	1127.59
2007	87.98	197.10	21.90	1055.70
2008	92.71	185.70	17.89	1112.50
2009	105.62	205.30	16.40	1267.40
2010	91.76	212.50	19.40	1101.10
Mean	83.03	170.66	16.52	996.62

3.4.2 Rainfall

Rainfall has a significant role in a hydrogeological study and as such, serious consideration has been given to ensure the consistency and reliability of the available data. The alluvial basin of Kastoria is covered by several of rainfall stations, which are of more than adequate number. However, to achieve better reliability in terms of the method used to spatially distribute the rainfall two more station were taken also into account that are outside the wider study area, providing a broader hydrological network and thus a better understating of the distribution and pattern of precipitation. The latter, as discussed in the next Chapter of the present thesis, is in close hydrogeological interaction with the aquifer system of the alluvial basin. Rainfall records are available as monthly totals for the periods defined in Table 7. Figure 12 and Table 8 summarize rainfall data as mean monthly values. Some of the records were incomplete, so the period of time covered by them is not consistent. Those missing values were filled using the mean value of all corresponding months. Fig. 13 presents the mean annual precipitation relationship with elevation. This was done with linear trendline and the use of four rainfall stations of Vissinia, Kastoria, Kleisoura and Argos Orestiko. The linear analysis yielded Y=0.533X+291.58 with R^2~=0.9 (Fig. 13), a result which is similar to the one produced by Vafeiadis (1983) and IGME (2010) for the eastern region of W.D GR 09.

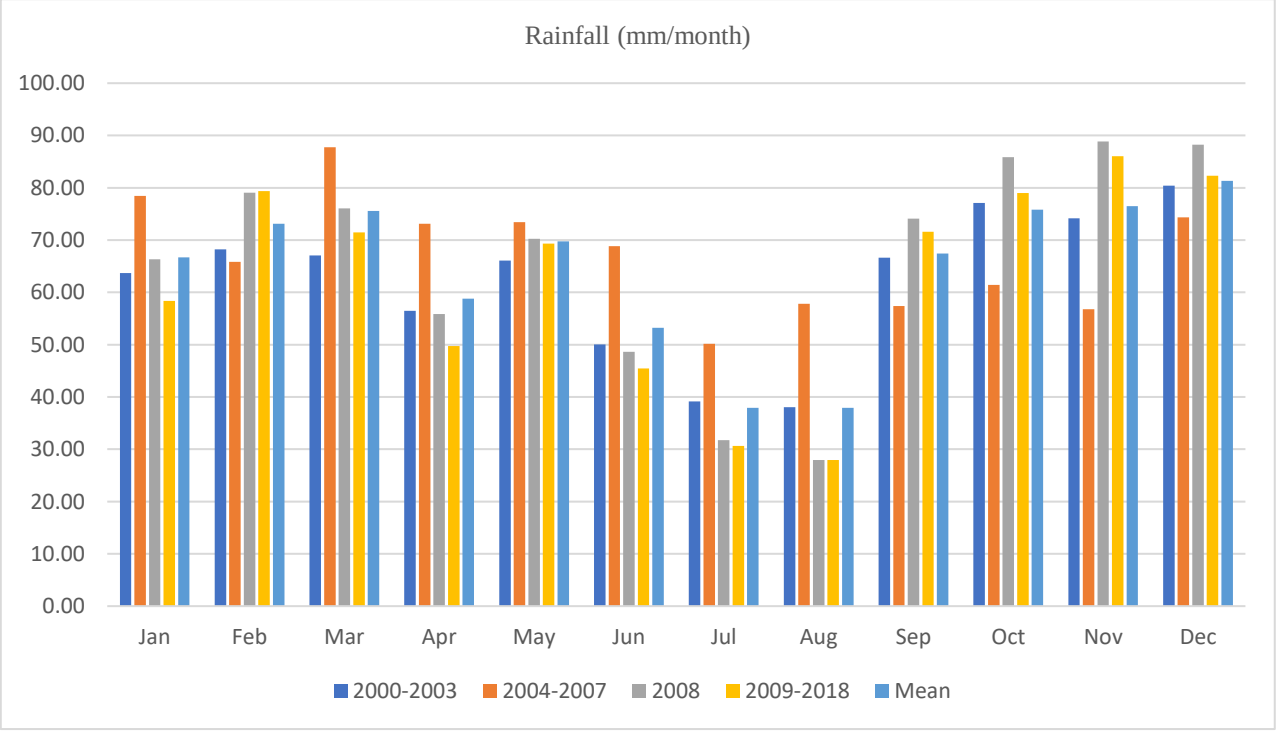

Figure 12 - Mean Monthly Rainfall for period 2000-2018 at Kastoria Basin

Table 7 - Monthly Rainfall Statistics for period 2000-2018 at Kastoria Basin

Month	Rainfall (mm/month)				
	2000-2003	2004-2007	2008	2009-2018	Mean
Jan	63.70	78.46	66.32	58.39	63.70
Feb	68.20	65.85	79.08	79.37	68.20
Mar	67.05	87.77	76.08	71.47	67.05
Apr	56.47	73.13	55.87	49.75	56.47
May	66.06	73.44	70.22	69.32	66.06
Jun	50.07	68.83	48.64	45.46	50.07
Jul	39.17	50.15	31.76	30.64	39.17
Aug	38.04	57.80	27.96	27.93	38.04
Sep	66.63	57.39	74.09	71.58	66.63
Oct	77.11	61.42	85.83	79.03	77.11
Nov	74.15	56.76	88.88	86.06	74.15
Dec	80.40	74.36	88.26	82.32	80.40
Sum	747.07	805.37	792.98	751.32	747.07

Table 8 - Annual Rainfall Statistics in mm for period 2000-2018 at Kastoria basin

Year	Mean	Max	Min
2000	57.94	91.21	24.06
2001	48.74	94.44	22.47
2002	74.71	201.13	26.93
2003	78.10	182.21	21.98
2004	71.66	140.53	19.67
2005	62.43	112.03	18.89
2006	59.25	103.01	20.16
2007	58.22	107.06	13.13
2008	48.50	106.90	4.92
2009	83.36	168.19	23.25
2010	79.68	168.09	14.22
2011	41.13	112.64	11.81
2012	58.85	109.92	15.49
2013	55.97	143.58	6.17
2014	61.90	150.54	16.66
2015	62.87	128.44	11.25
2016	65.54	213.23	5.55
2017	52.72	140.14	9.75
2018	68.01	137.38	5.12
Mean	62.61	137.41	15.34

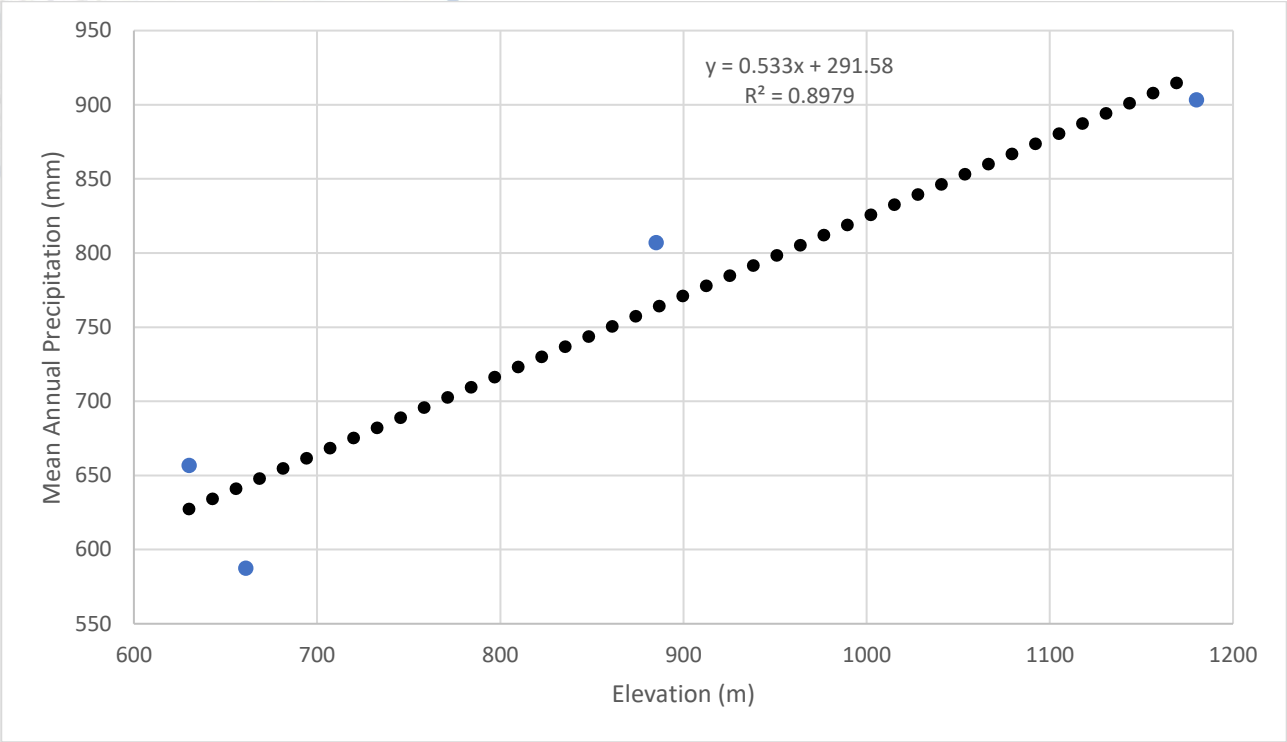

Figure 13 - Mean Annual Precipitation - Elevation Relationship

3.4.2.1 Rainfall pattern

Spatial distribution of precipitation is of significant importance in hydrology. According to Luo et al. (2010), Radial Basis Function Network, Kriging, Inverse Distance Weighting are widely used methods for such calculations. However, there are several more methods to determine the characteristics of precipitation over a catchment described in the literature, including the Arithmetic Mean, the Thiessen Polygons, the Isohyetal Method, the Hypsometric and the Multiquadratic Methods (Shaw, 1994; Panagopoulos, 1996). In this thesis, Radial Basis Function Network (Multiquadric), coded by Chirokov 2006, was used as a free mesh approach to spatially calculate the rainfall in the study area. This is done in an automated fashion via a MATLAB algorithm, developed in the framework of this thesis, that incorporates the aforementioned R. B function.

As mentioned earlier, R. B function was used to interpolate the spatial pattern of precipitation. The average annual rainfall for 19 years is 730 mm, between 2000 and 2018, which interpolated values is close to the one (~747 mm) calculated by simple statistics shown at Table 7 & 8. Fig. 14 and 15 depict the pattern of rainfall. Both figures depict the same pattern. They also present higher values of precipitation (>900 m of altitude) to places with a higher altitude at the eastern side of the basin while presenting low values at the western side. The plains of Kastoria basin receives relatively high amounts of rainfall while most of the rocky part of the basin receives a high amount of rainfall ranging from 750 mm to 1000 mm (Fig. 16). Also, mean monthly precipitation figures for the entire Kastoria basin along with a mean annula precipitation figure for the entire W.D GR 09 are passed at APPENDIX C.

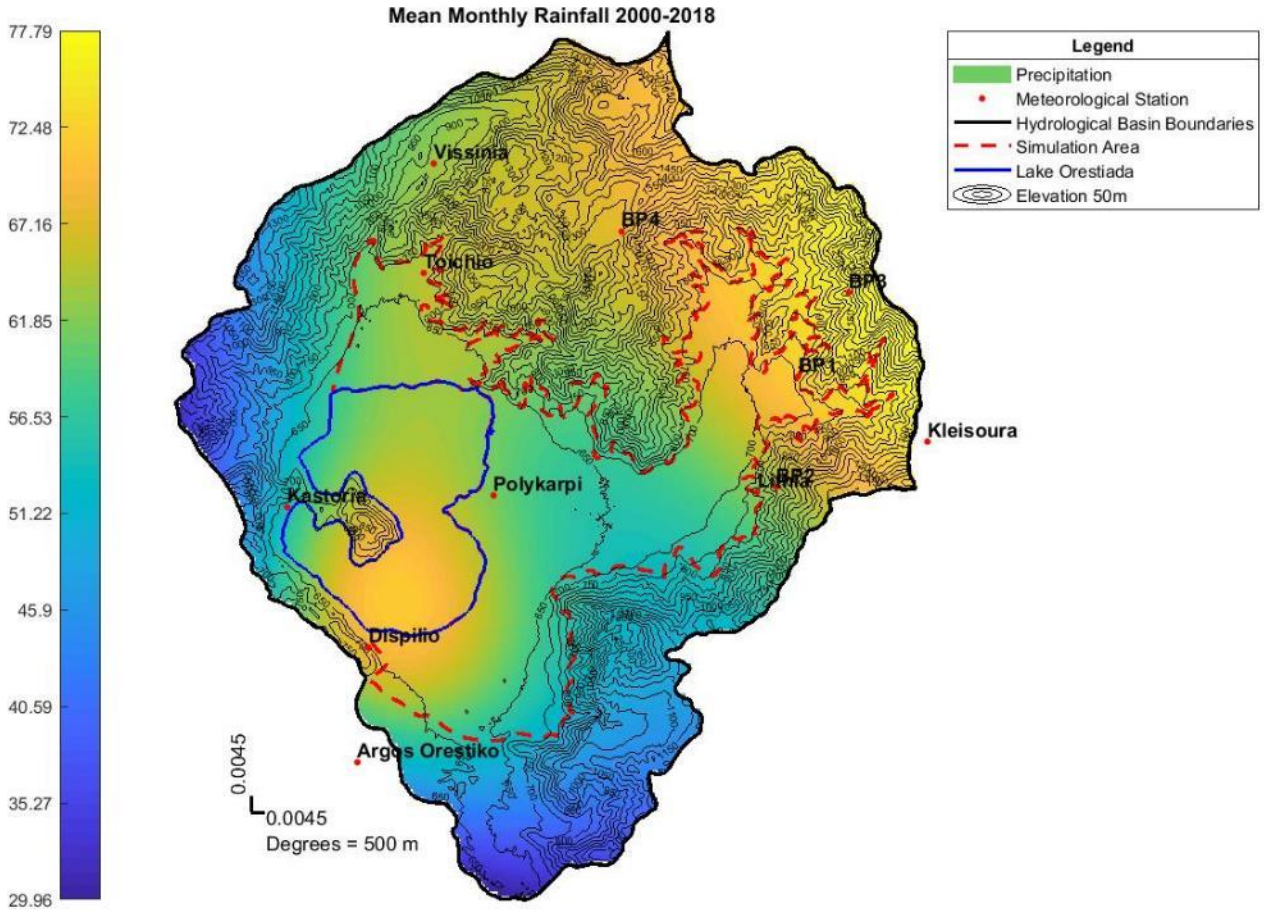

Figure 14 – Mean Monthly Rainfall for years 2000-2018

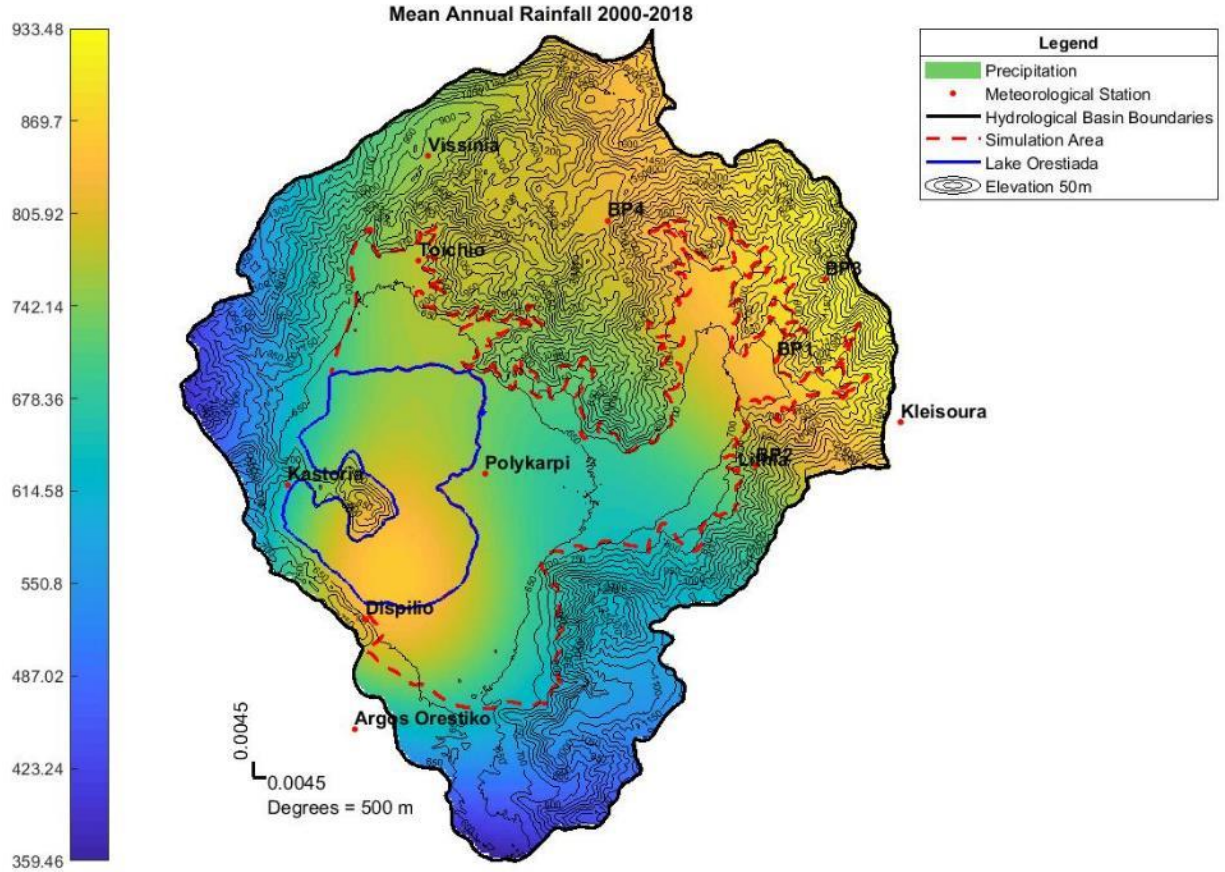

Figure 15 - Mean Annual Rainfall 2000-2018

During this period 52.6% of the years deviated below the average, indicating that dry spells prevail over wet ones (Table 8 & Fig. 16).

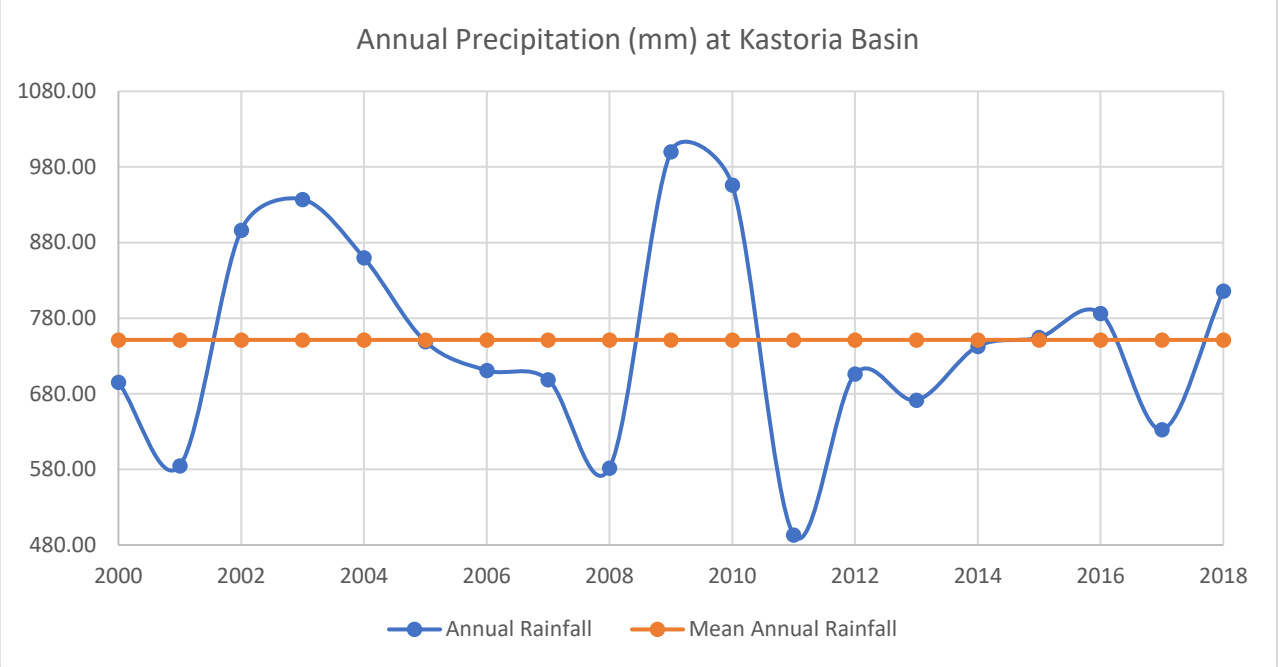

Figure 16 - Annual Rainfall at Kastoria Basin for period 2000-2018

The bulk of the rainfall mainly occurs during the winter and autumn months and to a lesser extent during early spring (Table 9). During at the dry period (June-September), only individual events are experienced. Rainfall intensity is inversely proportional to the "wetness" of the month. Towards the dry months the rainfall intensity increases and the duration decreases while during winter time rainfall events are of low intensity and of long duration. This fraction of the rainfall eventually contributes to aquifer recharge. Since year 2000 rainfall events have been concentrated in fewer months, and are characterized by very high intensity and low duration. Such a pattern leads to water clogged-soil, which impedes percolation and recharge. This in turn causes considerably increased runoff, commonly resulting in extensive flooding of land (Panagopoulos, 1996). Severe floods were reported in several months during period 2005-2007, i.e Mar-2005, Jan-2006 and Apr-2007 (Gianneli, 2009).

3.4.3 Evapotranspiration

Evapotranspiration is an important component of the hydrologic cycle as it can significantly affect the water budget of the natural. This necessitates its accurate estimation. Several empirical methods have been developed to derive evapotranspiration estimates. The Food and Agriculture Organization of the U.N. (F.A.O) recommends the Penman–Monteith method as the sole method to calculate reference evapotranspiration, wherever the required input data (i.e. temperature, relative humidity, solar radiation, wind speed) are available (e.g., Allen et al, 1998; Ampas et al, 2007). Other widely used methods are the FAO 24 Penman method, the FAO 24 Blaney and Criddle method (Doorenbos & Pruitt, 1977), the FAO 24 Makkink method, and the Hargreaves method (Hargreaves & Samani, 1982; 1985). Choosing one of those depend mainly upon the availability of the measured meteorological data. These may be categorized into one of the following classes of energy budget, aerodynamic transfer (or mass transfer), a combination of those and empirical methods.

The suitability of various evapotranspiration methods has been subject of research for many hydrologists and agriculturists, due to the different results they provide under different climatic conditions. Evapotranspiration research also includes comparison of numerous equations describing evaporation or evapotranspiration. Among the articles on comparison between different approaches is the work of Xu & Singh, 2002, which evaluated five empirical equation of ET_0 estimation with

daily datasets from Switzerland and of Antonopoulos & Antonopoulos, 2018, which compared the results of thirteen methods of evapotranspiration estimation using seven years of monthly meteorological data from Amynteo meteorological station of the National Meteorological Service.

In this thesis, the available data for the estimation of the reference evapotranspiration (ET_0) were only temperature. A comparison was made between temperature methods: the Blaney-Criddle method (Blaney-Criddle, 1950) and the Hargreaves method (Hargreaves-Samani, 1985). These methods were then compared to the mean monthly Penman-Monteith values of $\mathbf{ET_0}$ produced by Georgiou et al, 2000, who used meteorological data from meteorological station of Edessa, Katerini, Kozani, Ptolaimaida and Florina, which are found at basins adjacent to the one studied. Nineteen years of monthly temperature data of Argos Orestiko meteorological station of N.M.S, Kastoria, Toichio, Polikarpi and Kleisoura stations of meteo.gr were used for this comparison. These data were applied in the following Equations:

Blaney-Criddle

$$\boldsymbol{ET_b = p(0.457T_{mean} + 8.128),} \quad \textbf{[3.1]}$$

where,

$\boldsymbol{ET_b}$ is the reference evapotranspiration (mm d^{-1})

$\boldsymbol{T_{mean}}$ is the mean daily temperature (°C) given as $\boldsymbol{T_{mean} = (T_{max} + T_{min})/2}$

$\boldsymbol{p}$ is the mean daily percentage of annual daytime hours

Hargreaves-Samani

$$\boldsymbol{ET_h = 0.408(0.0023R_a(T_{mean} + 17.8)\sqrt{T_{max} - T_{min}},} \quad \textbf{[3.2]}$$

where the 0.408 =1/λ factor converts from MJ m^{-2} d^{-1} to mm d^{-1}

$\boldsymbol{ET_h}$ is the reference evapotranspiration (mm d^{-1})

$\boldsymbol{T_{mean}}$ is the mean daily temperature (°C) given as $\boldsymbol{T_{mean} = (T_{max} + T_{min})/2}$

$\boldsymbol{R_a}$ = extraterrestrial radiation (MJ m^{-2} d^{-1})

The following Tables depict the results from the comparison between the mean monthly Penman-Monteith values of evapotranspiration received from Georgiou et al., 2000 and those produced by the above equations yielded, by using monthly temperature data for 9 years, the following tables, which summarize the mean monthly percent change for the aforementioned meteorological station at the study basin for each of the two evapotranspiration estimation equations.

Table 9 - Monthly Means of Percent Change of Hargreaves method of Estimation of Evapotranspiration for five meteorological station at Kastoria basin

Hargreaves	Jan	Feb	Mar	Apr	May	Jun	Jul	Aug	Sep	Oct	Nov	Dec
Argos Orestiko	39.21	31.78	39.23	34.70	31.32	28.38	23.85	25.42	30.43	41.02	53.96	64.68
Kastoria	30.40	24.19	33.45	31.43	27.36	23.18	17.53	17.77	22.93	31.22	42.30	51.20
Kleisoura	-17.03	-12.99	-1.84	-0.42	-1.13	-3.19	-3.66	-3.95	-4.03	2.32	9.01	8.59
Lithia	32.57	23.88	19.56	9.66	5.23	-2.05	-9.41	-10.36	-2.74	26.96	54.37	48.34
Polykarpi	35.56	26.86	22.19	15.87	6.52	-0.67	-8.43	-9.56	-0.43	19.48	47.60	64.22
Toichio	35.03	25.07	22.06	7.11	3.44	-2.40	-10.48	-11.05	-1.89	18.19	35.21	48.90

Table 10 - Monthly Means of Percent Change of Blaney-Criddle method of Estimation of Evapotranspiration for five meteorological station at Kastoria basin

Blaney-Criddle	Jan	Feb	Mar	Apr	May	Jun	Jul	Aug	Sep	Oct	Nov	Dec
Argos Orestiko	243.44	150.05	103.92	56.74	41.03	33.12	23.64	29.32	60.21	129.75	221.25	300.05
Kastoria	257.74	160.09	111.00	62.87	45.06	35.66	25.21	30.82	62.93	135.26	237.28	322.77
Kleisoura	229.09	124.42	83.96	45.90	33.93	25.89	18.33	24.26	50.97	115.42	213.31	292.53
Lithia	65.87	36.92	19.54	5.14	-1.81	-4.15	-9.65	-6.42	7.68	63.87	131.63	105.59
Polykarpi	73.35	42.82	23.88	13.99	-0.10	-2.32	-8.36	-5.31	11.25	49.97	116.14	147.50
Toichio	72.02	39.28	23.66	1.51	-4.16	-4.62	-11.07	-7.37	9.00	47.56	87.80	107.09

In summary, the Hargreaves method generally overestimates ET_0 at Argos Orestiko and Kastoria stations while underestimates at the station of Kleisoura thought out the year. At the stations of Lithia, Polykarpi and Toichio, ET_0 is slightly underestimated for months June, July, August and September while the other months of the year its overestimated with similar percentages observed at the rest of the stations. The Blaney-Criddle method shows similar percentages for most of the months of the year for stations Lithia, Polykarpi and Toichio, apart from the winter months where it significantly overestimates ET_0 by 1-3 times the ones yielded by the Hargreaves method. The reference evapotranspiration is overestimated by 5-10 times at the stations of Argos Orestiko, Kastoria and Kleisoura apart from the summer months where the results are similar with the ones form Hargreaves methods. The significant overestimation of the Blaney-Criddle forbids its use for the estimation of the reference evapotranspiration at the study area. Thus, in this study ET_0 will be calculated with the Hargreaves method.

Tables 11 & 12 summarize ***ET_0*** data as monthly means and annual values, respectively, calculated with the Hargreaves method for the reason stated above. Some of the records were incomplete, so the period of time covered by them is not consistent. Those missing values were filled using the mean value of all corresponding months of the adjacent years.

Table 11 - Mean Monthly Reference Evapotranspiration Statistics for period 2000-2018 at Kastoria Basin

Hargreaves ET_0 (mm/month)			
Month	**2000-2009**	**2010-2010**	**Mean**
Jan	0.77	0.66	0.71
Feb	1.24	1.09	1.16
Mar	2.15	1.85	2.00
Apr	3.18	3.12	3.15
May	4.63	4.03	4.33
Jun	5.75	5.00	5.37
Jul	6.08	5.42	5.75
Aug	5.46	4.85	5.15
Sep	3.58	3.23	3.41
Oct	2.22	1.85	2.03
Nov	1.20	1.06	1.13
Dec	0.68	0.68	0.68
Sum	36.95	32.82	34.89

Table 12 - Annual Reference Evapotranspiration Statistics in mm for period 2000-2018 at Kastoria basin

Hargreaves ET_0 (mm)				
Year	**Mean**	**Max**	**Min**	**Sum**
2000	3.16	6.42	0.62	37.97
2001	3.20	6.18	0.49	38.41
2002	2.94	5.78	0.54	35.30
2003	3.03	6.17	0.66	36.38
2004	2.97	5.95	0.71	35.65
2005	3.01	5.93	0.68	36.15
2006	3.03	5.75	0.63	36.37
2007	3.23	6.68	0.59	38.79
2008	3.17	6.17	0.70	38.01
2009	3.04	6.07	0.73	36.48
2010	2.71	5.80	0.53	32.47
2011	2.69	6.37	0.37	32.27
2012	2.85	6.88	0.45	34.25
2013	2.77	5.81	0.57	33.23
2014	2.68	5.97	0.53	32.18
2015	2.68	6.48	0.49	32.10
2016	2.70	5.98	0.50	32.42
2017	2.80	6.42	0.17	33.65
2018	2.74	5.90	0.48	32.84
Mean	2.92	6.14	0.55	35.00

3.4.3.1 Evapotranspiration Pattern

In order to also achieve better reliability in terms of the method used to spatially represent the reference evapotranspiration, like implemented with the rainfall, more than three station were taken into account, two outside of them located the wider study area, providing a broader hydrological network and thus a better understanding of the distribution and the pattern of ET_0 for the periods defined in Table 9. The R.B function were also used in this case.

The average annual reference evapotranspiration for 19 years is 35 mm, between 2000 and 2018, whereas the interpolated values are close to the one (~12.7 mm) calculated by simple statistics shown at Table 11 & 12. Figures 17, 18 and 19 depict the pattern of ET_0 at monthly means values, mean annual and mean annual values for the growing period only, respectively. All three figures depict the same pattern. They also present lower values of ET_0 (>900 m of altitude) to places with a higher altitude as at the eastern side of the basin while presenting higher values at the middle and southwestern side.

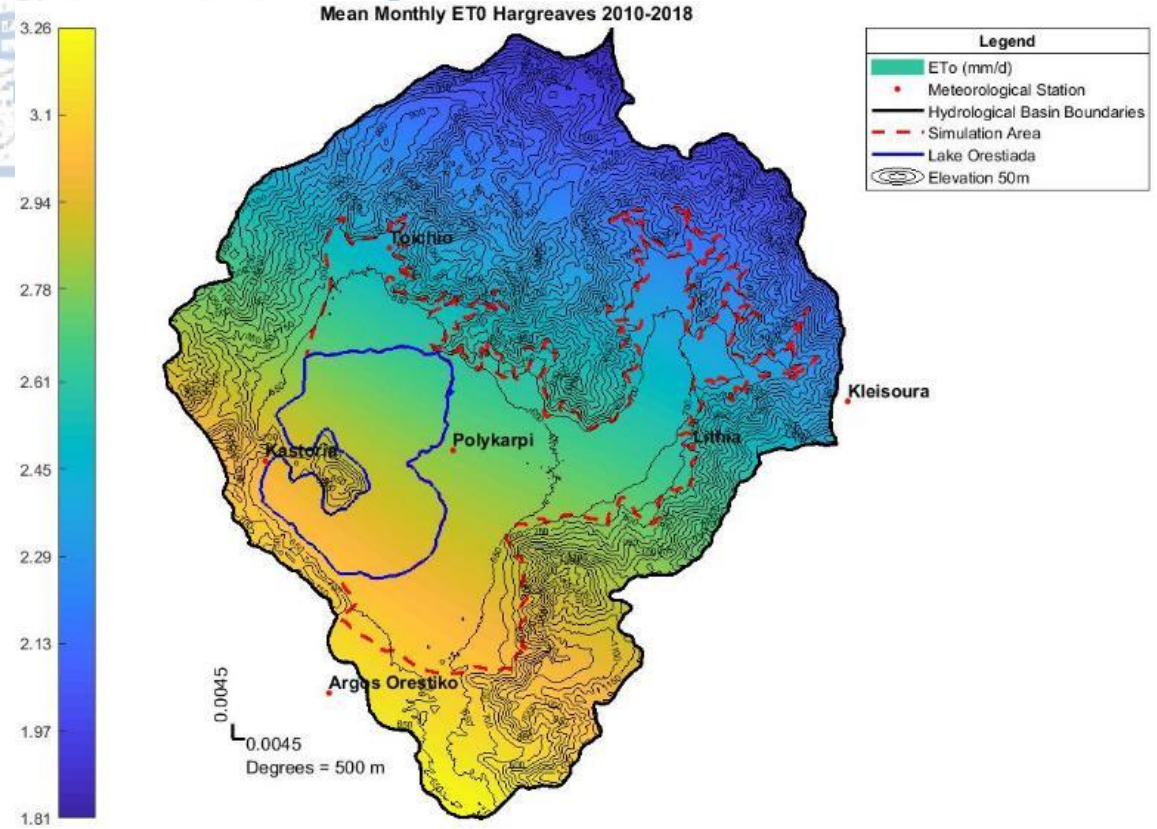

Figure 17 - Mean Monthly ET_0 for the period 2010-2018 estimated with the Hargreaves method

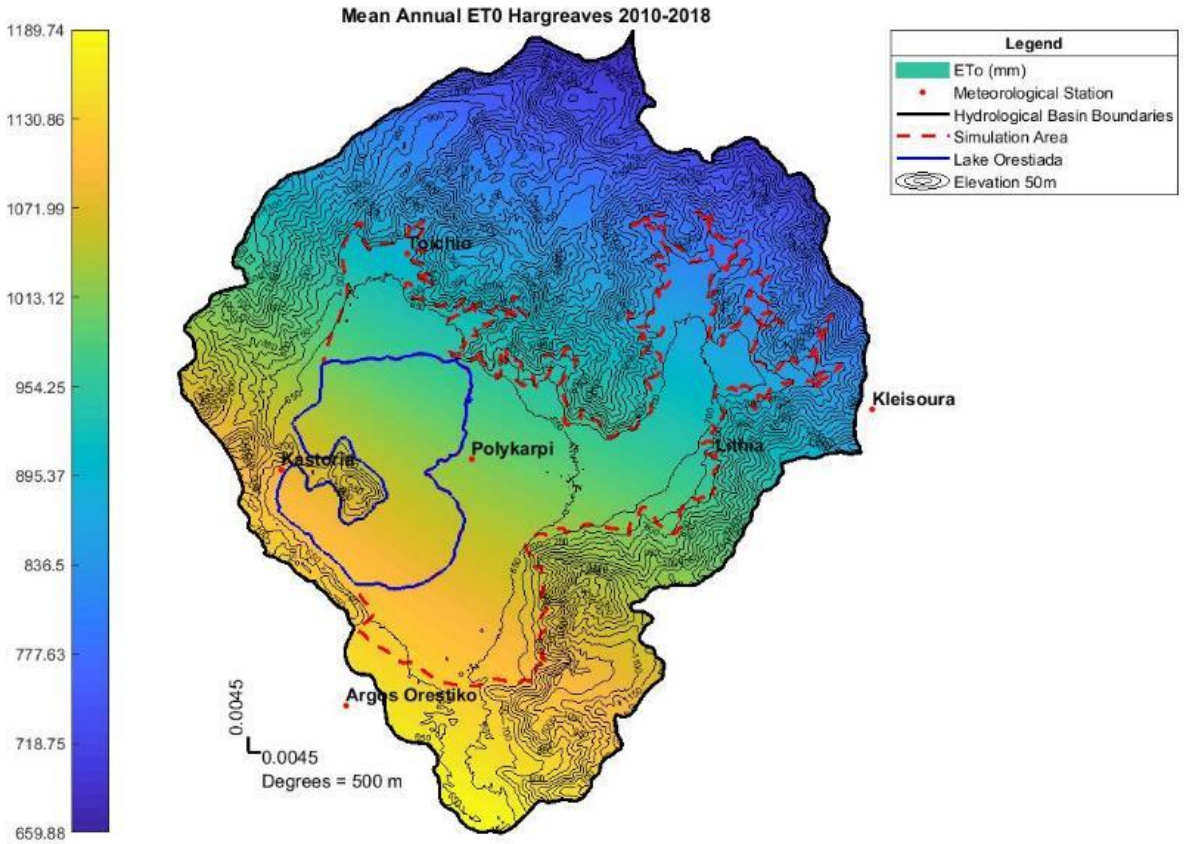

Figure 18 - Mean Annual ET_0 for period 2010-2018 estimated with the Hargreaves method

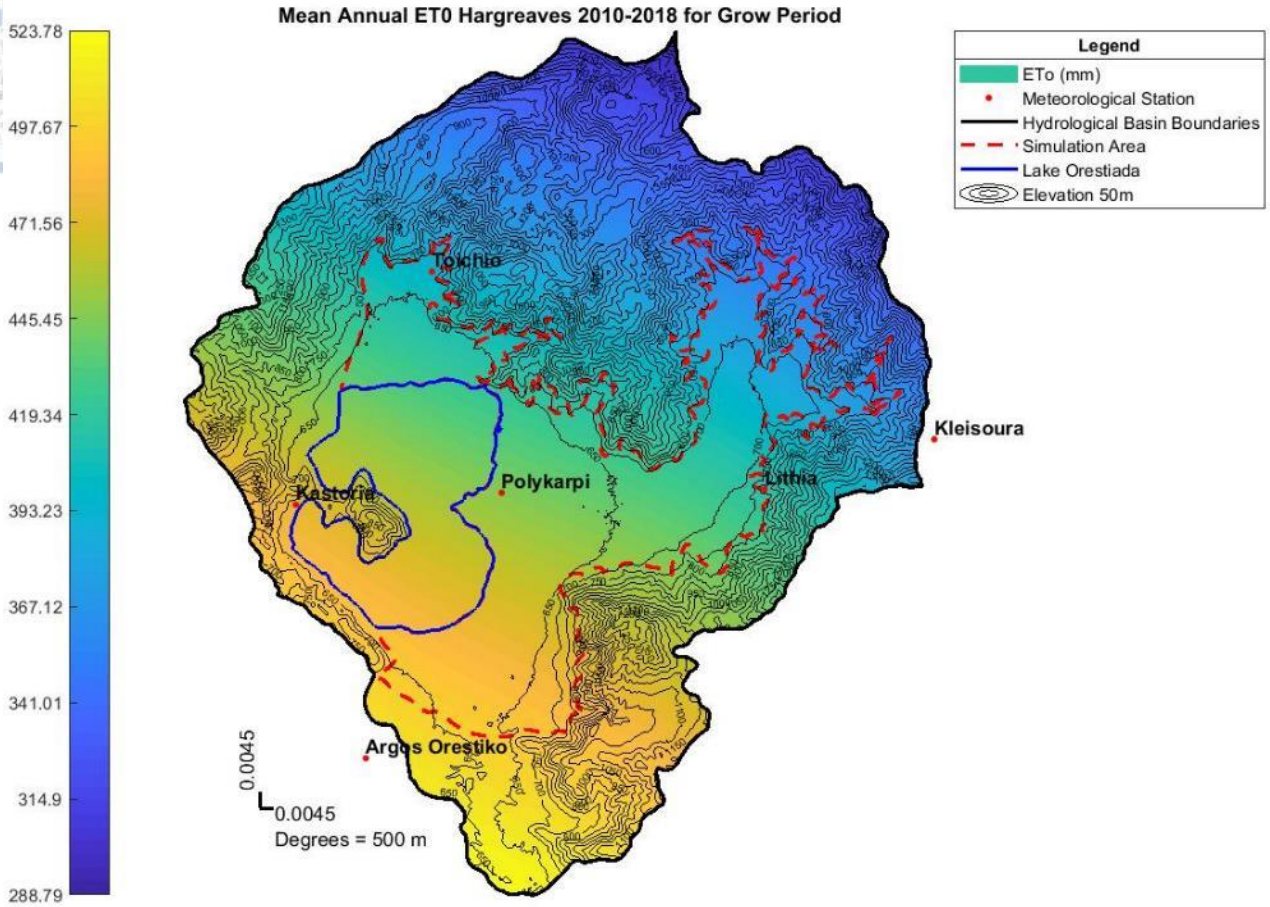

Figure 19 - Mean Annual ET_0 for Grow Period of 2010-2018 estimated with the Hargreaves method

3.4.4 Climate Classification Assessment

The climate of the Mediterranean region can be characterized by the Emberger formula, which gives a strong emphasis to annual changes in temperature. The rainfall quotient, Q, value for the studied region and the value of m are compiled climatic charts of Emberger modified by Sauvage (1930).

$$\boldsymbol{Q = \frac{2000P}{(Mk^2 - mk^2)}}$$

P: Annual Rainfall in mm
Mk: Mean temperature of maximum measured temperature of the hottest month in Kelvin
mk: Mean temperature of minimum measured temperature of the coldest month in Kelvin

At the Climate Diagram for Greece three bioclimatic categories can be distinguished "semi-dry", "wet" and "semi-humid" and four sub-categories based on the value of m (in °C degrees) in "hot winter", "mild winter", "winter cold" and "severe winter" (Mavromattis, 1980)

Thus, the following bioclimatic combinations are distinguished:

- Mediterranean very dry climate
- Mediterranean dry climate
- Mediterranean semi-dry climate
- Mediterranean sub-humid climate
- Mediterranean humid climate
- Mediterranean hyperhumid-climate
- Mediterranean climate of high mountains

The distinction of the sub-categories of each bioclimatic category is in five variants "warm", "temperate", "cool", "cold" and "very cold" is based on the average of the coldest month temperatures (m °C) as follows:

- m> 7 °C = warm underfloor, winter warm without frost
- 3 °C <m <7 °C = temperate, winter mild, frost rare
- 0 °C <m <3 °C = cool, winter chilly, frequent frost
- -10 °C <m <0 °C = chilly, severe winter, cold shade, long-term frosts
- m <-10 °C = very cold, winter very severe, frosts prolonged

By using the data generated by R.B function (P=800 mm) as well as the temperature data from the sources listed at Table 9 (M=30.5°C and m=-6.6°C) and the following modified equation of Emberger, that calculates Q equal to 75.63. This characterizes the climate of Kastoria basin, by these recent climatic data, as ***semi-humid with severe winters*** per Mavromattis, 1980.

3.4.5 Future Climate Projections

The Mediterranean region has been characterized as the planet's hot spot in terms of climate change effects (Giorgi et al., 2006). It's also the most vulnerable European region in terms of climate change impacts (Schroter et al., 2005; Navarra & Tubiana, 2013; Giorgi & Lionello, 2008) and is expected to witness a decrement in water resources due to climate change. This is attributed to the significant predicted increase in above average precipitation and decrease in annual precipitation with fewer wet days and drier summers (IPCC, 2007). This has been presented in several studies. Alpert et al., 2008 support this and further suggest greater decrease in rainfall, increase in temperatures and a greater tendency towards the aforementioned extreme. Moreover, Dubrovsky et al., 2014 based on future trends of 16 GCM runs suggested that a significant increase in temperature for the period 2070-2099, close to the end of the current century, relative to the control period 1961-1990. Seasonally, rainfall is expected to decrease 5-30% on an annual basis for the Mediterranean area, from north to south. In regard to temperature, the increase is expected to be higher in the summer and lower during the winter and spring, with average increase of 3-5 °C. Jacobcit et al. 2014, reviewed a wide number of studies about projected climate change that altogether cover the Mediterranean region. Precipitation for the entire Mediterranean points a downward trend for spring, summer and autumn while in winter global climate models indicate a general rainfall decrease in contrast to several statistical downscaling results that show increases in rainfall. Greece, found at the eastern part of the Mediterranean, shows an increasing trend in future temperature variation while precipitation is expected to decrease in amount and wet day occurrence (Tolika et al., 2012). The results of transient high-resolution RCM simulation by Zanis et al., 2015 indicate small changes, as increasing annual temperature by 1.8 °C and decreasing/increasing precipitation for the early-future period 2021-2050 while towards the end of the century more severe changes are expected i.e 3.4 to 4.2 °C of temperature increase and up to 40% decrease in precipitation. Summer presents the largest future increase in average temperature while winter and spring show the largest decreases in precipitation. In addition, extreme precipitation events are expected to be increased in Greece (Tolika et al., 2008).

The above described climate changes during the twenty-first century are expected to significantly affect water resources availability in the Mediterranean region. Studies that indicate water reduction attributed to climate change as a consequence have already been conducted (Garcia-Ruiz et al., 2011; Ludwig et al., 2011). According to the European Environment Agency (2009), several studies that aim to assess the potential effects of climate change at the water resources in the Mediterranean region have been conducted. They have concluded, in common, that the water resources availability is going to decrease. More specifically, fresh water availability at the Mediterranean region is expected to decrease between 30% to 50% by 2050 (Milano et al., 2013). Local studies of climate change impacts in water resources have also been conducted as reported at a previous Chap-

ter. In addition to their findings, Koutroulis et al. (2016) presented a significant reduction in groundwater level, as result of decreased groundwater recharge and increased groundwater abstraction of irrigations for Crete island while Kalogeropoulos & Chalkias (2013) suggested significant decrease in surface runoff for the next 50 years at a catchment of Andros island. Similar results are also suggested by Abdo et al. (2009) for the Gilgel Abay catchment in Lake Tana basin, Ethiopia, where rainfall will decrease by 20% while runoff will increase by 33% towards the end of the century.

Taking into account all the above, Chapter 2 and the necessity to develop climate change impact assessment studies on the local scale, to construct sustainable development plans, the careful evaluation of climate change data sets seems to be indispensable to comprehend climate change impact on water resources availability and spatio-temporal distribution. Given the fact that agricultural activities are the dominant water consumer in Kastoria basin accounting for almost the entire water use (Hellenic Ministry for the Environment, Energy and Climate Change-Special Secretariat of Water, 2014), precipitation and temperature evolution area expected to significantly affect water resources availability in the form of reduced effective precipitation and increase of crop water demand and indirect availability in the form of groundwater recharge and surface runoff, all of which processes are vital factors of the water balance of the basin and of the water balance of Kastoria Lake.

3.4.5.1 Climate data & bias correction

Monthly precipitation data were collected form 4 meteorological station located in the wider Kastoria basin area (Fig. 20). Those data cover a period of twenty years between 1986 to 2005 (control period). For 2 of those stations, average monthly temperature was also available. Information regarding the four meteorological stations can be found at Table 2. GCMs has been widely applied in climate change impact research, as mentioned in Chapter 2. However, Greece is a country that presents complexity at its climate characteristics. Thus, the controlling factors cannot be adequately represented by GCMs (Tolika et al., 2012) and, therefore, the application of RCMs, which have a finer resolution is necessary (Tolika et al., 2016). Consequently, precipitation and temperature data were extracted from the EURO-CORDEX project, in which RCMs were used to produce simulation of reginal climate at fine grids, e.g. 12.5 or 50 km resolution (Gobiet & Jacob, 2011). These simulations are driven by reanalysis data for the control period and by several GCMs under three emissions scenarios, e.g RCP 2.6, RCP 4.5 and RCP 8.5. Fifty-three RCMs were received from the EUROCORDEX experiment and were considered for use. However, such a number of models is cumbersome to handle and also, it's not certain that better results will be produced than using less models. Having in mind that RCMs present very different results meaning increase and/or decrease in precipitation and temperature and also that bias-correction might not always improve RCM results in terms of representing observed pattern for a given bias-correction method and a certain type of data e.g monthly data, only ten RCMs were chosen out of fifty-three all of which displayed mainly decrease in precipitation, increase in temperature and improvement in representing observed patterns after being bias-corrected. Two of those models are under the RCP 2.6 emission scenario while the rest of the models are equally divided into two groups under RCP 4.5 and RCP 8.5. The names and the hereafter names of the selected models are illustrated to the table found below.

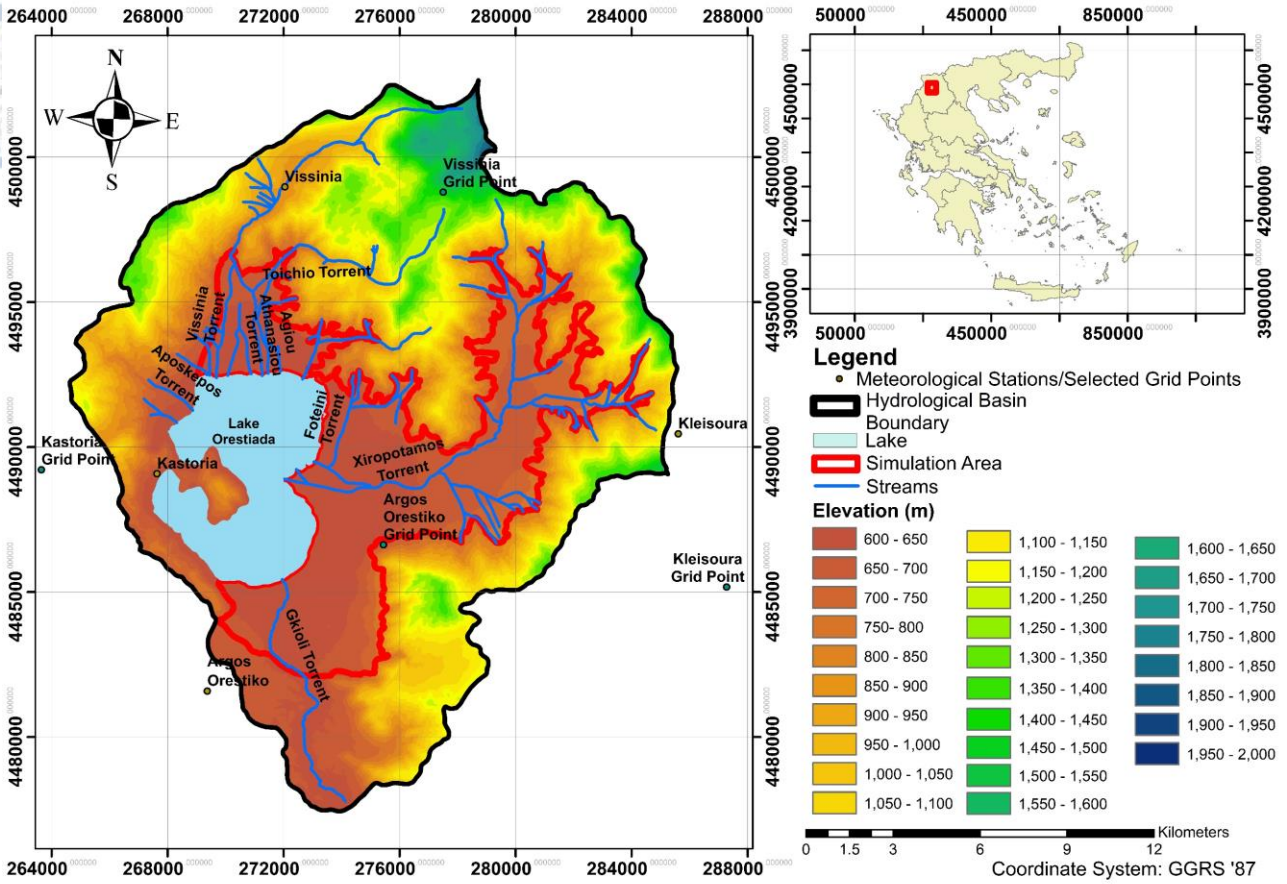

Figure 20 - Stations used to perform bias-correction and the corresponding grid-points extracted from the RCMs

Table 13 - Original Names and Hereafter Names of the selected RCMs

RCP		**RCP 2.6**		**RCP 4.5**				**RCP 8.5**				Total Number
EUR-11		RCMs										
		REMO2015	**REMO2009**	**WRF331F**	**RCA4**	**REMO2009**	**RCA4**	**CCLM4-8-17**	**CCLM4-8-17**	**REMO2009**	**RCA4**	
Institution - GCM	IPSL-IPSL-CM5A-MR	X										1
	MPI-M-MPI-ESM-LR		X									1
	IPSL-IPSL-CM5A-MR			X								1
	MOHC-HadGEM2-ES				X							1
	MPI-M-MPI-ESM-LR					X						1
	MPI-M-MPI-ESM-LR						X					1
	CNRM-CERFACS-CNRM-CM5							X				1
	MPI-M-MPI-ESM-LR								X			1
	MPI-M-MPI-ESM-LR									X		1
	MPI-M-MPI-ESM-LR										X	1
Total Number		1	1	1	1	1	1	1	1	1	1	
Hereafter Name		**RCP 2.6 A**	**RCP 2.6 B**	**RCP 4.5 A**	**RCP 4.5 B**	**RCP 4.5 C**	**RCP 4.5 D**	**RCP 8.5 A**	**RCP 8.5 B**	**RCP 8.5 C**	**RCP 8.5 D**	10
Reference		Jacob et al. (2012)	Jacob et al. (2012)	Skamarock et al. (2008)	Kupiainen et al. (2011)	Jacob et al. (2012)	Kupiainen et al. (2011)	Rockel et al. (2008)	Rockel et al. (2008)	Jacob et al. (2012)	Kupiainen et al. (2011)	

To improve local climate variability representation on regional and local assessment of climate change effects, bias-correction was applied in RCMs output via a custom MATLAB code. A wide range of bias-correction methods are proposed and used in the scientific community. The sim-

ple methods have the advantage of altering the RCMs' results as little as possible (Graham et al., 2007). The advantages and disadvantages of the most widely applied simple bias-correction methods, namely the delta change and linear scaling, are presented by Teutschbein & Seibert, 2013.

Linear scaling was applied for the purposes of this study, which has been previously used in several studies for the assessment of climate change impacts at river basin scale (Bosshard et al., 2013; Fiseha et al., 2014). A scaling factor was calculated for each calendar month for both precipitation and temperature. This factor is the ratio between the average observed and average simulated monthly precipitation for the historical period 1986-2005. Those scaling factors were subsequently multiplied by monthly precipitation data and added to the monthly temperature data for the each of the three sub-periods for the projected period, as shown at the equations found below. For each station of observed data used the nearest grid point were chosen.

$$P^* = P\left[\frac{\mu_m(P_{obs})}{\mu_m(P_{contr})}\right], \quad [3.3]$$

$$T^* = T + \mu_m(T_{obs}) - \mu_m(T_{contr}), \quad [3.4]$$

where:

P*=bias-corrected Precipitation
T*= bias-corrected Temperature
$\mathbf{P_{obs}}$=observed Precipitation
$\mathbf{T_{obs}}$= observed Temperature
$\mathbf{P_{contr}}$= control period Precipitation
$\mathbf{T_{contr}}$= control period Temperature
P= RCM Precipitation
T= RCM Temperature
μ_m= mean within monthly interval

The projected period 2019-2078 was divided into three equal sub-periods of 20 years each to assess future trends in precipitation temporal variations, e.g 2019-2038, 2039-2058, 2059-2078. The results were later analyzed on monthly, seasonal and annual basis for all sub-periods and compared to the corresponding precipitation and temperature data of the period 1986-2005.

The performance of each model to represent observed precipitation and temperature variation patterns was assessed, along with the performance of the chosen bias-correction method, with the construction of Taylor diagrams (Taylor, 2001), since they provide an efficient graphical method to present how well simulated patterns match the observed ones. Taylor diagrams are incorporating correlation coefficient (Pearson's for precipitation and Spearman's for temperature), centered root mean square difference (cRMSD) and standard deviation into a single diagram and, therefore, they provide a clear overview of similarity between simulated and observed data.

3.4.5.1.1 Future trends in precipitation variation

The Taylor diagram compiled by raw and bias-corrected RCM precipitation data for the period 1986–2005, is presented in Figure 21 ,while a summarizing table with the Taylor diagram data is passed to APPENDIX D. Points that are found closer to the "observed" quadrant of standard deviation and demonstrate higher correlation indicate better representation of observed patterns. With regard to raw RCM precipitation data, correlation coefficient ranged approximately between -0.12 and 0.2 for all RCMs while standard deviation 1.1-1.6, 0.9-1.55, 0.8-1.55, for the RCMs for each RCP. The corresponding cRMSD ranged between 2.5 and 1.75 for all RCMs. All RCMs were found to underestimate standard deviation compared to that of the observed data and, therefore, they indicate lower precipitation variation compared to the observed. The bias-correction improved correlation coefficient for the chosen RCMs as it was increased by more than 0.01 units, which is evidence of improvement, while improvement was also observed for the standard deviation. These improvements indicate better performance after the bias-correction application.

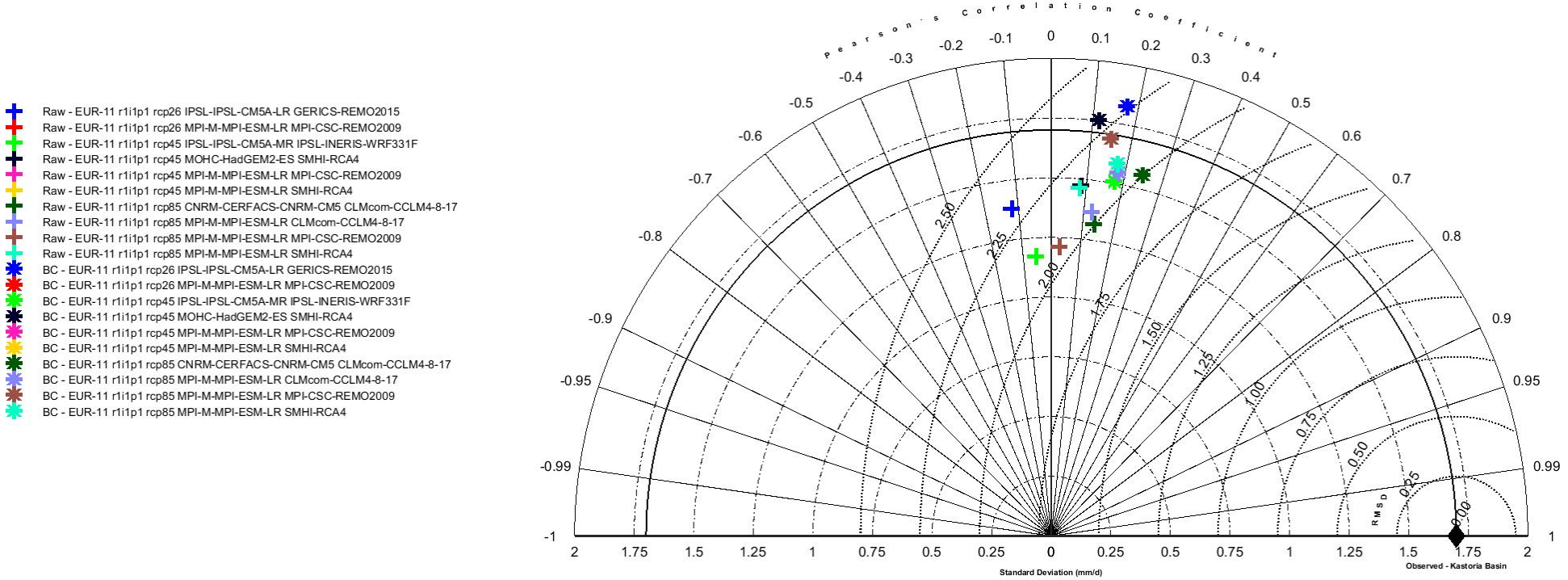

Figure 21 - Taylor diagram of Raw and bias-corrected (BC) EUR-11 RCM precipitation data for the control period 1986-2005

Annual temporal variation of precipitation was assessed for the three sub-periods and compared to the median total annual precipitation of the control period (1986–2005), which is 778.54 mm and the results are illustrated in Fig. 22. A wide range of annual precipitation change is indicated for all RCM–GCM combinations and all sub-periods. The general point of the results illustrated in Fig. 21 is that precipitation is expected to be significantly decreased, especially during the period 2059-2078. Climate change signal for the period 2019–2038 is not very clear as highly controversial estimates are generated; RCP 2.6 A, B, RCP 4.5 A, B, C and RCP 8.5 A indicate a small decrease or increase of precipitation by 10.33, 19.37, 6.7, -8.29, 12.31, -3.75 mm, respectively on the median, while RCP 4.5 D and RCP 8.5 B, C, D indicates annual precipitation decrement by 86.35, 51.89, 54.88 and 102.66, respectively. For the next sub-period of 2039-2058, all RCMs present decrease in precipitation between 17.73 and 115.99 mm, except RCP 8.5 A, whose median is almost equal to the median of the observed data of the control period while for the final sub-period all RCMs present decrease in precipitation between 9.08 and 122.39 mm, except from RCP 4.5 A, D and RCP 8.5 A, whose median present a slight increment in respect to the median of the observed data of the control period.

When comparing the temporal change of annual precipitation for each chosen model, different trends are indicated. RCP 2.6 A, RCP 4.5 A, C and RCP 8.5 B during the second and third sub-periods present even greater reduction in precipitation compared to the first sub-period. The second sub-period RCP 4.5 D and RCP 8.5 C, D present increase but are still reduced compared to the median of the control period. Also, RCP 2.6 B and RCP 4.5 B present a slight decrease while RCP 8.5 A present a slight increase, where it also shows increase compared to the control period. Finally, during the third sub-period all models present decrease except from models RCP 4.5 A, D and RCP 8.5 A, which present a slight increment.

To identify temporal trends in precipitation variation on a seasonal basis, box-plots of seasonal total precipitation were created for all sub-periods and RCMs., which are presented in Fig. In general, there are some clear variation trends identified when the precipitation for the two sub-periods are compared to the control period. All RCMs present increase or decrease during the first sub-period and decrease or increase during the second while decrease with a few exceptions as mentioned earlier.

Concerning the autumn season (Fig. 23), there is a general trend observed which indicates wider seasonal precipitation variation range and increment in precipitation extremes, either by little or by more. The high autumn precipitation extremes are increasing the potential negative impact on agricultural production of crops such as cotton. Its cultivation period is usually between end of October and middle November. RCP 2.6 B, RCP 4.5 A and RCP 8.5 B, D present decrease by 5.6 mm, 5 mm, 5.58 mm and 25 mm, respectively, during the first sub-period while during the second sub-period present increase by 23mm, 30 mm, respectively for the first two models. RCP 8.5 B presents a decrease by 25 mm and RCP 8.5 D presents a slight decrease of 1.9 mm. During the third sub-period, models RCP 2.6 A, RCP 4.5 C, RCP 8.5 B and C present 9.61, 6.66, 14.71, 12.81 mm decrease respectively while models RCP 2.6 B, RCP 4.5 A, B, D, RCP 8.5 A and D present 24.71, 27.89, 46.52, 38.85, 20.72 and 6.47 mm increase respectively. From all the chosen RCMs, only RCP 8.5 B presents decrease for all sub-periods, the highest autumn precipitation decrement is presented by RCP 8.5 D for the period 2019-2038 and it is equal to 25 mm.

Concerning the winter season (Fig. 24), only RCP 4.5 A and RCP 8.5 C present a decreasing trend for the first two sub-periods only. All other models present increments or decrements in each sub-period, either low or moderate. Similarly, to autumn season, there is a general trend according to which winter precipitation variation range is wider compared to the corresponding variation range of the control period, thus indicating increment in precipitation extremes, either low or high, for most of the examined model combinations and sub-periods. The highest decrement is presented by RCP 2.6 B model at the third sub-period and it is equal to 47.15 mm.

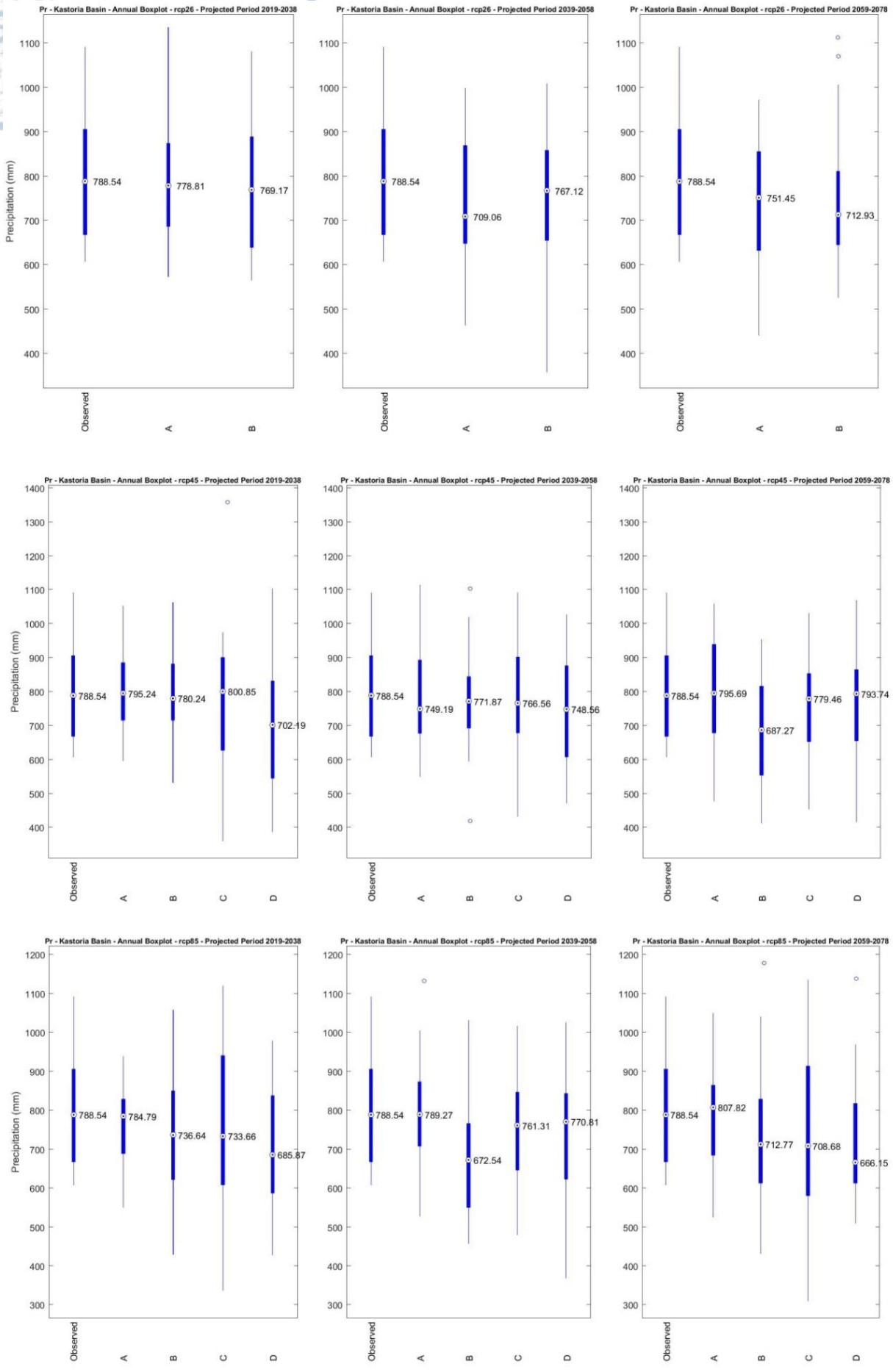

Figure 22 - Box-plots of total annual precipitation variation according to the results from the ten selected RCMs for the periods 2019-2038, 2039-2058 and 2059-2078

Concerning spring precipitation variation (Fig. 25), RCP 2.6 A, RCP 4.5 A, B, D, RCP 8.5 B, C and D present decrement for both sub-periods, ranging from -5.5 to -49 mm for the first period and -8 to -95 mm for the second period while 7 to 67 mm for the third period. RCP 2.6 B and RCP 4.5 C present increment for the first period, 1.2 mm, 10 mm, respectively, and decrement for the second sub-period, -15.3 mm and -9.6, respectively. RCP 8.5 A presents as slight increment on both sub-periods. As in autumn and winter, there is a general trend according to which spring precipitation variation range is wider compared to the corresponding variation range of the control period, thus indicating increment in precipitation extremes, either low or high, for most of the examined model combinations and sub-periods.

Finally, summer precipitation variation (Fig. 26) follows the general trends observed at the rest of the seasons for only for models under RCP 8.5. Models under RCP 2.6 and RCP 4.5 present narrower seasonal variation range while models under RCP 8.5 present wider range than the observed variation range. RCP 2.6 A, B, RCP 4.5 B, C, D, RCP 8.5 A, B, C, and D present constant decrement at both sub-periods, ranging from -2 to -54 mm for the first period, -15 to -61 mm for the second and from -19 to -58 for the third. RCP 2.6 A and RCP 8.5 A present decrement for the all sub-periods, by 18 and 54 mm for the first, and by 14 and 21 mm for the second sub-period, respectively while RCP 4.5 A present increment for the first sub-period by 15 mm, 4 mm for the second and 13 mm for the third. Moreover, summer precipitation variation indicates total dry summer periods for RCP 2.6 A, B, RCP 4.5 B, C, D, RCP 8.5 B, C, and D models.

In complement to annual and seasonal precipitation variation, monthly precipitation variation was also assessed. The cumulative frequency diagrams for the three sub-periods and for each RCMs chosen are presented in Fig. 27. A significant correction of precipitation CDFs for all RCMs has been achieved. These diagrams indicate that at the RCMs indicate maximum monthly precipitation greater than the corresponding maximum of the control period and, therefore, increment in monthly precipitation extremes is presented by most of the RCMs, either raw or bias-corrected. This is also proved from the fact that for cumulative frequency values > 70-75%, higher precipitation values are indicated for most RCMs and sub-periods. For cumulative frequency values < 70-75%, RCP 2.6 and RCP 8.5 RCMs are presenting lower monthly precipitation for both sub-periods. RCP 4.5 A and B indicate significantly different variation patterns for the rest of the RCMs, as for cumulative frequency values < 70% it presents monthly precipitation values which are close to the corresponding values of the historical period.

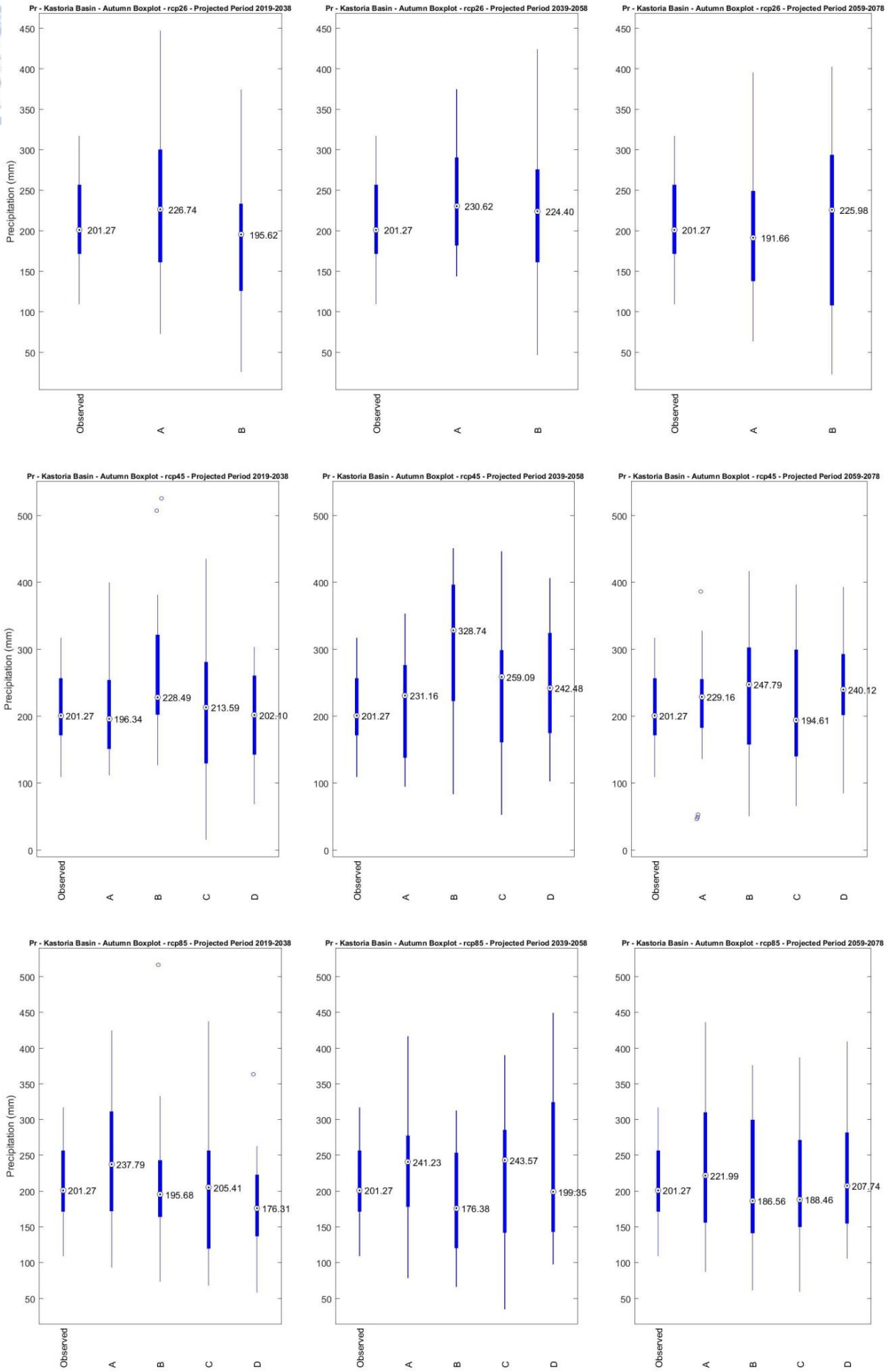

Figure 23 - Box-plots of autumn total precipitation variation according to results from the selected models for the periods 2019-2038, 2039-2058 and 2059-2078

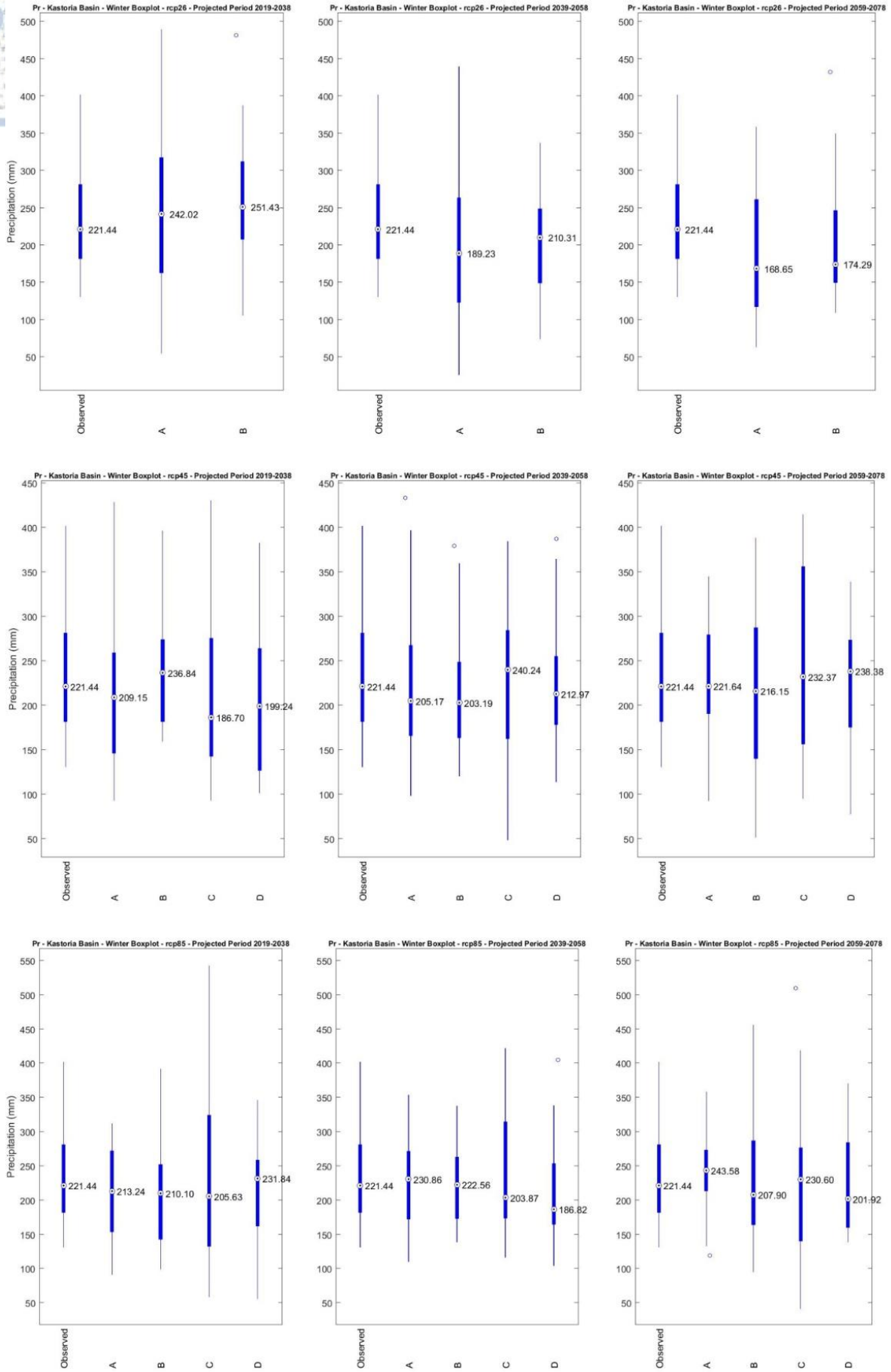

Figure 24 - Box-plots of winter total precipitation variation according to results from the selected models for the periods 2019-2038, 2039-2058 and 2059-2078

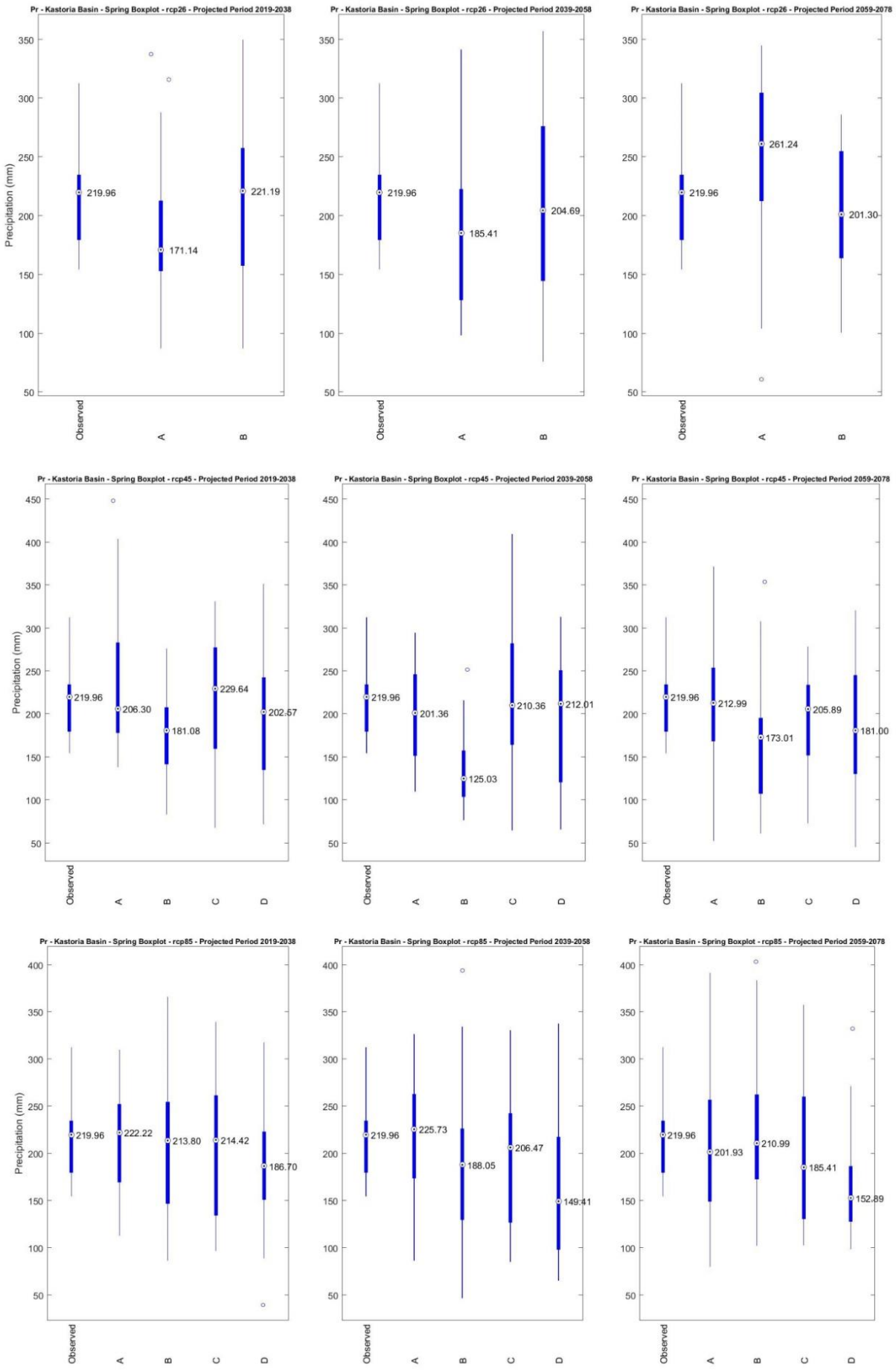

Figure 25 - Box-plots of spring total precipitation variation according to results from the selected models for the periods 2019-2038, 2039-2058 and 2059-2078

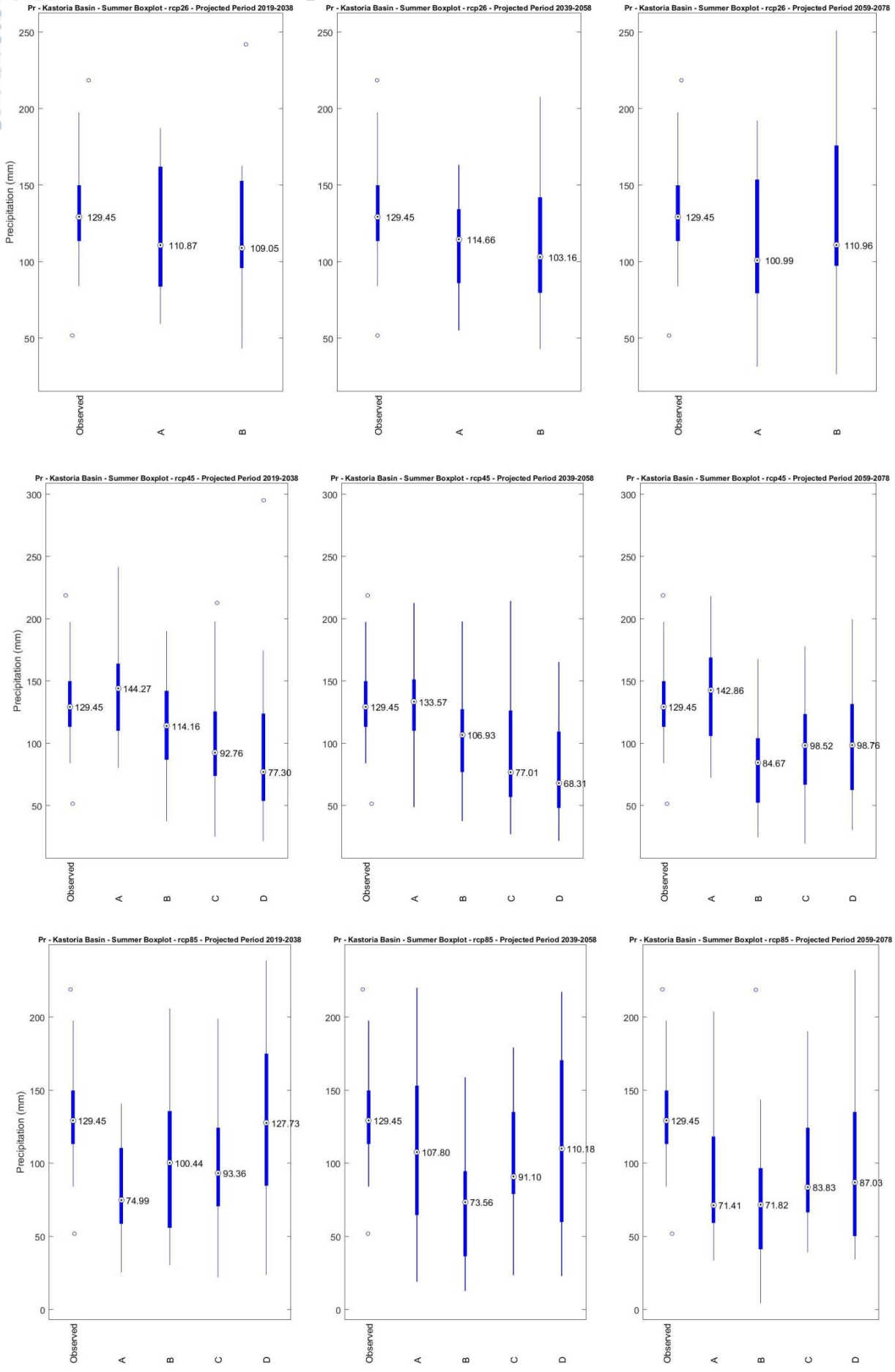

Figure 26 - Box-plots of summer total precipitation variation according to results from the selected models for the periods 2019-2038, 2039-2058 and 2059-2078

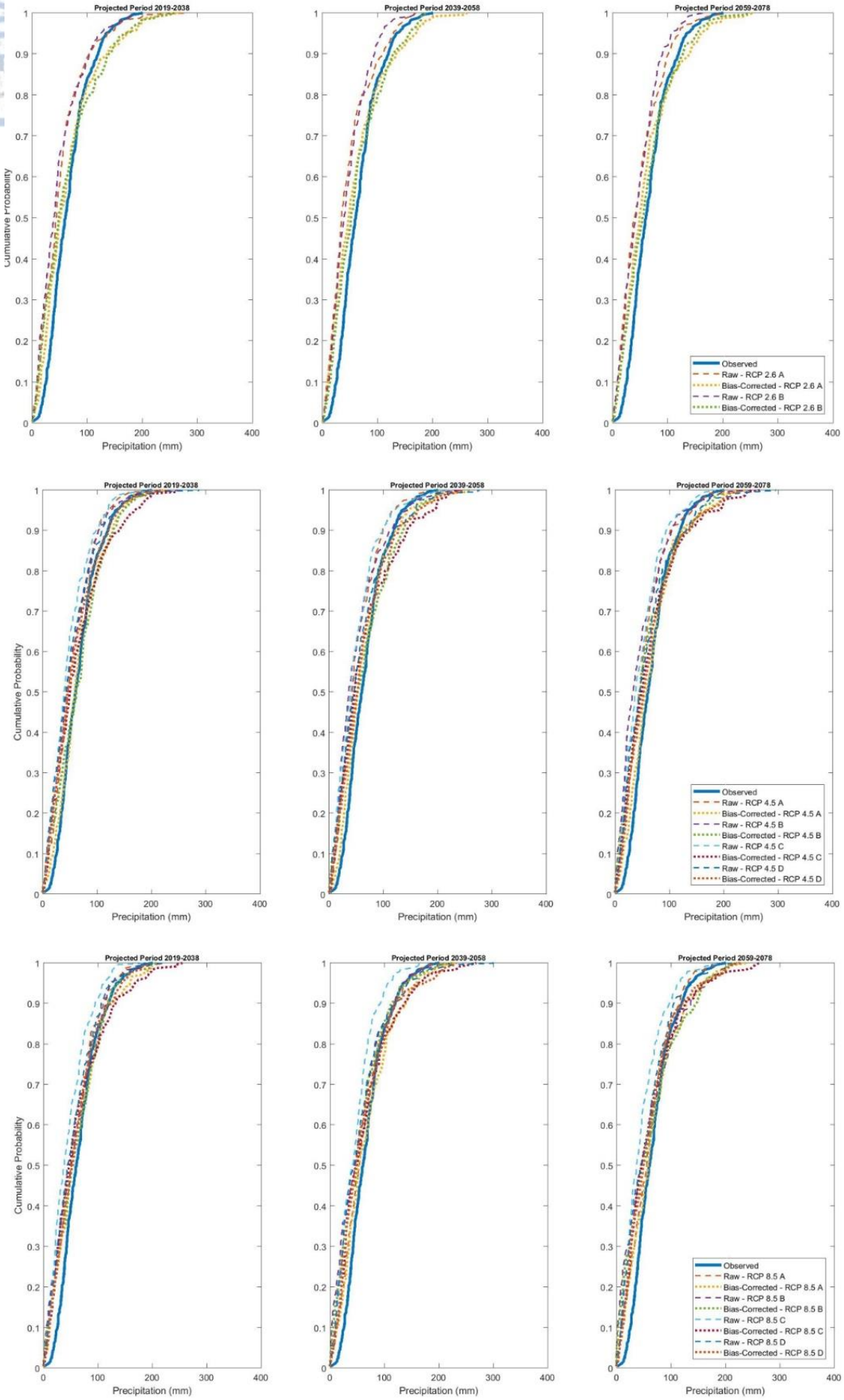

Figure 27 - Cumulative frequency diagram of monthly precipitation for the control period (1986-2005) and the selected RCMs for the three sub-periods

3.4.5.1.2 Future trends in temperature variations

The Taylor diagram compiled by the raw and bias-corrected RCMs temperature data for the period 1986–2005 is presented in Fig. 28. Points that are found closer to the "observed" quadrant of standard deviation and demonstrate higher correlation indicate better representation of observed patterns. With regard to raw RCM temperature data, correlation coefficient ranged between 0.91 and 0.95, while standard deviation ranged between 6 – 8.6 °C for the RCMs of RCP 2.6, 6.7 – 9 °C for the RCMs of RCP 4.5 and 6.3 – 9 °C for the RCMs of RCP 8.5. The corresponding range for cRMSD was 2.43 °C to 3.16 °C, 2.39 °C to 3.16 °C and 2.36 °C to 3.15 °C. Since correlation coefficient values of all RCMs raw temperature data are similar, the best performance is presented by those whose standard deviation is closer to the observed one. All RCMs were found to either underestimate or overestimate standard deviation and, therefore, they indicate higher temperature variation compared to the observed. The bias-correction procedure improved correlation coefficient since it was found to be increased by more than 0.01 units of temperature for all RCMs, while significant improvement was observed for standard deviation for all RCMs since it matches the observed one. After bias-correction, all RCM performance was found to be similar.

Average annual temperature variation for the three sub-periods is presented in Fig. 29. Despite the fact that all RCM–GCM combinations are indicating temperature increase during the period 2019–2078, with the exception of RCMs RCP 8.5 A and B, which present a slight decrease for the first sub-period only, the variation range of temperature increase produced by most RCMs is large. RCP 2.6 A and RCP 8.5 D present smaller variation range in comparison to the one observed, only for the first sub-period while RCP 4.5 A for the second sub-period only. RCP 4.5 A, RCP 8.5 A and RCP 8.5 B present variation range similar to the one observed for the first sub-period. Still, clearer trends are depicted for all selected models, compared to the afore-discussed precipitation trends. Depending on the period, the highest temperature increment is indicated by a different model. For the first two sub-periods the highest increase of temperature is indicated by RCP 2.6 A. For the third and final sub-period the highest increase is present by RCP 8.5 C. The lowest temperature increase is demonstrated for the RCP 4.5 C for first two sub-periods. For the third sub-period lowest increase is presented by RCP 2.6 B. For the first sub-period, the temperature increase ranges between 0.16 °C to 1.41 °C, while the corresponding range for the second sub-period is 0.43 °C to 2.6 °C while for the third 0.32 to 2.8 °C. The highest temperature increase is presented for all models during the third sub-period except those under RCP 2.6. The comparison of temporal change of temperature for each RCM indicates almost non-linear temperature increase for all RCMs model except from RCP 8.5 A and B, which present a slight decrease of the first sub-period only.

Moreover, similarly to temperature variation for most seasons, it is worth mentioning that for RCMs RCP 2.6 A, RCP 4.5 A and B the minimum average annual temperature is higher than the maximum average annual temperature observed during the control period, thus indicating significant difference in annual temperature variation pattern. RCP 2.6 B, RCP 4.5 C, D, RCP 8.5 A, B, C and D models do not indicate climate change for the first period, unlike at the second and third one, because their inter-quartile range overlap with the corresponding inter-quartile range of the control period. RCP 8.5 A and B RCMs results indicate the weakest climate change signal, for the first period, because the inter-quartile ranges of annual temperature variation they present almost overlaps with the corresponding inter-quartile range of the control period.

With regards to autumn average temperature variation, box-plots for the results of all selected RCMs and the three sub-periods were created and compared to the results of historical period (Fig. 30). The results of RCP 4.5 B autumn temperature, for all three sub-periods, is estimated to be decreased compared to the historical period. RCP 2.6 A, B, RCP 4.5 A, C and D demonstrate increased seasonal temperature for all sub-periods. Concerning autumn, the overall strongest climate change signal is on the median presented by RCP 2.6 A with temperature increment ranging between 1.75 (sub-period 2019–2038), 2.16 °C (sub-period 2039–2058) and 2.58 °C (sub-period 2059-2078). Moreover, it is interesting to mention that according to RCP 2.6 A, minimum median autumn temperature is higher than the maximum median autumn temperature observed during the

historical period, for all sub-periods, thus indicating significant difference in autumn temperature variation pattern. Other models e.g. RCP 2.6 B, RCP 4.5 A, C, D, according to which their inter-quartile range partially overlap with the corresponding inter-quartile range of the historical period but still present a higher median than the one at the control period. Significantly different variation pattern is presented by RCP 8.5 C and D, for which autumn temperature illustrates milder increment of 0.15 and 0.28 °C for the first sub-period, while at the rest of the sub-periods higher increment. RCP 8.5 A and B present a mild decrement and a moderate one respectively, only for the first sub-period.

In terms of winter temperature variation (Fig. 31), the overall strongest climate change signal is indicated by RCP 2.6 A, which illustrates, on the median, temperature increment of 1.81 for the first sub-period, 2.51°C for the second sub-period and 3 °C for the third sub-period. Significant winter temperature increase is also presented by RCP 2.6 B and for the models under RCP 4.5 for all sub-periods. The lowest winter temperature increase is illustrated by RCP 2.6 B, RCP 4.5 C, D and RCP 8.5 A of 0.15, 0.4, 0.16 and 0.08 °C during the first period, by RCP 2.6 B, RCP 8.5 B and D of 0.16, 0.41, 0.58 °C during the second period and by RCP 2.6 B and RCP 4.5 C of 0.59 and 0.42 °C, respectively. The inter-quartile variation ranges for most models and periods does not overlap with the corresponding range of the historical period, thus indicating significant difference in winter temperature patterns while wider temperature variation ranges are demonstrated for all periods by most models.

Compared to autumn and winter, spring average temperature (Fig. 30-32) indicates lower but significant increase compared to the historical period. Spring temperature is constantly increasing during the period 2019–2078 from mild values of 0.34 °C (RCP 4.5 D) to more significant of 5.26 °C (RCP 4.5 B). RCP 4.5 C, RCP 8.5 C and D during the first sub-period do not present any increment compared to the control period. Also, RCP 8.5 A and B present a slight decrease for the first sub-period only.

Considering that the study area is dominated by summer crops, any changes in summer temperature variation can potentially affect agricultural production. Among the four seasons, summer presents the strongest climate change signal with temperature increment on the median by up to 2.44 °C right from the first sub-period for all models. More specifically, the overall higher temperature increment is presented by RCP 8.5 D (1.06-4.05 °C) followed by RCP 8.5 C (1.44–3.62 °C), RCP 4.5 B (1.01–2.53 °C), RCP 4.5 D (1.21–2.28 °C), and then by RCP 8.5 A (0.49-2 °C), while the lowest temperature increment is presented by then by RCP 2.6 B, RCP 4.5 B, RCP 8.5 B, which have the same increment of 1 – 2 °C. Similarly to spring, summer temperature presents increase during the period 2019–2078 for all selected models, while the significant differences in variation range and inter-quartile ranges indicate the important differences in temperature variation patterns.

Similarly to precipitation, cumulative frequency diagrams of average monthly temperature for the four sub-periods and for each RCM are presented in Fig. 34. Concerning the sub-period 2019–2038, the widest monthly temperature variation range is presented by RCP 2.6 B, according to which minimum monthly temperature that is expected to be observed during the period 2019–2038 is a bit lower than the corresponding temperature observed during the historical period. All the other models demonstrate higher minimum monthly temperatures that are exceeding or are close to the one observed. The strongest climate change signal is presented by all models for all sub-periods, due to the fact that observed monthly temperature is mostly higher than similar for the whole range of cumulative frequency curve. The lowest climate change signal is demonstrated by the models under RCP 8.5 for the first period only, as the cumulative frequency curve for RCP 8.5 models of the first period is very close to the corresponding curve of the historical period, except from cumulative frequency values > 0.7 for which significantly higher monthly temperature values are indicated by the RCP 8.5 models of the first period compared to the control period. The cumulative frequency curves for the rest of the models, including the model results for the sub-periods presented in Fig. 34 are shifting steadily to the right, thus indicating further increment in average monthly temperature compared to the historical period and a tendency to overestimate average monthly temperature.

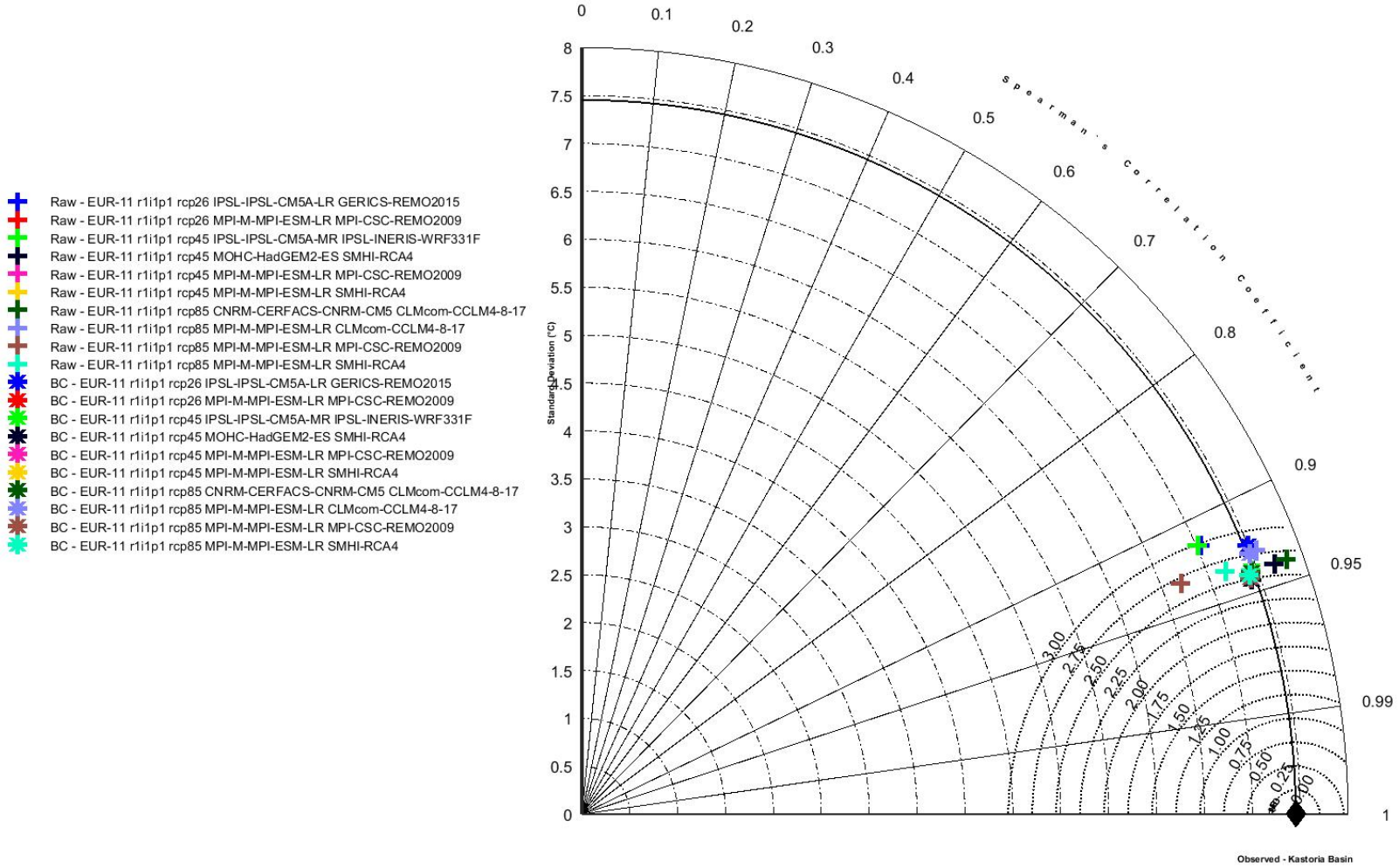

Figure 28 - Taylor diagram of Raw and bias-corrected (BC) RCM temperature data of the selected EUR-11 RCMs for the control period 1986-2005

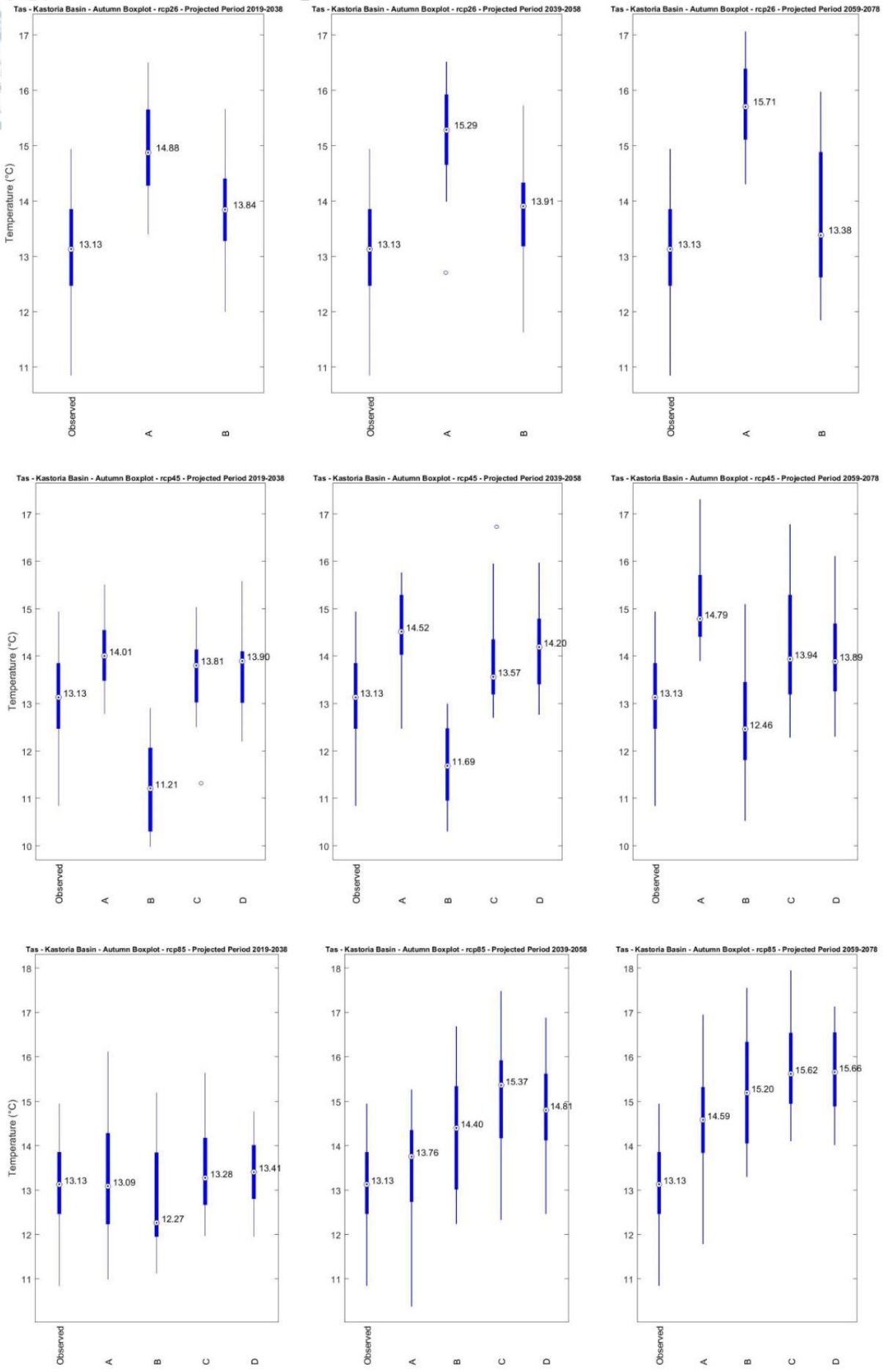

Figure 29 - Box-plots of average annual temperature variation according to results from the selected RCMs for the periods 2019-2038, 2039-2058 and 2059-2078

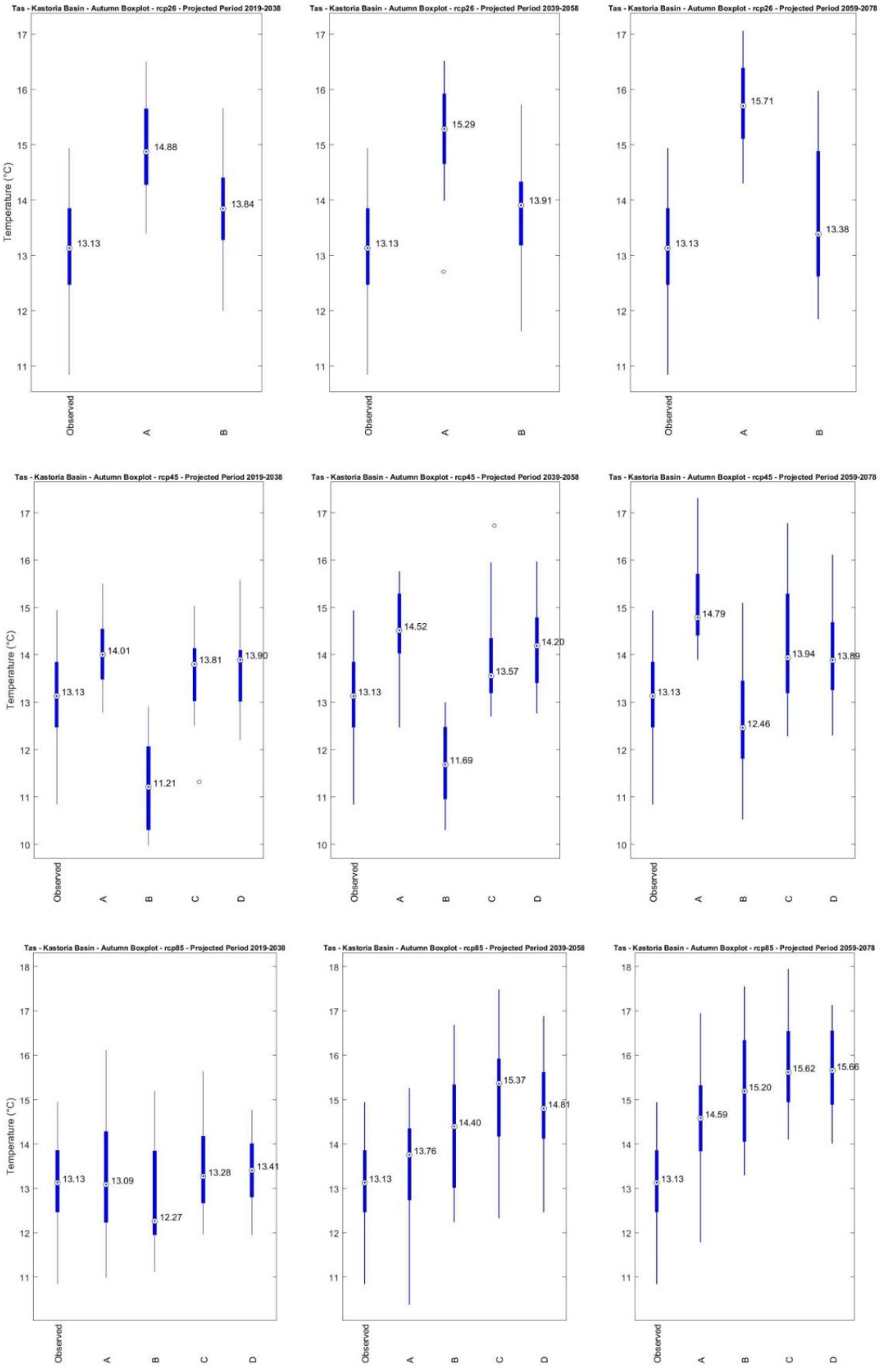

Figure 30 - Box-plots of autumn average temperature variation according to the results of the selected models for the periods 2019-2038, 2039-2058 and 2059-2078

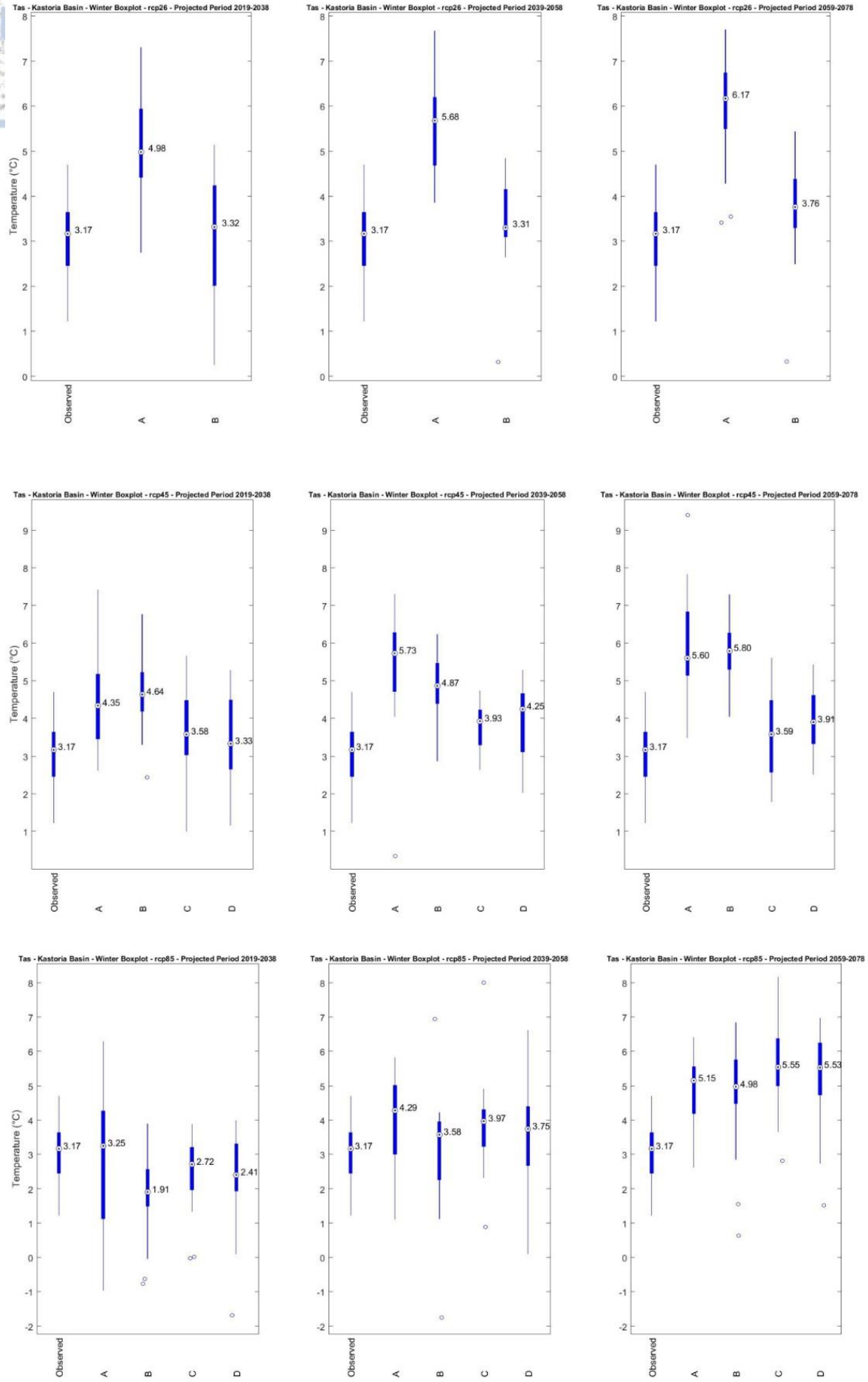

Figure 31 - Box-plots of winter average temperature variation according to the results of the selected models for the periods 2019-2038, 2039-2058 and 2059-2078

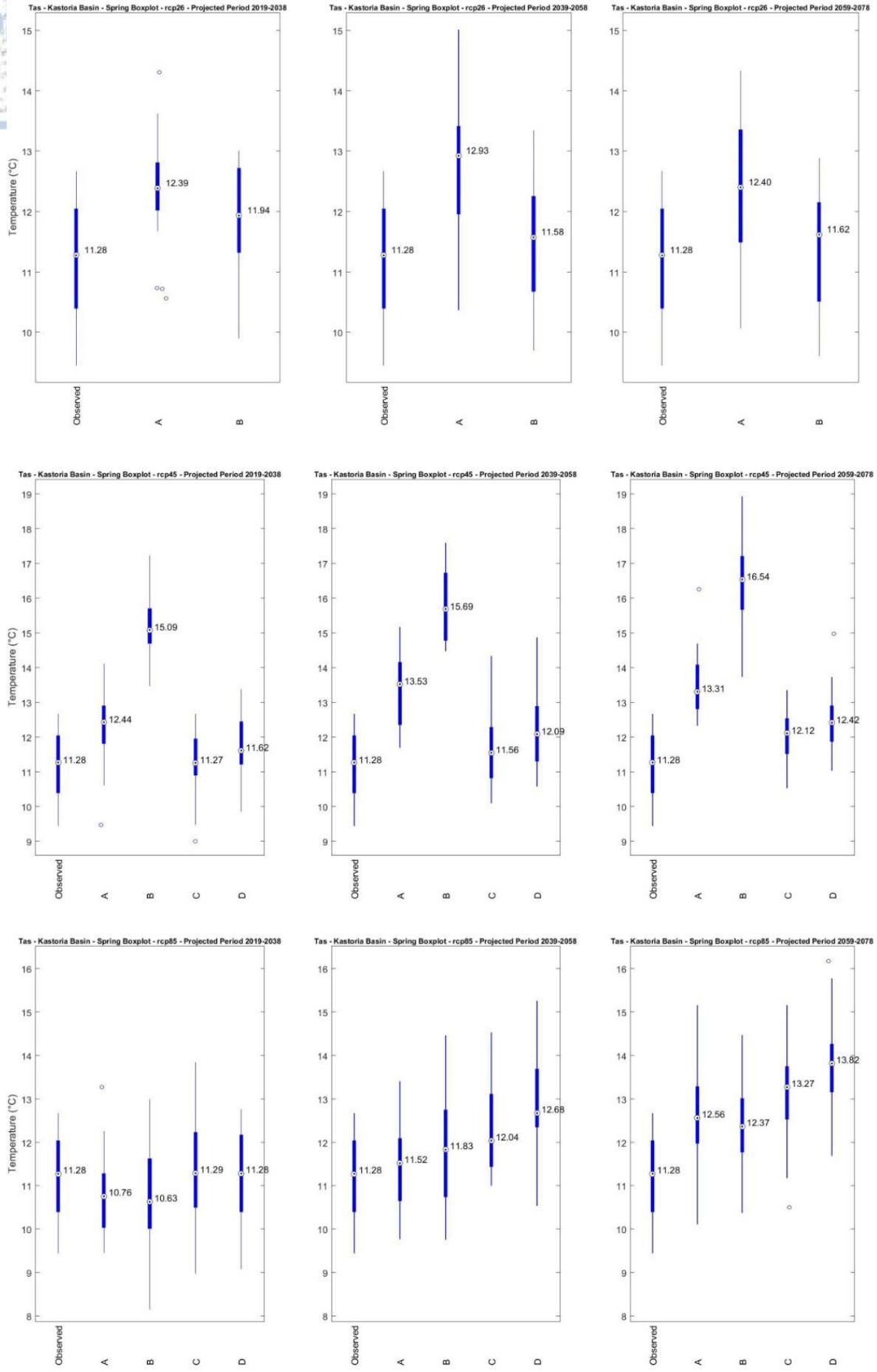

Figure 32 - Box-plots of spring average temperature variation according to the results of the selected models for the periods 2019-2038, 2039-2058 and 2059-2078

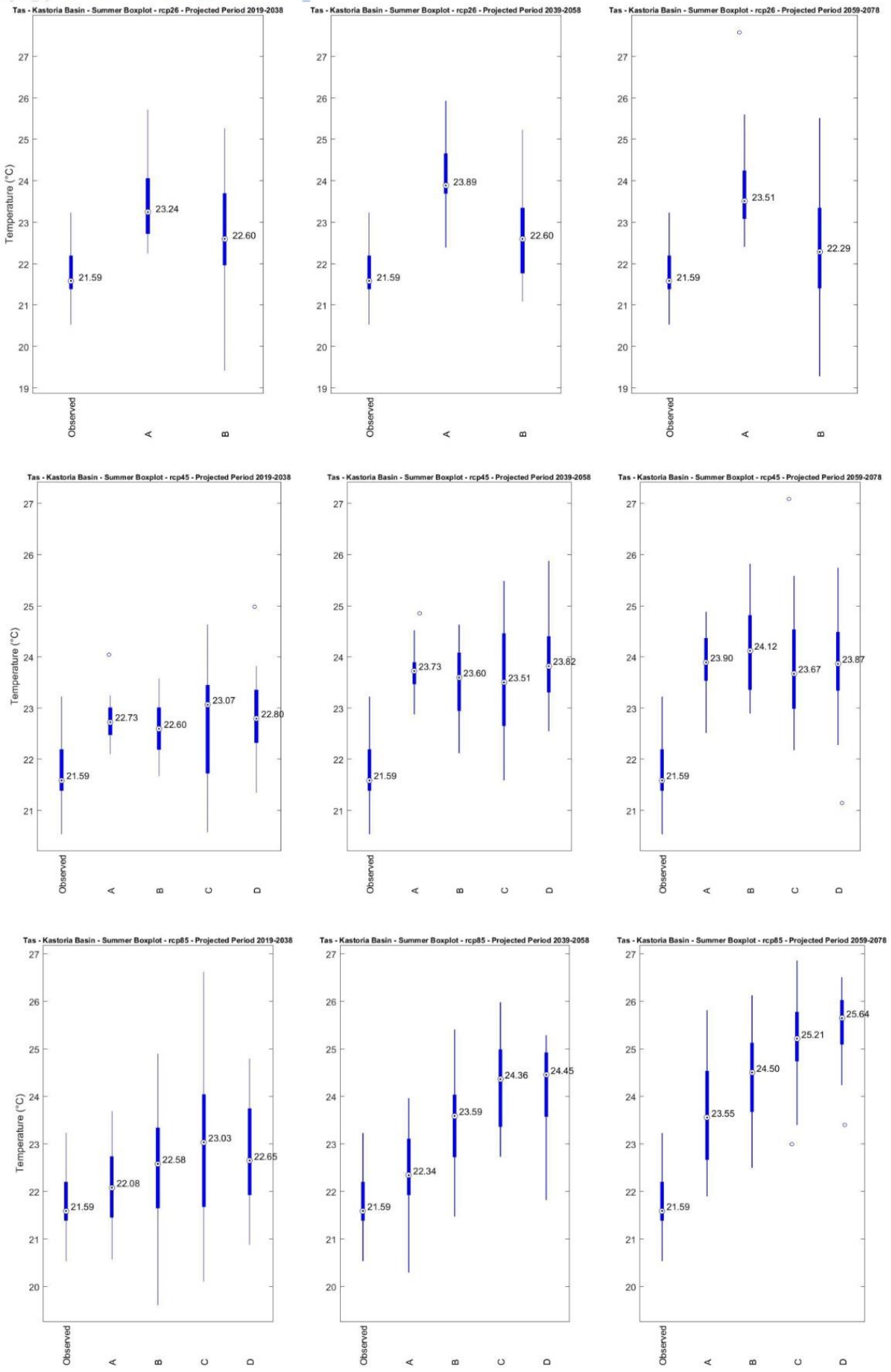

Figure 33 - Box-plots of summer average temperature variation according to the results of the selected models for the periods 2019-2038, 2039-2058 and 2059-2078

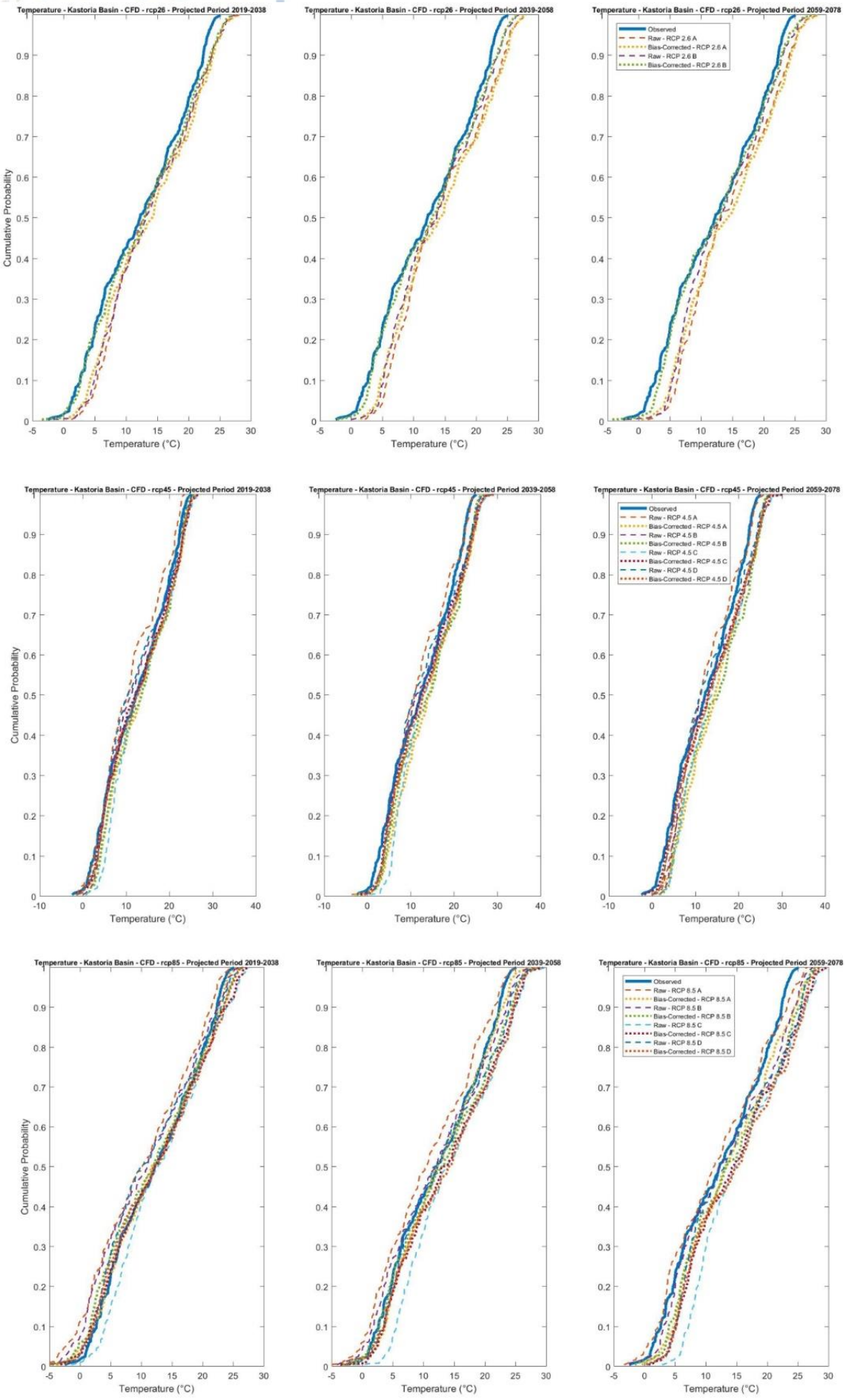

Figure 34 - Cumulative frequency diagram of monthly temperature for the control period (1986-2005) and the selected RCMs for the two sub-periods

3.4.5.1.3 Discussion of Results

Clearly, precipitation and temperature are crucial parameters at shaping the water budget, especially so under climate change conditions in cultivated basins, such as the study basin. Hence, the presented results of the estimated shift in precipitation and temperature patterns are expected to affect future water resource availability and status. Since RCMs have been found to partially reproduce climate pattern in Europe (Jacob et al., 2007; Christensen & Christensen, 2010) and taking into account the regional character of this study, it was chosen to include RCMs that have been proved in the literature to reproduce satisfactorily climate patterns in Mediterranean conditions. Overall, the strongest signal taken from projected climate data is precipitation decrease and temperature increase, since annual precipitation change for the period 2019–2078 was on the average about − 50 mm (or – 6.1%), ranging between – 1.5 (or – 0.18%) and - 131 mm (or – 16.3%), while the corresponding change for temperature was 2.46 °C, ranging between 0.3 and 5.44 °C. The presented, in this section, trends have been evaluated based on RCM data, indicating higher resolution than GCMs, which was further bias-corrected, thus representing a higher local representativeness.

When aggregating precipitation data from the selected RCMs for the two future periods and comparing to the period 1986–2005, winter precipitation decrement ranges between 5% (period 2019–2038) and 6.1% (period 2059-2078). Temperature increase for winter ranges between 0.25 °C (period 2019–2038) and 1.83 °C (period 2059-2078). Taking into account that the winter season is the wettest period for Kastoria basin, completely without crop growing due to heavy snowing, precipitation significantly contributes to the replenishment of water consumed during the irrigation period through groundwater recharge while also adding to the water balance of lake Kastoria by recharging it with surface run-off and by the lateral discharge of the alluvial aquifer of Kastoria to the lake. Therefore, the decrement of winter precipitation and the corresponding increment in potential evapotranspiration is expected to significantly stress the availability of water resources during winter in two ways: (a) decrement in groundwater recharge and (b) increment in potential evapotranspiration. Finally, the increased variation and inter-quartile range presented for mainly the second and third sub-period and for most RCMs constitute an indicator of increment in precipitation extremes, either low or high, and therefore increased risk for effective water resources management due to increased flooding potential, which is already dominant (in case of high extremes) or droughts (in case of low extremes, though few in number). The corresponding precipitation decrease for spring during the period 2019–2058 ranges between 4.71 (period 2019–2038) and 7.2% (period 2059-2078), while temperature increase ranges between 0.65 (period 2019–2038) and 1.77 °C (period 2059–2078). Similarly to winter, early spring is a period of significant precipitation contribution to groundwater recharge and, therefore, precipitation decrement is expected to result in groundwater recharge decrement. Moreover, spring period is very significant for the development of rainfed winter crops, the cultivation period of which usually ends at early summer and combined to potential evapotranspiration increase as a result of the increased temperature, the water stress of winter crops is expected to be increased. Moreover, spring season constitutes the sowing period for summer crops in Kastoria Basin.

Taking into account the elevated water needs indicated by temperature increase, in combination with reduced water availability as a result of precipitation decrease, the water stress indicated by summer crops during the spring period is significant. Since agricultural activities and especially summer crops are dominating water consumption in Kastoria basin, summer precipitation is of high importance and the demonstrated decreasing trend ranging between 16 (period 2019–2038) and 21.4% (period 2059–2078) reflects the necessity for increased irrigation to satisfy water demand of the summer crops. Water demand is expected to further increase in response to temperature increase which ranges between 0.96 and 2.3 °C, as a result of the increased potential evapotranspiration. It has to be mentioned that crops that are not tolerant to the temperature increase will suffer from temperature stress, leading to decreased agricultural production, thus posing another risk except from water resource availability reduction. Concerning the autumn season, precipitation data aggregation from the selected RCMs indicates that seasonal precipitation change may vary on average from

0.55% (period 2019-2038) to 2.35% (period 2059-2078), while corresponding temperature increase ranges between 0.28 and 1.52°C. Due to the fact that for the most significant crops cultivated in Kastoria Basin, cultivation period extends to autumn, the significant change in autumn temperature variation can potentially increase water demand during early autumn and affect crop growth behavior. The aforementioned trends are expected to lead to an acute water-deficit condition, since potential evapotranspiration shall increase with parallel decrease of precipitation share to irrigation, and obviously effective precipitation for natural groundwater replenishment is expected to further decrease over specific years and/or periods. Consequently, water demands will need to be catered for by either groundwater abstractions, thus inducing water-deficient budget conditions at KB, as described above. Moreover, as deduced from the presented results, during the wet seasons and especially during winter, a high precipitation intensity variability is anticipated along with overall decrease in total precipitation heights that could potentially lead to: (a) increased flash flood events, (b) soil clogging effects, (c) decreased natural recharge of Kastoria Lake. All three phenomena may trigger extensive soil erosion leading to desertification, magnification of existing or triggering of new groundwater depletion conditions (that may eventually lead to mining) and fresh water reserves pollution.

3.4.6 Future Climate Classification Assessment

For future climate assessment using the Embreger Equation (see section 3.4.4) and the results of the selected RCMs for each sub-period yielded that the rainfall quotient, **Q**, raises slightly making the climate more humid inside the range for sub-humid characterization. In addition, the m value also increased, for most of the RCMs and sub-period within the range of the "chilly, severe winter, cold shade, long-term frosts" category. This is an indication of climate change.

Table 14 – Projections of Climate Change at the end of the projected period

Sub-period	RCP Name	Q	m	Description
2019-2038	RCP 2.6 A	95.70	0.24	cool, winter chilly, frequent frost
	RCP 2.6 B	95.72	-3.49	chilly, severe winter, cold shade, long-term frosts
	RCP 4.5 A	96.58	-1.42	chilly, severe winter, cold shade, long-term frosts
	RCP 4.5 B	98.39	0.59	cool, winter chilly, frequent frost
	RCP 4.5 C	97.16	-1.47	chilly, severe winter, cold shade, long-term frosts
	RCP 4.5 D	95.63	-1.59	chilly, severe winter, cold shade, long-term frosts
	RCP 8.5 A	93.67	-3.80	chilly, severe winter, cold shade, long-term frosts
	RCP 8.5 B	89.89	-4.63	chilly, severe winter, cold shade, long-term frosts
	RCP 8.5 C	92.01	-3.22	chilly, severe winter, cold shade, long-term frosts
	RCP 8.5 D	85.04	-5.49	chilly, severe winter, cold shade, long-term frosts
2039-2058	RCP 2.6 A	98.63	1.52	cool, winter chilly, frequent frost
	RCP 2.6 B	99.61	-2.27	chilly, severe winter, cold shade, long-term frosts
	RCP 4.5 A	96.87	-3.02	chilly, severe winter, cold shade, long-term frosts
	RCP 4.5 B	94.69	-0.66	chilly, severe winter, cold shade, long-term frosts
	RCP 4.5 C	99.05	-1.66	chilly, severe winter, cold shade, long-term frosts
	RCP 4.5 D	94.20	-0.80	chilly, severe winter, cold shade, long-term frosts
	RCP 8.5 A	92.70	-2.38	chilly, severe winter, cold shade, long-term frosts
	RCP 8.5 B	78.69	-3.25	chilly, severe winter, cold shade, long-term frosts
	RCP 8.5 C	86.86	-3.55	chilly, severe winter, cold shade, long-term frosts
	RCP 8.5 D	88.08	-2.78	chilly, severe winter, cold shade, long-term frosts
2059-2078	RCP 2.6 A	97.85	0.46	cool, winter chilly, frequent frost
	RCP 2.6 B	89.55	-4.22	chilly, severe winter, cold shade, long-term frosts
	RCP 4.5 A	96.47	1.73	cool, winter chilly, frequent frost
	RCP 4.5 B	92.94	1.67	cool, winter chilly, frequent frost

	RCP 4.5 C	87.63	-1.81	chilly, severe winter, cold shade, long-term frosts
	RCP 4.5 D	97.16	-0.14	chilly, severe winter, cold shade, long-term frosts
	RCP 8.5 A	96.17	-0.43	chilly, severe winter, cold shade, long-term frosts
	RCP 8.5 B	94.26	-1.58	chilly, severe winter, cold shade, long-term frosts
	RCP 8.5 C	94.55	0.63	cool, winter chilly, frequent frost
	RCP 8.5 D	95.36	0.27	cool, winter chilly, frequent frost

3.5 Surface Hydrology of Kastoria Basin

The broader study area is the lake's catchment area of Kastoria. The surface of this basin covers an area of 315 km^2 and is subdivided into 11 sub-basins (Table 15) of which:

- 9 sub-basins refer to the main torrents, which have hydrological values (Fig. 35)
- 1 concerns the sub-basin of the city of Kastoria, whose surface run-off is entering the lake through the rainwater drainage pipes.
- 1 concerns the sub-basin of the area of Ampelokoipoi located southwest the basin of Kastoria, whose surface waters are led to Gkioli torrent and end up in River Aliakmonas, while groundwater contribute to the lake.

Table 15 - Torrents and sub-basins of Lake Kastoria Watershed (Tolikas & Mylopoulos, 2000)

No.	Area or Sub-basin	Area (km^2)
1	Fountoukli torrent	4.19
2	Aposkepou torrent	8.3
3	Vissinia torrent	48.46
4	Agiou Athanasiou torrent	2.14
5	Toichio torrent	23.25
6	Metamorphosis torrent	12.28
7	Foteinis torrent	9.87
8	Xiropotamos torrent	113.44
9	Istakos torrent	9.46
10	Kastorias - Dispilio	12.64
11	Ampelokoipoi	23.47
Summary of Area	-	267.5
Lake Kastoria Area	-	27.9

All the above torrents discharge into lake of Kastoria, which in turn discharges Gkioli stream. This stream is located in the southern part of the lake and its waters end up in Aliakmonas.

The hydrological basin of the lake is morphologically structured into two areas as follows:

- The mountainous area, which constitutes most of the basin and is characterized by a relatively dense hydrographic network. It is comprised of the sub-basins Aposkepos, Krisininias, Toichio, Metamorphosis, Fotini and Xiropotamos.
- The lowland area, which exist in the lakeside area mainly between Odessa, Mavrochori and Dispilio.

The rocky formations that are basement rocks of basin provide a lot of erosion materials to the above-mentioned torrents, due to the harsh climate which presents intense temperature changes and significant precipitation. Tolikas and Mylopoulos, 2000, also, suggest that the Xiropotamos sub-basin presents the largest annual material load value compared to the other torrents.

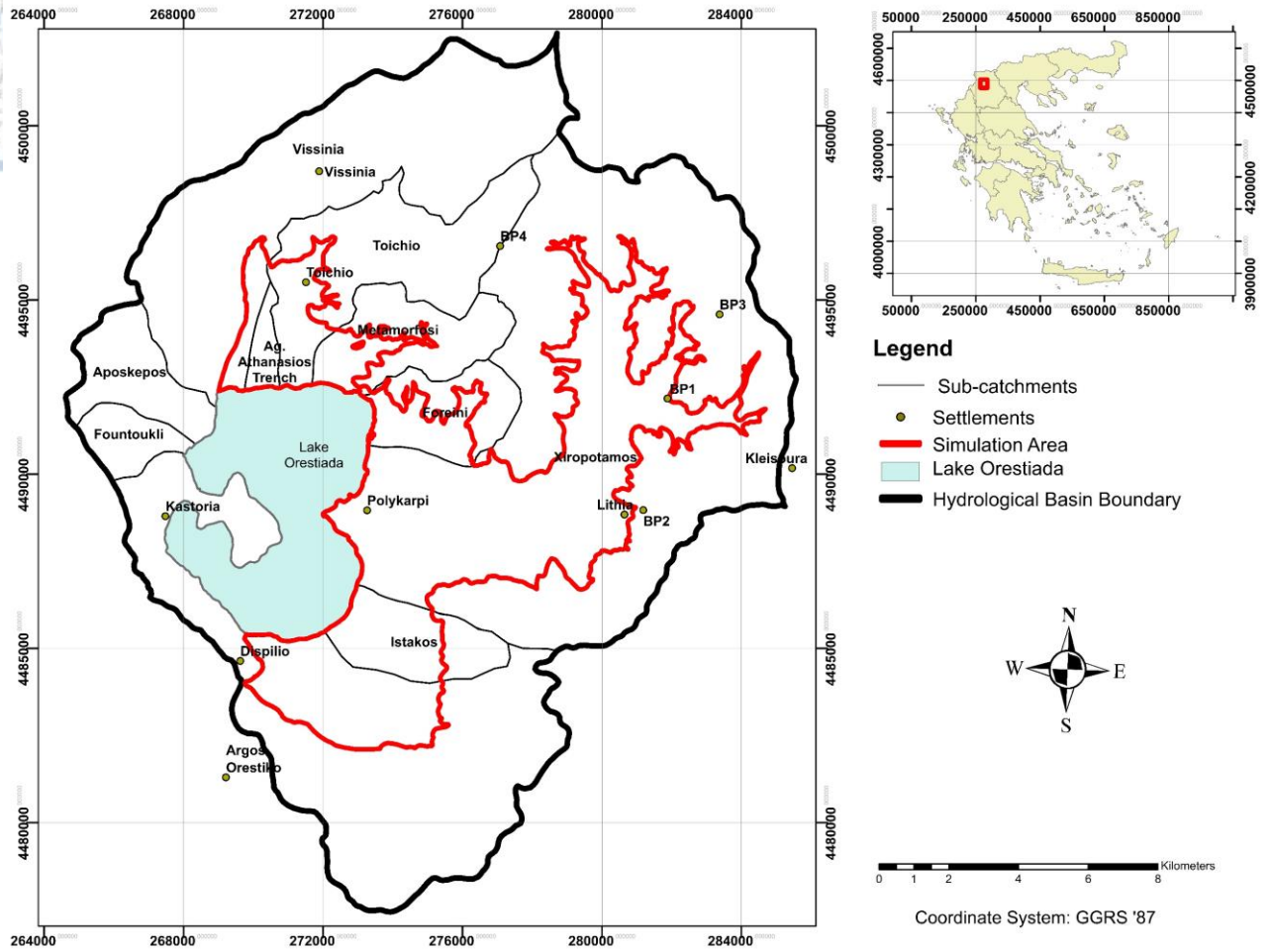

Figure 35 - Nine sub-basins of Kastoria basin (adapted from Tolikas & Mylopoulos, 2000)

3.5.1 Surface Runoff

Surface runoff refers to the percentage of the rainfall that flows along the earth's surface when its falls on the latter and after following a certain route it enters the hydrographic network. The outflow of the basin is dependent by many climatic, morphological factors and the geology of the rocks found in the basin. All of those are a fundamental factor in the surface runoff. The studied basin for its largest part consists of gneiss and metamorphosed shale rocks that are considered generally impervious formations, therefore having a relatively large surface runoff factor, in this case R=35%. In contrast, the carbonate rocks of the basin are almost fractured or karstified, so they have small or no surface runoff, in this case R=0.4-0.5%. The loose Quaternary formations that are found at plains of the basin have a significant effect on the run-off characteristics, while the other geological formations i.e ophiolites and Neogene sediments account for less than 2% of the entire surface of the basin and are of no particular importance, as also mentioned in a previous Chapter. The total runoff is the sum surface and sub-surface runoff, which both go into the lake. The magnitude of former is the result of the regulation of the water level of the lake, that is being made by the Municipality of Kastoria and is basically the discharge of the Gkioli stream which discharges into Aliakmonas river. This means that the surface runoff coefficient of the entire basin cannot be directly estimated. Therefore, it was indirectly calculated as the unknown factor of the water balance of the entire basin and it's equal to R=0.14 (Vafeiadis, 1983).

3.5.2 Lake Orestiada

The lake of Kastoria or lake Orestiada is located in the southwestern part of Kastoria basin, which is a residual form of the larger Neogene-Quaternary lakes that dominated the area of Macedonia. These lakes originated from the tectonic valleys that formed in the Western Macedonia re-

gion during the neotectonic stage of the Alpine orogenesis that began in Tortonio, as mentioned earlier. Lake Orestiada is found enclosed by mountains Heloni and Verno at north, Askio, Tsouka, Korissos and Pyrgos at southeast, Vigla, Samarina at the west, Ouxi and Kainaki mountains at the east.

The shape of the lake is ellipsoidal with a large axis of direction from S to N, 7 km long and a small axis of direction from E to W, 5.5 km long. The rocky carbonate peninsula Koritsa (maximum elevation of 890 m) divides the lake in two almost equal parts. The total area of the lake is approximately 27.9 km^2, the average depth of water 4.40 m, the maximum depth is 9.1 m near the northernmost end of the peninsula, the total water volume is 112 x 10^6 m^3 and the perimeter is 33.6 km. The bottom of the lake close to the perimeter of the alluvial zone tangent to the lake smoothly deepens up to the depth of 5 m while its deeper parts are located NNE and SSW of the peninsula. Erosion materials expand the delta of the Xiropotamos torrent towards the Koritsa peninsula, which tend to separate the lake into two parts (north and south). This also makes an uneven interface of hydraulic communication, in terms of depth, due the deposition of materials by the basin's torrents.

Rain water, several streams and underwater springs recharge the lake while its water level is maintained by the Municipality of Kastoria by discharging the excess water at the south part of Kastoria basin via the Gkioli stream, which exist mostly on the impermeable Neogene deposits. The maximum and minimum water level allowed is +630.27 m and +628.8 m respectively. Vafeiadis (1983) and IGME (2005) studied the water balance of the lake and concluded that, in general, its lowest level occurs in October, the highest in April or May and its annual fluctuation ranges between 0.40-0.60 m.

3.5.2.1 Water Balance of Lake Orestiada

The water balance of the lake is regulated by the amount of water entering and coming out of it. The water amount that contributes to the lake recharge includes the precipitation mount that falls directly on its surface, surface runoff of small and large torrents and groundwater water inflows both from karst and granular aquifers that discharge in the lake. On the other hand, the water that outflows from lake is the one that discharges, as surplus, with the Gkioli stream to the Aliakmonas River as well as the one that evaporates from its surface.

This water balance was quantified by Vafeiadis (1983) and Tolikas & Mylopoulos (2000). The latter are presented below in a tabulated form.

Table 16 - Water Balance of Lake Orestiada

Inflow (m^3)	Precipitation on the surface of the lake	$16.5x10^6$
	Surface & underground inflow to the lake	$76.2x10^6$
	Inflow from under water karst springs	Cannot be estimated
Outflow (m^3)	Evaporation	$23.3x10^6$
	Direct water abstractions from the lake	Cannot be estimated
	Surface outflow from the lake via Gkioli stream	$61x10^6$

The streams that discharge into the lake are classified in terms of size into three categories:

- Medium-sized torrents, only Xiropotamos sub-basin belongs in this class, with a catchment area of 104.1 km^2, which occupies 51.29% of Kastoria basin
- Small size torrents, all streams that discharge into the lake, with catchment area less than 5 km^2
- Intermediate drainage surfaces, the interposed surfaces between the mountain basins of the streams mentioned, as well as surface areas with a catchment area of more than 5 km^2

The estuaries of these torrents are mainly concentrated in the NE quarter of the lake's perimeter, and extend to a coastline of 10 km. The stream of Aposkepos discharges independently into the lake. The torrents of Vissinia, Toichio and Metamorphosis converge close to their estuaries in the lake and form a single delta. Lastly, Xiropotamos forms an imposing delta to its estuaries.

Underwater karst springs exist at the south-west part of the lake but there are no measurements or estimates of their discharge rates. During winter periods the entire surface of the lake covered by an ice layer except from the area close to the underwater karst springs where such an ice sheet is not observed.

3.6 Hydrogeology – Groundwater Hydrology of Kastoria Basin

In this Chapter, the important hydrogeological units of the study area are presented (Fig. 36) and their characteristics analyzed. An extensive aquifer system is present in the alluvial deposits of the Kastoria basin and is in strong hydraulic interaction with the karstified limestones in the south-eastern part of the basin. The nature of hydraulic interaction between the karst and alluvial aquifers themselves, as well as between them and the river that flow across the study area is also examined. Finally, the water balance of the aquifer system in the study area is also discussed.

3.6.1 Hydrogeological units

As discussed in Chapter 1, the following geological formations are present in the study area:

3.6.1.1 Crystalline bedrock

The hydrogeological properties of this formation were examined in previous studies and were found to have very poor hydrogeologic properties in terms of infiltration and hydraulic conductivity including the faults, which are filled with filling material. Because of the mechanical properties of this formation, the effect of the imposed tectonic stresses resulted to mainly plastic deformation while limited evidence of brittle deformation was found. This means that despite the large spatial distribution of this formation the aforementioned brittle tectonic features have not enough distribution themselves to attribute a hydrogeological importance to this formation (Vafeiadis, 1983, MinAgric, 2013).

An unfractured metamorphosed rock has porosity of less than 3% and its fractures are small and usually do not communicate hydraulically with each other. However, along preferential flow ways that can exist in such rocks i.e fracture zones, discontinuous surfaces and mylonitizied zones secondary porosity can exist that allows the storage of relatively good quantities of groundwater (Vafeiadis, 1983).

In this case, field evidence and study of borehole lithological sections taken from previous studies mostly carried out by IGME, 2010 and personal communication with IGME, 2018, suggest that in the study area the weathered zone only extends a few meters in depth, thus it is insignificant in terms of hydrogeological importance. Furthermore, the joints-fractures that can be seen on the surface, rapidly reduce and disappear in the deeper parts of the formation.

The hydrogeological importance of this formation is therefore very small and does not contribute significantly to the recharge of the alluvial aquifer system. Water from small springs emerging from the joints of this formation, is known to have been used in the past to cover for limited drinking water needs.

3.6.1.2 Karstified limestones

This group is consisted of the Triassic-Jurassic limestones of the Korissos, Dispilio, Kastoria and Aposkepos-Kefalari. Their thickness can reach more 400 m, present thick layers without shale intercalations and the degree of karstification is very high. They present a spatial extent of almost 36 km^2 altogether it becomes apparent that these formations should be regarded as aquifers in their

own respect. As will be discussed later in this Chapter, this formation is of significant importance to the water resources of the region. Two major springs are found at those formations that discharge the karst systems.

The permeability of karstified limestones is anisotropic, being of dual porosity. The primary, or matrix porosity and the secondary porosity due to caves, joints, karst channels and other karst phenomena developed in the rock mass. The water flow within the karst body preferentially travels through fractures and generally karst elements, which are not clogged with clogging material. The vertical permeability to carbonates, is usually 2 to 10 times greater than the horizontal one.

In this case, the secondary vertical permeability but also the horizontal one is high, with the former being greater. This conclusion is strengthened by the fact that many karst phenomena exist at the limestones of Kastoria basin e.g dolines, caves, sinks, etc., the large infiltration rates calculated for the limestones and significant karst springs found at their body (Vafeiadis, 1983).

3.6.1.2.1 Characteristics of Korissos karst system

The Korissos karstified limestones have an inclination of WNW. Vafeiadis, 1983 and IGME, 2010 suggest that these limestones do not discharge their water directly into the lake. This conclusion is further strengthened by the occurrence of significant karst spring of Militsa, which are found at 24 m elevation above the lake's water level. However, the karst water is indirectly discharged to the lake via the granular aquifer of the plains Ampelokipoi-Crepene, which is a part of the larger alluvial aquifer of Kastoria basin. Lastly, the secondary permeability is particularly important in these rocks because they inter-connect the flow of the karst water in their mass.

Practically no soil cover or vegetation exists, which suggests that infiltration rate is quite high, as will be discussed in a subsequent Section. Impressive karst formations such as caves or big caverns do not exist, implying that the karstification has developed in a homogeneous pattern rather than in a few large karst channels. This is also supported from the analysis of the spring hydrographs which drain the karst water.

3.6.1.3 Post-alpine deposits

The main aquifer system is formed within these sediments, the total thickness of which exceeds 300 m in places. Those deposits consist of two parts: the one being the Neogene deposits and the other the Quaternary deposits.

The Neogene deposits are found in the southern part of the area in the form of old alluvial terraces as mentioned earlier. Vafeiadis, 1983 assessed the lithological and hydrogeological data of the boreholes drilled at those formations and concluded that fine clayey-marly sediments prevail. The thickness of the coarse-grained layers is small along with the stored water there. This is due to the fact of the low permeability of aforementioned strata, which are mainly sandstones, compacted sand and the poor recharge conditions.

Quaternary deposits present a variety of hydrogeological responses depending on location, thickness and granulometry, and are of fluvio-torrential origin. Their thickness varies greatly. This generally increases from the edges of the basin towards its center. Next to the perimeter of the flat land and at the upstream plateau of Xiropotamos, the thickness of the deposits is small, about 120m. In the main plain area of Kastoria the deposits present horizontally differentiated layers of coarse- and fine-grained materials. High hydraulic conductivities were observed by Vafeiadis, 1983 at certain places of the alluvial aquifer. They are attributed to the coarse-grained formations.

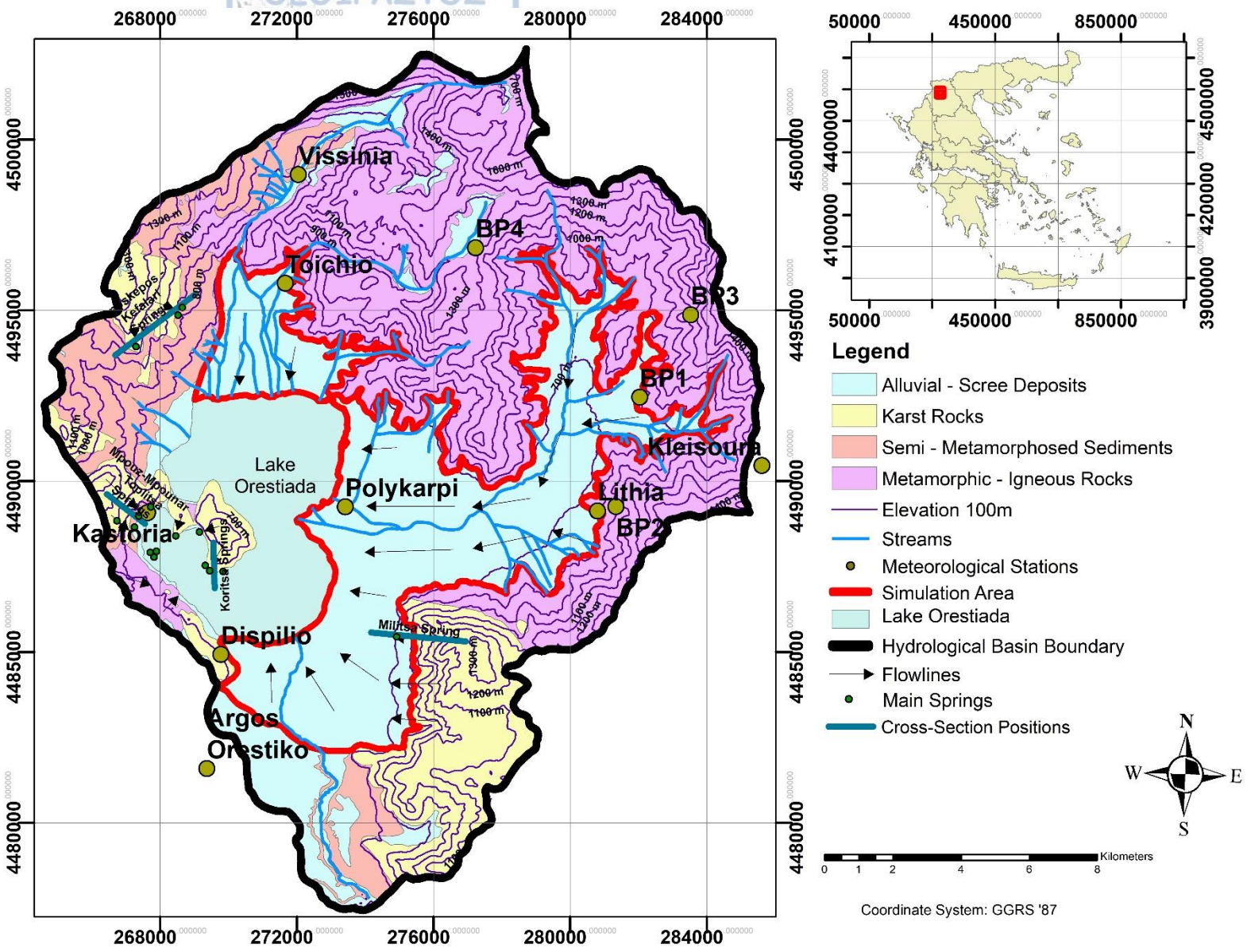

Figure 36 - Hydrogeological map of Kastoria Basin

3.6.2 Springs of Kastoria Basin

In this Section the springs are being described, their characteristics and their role in the water balance of the study basin are analyzed. The type of springs that exist in the study basin are: Contact springs, due to the existence of permeable cover, springs that exist due to discontinuities (faults) of impermeable rocks of the crystalline bedrock and karst springs, which exist due to the dissolution of carbonated rocks. This classification is based upon the type of aquifer and the nature of the water circulation inside the various rocks (Vafeiadis, 1983).

3.6.2.1 Contact Springs

This category includes the springs that appear at the contact of the impermeable crystalline bedrock with overlying permeable brittle material that come from the erosion of the bedrock. Those materials are of very small extent. Also, at this category belong the springs that form at the base of certain screes of the basin. Such springs have been identified in several mountainous regions in previous studies. The springs of this category do not present sufficient flow rates; thus, making them insignificant.

3.6.2.2 Springs in fractures

This category includes the springs that appear in fractures zones of impermeable rocks, e.g the metamorphic and semi-metamorphic rocks. These zones with secondary permeability and active porosity that supplies the springs of this categories as a result of the existence of discontinuities caused by fractures that favor and accelerate the weathering of the rocks. Their existence is purely based to brittle nature of the rock and to that the discontinuities do not clog with clay material because of the weathering resistant nature. Such springs of some significance occur in relatively high-altitude areas, which are characterized rainfall, snowfall and forests. These like those of the previous type don't show any significant discharge.

3.6.2.3 Karst Springs

Remarkable karst springs occur at the appearances of the Mesozoic carbonate rocks of the studied area. The limestone mass of the Korissos karst system heights presents two major spring named Militsa and Istakos. Also, there are other three that have small discharge rate, of seasonal character and therefore, they won't be described in this study. At the limestone mass adjacent to village Dispilio a small discharge spring is found while at northwest side of the basin two spring of medium discharge are found named, Aposkepos spring and Kefalari springs, which have ad distance of 250 m from each other. The Mpouz-Mpounar and Toplitsa springs exist adjacent of southwestern side of the lake while Koritsa spring exist at the limestones found at south side of the 'peninsula' of Kastoria. Finally, some underwater karst spring are found inside the lake at two locations (Fig. 36). Below a detailed description of these karst springs is presented.

3.6.2.3.1 Karst Aquifer of Mount Koritsa, Lake Kastoria

The limestones of Mount Koritsa, which extend within the Lake Kastoria, have the same characteristics as the rest of the limestones described in this section. This karst aquifer is isolated due to the existence of the impermeable rocks that exist west of this aquifer (Fig. 36). The discharge of the karst water happens directly into the lake during the wet season while the dry period the lake recharges the aquifer. In addition, this aquifer cannot be exploited because the aquifer receives a bit degraded water from the lake and especially because the city of Kastoria is built on the first and second protection zone of the aquifer. The hydrogeological cross-section below shows the aquifer hydraulic communication and of the lake.

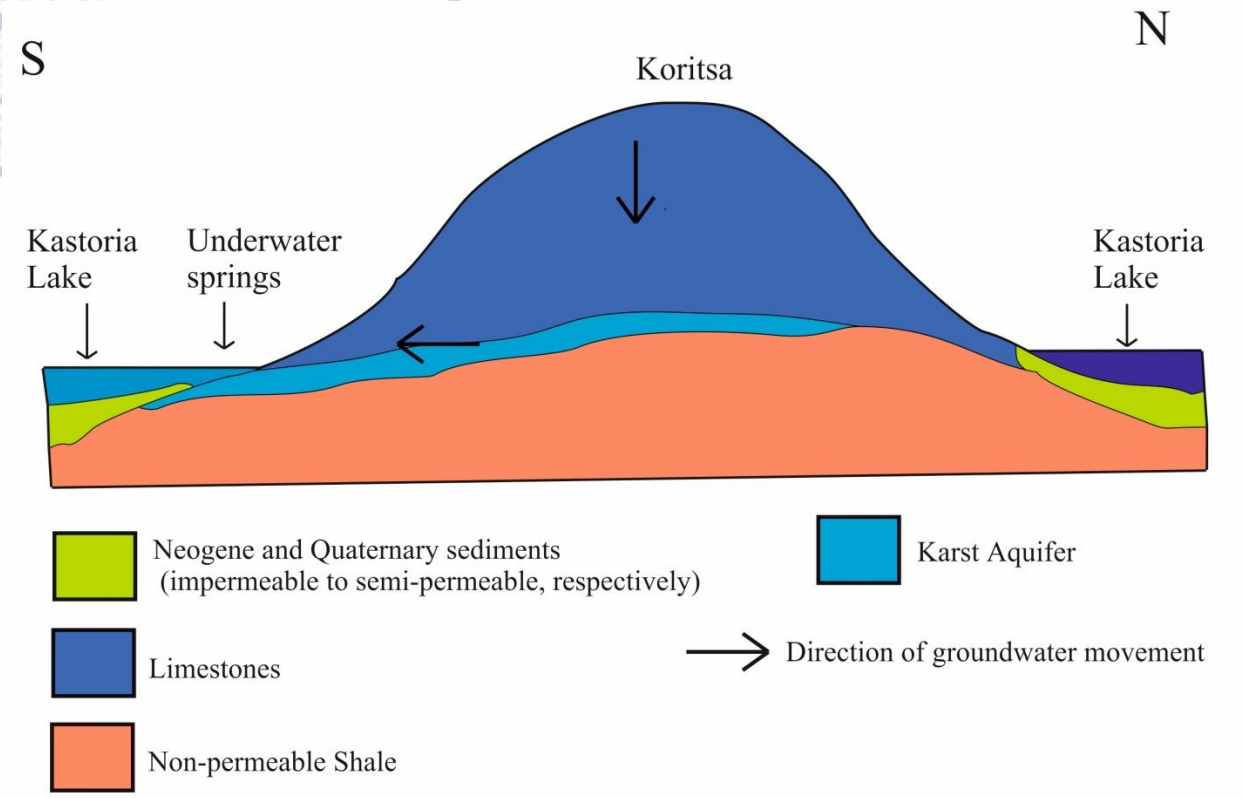

Figure 37 - Hydrogeological cross-section of Koritsa Heights (IGME, 2005)

3.6.2.3.2 Karst Springs of Aposkepos, Kefalari

These springs are karst springs of the karst aquifer found at north-west region of the study basin. The limestone at this region is onlap the impermeable bedrock. The springs discharge at three locations (Fig. 36) two at Kefalari and one at Aposkepos, as mentioned earlier in this section, with discharge rate of 17.52 lit/sec and 14 lit/sec, respectively, meaning these aquifers have small annual renewable amounts. Also, they have the same recharge area (Vafeiadis, 1983; IGME,2005).

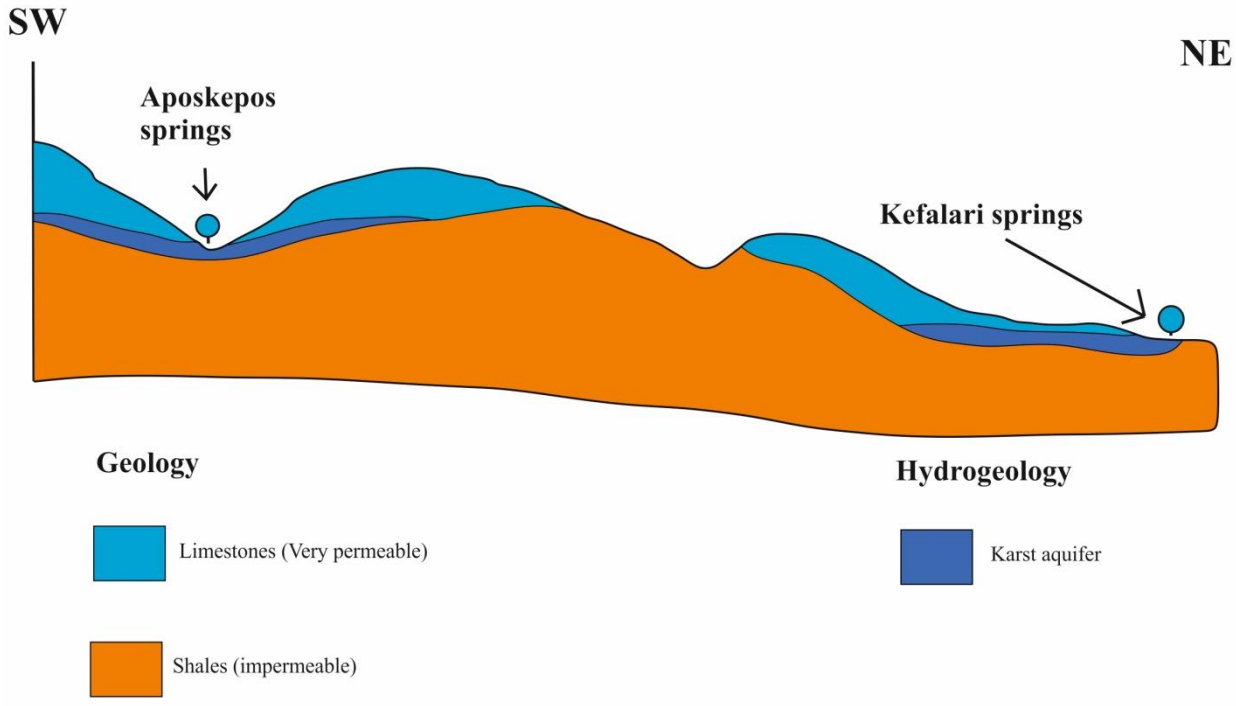

Figure 38 - Hydrogeological cross-section of Aposkepos and Kefalari springs (IMGE, 2005)

3.6.2.3.3 Karst Springs of Mpouz-Mpounar and Toplitsa

The springs of Mpouz-Mpounar and Toplitsa are of karst contact type (Fig. 39). They have an altitude just above from +625 m (Fig. 36).

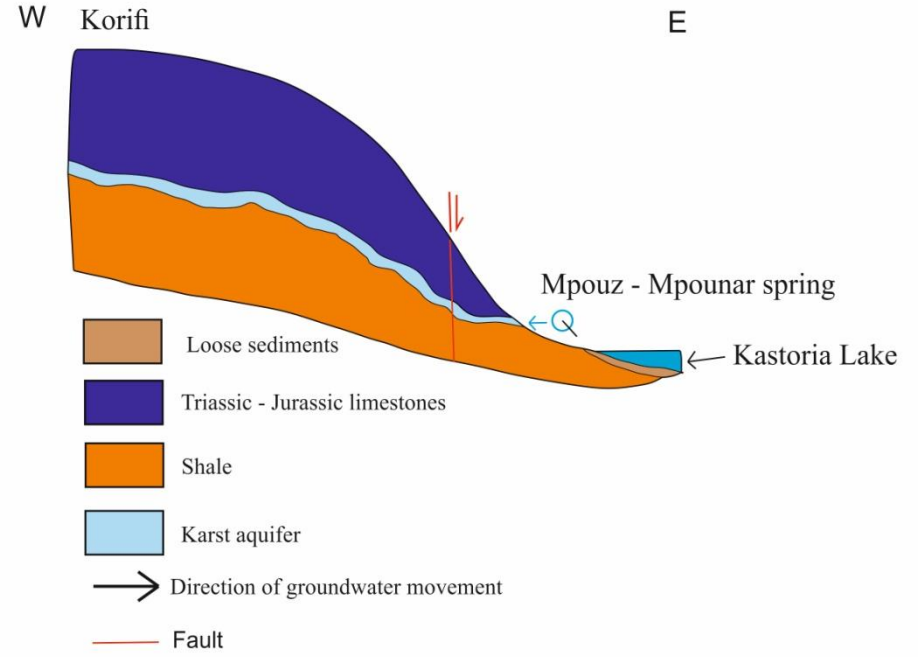

Figure 39 - Hydrogeological cross-section of Mpouz-Mpounar Spring (IGME, 2005)

3.6.2.3.4 Militsa Spring

South-east of Kastoria lake a large mass of limestone exists, this is the same limestone of Triassic-Jurassic age like those described above. However, this one has great thickness. This favors the existence of major karst springs e.g Istakos Mavrochori and Militsa springs, with discharge rates of 29.5 lit/sec and 44 lit/sec, respectively. The karst aquifer discharges through these two major springs (Vafeiadis, 1983).

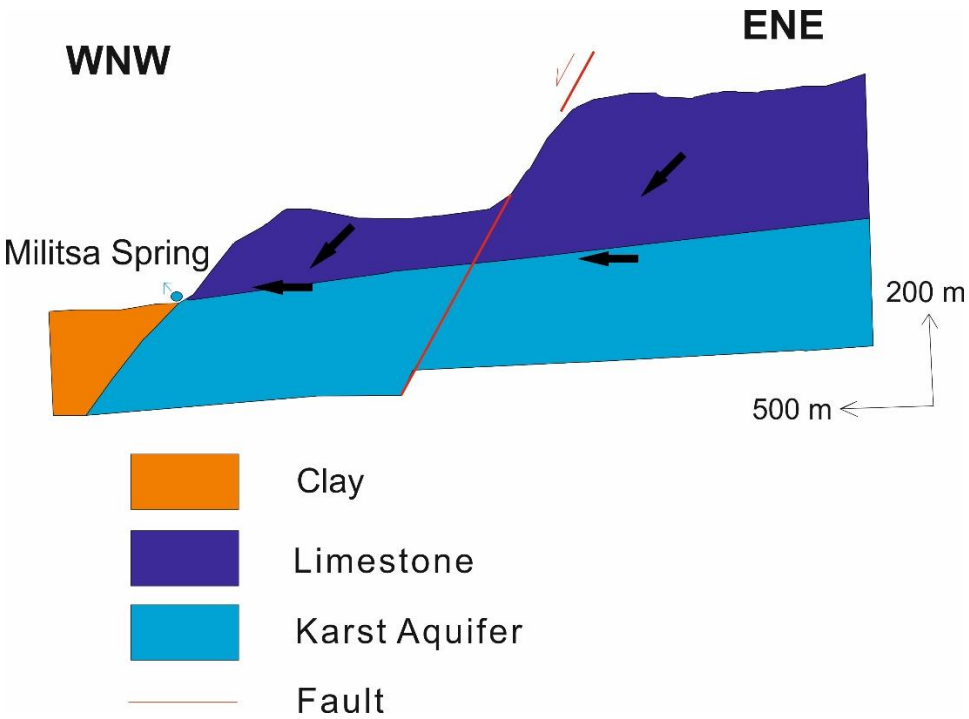

Figure 40 - Hydrogeological cross-section of Militsa spring (IGME, 2005)

In summary, most of the springs found at Kastoria basin are of small discharge and do not contribute to the water balance of the lake.

3.6.3 Granular aquifer sub-system of Kastoria

CODE: GR0900021
Name: Granular Aquifer Sub-system of Kastoria

The Granular Aquifer subsystem of Kastoria is characterized as main, granular and is located perimetrically and in contact (East, South, West) of the homonymous lake. Granular Aquifer subsystem of Kastoria (CODE: GR0900021) is included in the aquifer system (CODE: GR0900020) along with the GR0900022 granular subsystem of Mesopotamia - Xiliodendro, Kastoria. The two subsystems are separated by the molassic sediments of the Mid-Hellenic trench, which acts as an impermeable boundary so that it is not possible for a hydraulic communication to exist between the two other subsystems. Also, they are consisted of Quaternary deposits (alternations of sand, clay, sand-pebbles), whose main feature is the rapid alternation of the grain size in both the horizontal and vertical directions as well as the position - prevalence of one or the other lithological type. GR0900021 is associated with Kastoria Lake (GR1320003), whose water volume eventually discharge to River Aliakmonas via the stream Gkioli (GR1320001).

Below are the main features of the GR0900021 subsystem.

3.6.3.1 Description of the aquifer

The Kastoria granular aquifer subsystem consists of mainly medium – grained formations. The constant alternation of these horizons with clayey materials constitutes the vertical anisotropy of the system and creates the proper conditions for the development of partially confined aquifers at certain deep locations. This area is dominated by unconfined aquifer while deeper partially confined aquifer layers exist. The recharge of the system is carried out by deep percolation of precipitation, infiltration of surface waters (mainly from the torrents of the area), the irrigation returns and the lateral recharge from the Korissos karst system. The natural underground discharge of the system is towards the lake of Kastoria. Groundwater is used for irrigation (primarily) and secondarily for water supply only for the settlements close the mountainous regions. The summarized characteristics of the system are as follows:

Area: 77 km²
Renewable water amount: 20 x 10^6 m^3/year
Water balance: positive

3.6.3.1.1 Structure

3.6.3.1.1.1 Lithology

The Kastoria basin contains alluvial deposits of mixed fluvial, lacustrine and fluvio-torrential origin. Study of the tectonic history of the area, stratigraphic data prove that sedimentation of the alluvial basin is controlled by the following two factors: Climatic conditions and tectonic evolution. Examination of the borehole lithological sections made by Vafeiadis, (1983), those provided by the TOEV of Korissos-Lithias, indicates a high degree of heterogeneity along the River Xiropotamos and its upstream plain and a high degree of vertical heterogeneity at the south part of the basin.

The Miocene sediments were deposited at the south part of the basin and consist of alternating layers of clays, marls, sandstones and conglomerates to a lesser extent in the form of old fluvial terraces. These sediments at their largest part consist of fine-grained clayey marly sediments. The thickness of the more coarse-grained parts (mainly sand and sandstones) is small and have unfavorable lateral recharge conditions; thus, resulting in low pumping rates. The Quaternary

sediments, on the other hand, present a different response in terms of hydrogeology, depending on their thickness, which increases from the basin's boundaries towards the center, particle composition and location.

IGME, 2010 carried out geoelectrical surveys at this basin (Fig. 41). Analysis of the results revealed low to medium electrical resistivity layers, presenting an unconfined aquifer, at the central area of Kastoria Plains and along the most of the lower part of torrent Xiropotamos while in the northern and northeastern part of the study area, namely the upstream of torrent Xiropotamos, layers of coarse grained content are found, indicating high effective porosity. Furthermore, a lithological transition from coarse, low clay content deposits in the NE, to mostly finer, higher silt and clay content material of lacustrine environment towards the central part of the basin was indicated. The same trend was concluded from the study of the borehole lithological sections by Vafeiadis, 1983.

Further examination of borehole lithology showed that the alluvium composition is generally fine in its upper parts at some areas. Below these parts a sequence consisting of alternating bands of fine and coarse materials is observed in the central parts. Coarse and fine sediments exist at equal proportions within the basin. However, because of the relatively sharp vertical variations that characterize the alluvial sediments a typical sequence cannot be defined for the entire basin. However, such a typical sequence can be defined the Kastoria plains (Fig. 40)

Torrent Xiropotamos has a torrential character and flows at steep slopes at the upper areas while it flows at gentler slopes (Fig. 3), before discharging at Lake Orestiada. The existing slope-break on entering the plains' area in deposition of its stream-load which consists of angular and rounded pebbles of mainly metamorphic origin, mixed with less coarse and more fine materials. Consequently, an extensive marginal fan of several tens of meters has developed in the western part of the study area, which is the Kastoria plains.

3.6.3.1.1.2 Geometry

As discussed in the previous Chapter, the Kastoria alluvial aquifer system forms the central, north, northeastern and southern part of Kastoria basin. It is bounded by the crystalline rocks in the north, northeast and at the east, by crystalline limestones in the south-east, by the impermeable Neogene formations in the south, which most of them exist outside the local base level (see section 3.1) and Lake Orestiada in the west.

The Holocene deposits present little to some porosity and they are small in thickness, but with the underlying Pleio-Pleistocene deposits are capable of housing a substantial aquifer. The Pleistocene and Pleio-Pleistocene deposits present significant porosity and can store groundwater so to form the aforementioned substantial aquifer in the plains of Kastoria basin. The loose sediments of the quaternary deposits of Kastoria basin found north, east and south of the lake consist of alternations of sand, gravel, clay and marl. The water supply is mainly located in the sandy pebbles formations, where they form unconfined and confined aquifers down below at the deepest points. The groundwater potential developed in the above formations is remarkable and its level is a few meters below its surface terrain, due to the great hydraulic connection between the permeable layers. The hydrogeological map, found in Fig. 36, shows the spatial extent area of the aquifer of these deposits, of course, without being precisely delineated.

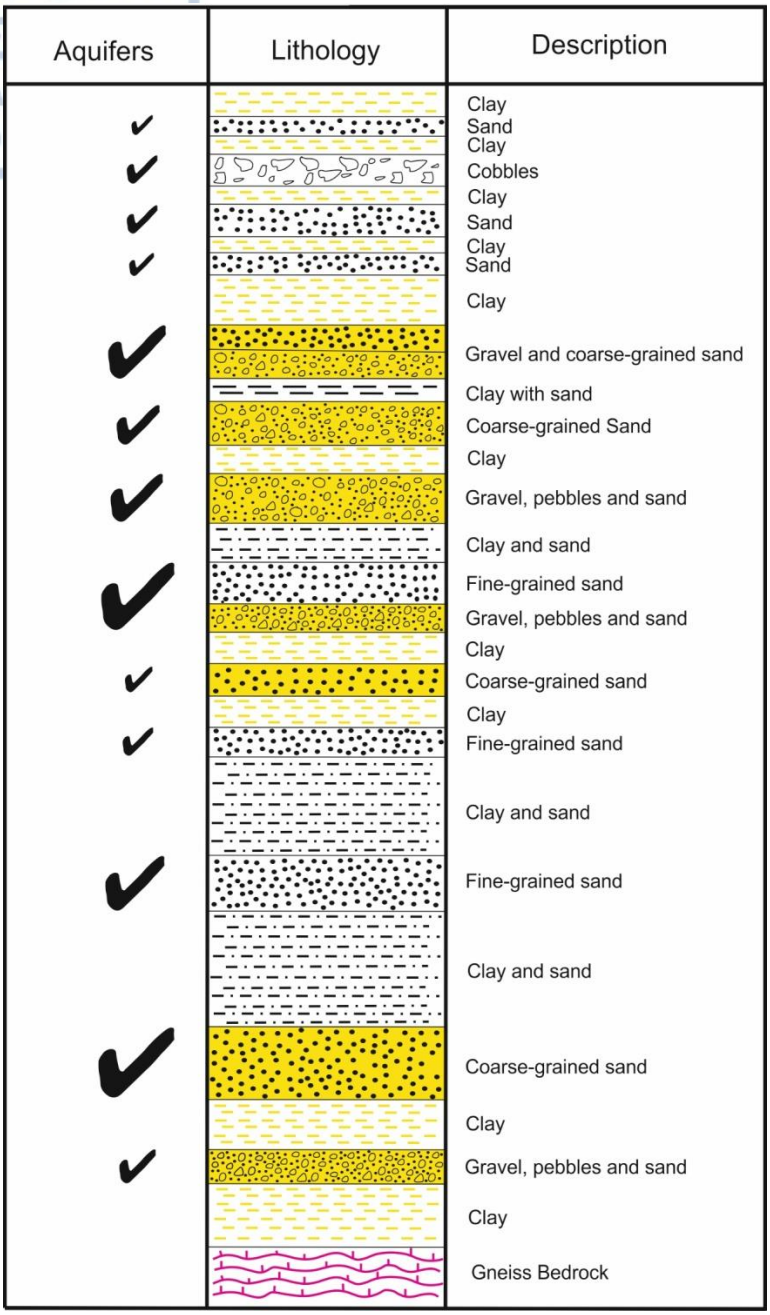

Figure 41 - Typical Stratigraphic Sequence of the Quaternary sediments of the plains area perimetrically of Kastoria Lake (adapted from IGME, 2005)

The above lithological section shows the layers of the Quaternary loose sediments around the lake and the corresponding aquifer layers, which constitutes the known alluvial aquifer of Kastoria, whose water supplies a large number of irrigation wells as well as well for domestic use.

Neogene deposits include the molassic sediments and are found directly below all previously mentioned deposits. In hydrogeological terms, they do not appear to have any porosity at all so they cannot house any groundwater, meaning that they are characterized as watertight formations and their role is as a regulator of the groundwater flow of the overlying permeable formations. Thus, the Neogene sediments lack any groundwater except very few cases where the present very limited and local porosity.

The molassic formations are made up of the Tsotili and Pentalofos formations, which are sediments of Oligocenic age. They are deposited in the Mid-Hellenic trench and consist of marl, clay, conglomerates and sandstones. These sediments of the Molassic formations extend beneath the aforementioned Quaternary deposits, in terms of Stratigraphy, so they have a very large spatial extent and a great thickness. Also, they don't present any porosity in their mass either primary or secondary, despite their significant extent. Their hydrogeological importance significance, however,

lies in the fact that they act as regulators of the groundwater movement, as mentioned in a previous chapter.

The Paleozoic gneisses and granite gneisses form the basin bedrock, whose depth varies with location. The thickness of the Quaternary alluvial deposits located in Kastoria basin is set by the bedrock depth distribution. Their strong heterogeneity presents some trends in terms to the distribution of their lithology, as previously discussed. Based on the analysis of these trends, derived from ERTs (Electrical Resistivity Tomography) provided by IGME, 2010 and observation made by TOEV Korissos-Lithias and IGME during borehole drilling, resulted to following conclusions about the geometry of the alluvium of Kastoria basin.

Finally, based on the above, the following two units can be distinguished in the alluvium, that's excluding the appearances of weathered bedrock and limestones as found by the aforementioned geophysical survey, which are limited in both number and extent. These exist perimetrically to the lake while the lower one is also found as a single at the upper section of the Xiropotamos torrent.

1. Upper alluvium perimetrically to the lake, where fine thin layered materials with clay content exist along with some bands of sands and gravel. Between these layers medium grained sand exists. These bands present a limited spatial extent. The thickness of this part is varying from 10 m to 70 m.
2. Lower coarse alluvium which has a variable thickness of 350-400m or more for the plains area, where it presents thicker layers of more coarse material along with small participation of finer sediments. At the upper section of Xiropotamos torrent only the second unit of alluvium is found. The reason of this change is mentioned in the previous section.

Below a more detailed description of the alluvium is presented based mainly on the geophysical survey made by IGME for the north, central and eastern part of the basin.

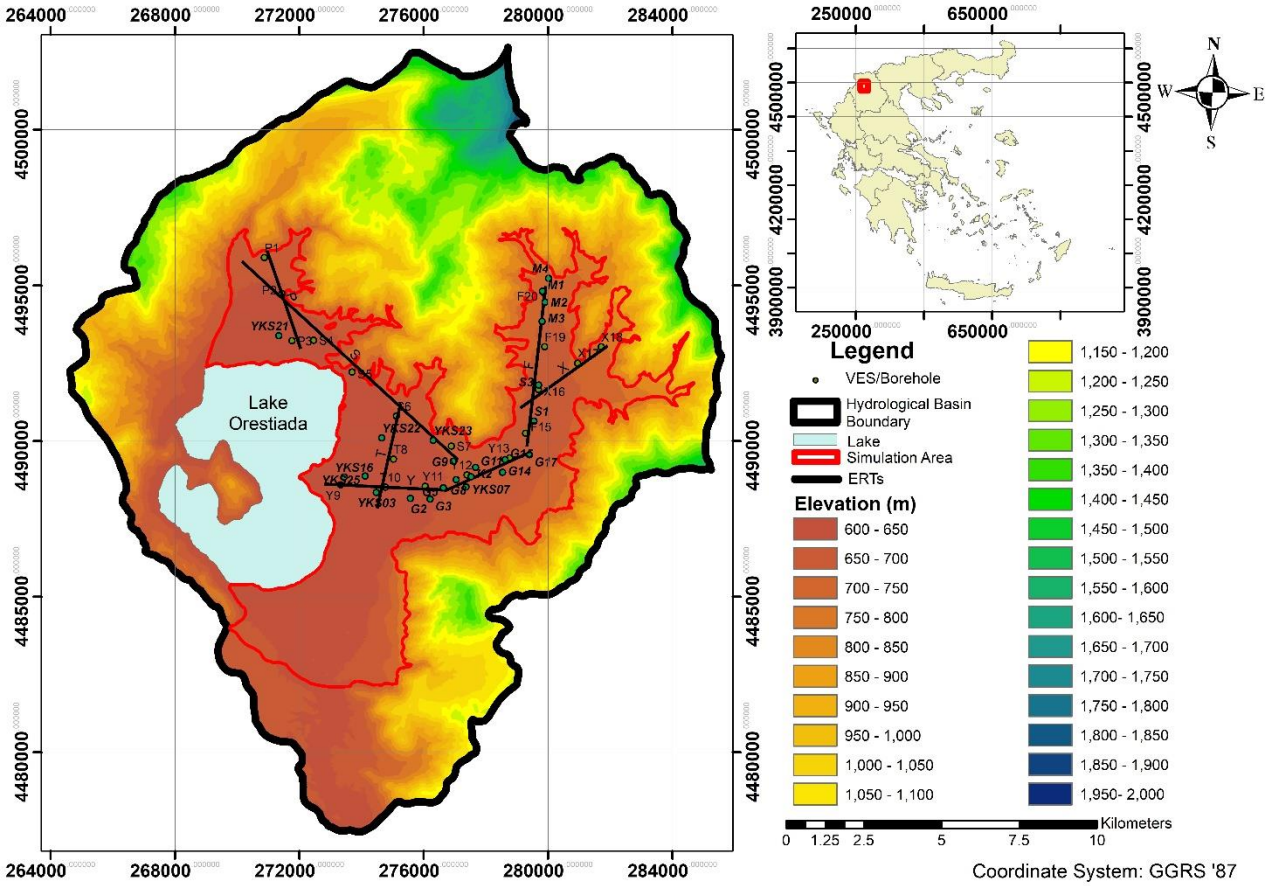

Figure 42 - Location of ERTs, VES and boreholes used for the ERTs (data form IGME, 2010 and Gianneli, 2009)

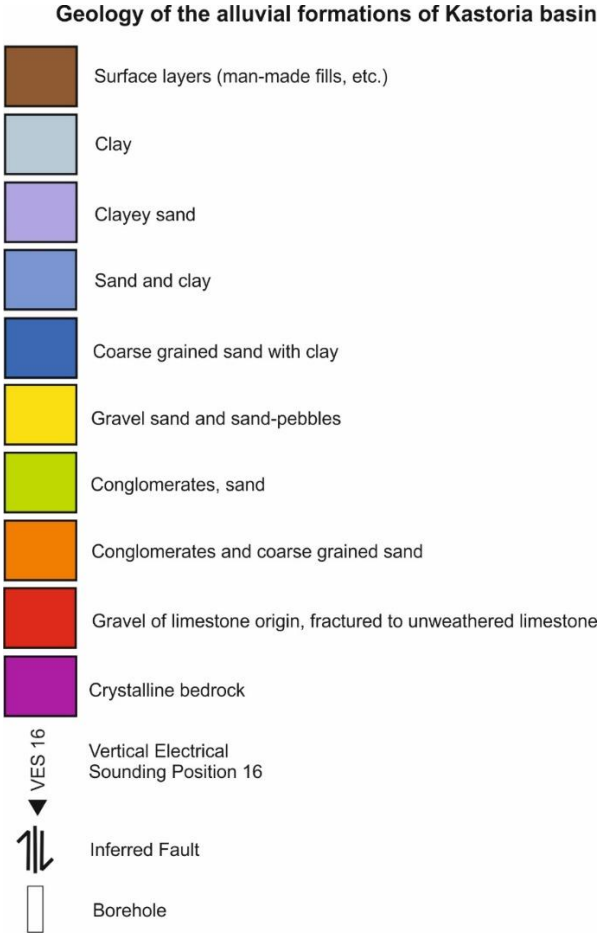

Figure 43 - Legend of ERTs

- ERT S: The top layers between the village of Toichio and the Synora area are a few meters to 32 m thick, consisting of man-made fills, fills, gravel, sand and sand pebbles. Sands, sand pebbles with gravel are found below, 5 to 30 m thick and up to 50 m at certain places. Underlying those materials sands and some conglomerates or gravel can be found. Conglomerates with gravel and sand are found directly below. Their thickness ranges from 50 to 100 m and maybe over 300 m down below. Finally, at the of the sequence carbonates and the crystalline bedrock are found.

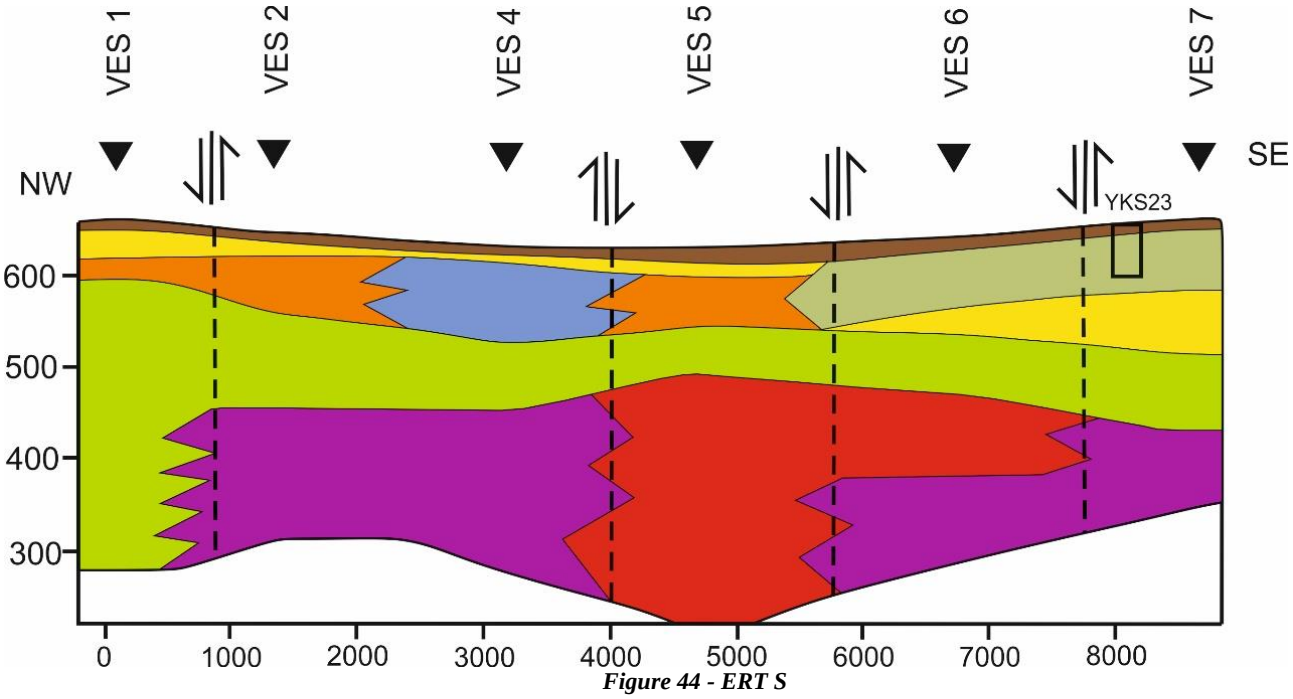

Figure 44 - ERT S

- ERT T: Man-made fills, fills, sands and clays make up the surface layers of about 15m thick, between the villages of Fotini and Mavrochori. Below clay with the participation of coarse-grained sand of a 30-40 m thickness are found. Underlying the last layer coarse sands with gravel and a little clay of about 40 meters thick exist while directly below clay with some coarse-grained sand is found of about 25-55 m thick. Next, sands and sand pebbles exist up to the depth of 170 m. In contrast, close to VES. 8 and 10 less cohesive sediments such as sands, both coarse and fine grained, with clay intercalation exist.

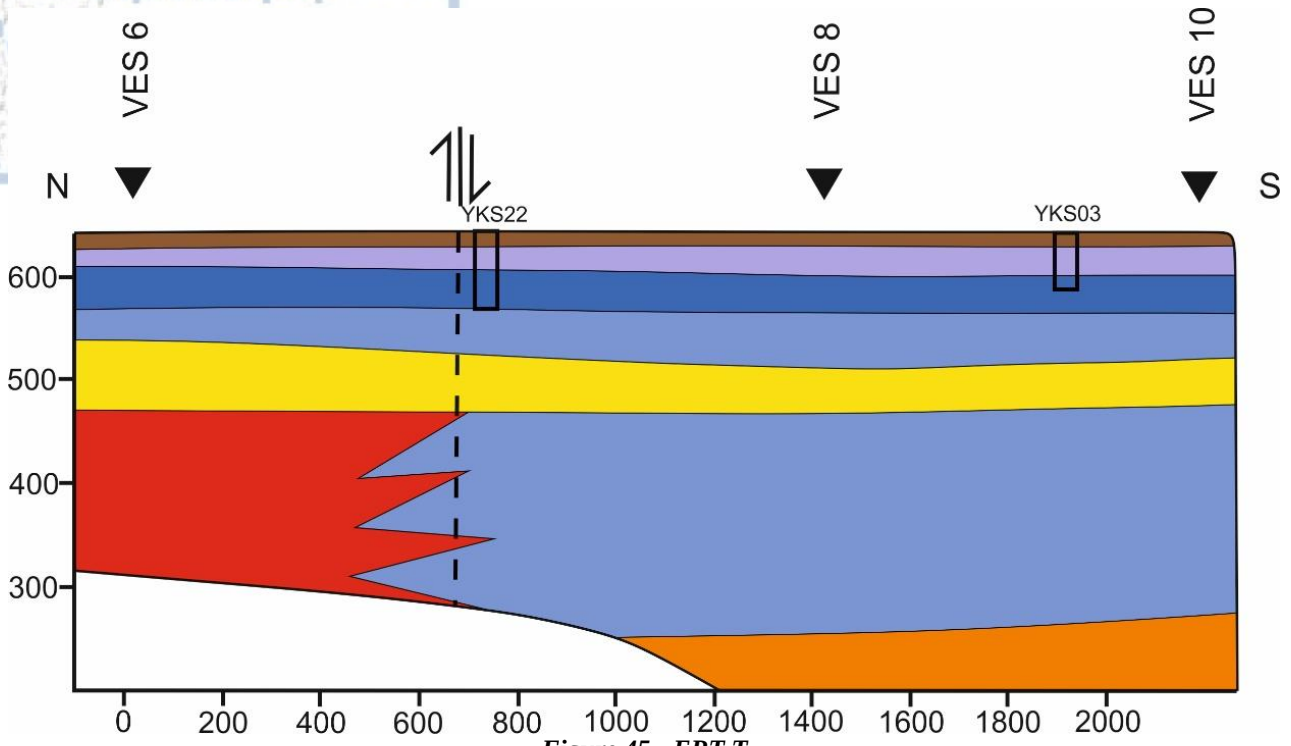

Figure 45 - ERT T

- ERT Y: The thickness of the surface layers, between the villages Mavrochori and Lithia, is about 20 m and consist of man-made fills, fills, etc. Below the layers are made of alternations of coarse sands with clays and fine sands of about 30-130 m thick in total. Up to the depths of 180 - 220 m, conglomerates can be found. Close to the center of the plains of Kastoria fine sands with clay intercalations are found. Rural measurements should have leaked, therefore cannot be taken into account, so in this section the e. layer is presented without color and with question mark. At VES. 13, coarse-grained sands are found about 70 m thick, VES. 9 clay prevail while at VES. 10 coarser material like sand pebbles and gravel exist. At the rest of the survey, the crystalline bedrock was located.

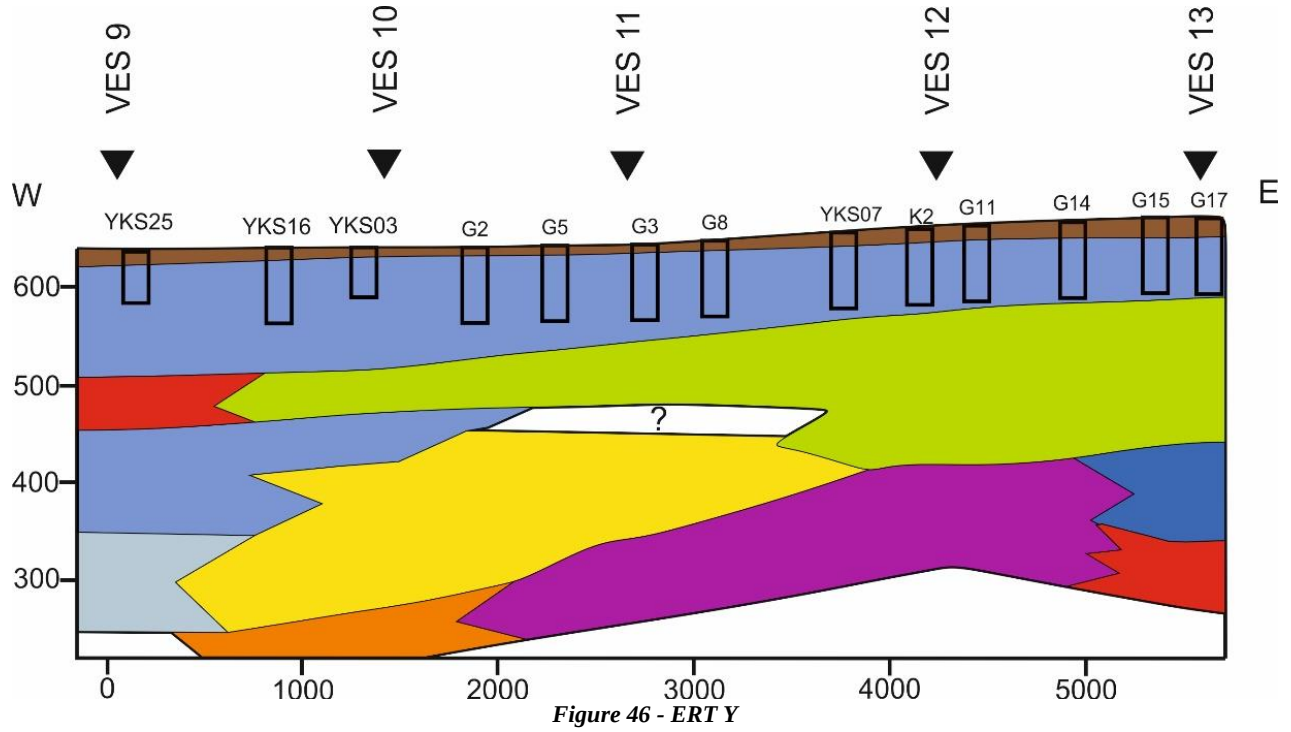

Figure 46 - ERT Y

- ERT F: Between the villages of Melissotopos and Stapototamos, surface layers, 10 to 25 m thick, consist of man-made fills, fills, etc. Below and up to 60-140 meters, the underlying is made of alternations of sand, sand pebbles and gravel. At VES. 20 and 16 the gravel part of the layers is greater. The underlaying carbonate layer is about 65-140 m and finally the crystalline bedrock.

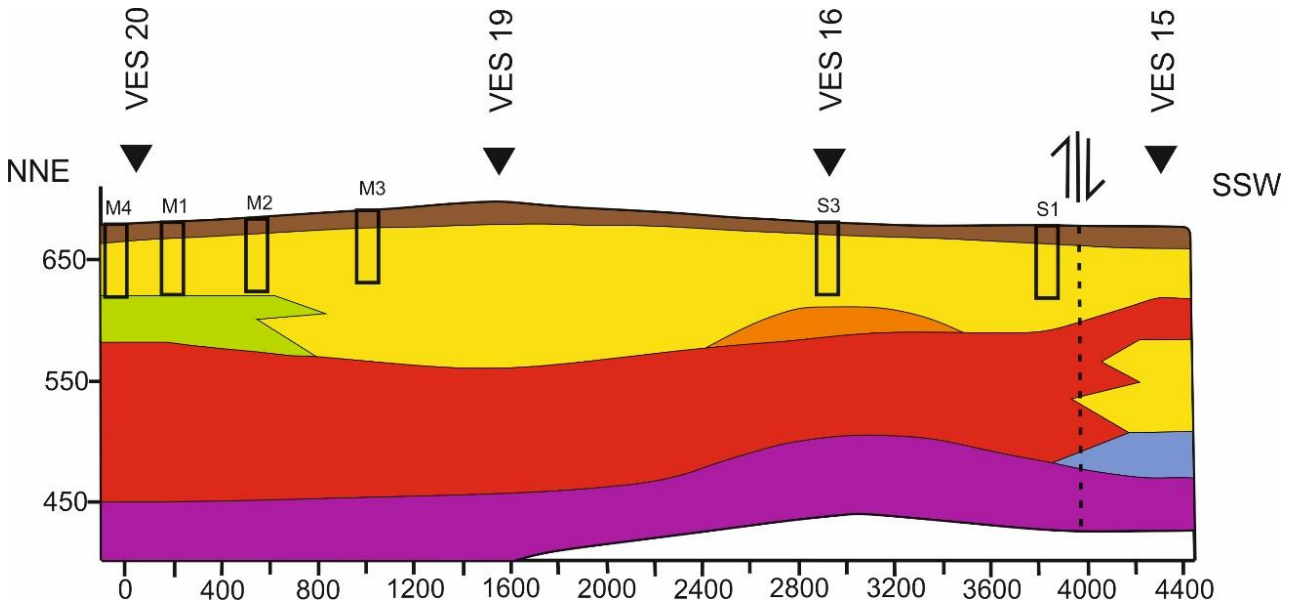

Figure 47 - ERT F

- ERT X: East of the village Stavropotamos, the surface layers for the first 13-25 m are made of man-made fills, fills and alternations of sand, clay and gravel. Below and up to the depths of 60-80 m, coarse-grained sands with intercalations of clay and sand. Also, between the afore-mentioned layers there are more coherent materials with the possible participation sand pebbles and/or fine sands. Underlying below with a 30 to 50 meters thickness carbonate rocks can be found. Finally, from the depths of 165 to 220 m and below the crystalline bedrock is found.

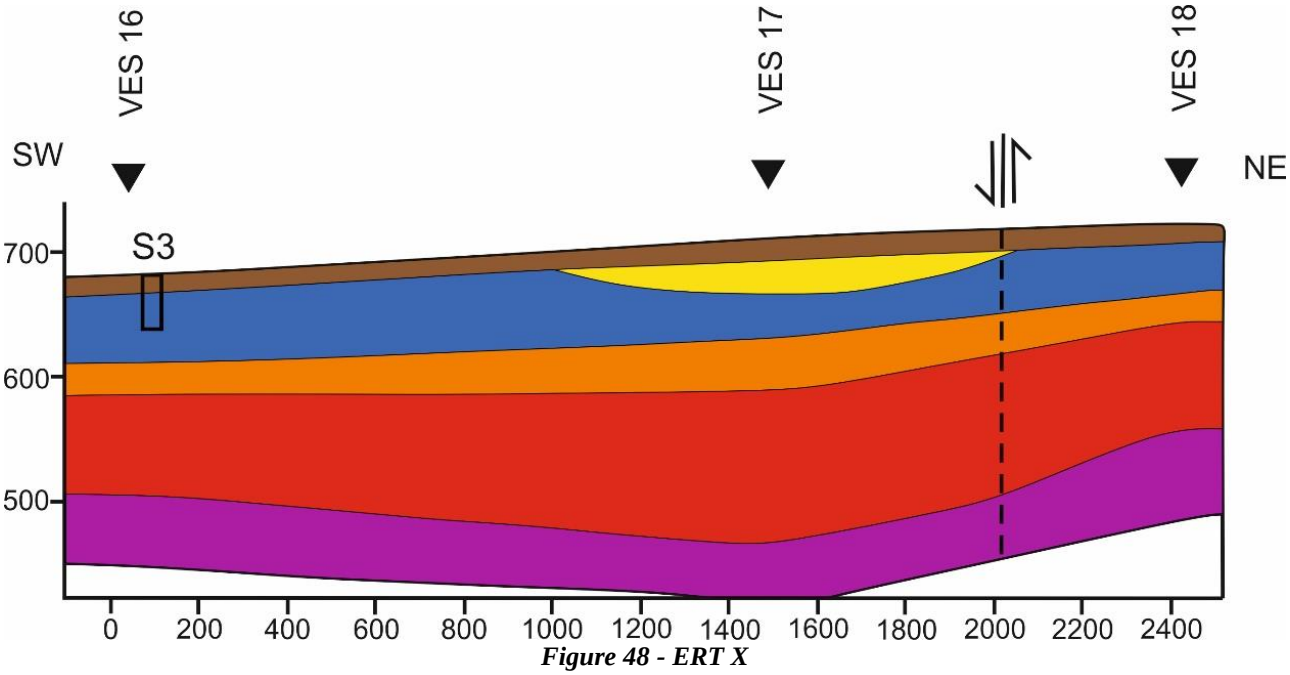

Figure 48 - ERT X

- ERT P: The formations between the villages of Toichio and Metamorphosis, for the first layers 9-20 m thick, are composed of alternating layers that consist of sands, pebbles, gravel and clays. There is also faults between the VESs of IGME. Up to the depth of 70-110 m, there are

alternations of gravel, sand and sand-pebbles. Conglomerates with sand prevail, from below and to greater depths until the crystalline bedrock.

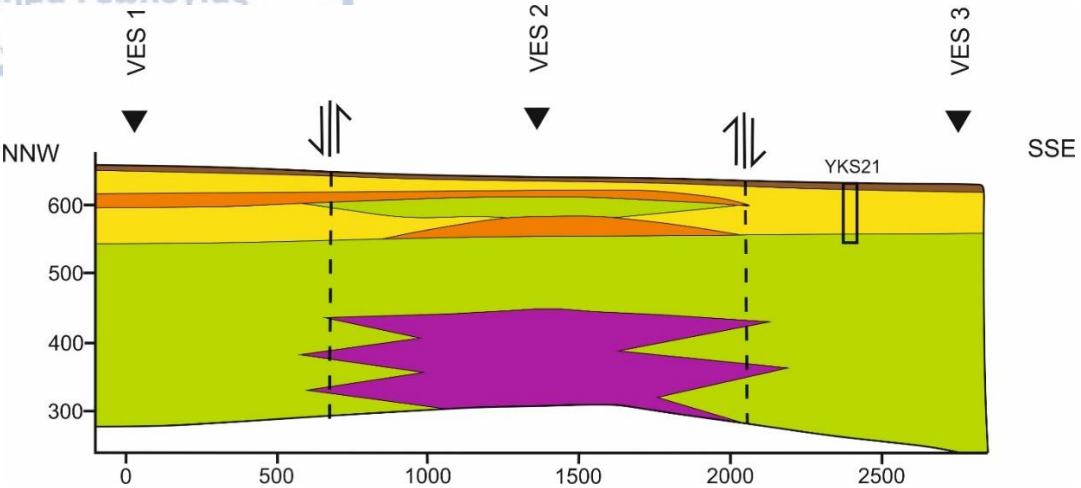

Figure 49 - ERT P

3.6.4 Hydraulic Parameters

In the study of a hydrological basin, the determination of the hydraulic parameters of aquifers is of primary importance because they are key elements for estimating the potential of the aquifers present; thus, determining how they can be exploited in a sustainable way. The hydraulic parameters needed for such a determination are: the hydraulic conductivity (k), which expresses how easily the water flows in the porous media, transmissivity (T), which expresses the capability of an aquifer to transmit water to a directly adjacent location and storativity (S), which defines the volume of water released or stored in the surface unit of 1 m^2 of the aquifer, when its pressure level changes for a unit of length to 1 m. Some of methods known from literature that are used in calculating those parameters are: Thiem, Theis, Jacob, Chow, Jacob-Lohman; Hantush-Jacob and Walton and Boulton.

Vafeiadis (1983) performed a total of twelve pumping tests over the years 1980-81 in the lowland area while Gianneli (2009) performed three at the south part of the upstream part of Xiropotamos. The depth of the wells that were pumped in both those theses ranged from >50 m to 100 m. The summarized results of those pumping tests are summarized at the table below while their position is illustrated at Fig. 50.

Table 17 - Hydraulic Parameters of 15 boreholes at Kastoria basin

ID Num.	Name	S	k (m/s)	T (m^2/s)
1	G12	9.20E-03	1.50E-04	1.10E-02
2	B7	1.50E-03	2.80E-05	1.40E-03
3	B6	2.30E-04	5.00E-05	2.00E-03
4	A1	-	1.90E-04	6.90E-04
5	A2	2.00E-02	3.17E-04	4.78E-03
6	A3	2.00E-02	3.16E-06	1.09E-02
7	A4	2.85E-03	1.37E-06	2.47E-02
8	A5	-	2.80E-03	8.50E-03
9	A6	-	4.43E-04	4.00E-04
10	A7	-	5.10E-04	8.17E-03
11	A8	-	5.20E-05	1.20E-03
12	A9	3.30E-02	2.80E-04	5.28E-03
13	A10	-	2.80E-04	5.28E-03
14	A11	2.90E-04	6.00E-05	2.90E-04
15	A12	3.30E-05	1.46E-04	7.30E-03
Mean	-	9.68E-03	3.54E-04	6.13E-03

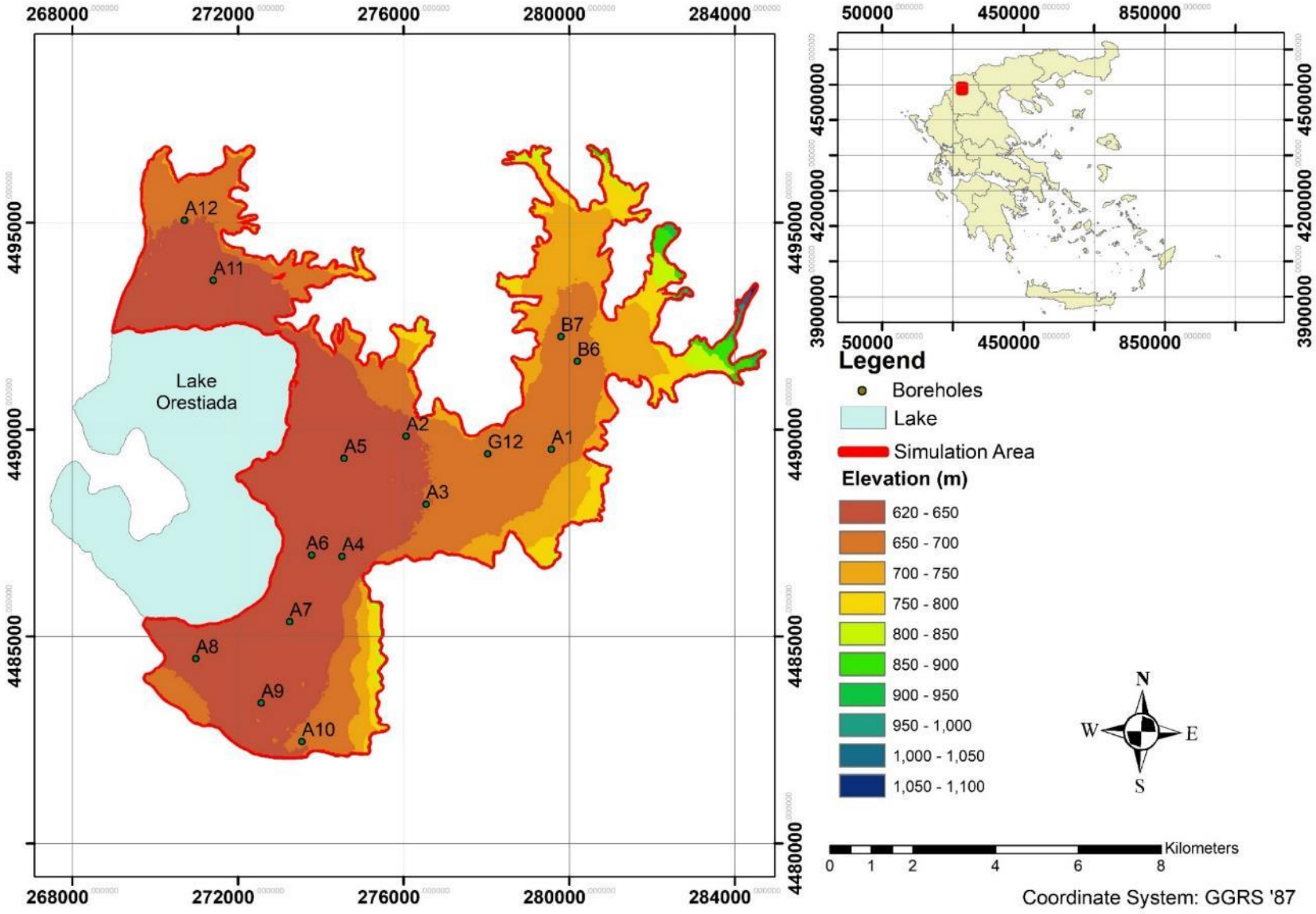

Figure 50 - Location of 15 Boreholes with the Hydraulic Parameters

3.6.5 Piezometry

The study of piezometry of the study area was based on the water table measurements performed by Gianneli (2009) and IGME (2010) as well as Vafeiadis (1983). Available monitoring points have an adequate spatial distribution within the boundaries of the study area. The following discussion will present that the available monitoring boreholes adequately describe the piezometry of the studied alluvial aquifer system.

Data records are available for 60 monitoring points that cover two periods between 2003-2008 and between 2010-2012. The records consist of measurements performed at the end of wet and dry period of each hydrologic year. A map showing the position of the monitoring points, is illustrated in Fig. 51.

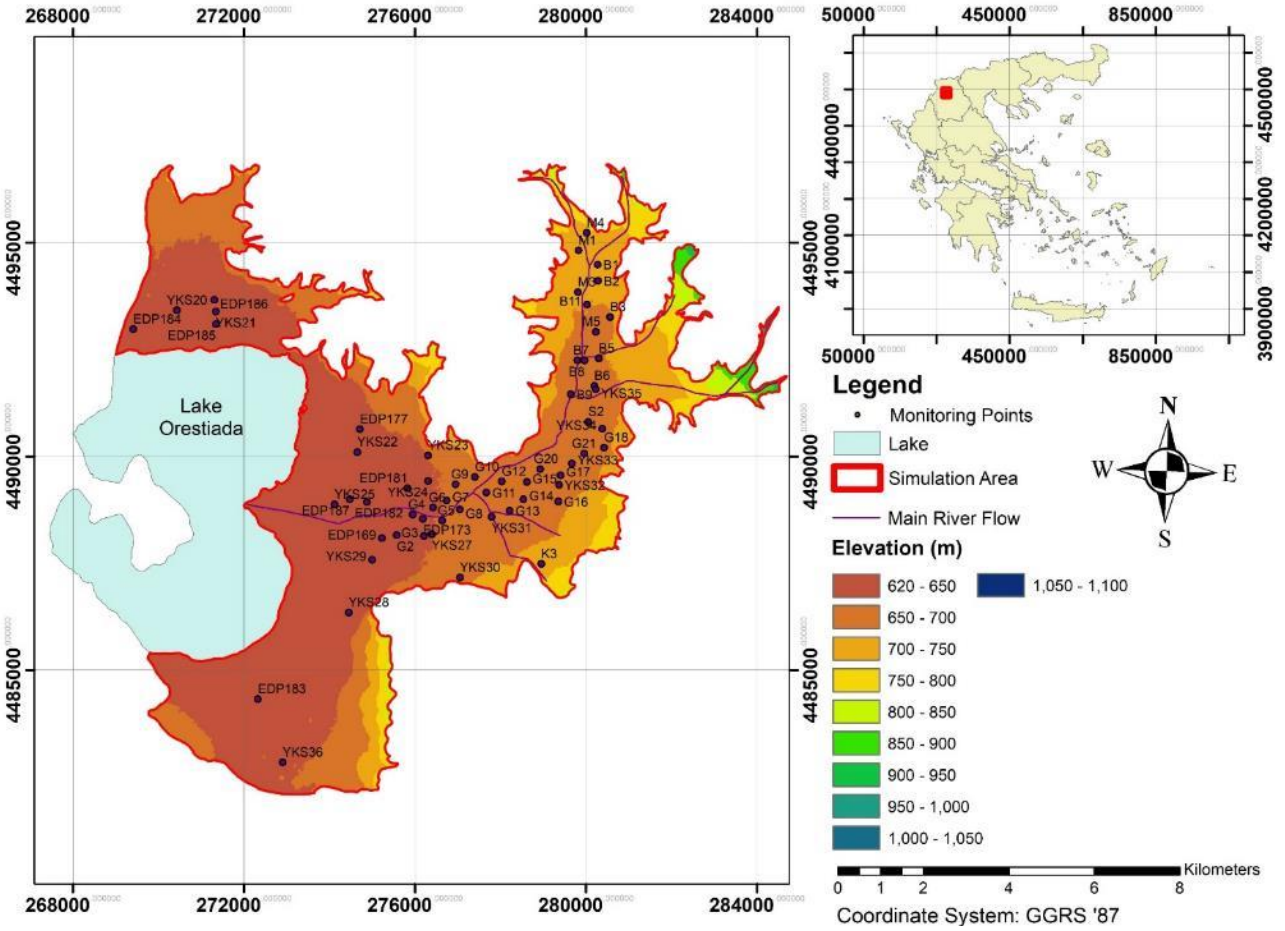

Figure 51 - Position of the 60 Monitoring Points in the Simulation Area

A number of limitations apply to the usefulness of the available data as a means to study the evolution of the water table:

- Some data records are missing from the data inventory. It was thought that data generation to fills those missing would have been accurate, because there are not any significant localized factors such as lithological variations since the studied aquifer system is alluvial to its entirety and generally of small extent but still, they are of fluvio-torrential origin so some uncertainty can be expected. Also, abstraction patterns within the aquifer system remain the same in terms of spatial distribution. Thus, the missing records were filled with the mean value of all the records of each corresponding period for each borehole.
- Study of the vertical hydraulic gradients proved to be very difficult as no multi-depth dedicated piezometers and/or boreholes exist for each aquifer layer. Due to the small extent and thickness of the individual aquifer layers no significant vertical hydraulic gradients are ex-

pected. Also, impermeable layers within the aquifers are of small extent in 3D space so it assumed that entire alluvial aquifer system to be one layer.

The official end of the irrigation period is 15/9 and most of the irrigation use is terminated in the end of September. It was therefore thought that the measured water levels would not be strongly affected by localized depression cones from individual pumping wells as they would have significantly affected the regional piezometry situation of the aquifer (IGME & Municipality of Kastoria, personal communication 2018).

3.6.5.1 Transient piezometric data

Piezometric maps for the aquifer was based on the filled sets of measurements. It therefore follows, that piezometric isolines drawn for this aquifer are to an extent arbitrary. Also, due to fact that the exact dates of the beginning and end of irrigation period are unknown, the measurements performed later than 2010 present somewhat large drawdowns as shown at Fig. 52. This leads to an increase of groundwater flow velocity.

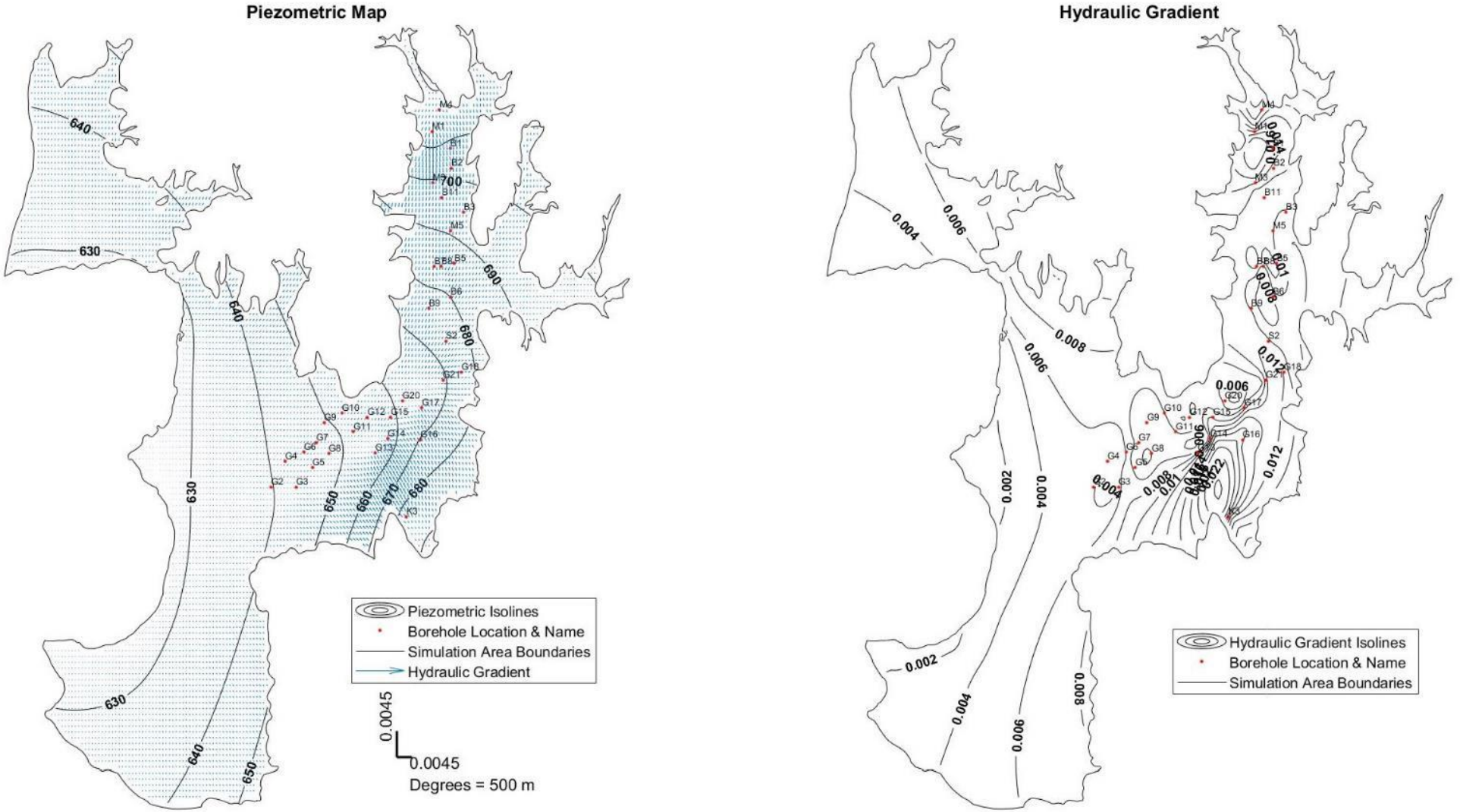

Figure 52 - Piezometric map for May 2004

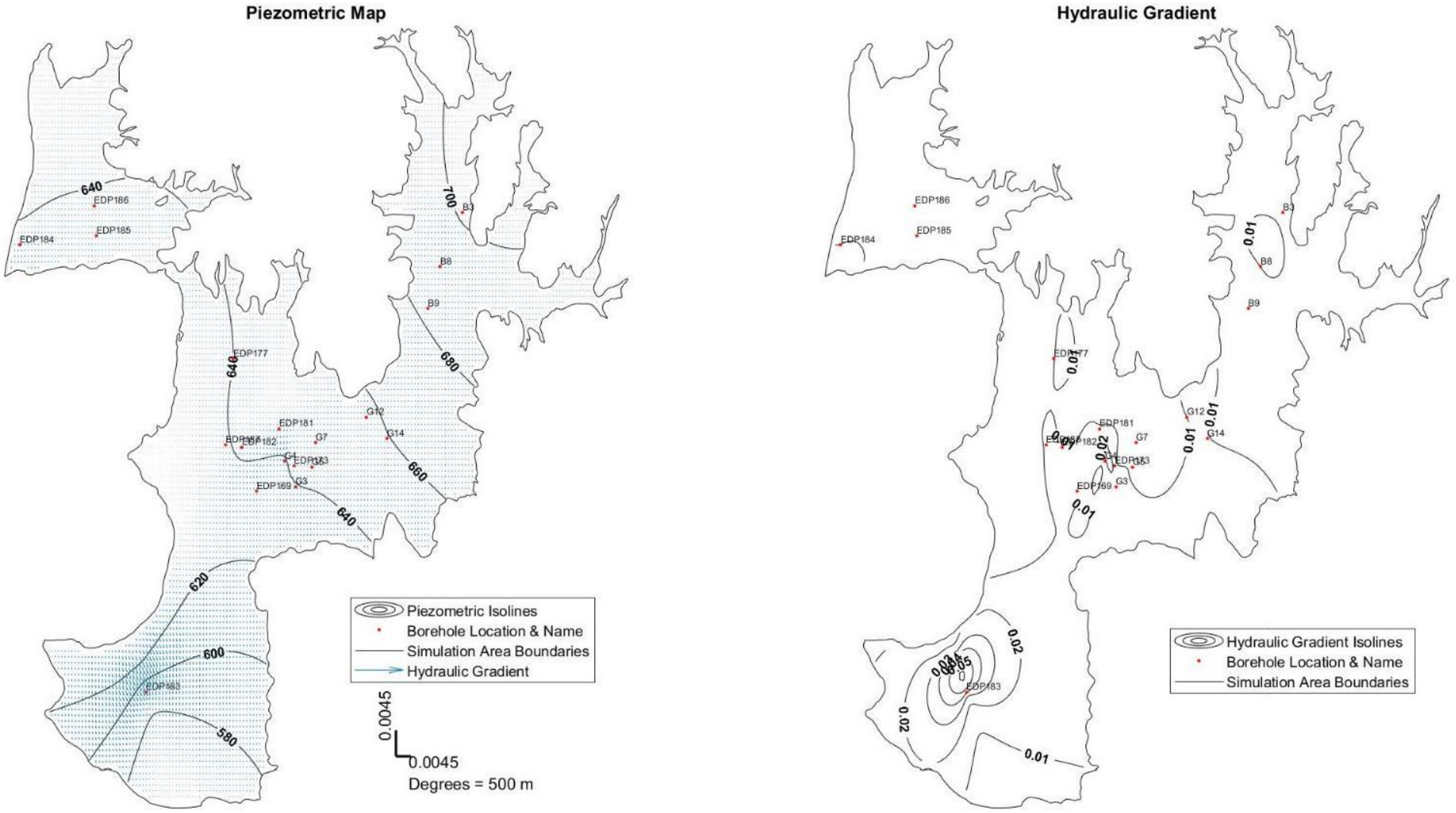

Figure 53 - Piezometric map for May 2012

Vafeiadis (1983) compiled piezometric maps for October 1979 and May 1980 and then outlined the following observations:

- The piezometric isolines, at the larger part of the alluvial aquifer of Kastoria plains, are straight, parallel and of non-equal distance from one another corresponding to cylindrical aquifers
- In the plains section NE of the lake, piezometric surface has conical shapes inferring radial type of aquifer layers
- The groundwater flow lines in the upstream section of river Xiropotamos converge towards the torrent. Downstream of Xiropotamos torrent the flow lines deviated from each other. At the area found next to the perimeter of the lake, the flow lines are parallel or nearly parallel. These observations suggest that Xiropotamos in certain parts acts as effluent and at others as influent

Observations made from the compiled piezometric maps, at the beginning and the end of the irrigation period, of Vafeiadis, 1983; Gianneli, 2009 and those compiled, by a custom MATLAB code with Ordinary Kriging Method (Schwanghart, 2010), on the framework of this thesis indicate that the hydraulic gradient, as presented by the density of the piezometric isolines, of the groundwater's piezometric surface in the upstream zones are generally greater than those found at the Kastoria plains. Decrement of the hydraulic gradient is attributed to the decrement of the dip angle of the impermeable bedrock from upstream to downstream and to the increment of the hydraulic conductivity, due to thicker aquifer layers downstream.

Also, as observed from the piezometric isolines, using the Kastoria Lake as reference, a wide range of hydraulic head values are present in terms of spatial distribution of each hydrologic year studied. At the Xiropotamos torrent basin, during the irrigation period high values are found as a mean e.g. +40-60 m. At the basin of Lakkos torrent, which is found north of the lake, and the rest of Kastoria plains the hydraulic load increases from the south towards the north and reaches values of up to +20 m. At the southern part of the basin some negative values are observed. This happens due to pumping but more importantly the nature of the formation there that does not allow for a quick lateral recharge of the aquifer layers. In contrast, at the north-eastern part of Kastoria basin hydraulic loads are of +60-80 m which is of higher elevation. All of these observations generally agree with the observations of Vafeiadis, 1983 made almost 20 year earlier, including the ones made at the south part of the basin where negative hydraulic loads are found after each irrigation period. A mean piezometric surface of all available data is presented at the following figure.

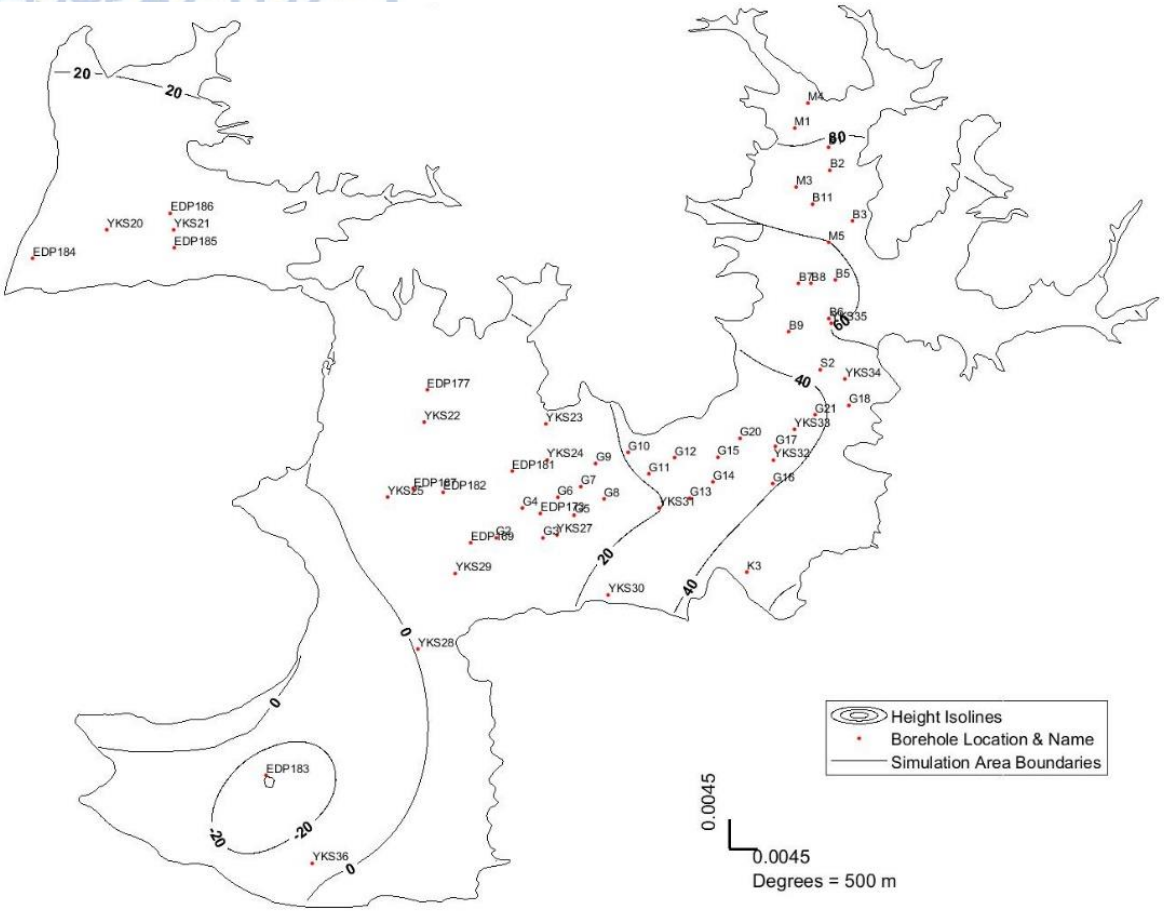

Figure 54 - Piezometric Isolines using Kastoria Lake as a reference

The average linear velocity in the aquifer can be calculated from the following equation (Fetter, 1992):

$$\boldsymbol{ALV} = \frac{\boldsymbol{v}}{\boldsymbol{n}}$$

where:

ALV = Average linear velocity, (m/d)

v = Darcian velocity, $v = k.i$, (m/d)

n = Effective (or interconnected) porosity

k = Hydraulic conductivity, (m/d)

i = Hydraulic gradient, $i = \frac{dh}{dl}$

Using the above equation, the mean hydraulic conductivity close to the Korissos karst aquifer, based on the obtained results from the Ordinary Kriging interpolation is k=8.77 m/d. A value of 0.1% for effective porosity was considered to be reasonable for the studied environment. Finally, the mean hydraulic gradients were calculated, from the compiled piezometric maps, to be i=7.9 x 10^{-3} in May 2004 and i=1 x 10^{-2} in May 2012.

Hence: $ALV_{May\ 2004}$=0.69 m/d=253 m/a and $ALV_{May\ 2012}$=0.87m/d=320 m/a.

Groundwater flow velocities are therefore increasing with time as a result of the declined piezometric surface imposed by the exploitation of the water resources. As mentioned earlier, this happens due to the depression cones created by pumping.

The irrigation returns and rainfall constitute a significant source of recharge to the system while also receives some recharge from the Xiropotamos torrent. Also, the system witnesses a slightly positive increment after the 2000s, as stated earlier. Therefore, if the existing

policy is to maintain this positive trend for a long period of time, the aquifer should be over-exploited.

In the studied case, the resources of the system are covering irrigation, domestic demands and water demands of livestock, and no significant known change in the development policy of the region is planned or can be foreseen. Consequently, the water resources of the system should be maintained at an economically viable depth, herein defined as less than the design of the existing wells permits. In parallel, the imposed stresses have not changed over the years. Under these considerations, the previously discussed trends of the piezometric surface evolution, suggest that the system is not being over-exploited as also suggested by IGME (2010) and Municipality of Kastoria (2015).

3.6.6 Torrent-aquifer interaction

Torrent Xiropotamos flows across a significant part of the study area, as illustrated in Figure 55. Torrent Xiropotamos is a small torrent, which almost always is perennial throughout the year. Observation of the torrent bed, suggests that the deposited sediments are of fluvio-torrential origin. Therefore, it follows that the hydraulic conductivity values of the torrents' bed are moderate. As a result, the hydraulic interaction between the river and each local part of the aquifer can also be characterized. To study the direction and the pattern of the existing hydraulic interaction between the river and the aquifer, the transmission losses along a segment of the river were calculated using Gianneli, 2009 data, the description given by Vafeiadis, 1983 and the following equation (Lerner et al., 1990):

$$\boldsymbol{\Delta Q = Q_{up} - Q_{down} + \Sigma Q_{in} - \Sigma Q_{out} - E_a - \frac{\delta S}{\delta t}}, \quad \textbf{[3.1]}$$

where:
$\boldsymbol{\Delta Q}$ = Transmission losses (m^3/d)
$\boldsymbol{Q_{up}}$ = Flow rate at upstream end of segment (m^3/d)
$\boldsymbol{Q_{down}}$ = Flow rate at downstream end of segment (m^3/d)
$\boldsymbol{Q_{in}}$ = Inflows from tributaries and irrigation returns (m^3/d)
$\boldsymbol{Q_{out}}$ = Outflows for water supply and irrigation (m^3/d)
$\boldsymbol{E_a}$ = Evaporation from water surface or river bed (m^3/d)
$\frac{\boldsymbol{\delta S}}{\boldsymbol{\delta t}}$ = Rate of change in channel or unsaturated zone storage (m^3/d)

Due to the fact that no large tributaries exist, the abstractions from the river as well as the inflows to the river are existent and that the evaporative losses are negligible, because of the size of the river and most importantly the presence of a lake right before the river, the change in storage are non-existent, compared to $\boldsymbol{Q_{up}}$ and $\boldsymbol{Q_{down}}$, Equation [4.6] can be simplified to:

$$\boldsymbol{\Delta Q = Q_{up} - Q_{down}}, \quad \textbf{[3.2]}$$

Provided that the above-mentioned assumptions are true, positive transmission losses along a studied segment calculated using Equation [3.2], would indicate that the river is acting as an influent, thus infiltrating water in the unsaturated zone which will eventually reach the water table and contribute to the aquifer's recharge. In contrast, negative transmissions losses along a studied segment calculated using Equation [3.2] indicate that the river acts as effluent, where the groundwater contributes the river discharge. The validity of the assumptions made is discussed later in this Section.

Finally, Vafeiadis (1983) suggested, by analyzing one hydrologic year worth of monthly flow rate measurements taken at measuring points A, B1, B2, G and D (Fig. 55), that:

i) In the upstream zone at section A-B1. The effluent rates are elevated in the summer months, mainly between June-October while the winter months, more water reaches the groundwater table because of higher average flow rates. Average annual water infiltration volume in section A-B1 was estimated to be of 44 lit/sec= 1,387,584 m^3/year. However, infiltrations also occur in the small tributaries of the Mellisopotamos stream and by taking into account the greater discharge rates and longer route that the water takes in the alluvial deposits, the infiltration must be greater than those of Koutouri torrent. The total filtration supply in the upstream part of Xipotamos river was estimated to be 120 lit/sec= 3,784,320 m^3/year.

ii) For section B-G of Xiropotamos. Vafeiadis' measurements show that the aquifer is discharging into the stream. The transmission losses between the two positions do not represent astutely the discharge of the aquifer, at least the winter-rainy season due to the fact that small torrents increase the flow of Xiropotamos at position G. However, Vafeiadis states that the discharge of the aquifer does exist due to the flow measurements where transmission losses in the B-G sections in the summer-dry months represents the discharge of aquifer. The same is also dictated by the compiled piezometric maps both older, compiled for Vafeiadis, 1983 and modern, compiled in the framework of this thesis.

iii) In the downstream section, section G-D, of Xiropotamos, between July and February infiltration rates are high, while from March to September they are reduced to a minimum. This decrement is attributed to the saturation of uppermost aquifer layers. The average annual infiltration in this section of the Xiropotamos river was estimated to be is approximately 40 lit/sec.

In conclusion, significant infiltration occurs of take place in the upstream zone of Xipotamos. Discharges of the aquifer are taking place in the section between Stavropotamos – Korissos with part of the water discharged being infiltrated in the downstream zone.

3.6.6.1 Transmission losses calculation

Calculation of more recent transmission losses was performed using the measurement data from Gianneli, 2009 taken at three locations (P1, P2, P3). The first station is located in the northern edge of the simulation area, the second one is at the eastern side, while the third one is located downstream in the western part of the simulation area as shown at Fig. 55. Flow rates were measured using a current meter.

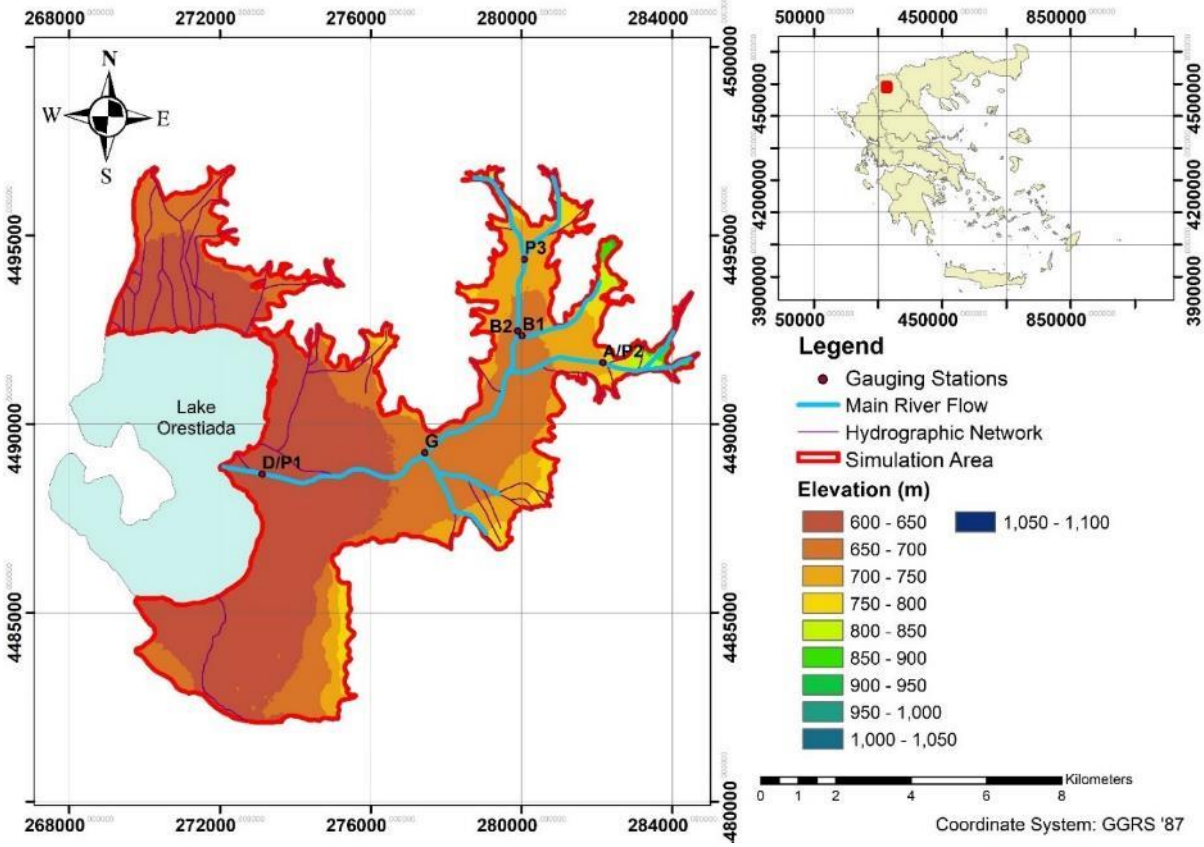

Figure 55 - Location of main river flow and stage gauging stations.

Measurements of the flow rates were taken once roughly every 15 days by Gianneli (2009) for three hydrological years between 2003-2007. The accuracy of the existing data is limited by a number of factors, the most important of which are discussed below:

1. Because of the lack of autographic recorders, measurements were made once every 15 days. As a result, the measured flow rates represent the response of the system to a particular instance within the month and not an average trend. Consequently, the response of the river to a prolonged rainfall event will not be depicted if the measurements were taken just before the event occurred. Similarly, if measurements were taken just after a rainfall event followed by a drought period during the rest of the month, the obtained response will also be misleading. In addition to the above, monitoring in the stations does not always take place at the same time as it should be, which constitutes an additional potential source of error, since in the time lag between the measurements at adjacent gauging stations a major rainfall event might have occurred.

2. Shaw (1994) suggests that flow rate and stage measurements should be made at a segment of the river where the flow is well regulated and the cross-section area is fixed. Monitored river water velocity at a specific location within the river channel defines the measured flow rate. Such measurements will not be directly comparable because the

differences in the calculated velocities will not only reflect the changes in the river flow rates, but will also be a result of the altered cross section of the river channel if the cross-sectional area of the river channel at a specific gauging station is somehow altered between two measurements. At this case the cross-section of Xiropotamos river could be widened by erosion processes during flooding. As no correction factors are incorporated to account for these changes, it is believed that the obtained measurements are not accurate. Considering the above discussed limitations of the available data records, the transmission losses hydrographs were studied, in an attempt to examine the hydraulic relation between the River Xiropotamos and the aquifer.

3.6.6.1.1 Transmission losses between gauging stations P3/P2-P1

Using Equation [3.2], the transmission losses were calculated between the gauging stations P3/P2-P1 and the results were plotted on a graph, as illustrated in Fig. 56.

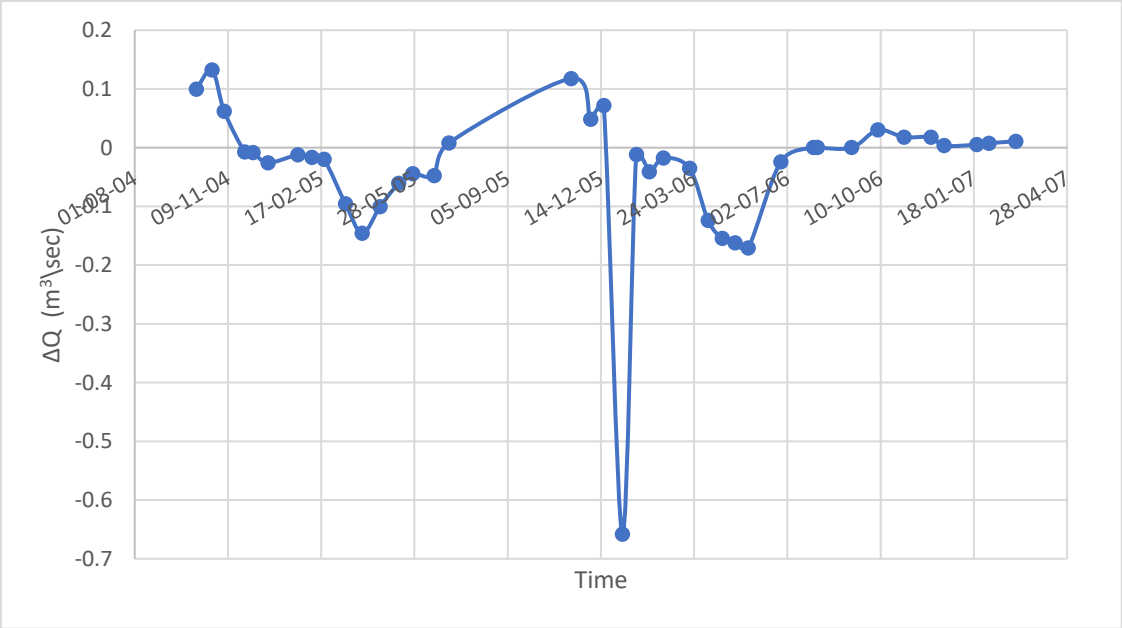

Figure 56 - Transmission losses between gauging stations P3/P2-P1

The following trends are observed in the obtained plot:

1. During spring, the river is acting mainly an influent, thus it infiltrates water into the unsaturated zone, which eventually reaches the water table and recharges the aquifer. However, as observed in the transmission losses plot (Fig. 56), the infiltrated rates are quite limited compared to the effluent.
2. The river acts as an effluent stream mainly during winter and autumn. As deduced from the study of the compiled piezometric maps, the water table of the aquifer lies above the river bed, raised by rainfall percolation due to significant infiltration coefficient 'I'. Thus, the water received from the river finds its origins in the irrigation returns and the infiltrated rainfall, which is stored in perched water tables within the unsaturated zone.
3. In the summer, the river acts mostly as an effluent with very limited discharge.

The evaporative losses to be negligible due to the size of the river and the existence of the lake of Kastoria nearby. The length of the studied segment is about 13790 m, while the average width of the river is 0.9 m. Also, most of the river banks are almost vertical.

Therefore, the river bed should remain saturated during the entire year and as a result the changes in the river bed storage should again be negligible.

From the above discussion, it follows that the assumptions set for the use of Equation [3.2] are generally truthful. The measured flow rates are not accurate and therefore the calculated transmission losses cannot be used for quantitative analysis, as earlier discussed. Indications of such errors, are the extreme transmission losses that appear on the relevant plot Fig. 56. However, it is believed that the above study provides an overall accurate qualitative indication of the hydraulic relationship and its trend between the Torrent Xiropotamos and the unsaturated zone above the aquifer. The following table summarizes the measurements taken by Gianneli, 2009, at mean seasonal values, the inflows/outflow of the aquifer as a result of torrent-aquifer interaction. Note that these values include the increase of flow rate induced by storm events and that in autumn the torrent charges the aquifer due to the drawdown created by irrigation pumping while the rest of the year the aquifer recharges the torrent.

Table 18 – Seasonal values of inflows/outflows of the aquifer due to the hydraulic interaction with the torrent Xiropotamos (+ denotes influent behavior while - denotes effluent behavior)

Season	**Winter**	**Spring**	**Summer**	**Autumn**
m^3/d	-3080.15	-9266.07	-1175.02	+5789.34

3.6.7 Water balance

A general water balance of the alluvial aquifer system was calculated for year 2004. This year over which the balance was calculated was selected on the basis of the following criteria: The year selected should be during and over which the aquifer system would be in dynamic steady state conditions. This will allow the water balance calculations to be simplified, since no significant changes in the water storage of the system would occur, hence less inaccuracies would be incorporated into the calculations. Ideally, this year would have to be of average rainfall preceded by years also characterized by average or at least not extreme rainfall, during which no abstractions existed. However, as such conditions could not be met since abstractions in this aquifer system do exist from the 80s, a close approximation was considered.

The selected year is characterized by average rainfall with no extreme values during the previous years (see section 3.4.2). Hence, during 2004 the recharge to the aquifer system which is controlled mainly by rainfall, should have also been in average terms. In parallel, during the 2000s the abstractions imposed are generally steady and do not present any fluctuations. Consequently, the aquifer system was not intensively stressed and it should therefore be in dynamic steady state in average terms. This average, was decided that it is most appropriately obtained over a year, as during this period the system's losses from abstractions are assumed to have been offset by recharge.

As previously discussed, the earliest feasible year would be the most appropriate for the water balance calculations as the imposed abstractions would have been the minimum of the successive and following years. Since the existing inventory starts is short and sparse, the selected year is the best possible option.

3.6.7.1 Recharge and discharge areas

Water balance estimation of an aquifer system requires identification of the recharge and discharge areas (Fig. 57). Those boundaries are listed below.

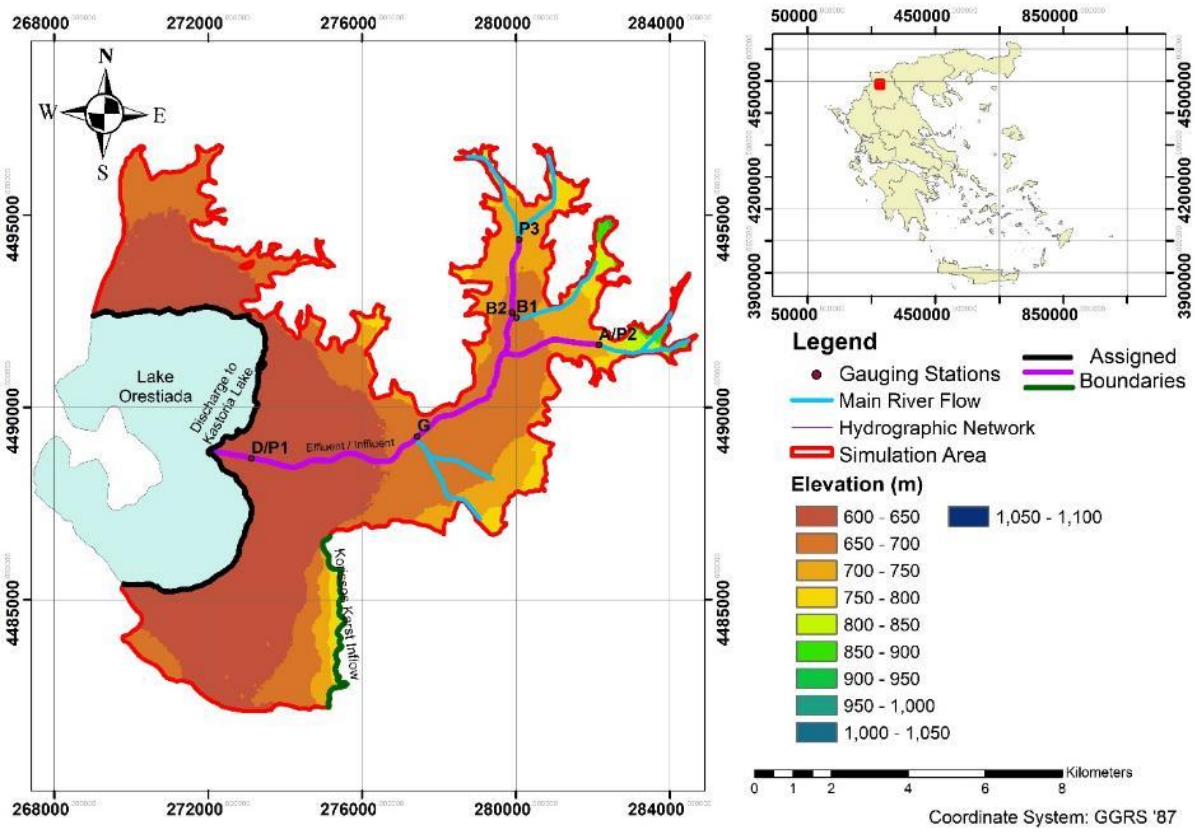

Figure 57 - Recharge and Discharge areas. Rainfall Infiltration happens to the entire simulation area.

3.6.7.1.1 Recharge areas

The alluvial aquifer system is mainly recharged by rainfall infiltration and at the southern part, in addition, is recharged by the steady crossflow from the Korissos karst system found at the southeastern margin of the basin. Crossflow from the crystalline bedrock might also exist, but it is thought to be of minor importance; thus, negligible (Vafeiadis, 1983; Gianneli, 2009; Ministry of Agriculture, 2012). Direct infiltration from rainfall contributes to the recharge of the system and its significance is upmost importance to this system along with the irrigation returns during the irrigation period that also make a significant contribution to the recharge of the system.

3.6.7.1.2 Discharge areas

Discharge of the groundwater occurs only in the Kastoria Lake due to the fact that the geometry and geology of the system along the area in question is such that it does not allow groundwater flow out of the basin because of the impermeable formations found at the southern margin of the basin but also due to the different base level lake Kastoria has than the rest of the River Aliakmonas catchment, as described in a previous Chapter. In addition, discharge of the system also happens when Xiropotamos acts as effluent, as indicated by the analysis of the calculated transmission losses (Fig. 56).

Evaporation may also account for losses from an aquifer; however, because the water table is not very shallow and the mean actual potential evaporation does not exceed 1200.0 mm, as calculated in a previous Chapter, no evaporative losses are expected from it, as experienced in arid climates (Wright et al., 1982). Therefore, evapotranspiration losses only occur in the form of transpiration losses from the plants. These are accounted for in the

calculation of the groundwater abstractions from the system, as it will be discussed in Chapter 4.

Apart from the natural discharge area artificial discharge also exists in the form of abstractions mainly for irrigation. The main elements of the water balance as deduced from the discussion above, are illustrated in the block diagram of Figure 58.

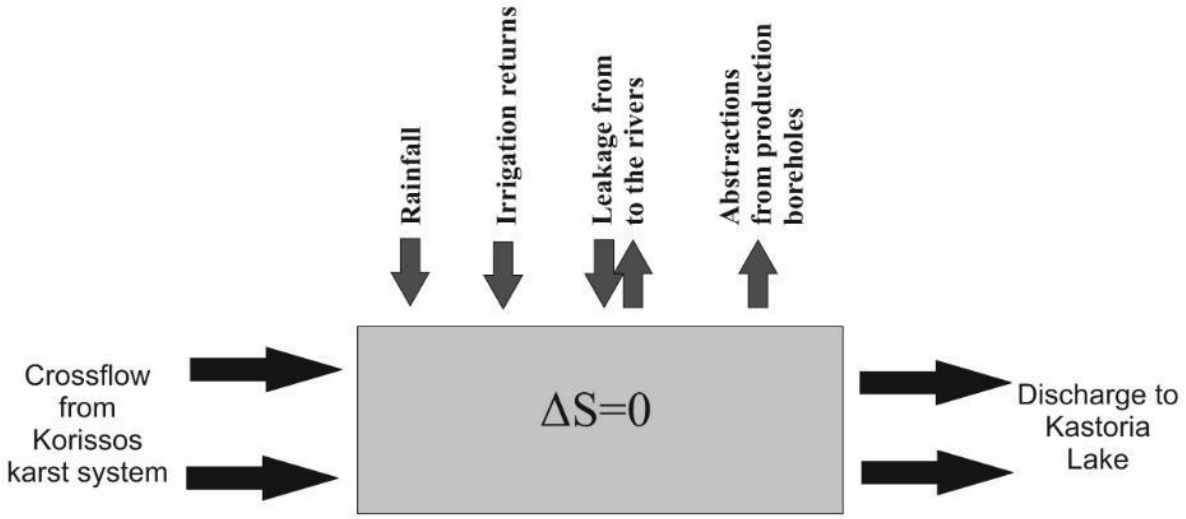

Figure 58 - Block diagram of water balance elements in the study area

3.6.7.2 Calculation of water balance

The basic water balance equation for the studied system is:

$$\sum Q_{in} = \sum Q_{out} \pm \Delta S, \quad \text{[3.3]}$$

where:

ΣQ_{in} = Total inflow to the system, (m^3/d)

ΣQ_{out} = Total outflow from the system, (m^3/d)

ΔS = Change in storage of system, (m^3/d)

Since during the period of time the water balance is being calculated, the system is assumed to be in dynamic steady state conditions, the change in storage S=0 and therefore Equation [15.4] can be simplified to:

$$\sum Q_{in} = \sum Q_{out}, \quad \text{[3.4]}$$

Analysis of the above equation yields:

$$\sum Q_{in} = Q_{karst} + Q_{prec.\ basin} + Q_{ir.\ ret.} + Q_{river\ in}, \quad \text{[3.5]}$$

$$\sum Q_{out} = Q_{abstrac.} + Q_{river\ out} + Q_{lake\ out}, \quad \text{[3.6]}$$

where:

Q_{karst} = Crossflow from the karst system

$Q_{prec.\ basin}$ = Infiltrated rainfall over the alluvial basin

$Q_{ir.\ ret}$ = Irrigation returns

$Q_{river\ in}$ = Influent from the rivers

$Q_{abstract.}$ = Abstractions from boreholes and wells

$Q_{river\ out}$ = Effluent to the rivers

$Q_{lake\ out}$ = Discharge towards lake Kastoria

All of the above flow rates are in m^3/d. Overland flow out of the study area is no existent due controlled outflow discharge of the lake through Gkioli steam.

Calculation for the abstracted water volume for domestic use used ELSTAT's data for the population consensuses carried out in 2001 and 2011. The daily consumption of water for domestic use was arbitrarily selected as 220 liters of daily water consumption per capita. This complies with law D11/F16/8600/1991 (Doc. Num: B' 174). The following equation was also used to project the future population growth.

$$\boldsymbol{\Pi_m = \frac{t_m - t_2}{t_2 - t_1}(\Pi_2 - \Pi_1) + \Pi_2,} \quad \textbf{[3.7]}$$

In the following part of the section is a discussion of the estimation of each flow element of the water balance.

3.6.7.2.1 Crossflow from the Korissos karst system

The crossflow from the karst system to alluvial aquifer system was calculated as the remainder from the water balance of the karst, assuming that the system is in dynamic steady state conditions, as also assumed for the alluvial aquifer system. Using Equations [3.4 and 3.5], the water balance for the karst system was calculated as:

$$\sum \boldsymbol{Q_{in}^{karst}} = \sum \boldsymbol{Q_{out}^{karst}}$$

$$\sum \boldsymbol{Q_{in}^{karst}} = \boldsymbol{Q_{rain}^{karst}}$$

$$\sum \boldsymbol{Q_{out}^{karst}} = \boldsymbol{Q_{karst} - Q_{springs}}$$

The above equations yield the following:

$$\boldsymbol{Q_{karst} = Q_{rain}^{karst} * I - Q_{springs}}$$

$\mathbf{Q_{rain\ karst}}$ = Recharge from infiltrated rainfall over the karst outcrop
$\mathbf{Q_{springs}}$ = Discharge from Korissos karst springs
$\mathbf{Q_{karst}}$ = Crossflow from the Korissos karst system
I=0.53, karst infiltration coefficient as proposed by Vafeiadis, 1983
All the flow rates are in m^3/d.

Calculation of the crossflow from the karst system was based on Darcy's law (Darcy, 1856), due to the not very well-known characteristics of the karst system:

$$\boldsymbol{Q_{karst} = A.k.i}$$

$$\boldsymbol{A = L.D}$$

By substituting the second equation into the first:

$$\boldsymbol{Q_{karst} = L.D.k.i,} \quad \textbf{[3.8]}$$

$\boldsymbol{Q_{karst}}$ = Crossflow rate, (m^3/d)
$\boldsymbol{L}$ = Length of interface area, (m)
$\boldsymbol{D}$ = Saturated depth of interface area, (m)
$\boldsymbol{k}$ = Hydraulic conductivity of the interface, (m/d)
$\boldsymbol{i}$ = Hydraulic gradient across the interface

$\mathbf{Q_{springs}}$ is ignored because of the higher elevation of the springs in comparison to the interface of the between the alluvial aquifer and the Korissos karst system.

The area of the interface between the Korissos karst system and the alluvial aquifer, Fig. 56, was calculated from the geological sections drawn, the compiled geological map, to be A=114,220 m^2. The hydraulic conductivity of the interface was calculated by pumping tests at nearby boreholes to be k=6.18 m/d, while the hydraulic gradient was calculated between the basin and the Militsa spring, where the closest reference to piezometry exists, to be i=0.01. Thus, applying Equation [3.8] yields: $\boldsymbol{Q_{karst}}$ **= 7,058 m^3/d**.

3.6.7.2.2 Infiltrated rainfall over the basin

The infiltration rate of rainfall over the Kastoria basin was estimated to be 15.8% of the rainfall depth by Vafeiadis, 1983, which is with close agreement with IGME, 2010 estimation of 20% infiltration rate. This was done by dividing the study area into infiltration zones, according to the lithology of the system. Apart from the lithological characters, the characterization of the infiltration capacity of the soils was taken into consideration. The areal extent of the studied basin without the lake and the Korissos karst system is almost 269 km^2, whilst the mean rainfall over the basin is about 950 mm/a, (see Chapter 3). Hence, the infiltrated rainfall that enters the alluvial part of the basin over the simulation area is: $\boldsymbol{Q_{rain\ basin}}$ **= 112,022 m^3/d**.

3.6.7.2.3 Abstractions from boreholes and wells

No specific data regarding the abstractions from boreholes exist for the period of interest. As it will be discussed in Chapter 4, the calculation of the abstracted volumes was based on the surface area and the population supplied by each irrigation, domestic and herd watering supply boreholes respectively. Following this method, the average abstraction rate for the year of interest was calculated to be: $\boldsymbol{Q_{abstrac.}}$ **= 42,561 m^3/d**.

3.6.7.2.4 Irrigation returns

Field irrigation returns account for the amount of water applied to fields during the dry period. A part of Chapter 6 discusses that the irrigation returns were estimated to be 10.0% of the water abstracted from borehole. Having estimated the abstracted rate for irrigation purposes to 41,861 m^3/d, it follows that the irrigation returns are: $\boldsymbol{Q_{ir.ret.}}$ **= 4,186 m^3/d**.

3.6.7.2.5 Discharge to Lake Kastoria

The alluvial aquifer of Kastoria discharges to Kastoria lake happens only from the south, east and north side of the lake because the west side is dominated by Neogene formations, which are impermeable. The area of the interface between the lake and the alluvial aquifer of Kastoria was calculated to be A=80,000 m^2, with an effective depth of 5 m. The mean hydraulic conductivity of the interface was calculated to be k=220 m/d, while the hydraulic gradient was calculated from the closest reference to piezometry exists, to be i=0.004. Thus, applying Equation [3.8], in a similar fashion, yields: $\boldsymbol{Q_{lake\ out}}$ **= 70,400 m^3/d**.

3.6.7.2.6 Influent-effluent to the rivers

As argued in a previous Section, scarcity and unreliability of the river flow rate data, prohibits the quantitative analysis of flows between the aforementioned torrent and the alluvial system. However, the study of the river hydrographs, and the compiled piezometric maps showed that a bidirectional hydraulic relationship exists between the aquifer system and the river. It was suggested that the rivers recharge the aquifer system, mainly along its upper and lower segments, whilst the aquifer system discharges water into the rivers primarily along the middle segment, of whom a big part infiltrates into the lower segment, as also observed by Vafeiadis, 1983. Based on these findings, it was assumed that the sum of the estimated seasonal values, **7,732 m^3/d**, (Table. 16) recharges the designated segment of torrent Xiropotamos at Fig. 57.

3.6.7.2.7 Summarized Results

If all the stated hypothesizes hold and provided that the system is indeed in dynamic steady state conditions, then by substituting the calculated flow terms in Equation 3.4, yields:

$\sum Q_{in} = 123{,}266\ m^3/d$
$\sum Q_{out} = 120{,}693\ m^3/d$

Thus, by subtracting the two above numbers: $\Delta \sum Q = -2{,}573\ m^3/d$.

The calculated deviation of 2.1% from a perfectly closed water balance can be attributed to the imperfections of the most of the calculations of the water balance elements because they were performed under simplifications and assumptions due to uncertainties or lack of accurate data, as discussed earlier. Although reasonable, these simplifications are potential sources of errors. It should also be noted that in a natural system, especially under human intervention, steady state conditions cannot be obtained to a full extent. Under favorable situations, however, as in the current study, the system may be accepted to be in approximated steady state conditions. Such an approximation would inevitably incorporate an error. In addition to the above, the hypothesis regarding the influent and effluent volumes of river Xiropotamos was based purely on scarce qualitative data and observations. Thus, another source of potential error was incorporated in the calculations. The inflows/outflow of the aquifer that were presented above are summarized at the table below.

Table 19 - Water balance of the alluvial aquifer of Kastoria

m^3/d	Inflows	Outflows
Abstractions from wells and boreholes	-	41,561
Irrigation Returns	4,186	-
Lake Kastoria	-	70,400
Influent/Effluent at Xiropotamos river	-	7,732
Infiltrated Rainfall	112,022	-
Cross-flow from Korissos Karst system	7,058	-
Summary	120,693	123,266

As an overall appraisal, considering the above problems the accuracy of the obtained result is very satisfactory. The calculated water balance served as a reference and guideline to the initial calibration of the designed groundwater flow model of the study area and as such it proved to be essential.

3.7.1 Future Climate Change Impact at Korissos karst system

Climate Change impact on Korissos karst system was evaluated based on the bias-corrected results of the ten selected RCMs. The infiltration coefficient, I=0.54, proposed by Vafeiadis, 1983 was used to estimate the infiltration amount that recharges the karst system. The observed precipitation used at this assessment were during 2000-2018 in contrast to the ones used for the bias-correction procedure (1986-2005). As presented at the figure below the decrease in precipitation causes a severe impact on the karst water reverse. The results presented at this section follow the trends assessed at section 3.4.5.1.1 since the rely only on precipitation.

Annual temporal variation of infiltrated water amount at Korissos karst system was assessed for the three sub-periods and compared to the median total annual precipitation of the control period (2000-2018), which is 6.13×10^6 m^3 and the results are illustrated in Fig. 59. The general point of the results illustrated in Fig. 59 is that the infiltrated amount and therefore the stored water amount in the karst system is expected to be significantly decreased by

the period 2059-2078. RCP 2.6 A present a slight decrease for the second period while at the rest of the sub-period presents a slight decrease. RCP 2.6 B present a slight increase only for the first sub-period while slight decreases during the rest of the sub-periods. RCP 4.5 A presents a slight increase for the first sub-period, a slight decrease for the second and for the third a significant increase by approximately a million cubic meters. RCP 4.5 B present slight increase for the first sub-period in contrast to the rest of the sub-periods where it presents moderate decrease. RCP 4.5 C, D present slight to moderate decrease throughout the projected period. RCP 8.5 A indicate a small increase during the second sub-period while it presents decrease of 0.75 x 10^6 m^3 for the rest of the sub-periods. The rest of the models under RCP 8.5 present slight increase from 0.07 x 10^6 m^3 (RCP 8.5 C) to 0.3 x 10^6 m^3 (RCP 8.5 D) for the first sub-period. At the other two sub-periods they present moderate decrease from 0.32 x 10^6 to 1.3 x 10^6 m^3. Finally, when comparing the temporal change of annual precipitation for each chosen model, different trends are indicated. Most models yield slight increase during the first sub-period in contrast to the other two sub-periods where slight to moderate decrease can noticed, compared to the control period.

Apart from the impact at the karst system storage the impact on the flow at the subsurfaced interface between the karst systems and the neighboring alluvial aquifer must also be assessed to maintain the already positive water balance of the aquifer. The interface provides a steady flow flux towards the aquifer at all times, as mentioned at the previous section. The corresponding water amount of this steady flux is approximately equal to 2.6 x 10^6 m^3, which is an amount far lower the projected infiltrated water in the Korissos karst system. This ensures that the interface will recharge the aquifer with same amount of water that it does today. Finally, it's worth mentioning that the two springs that are found at this karst system, which are at a higher elevation than the interface, is possible to be affected by the reduced precipitation.

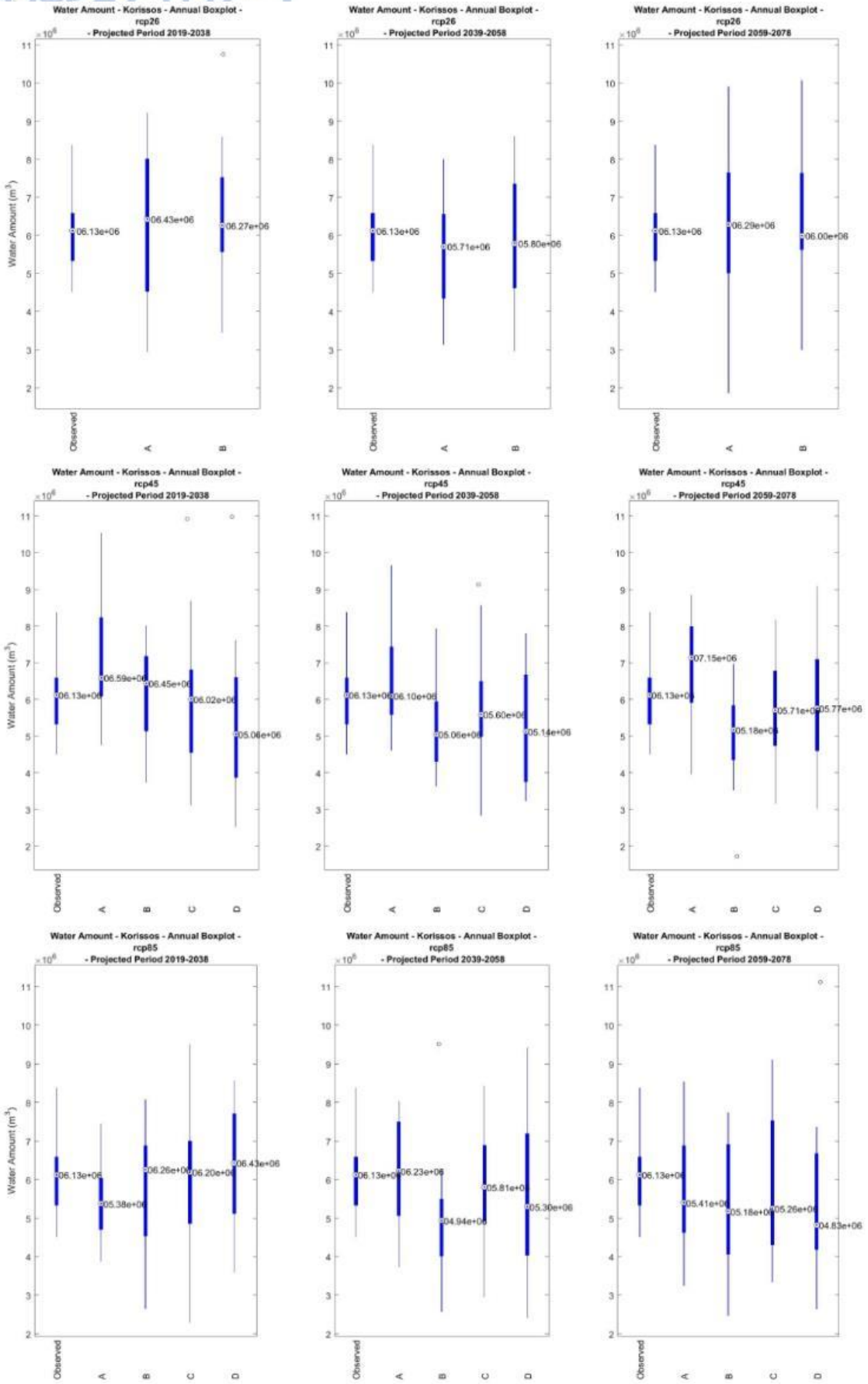

Figure 59 - Box-plots of total annual infiltrated precipitation amount variation for Korissos karst system according to the results from the ten chose RCMs for the periods 2019-2038, 2039-2058 and 2059-2078

CHAPTER 4. Groundwater flow modelling

In this Chapter, the mathematical groundwater flow modeling implementation, undertaken as part of the current study, is discussed. Modeling of the studied aquifer system was based on the obtained results from the geological, hydrological, hydrogeological and geophysical studies discussed in the previous Chapters. The objective of this implementation is to simulate, hence validate the flow mechanisms of the system and in parallel to extend the understanding developed so far from the application of conventional methods of hydrogeological studies conducted by Vafeiadis, 1983 and Gianneli, 2009. Furthermore, a number of future exploitation scenarios of the groundwater resources were considered, aiming to a guide solution which would ensure the sustainability of the groundwater resources that are a key issue to the ecologic stability of the studied region.

Mathematical groundwater flow modeling is a well-established groundwater resources management tool, which has been applied in numerous occasions around the world (Anderson et al., 1991). In this case, known techniques and methods were employed in a vulnerable hydrogeological environment of complex structure and evolution characterized by typical Mediterranean climatic conditions, to address the problem of sustainability of the groundwater resources. As revealed from the discussions in the previous Chapters the available data are limited. This FEFLOW model implementation complies with the general procedure of modelling groundwater aquifers. It therefore constructs, refines and verifies a groundwater flow model which subsequently is used as a comprehensive tool for the potential management of the groundwater resources.

The designed model will provide a comprehensive, relatively easy to use yet reliable and efficient management tool in the hands of the decision makers. In the subsequent sections the general setup of the model will be discussed and each step of the model implementation will be analyzed. Finally, the examined predictive scenarios will be presented in view of the implications to the sustainability of the groundwater resources of the study aquifer system.

4.1 Model design

A mathematical model is a tool designed to represent a simplification of reality. Only implemented as a simplification because in truth, reality is too complex to represent. Mathematical models have been used since the late 19th century, however it was not before the early 1960s when the development of the computer systems saw a fast pace, that models were more widely used (Wang et al., 1982). This fast development allowed modelers to use more complex and data hungry models that require more computational effort. The steps followed to design and operate this model are illustrated in Figure 60 and discussed in detail in the following sections.

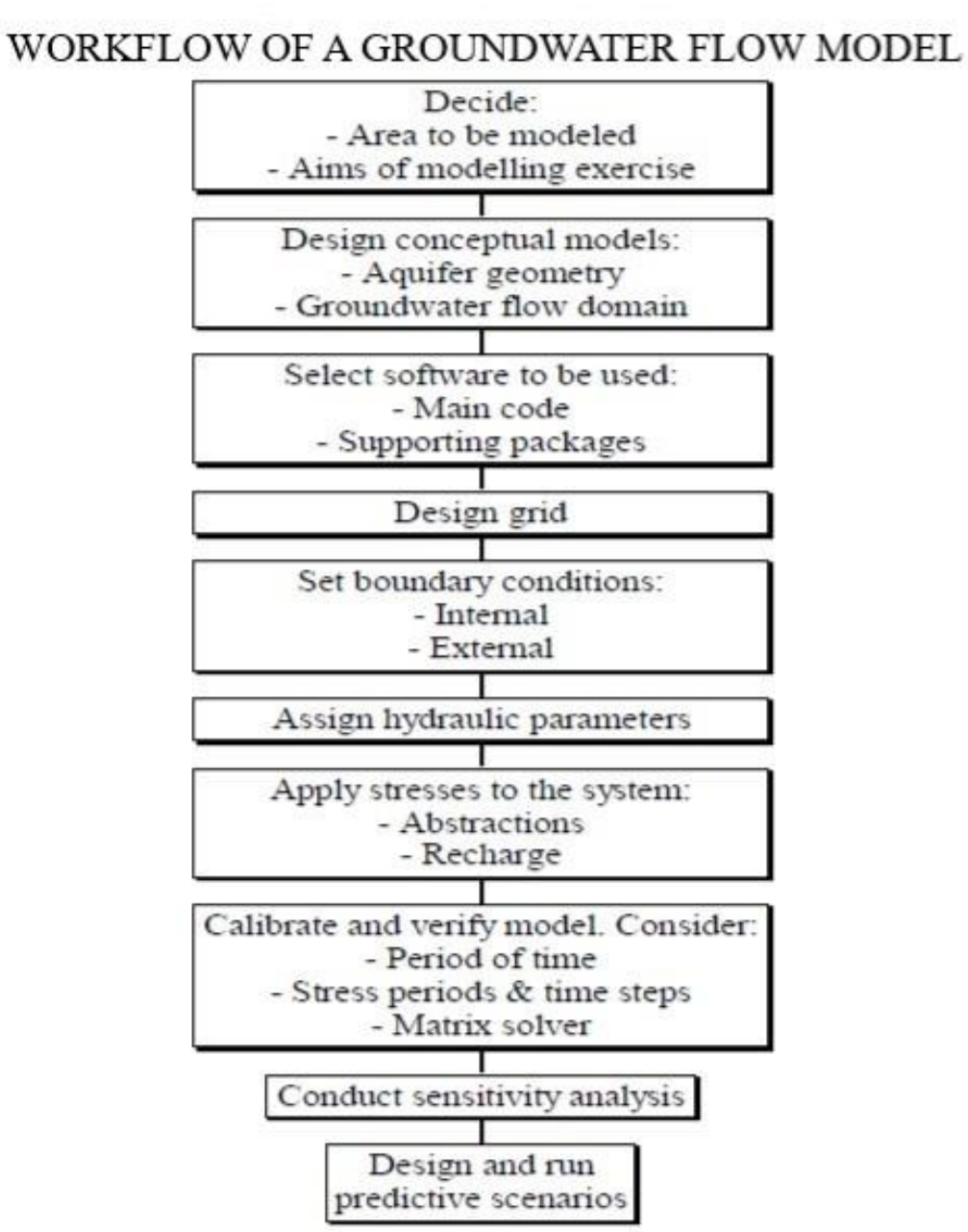

Figure 60 - Workflow of a Groundwater Flow Model (Panagopoulos, 1996)

4.2 Simulation area

The first of a number of decisions before a mathematical model is designed is the aim of the model implementation. This will determine to an extent the area to be modeled and its configuration in the model's design. The area of interest and consequently the area initially selected to be modeled is the alluvial aquifer system of Kastoria, bounded by the crystalline bedrock to the north and the east, the Korissos karst system to the south-east, Lake Orestiada to the west and the impermeable Neogene sediments found south of the modeled area. Although a strong hydraulic relation exists between the southern part of the alluvial aquifer system and the Korissos karst system, the latter was not included in the model, as not enough data exist for the karst system to enable modeling of this type of aquifer.

4.3 Selection of software

The selection of the software used in this implementation was based on the following criteria: The software and hardware availability, the accuracy required from the designed model, the aim of the model, the ease of use and versatility offered by the software. Three stages can be distinguished in the modeling procedure: Preprocessing, processing and post-processing. FEFLOW v.7.2 is a self-contained software package which can serve the last two stages. The first stage is served by ArcMap and MATLAB programs as mentioned at previous Chapters.

4.4 Mesh design

In a numerical model, a discretized domain is created consisting of an array of computational nodes and associated finite difference blocks or finite elements, in this case finite elements (Wang & Anderson, 1982; Anderson et al., 1991). This nodal mesh forms the framework of the numerical model and its design, in terms of discretization, defines the results' spatial detail, which were obtained from the simulation.

Finite element mesh designs offer more accurate representation of the geometry of the simulated aquifer system and also a more natural representation of the boundary conditions that could significantly affect the solution obtained from a model (Wang & Andersson, 1982). These advantages however only become important when supported by sufficient and accurate input data. Considering the advantages of the finite elements method and that nowadays computers have enough processing power to compute complex models, the current implementation was based on the finite element method. The number individual finite element; thus, the overall dimension of the mesh determines the accuracy of representation of the flow within the modelled domain. Numerical computation of groundwater does not require high discretization when computed by the finite element method. However, it's important to point out that that large finite elements result in fewer computational nodes and require less averaged data over larger areas of the modelled domain; however, the obtained accuracy is low. On the other hand, small finite elements can result to a more accurate representation of the groundwater flow but data and consequently computational effort requirements are higher (Anderson et al., 1991). As a general rule for this thesis, small dimension elements are placed around the abstraction boreholes and along the river Xiropotamos whereas a coarser mesh is placed at the remaining parts of the modelled domain.

The modeled domain is delineated by the crystalline bedrock to the north and at the east, the Korissos karst system to the southeast, Neogene formations at the south and the Lake Orestiada at the west. As illustrated in Fig. 60, the designed mesh is refined along the

river Xiropotamos, around the boreholes and at the west and south eastern borders of the modelled area as necessary for the following reasons:

- The Korissos karst system in the southeastern margin of the simulation area has a significant role in the recharge of the southern part of the system as it was discussed in the previous Chapters. It was therefore expected that a major control to the flow domain of the southern part of the system is exerted by the hydrogeological setup of that area.
- A significant contrast between the hydraulic conductivities of the central part of the plain area and the rest of the studied area was indicated from the pumping test analyses and was anticipated because of the lithological setup of the alluvium as presented by IGME's geophysical survey. Such contrasts usually result in numerical instabilities in the solution of a model or sometimes to non-convergence, that may be prevented with local refinement (Anderson et al., 1991; Wang et al., 1982).
- Most of the production boreholes are located along the river. The stresses imposed to the model as a result of the abstractions from them were expected to affect the flow of that area.
- As discussed earlier in the Chapter, the aim of the projected simulations was to examine the sustainability of the groundwater resources under various exploitation scenarios. The assessment criterion adopted was the viability of the existing production boreholes under each of the alternative groundwater management plans. Hence, a detailed representation of the existing abstraction areas was required in the modeled domain.

The mesh design, as illustrated in Fig. 61, was able to accurately simulate the groundwater flow system of the main study area without any influences from the assigned boundary conditions. It consists of 96,647 computational nodes distributed at the vertices of trigonal elements on a 2D horizontal plane, which represents the simulated aquifer. It is declared as an unconfined aquifer and each finite element of the layer is described by its hydraulic conductivity value, k, which describes both horizontal dimensions. These will be discussed in the next section of the Chapter.

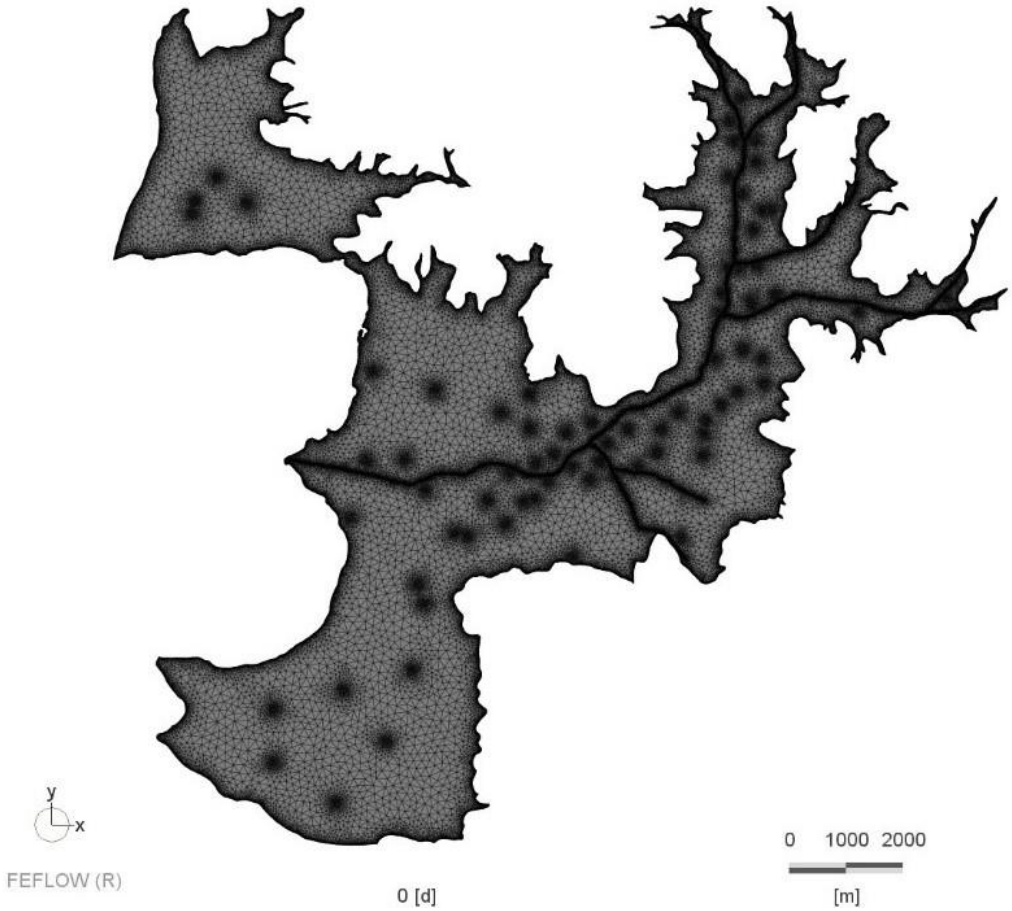

Figure 61 - 2D horizontal mesh of the modelled area

4.5 Boundary conditions

The boundary conditions are a fundamental part of any numerical model and their appropriate definition is crucial to the dependability of the results obtained from the simulations. Models often fail to represent their respective system as a result of inaccurate or illogical setup of these conditions. Because of their importance, a discussion of the existing types, principles and limitations in applying them on a model is presented in this Section.

The boundary conditions are the means of communication and connection of the modelled domain to the ambient non modelled environment. They are mathematical statements that specify the dependent variable (head) of the governing equation or the derivative of it (flux) at the boundaries of the modelled domain (Anderson et al., 1991). Boundary conditions therefore constrain the numerical solution, produced by the chosen solver, of the governing equation making it unique (Wang & Andersson, 1982). Boundary condition are defined to the edges of the modelled domain; thus, being external, or they can be set inside the modelled domain; thus, being internal in which case they specify the hydraulic interaction between any internal part of the modelled domain with an external source or sink.

It is suggested that the assigned boundaries conditions in an ideal situation should coincide with the setup of the physical system such as impermeable formations or large bodies of surface water, or the hydrological boundaries of the modelled aquifer system (Wang & Andersson, 1982). Boundary conditions defined as an attempt to represent the reality, could possibly reduce the potential errors in representing the flow domain, however they do not always ensure their influence because of the uncertainties found in the complexity of reality and the inherent instabilities of numerical methods, as it was experienced in the current model implementation (see later in this Chapter). Boundary conditions can be grouped in three catego-

ries: 1. Specified head, or Dirichlet conditions, 2. Specified flow, or Neuman conditions and 3. Head dependent flow, or Cauchy conditions (Wang & Andersson, 1982; Diersch, 2009). The characteristics of each of these three types are discussed below.

4.5.1 Specified heads

The groundwater potential is assigned as a fixed value on the boundary elements, which a-priori implies an infinite amount of water entering the domain. This dictates that the specified heads should be used with great caution because they may introduce large errors in the water balance of the model. Specified hydraulic heads are ideal to represent the sea or a large lake that interfaces the modelled domain, whilst they are often used to reasonably approximate large springs (Anderson et al., 1991; Diersch, 2009). As heads are usually readily available, they are easy to implement in a model design. In the specified head boundaries, the water entering or leaving the aquifer from a series of elements is constant for each stress period of the simulation. Since the flux across the boundary is proportional to the hydraulic gradient at the direction of water flow that is defined by the former, the mathematical expression of this boundary type is where *n* is the said direction and *C* the constant flux value, which can be either constrained to limit the flow the water that traverses that boundary or unconstrained (Diersch, 2009).

A special case of boundary conditions is the no flow boundary where C equals to 0. No flux across the interface exists. This condition applies to the boundary between the aquifer system and an impermeable boundary where. In parallel, it can adequately represent the boundary along a groundwater divide.

Specified or fixed flow boundaries offer a representation of crossflow to the modeled domain from an adjacent aquifer and vice versa and can accurately represent abstractions from, or artificial recharge to a modelled system. Fluxes however, cannot be directly measured so calculations have to be made in the case of crossflow representation based on the hydraulic conductivity and gradient but not to the amount of water available in the physical system. This can overestimate or underestimate the crossflow flux. Such calculations incorporate a potential error due to uncertainties of the physical system, but it can be used when no other option will be applicable.

4.5.2 Head dependent flow

The flux across a boundary element depends on the hydraulic gradient between a fixed head value assigned to an external source-sink and the calculated head in the boundary element of the modelled domain. Head dependent boundaries may be used to realistically represent ponds, rivers, drains, or crossflows into or out of the modelled domain. Although it is generally the most realistic type of boundary, it can potentially produce large errors, as the hydraulic conductivity is practically an unknown term.

4.5.3 Assigned boundary conditions

The type of boundary conditions that were applied, were chosen for their ability to astutely represent the expected reality. These conditions are illustrated in Fig. 62 and their implementation is discussed below.

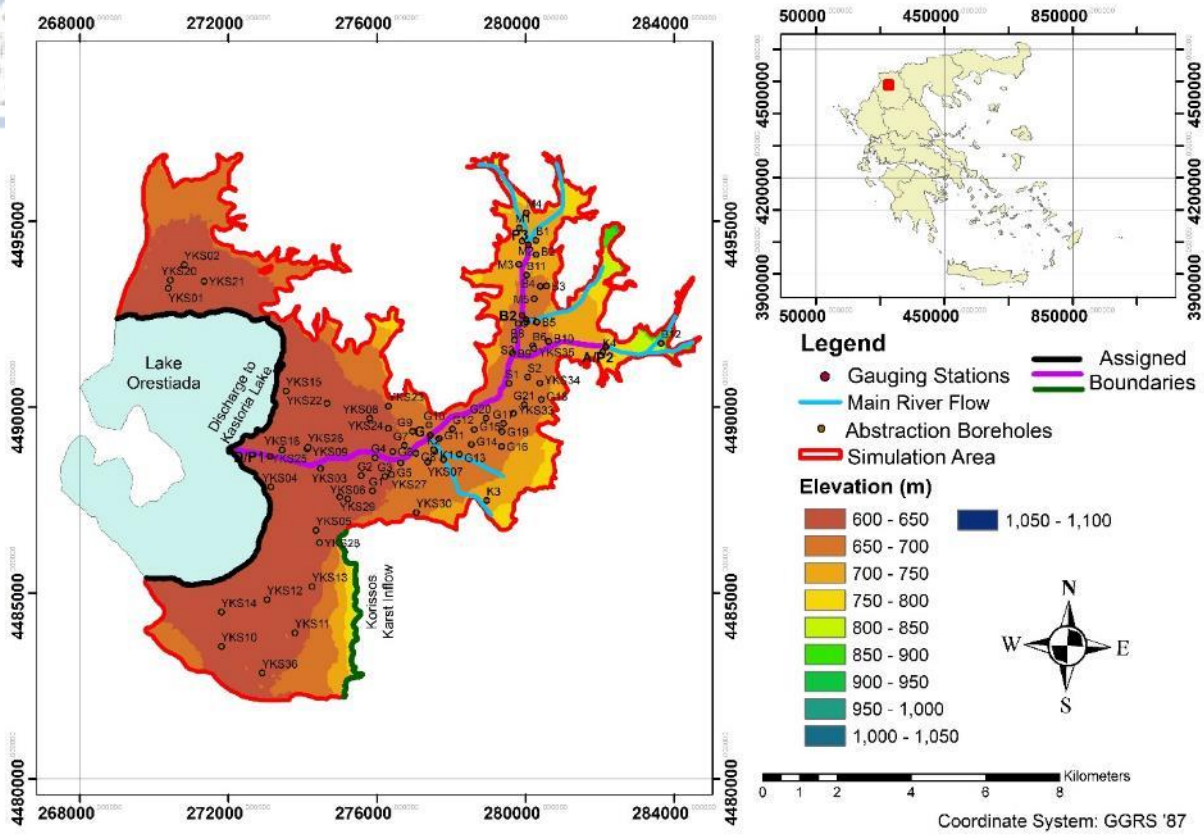

Figure 62 - Assigned Boundary Conditions

4.5.3.1 Western boundary

Constant head boundaries were assigned along Lake Kastoria, where the alluvial Kastoria aquifer discharges underground, as illustrated in Fig. 62. As discussed earlier, the annual variability of the water level of the lake is very small, due to the control imposed to it by the Municipality of Kastoria. The chosen value. 629.535 m, is the mean between the maximum and minimum allowed water level.

4.5.3.2 Southeastern boundary

Constant head boundaries were assigned along the Korissos karst system in the southeastern edge of the model, as illustrated in Fig. 62. As discussed earlier in this Chapter, fixed or constant head boundaries imply an infinite source of water which almost certainly cannot be sustained for a long period of time. However, it was thought that if the flow generated by the assigned heads were properly constrained during the entire simulation a reasonable approximation could be obtained, as justified by the following observations:

- Over a period of 29 years, the borehole hydrographs in the vicinity of the karst system and Militsa spring hydrographs in the Korissos karst system suggest that the annual fluctuation and the total decline of the water levels are not substantial. Hence, the karstified limestones is capable of suppling enough water to maintain the water levels almost constant for specific stress periods i.e winter-summer.
- Study of the lithological sections of boreholes drilled in the karst (Soulios et al., 1985) and the description of the characteristics given by Vafeiadis, 1983, revealed the existence of large conduits and high anisotropy as mentioned in a previous Chapter. Moreover, the examination of the karst spring hydrographs suggested that the limestones in question are

characterized by a homogeneous, well developed karst system as discussed in Chapter 4; thus, characterizing the crossflow of steady nature, as mentioned at Section 3.6.7.1.1.

In addition to the above, analysis of the few pumping tests, as provided by Soulios et al., 1985, conducted in boreholes located on the Korissos karst system resulted in very large values of transmissivity and as expected, extremely low values of storativity, as mentioned in a previous Chapter. These observations suggest that at the modelled domain the hydraulic behavior of the karst system can be effectively approximated to that of an open surface water body.

Constant and constrained head boundaries were also set at the Korissos karst system for transient state simulation. The model was calibrated for steady state conditions with constant and constrained heads assigned along the alluvial aquifer – Korissos karst system interface. Subsequently, these calibrated values were assigned to the transient simulation along the interface.

4.5.3.3 Torrent Xiropotamos

The Fluid flux boundary conditions was used to assign the amount of influent or effluent amount water correspondingly along the courses of the River Xiropotamos (Fig. 62). The flux across a river is calculated as a water budget function – fluid source of the transmission losses. However, as discussed in Chapter 4 the available discharge inventories exist only for a four-year period, which is short period compared to the 19 years of the modelling period, also, in comparison to the length of the projected period. Hence, they were used for producing seasonal values that are assigned along the elements of the river as constant within each season.

Considering the fact that the limited available data and that boundary conditions essentially act as a means of representing the hydraulic interaction between the modelled domain and the surrounding environment, any value that approximates torrent-aquifer realistically would be acceptable. The Fluid flux BC was set along with torrent stages to every element. Consequently, the assigned values (Table 16) were adjusted to fulfill the water balance and hydraulic head distribution in the alluvial aquifer system, during the calibration process.

4.5.3.4 Abstraction Boreholes

The Well BC was used to assign the estimated abstracted water volume at the 78 main abstraction boreholes. The assigned values were calculated in m^3/d and was initially assigned evenly to all of those boreholes. The final values of the well rates are the calibrated ones through a trial and error procedure.

4.5.4 Hydraulic parameters

The hydraulic parameters values that were used as input data in this model implementation have been obtained from pumping tests, which basically are point measurements, and are not enough to cover the entire modeled system by themselves especially when its structure is complicated with a substantial degree of heterogeneity. The study area presents a degree of complexity at some places as stated in a previous chapter. Inevitably, the assigned hydraulic parameters will only be an approximation of the reality and at the areas of increased complexity are expected to produce larger errors from the obtained solution. An optimum number of different values for each one of the hydraulic parameters has to be assigned, depending on the degree of complexity of the modeled system and the available measurements. Increasing the number of values will probably decrease the accuracy of the solution as the uncertainty of

each assigned value, due to the unknown complexity of the lithology, will increase while reducing the number of values will result in an over-simplification of the problem, hence increasing the error of the obtained solution (Yeh, 1986). At this study a stochastic approach was used to calibrate the hydraulic parameters using PEST (Doherty, 2015).

4.5.4.1 Hydraulic conductivity

Hydraulic conductivities should be used instead of transmissivities in the designed model, so that hydraulic parameters will remain constant throughout the entire simulation period. As opposed to an individual hydraulic conductivity value for each element, the Ordinary Kriging interpolation method was used to produce a spatial distribution of the hydraulic parameters. This was done by taken into account the aquifer zones proposed by Vafeiadis (1983) characterized by the same hydraulic characteristics and the geo-hydrological characteristics of the modelled aquifer system as these were described in Chapters 3. The assigned values were then adjusted using PEST using the pilot method, as stated earlier, during the calibration process, which resulted in the distribution illustrated in Fig. 63. PEST and the chosen method were employed to try to alleviate some of the inherent uncertainty imposed by the fluvio-torrential origin of the simulated area. The large values in hydraulic conductivity are attributed in coarse-grained layers of the Quaternary deposits, as mentioned at section 3.6.1.3.

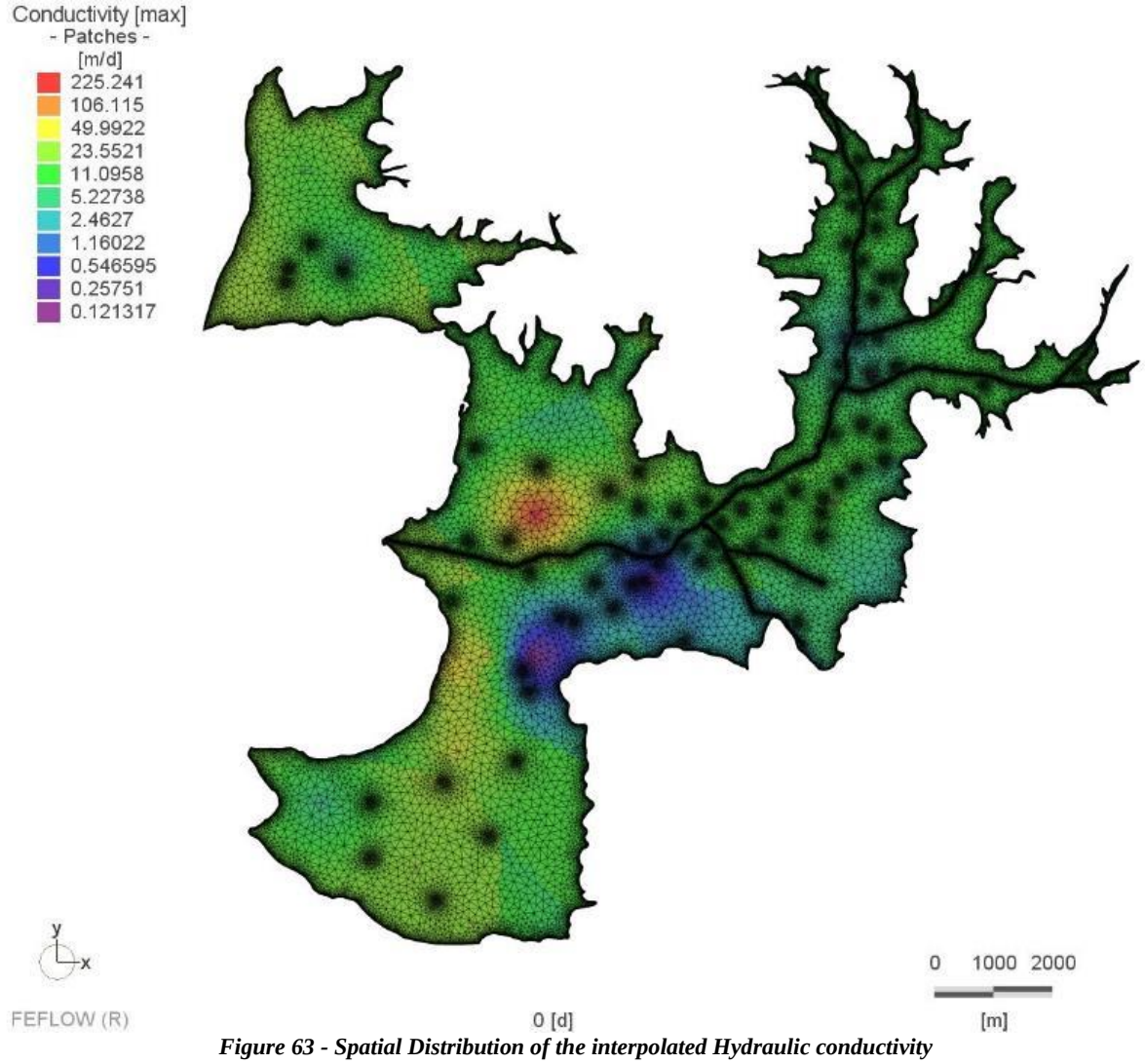

Figure 63 - Spatial Distribution of the interpolated Hydraulic conductivity

Calibration of the hydraulic conductivity was performed with the PEST tool on the basis of altering the assigned conductivity values produced by the Ordinary Kriging interpolation method, conforming to the distribution trend as this had been dictated by the geological and lithological characteristics of the system (see Section 3.6).

The spatial distribution of hydraulic conductivity in accordance with the results obtained from the examination of the geological and the hydrogeological data, as these were analyzed in the previous Chapters:

- Reduction towards the east-southeastern part of the simulation area, close to the A3 and A4 boreholes.
- Hydraulic conductivities are higher in the rest of the area. The highest values are observed at A5 borehole.

Such a ratio is expected in this type of hydrogeological environment, due to the orientation of clay minerals and the layered structure of the deposited sediments. In the current modelling implementation, it was assumed that the modelled aquifer system is homogeneous and isotropic in the horizontal directions.

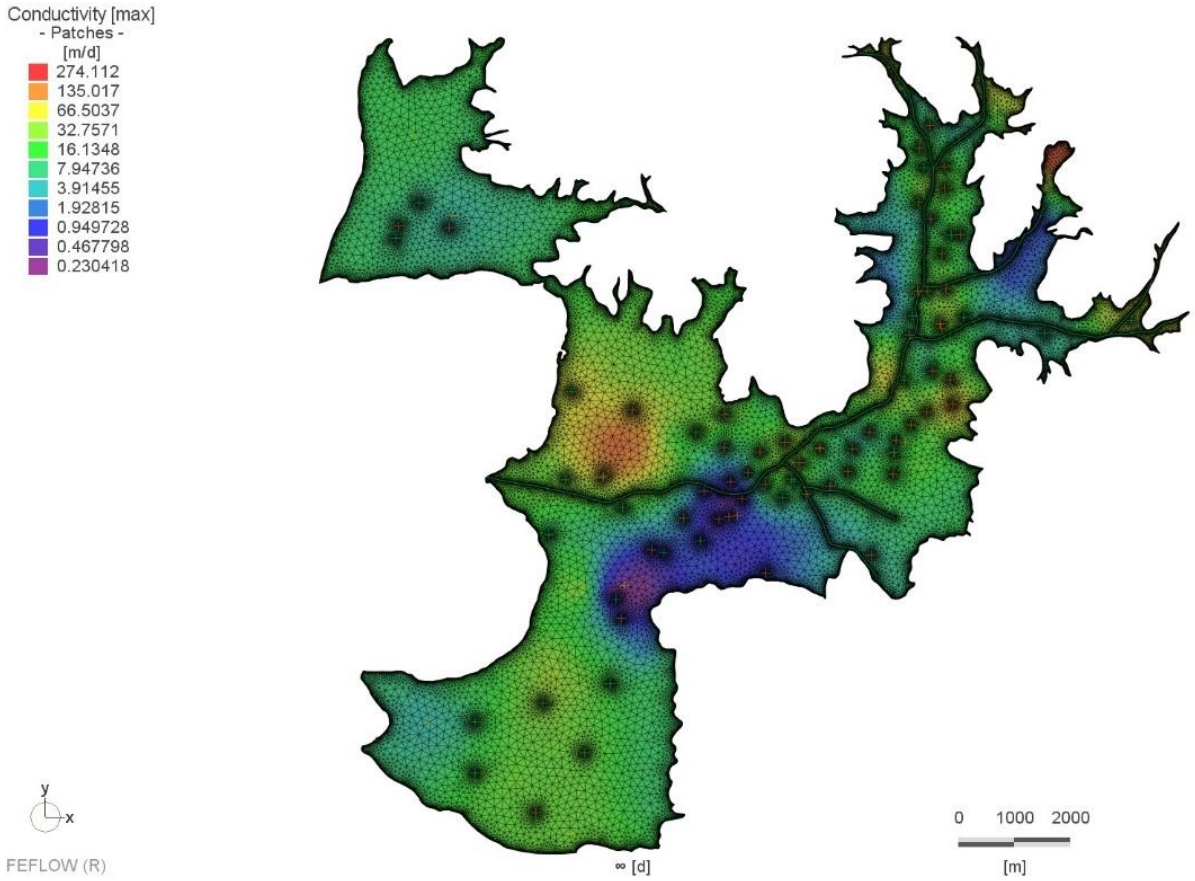

Figure 64 - Calibrated hydraulic conductivity as produced by PEST

5.5.4.2 Storativity

As with the hydraulic conductivities, the initial distribution of storativity was based on the results from the pumping test analyses and the lithological characteristics presented by Vafeiadis, 1983 and Gianneli, 2009. These values have a spatial distribution that covers almost the entire simulation area, which were adjusted during the calibration procedure with

the PEST tool in a similar fashion as with hydraulic conductivity. This parameter was not very sensitive so it won't be discussed further.

4.5.5 Applied stresses

In this Section, the method proposed by Panagopoulos, 1996 is largely followed to calculate the groundwater abstractions and the irrigation returns. As discussed in Chapter 1 and earlier in this Chapter, the groundwater resources exploitation in Greece has been intensified since mid-80s (HAO "DEMETER", personal communication 2018). However, to this general rule Kastoria basin is an exception as mentioned earlier. As a result, the abstracted water volumes have stressed the corresponding system; thus, disrupting its equilibrium. Because of this reason, in this context the above-mentioned parameters are considered as hydraulic stresses (Fig. 65).

Abstractions from the production boreholes and irrigation returns are calculated by a custom MATLAB code that receives the ET_0 values calculated by the Hargreaves-Samani method, the crop coefficients K_c proposed by the Greek Ministry of Agriculture, 1989 and the crop area data received from OPEKEPE. Following, is a description of the methods and techniques employed in the calculation of the applied stresses.

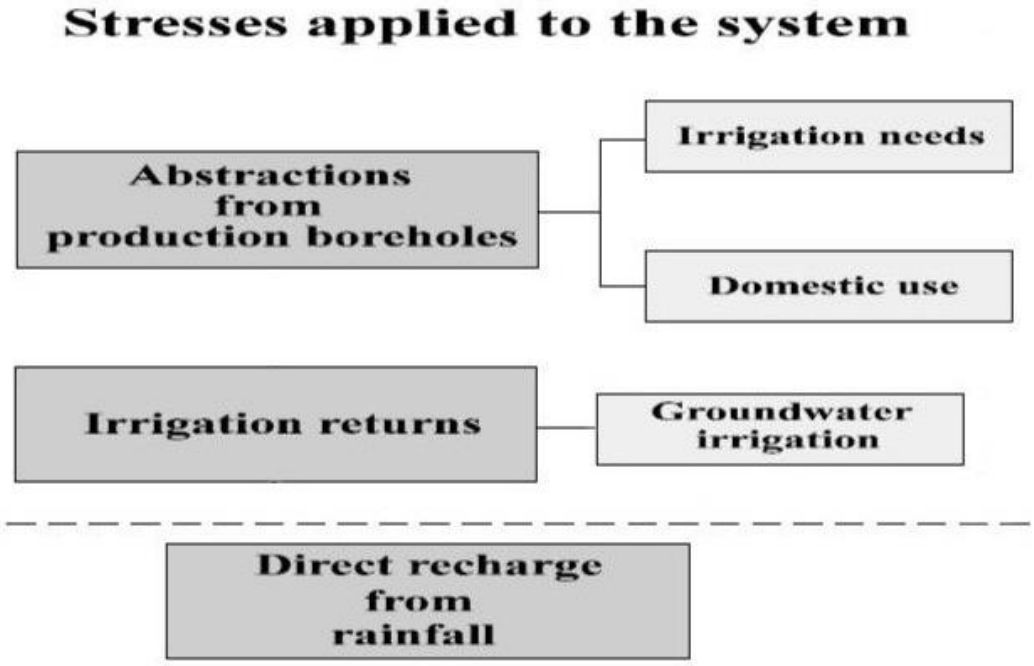

Figure 65 - Stress applied to the modelled system

4.5.5.1 Abstractions from the production boreholes

As discussed in Chapter 1, the main water use in the study area is for irrigation purposes. A significantly smaller fraction is used to cover domestic needs. The karst springs that discharge the fractured and karstified carbonate rock aquifers of the Kastoria area were not included in the model as they do not interact with the flow system of the modelled domain (see Section 3.6.7.2.1).

Well rate information was available only for the productive boreholes found perimetrically of the lake, provided by IGME. For the rest of the boreholes that cover the eastern part of the modelled area an initial value was calculated and then optimized at the calibration procedure. Water abstraction volumes were calculated monthly only for the summer irrigation period. Crop type and crop area data were received from Payment and Control Agency for

Guidance and Guarantee Community Aid (OPEKEPE in Greek) and crop coefficient K_c from the Greek Ministry of Agriculture, 1989 (Doc. Num: 438). The totally abstracted volumes from each borehole for irrigation use were therefore indirectly calculated using the afore described data.

Various methods to estimate the crop water requirements based on the calculation of evapotranspiration are quoted in the literature (Hansen et al., 1979). Three steps are suggested to be followed in such calculations (Doorenbos & Pruitt, 1977):

i. Calculation of the effect of climate on crop water requirements as this is given by the potential evapotranspiration ET_0
ii. Estimation of the effect of the crop characteristics on the crop water requirements as this is given by the crop factor K_c
iii. Evaluation of the effect of local conditions and agricultural practices on crop water requirements.

In the current study, the crop water requirements suggested in the aforementioned Ministry of Agriculture Directive, 1989, were adopted as a guideline in the performed calculation. It is believed that the produced estimates are as realistic as possible since the followed guidelines are adapted to the specific field characteristics of Water District GR 09. The proposed crop water requirements are calculated for each crop type and month of the irrigation period (1st May-31st September) for Water District GR 09.

Having determined the reference evapotranspiration for the simulation area at Section Chapter 3.4.3, the crop water requirements ET_c, were calculated from the following Equation (Doorenbos & Pruitt, 1977):

$$ET_c = K_c . ET_0, \quad \text{[4.1]}$$

And the total irrigation amount from Equation 4.2:

$$IR = ET_{total} - P_{eff}, \quad \text{[4.2]}$$

The effective rainfall (P_{eff}) was calculated in relation to monthly precipitation (P) according to the following equations (FAO, 1986):

$$P_{eff} = 0.8P - 24, \ P < 70\ mm, \quad \text{[4.3]}$$
$$P_{eff} = 0.6P - 10, \ P > 70\ mm, \quad \text{[4.4]}$$

Mean monthly figures of precipitation and effective precipitation can be found at APPENDIX C. Considering that there is a tendency towards over-irrigation, the maximum recommended crop water requirements suggested in the aforementioned Directive were also taken into account during the calibration process. Two compensation factors were applied on these values to account for losses in the pipe distribution network from the production boreholes to the irrigated fields and for the efficiency of the practiced irrigation techniques:

1. According to the Greek Ministry of Agriculture 1989, the efficiency of overhead irrigation which is commonly practiced in the study area varies between 75.0 and 85.0%. In the current study an average efficiency of 80.0% is accepted.
2. Losses to the distribution network were arbitrarily taken to be 5.0% of the water requirements because only about 50% of the irrigation water is distributed through the public domain distribution network.

The corrected crop water requirements were therefore calculated as:

$$ET_{total} = ET_c + A + B, \quad [4.5]$$
$$A = (1 - E).ET_c, \quad [4.6]$$
$$B = L.(ET_c + A), \quad [4.7]$$

By substituting Equations 4.6 and 4.7 into 4.5, the latter yields:

$$ET_{total} = 1.26ET_c\ , \quad [4.8]$$

where:

ET_{total} = Corrected crop water requirements.

ET_c = Crop water requirements as calculated from Equation [4.1].

A = Correction factor accounting for the efficiency "E" of the irrigation practices, E=80%.

B = Correction factor accounting for the losses "L" in the distribution network, L=5%.

Finally, by substituting Equation [4.8] into [4.2], the following equation is produced:

$$IR = 1.26ET_c - P_{eff}, \quad [4.9]$$

The calculated ET_{total} amount was then evenly distributed to all 78 available boreholes due to the unavailability of the spatial distribution of crop types.

Apart from the boreholes owned by the local irrigation organizations a large number of private boreholes tap the aquifer in the study area. No official records exist as to the number and geographical distribution of these boreholes and consequently no data is available on the volumes abstracted from them.

However, it had been estimated that the total abstracted water from these boreholes should account for about equal or a little more of the volume abstracted from the public domain boreholes. (TOEVs of Kastoria basin, personal communication, 2018). Irrigation may start before the beginning of the official period (1st May) and may last after the end of it (31st September), depending on the meteorological conditions of each year. Due to the low temperature during the winter crops are not cultivated so no winter irrigation happens.

Domestic water is supplied by springs and public domain boreholes. Communities that are close to springs do not receive water from boreholes. As with the groundwater abstracted for irrigation purposes, no reliable data records are available with regards to the annual domestic use groundwater consumption. Consequently, the required figures were calculated based on the population of each settlement and on the per capita guideline consumption figures. This was done only for settlements that are found at the mountainous region.

Population of the villages and towns in the study area was obtained from the national censuses conducted in 2001 and 2011 by the National Statistics Service of Greece (2001; 2011). The obtained figures were interpolated to estimate the population in the years between the censuses.

4.5.5.2 Irrigation returns

Irrigation returns in the study area occur at the irrigated fields near the groundwater boreholes. As no conclusive data exist at the irrigated area, the following assumptions that were based on estimates provided by the Municipality of Kastoria and the TOEVs of the study basin had to be made in order to accommodate the required irrigation return calculations (Municipality of Kastoria and the TOEVs of the study basin personal communication, 2018):

- Irrigation returns were applied in the elements of the entire modeled area since there are no data for the location of each crop cultivated

- A single irrigation returns coefficient was chosen for the entire simulated area, IRR_coeff=0.1

4.5.5.3 Direct recharge from rainfall

Direct recharge from rainfall was accounted for in the designed model using a custom MATLAB code developed in the framework of this thesis. Recharge was specified in terms of rainfall depth and it was applied on the top of the active slice of the model as monthly values. A single infiltration coefficient, I=15.8%, was chosen for the entire modelled area, based on the characteristics of the soil cover, the lithological characteristics of the modelled aquifer system's greater area as mentioned in section 3.6.

4.6 Calibration-verification of model

Calibration is the most significant stage in the creation of a defendable numerical model. It consists of solving the "inverse problem" by an optimization process of the assigned hydraulic parameters and the applied stresses to produce acceptable hydraulic head distribution and water balance in the modelled domain (Anderson & Woessner, 1991). A deterministic approach is used to produce a solution to the inverse problem by altering the parameters under calibration manually in a trial and error procedure, or through a stochastic approach in which the above procedure is automated using statistical criteria. The possible solution to a model is not unique because of the uncertainty of the modelled parameters.

Deterministic approaches derived their accuracy on experience of the modeler in terms of the adopted methodology and the number of hydraulic parameters examined to reach calibration and therefore producing a physically sound solution. In contrast, stochastic approaches do not require prior insight and experience by analyzing the spectrum of possible solutions and consequently the uncertainty range associated with parameters.

The following hydraulic parameters were considered during the calibration process: hydraulic conductivity and storativity. The crossflow from the south-eastern edge of the model, the borehole abstractions and therefore the irrigation returns were also considered during the calibration because the values were not accurately known for all available boreholes, as discussed in the previous Chapter.

4.6.1 Calibration stages

A complex groundwater flow system parameter calibration can be a time consuming and elaborate procedure, as stated earlier, as the areal distribution of numerous implicitly associated parameters has to be optimized in an interdependent combination. A step calibration procedure was adopted during this implementation to minimize the time need for the calibration of the model. It consists of analyzing the model in successive designs of increased complexity in terms of astutely representing reality and calibrating each one starting from the simplest. The most significant advantage of this technique is that the number of variables to be calibrated are minimized in the simplest design and progressively increase with the design complexity (Wang & Andersson, 1982). After that PEST was used to make the final calibration of the hydraulic conductivity. A similar approach was adopted in the current implementation, as discussed below:

- Dynamic steady state calibration of single layer model: For the current stage of calibration, the year of 2006 was selected as the most suitable period which best met the selected criteria as these have been discussed in Chapter 4. The aquifer was assumed to consist of a single layer of 100 m thick, as stated in an earlier Chapter. Moreover, because a

steady state problem is not time dependent the solution does not rely on the storativity of the aquifer; thus, this parameter is not accounted for. The calibrated hydraulic parameters e.g hydraulic conductivity provided useful information regarding their distribution pattern across the modelled domain.

- Transient state calibration: The 2D single layer model was calibrated for the period 2004 –2008 (Gianneli, 2009 and IGME, 2010 data) and further verified during the period 2010-2012 (MinAgric, 2013). Selection of the stress period length was dictated by the lack of accurate data during the stated period of time. The abstractions that are effectively the ones applied on the modelled system occur during the irrigation period (summer time). In the selected stress period length, the applied stresses were therefore spread over a longer period of time and Well BC in 2D models in FEFLOW abstract water along the depth of entire column, hence their effects over the system were not as intensive as in reality. Consequently, the storativity which was then introduced as an extra variable to the problem, was not a very sensitive parameter and therefore did not significantly influence the calibration procedure. Under these conditions, calibration of the storativity values was achieved.

The prolonged period of the transient state calibration ensured the correct setup of the model and verified its reliability to simulate the groundwater evolution of the studied aquifer system.

4.6.2 Calibration criteria

As discussed below, three criteria where considered to assess the precision of the performed calibration:

4.6.2.1 Distribution of heads

A number of observation points were chosen as the calibration target of the simulated hydraulic head. The spatial distribution of the used target heads is illustrated in Fig. 66.

At the end of each calibration run, their values were compared to the corresponding heads that were calculated by the model, either in terms of single values (steady state calibration), or in terms of borehole hydrographs (transient state calibration). The deviation of allowed residuals between target and modelled heads was 0.5 m. The above stated figures were considered to be quite high given the related uncertainty of the lithology of the system (see Section 3.6.5), and the fact that monitored heads represent point values in 3D space as opposed to modelled heads that are an average of the regional conditions.

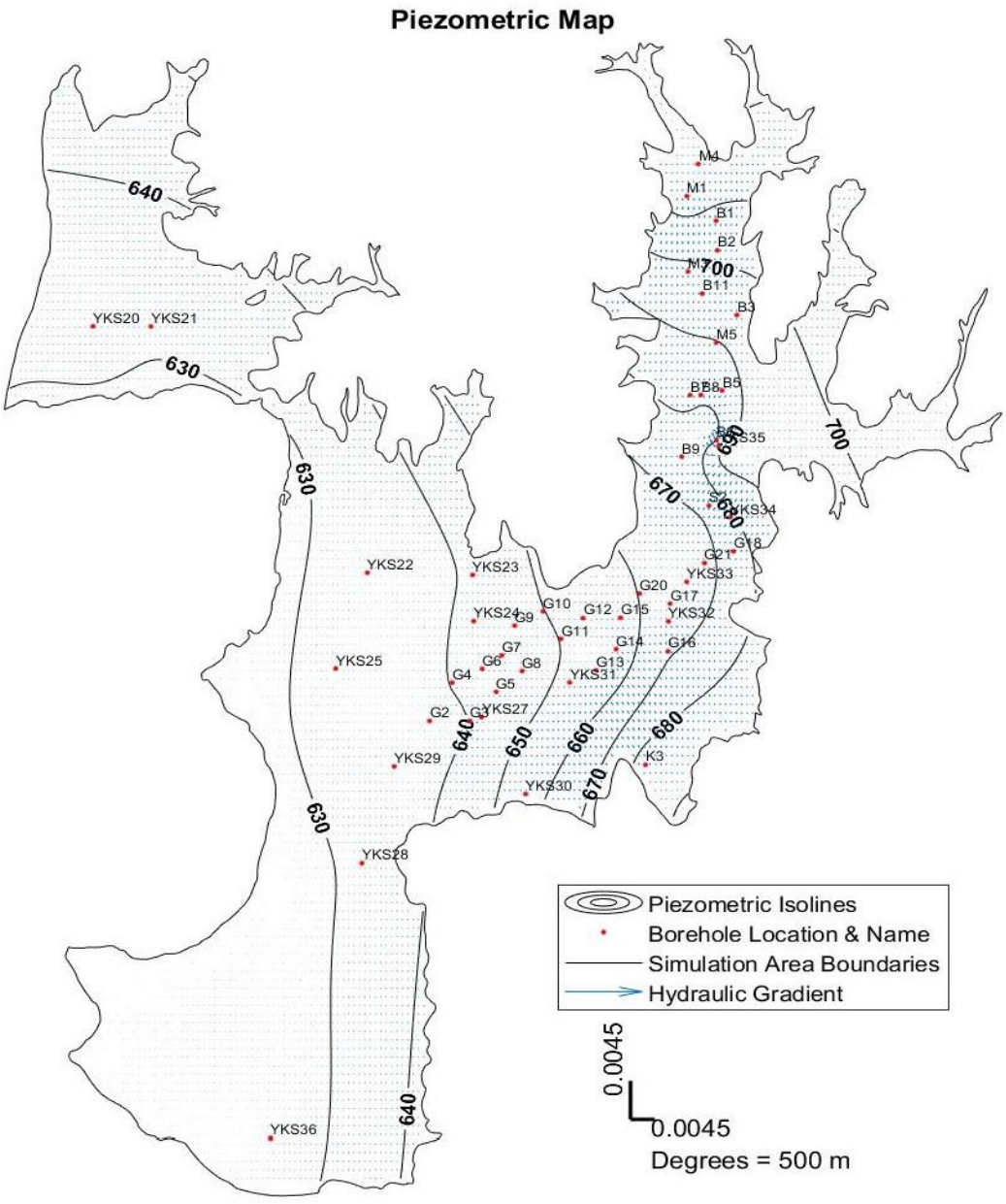

Figure 66 - Distribution of target heads in the modelled domain

4.6.2.2 Calculated water balance

A solution to a groundwater flow model is not explicit due to the fact that a number of different sets of hydraulic parameter configurations may produce an almost identical distribution of hydraulic heads that meet the selected calibration criteria. However, not all of them provide a realistic representation of an aquifer system in respect of groundwater flow evolution. Produced water balance that has a reasonable agreement with hand calculation ensures that the obtained solution adequately represents the general flow mechanisms in the modelled domain. This criterion was considered important during calibration, especially in the steady state calibration as accurate hand calculations can be easily calculated due to the lack of time-steps (see Chapter 4).

For every simulation, FEFLOW calculates the produced inflows and outflows from the modelled domain. This difference between those values is termed as the residual error of the numerical computation and offers a useful initial assessment of the obtained solution in terms of general groundwater flow.

4.6.2.3 Statistical analysis

Quality of a model design is measured using statistical criteria or parameters (Anderson et al., 1991; Wang & Anderson, 1982). A number of statistical parameters based on the head residuals were calculated using a custom MATLAB code. Residuals were calculated automatically by FEFLOW, and plotted as error bars, by subtracting the computed heads from the observed heads, hence, a negative residual indicates over-predicted modelled heads and vice versa. For the transient state calibration, the following functions of statistical criteria were programmed into FEFLOW; thus, created a simple and efficient way of evaluating the level of calibration of the transient model.

The following parameters were considered for each stress period of the simulation: Head residuals, residual mean, residual standard deviation, absolute residual mean, ratio of residual standard deviation to calculated head range across the modelled domain, slope and intercept of linear regression between modelled-measured heads and Pearson product moment correlation coefficient. The definition and description of the use of each of the above parameters is described below, whilst the used notation is submitted in the end of this discussion:

Standard deviation of the residual heads: It was calculated for each stress period as:

$$\boldsymbol{SD = \sqrt{\frac{n\sum \bar{h}_r^2 - \left(\sum \bar{h}_r\right)^2}{n(n-1)}}}, \quad \textbf{[4.10]}$$

It measures the spread of the residuals across the modelled domain and its value should be as close to 0.0 as possible.

Ratio of residual standard deviation to head change across modelled domain: It was calculated for each stress period of the simulation as: $\boldsymbol{r = \frac{SD}{(h_{max} - h_{min})_m}}$, **[4.11]**

It is considered to be one of the most objective indexes of calibration and its value should be lower than 0.1 to 0.15 (Geraghty & Miller, 1993).

Slope and intercept of linear regression $y = ax + b$ between modelled and target heads: They were calculated for each pair of target-modelled heads and every stress period. Slope was calculated as: $\boldsymbol{a = \frac{n\sum h_f h_m - (\sum h_f)(\sum h_m)}{n\sum h_f^2 - \left(\sum h_f\right)^2}}$, **[4.12]**

and its value should be as near to 1.0 as possible, while the intercept was calculated as:

$\boldsymbol{b = \bar{h}_m - a\bar{h}_f}$, **[4.13]**

and its value should be as close to 0.0 as possible. Both parameters are indices of the bias of the solution against over-predicted or under-predicted heads.

Pearson product moment correlation coefficient: This statistical parameter complements the values of the slope and intercept of a linear regression line in that it measures the fit of the regression line to the projected points. It was calculated as:

$$\boldsymbol{R = \frac{n(\sum h_f h_m) - (\sum h_f) - (\sum h_m)}{\sqrt{\left[n\sum {h_f}^2 - \left(\sum h_f\right)^2\right] \cdot \left[n\sum {h_m}^2 - (\sum h_m)^2\right]}}}, \quad \textbf{[4.14]}$$

and it is an index of the proximity of the obtained calibration to the target heads. In ideal conditions its value should be 1.0.

Root Mean Square Error: This statistical parameter complements model efficiency; in this case in each stress period. It was calculated as: **RMSE** = $\sqrt{\frac{\sum_{t=1}^{n}(h_m - h_f)^2}{n}}$, ... **[4.15]** and it is an index of the proximity of the obtained calibration to the target heads. In ideal conditions its value should be 0.0.
The notation of the symbols used in Equations [4.10] to [4.15] is as follows:

h_r = Residual heads.
h_f = Target heads.
h_m = Model calculated heads.
n = Number of considered heads.
SD = Residual standard deviation.
r = Ratio of residual standard deviation to range of calculated heads across the modelled domain.
$(h_{max}-h_{min})_m$ = Range of calculated heads across the modelled domain.
a = Slope of linear regression.
b = Intercept of linear regression.
R = Pearson's correlation coefficient.
RMSE = Root Mean Squared Error.

4.6.3 Starting conditions

At the beginning of a simulation period or transient simulation of a mathematical groundwater flow model, definition of initial conditions consists of specifying hydraulic head distribution that represents the average flow conditions of modelled domain (Franke et al., 1987). In transient state simulations, definition of a specific problem requires definition of both specific boundaries and initial conditions. Also, such a definition is mandatory as Rushton & Wedderburn, 1973 demonstrated. In that case if incorrect starting heads are used, convergence time is increased dramatically and convergence itself can probably lead to inaccurate results. The following starting conditions were used in the calibration of the model:

4.6.3.1 Steady state calibration

As discussed in Chapter 4, the year of 2006 was selected as the calibration period. Studying the compiled borehole hydrographs, it was concluded that hydraulic heads in October and in May are having an average value over the entire year thus, best representing the steady state conditions. For the calibration of the steady state model, the heads in May were used.

4.6.3.2 Transient state calibration

The heads produced from the dynamic steady state calibration were used in the transient simulation as initial conditions.

4.6.4 Single layer model design – 2D horizontal

The compiled piezometry of the aquifer was used as reference during the steady state calibration. Fluid Flux boundaries conditions were assigned along the river course to account for the river-aquifer hydraulic interaction. Hydraulic head boundaries were assigned for the Korissos karst system crossflow as well as at the Kastoria lake found at the western edge of the modelled area (see Section 6.2.4). Flow constraints were applied to the latter to limit the

inflow of water into the modelled area at the flow rate calculated at Section 3.6.7.2.1, as mentioned earlier.

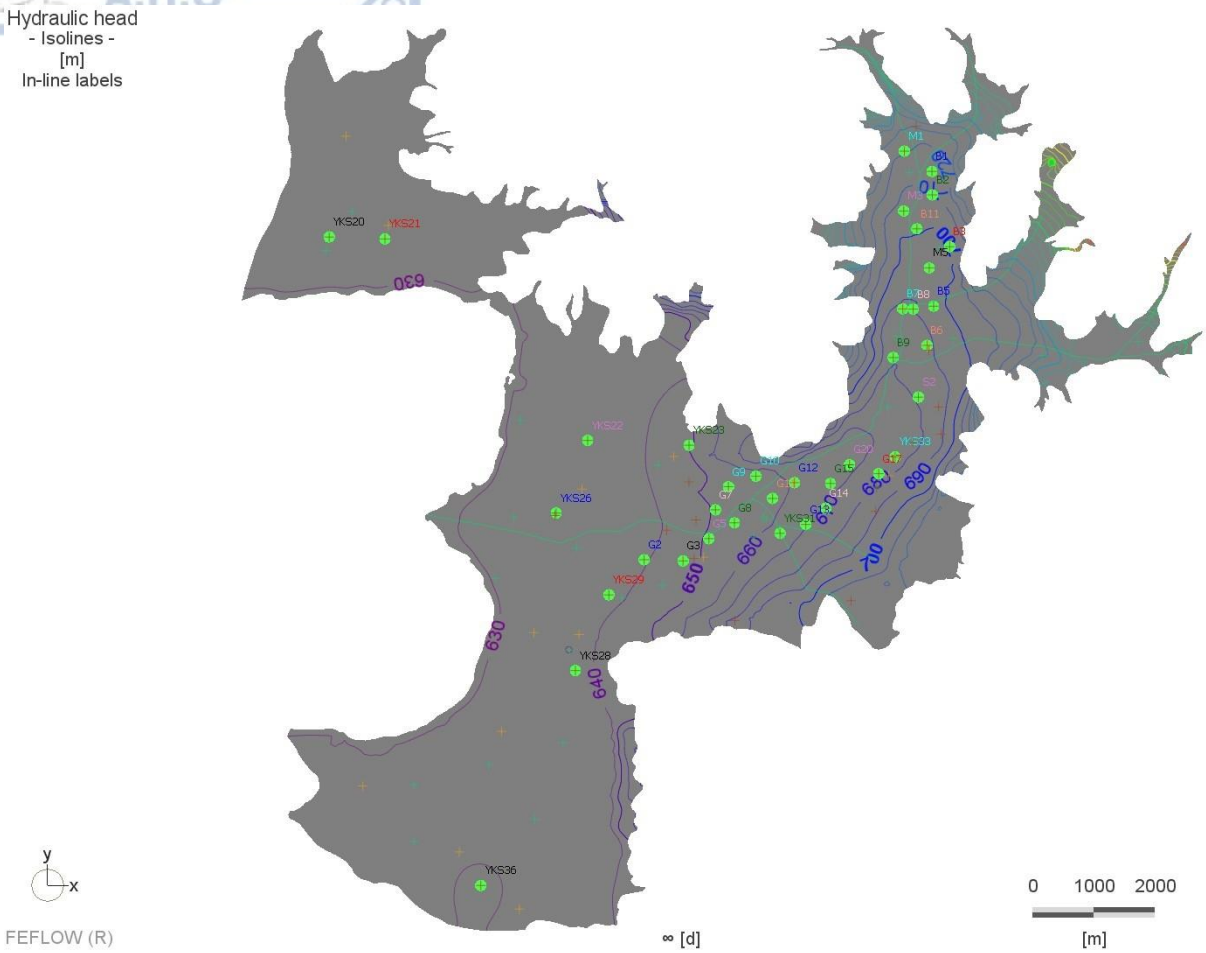

Figure 67 - Calibrated steady state piezometric map. The green dots are the selected calibration points

As discussed in Chapter 3, due to the lack of adequate and reliable time-series data, the effluent and influent volumes of torrent Xiropotamos cannot be calculated for the entire simulation period. However, it had been accepted that the seasonally calculated volumes of water that are either effluent or influent largely represents the average river-aquifer interaction. Hence, river leakage is herein examined in this context. Based on the above categorization, the water balance produced from the single layer model was examined. As illustrated in Table 6.3, the produced water balance agrees with the reference balance, indicating that the designed model adequately simulates the groundwater flow system. Also, this choice of 2D modelling of the area is further supported by the setup of the aquifer layers display a minimal vertical hydraulic gradient.

4.6.4.1 Steady state calibration

As illustrated in Fig. 67, the calibrated piezometry comply well enough with the compiled piezometric maps for the examined period of time. At the southernmost part of the Kastoria Lake, the simulated piezometry deviates from the reference map. However, as illustrated in Fig. 69 the field data density at that area is sparse and there the aquifer layers do not easily recharge from adjacent ones; therefore, the confidence level of the reference map is low. Hence, it cannot be safely claimed whether the observed deviation is due to drawing inaccuracy of the reference maps, due to the nature of aquifer layers, the sparsity of the observed

data and the abstraction regime, which is also an unknown factor. It is believed that all of the above-mentioned possibilities are involved to a certain extent.

As observed in Table 20, the water balance produced by the model agrees well with the reference water balance, with the exception of the volume abstracted from the boreholes which is predicted to be significantly higher than the reference one. This deviation is attributed to existence of active private groundwater boreholes for which only estimates were made due to lack of official data, as discussed in a previous Section. It is therefore suggested that these abstractions were underestimated and therefore calibrated. Groundwater abstraction are considered the most significant part of the groundwater resources exploitation due to the characteristics of the aquifer system. Studying the distribution of the produced river leakage fluxes it is evident that the River Xiropotamos does have a moderate hydraulic interaction with the studied aquifer system, for the bulk of the studied segment, as it had been suggested in Chapters 3 by the hydrogeological data.

Table 20 - Water balance of the dynamic steady state model

Water Balance Elements (m^3/d)	Hand Calculated Inflows	Modelled Inflows	Hand Calculated Outflows	Modelled Outflows
Recharge	136,567	137,580	-	-
Korissos karst system	7,098	7,123	-	-
Well abstractions	-	-	16,530	17,168
Xiropotamos torrent	-	-	7,732	8,251
Kastoria Lake	-	-	118,763	118,390
Total	143,665	144,703	143,025	143,809

The performed statistical analysis of the obtained piezometry showed that the maximum residual between modelled and target heads was 0.5 m whereas most of them where calculated to be less than 0.5 m, thus complying with the limits discussed earlier in this Chapter. The ratio of the residual standard deviation to the calculated range of heads across the modelled domain was calculated to be r=0.05, hence one order of magnitude less than the guideline values of r=0.1 to r= 0.15. The complete results of the statistical analysis are presented below. From the above discussion it follows that the heads distribution and the statistical analysis of the residual heads' calibration criteria are met.

Table 21 – Statistical Parameters for the steady state model

Statistical Parameter	Value
r	0.05
SD	0.43
a	0.96
b	0.21
R	0.987
RMSE	0.55

4.6.4.2 Transient state calibration

The transient state calibration as well as its validation was completed in one stage at periods 2004-2008 (received from Gianneli, 2009 and IGME, 2010) and 2011-2012 (received from MinAgric, 2013), respectively. The hydraulic head results of the steady-state model were as initials conditions. Each simulated year was divided to two stress periods, e.g winter stress period of 212 days and the summer stress period of 153 days. This was done because during the winter stress period only recharge occurs while in the summer period both irrigation abstraction and recharge happens, but with the former at small extent than the recharge of the winter stress period. The time steps of the transient model were set as 1 month long. This automatically ensures short initial time steps and a limited number of total steps per

stress period, thus reducing the risk of serious numerical oscillations and in parallel keeping the total simulation time within reasonable limits. The results were stored also in a monthly step.

Setup of the boundary conditions and the applied stresses in each stress period of the designed models was performed as follows:

- Applied stresses: Groundwater abstractions and irrigation returns were calculated for each summer stress period as it has been discussed earlier in this Chapter. A factor was applied to every accounted abstraction borehole using a ratio of the abstracted volume for the entire basin that were calibrated during the steady state model to calculated abstract volume at the period of interest. Also, changes of the recharge received from rainfall infiltration over the alluvial basin were calculated by multiplying the "I" recharge coefficient.
- Boundary conditions: The constraints placed at the hydraulic heads at the assigned heads boundaries were adjusted for each stress period based on the available piezometry inventory, whereas the hydraulic conductivity was assumed to be constant and equal to those assigned in the steady state calibration. The fluid flux BC placed at the torrent used the seasonal values calculated at an earlier chapter.

Finally, the ratio of the average residual standard deviation to the observed range of heads across the model, over the entire simulation period was calculated to be r=0.283 while the RMSE to be equal to 0.785. The complete results of the conducted statistical analysis are submitted below.

Table 22 - Statistical parameters of each stress-period for the transient state model

Type	Date	SD	RMSE	R	a	b	r
Calibration	01-05-04	0.17	0.280	0.965	0.93	0.67	0.158
	31-10-04	0.14	0.300	0.945	0.92	-0.27	0.182
	01-05-05	0.09	0.445	0.938	0.94	-0.37	0.469
	30-09-05	0.21	0.290	0.961	0.93	-0.94	0.131
	01-05-06	0.12	0.276	0.948	0.94	-0.92	0.233
	31-10-06	0.09	0.350	0.936	0.94	0.23	0.171
	01-06-07	0.15	0.454	0.916	0.91	0.06	0.280
	01-10-07	1.00	1.132	0.912	0.91	-2.07	0.147
	25-10-07	2.29	2.188	0.927	0.94	39.83	0.271
	17-12-08	0.21	0.550	0.933	0.94	2.96	0.422
Validation	31-10-10	0.99	0.949	0.935	0.94	-26.48	0.376
	01-05-11	1.27	1.389	0.935	0.89	-28.55	0.378
	31-10-11	1.00	0.957	0.934	0.88	-26.79	0.376
	01-05-12	1.28	1.432	0.920	0.88	-31.47	0.372

4.6.4.3 Results

Examination of the produced water balance of the studied aquifer system concluded the following:

- Groundwater abstractions decreased slightly after 2000, as it was discussed in Chapter 1. However, the real water abstractions are higher than that calculated using the available data as discussed in a previous Section. The observed deviation at the statistical

analysis was attributed both to poor quality data on the area irrigated from each of the production boreholes and probably to excessive waste of the groundwater resources in terms of irrigation techniques. It is also suggested that the private, non-registered production boreholes are more than those initially estimated and likewise is the total volume of water abstracted from them

- The torrent Xiropotamos-aquifer interaction displays a moderate influence at the water balance of the studied aquifer system
- The storage of the aquifer system exhibits a positive trend
- The mean annual sub-surface flow or discharge of the aquifer to the lake equals approximately to 36 x 10^6 m^3

The above statements are consistent with the conclusions drawn from the study of the hydrogeological data (Section 3.6). It is therefore suggested that due to the imposed exploitation regime, the studied system indicates a highly positive recharge trend that could potentially be exploited to expand agricultural activities, having serious implications to the development of the region.

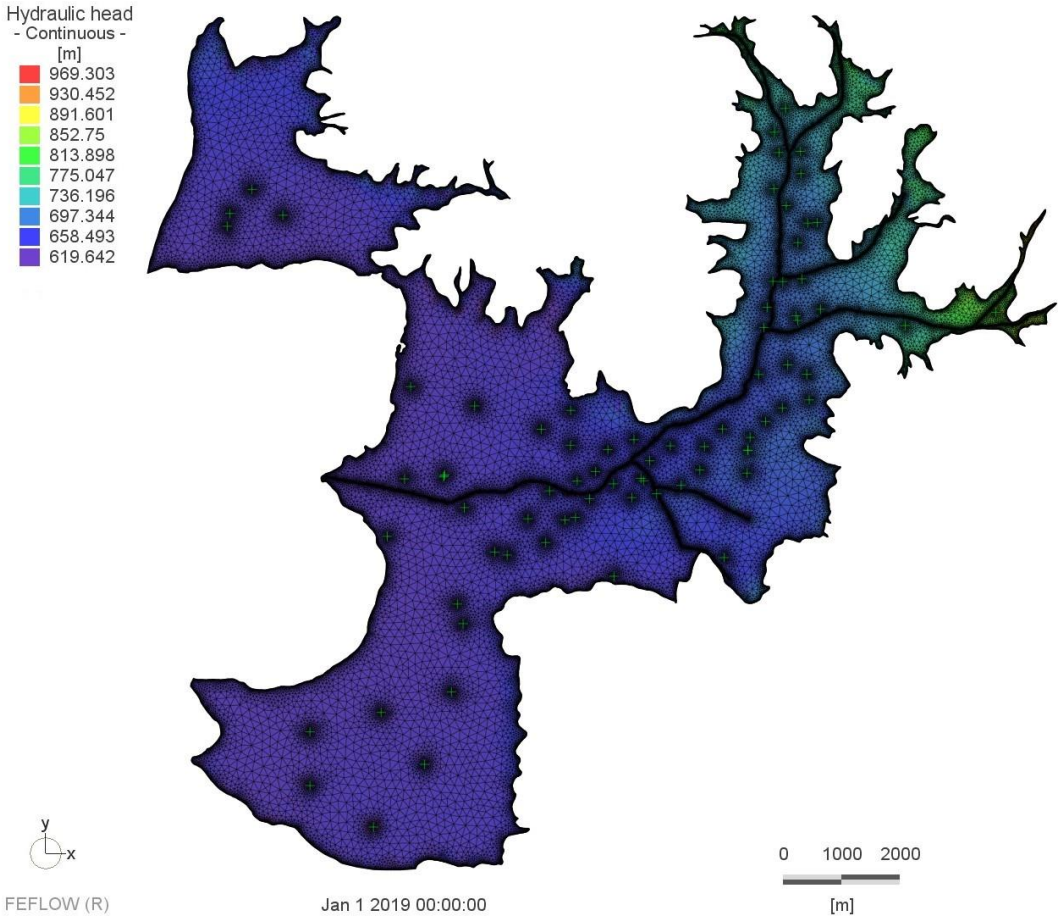

Figure 68 - Hydraulic head distribution for the last time step of the transient simulation

4.7 Future groundwater management

Accurate and reliable predictive simulations are based on a well-established model (Wang et al., 1982; Doherty, 2015). The described calibration procedure ensured that such a model was constructed. As a result, the examined management scenarios that are discussed in this Chapter provide a realistic insight in the future evolution of the groundwater resources of the studied system. The proposed management scenarios are planned by receiving data from

RCMs of EUROCORDEX (EUR-11) and are based on the proposed management plans by the Municipality of Kastoria, 2015 and the Ministry of Environment & Energy, 2014 for Kastoria basin. The irrigation regime is unlikely to change significantly in such a way to be unpredictable and the water level of the lake is managed by the Municipality of Kastoria; thus, making an extension of the original transient simulation acceptable and defendable. The last year simulated in the predictive models is year 2078. Low confidence level predictions would potentially be produced by a longer period. In this implementation ten groundwater management alternatives were examined in terms of the implications to the sustainability of the resources of the aquifer system, based upon the analyzed results of ten RCMs as presented in Section 3.4.5. The aim of proposed plans was to devise a feasible groundwater management options which would ensure sustainability of the resources and consequently possible future agricultural developments of the region, which mainly depends on them. In assessing the feasibility of the examined scenarios, the following criteria were adopted: 1. The model layer must not be dewatered. This criterion was met by all ten of the examined scenarios and is therefore not discussed further in this study. 2. In order for a future water management plan to be economically feasible, all the existing boreholes should be operational, thus avoiding the prohibitive cost of the construction of new deeper installations to cover the irrigation and domestic demands. A borehole was deemed operational if the predicted piezometric surface was higher than the middle of its screened section, the depth to which is herein referred to as the critical depth. The construction characteristics of the boreholes in the study area suggests that no borehole exceeds 100 m depth. The deep boreholes are found mainly around the southern part of the basin and along the main part of torrent Xiropotamos while shallower boreholes can be found at any part of the study area. The existence of many private boreholes whose location and actual depth are not available, though they do not exceed 100 m; thus, it does not forbid the creation of a map of the areal distribution of the critical depth over the studied region (Fig. 69). The critical depth of each borehole was assumed to be half of its total depth. Depression cones are a result of pumping is a localized effect and are therefore not accounted for in the simulated heads distribution. The produced map only served as a working hypothesis and as such it does not imply the existence of these abrupt variations.

Setup of the transient projected models was based on the methodology followed the design of the transient model and the RCM's results presented in section 3.4.5. Since no official guidelines exist to suggest that any major changes will be implemented on the currently irrigated crop patterns. Hence, as an initial approach it was assumed that the irrigation pattern over the entire simulation period remains identical to that of the last year of the transient state calibration. This is further supported by the decline of the population at the settlements found within the simulated area as projected in this thesis and by the land use of CORINE 2000, 2006, 2012 and 2018, which do not show any change throughout the 19 years these data cover. However, it was assumed that irrigation practice will progressively change to tickle; thus, slightly reducing the irrigation amount needed. Also, the mean seasonal values calculated for the aquifer-Xiropotamos torrent interaction were also used for the projected period.

For each examined scenario the map of the predicted depth to the water levels was compiled for the last simulated step since precipitation accounts for most of the recharge of the system. These maps were compared to the map of the minimum allowable water level. One area was distinguished in some of the projected scenarios, where the water level drops a few meters below the minimum set by the following figure; thus, signifying reduction. However, this happens specifically at the area of the boreholes of the public irrigation system since they supply the biggest part of the irrigation demand of the area, including the middle plains of Kastoria. Also, this reduction quickly decreases over time due to the high level of precipitation recharge and the lateral hydraulic communication with the northeastern part of the aquifer which of higher elevation and also of higher precipitation and recharge.

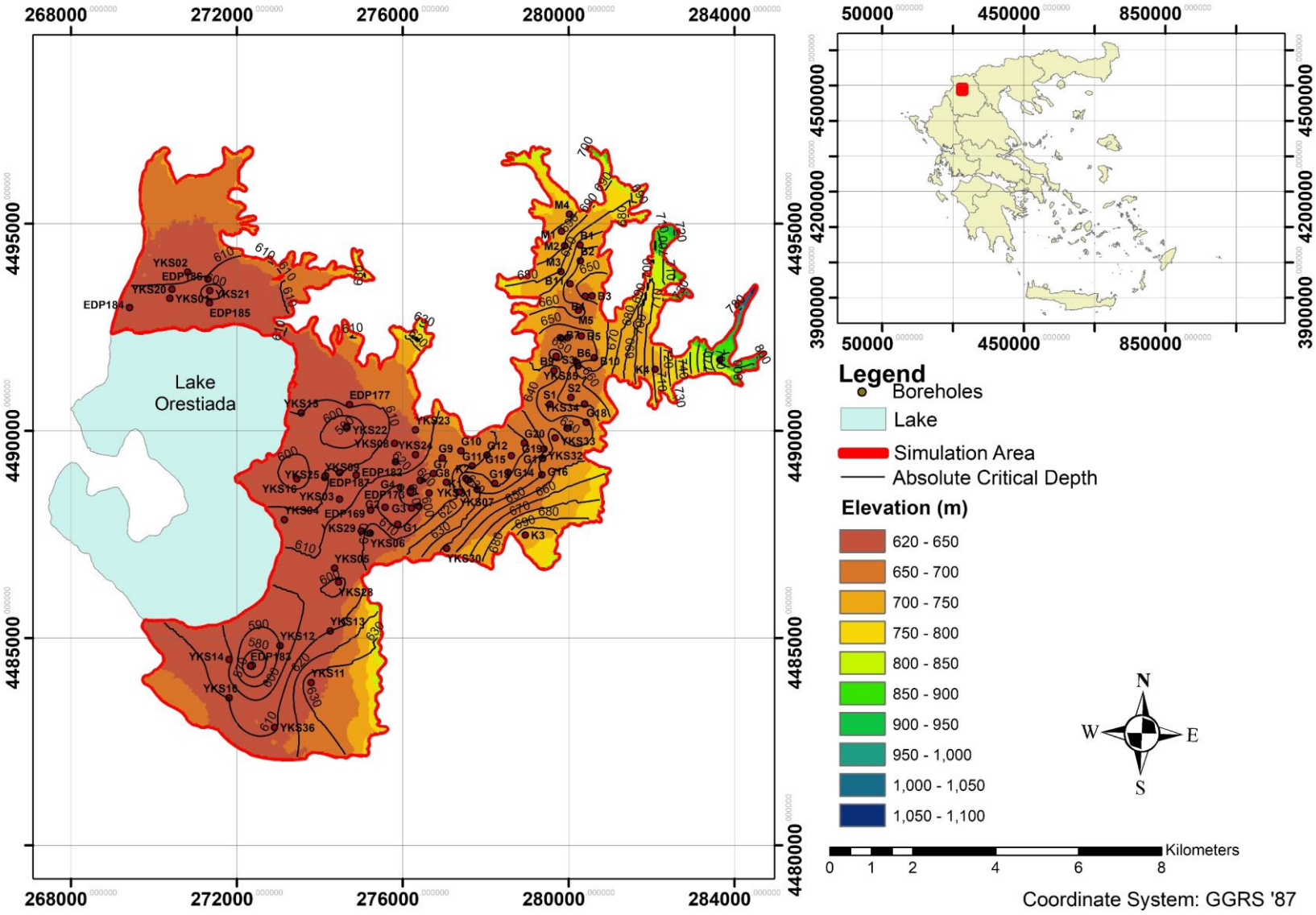

Figure 69 - Absolute critical water levels in the designed model

4.7.1 Summarized Results

Models RCP 2.6 A, RCP 4.5 A, C and RCP 8.5 A present water level reduction below the set minimum. However, this happens only at the vicinity of certain boreholes of the public irrigation boreholes', due to high pumping rates, which are overestimated as mentioned in an earlier section, by being close to no flow boundaries and because of the low hydraulic conductivity, which both negate lateral recharge of the aquifer layers found there. This happens especially in the southern part of the middle section. Moreover, this depression almost disappears at the start of the next summer stress period, due to the high rainfall recharge, as mentioned earlier. The hydraulic head distribution at 1 Jan 2078 for each examined scenario can be found below.

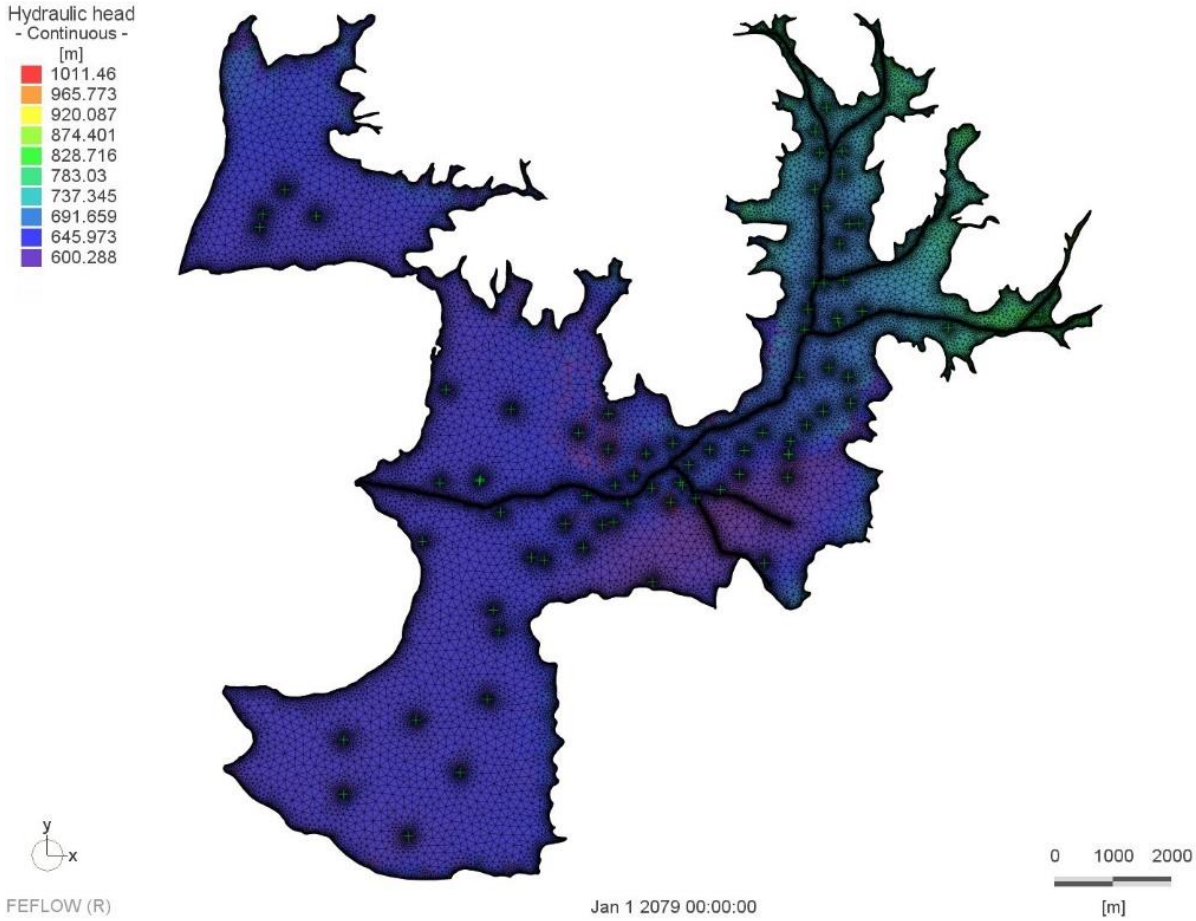

Figure 70 - Hydraulic head distribution at 1 Jan 2079 for RCP 2.6 A

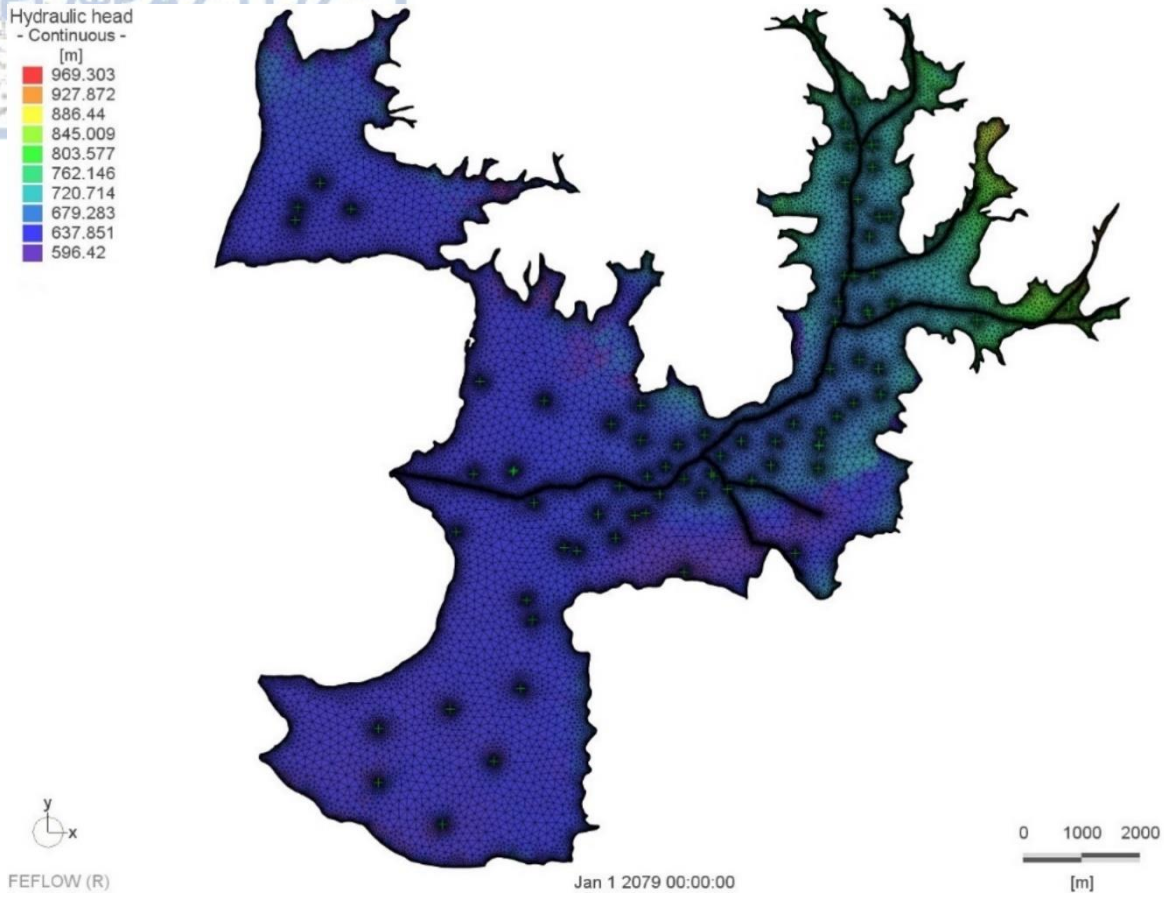

Figure 71 - Hydraulic head distribution at 1 Jan 2079 for RCP 2.6 B

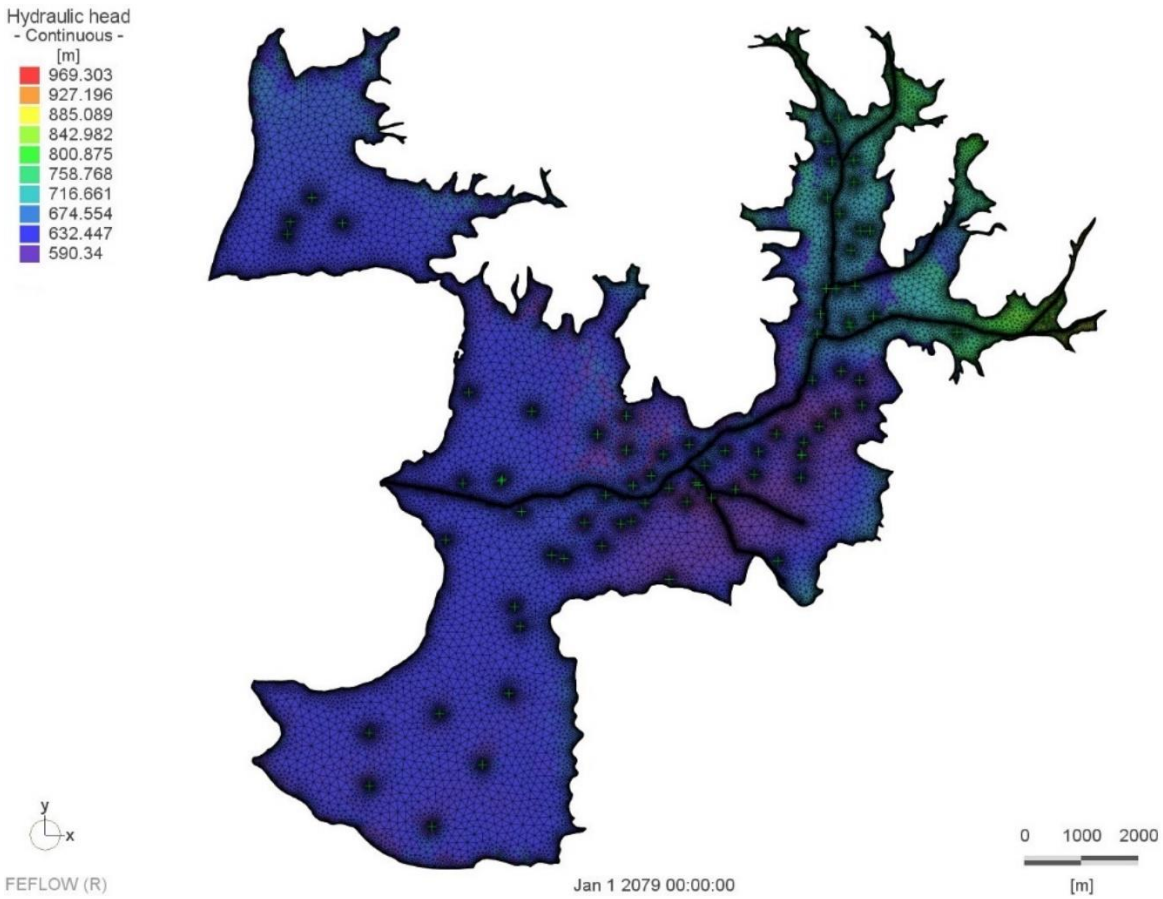

Figure 72 - Hydraulic head distribution at 1 Jan 2079 for RCP 4.5 A

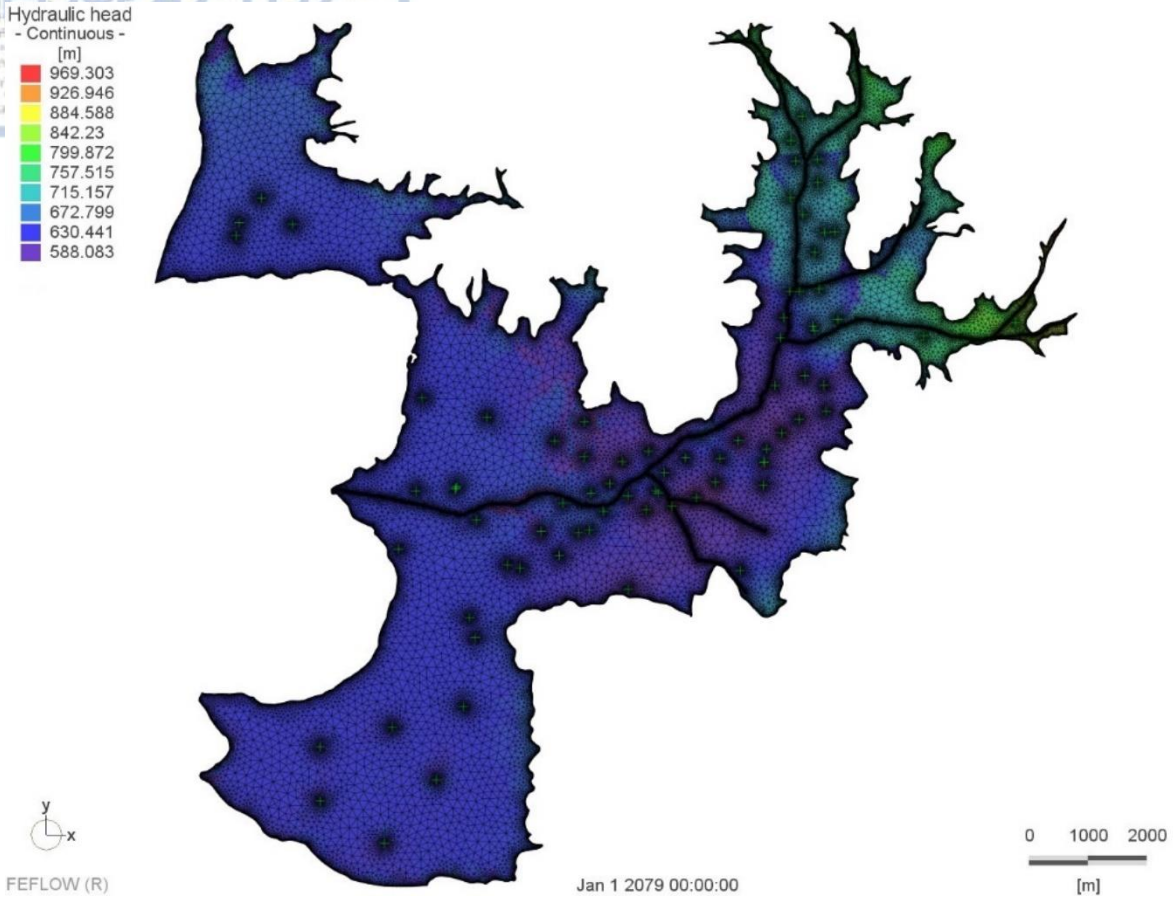

Figure 73 - Hydraulic head distribution at 1 Jan 2079 for RCP 4.5 B

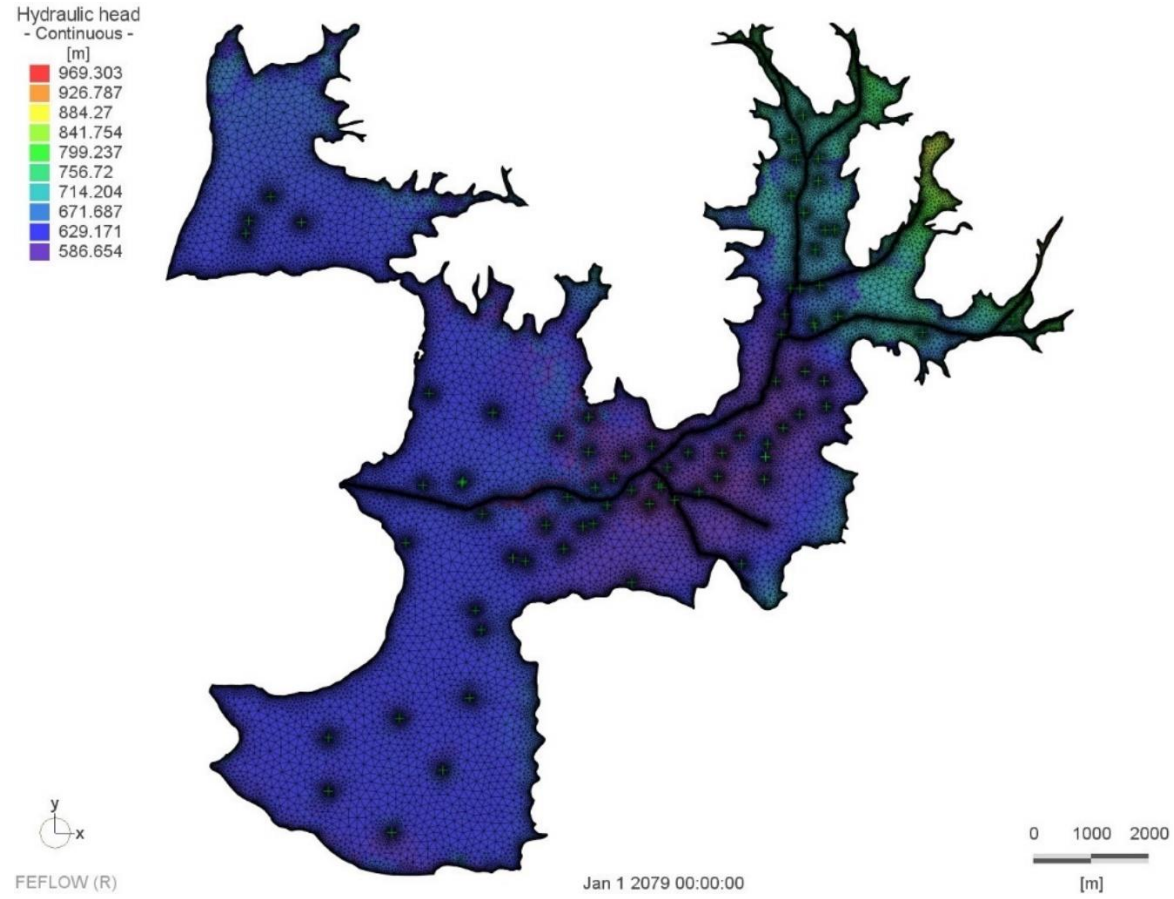

Figure 74 - Hydraulic head distribution at 1 Jan 2079 for RCP 4.5 C

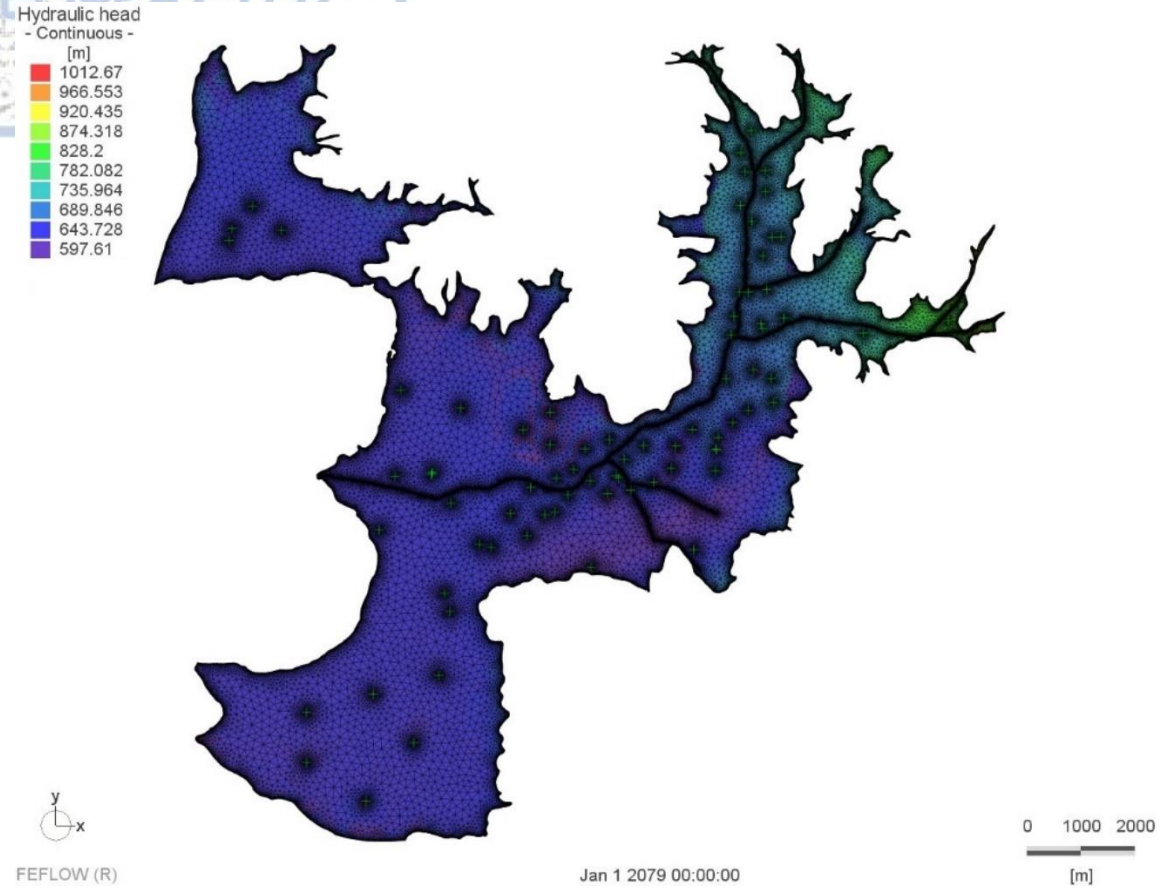

Figure 75 - Hydraulic head distribution at 1 Jan 2079 for RCP 4.5 D

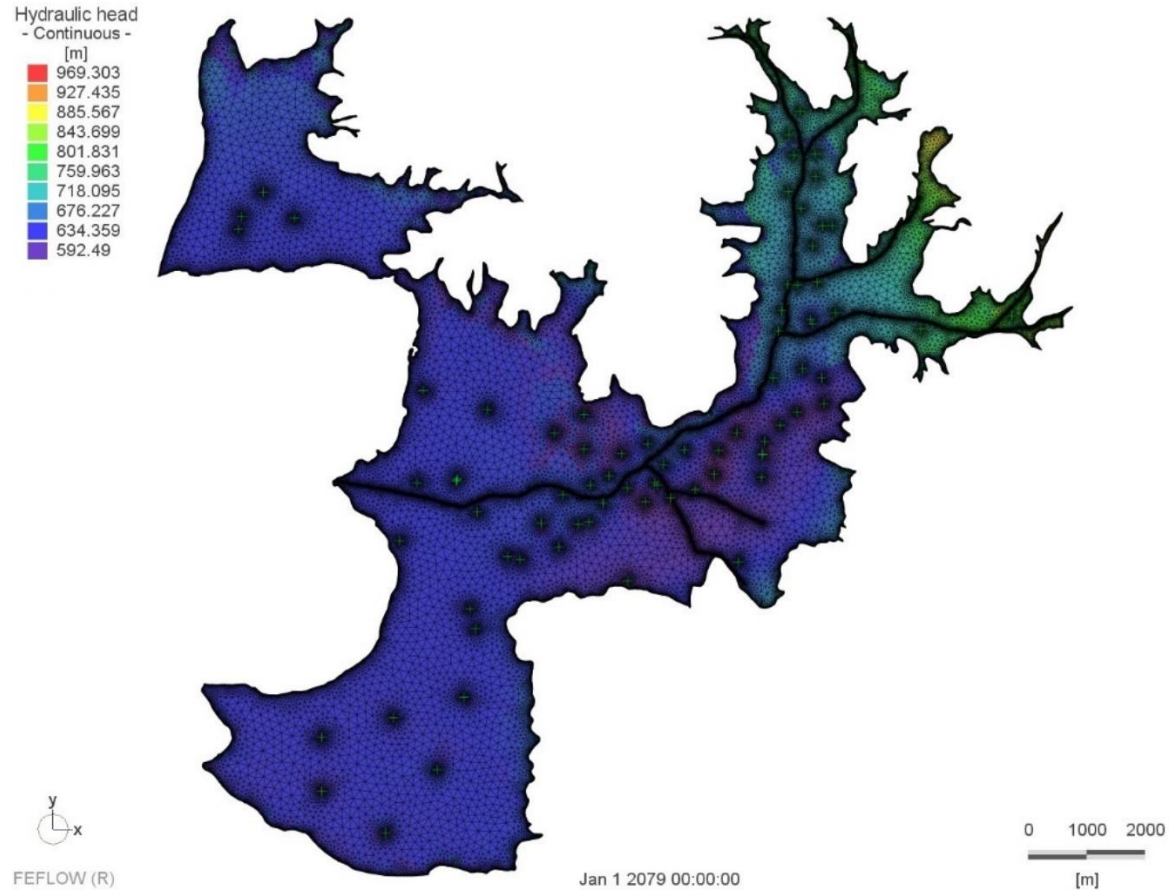

Figure 76 - Hydraulic head distribution at 1 Jan 2079 for RCP 8.5 A

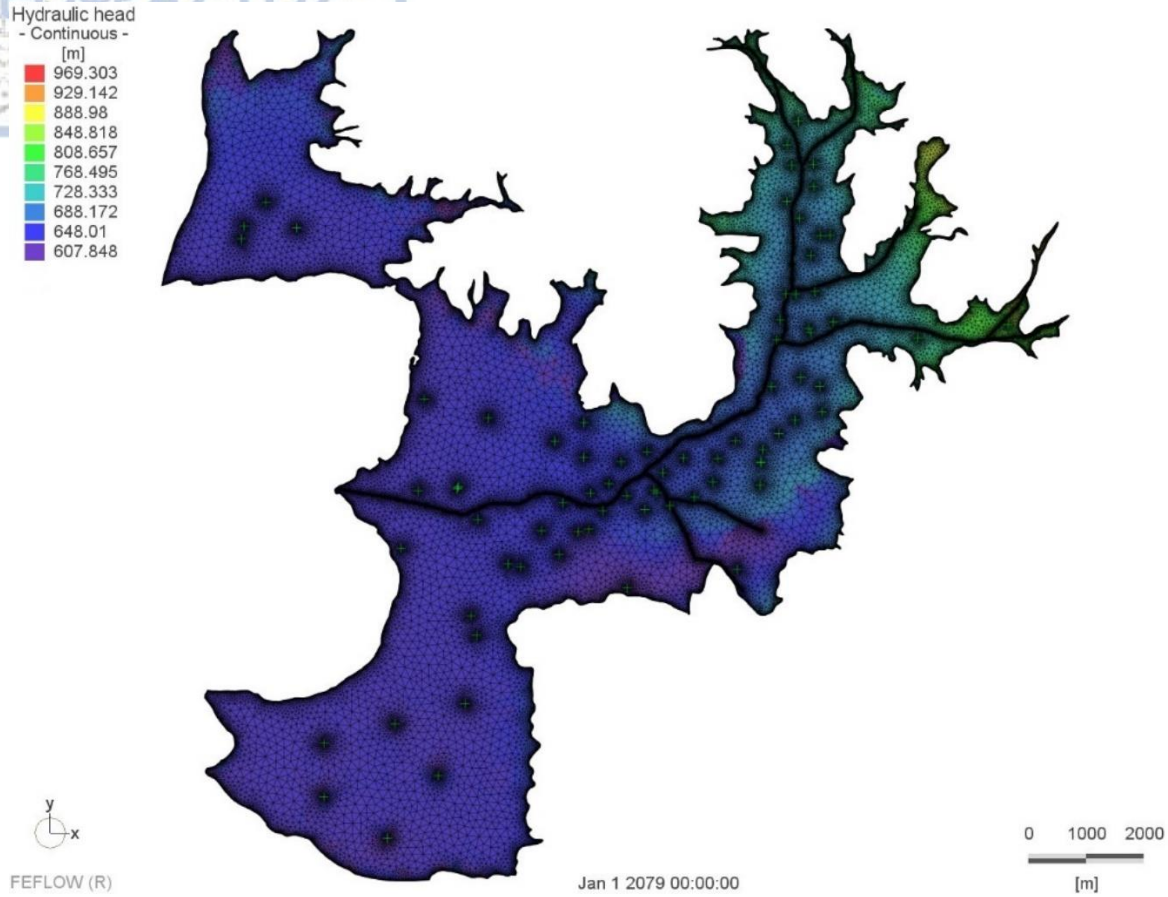

Figure 77 - Hydraulic head distribution at 1 Jan 2079 for RCP 8.5 B

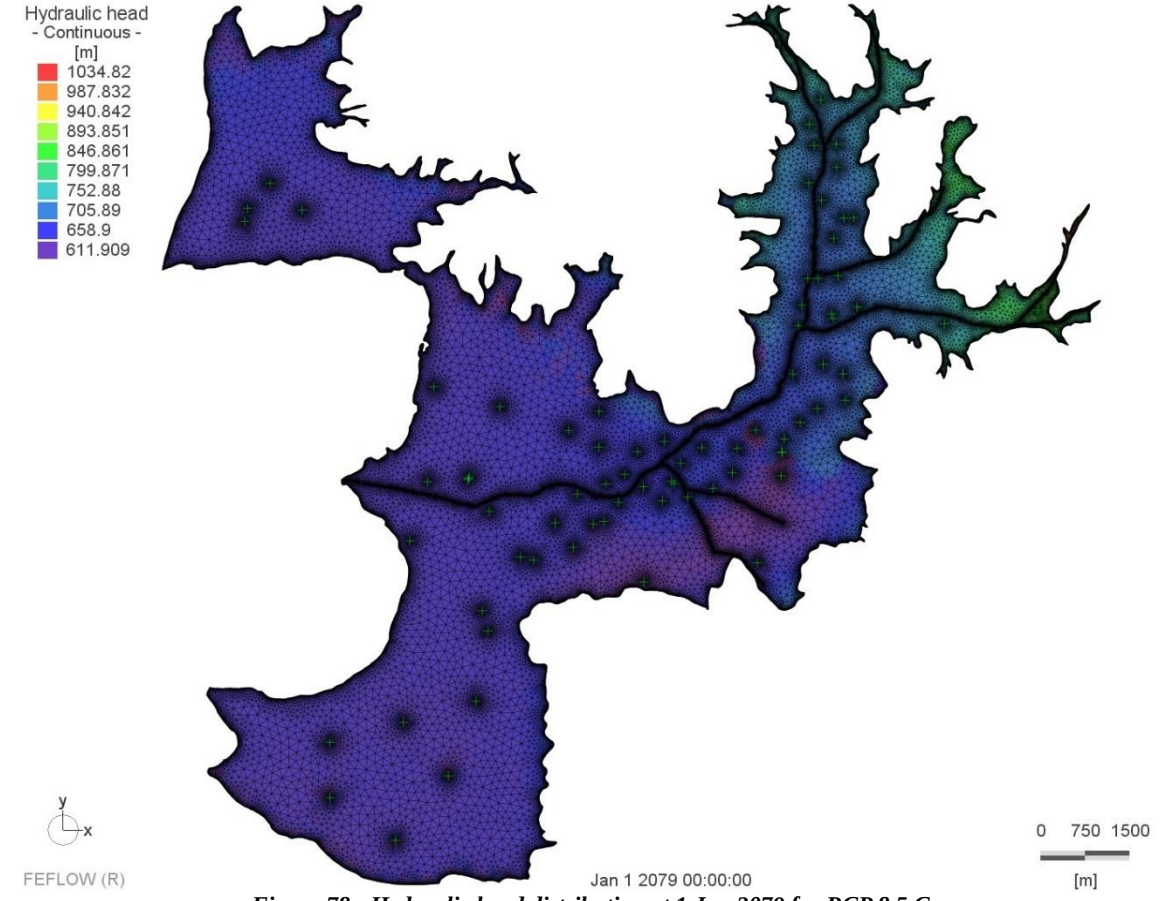

Figure 78 - Hydraulic head distribution at 1 Jan 2079 for RCP 8.5 C

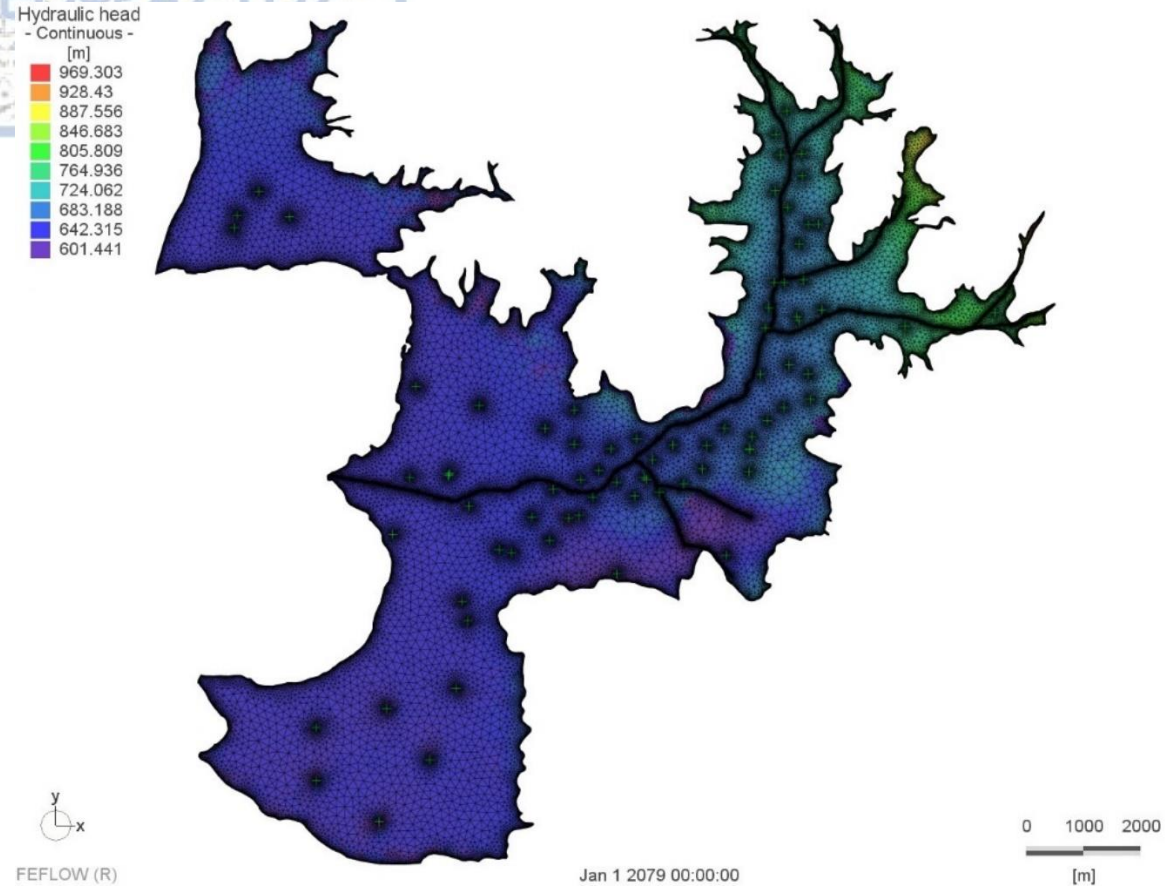

Figure 79 - Hydraulic head distribution at 1 Jan 2079 for RCP 8.5 D

4.7.2 Calculation of Projected Water Balance of Kastoria Lake

For the compilation of the water balance of Lake Kastoria, which is considered as a reservoir, the continuity equation is used (Sakkas, 1989):

$$\frac{dS}{dt} = I - Q, \quad \text{[4.16]}$$

where **S** = the volume of the reservoir water at a given time,
t = time
I = total supply of inputs to the reservoir
Q = total flow of water from the reservoir

For a given time, in this case year, Eq. could be written as:

$$\Delta S = V_{in} - V_{out}, \quad \text{[4.17]}$$

where

$$V_{IN} = I\Delta t, \quad \text{[4.18]}$$
$$V_{OUT} = Q\Delta t, \quad \text{[4.19]}$$

are the total inflow and outflow volumes respectively for every given year.

Inflows to the lake are the rainfall that falls to its surface and the runoff from the land section of the basin (surface and underground). Outflows from the lake include evaporation

from its surface and discharge through the Gkioli stream to the Aliakmon River. Underground outflows exist towards the alluvial aquifers of the area, south of the lake, according to Vafeiadis, 1983 are negligible and therefore not taken into account. With these assumptions, Eq. 1 are written in the form:

$$\boldsymbol{V_{IN} = V_P + V_R + V_A,} \quad \textbf{[4.20]}$$
$$\boldsymbol{V_{OUT} = V_E + V_G,} \quad \textbf{[4.21]}$$

where

$\mathbf{V_P}$ = annual precipitation volume that falls directly onto the lake surface
$\mathbf{V_R}$ = annual surface runoff
$\mathbf{V_A}$ = annual lateral recharge from the Kastoria Aquifer sub-system
$\mathbf{V_E}$ = annual evaporation from surface of the lake
$\mathbf{V_G}$ = annual volume of water that discharges from Kastoria lake to river Aliakmonas via the Gkioli stream

The change in water storage, **ΔS**, in the lake for a reference duration of a year is assumed to be zero, due the control of the lake's water level by the Municipality of Kastoria. This assumption along with the above equations yield the equation that calculates the annual water balance of Kastoria Lake.

$$\boldsymbol{V_{IN} - V_{OUT} = \Delta S \Rightarrow}$$
$$\boldsymbol{V_P + V_R + V_A - V_E - V_G = 0 \Rightarrow}$$
$$\boldsymbol{V_G = V_P + V_R + V_A - V_E,} \quad \textbf{[4.22]}$$

Moreover, the water balance elements stated earlier are calculated separately and then are substituted in the above equation. The calculation workflow for each water balance elements is stated below.

- The annual precipitation volume that falls directly onto the lake surface ($\boldsymbol{V_P}$) is calculated by multiplying the rainfall height as meters with the area of the surface area
- The annual runoff ($\boldsymbol{V_R}$) is calculated by multiplying the total runoff coefficient estimated by Vafeiadis, 1983 for the entire basin with the annual precipitation volume of the entire basin presented at section 3.5.1
- The annual lateral recharge from the Kastoria Aquifer sub-system ($\boldsymbol{V_A}$) is calculated by the FeFLOW model implementation of this thesis
- The annual evaporation from surface of the lake ($\boldsymbol{V_E}$) is calculated from equation $\boldsymbol{E=K_wET_0}$. by using the $K_w=0.85$ coefficient proposed at FAO-56, 1986, for the estimation of evaporative losses from open water bodies at sub-humid climate zones and multiplying it with the calculated Hargreaves-Samani reference evapotranspiration
- The annual volume of water that discharges from Kastoria lake to river Aliakmonas via the Gkioli stream ($\boldsymbol{V_G}$) is calculated indirectly from the above equation

Calculation errors are yielded from this equation because the conceptual model imperfection that are inherited from the analytical calculation methods and from the numerical errors yielded from the numerical simulation of the FeFLOW model for the annual lateral recharge from the aquifer. However, those errors are summed at the $\boldsymbol{V_G}$ volume, due to the fact that the $\boldsymbol{V_G}$ is the water balance element that is being calculated though this procedure. This done to assess the impact climate change has to the water balance of the lake by assessing the deviation the calculated $\boldsymbol{V_G}$ value has from the value of 51 x 10^6 m^3 proposed by the current

study. For example, the closer the calculated V_G is to reference value the less the impact to the water balance of the lake. However, this procedure does not include the material load that the torrents deposit into the lake. This water load takes the place of the water in the lake reducing its capacity to store water at the given maximum and minimum water level suggested by the management plan of W.D GR 09.

4.7.2.1 Precipitation on the surface of the lake

Precipitation received by the surface of the lake was calculated with the procedure described above. The observed precipitation used at this assessment were during 2000-2018 in contrast to the ones used for the bias-correction procedure (1986-2005) as at section 3.7. As presented at the figure below the decrease in precipitation reduces significantly the water amount received by the surface for most models. The results presented at this section follow the trends assessed at section 3.4.5.1.1 since the rely only on precipitation. RCP 2.6 A present a slight decrease at the first and third sub-period while RCP 4.5 A present this for the first sub-period only. At the rest of the sub-periods they present significant decrease. The rest of the models present significant decrease right from the first sub-period, which become more severe towards the end of the century.

Annual temporal variation of the precipitation received by the surface of the lake was assessed for the three sub-periods and compared to the median total annual precipitation of the control period (2000-2018), which is 19.58 x 10^6 m^3 and the results are illustrated in Fig. 80. The general point of the results illustrated in Fig. 80 is that the amount received by the surface of the lake from precipitation is expected to be significantly decreased, especially during the period 2059-2078. RCP 4.5 A present a slight decrease for the second sub-period only. RCP 2.6 A and RCP 4.5 A present a slight decrease at the first sub-period only, as mentioned earlier, of 1.3 and 1.09 million cubic meters, respectively. The rest of the models present significant reduction on the water amount received by the surface of the lake from 1.4 (-7.87%) to 3.69 x 10^6 m^3 (-18.85%) for the first sub-period, from 1.4 (-7.87%) to 3.69 x 10^6 m^3 (-18.85%) for the second and from -1.4 to -5.61 x 10^6 m^3 for the third sub-period. For most of the models the inter-quantile range partially overlap with the one of the observed data, meaning also a significant reduction.

When comparing the temporal change for each selected model, similar trends are indicated. Most models present even greater reduction in water amount during the second and third sub-periods compared to the first sub-period. During the third sub-period RCP 2.6 B, RCP 4.5 A, D and all the models under RCP 8.5 present increase compared to the other sub-periods but it's still reduced compared to the control period. Consequently, the reduced precipitation will decrease the water amount of direct rainfall recharge the lake receives.

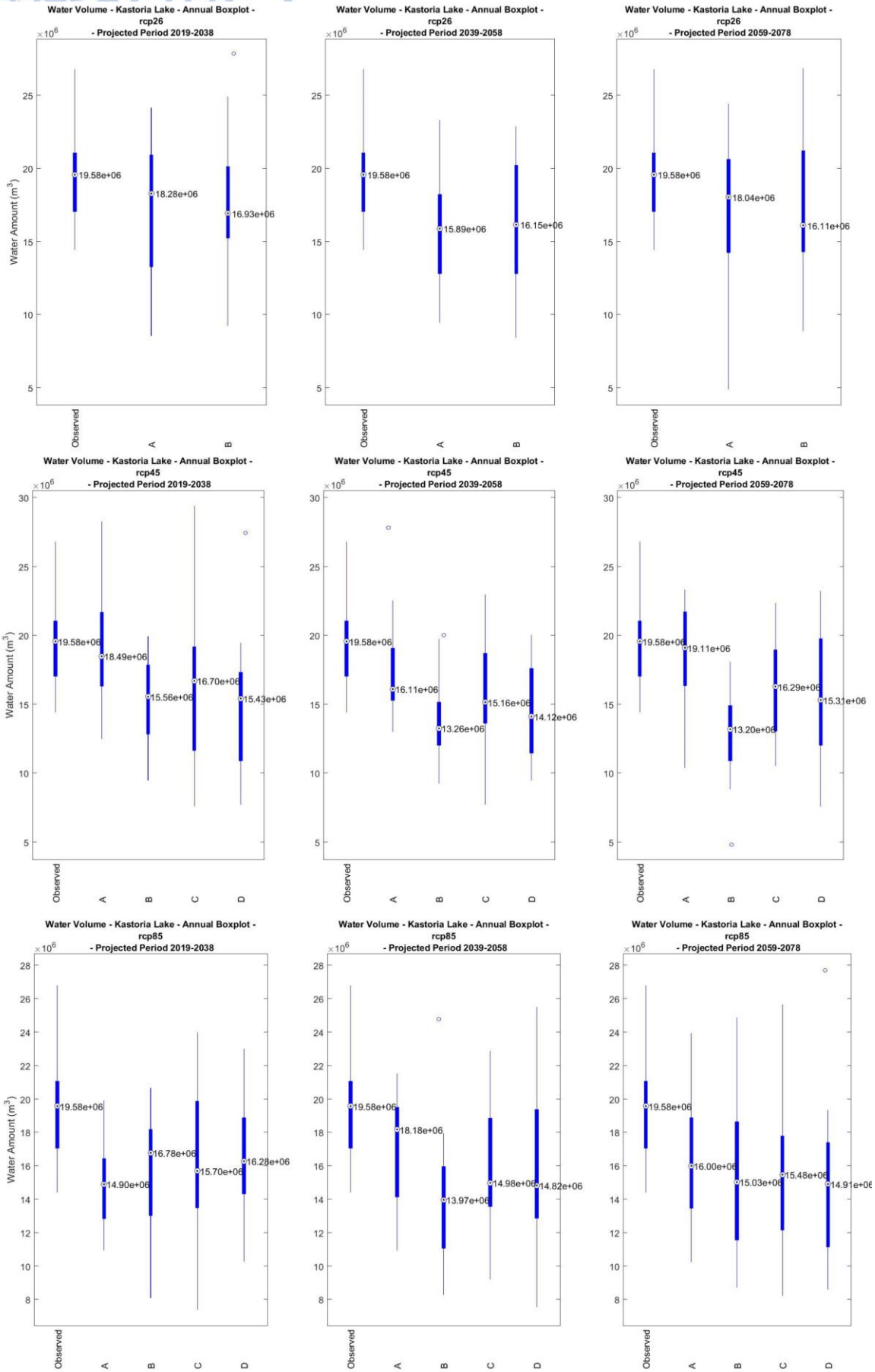

Figure 80 - Box-plots of total annual precipitation amount variation received by the surface of the Kastoria lake according to the results from the ten chose RCMs for the periods 2019-2038, 2039-2058 and 2059-2078

4.7.2.2 Evaporation from the surface of Kastoria lake

Evaporation from the surface of the lake was calculated with the procedure described above. The observed evaporation data used at this assessment were during 2000-2011, since they were the only data available. As presented at Fig. 81 the increase in evaporation severely increases throughout the projected period. All models present significant increase in every sub-period.

Annual temporal variation of evaporation from the surface of the lake was assessed for the three sub-periods and compared to the median total annual evaporation of the control period, which is 29 x 10^6 m^3 and the results are illustrated in Fig. 81. The general point of the results illustrated in Fig. 81 is that the amount evaporated from the surface of the lake is expected to be significantly increased. RCP 2.6 A and RCP 4.5 D present significant increase during the first two sub-periods and a slight decrease but still it's higher when compared to the control period. The increase of the evaporation ranges from 4.99 (11.59%) to 3.36 (17.21%) million cubic meters for the first sub-period, from 3.18 (10.97%) to 6.95 (23.97%) for the second and from 2.85 (9.83%) to 6.34 (21.86%) for the third sub-period. It is evident that during the second sub-period slightly more water will be evaporated than the evaporation amount of the third sub-period.

When comparing the temporal change for each selected model, similar trends are indicated. Most models present even greater increase in evaporation during the second and third sub-periods compared to the first sub-period at which evaporation is already high. Consequently, large amounts of water are being evaporated for the lake both in present and future.

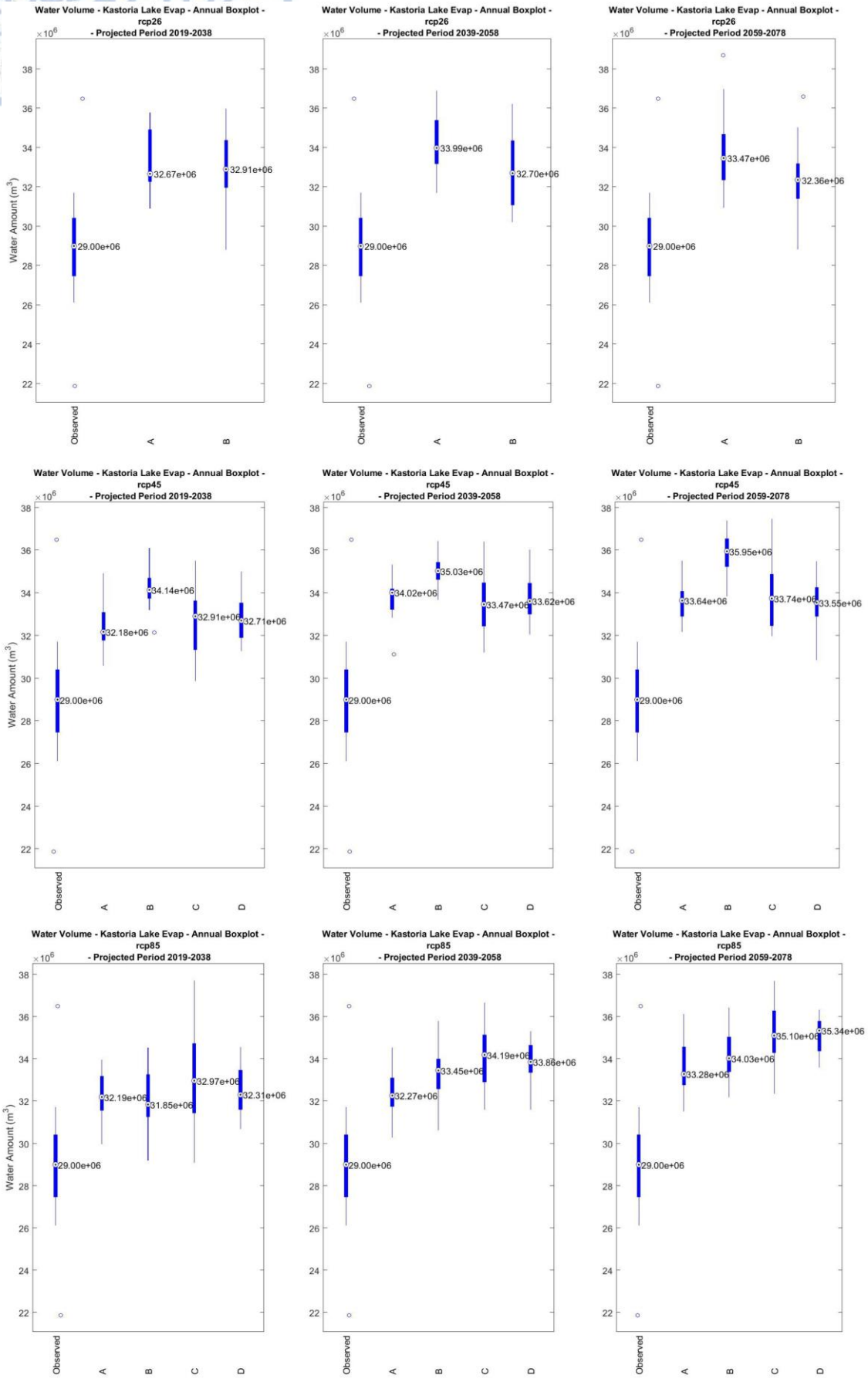

Figure 81 - Box-plots of total annual evaporation amount variation from the surface of the Kastoria lake according to the results from the ten selected RCMs for the periods 2019-2038, 2039-2058 and 2059-2078

4.7.2.3 Surface runoff at Kastoria Basin

Surface runoff at the basin of Kastoria was calculated with the procedure described above. The observed precipitation used at this assessment were during 2000-2018 in contrast to the ones used for the bias-correction procedure (1986-2005) as at section 3.7.

Annual temporal variation of the surface runoff received by the surface of the lake was assessed for the three sub-periods and compared to the median total annual precipitation of the control period (1986–2005), which is 29.77 x 10^6 m^3 and the results are illustrated in Fig. 82. The general point of the results illustrated in Fig. 82 is that surface runoff remains largely the same as the observed, towards the end of the century, since the increase of the projected surface runoff at each sub-period does not exceed 5 million cubic meters with the exception of RCP 4.5 A at the third sub-period. It also presents increase for all sub-periods. RCP 4.5 D present a slight decrease throughout the projected period. Models under RCP 2.6 present increase of surface runoff throughout the projected period. Slight increase is presented by RCP 2.6 A, B, RCP 4.5 A, B, C (15.18%, 8.53%, 5.68%) and RCP 8.5 B, C, D during the first sub-period, decrease for models B, C, D under RCP 4.5 (7.09%, 2.59%, 7.19%) and 8.5 (12.13%, 5.11%, 5.74%) for the second sub-period while increase for models RCP 4.5 A and RCP 8.5 A (9.54%, 12.66%) and decrease for models B, C, D (7.29%, 2.18%, 3.83%) and A, B, C, D (0.84%, 6.28%, 1.11%, 4.57%) under RCP 4.5 and RCP 8.5 for the third sub-period, respectively, while increase for RCP 4.5 A (18.64%). For most of the models the inter-quantile range partially overlap with the one of the observed data, meaning mostly an increase in surface runoff, due to extreme precipitation events.

When comparing the temporal change for each selected model, similar trends are indicated. Most models present mostly equal quantity of surface runoff in water amount during the second and third sub-periods compared to the first sub-period. During the third sub-period RCP 4.5 B, C, D and RCP 8.5 models a slight decrease compared to the other sub-periods but it's still reduced compared to the control period. Consequently, the reduced precipitation will decrease the water amount of surface runoff towards the end of the century for most models.

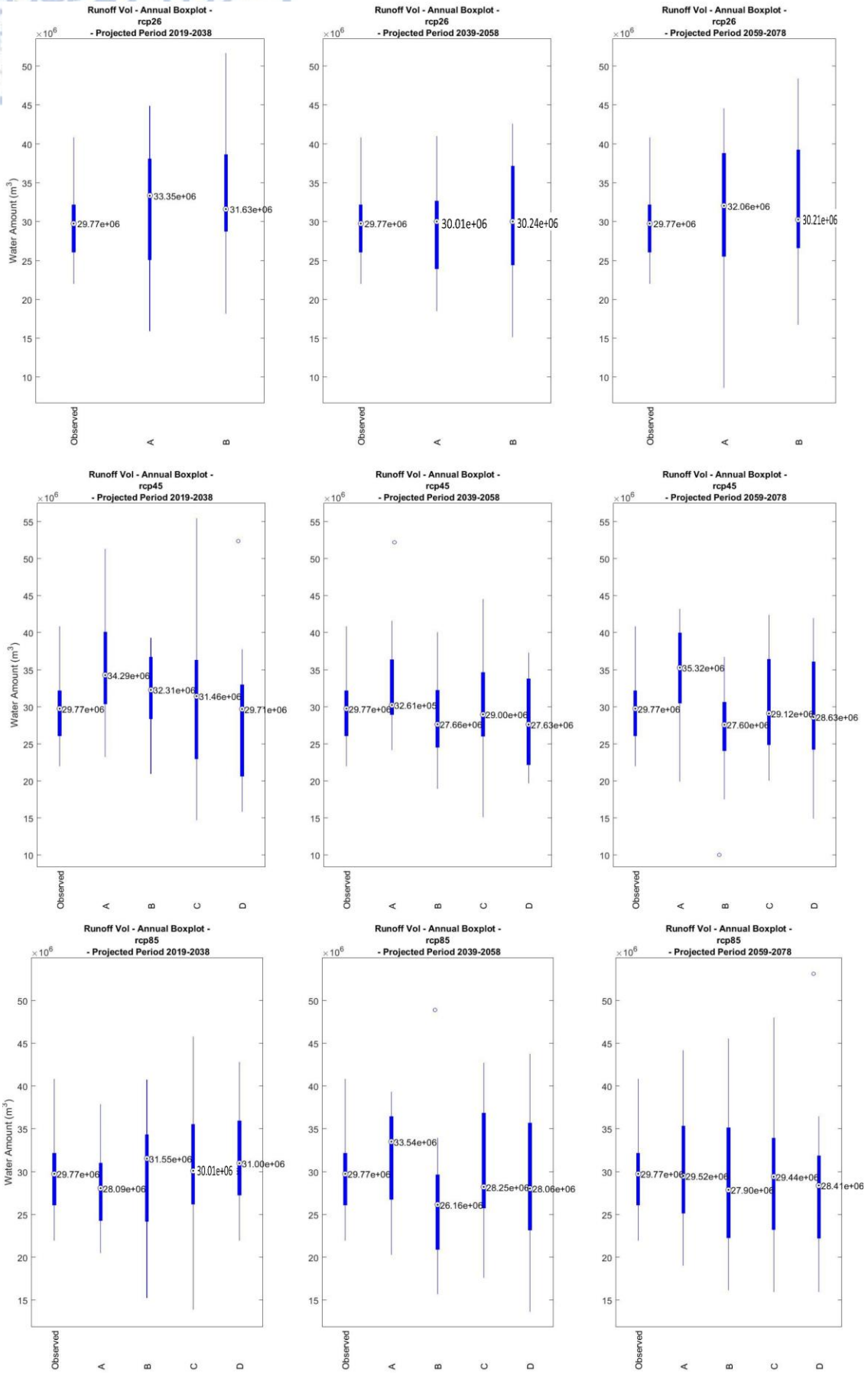

Figure 82 - Box-plots of annual surface runoff amount variation at Kastoria basin according to the results from the ten selected RCMs for the periods 2019-2038, 2039-2058 and 2059-2078

4.7.2.4 Sub-surface runoff at Kastoria Basin

Subsurface runoff at the basin of Kastoria was calculated with the FEFLOW program as outflow to the lake that borders the Kastoria alluvial aquifer. The observed precipitation used at this assessment were during 2000-2018 in contrast to the ones used for the bias-correction procedure (1986-2005) as at section 3.7.

Annual temporal variation of the subsurface runoff received as inflow by the lake was assessed for the three sub-periods and compared to the median total annual precipitation of the control period (2000–2018), which is 36.98 x 10^6 m^3 and the results are illustrated in Fig. 83. The general point of the results illustrated in Fig. 83 is that subsurface runoff reduces throughout the projected period compared to the observed period, since the increase of the projected irrigation demand and reduced projected precipitation lowers the amount of outflow to the lake. Models RCP 2.6 B, RCP 4.5 A present a slight increase for the first sub-period only, while RCP 4.5 D and RCP 8.5 A present that slight increase at the third sub-period. The rest of the models and the corresponding sub-periods present a reduction of 1.08 to 3.97 x 10^6 m^3 (3.91% to 10.74%) for the first sub-period, 0.88 to 5.76 x 10^6 m^3 (2.38% to 15.58%) for the second sub-period and 0.32 to 5.84 (0.84% to 15.79%) for the third sub-period. For most of the models the inter-quantile range partially overlap with the one of the observed data, also meaning mostly a decrease in subsurface runoff.

When comparing the temporal change for each selected model, similar trends are indicated. Most models present reduction of subsurface runoff in water amount during the second and third sub-periods compared to the first sub-period and the observed one. Consequently, the increase irrigation water demand and reduced precipitation will decrease the water amount of subsurface runoff to the lake towards the end of the century for most models.

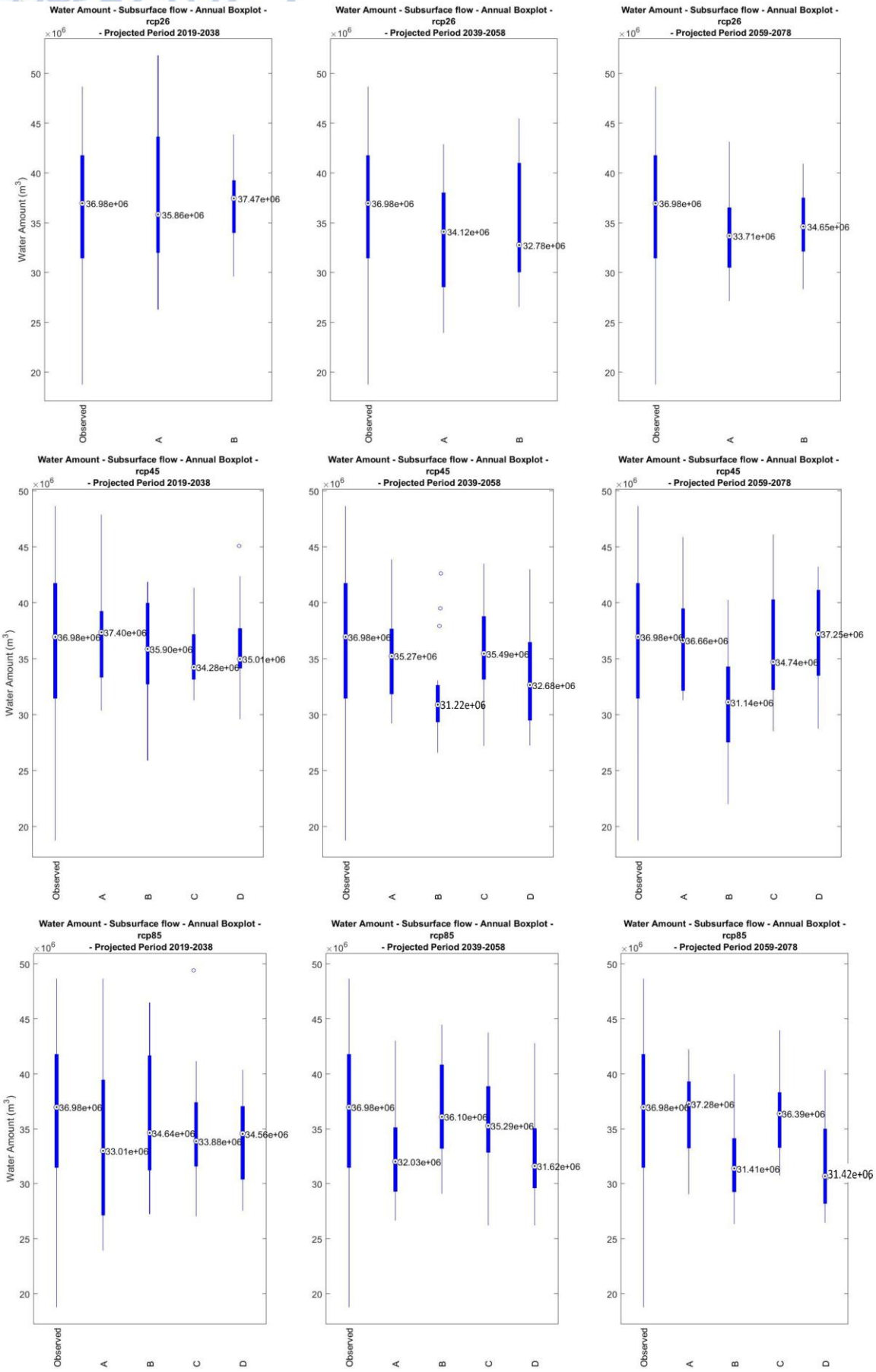

Figure 83 - Box-plots of annual sub-surface runoff amount variation at Kastoria basin according to the results from the ten selected RCMs for the periods 2019-2038, 2039-2058 and 2059-2078

4.7.2.5 Outflow from Kastoria Lake to Gkioli stream

Outflow from Kastoria Lake to Gkioli stream was calculated with the procedure described at the beginning of section 3.8 with the FEFLOW program. The observed precipitation used at this assessment were during 2000-2018 in contrast to the ones used for the bias-correction procedure (1986-2005) as at section 3.7.

Annual temporal variation of the outflow from Kastoria lake to Gkioli stream was assessed for the three sub-periods and compared to the median total annual outflow of the control period (2000–2018), which is 51.34 x 10^6 m^3 and the results are illustrated in Fig. 84. The general point of the results illustrated in Fig. 84 is that this specific outflow reduces throughout the projected period compared to the observed period. Models RCP 2.6 A, RCP 4.5 A, B, C present a slight to moderate increase for the first sub-period, while RCP 8.5 A present that slight increase at the second sub-period and a moderate increase during the third sub-period by 6.43 (12.52%). The rest of the models and the corresponding sub-periods present a reduction of 0.04 to 5.88 x 10^6 m^3 (0.08% to 11.45%) for the first sub-period, 1.89 to 15.81 x 10^6 m^3 (3.68% to 30.79%) for the second sub-period and 2.56 to 13.71 x 10^6 m^3 (4.99% to 26.7%) for the third sub-period. For most of the models the inter-quantile range partially overlap with the one of the observed data, also meaning mostly a decrease in total runoff.

When comparing the temporal change for each selected model, similar trends are indicated. Most models present reduction of total runoff in water amount during the second and third sub-periods compared to the first sub-period and the observed one. Consequently, the increase in irrigation water demand, reduced precipitation in terms of recharge to aquifer and the surface of the lake by direct recharge, increased evaporation will decrease the water amount of total runoff to the lake towards the end of the century for most models, even by a slight to moderate increase in surface runoff, as described at the previous section. This reduction, however, only reduced the ample amount of total runoff meaning that the water level of lake Kastoria will still be between the pre-defined range given proper management.

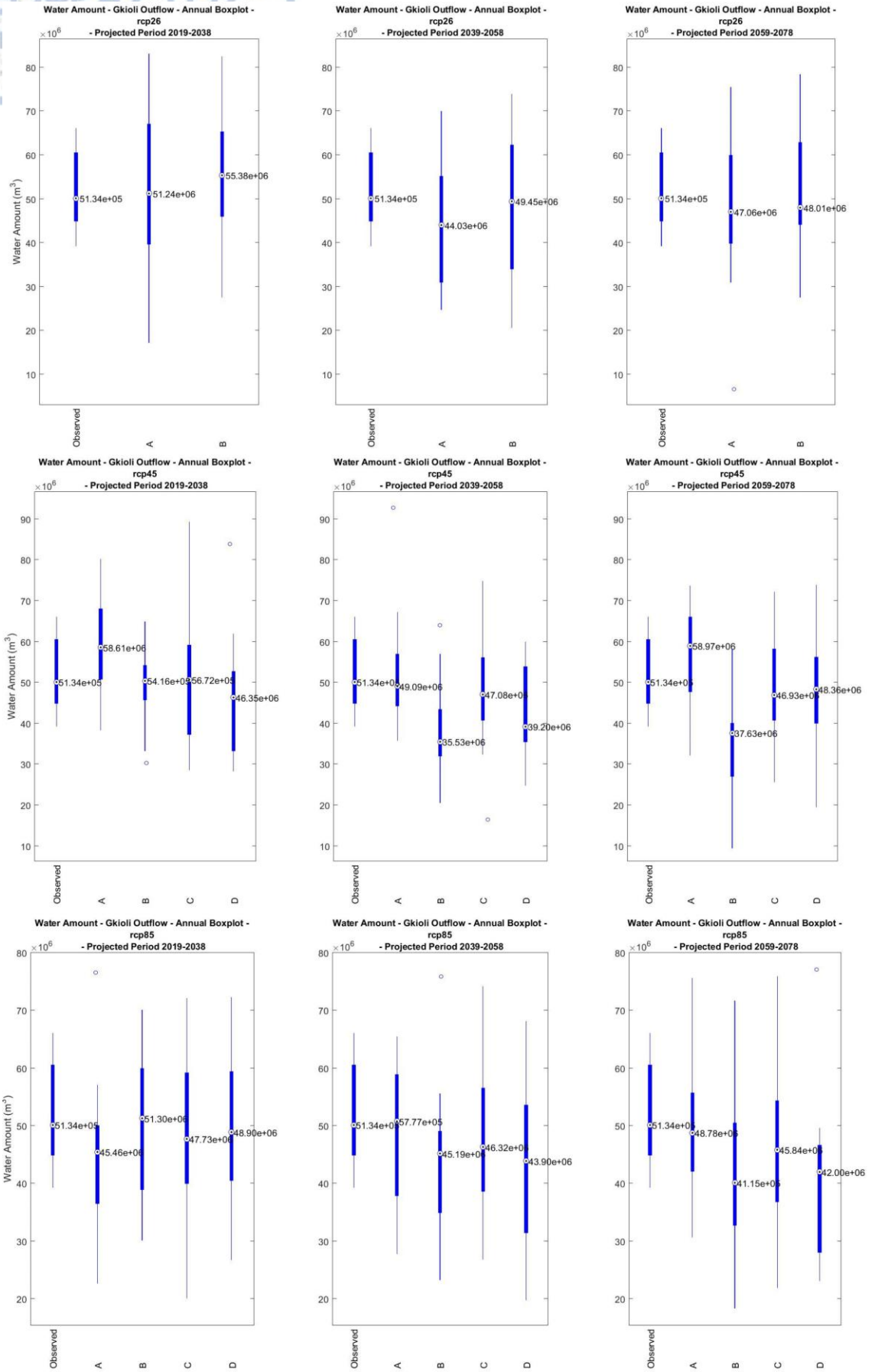

Figure 84 - Box-plots of annual total runoff amount variation at Kastoria basin according to the results from the ten selected RCMs for the periods 2019-2038, 2039-2058 and 2059-2078

4.7.2.6 Guide scenario

A rational groundwater management plan was examined in total, under which the abstracted volumes will not significantly and permanently reduce the water table level of the alluvial aquifer of Kastoria. In parallel, irrigation practices will gradually change to trickle irrigation, thus reducing irrigation returns to 5% of the applied irrigation water. As discussed earlier, this way the expected groundwater abstractions will be also reduced slightly. Observation of Fig. 69 - 78, suggests that under this groundwater management scenarios practically no problematic areas are predicted to occur; thus, all the existing productive boreholes will remain fully operational. At the area of the bulk of the public irrigation network's boreholes the water table level will be reduced slightly below the set minimum only for two models. This happens due to increased irrigation needs. However, this won't be a potential risk for the far future (towards the year 2078) viability of the boreholes located there. Also, because of the limited extent of the study area it is suggested that at a minimal socio-economical hence political cost will come forth which the decision makers will be able to regulate groundwater abstractions there, thus ensuring the long-term viability of the existing installations. Such a regulation can be succeeded by swapping to crops that have lower irrigation needs.

As it follows from the discussion above, under the existing borehole configuration, the guide scenario is the viable groundwater management plan, which ensures long-term sustainability of the groundwater resources and consequently uninterrupted development of that economic element of the study area. As discussed earlier, this management plan does not allow for any increase of the irrigated land under the currently cultivated crop scheme, due to the fact that such an operation does not form part of the future development policy plan of the region and was therefore not examined in the current study. Should alternative crops that have reduced irrigation needs were considered, the total irrigated land could increase without any subsequent increase in the abstracted groundwater.

Study of the predicted piezometry at the end of the projected period, suggests that a vertical downwards hydraulic gradient will have been developed only to the area of certain irrigation boreholes of the public network (Fig. 69-78). This, however, is not permanent and disappears until May of the next year. Moreover, analysis of the water balance elements of the lake Kastoria showed that increased evaporation and decreased subsurface inflow to the lake will decrease the total runoff of the basin but it will not reduce the water level of the lake as a result, due to the latter is being regulated by the Municipality of Kastoria. Reliable study of the likelihood of the occurrence of this phenomenon would require expansion of the model to 3D coupled with the surface water elements of the basin, especially to the lake itself.

CHAPTER 5. CONCLUSIONS AND PROPOSALS

5.1 Summary

It has been shown that a substantial aquifer system is present in the basin of Kastoria, the resources of which cover most of the irrigation demands or the agriculture practiced in the region. The available geological, hydrological and hydrogeological data are moderate in quantity at certain parts of the modelled area and with limited quality because some of them like the torrent Xiropotamos discharge data are of limited temporal extent and non-standardized. However, using this information it has been shown that a conceptual understanding of the mechanisms involved in the groundwater flow evolution and exploitation was possible to be developed. Based on the developed understanding, the existing databases that were used to build a comprehensive numerical groundwater flow model, which was able to astutely simulate the flow mechanism of the study, as showed by the statistical analysis of the transient simulation, despite the uncertainty involving flow mechanics and groundwater abstractions. PEST was employed to alleviate some of this uncertainty, thus, producing a global RMSE for the entire simulation period that equals to 0.785. Consequently, it has been demonstrated that the FeFLOW groundwater modelling system can be effectively used in planning a viable water management policy which ensures the long-term groundwater resources sustainability of the studied aquifer system; thus, securing the economic growth of the region. In addition, to ensure the long-term groundwater resources sustainability of the studied aquifer system RCM results were extracted from the EUROCORDEX project. The results are of high resolution, and it was believed that those RCM results will be able to represent future climatic pattern at the study area. Ten RCMs were selected because after bias-correction it is proved that they can represent future climate patterns at the study area, as shown by the corresponding Taylor diagrams there is an improvement of the correlation coefficient by at least 0.03 mm/day in precipitation and at least 0.01 unit of temperature. Future climate characterization as per Mavrommatis, 1980 will practically remain the same as it today i.e sub-humid with severe winters. Precipitation will reduce by mean annual values of 44, 48 and 53 mm for each sub-period (or by 5.52%, 6.04%, 6.62% respectively) and temperature will increase by mean annual values of 1.08°C, 2.57°C and 3.71°C for each sub-period. However, these projections cannot be verified and bear an increasing amount of uncertainty towards the future (Chapter 4). These flaws are inherited from the way RCMs are made.

The examined area presents most of the rock formations found at W.D GR 09 and its was brought to its current form by three tectonic events. The alluvial aquifer system of Kastoria is of fluvio-torrential origin bearing the general characteristics of the alluvial basins of Water District GR 09 as well as most basin of Greece, in terms of general hydrogeological characteristics and data availability. It therefore follows that the current model implementation can be applied to most alluvial aquifer systems located at Greece. The workflow followed in this study provides a standard for the studying of similar environments in the country and subsequently for the development of an approach that will enable the planning of an effective and viable long-term groundwater resources management policies. Such planning is more essential now than ever before because of climatic changes that have resulted in intensified exploitation of the available resources at Greece. A viable long-term groundwater management policy will ensure the sustainability of the resources and consequently it will secure the development and economic growth of the country.

5.2 Conceptual model

A key aspect in the implementation the management of groundwater resources is the development of a conceptual model of the groundwater flow evolution of the studied system. In this case alternating layers with moderate vertical and lateral hydraulic connection can be simulated as one layer. This is further supported as a true fact because this setup of layers created an unconfined aquifer. The main recharge element of the alluvial aquifer of Kastoria is precipitation, due to the high infiltration rate of 15.8%. The Korissos karst system in the southeastern margin of the basin recharges the south part of the aquifer in addition to the precipitation recharge. The torrent Xiropotamos proves a moderate hydraulic interaction with aquifer, as proved by the current model implementation. by being recharged from the aquifer for most of the year because of the high water table level, while the rest of the year, namely autumn, the torrent recharges the aquifer because of the water abstractions during the irrigation period. Also, the water table level will drop more significantly during the irrigation period but due to the still significant infiltration rate the annual water table level range will largely remain the same of 0.5 to 2.5 m compared to the current one 0.5 to 2.1 m, excluding extreme drawdown that are found locally at the boreholes of the public irrigation network.

As a result of the intensification of the exploitation regime due to climate change, torrent Xiropotamos will most likely recharge the aquifer at most times opposed to the current hydraulic interaction. Direct recharge from precipitation will reduce and water abstractions will intensify as a result of higher evapotranspiration rates reducing slightly the water table level and the lateral flow that recharges the lake. Korissos karst system will still provide the steady flow flux of 7,058 m^3/d that provides today towards the end of the century but its water reserves will be reduced. Also, this reduction in precipitation could possibly affect the two springs that are found there. Kastoria lake water level will drop, if left unchecked, due to higher evaporation i.e mean annual values of 3.79, 4.64, 5.06 x 10^6 m^3 for each sub-period respectively (or by 13.06%, 15.97%, 17.41% respectively), reduced precipitation i.e mean annual values of 3.17, 3.99, 3.64 x 10^6 m^3 for each sub-period (or by 16.14%, 20.36%, 18.54% respectively) and lower lateral flow volumes from the alluvial aquifer of Kastoria i.e mean annual values of 0.48, 2, 1.6 x 10^6 m^3 for each sub-period (or by 1.34%, 5.4%, 4.43% respectively). Extreme precipitation events will mainly increase as will surface runoff as consequent, as also proposed by many previous studies and the current one i.e mean annual values of 1.3, -0.38, 0.17 x 10^6 m^3 for each sub-period respectively (or by 4.34%, -1.25%, 0.56% respectively). This will probably increase the inflow of solid material to the lake reducing its capacity as a water reservoir. Finally, the overall decrease in mean annual total runoff or discharge volume to river Aliakmonas through the Gkioli stream will be 1.89, 6.7, 5.87 x 10^6 m^3 for each sub-period (or by 3.6%, 12.79%, 11.2% respectively).

The economy of this particular region is based on irrigated agriculture the demand for which is covered by groundwater abstractions. The designed numerical model verified the developed conceptual model in terms of representation of the main groundwater flow mechanisms involved in both the evolution of the system and its hydraulic parameters. This adds to the defendability of the value of the model as a tool by proving its usefulness and effectiveness for the management of the groundwater resources of the system for which it was intended.

5.3 Proposals for future work

During the course of the current research it became apparent that the elaborated results could have been enhanced by the use of additional high-quality data. Towards this direction, the following steps are proposed to be taken:

- Several stage gauging stations, that comply with the norms set in the literature, must be placed at the junctions of the torrent Xiropotamos in order to provide accurate, consistent and frequent data. This is considered to be essential for the realistic calculation of transmission losses and the rational management of the river water and its material load during flooding
- The current 2D model implementation must be expanded to 3D to also assess the quality of the groundwater not only because safe, clean irrigation and drinking water must be provided but also because Kastoria lake is a protected part of the local ecosystem; thus, its evolution must regulated, according to the norms set by various environmental protection agencies, and kept safe for future generations
- Monitoring of the soil moisture deficit and calculation of the root constant and the wilting point of the cultivated crops, complemented by daily or ten days potential evaporation data would enable setting up a soil moisture balance model which would provide a detailed study of the recharge from precipitation and from the irrigation returns. The results from such a study would improve the quality of every designed model and would also provide indications of the groundwater resources pollution risk from the low-quality irrigation return waters.
- Development of an effective groundwater abstractions monitoring plan is imperative to all safe management scenarios. Inadequate knowledge of the abstracted volumes limits the reliability and effectiveness of any designed water resources management policy. A detailed inventory of the production boreholes should be created and flow meters should be installed and monitored.

Materialization of the above discussed proposals would require the investment of a large capital. However, continuous monitoring of quality data is essential for the frequent update of the developed numerical model, if its integrity is to be maintained. It should be reminded that a reliable model is a valuable tool for the design of viable groundwater management policies that can guarantee the long-term sustainability of the resources, thus, ensuring the socio-economic development of the region.

Further extension of the conducted research could include the following:

Based on the developed mathematical model as well as its further expansion to 3D, it is proposed that an model implementation must be undertaken to examine the feasibility of an augmentation scheme of the lake, in which the reduction of the water level Kastoria lake will be recharged with a part of the discharge of the River Aliakmonas during the wet months. One other measure is to construct small dams and then pump the water from their reservoir to the lake and the aquifer after ensuring that is without sediments. This water taken from the reservoir of the small dams could also be used to artificially recharge the alluvial aquifer system through the existing, or new purpose-built injection boreholes. Such a scheme could potentially establish a new balance in the system, thus providing the means to support the optimal management of the irrigated land. A number of constraints however have to considered in order to assess the viability of such an operation, including the quality compatibility of the river water with that of the lake and the groundwater, the construction and maintenance cost and the life expectancy of such an endeavor.

The results of the RCM-based predictive scenarios indicated that in the future the studied system will present slightly larger water table level range of the alluvial aquifer system of Kastoria accompanied with a reduced lateral flow flux to lake. Groundwater flow modelling is an intriguing though time consuming task as likewise is its constant updating which is essential in maintaining its integrity. A geographical information system (GIS) could enhance

and shorten this procedure by automating the calculation of the hydraulic stresses applied to the model, due to the fact that the studied system is not a complex one. Development of an automated interface between this system and the groundwater flow modelling package used in this study will result in a powerful and time efficient integrated platform, which would considerably simplify the task of modelling and provide better control over the modelled parameters, thus rendering it an even more appealing water management tool.

APPENDIX A. Western Macedonia Water District (GR 09)

The Water District of Western Macedonia (GR 09) is found at the northeastern part of Greece and borders, geographically, with FYROM at the north and in the east, from north to south, it is bordered by Mount Paiko, the Mid-Hellenic Trench and the Thermaikos Gulf. Mounts Olympos, Kamvounia mountain range and Hasia border with GR 09 at the south, from east to the west. Lastly, at the west, from the south to the north, it is bordered by Mounts Lygkos and Voio and the Greek-Albanian border. Also, regarding its relative position to rest of Greece, of Central Macedonia (GR 10) is at the east side, of Thessaly (GR 08) at the south and of Epirus (GR 05) at the west. It consists of seven regional units, namely R.U Grevena, R.U Imathias, R.U Kastoria, R.U Kozani, R.U Pella, R.U Pierias and R.U Florina.

Water District GR 09, includes Aliakmon basin and Prespa Lake, presents complex geological, tectonic and hydrogeological regime as it includes four tectonic units, which from the west to the east are: a) Pindos zone with Mount Grammos, b) the Sub-Pelagonian – Pelagonian zones in Kastoria and a small part of the Mid-Hellenic trench, c) the bulk of Mid-Hellenic trench in Grevena, d) the Pelagonian zone in the regions of the Prefectures of Kozani, Florina and the area of Almopia, which is its Sub-area Axios area on Vermio mountain. The stratigraphy is complemented, at its upper part, by the molassic sediments of Mid-Hellenic trench, the Neogene deposits and Quaternary deposits.

Tectonic setting and stratigraphy are important factors both in the development of aquifers and springs but also in the general groundwater movement. The tectonic units, mentioned above, influenced the creation of underground aquifers in a different way either due to particular tectonics or due to of their particular stratigraphy. Extensive karstic aquifers are found in the Pelagonian unit area, due to the existence of Triassic-Jurassic karstified limestones that discharge their water supply from karstic springs i.e. in the area of Kastoria (springs of Korissos, Germas, Graves, Koromilia, Dodlikas etc.). The same phenomenon happens in the Prefecture of Kozani, where karst aquifers developed in the aforementioned Triassic-Jurassic limestones discharge to a large extent in the county of Edessa (karst springs of Voda and Agra) as well as in Kozani in the underwater karst springs of Neraida, which today are covered by the waters of the artificial lake of Polyfytos. At the Mid-Hellenic trench, in the regions of Grevena, the south part of the Prefecture of Kastoria and in the western part of the Prefecture of Kozani, there are no groundwater aquifers of any kind because the rocks of the Molassic sediments are non-permeable. Almopia zone, found partly in the prefectures of Kozani and Imatheias - Pellas at the Vermio mountain, consists of large masses of limestone and carbonite conglomerates, which have been placed by tectonics on top of the impermiable flysch. The inclination of the bedding of these formations leads the groundwater to the east. The aforementioned limestones extend largely to the Vermio mountain. Extensive karstification allowed for karst aquifers to develop, which discharge at the springs found at the east foot of mount Vermio.

Large and extensive alluvial aquifers exist in the Quaternary formations deposited in the major tectonic basin of Ptolemais, in the basins of Florina, Kastoria, Grevena, while in the Neogene formations aquifers are have a low porosity.

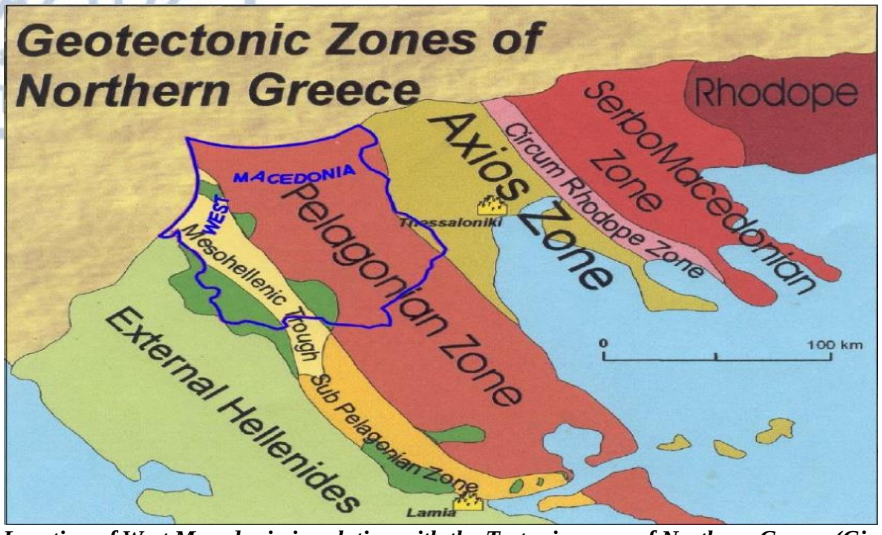

Figure 85 - Location of West Macedonia in relation with the Tectonic zones of Northern Greece (Gianneli, 2009)

A.1 Lithology of WD GR 09

The geological formations that make up the area, from younger to older, are described below and presented in Fig 2. (modified after IGME, 2010).

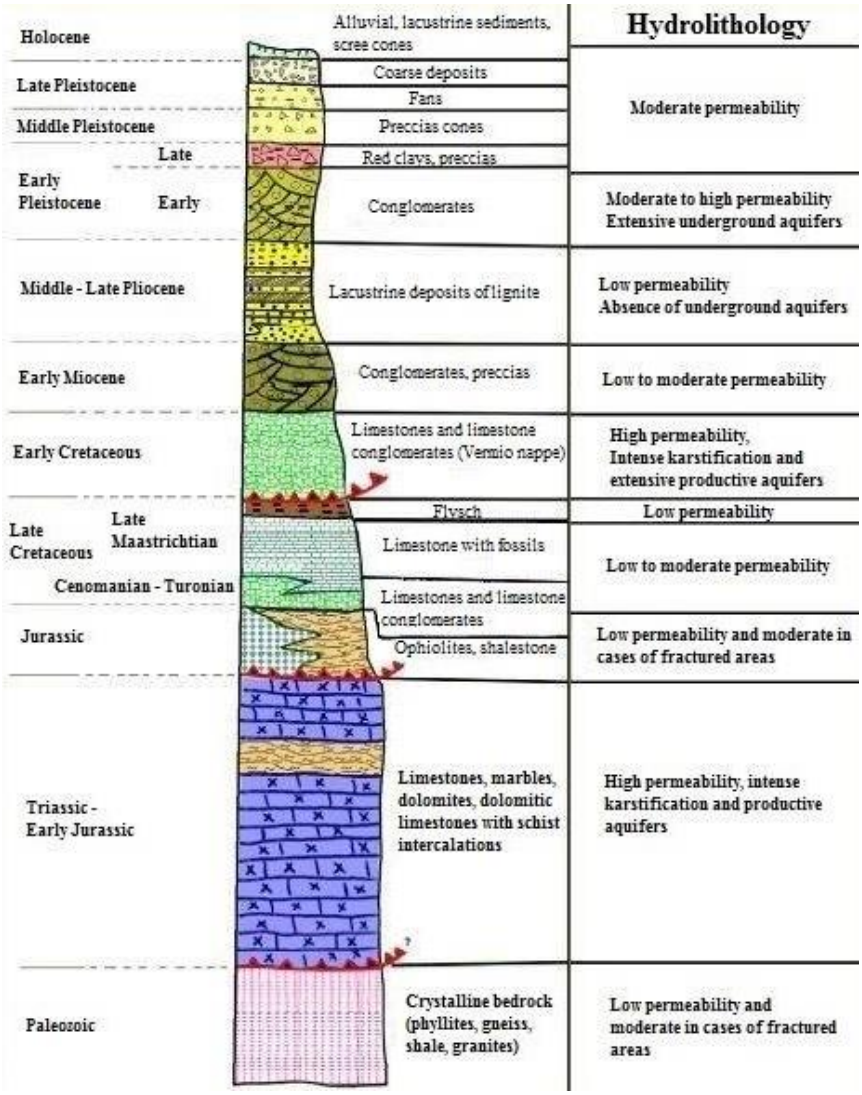

Figure 86 - Synthetic Stratigraphic Column of W.D GR 09

A.1.1. Silting and fluvio-torrential deposits of the Quaternary

The Quaternary deposits consist of fluvial deposits that include clays, sands with a small or large percentage of fine grain materials and screes. The Quaternary deposits include modern deposits with inconsistent materials (sands, clays, pebbles) found in riverbeds and fluvial torrents. At places of gentle morphology, the outskirts of the Neogene basins, old and modern screes, fluvio-torrential deposits, conglomerates, sandstones, sand are found. The fluvio-torrential deposits are with varying degrees of consistency and overlap the molassic formations along with the Neogene formations. Their average thickness is approximately 100 m. They cover large sections of the basins of Kozani, Ptolemaida, Kastoria, Grevena, Florina and one either side of river Aliakmonas.

In these deposits extensive alluvial aquifers were developed, which have a high productivity and due to that they are utilized for water abstraction. This activity, however, causes the water table level to drop; thus, presenting a decline in water reserves.

A.1.2. Neogene Lacustrine deposits

Those deposits consist mainly of marls, clays and marly limestones, with interferences of sand and gravel of small extent. Aquifer of very little significance develop only inside the intermediary layers of gravel. These deposits occupy small areas in WD GR 09. The Quaternary deposits overlap and completely cover these formations.

A.1.3 Quaternary sediments

Tectonic activities caused the upward and downward movement of the W. D's regions after the deposition of Neogene sediments, during early Pleistocene. New trench-like sub-basins and crevasses were created and so began intense weathering and then erosion, both in the outcrops and in the high-mountain ranges which created new abundant material, ranging from gravel to clay, silt and sand to be deposited on the existing sediments in the area. These materials consist the Quaternary fluvio-torrential deposits and the alluvial fans of the sub-basins. Many times, these deposits caused the river bed to move their position along with their carrying capacity. This phenomenon formed crossed layers that overlap unformibly on the Pleistocene deposits.

Quaternary sediments consist of alternating intercalations of conglomerates, either loose or consistent, sandstones, sand, clay with gravels, whose consistency range from carbonate, shale, ophiolithic, chert depend on their source rock. The erosion of the weather material from the and the neighboring mountain ranges continued to take place resulting in the thick Quaternary sediments, which appear in the sub-basins of the southern field of Ptolemaida, Amynteon, Galatea - Olympiada and in smaller sub-bastions that today constitute the homonymous alluvial aquifers.

A.1.4 Neogene sediments of the Mid-Hellenic Trench

The Neogene deposits occur only superficially on the rocky outcrops and are a few meters thick. These deposits were deposited after the creation of the Great Tectonic trench that starts south from Servia, Kozani and continues up north reaches up to FYROM. These consist of three distinct categories, as dictated by the studies of the Lignite Research Directorate of IGME:

i. the upper row (overlaps the lignite)
ii. the Lignite-rich series

iii. the lower row (underlying lignite)

A.1.5 Molassic sediments of the Mid-Hellenic Trench

The molassic formations consist of the Tsotyli, Pentalofos, Eptachorion, Tsarnos series, that were deposited in the Mid-Hellenic Trench. These series generally consist of marls, clays, conglomerates, breccias and sandstones in an alternating scheme. Those sediments extend below the Quaternary and Neogene deposits and have great thickness. They cover a very large area, mainly in the prefectures of Grevena, Kastoria and Kozani. Aquifers does not exist in these formations because they do not have porosity of any kind. Their hydrogeological significance lies in the fact that they are impermiable layers, which act as regulators of groundwater movement and storage of overlying fluvio-torrential deposits.

A.1.6 Flysch

Flysch has a large spatial extent at the W.D GR 09 and is found in relatively large areas in almost all the tectonic zones, Sub-Pelagonian, Pelagonian and the Almopia zone. It consists of a variety of rocks like sandstones, conglomerates and marls. It is of none hydrogeological interest since it lacks porosity. However, it is responsible for the creation of the overlying karst aquifers at Mount Vermio, as well as in the movement of the underground because its eastern wise slope guides the groundwater to springs that are located at the eastern side of mount Vermio.

A.1.7 Heterochonous limestones and carbonate conglomerates of Mount Vermio

Those limestones are of Cretaceous age and are part of Mount Vermio nappe. They exist onlap of Pelagonian zone and consist mainly of them limestones and limestone conglomerates, whose gravel are exclusively come from the white Triassic-Jurassic marbles of the Pelagonian zone. They occupy a very large area and have a large thickness at the location of Mount Vermio mountain. They also are strongly karstified so they have a very large porosity. Because of this, extensive karstic aquifers develop at their mass. These limestones belong to the area of Almopia and are thrusted upon the flysch of the Pelagonian zone, which is impermiable as mentioned earlier.

A.1.8. Cretaceous limestones of pelagic, sub-seminal and belt Axios

The appearance of these limestones is of small extent in all the tectonic units of the W.D GR 09. They are onlap and have a lot of different clastic materials in their body i.e. rudders limestones, marly limestones, neritic phase limestones with fragments of rudders and gastropods. They appear plated and dark-gray with lenticular intercalations of sandstones and clay shale and have not been karstified to a large extent. In West Vermio, the lower layer of these limestones is composed from marly limestones, which do not have any porosity.

A.1.9. Ophiolithic complex

It consists of a wide range of rocks such as ophiolithic conglomerates, doleritic breccia, serpentinite, dakites, diorites, andesitic, basaltic, diavasic lava, gabbro, pyroxenites, peridotites, dounites. These ophiolithic rocks appear mainly in Pindos and Pelagonian zones at the mountain ranges of Vourinos and Pindos and are considered to be thrusted on top the Triassic-Jurassic limestones. They have no porosity except at the tectonic discontinuities and

at the fracture's zones. These rocks are heavily fractured with fractures, which are either open or clogged with sediments.

A.1.10 Triassic-Jurassic limestones

The Triassic-Jurassic limestones consist of limestone, dolomitic limestones and dolomites, unpaved or thick-bedding of varying degree of recrystallization. They exist on a large area on Mount Vermio, Aschio, Mount Vorra, Pieria mountains, mountains of Prespa and Vernos, Kastoria. Their most important characteristic is that they are karstified to a great extent. In the Triassic-Jurassic series, we see white-ash, ash, white, black limestones with varying degrees of recrystallization, either thick or unpaved and thin-layered, white marble, and dolomitic limestones. They are heavily fractured and karstified, with interference of shales at northwest side of Mount Vermio. The various lithological types of these carbonate rocks do not appear as distinct horizons that develop from the older to the younger horizons, but they alternate irregularly. Each such alternation corresponds to changes of sedimentation conditions. Their total thickness exceeds 1000 m.

The geologic contact with the underlying crystalline bedrock is a tectonic contact and as presented at Askios and Voras mountains, where the contact is visible. Inside this contact there are many appearances of mylonitis and unconformable stratigraphic contacts in the inclinations of the carbonate nappe with the crystalline basement.

At Askios mountain, in the upper members of the carbonate series, shale-sandstone-chert-like beds of small thickness is entrapped along with ophiolite bodies. Such an appearance lies to the east of Galatenes. At the northwest side of Mount Vermio, Lower Grammatiko - Mesovouno, frequent intercalations can be encountered, as well as ophiolithic appearances as shown by IGME bore samples. At the south side of Mount Vermio, the lower horizons of the limestones, present an intercalation of 100 m thick slate while they overlay white marbles. Summarizing, these limestones appear strongly fractured and karstified, creating remarkable underground water reservoirs with a huge quantity of water reserves.

A.1.11 Crystalline bedrock of pre-Alpine age

The term "crystalline rock" includes a very large range of rocks i.e. schists, gneisses, gneiss slates, granites and other rocks. They inseparably, since they were affected by a number of metamorphic and tectonics events that move and transform them to their current, consisting of:

A.1.11.1 Slightly metamorphosed system

It consists of slightly metamorphosed conglomerates, sandstones and arkoses, that gradually changes to phyllites, greenschists and schists of various types, such as chloritic, sericitic, muscovitic shales, etc. The rock formations of younger age are fine-grained meta-sediments and contain traces of basic volcanoclastic rocks. It is believed that the volcanoclastic materials gave greenschists after metamorphic events that give sinologists. In several areas, intercalations of semi-crystalline limestones of 5-10 cm thickness are observed.

The main mineralogical components of these rocks are quartz, sericite, chlorite, muscovite and albite. The formations of the slightly metamorphosed system are usually on top of the formations of the strongly metamorphosed system.

A.1.11.2 Strongly metamorphosed Crystal-Paleozoic system

They occupy the upper horizon of the system except them schists. This system includes in a smaller extent cipolines, marbles, serpentinites and quartzites. They overlap ortho- and para-rocks, either with a conformity or not. Main mineralogical constituents are: quartz, felsic plagioclase, calcite, clinozoisite, biotite, muscovite, calcite, graphite at various proportions.

A.1.11.3 Gneisses

They occupy the lower horizons of the system and consist mainly from ortho- and para-gneisses with intercalations of slates in the form of lenses or beds layers and partly by amphibolites. The ortho- gneisses are characterized by granoblastic to porfyro-like microstructure and consist of quartz, feldspars and muscovite. The para-gneisses consist of quartz, felsic feldspars and muscovite. Amphibolites consist of amphiboles and epidote.

A.1.11.4 Granite Gneiss

It is a petrological zone that corresponds to the lower members of the strongly metamorphosed system. They have a gneiss to schist-like microstructure. The main minerals are: quartz, alkaline feldspars, felsic plagioclases and sericite. Secondary minerals are: muscovite, epidotite, alanite, titanite and metallic minerals.

A.1.11.5 Aplitic Granite of the Pyli, Florina (Plutonian Rocks)

Its main feature is that the minerals of this formation are almost completely felsic. It occurs in the form of small tectonic appearances at the area of the village of Pyli. The geologic contact, in some positions along, with the oldest rocks in the area show evidence of mylonitization. It presents granoblastic microstructure and oriented texture close to his contacts with the other rocks of the area. The main mineralogical components of this granite are quartz, alkali feldspars and felsic plagioclase.

A.1.11.6 Coarse-grained to porphyrous meta-granite

It intrudes the rocks of the Paleozoic basement and is characterized by intense fracturing and weathering. In some regions, it also intrudes into the Triassic-Jurassic carbonate rocks. Its schism increases in intensity from the inside to the outside and its main mineralogical components are quartz, K-feldspars (microcline, orthoclase), plagioclase, green hornblende and biotite. Secondary minerals are the epidote, sericite, chlorite, apatite, zircon and others.
Particular features of these rocks are:

- perthitic intergrowths of K-feldspars
- varying degree of chemical weathering of plagioclases
- intense tectonic deformation of its minerals
- recrystallization mainly of quartz and filling of discontinuities with fine-grained material
- appearances of stilpnomelane in a small or large proportion

In some areas, these rocks can be found arenitized and as arenites, a group of rocks with granular texture. Their composition comprises of various sized crystals of quartz, perthitized K-feldspars, sericitized plagioclase and phyllosilicate minerals. The arenitization

was induced by the intense tectonism, which influenced those granite rocks, and can reach up to the creation of mylonitis.

A.1.11.7 Amphibolitic and/or biotitic granite-granodiorite-monzogranite-diorite

A large group of rocks that extends to almost the whole area between Florina, Posideri and Agios Germanos. These rocks intrude or are found underlying the strongly metamorphosed system. They have granitic microstructure and are coarse-grained with a varying degree of composition from granite to diorite. They consist predominantly of quartz, K-feldspars, plagioclase, biotite and green hornblende. Secondary minerals are the muscovite, epidote, titanite, rutile, apatite, zirconium, etc. This formation is of Late Permian – Early Triassic age.

They are characterized by:

- perthitic intergrowth of K-feldspars
- slight to intense weathering of plagioclase
- tectonic deformation of its minerals
- recrystallization mainly of fine-grained biotite and quartz

In the zones of open cracks and diaclases resulting from fracturing, are secondary porosity and can provide a satisfactory quantity of water, i.e. in Dasochori, Grevena and, to lesser extent, in Deskati area, a competent such aquifer can be found that can provide a significant water supply of up to and 80 m^3/h. The fractured metamorphic formations and granites of Varnounta, which appear mainly on Mount Varnounta between Kastoria and Florina, can also provide an ample amount of groundwater.

A.2 General Morphology of Water District GR 09

The Western Macedonia Water District is located in the northwestern part of the Greece and borders with Albania and FYROM and has an area of 13,650 km^2. It consists of the Prefectures of Kozani, Grevena, Kastoria, Florina and the western part of the prefectures of Pella, Pieria and Imathia in the region of Central Macedonia.

Tectonics have defined the orientation of the mountain ranges, which have an NNW-SSE orientation like the mountains of Mount Vermio in the east, Varnounta-Askio and Vourinos mountains and the northern Pindos with Mount Grammos in the west and the south, which have ENE-WSW such as Kamvounia and Pieria mountains.

Neotectonic events in the area follows the above directions of the orographic axes, created the grabens, i.e. the large tectonic graben of Kozani-Ptolemaida-Florina-Monastery, where the thick sediments of large spatial extent were deposited (Neogene and Quaternary age). The plains of this large trench, with an average elevation of 600 m, south of the mountain range of the Kamvounia Mountains, east and west from the mountain ranges of Vermio, Askio and Mount Varnounta in Florina. In contrast, all the mountain that exist inside this water district have an average maximum elevation of approximately 2100 m.

A.3 Hydrology of W.D GR 09

A.3.1 Climate of W.D GR 09

Greece's climate is affected by climate phenomena induced mainly by Mediterranean Sea and so lies within the Mediterranean climatic region. Pindos mountain range has a northwest-southeast development. This serves as a natural barrier to induced by the wind de-

veloping from the west. As a result of this, the western part of the country receives precipitation of 1000 to 1200 mm annually, whereas the eastern part of the country, where the study area is, receives 400 to 700 mm. Most of the rainfall falls during the winter time. Snow falls happen mainly during the winter but are not rare between December and March (Vafeiadis, 1983; Gianneli, 2009). At this period snowfall is concentrated in the mountainous regions of the country. Data from meteorological stations in Greece suggests that the rainfall occurrence is about 95 days a year and the snowfall occurrence is about 6 days a year (Biel, 1944).

The climate of Western Macedonia differs from the other parts of Greece, due to its overall altitude and morphology. The climate of the region is characterized as continental Mediterranean. It's a temperate climate, with severe winters and mild summers, as opposed to the Mediterranean coastal climate of the country. Its plateaus have a southeast heading and no mountains intersect between them. The winds that blows form the north prevails, thus keeps the temperature at a low level, while creating snowfall conditions during the winter. Although the region of Western Macedonia belongs to the eastern continental part of the country that is characterized by less rainfall than the western one, the climate is more wet due to the combination of mountainous landscape and lakes. According to older bibliographic data, the climate of western Macedonia is transitional between Mediterranean and Continental climate. The climate of Western Macedonia is humid mesothelium, with a distribution of rainfall throughout the year, in accordance to the Koeppen classification. Based on Thornthwaite classification the climate of the study area is characterized as sub-humid deviant to humid, with moderate lack of water during the summer (Vafeiadis, 1983) and finally as semi-humid with severe winter per Mavromattis, 1980 as stated at the Kastoria lake management plans, 2015.

A.3.2 General Precipitation Characteristics of W.D GR 09

The area of the Water Department has been divided into three regions by IGME 2010, based on precipitation characteristics like uniformity of the precipitation distribution and rainfall-altitude association. In general, IGME's assessment of precipitation in the water district concludes that in the eastern region at Mount Vermio mountain range there is a ridge to its east that receives have increased rainfall in contrast to its west side. At the west region, it is concluded that the precipitation increased to the west. Finally, the central region receives a lower amount than both of the other regions. This difference in spatial distribution of precipitation presents that the morphology of the W.D GR 09, along with hydrogeological characteristics like percolations and runoff, plays a pivotal role on the recharge of its aquifers, which can affect water sources and in turn their management plans. The total rainfall amount that the W.D GR 09 receives per year is 9,974,135,193,694 m^3 with an average rainfall of 730 mm.

A.3.2.1 Eastern Region of W.D GR 09

The eastern region of GR 09 includes eastern side of Vermio mountain, Mount Voras and Pieria Mountains. Data received from various stations for 21 consecutive years (1980-2001) show fluctuations in annual rainfall that show periodically lower and higher values of precipitation for about every 2-3 years. Correlation of corrected annual precipitation data yielded the precipitation-altitude equation, which has a correlation coefficient of r=79.37%: Y = 0.4223X+573.94, where Y the precipitations at the respective altitude X. This equation suggests that the precipitation is increased by 42.23 mm per 100 m of elevation.

A.3.2.2 Western Region of W.D GR 09

The western region of the water district includes the area of Mounts Grammos and Pindos. This region receives increased rainfall like the eastern region and present the same fluctuation patterns. For this region, data received, and corrected, from various stations for 28 consecutive years (1980-2008) yield a r = 75.48% correlation equation: Y = 0.9094X + 10.442, where Y the precipitation at the respective altitude X. According to the above equation, the precipitation is increased by 90.94 mm per 100 m.

A.3.2.3 Central Region of W.D GR 09

The central region of the district includes the areas of the plains of Kastoria, Kozani, Grevena and Florina, the mountains of Triklarios, Askio, the northwest side of Vourino mountain, Kamvounia, the western side of mountain Vora and Vermio. The rainfall this receives is lower than the two aforementioned sectors. The fluctuations of annual rainfall follow the same pattern as the previous two regions. Average annual rainfall data yield the following equation for providing the correlation equation for precipitation-elevation relationship: Y = 0.4515X + 238.18, where Y the precipitations at the respective altitude X. The correlation coefficient of this equation r = 77.11%. According to the above equation, precipitation is increased by 45.15 mm per 100 meters of altitude.

A.4.1 General Percolation Characteristics

The rocks found in WD GR 09 are classified in four main categories in terms of permeability (IGME, 2010):

- Rocks with very high permeability, such as the karstified Triassic-Jurassic limestones and marbles, carbonate conglomerates and the limestones of Vermio nappe. The percolation coefficient of these rocks' ranges from 50 to 60%.
- high permeability rocks, such as the fluvial and fluvio-torrential deposits of the Quaternary sediments. Their percolation coefficient is about 20% of precipitation.
- Moderately permeable rocks, such as the fine-grained part of the Quaternary deposits and the slightly fractured crystalline and ophiolithic formations. Their percolation coefficient is about 5%.
- Rocks of very low permeability, such as the Neogene deposits, molassic formations, and most of the crystalline and ophiolites rocks. These rocks are almost impermiable therefore the surface runoff is predominant and reaches about 35%.

A.5.1 General Runoff Characteristics

Percolation and runoff are import factors of hydrology. Surface run-off is only predominant in the areas comprised of the molassic formations, Neogene sediments and the slightly fractured rocks. Most of the Prefecture of Grevena consists of the molassic sediments of the Mid-Hellenic Trench along with a part of the southwestern region of the Prefecture of Kastoria and the western part of the Prefecture of Kozani.

A.4 General Hydrogeological setting of W.D GR 09

The previous chapter describe the hydrological setting of the geological formations of the area of W.D GR 09, which includes and a part of the area of Central Macedonia. The hydrolithological properties i.e. porosity (either primary or secondary) of the rocks define the

movement and storage of water in their bodies and have an important role in the development of groundwater aquifers.

Based on such characteristics, the rocks in W.D GR 09 are divided in three main categories. Those are the karst limestone aquifers formations, the granular aquifers and the fractured aquifers of rocky outcrops and ophiolithic formations of limited productivity. A brief description is given below.

A.4.1 Granular of alluvial aquifers of Quaternary sediments

Quaternary deposits and modern silting materials consist of clays, gravel, breccia and conglomerates, cohesive or loose, sandstones, sands with a small or large percentage of finely grained clay materials with different types of intercalations. The above deposits cover large basins in the Grevena – Kozani area, Ptolemaida, Kastoria, Florina, also in the Aliakmonas, Venetikos and Sioutsa, Grevena rivers. They are mostly fluvial materials which came from the weathering processes that took place at the rock outcrops of the nearby mountain ranges and then transported by rivers and finally deposited on these basins. These formations exhibit significant porosity and they can store a lot of groundwater, especially when the participation of finely divided clay materials is absent or of small extent. Thus, extensive and productive aquifers exist in those formations, i.e in the Ptolemaida tectonic basin, in the Mid-Hellenic Trench, in the Grevena basin, in the basins of the Prefecture of Kastoria, in Florina and in other such places. The thickness of these aquifers varies widely and can reach 120 m with 50 m thick layers. They are productive aquifers, which can provide groundwater with pumping rates that can reach 200 m^3/h. Groundwater is mostly used for agricultural irrigation and industrial uses.

The aforementioned sediments that house the aquifers of Water District of Western Macedonia are found inside the great tectonic trench that begins with Servia, Kozani to up north to Ptolemaida, Amynteo, Florina and continues outside border to Monastir - Prileps of FYROM. These aquifers are of significant importance because they are extensive and are utilized both for water supply, industrial and irrigation use.

During the most recent syn-orogenic phases of neo-alpine folding (Pleiocene), followed by extensive fracturing faults of great length were created with an orientation of NW-SE to NNW-SSE. These faults created large grabens from Kozani to Florina and FYROM, where today constitute the tectonic trench that houses the aquifers of Water District of Western Macedonia.

After the deposition of Pleiocene sediments, the tectonic evolution further broke down this large graben into smaller ones i.e. Kozani-Servia, Sarigiol, Ptolemaida, lake of Petronas-Limnohori, Florina, which are separated from each other by the rift outcrops of the Koilon-Galanis, Komanos - Ag. Christoforou, Vegoras marsh. These outcrops provided all the clastic materials that fill those smaller grabens.

A.4.2 Karst aquifers of limestone and marble rocks

The limestones and marble appearances of the Pelagonian and Sub-Pelagonian zone have a great extent and a large thickness. They are found at Mounts Vermio, Voras, Pieria, Korissos, Verno and Triklariou Kastoria, Prespon. The various lithological types of these carbonate rocks do not appear as distinct horizons that develop smoothly from the older to younger but alternate irregularly, as a result of changes in sedimentation conditions and their total thickness exceeds 1000 meters. They are heavily fractured and karstified. Karstification is observed in various karstic forms such as sinks, caves etc.

Borehole drilling in the areas of the Perdika Dam, Komnina, Antigono, Pyrgoi, Pelargos, Lofoi, Veroia and elsewhere, revealed large cavities where the drilling mud got channeled in so it was not recovered. Karst structures also found at these rocks like dolines, uvalas and poljes. Internal karst cavities along with the existence of an underlying impermeable layer, which is a flow regulator, act as underground water storage. For example, at the northwest Vermio Mount these formation house extensive and highly productive aquifers with annual renewables amounts of 150 x 10^6 m^3 and a water table level at +510 m. The Sarygiol basin is mainly surrounded by the Triassic-Jurassic limestones, in which a very productive rich underground aquifer is found with a water table level at +290 m.

Apart from the aforementioned Triassic-Jurassic limestones of the Pelagonian and sub-Pelagonian zones limestone conglomerates of Cretaceous age and limestones of the Vermio nappe are also found in the area of W.D GR 09. Those limestone conglomerates consist mainly of limestones and gravel of the white Triassic-Jurassic marble of the Pelagonian zone. They occupy a very large area and are very thick at the Vermio Mountain. Also, they have undergone a severe karstification process as mentioned above; thus, developing extensive aquifers. These limestones formations belong to the Almopia zone and are thrusted on the flysch of the Pelagonian zone, which is an impermeable formation. The dip of the underlying flysch in its large extent inclines eastward so it guides the stored water of the overlying aquifers of these limestones eastward and is discharged at the eastern karst springs of Vermio Mount such as Agios Nikolaos of Naoussa and Agra spring of Edessa. However, at the west side of Vermio Mount, the same aquifers are of smaller extent; therefore, less productive. Evidently, these rocks are of great hydrogeological importance for W.D GR 09.

Finally, in the W.D GR 09 the indigenous Cretaceous age limestones of the Pelagonian zone are also found. The extent of these limestones is small in all three geotectonic zones of the Water District, therefore of small productivity. They do not have undergone significant karstification except at fractured zones, where a small degree of karstification is found. In the west side of Vermio mount, marly limestones with no significant porosity are found. In the North-West Vermio Mountain, the Cretaceous limestones of Pelagonian zone are in contact with the Triassic-Jurassic limestones. They present karstification and are a single hydrogeological unit with the aquifers of the Triadic-Jurassic limestones.

A.4.3 Fractured aquifer of the ophiolithic and crystalline rocks

Ophiolitic and crystalline rocks do not have primary porosity but only secondary porosity existent at discontinuities. These rocks are fractured at almost their entire extent, sometimes found with clogging material inside the fractures. The volume of the clogging material varies with depth. For example, at the places within the fractures where chemical weathering takes place from the surface and up to a certain depth the fractures are open, filled mostly with opal. In greater depth serpentinization occurs; therefore, the fractures are filled with serpentine. Serpentine comes from olivine, which absorbed water in its structure. This causes swelling and clogs any voids by swelling. Consequently, the chemical weathering-serpentinization relation in the ophiolithic formations play an important role in the groundwater circulation and therefore, sets appropriate conditions for the development of aquifers of small productivity that can cover the water supply of small municipalities.

Crystalline rocks also do not present any primary porosity but develop secondary porosity due to the tectonic strain that fractured the rock in a similar fashion with the ophiolithic rocks. However, there are areas where those formations behave like permeable formations having significant porosity with discharge rates reaching 100 m^3/h. For example, an area of significant extent with these rocks is the area of Dasochori Grevena in Deskati, where a high

productivity aquifer exists with annual renewables of 10 x 10^6 m^3. This aquifer is utilized for water supply and irrigation.

A.5 General Tectonic Setting of W.D GR 09

The Pelagonian zone consists the larger part of W.D GR 09 as mentioned earlier. For this reason, only the tectonic setting of the Pelagonian zone is described in this section. Its eastern part consists of a part of Almopia zone and in its western part formations of the Mid-Hellenic trench are encountered. The Pelagonian zone was an elevated area and was affected by the pre-Alpine orogenic phases i.e. Erkinian and Calidonian as suggested by Brunn, 1956. The great lithological variety of the metamorphosed rocks recommend that the mountain mass of Vernos-Varnounta, which is part of the Pelagonian, came from the metamorphosis of old sediments, excluding any slightly metamorphosed system (Kilias, 1980; Mountrakis, 2010).

Throughout the duration of the Alpine orogenesis the Pelagonian zone was a submarine ridge that was affected by the evolving tectonic setting of this orogenic phase i.e. folding, metamorphosis of rocks and temporary of the rock's emergencies out of the sea. The zone functioned as a ridge which was not continuous but separated by transverse trenches that were communicating with each other on either side of Pelagonian zone. The Mid-Hellenic trench in the area of Kozani, perpendicular to the Pelagonian zone's layout, divides the zone into the areas of North Pelagonian, of north-west Macedonia and Central Pelagonian zone, which includes the mountainous complexes of Pieria and Pelion (Brunn,1956; Mercier, 1968; Mountrakis, 2010).

The first tectonic event that affected the basement rocks happened during Paleozoic era before the Late Carboniferous, which created main foliation found at theses rocks along with small folds, while the second happened during the Late Jurassic, which affected the granite of Late Carboniferous age, the Permian-Early Triassic meta-clastic deposits and Triassic-Jurassic marbles (Mountrakis, 2010).

During the time of the second tectonic event, tectonic phases caused older rocks to fold with an NW axis. This phase, also, thrusted the ophiolites and the accompanying sea sediments called the Eohellenic nappe, parts of Axios-Vardar zone onto the limestones of Triassic-Jurassic age of the east side of Pelagonian zone while those pre-existing rocks were subjected to metamorphosis. Slip marks were created on the basement rocks along with intense fracturing close to this tectonic contact. This also created the nappe of Almopia, whose ophiolithic melanges are found at the east side of the Pelagonian zone (Mountrakis 1977, 1982, 1983, 1984, 2010). Vafeiadis, 1983 observed faults with clastite in their fracture zone at Kastoria basin, with NE-SW, N-S and NW-NE strike, found in the limestones of Triassic-Jurassic age and the thrusted ophiolites on top of the limestones.

The third and last tectonic phase were the brittle tectonic events, dictated by mainly vertical movements, that occurred during the Quaternary and created large fracture zones, which gave form to the current topography of Western Macedonia. This is suggested by the findings of Psilovikos, 1981 that the flattened surface at the area of Olympus present four stages of flattening and uplifting, which happened during Oligocene-Miocene, which uplifted the area by 2.100 to 2.400 m. These uplifting forces affected the South Balkan peninsula mountain ranges, including those found at Macedonia. Also, this event created the Middle Miocene is considered to be the early stage of the creation of the valleys of Western Macedonia. Some of those valleys were turned into lakes such as the lakes of Ohrid, Prespa, Maliki and Kastoria, that covered the area of Macedonia. For example, the lacustrine sediments of Pleiocene-Pleistocene age suggest that Lake Kastoria is a residual form of the such large lakes of the Neogene-Quaternary.

In summary, the presence of three main deformation events phases are found at the Pelagonian zone (Mountrakis, 2010). These three phases are linked with the deformation products mentioned above:

- P1- Orogenetic Period (Late Jurassic – Early Cretaceous) with axes, mainly NW-SE
- P2- Orogenetic Period (Late Cretaceous - Paleocene) with axes strike, mainly NE-SW
- P3- Orogenetic Period (Priambonian-Oligocene) with axes strike, mainly NW-SE to NNW-SSE

A.6 Geology of W.D GR 09

Hellenides, how Greek mountain ranges are called in literature, are distinguished in 12 tectonic units. Each such unit is defined by a sequence of geologic formations that had been deposited in the same palaeogeographic environment and then undergone the same deformation and metamorphosis during the Alpine orogenesis, followed by a period of tectonic relaxation that have yet to end. This last period, in turn gave way for the meta-alpine sediments which were deposited during the Neogene and Quaternary stratigraphic periods. The mountainous region, where most rock crops are found, in the study area is structured by formations of the Pelagonian tectonic zone, which is theorized to be remnant of the Kimmerian continent (Brunn, 1956, Aubouin, 1959). The stratigraphic sequence of this zone consists, typically, of a crystalline gneiss basement, gneissed granites, semi-metamorphic Permo-Triassic rocks, two carbonate nappes of Triassic-Jurassic age, ophiolites and Late Cretaceous transgressive sediments (Mountrakis, 2010). First, the Pelagonian zone is briefly described follow by an also short description of the Meta-Alpine Sediments that were deposited during the relaxation period after the Alpine orogenesis.

A.6.1 Pelagonian Zone

The Pelagonian zone consists 5 main stratigraphic sequences.

Paleozoic crystalline bedrock, consisting of ortho- and para- gneisses with intercalations of shales and intrusions of large masses of plutonic rocks. The crystalline background is structured from the lower layer, whose age is not accurately identified (high crystal transformation of crystalline rocks, with shales, cipolines, marbles of Paleozoic age (Brunn, 1956; Maratos, 1972; Mountrakis, 2010).

Kilias and Mountrakis, 1989 distinguish the crystalline bedrock of the Pelagonian that exists in the wider region of Macedonia, into three main masses:

- the mass of Vora,
- the mass of Vernus, where the pluton of Varnousa - Kastoria is found
- the mass of Pieria - Kamvounion, two important plutons are found: the pluton of Verdikousa - Deskatis and the Pieria pluton.

Neo-Paleozoic formations, which are made up of metamorphic rocks of sedimentary origin (shale – gneissed shales and amphibolites) with some local appearances of coarse crystalline marbles. These formations have been deposited nonformibly on the crystalline bedrock.

Triassic-Jurassic carbonite nappe, consisting of thick-strata of white colored and locally black limestones, which gradually change to pelagic sediments. These formations have undergone prasinoschistolithic metamorphic phase during Upper Jurassic – Down Cretaceous; thus, found recrystallized.

Ophiolites with the accompanying deep-sea sediments, which are found in the wider region of Vourinos and constitute the most important ophiolithic complex of the Greek area. An important tectonic event took place in the Lower Cretaceous, which resulted at thrusting the ophiolite complex on the medium- late Triassic - late Jurassic marble on the Neo-Paleozoic to the Early-Middle Triassic formations or on the crystalline bedrock. This tectonic event resulted in the creation of a unit of mixed formations specifically an ophiolithic mélange (Mountrakis, 2010).

Upper Cretaceous formations and flysch are found in the area of East Thessaly and in the region of Macedonia. They consist of crystalline limestone and marble (Mountrakis, 2010).

A.6.2 Meta-Alpine formations

A.6.2.1 Molassic sediments of the Mid-Hellenic Trench

The sediments of the Mid-Hellenic Trench extent to the wider area of Karditsa, Trikala, Kalambaka, Grevena and Kastoria to the Greek-Albanian border and continue further up-north in Albania.

According to Brunn 1956, the Mid-Hellenic Trench is consisted of the following formations:

Krania Series (Late Eocene): This series consists of the conglomerates, which are the lowest stratigraphic part of the Mid-Hellenic trench molassa, it has a maximum thickness of about 3,000 meters.

Eptachorion Series (Late Oligocene): This series is structured by exchanges of fine-grained sandstone and marls, and by rare, small strata of conglomerates and a few lignite appearances. Its thickness reaches from 600 up to 1,500 m.

Pentalofos-Meteora Series (Late Oligocene – Aquitanian): This series, the thickness of which reaches 3,000 meters, is composed from alternations of conglomerate-sandstone at the eastern part and sandstones to shandy marls to the rest of the area.

Tsotyli Series (Late Aquitanian – Bordigalian): This series is 600 m to 2,200 m thick and consists of exchanges of marls and sandstone. Also, at this series conglomerates with some appearances of lignite are found.

Kastonochorion Kastorias series or Ontria series (Late Bordigalian – Elbetio): This series consists of alternations of sandstones, limestones, marl and sandstone limestone with lignite layers and has a maximum thickness of about 400-500 m.

Orlia Series (Elvetio): This series is last series of the molassic sediments of the Mid-Hellenic trench. It is structured by, almost horizontal, layers of sandstone and organic limestones. The maximum thickness of the series is about 100 m.

A.6.2.2 Pleio-Pleistocene basins of the Mid-Hellenic Trench

Sediments newer age than that of those described above are Pleio-Pleistocene sediments and quaternary sediments are found throughout the water district of West Macedonia (GR 09). These geologic materials, which have a lake to river origin or of scree origin, have been deposited with unconformibly on the formations of the Mid-Hellenic Trench and on the older pre-Cenozoic rocks.

Significant tectonic stresses, after the deposition of the Elvetian age formations, lifted and otherwise affected the Miocene deposits, which formed trench like grabens where the Pleio-Pleistocene sediments were deposited. The major Pleio-Pleistocene basins are:

- the basin of Argos Orestiko

- the Neapolis - Sarantaporos basin
- the Grevena basin
- the Carpero basin

The sediments that are found at those basins are mostly gravel, pebbles, sand and marl with a varying degree of cementation and a large granulometric range. Sedimentation ends in the Middle Pleistocene.

The deposition of Pleio-Pleistocene sediments occurs on mesozoic rocks, within grabens that were created during alpine orogeny. It should be noted that not there is a single sedimentary basin but many small ones that are in communication which each other. The most important Pleio-Pleistocene basin in the area is the basin of Serbian-Kozani, which extends up north to Ptolemaida, Amynteo, Florina and continues to FYROM and Albania. This basin, which is the southern part of a large graben that begins from Monastir, which is located immediately downstream of the Ilarion Dam.

According bibliographic data, the basin is composed of an underlying formation layer, which is composed of clayey and sandy marls with marly limestone lenses and by more coarsed grained materials like tiles and pebbles. At the upper part of the layer, where fine grained materials are superior, horizons of clayey lignite are found. Its thickness exceeds 200m. - the middle layer of formations, where significant lignite horizons are located. The thickness of these horizons, which alternate with horizons of marls or clay, ranges from 15 up to 25m. The overall thickness of the middle layer, which is of no hydrogeological interest, reaches 150m. - the upper layer of formations is consisted of alternations of clay to sandy clay, with small layers of clay, sand, gravel, conglomerates and marly limestone. These formations, belonging to a lake-fluvial sedimentation phase, that has been deposited uncorfomirbly on an underlying sequence clayey-marly formations of a lake deposition phase. This basin is of particular interest since the extraction of lignite horizons presupposes the removal of any overlying Quaternary deposits, where significant granular aquifers exist.

A.6.2.3 Quaternary formations

These formations present significant extent throughout the region of Western Macedonia and consist of alternations, loose to semi-loose structure, coarse-medium grained clasts and finer grained clastic formation with a rapid granulometric change. The quaternary deposits of particular interest are they have deposited in the basins of Sarigiol, Ptolemaida, Amyntaio, Grevena (Western and Central region of the W.D EL09) as well as in the Aridaia, Giannitsa-Thessaloniki basins and its coastal zones at eastern section of the GR 09. The formations that are encountered are:

- Alluviums, screes, fluvial deposits: consist of loose clay-silt, sand, gravel, pebbles, in all possible granulometric combinations, cohesive and/or semi-cohesive structure, paleo-screes, as well as intercalations of loose to semi-cohesive conglomerates and sandstones. These deposits are of hydrogeological interest as extensive aquifers with varied productivity (depending on the geometric characteristics of the aquifer, the permeability materials, recharge conditions). The largest of the granular aquifers in question are abstracted with a significant number of hydro-wells for water, irrigation or other use.
- Neogene deposits: consist of marls, clays and marly limestones with sand and sand-pebbles. These formations are of little interest as they consist of impermiable formations. The alternations of sand-pebbles may present aquifers of very limited capabilities.

A.7 Water Resources of W.D EL 09

The average water supply in the Water district of Western Macedonia amounts to 3.2 x 10^9 m^3 annually. The water needs of the W.D EL 09 and part of the Central Macedonia (W.D EL10) are covered, as a quantity of water of approximately 500 x 10^6 m^3 is transported via the Aliakmonas-Axios canal to fulfil the irrigation needs of the Thessaloniki-Lagadas plain and the irrigation network of the Municipality of Alexandria, as well as an amount of 50 x 10^6 m^3 (with a maximum of 98 x 10^6 m^3 depending on needs) to meet the needs of the wider region of Thessaloniki (W.D EL 09 management plans, 2014).

Considerable aquifers exist, at Water District EL 09, within the Quaternary formations but also within the karst formations, while aquifers of smaller extent are found in fractured formations. A sort description of basic characteristics of such aquifers is found below:

A.7.1 Granular or Alluvial Aquifers

This category includes all quaternary formations, as well as sediments that were deposited at Pleiocene. Aquifers are developed at the coarse – medium grain clastic parts of these formations.

In the alluvial formations the following aquifer types develop:

- unconfined aquifers, commonly found in river beds and lakes
- a series of successive underground aquifers partially under pressure, which usually have partial hydraulic communication with the overlying unconfined aquifers
- series of successive underground aquifers under pressure

Successive underground aquifers, partly under pressure or under pressure, are formed due to the impermiable formation that exist between them.

The aquifers, at W.D EL 09, with the largest extent are alluvial formations and located in Kastoria, Grevena, Florina, Amynteo, Ptolemaida, Arnissa, Pella, Alamo, southern part of the Aliakmonas basin, Katerini and Kolindros.

A.7.2 Karst Aquifers

These systems are karstified carbonate formations. The circulation of water is done via the karst structures (enlarged cracks, troughs, conduits etc.) and depends on both the geometrical characteristics (openings width etc.) of the karst system and the filling of karst structures themselves. Karst springs discharge the system. Discharging of karst formations can usually happen towards to neighboring granular systems and towards the sea, that's if the karst systems is directly next to the sea so they can communicate hydraulically. Karst aquifers cover most of the area at West Macedonia's water district. They exist below alluvial aquifers and, in many cases, contribute their water supply to those neighboring aquifers. The most significant ones for W.D EL 09 are located in the area of Trikalario, Kastoria, NW Vermio – Askio mount, NE Vermio and Litochoro.

A.7.3 Fractured Aquifers

These aquifers exist in every kind of lithological formation of rocky structure (excluding carbonate formations), which presents a developed and continuous network of structural discontinuities and/or bands of intense fracturing, which are usually identified with large tectonic structures. The circulation of water is done only through the network of discontinuities i.e. diaclases as well at the interface that develops between the zone i.e. scree, created by gravity weathering and the underlying healthy bedrock. Within the aforementioned

circulation network there must not be any fine geological materials i.e the result of mylonitization due to tectonic movement, which are clay and silt because they act as a water tight bulkhead that prevents the movement of water. Fractured aquifers discharge at springs, that appear near river lines or in places where either healthy bedrock outcrop or heavily brittle deformated area exist and by lateral infiltration towards the two-sided formations.

Considerable fractured aquifers are mainly located in the eastern and southern parts of the Water district of Western Macedonia, in the regions of Grevena, Pieria, Naoussa, Almopia, Aridaia, Vourinos, Voras, Varnousa-Vernos and North Pindos.

The formations are distinguished in permiable, semi-permiable and impermiable, and then into further categories based on the capacity, extent and lithology of each formation, resulting in the following basic classification system:

- **Permeable formations:** micropermiable or porous formations and macropermiable or fractured formations.
- **Semi-permeable formations:** micropermiable or macropermiable formations. Also included in this category are all water-permeable formations, those with small extent, low-capacity; and limited significance.
- **Impermiable formations:** truly impermiable formations.

A.7.4 Aquifer Systems of W.D EL 09

Directive 2000/60 dictates that the characterization of groundwater systems is based on geological and hydrogeological characteristics like those stated above. The purpose of the first and initial designation of groundwater systems in Greece is to evaluate the water stresses that exist at each of those aquifers as well as the evaluation of the risks that any kind of stress impose on those systems resulting in failure to comply the objectives set of Directive 2000/60/EC. This designation was made by the Ministry of Environment, 2008 and IGME, 2010 and takes into account the location of the groundwater systems along with their boundaries, the general character of the overlying layers, the interaction with surface water ecosystems and/or terrestrial ecosystems and any effects (both quantitative and qualitative) that human activities might cause.

The groundwater systems that belong to W.D EL 09 were categorized into two groups, primary aquifer systems and secondary aquifer systems, as follows:

I. Primary Aquifer Systems
GR09AF010: Aquifer system Triklario of mount of Kastoria - Prespa
GR0900020: Granular Aquifer System of Kastoria
GR0900030: Granular Aquifer System of Grevena
GR090F040: Granular Aquifer System of Florina
GR0900050: Granular Aquifer System of Amyntaio of Florina
GR0900060: Granular Aquifer System of Ptolemaida
GR0900070: Aquifer System of SW Vermio Mount
GR0900080: Aquifer System of NW Vermio Mount
GR090F090: Aquifer System of NE Vermio Mount
GR0900100: Central and Eastern Vermio Mountain Aquifer System
GR0900110: Karst Aquifer System of SE Vermio Mountain (Veroia)
GR0900120: Granular Aquifer System of Almopias
GR0900130: Granular Aquifer System of Southern Aliakmonas River
GR0900140: Karst Aquifer System of Litochoro
GR0900150: Granular Aquifer System of Katerini

GR0900160: Granular Aquifer System of Kolindros

II. Secondary Aquifer Systems
GR0900170: Granular Aquifer System of Dasochori, Grevena
GR0900180: Granular Aquifer System of Trigokkia, Grevena
GR0900190: Granular Aquifer System of Paliouria, Grevena
GR0900200: Granular Aquifer System of the river bed of the river Sioucha
GR0900210: Granular Aquifer System of Aetias, Grevena
GR0900220: Karst Aquifer System of Korissos, Kastoria
GR0900230: Granular Aquifer System of Galateias – Emporiou, Kozani
GR0900240: Fractured Aquifer System of Pieria Mountains
GR0900250: Fractured Aquifer System of Naousa
GR0900260: Fractured Aquifer System of Almopia
GR090F270: Fractured Aquifer System of Aridaia
GR0900280: Fractured Aquifer System of Vourinou
GR090F290: Fractured Aquifer System of Voras
GR090F300: Fractured Aquifer System of Varnounta-Verno
GR0900310: Fractured Aquifer System of Northern Pindos
GR090F320: Granular Aquifer System of Veui-Flampouro
GR0900330: Granular Aquifer System of Nympheo-Vlastis
GR0900340: Granular Aquifer System of Filotas
GR090A350: Fractured Aquifer System of Mid-Hellenic Trench
GR0900360: Fractured Aquifer System of Elatis-Livadero

APPENDIX B. Theoretical Background (to be added at a later date)

APPENDIX C. Supplemental Figures

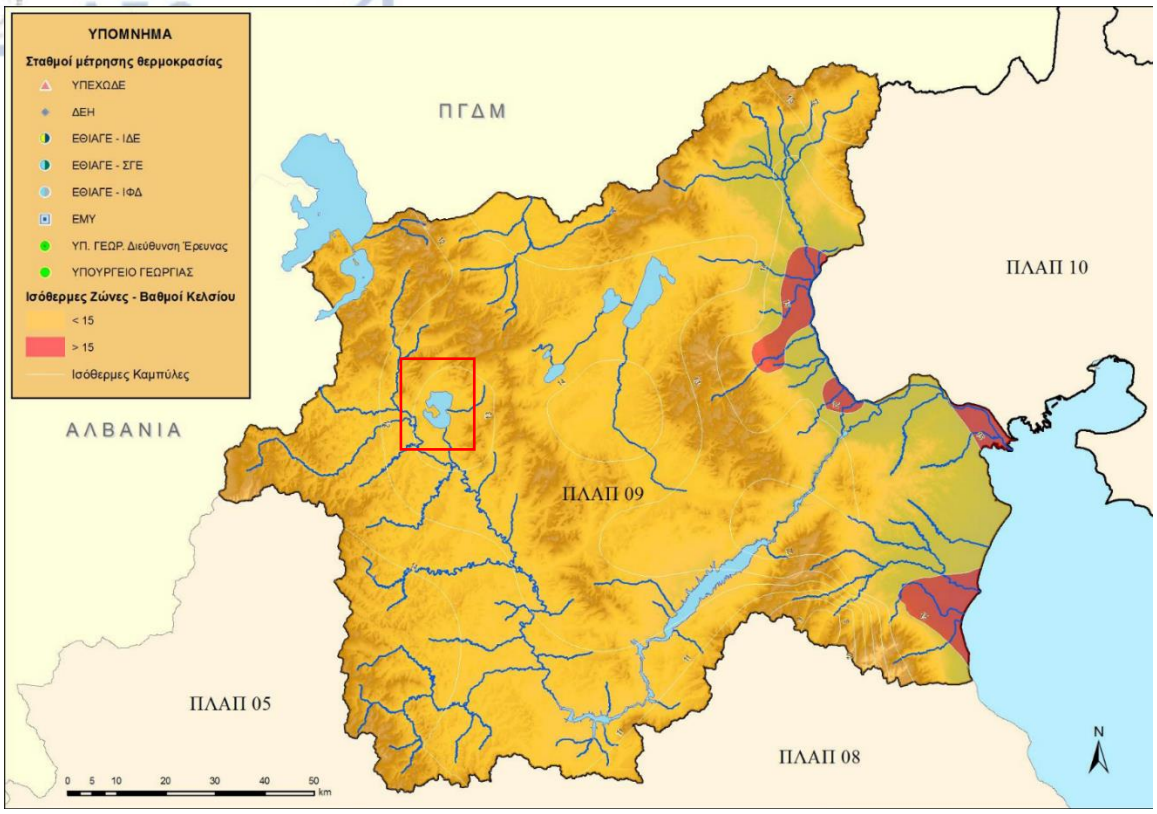

Figure 87 - Isothermal zone of 15 °C at EL 09 (YPAN, 2008). The red box roughly delineates the basin of Kastoria

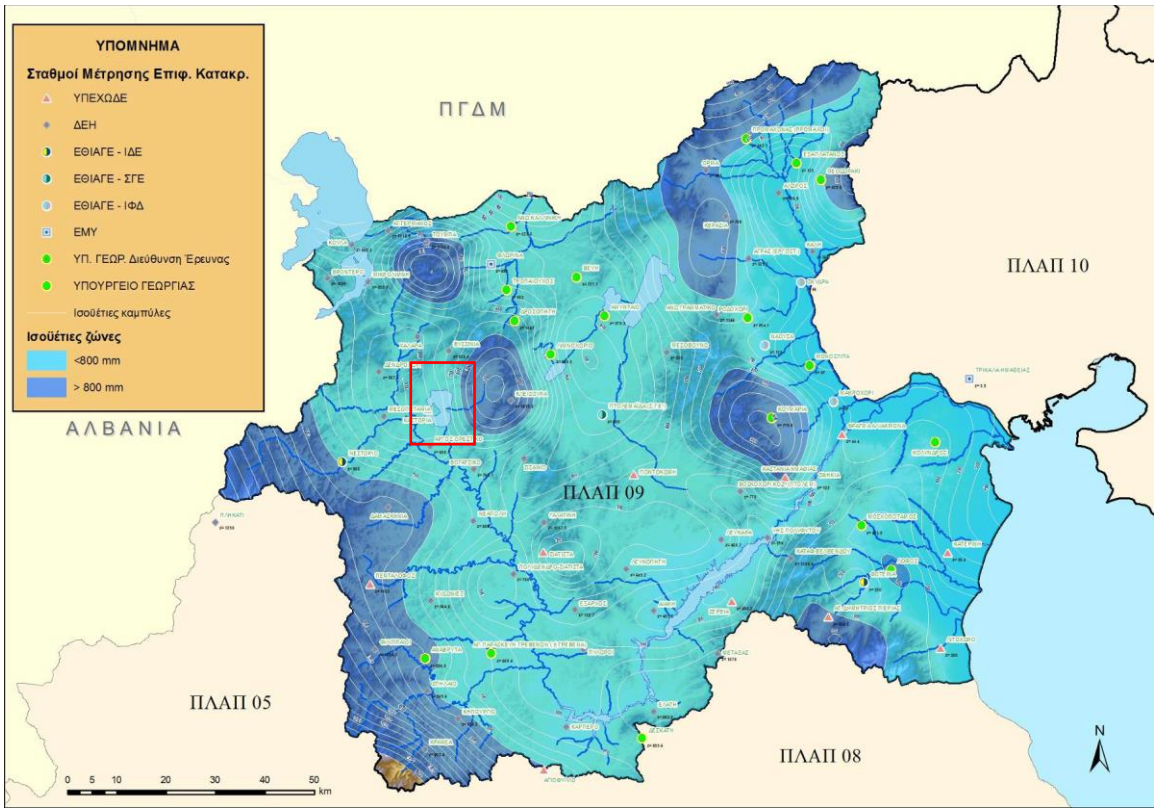

Figure 88 - Rainfall zone of 800 mm at EL 09 (YPAN, 2008). The red box roughly delineates the basin of Kastoria

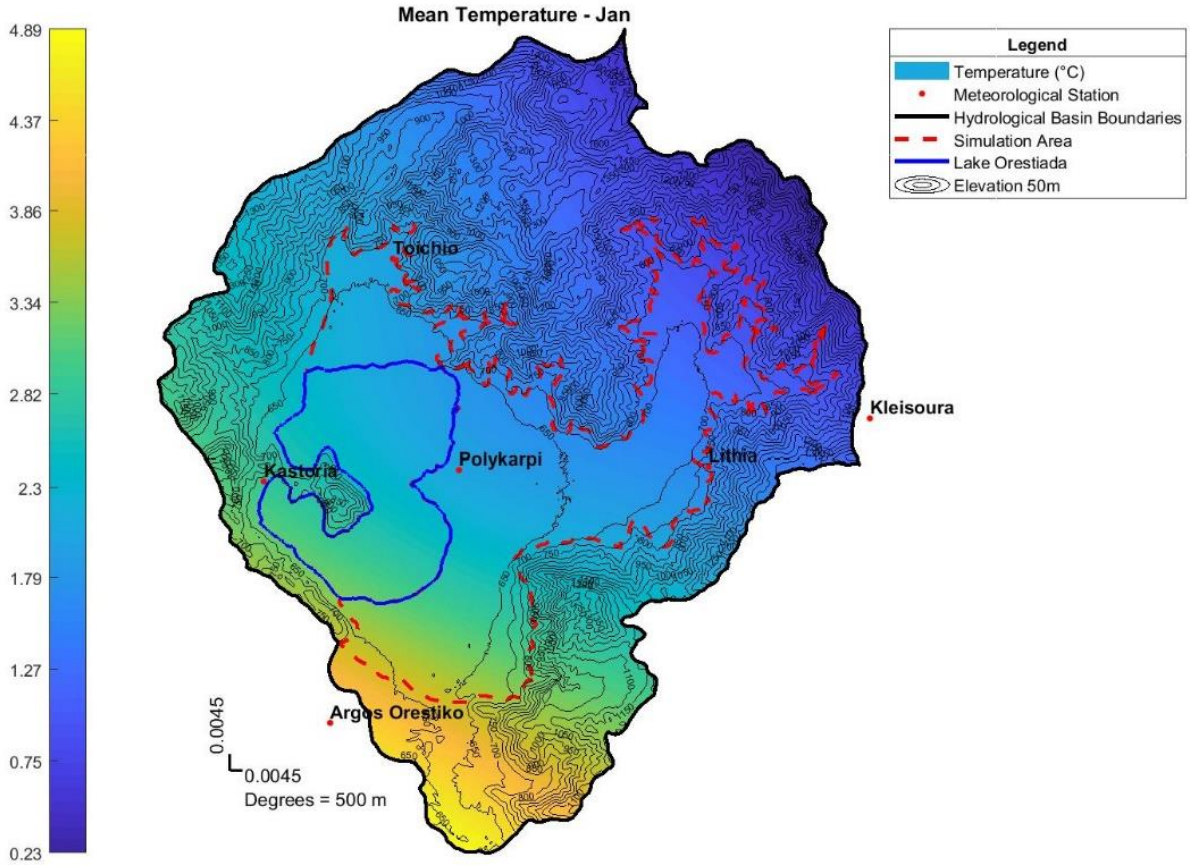

Figure 89 - Mean monthly Temperature of January at Kastoria basin

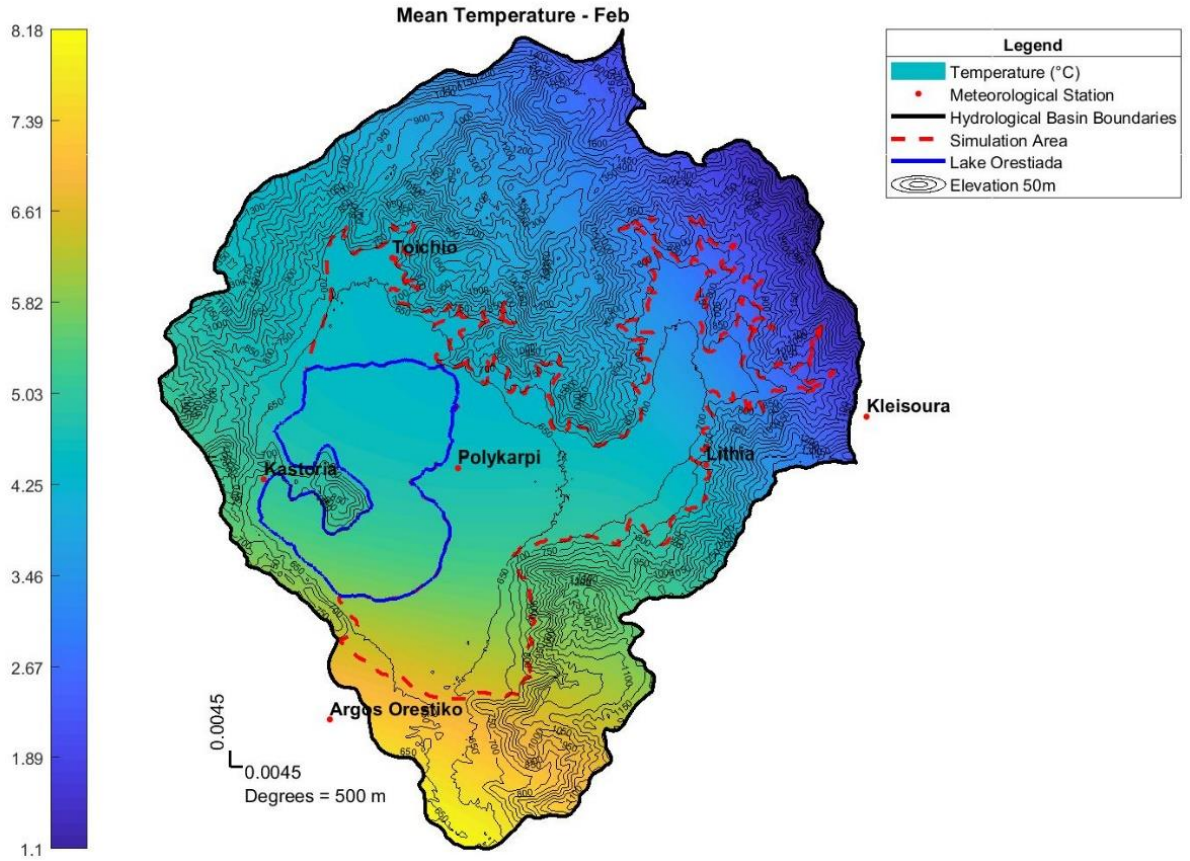

Figure 90 - Mean monthly Temperature of February at Kastoria basin

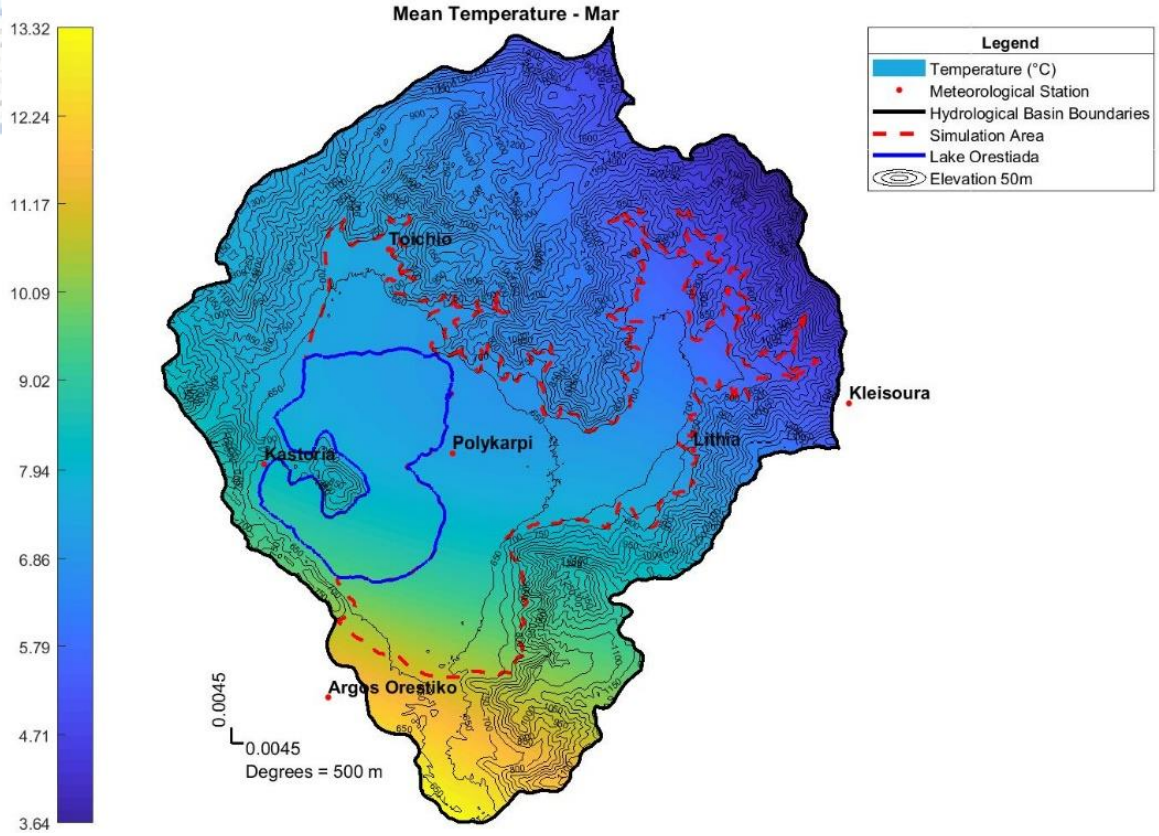

Figure 91 - Mean monthly Temperature of March at Kastoria basin

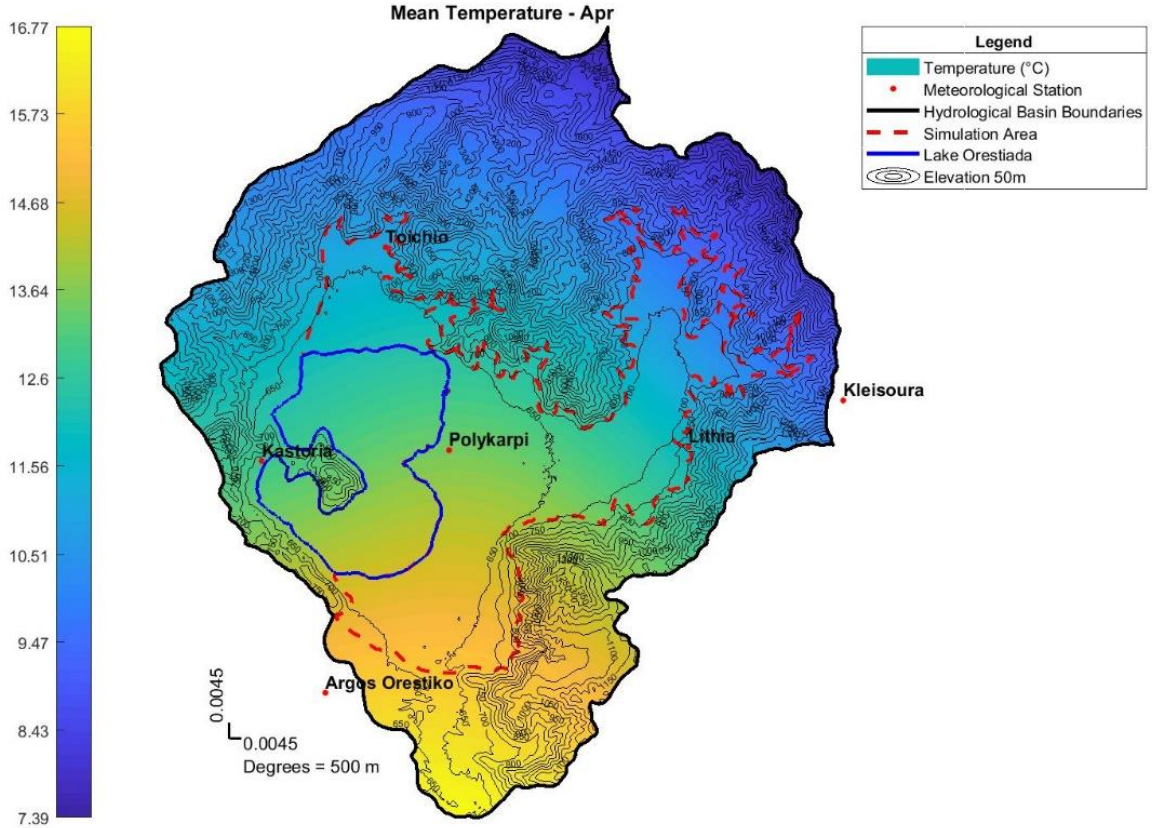

Figure 92 - Mean monthly Temperature of April at Kastoria basin

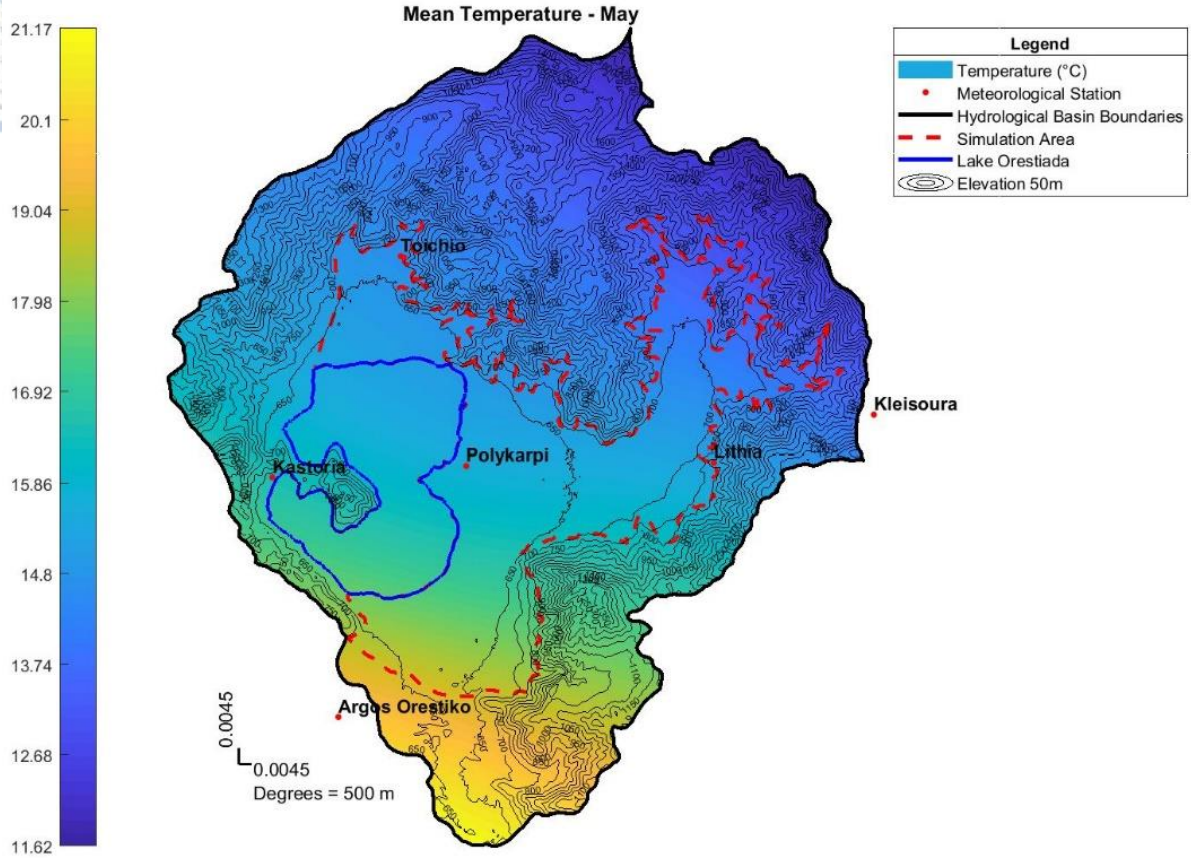

Figure 93 - Mean monthly Temperature of May at Kastoria basin

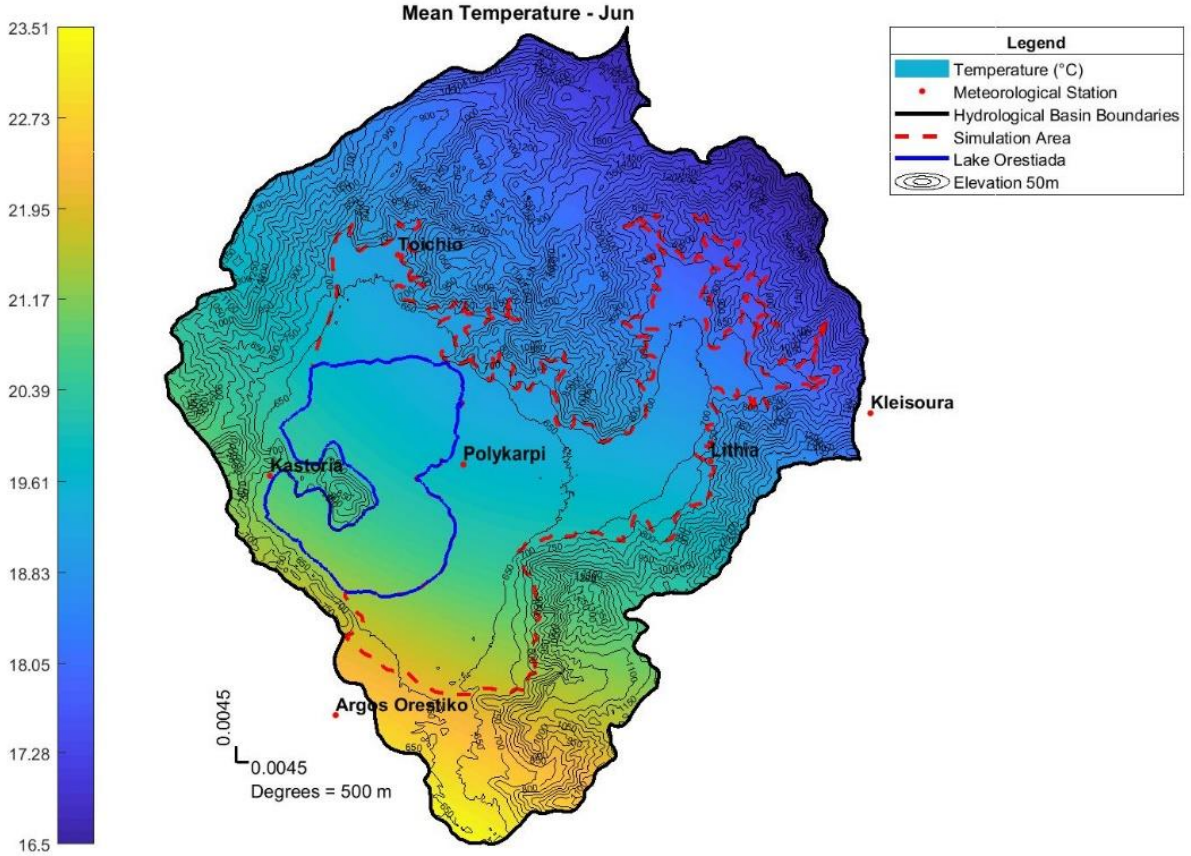

Figure 94 - Mean monthly Temperature of June at Kastoria basin

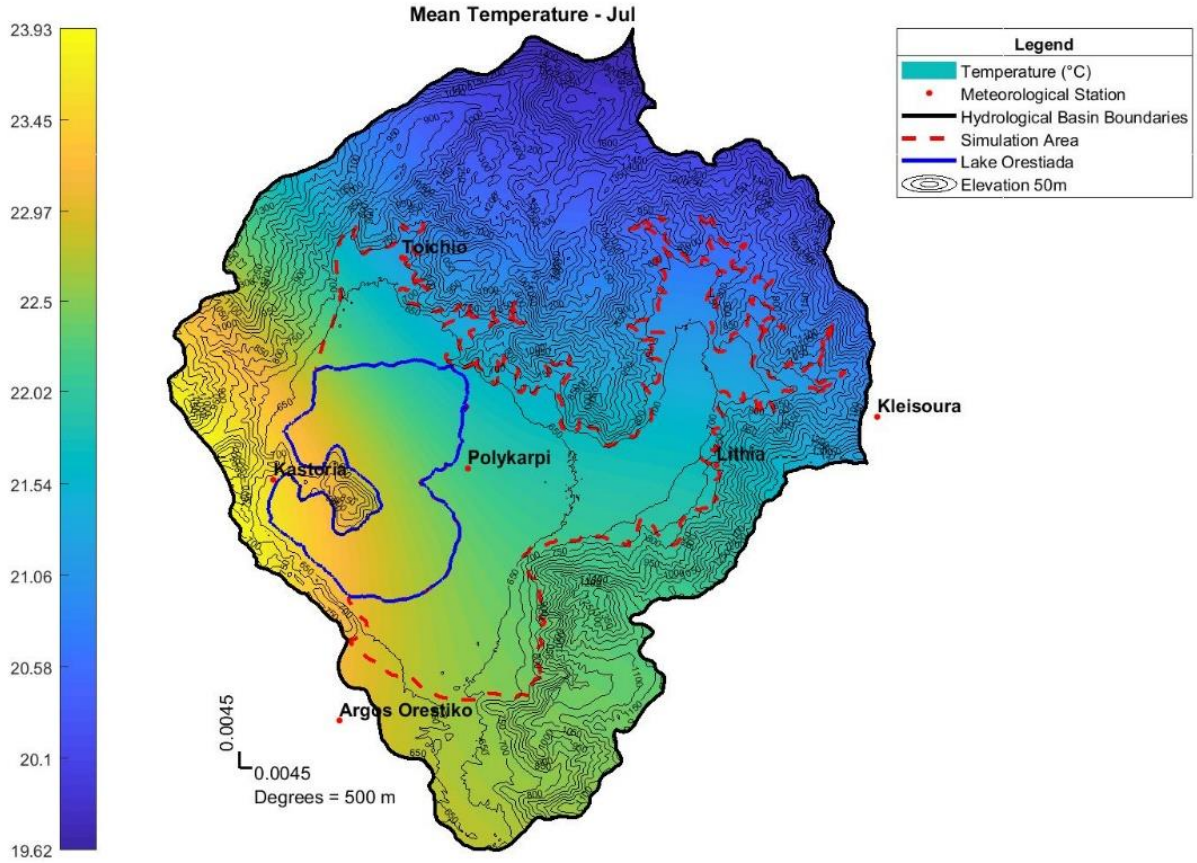

Figure 95 - Mean monthly Temperature of July at Kastoria basin

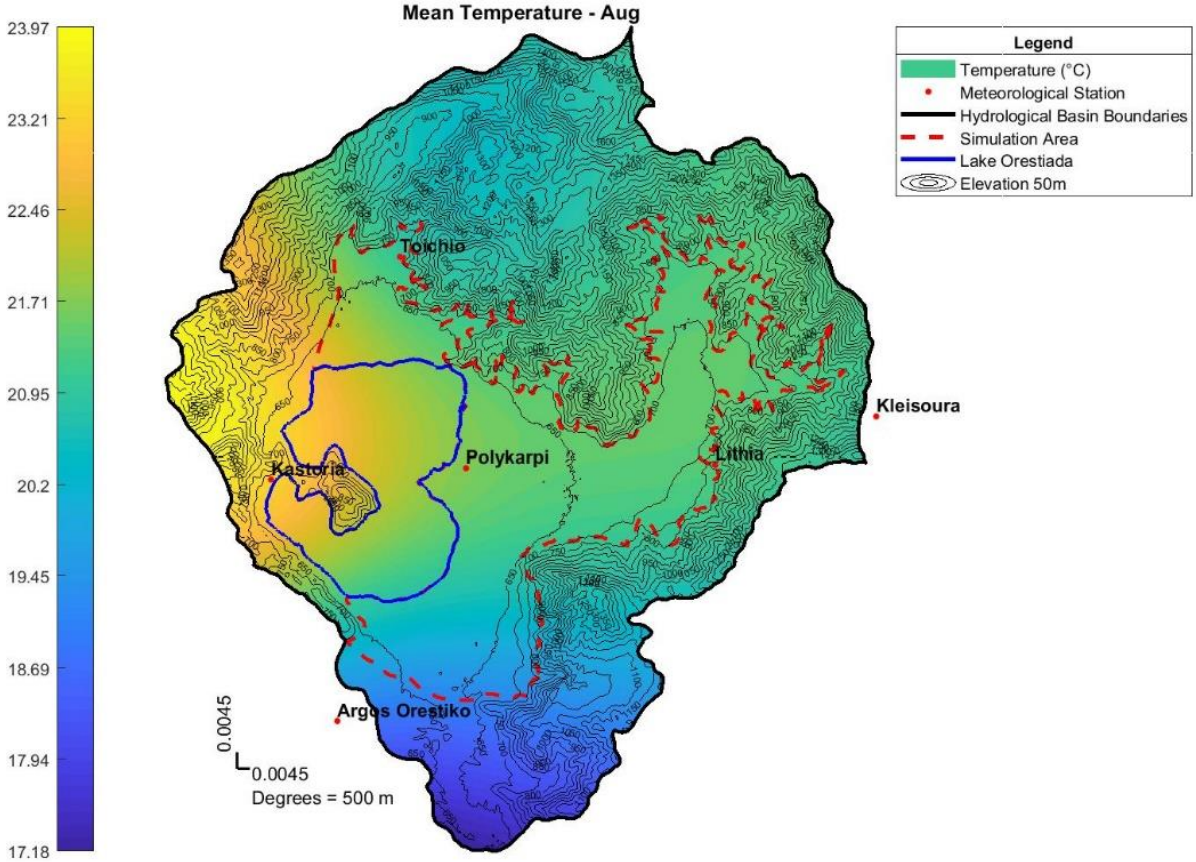

Figure 96 - Mean monthly Temperature of August at Kastoria basin

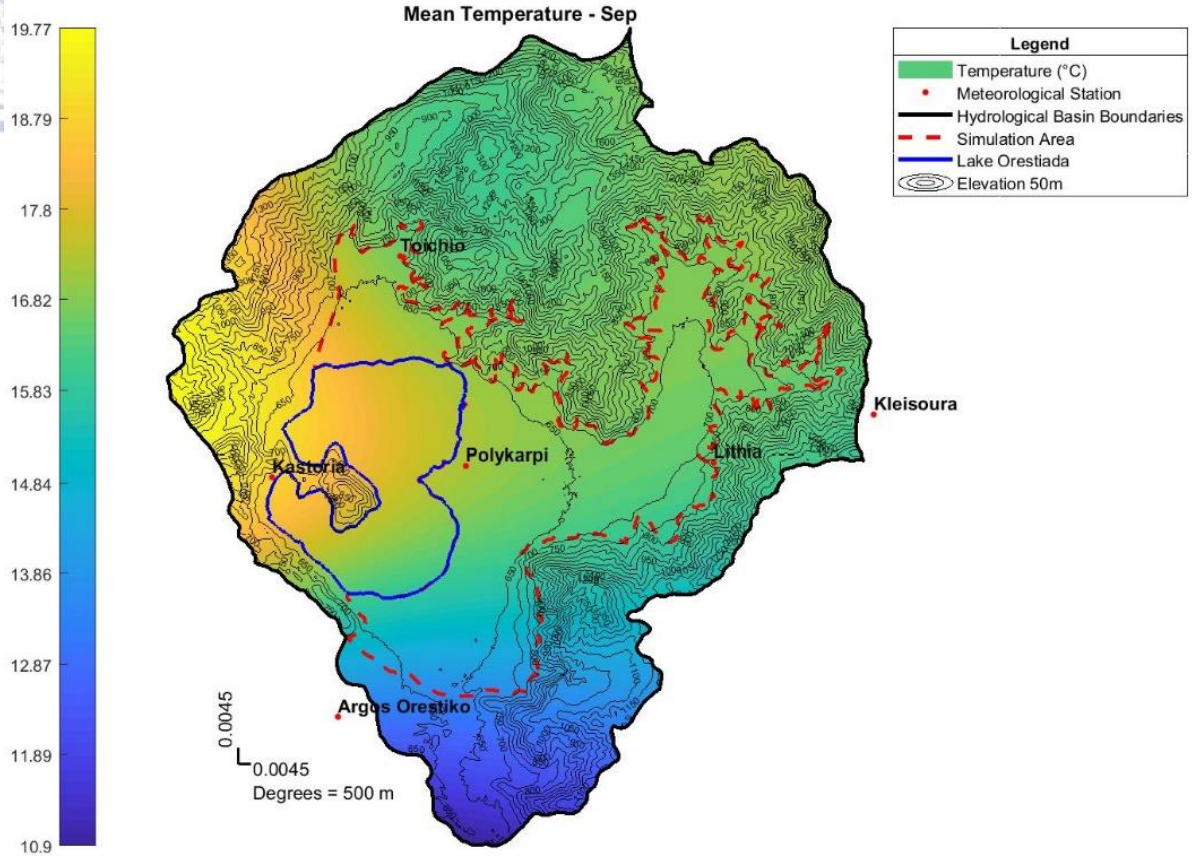

Figure 97 - Mean monthly Temperature of September at Kastoria basin

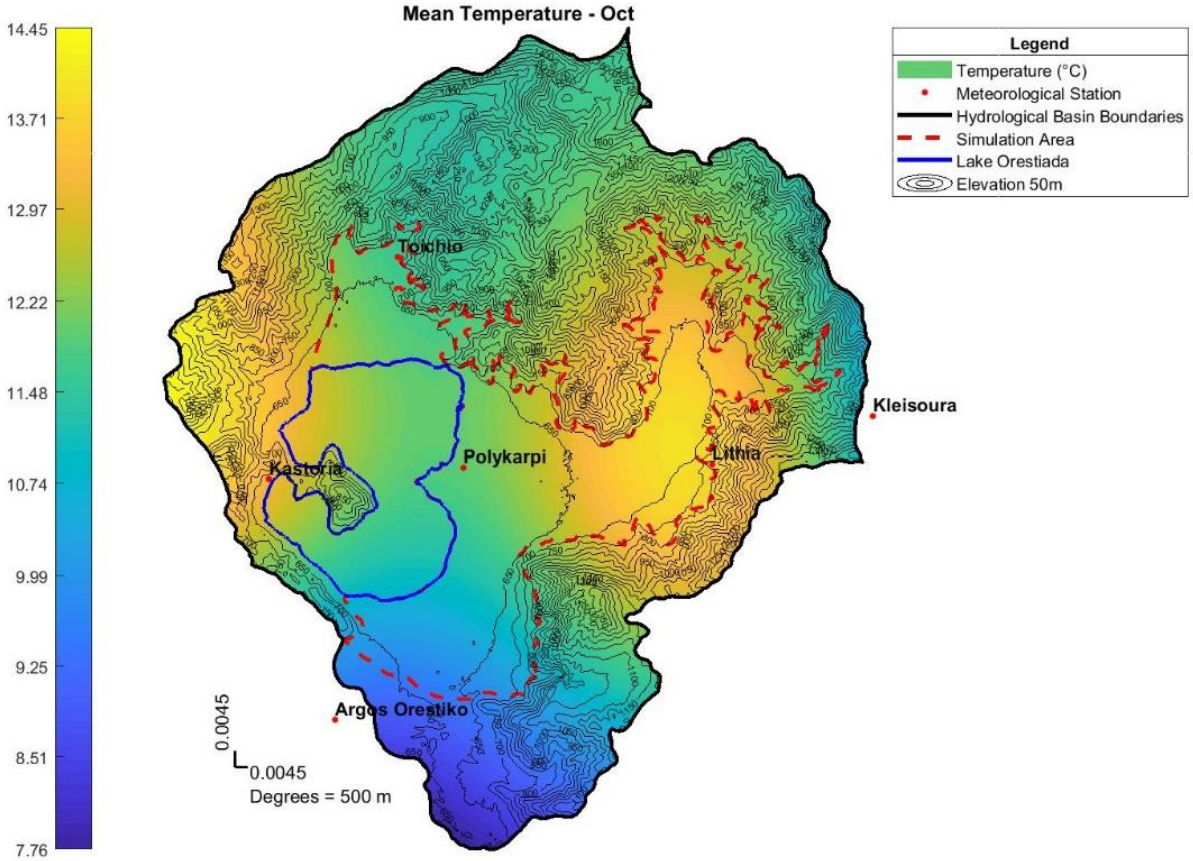

Figure 98 - Mean monthly Temperature of October at Kastoria basin

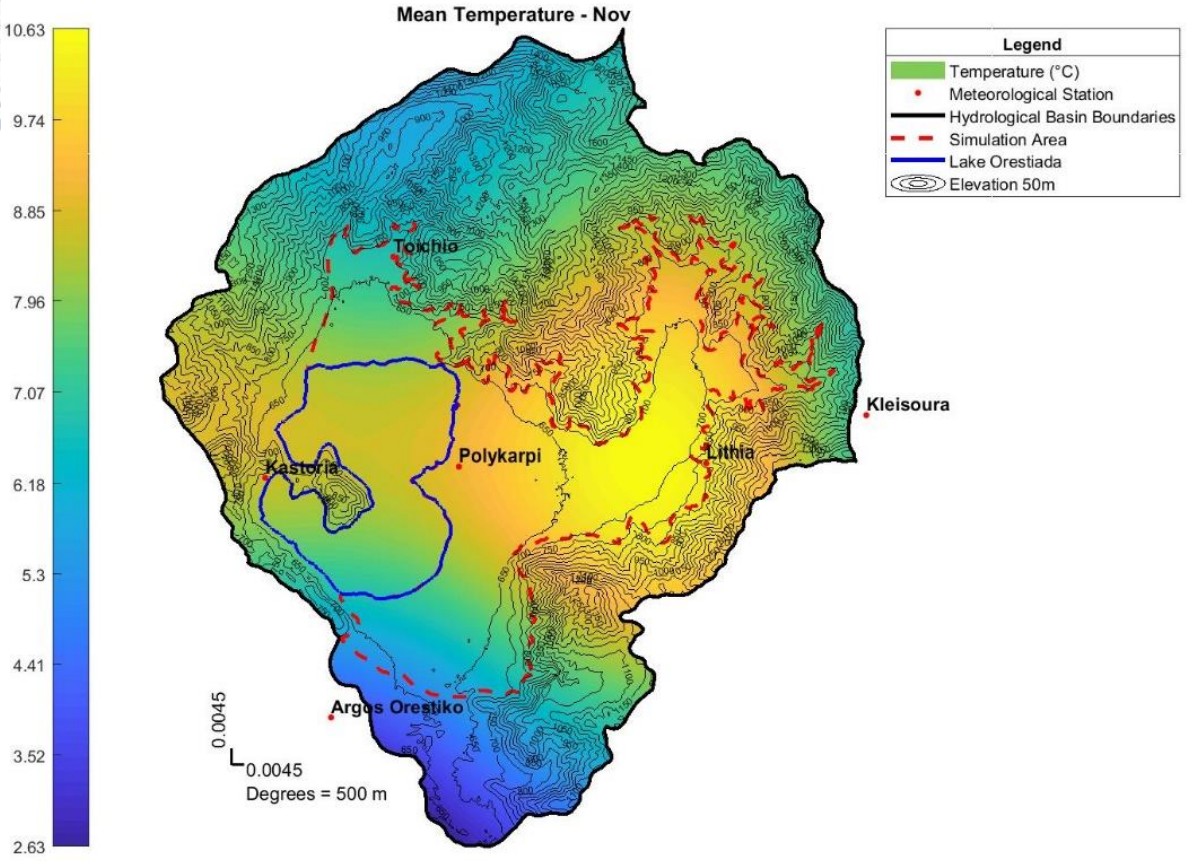

Figure 99 - Mean monthly Temperature of November at Kastoria basin

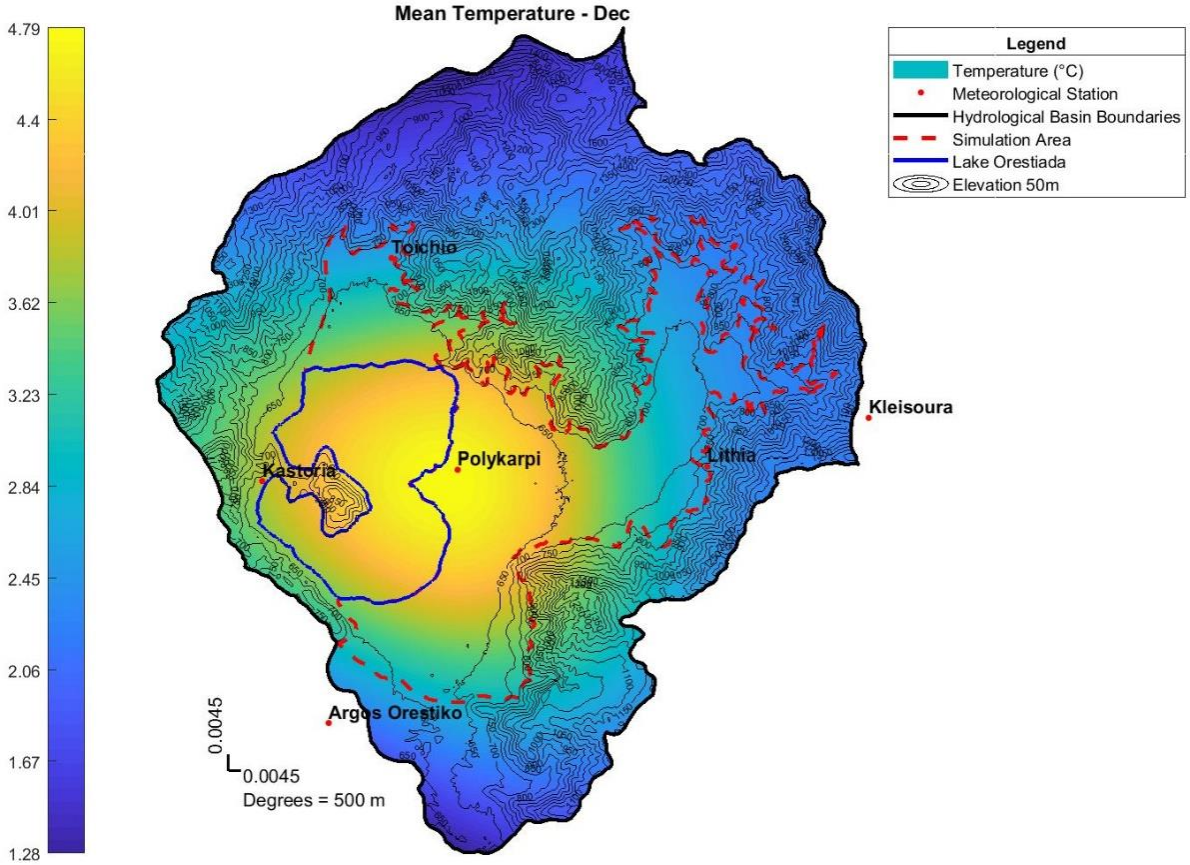

Figure 100 - Mean monthly Temperature of December at Kastoria basin

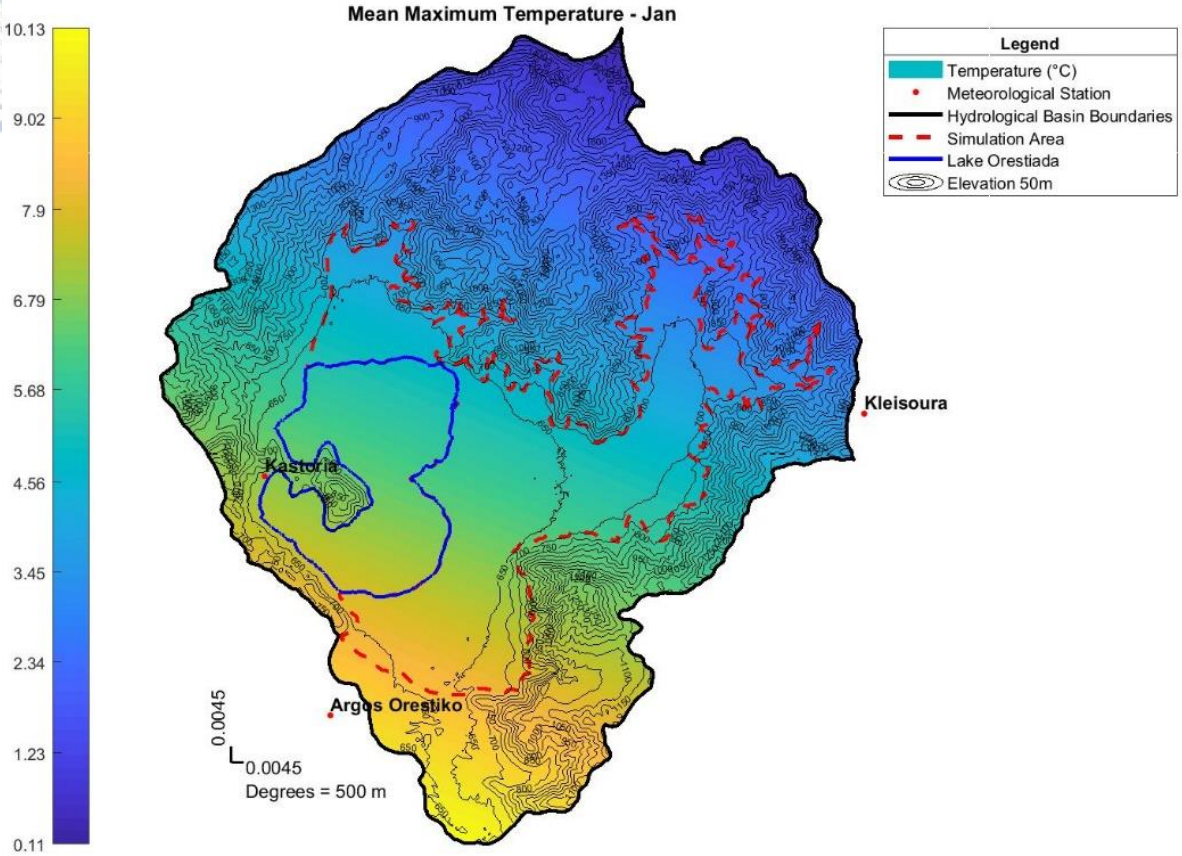

Figure 101 - Mean monthly Maximum Temperature of January at Kastoria basin

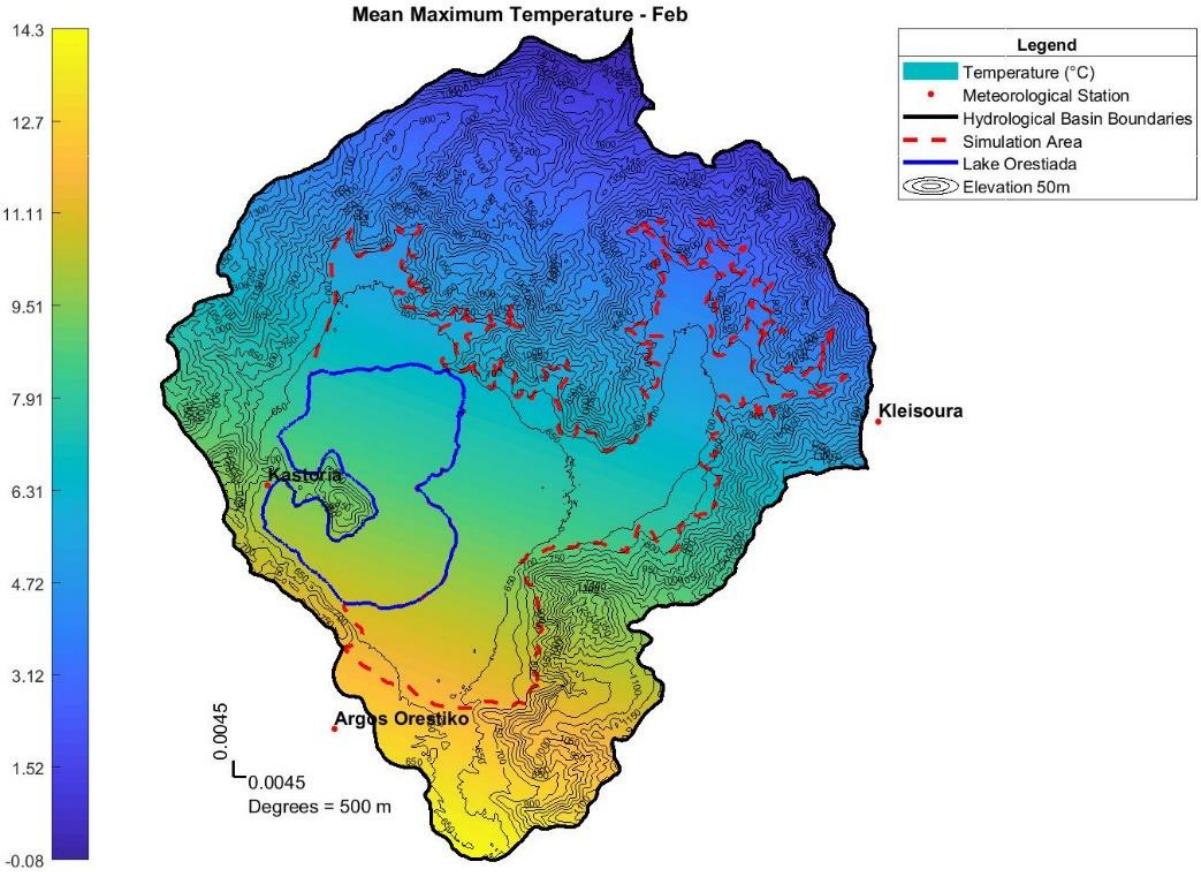

Figure 102 - Mean monthly Maximum Temperature of February at Kastoria basin

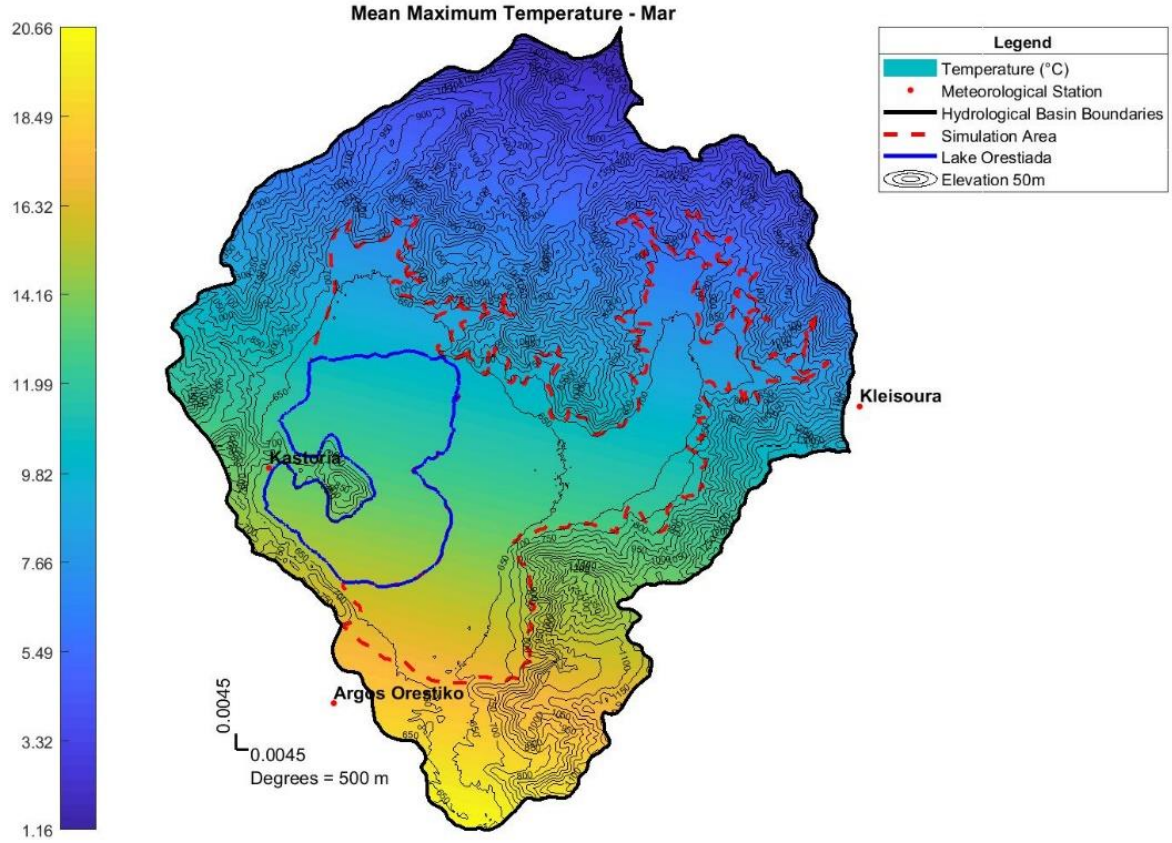

Figure 103 - Mean monthly Maximum Temperature of March at Kastoria basin

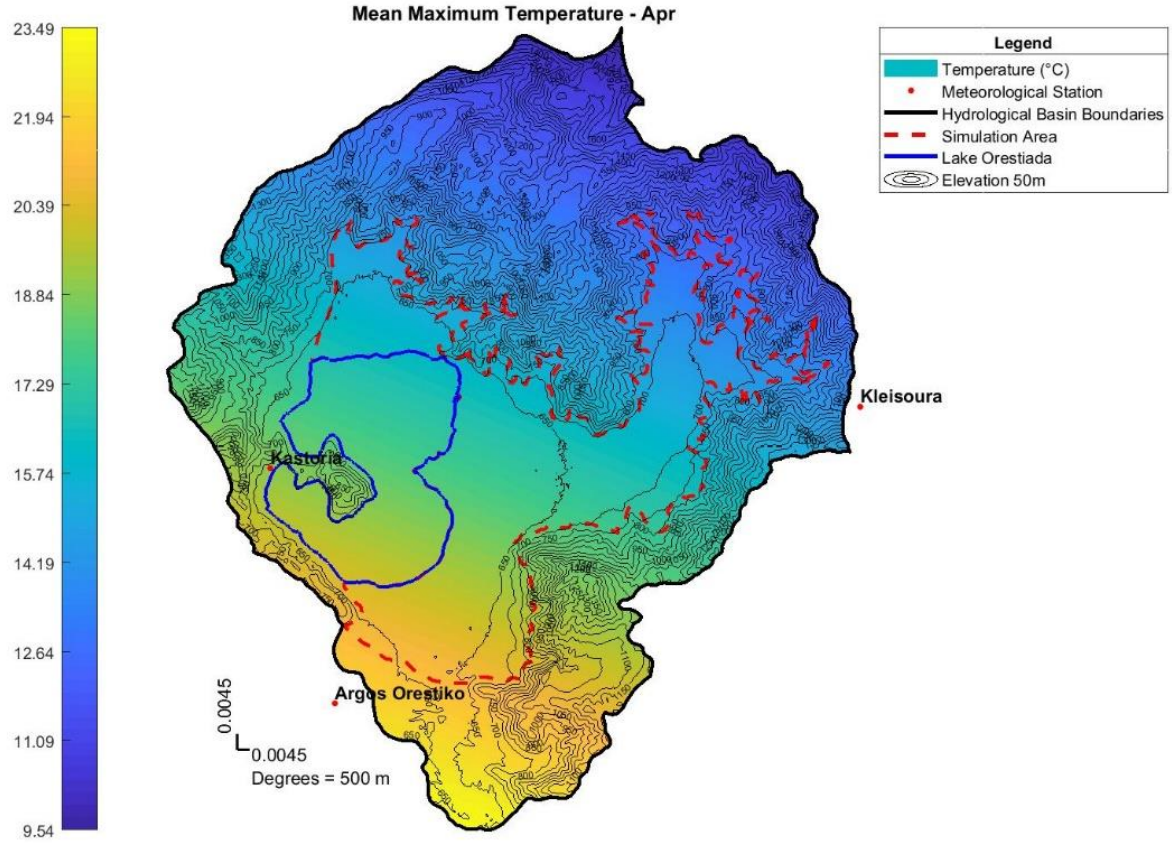

Figure 104 - Mean monthly Maximum Temperature of April at Kastoria basin

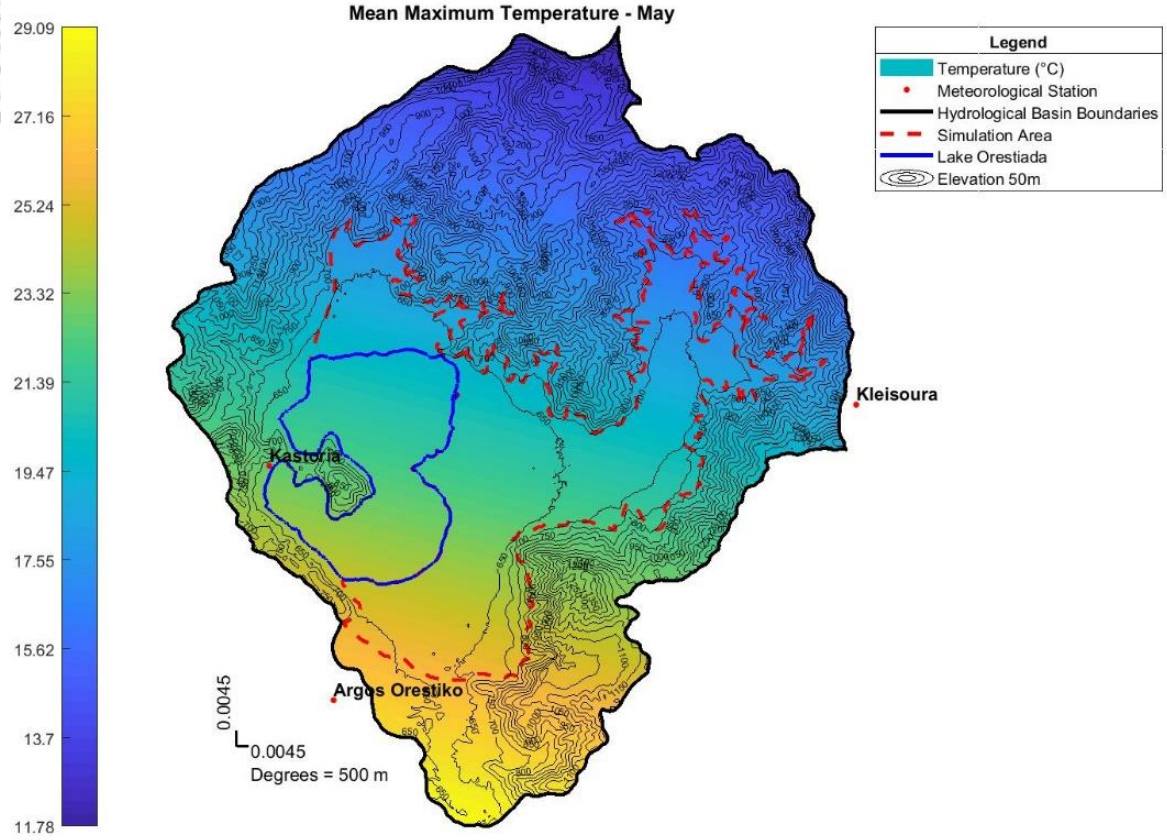

Figure 105 - Mean monthly Maximum Temperature of May at Kastoria basin

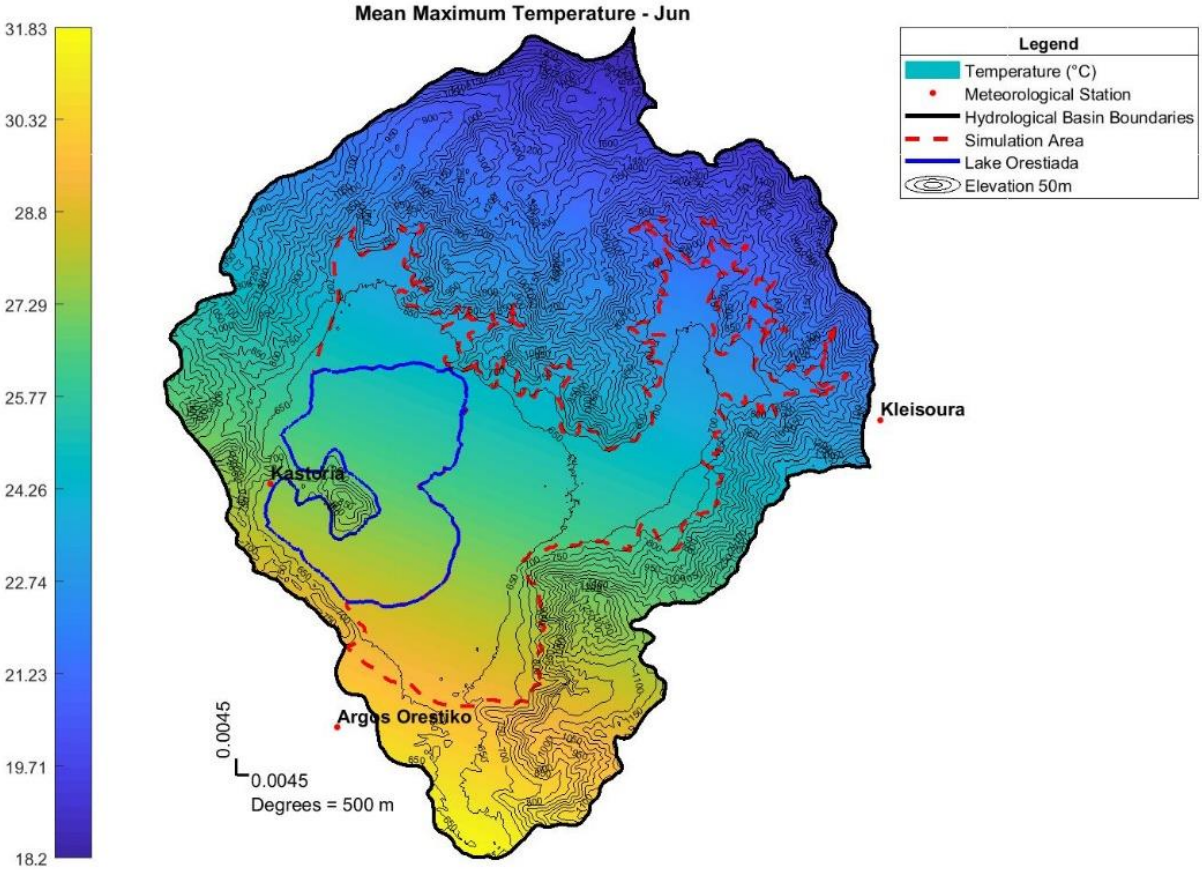

Figure 106 - Mean monthly Maximum Temperature of June at Kastoria basin

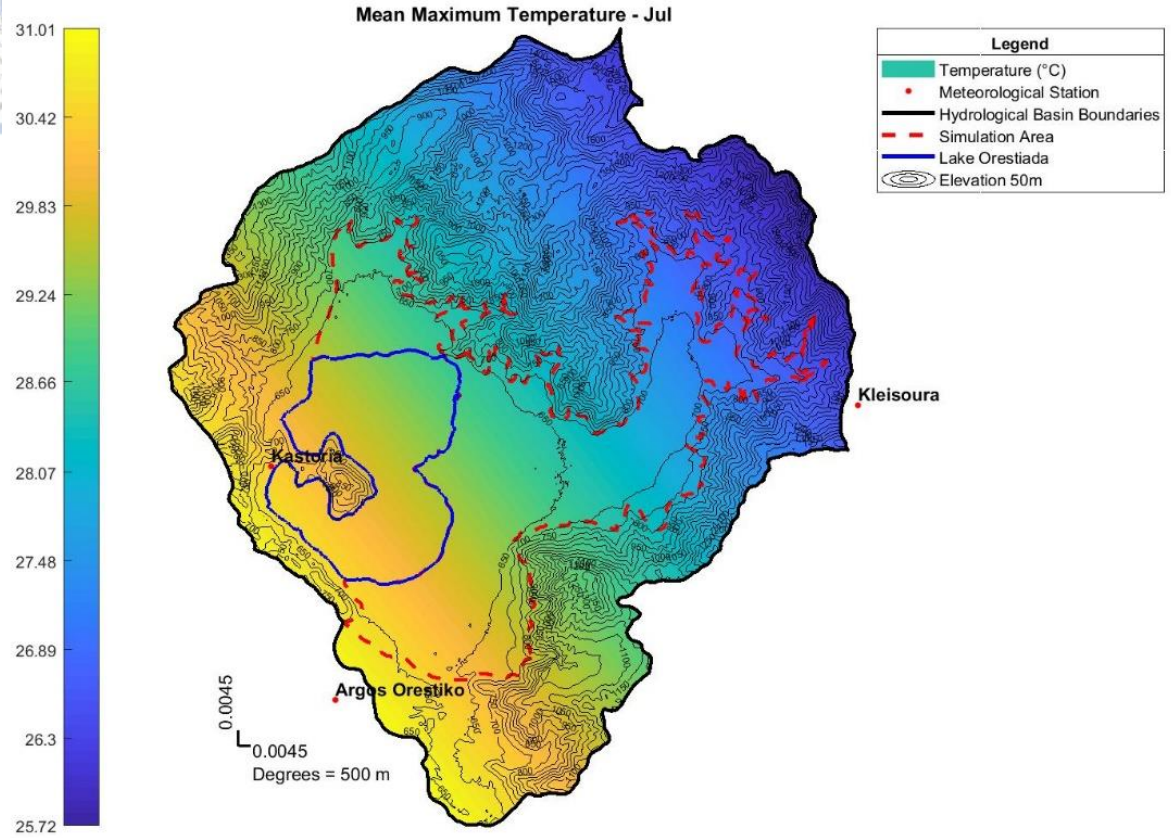

Figure 107 - Mean monthly Maximum Temperature of July at Kastoria basin

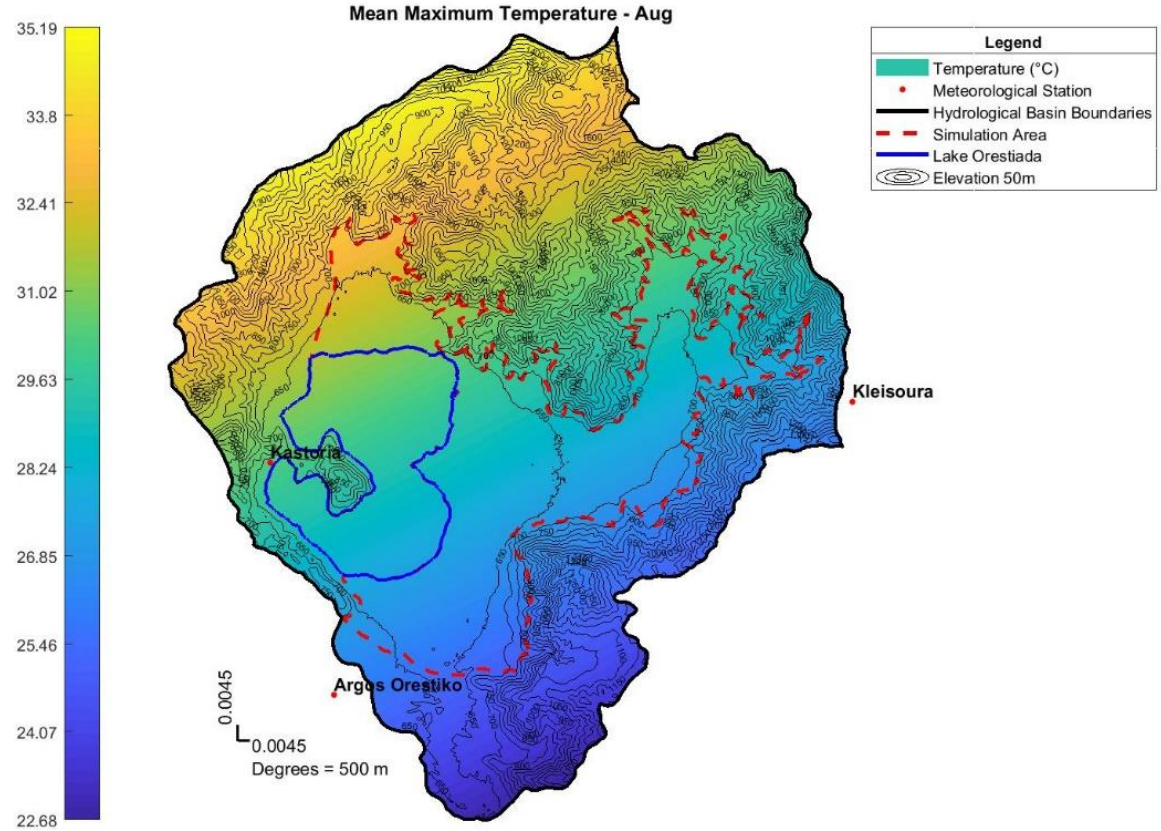

Figure 108 - Mean monthly Maximum Temperature of August at Kastoria basin

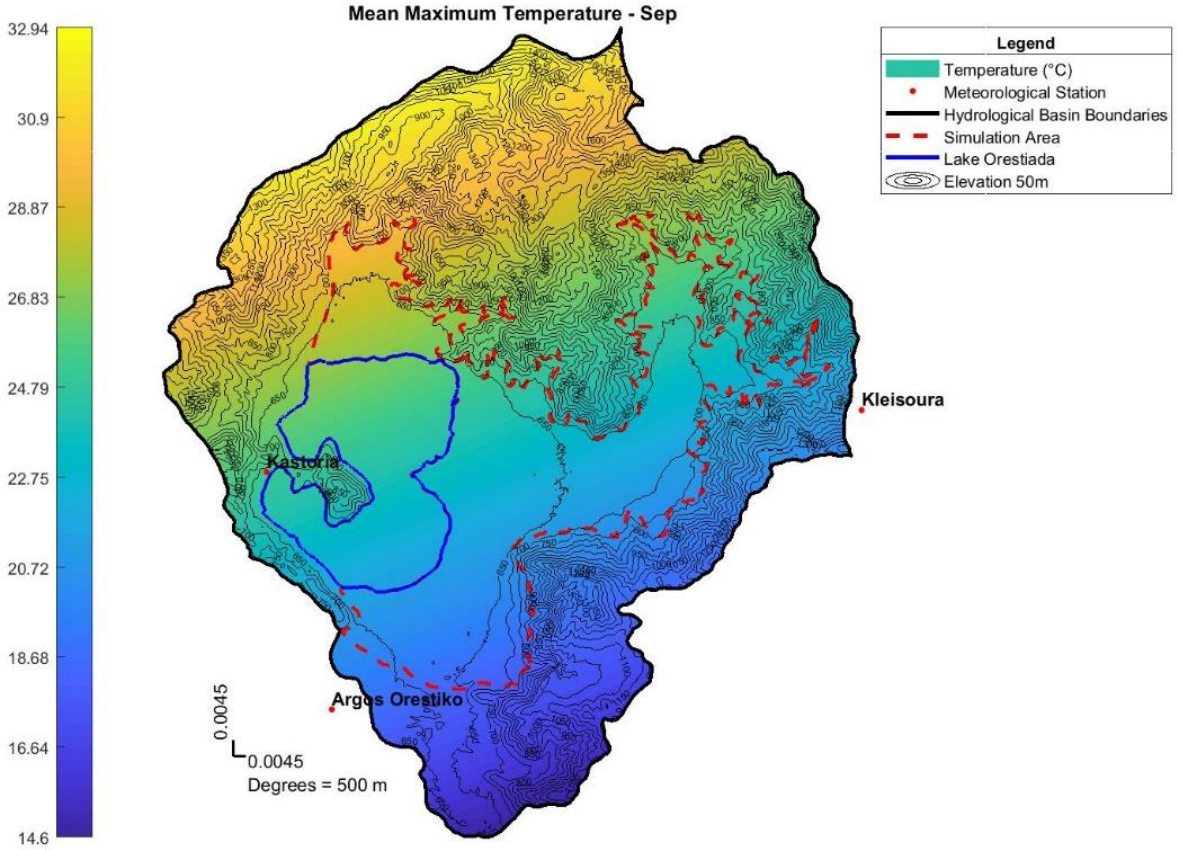

Figure 109 - Mean monthly Maximum Temperature of September at Kastoria basin

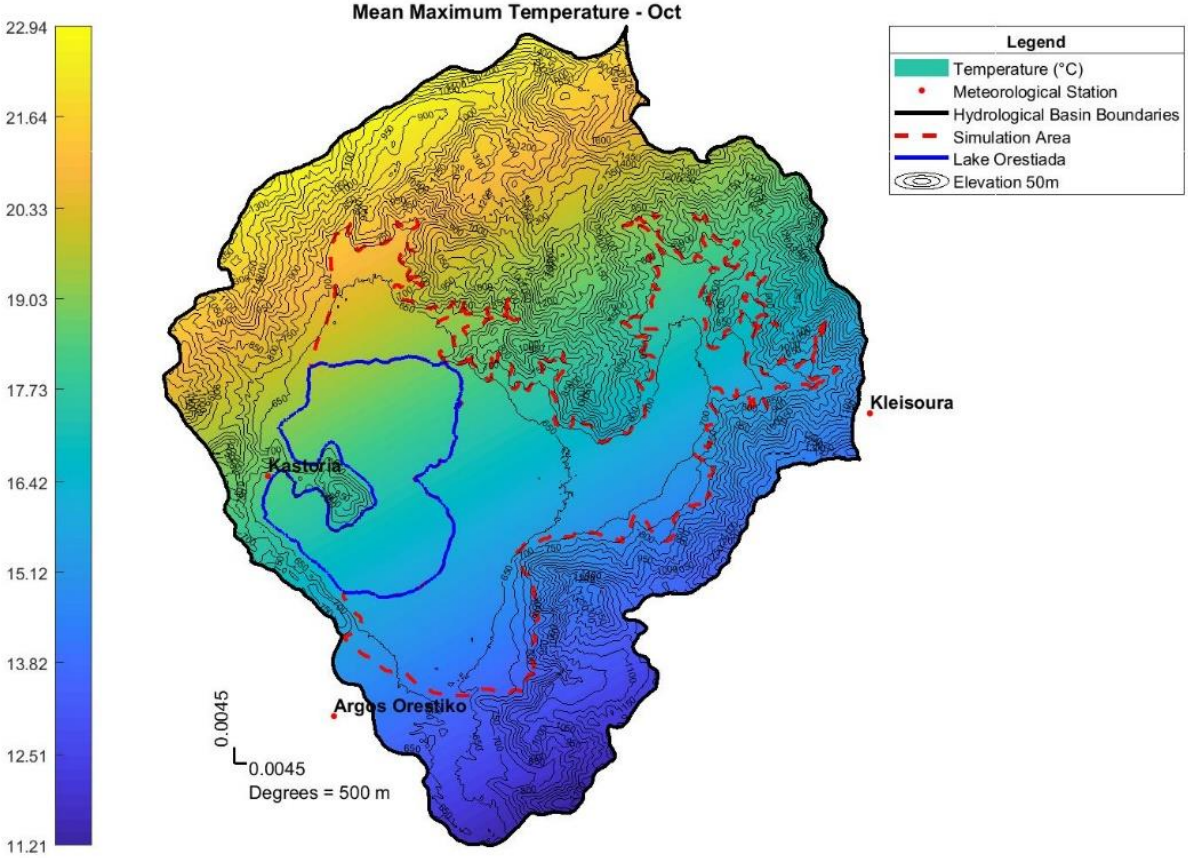

Figure 110 - Mean monthly Maximum Temperature of October at Kastoria basin

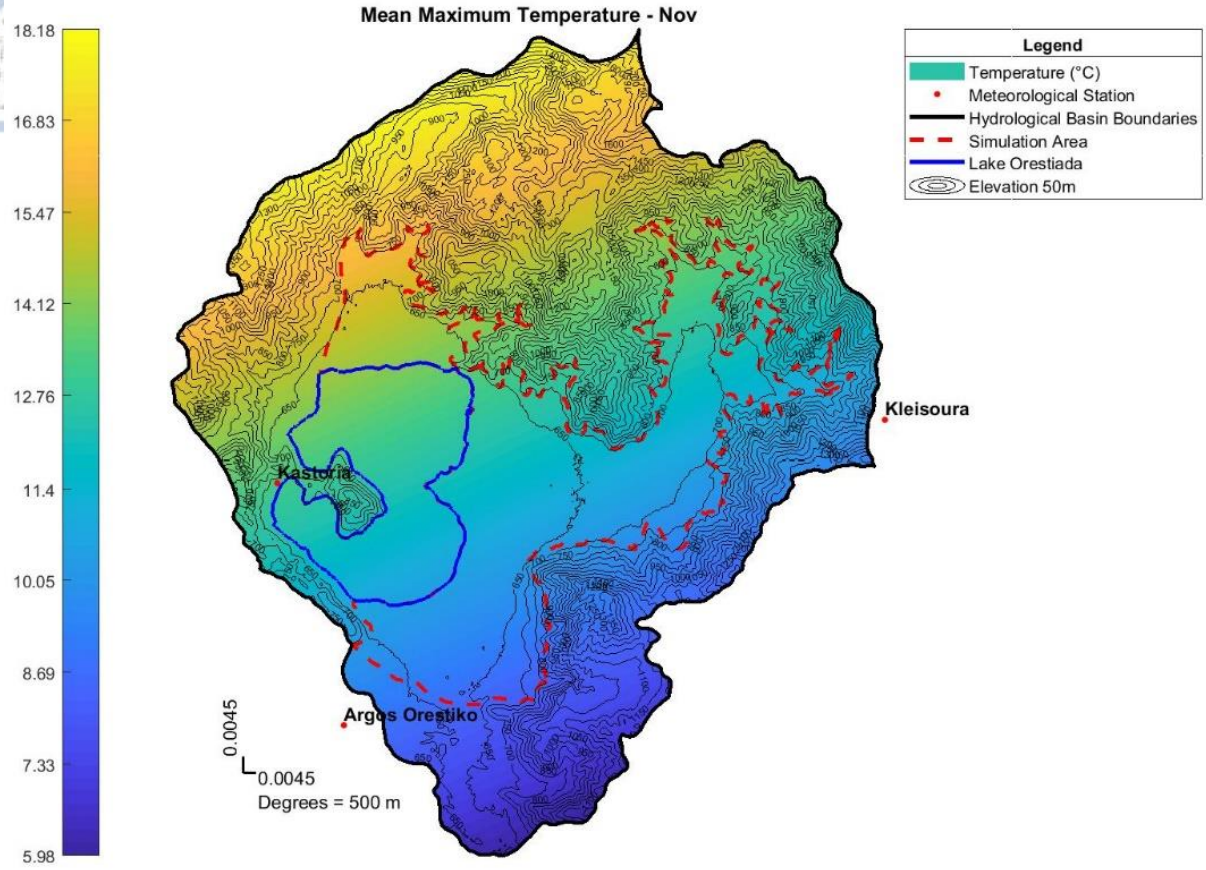

Figure 111 - Mean monthly Maximum Temperature of November at Kastoria basin

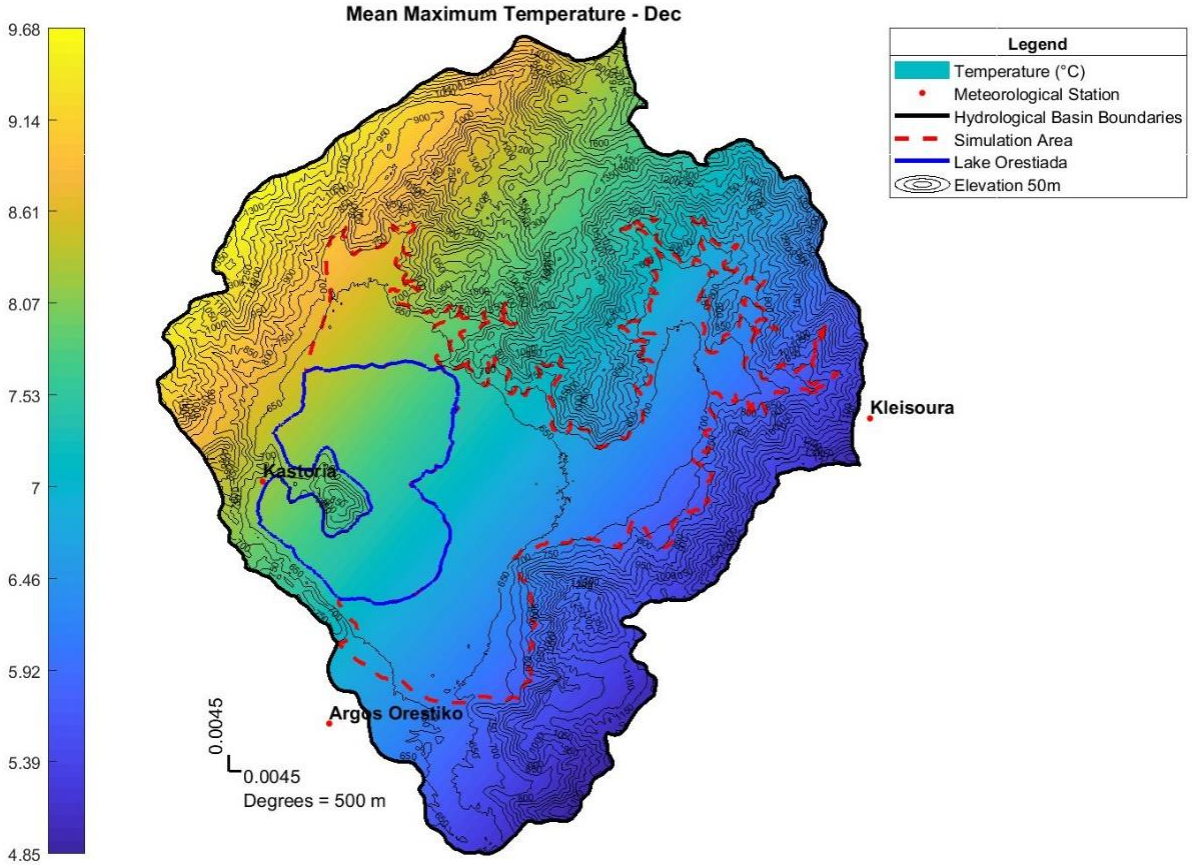

Figure 112- Mean monthly Maximum Temperature of December at Kastoria basin

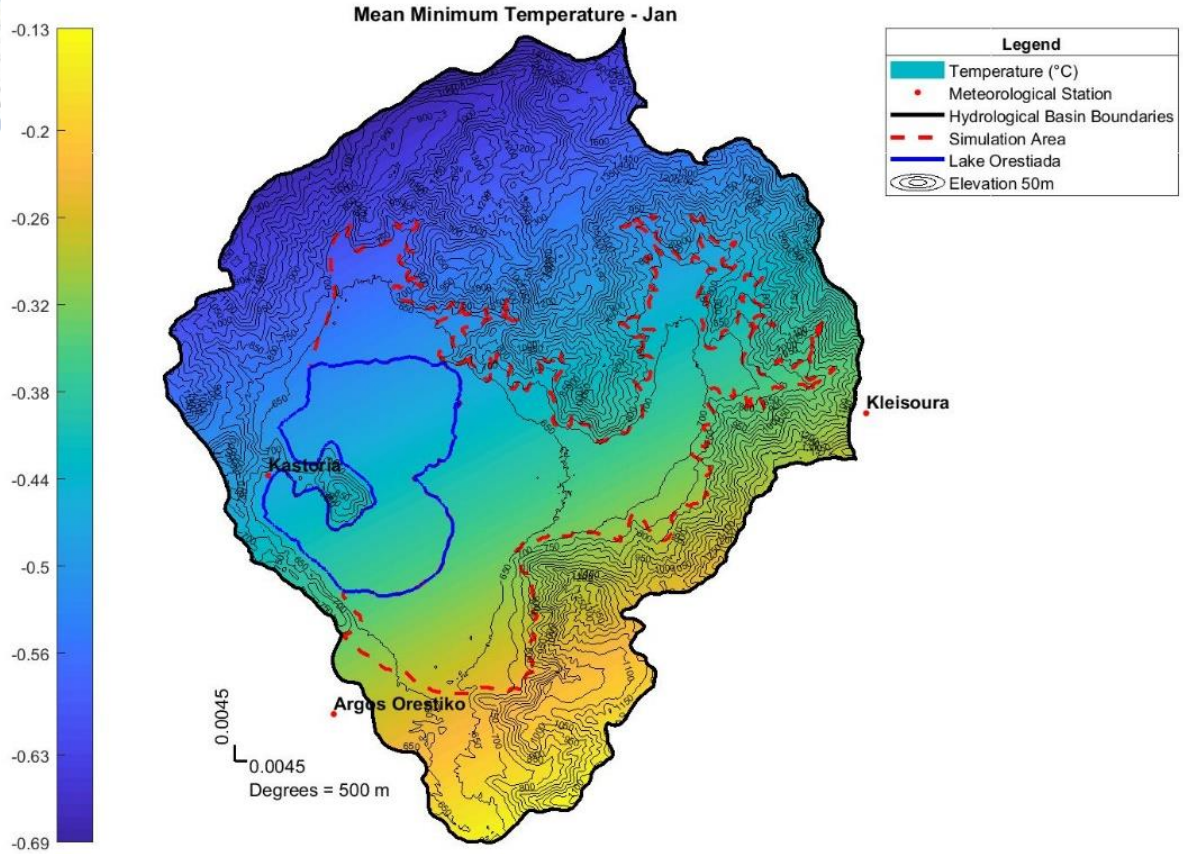

Figure 113 - Mean monthly Minimum Temperature of January at Kastoria basin

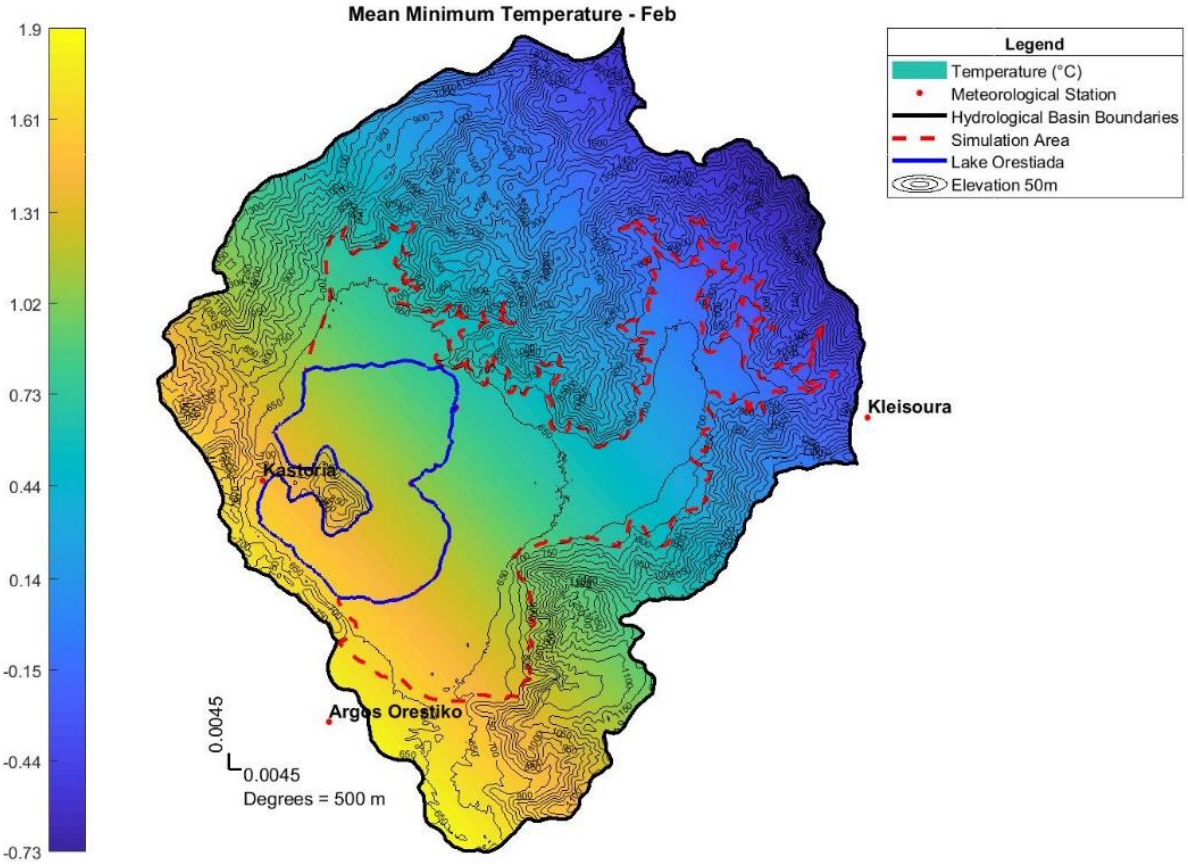

Figure 114 - Mean monthly Minimum Temperature of February at Kastoria basin

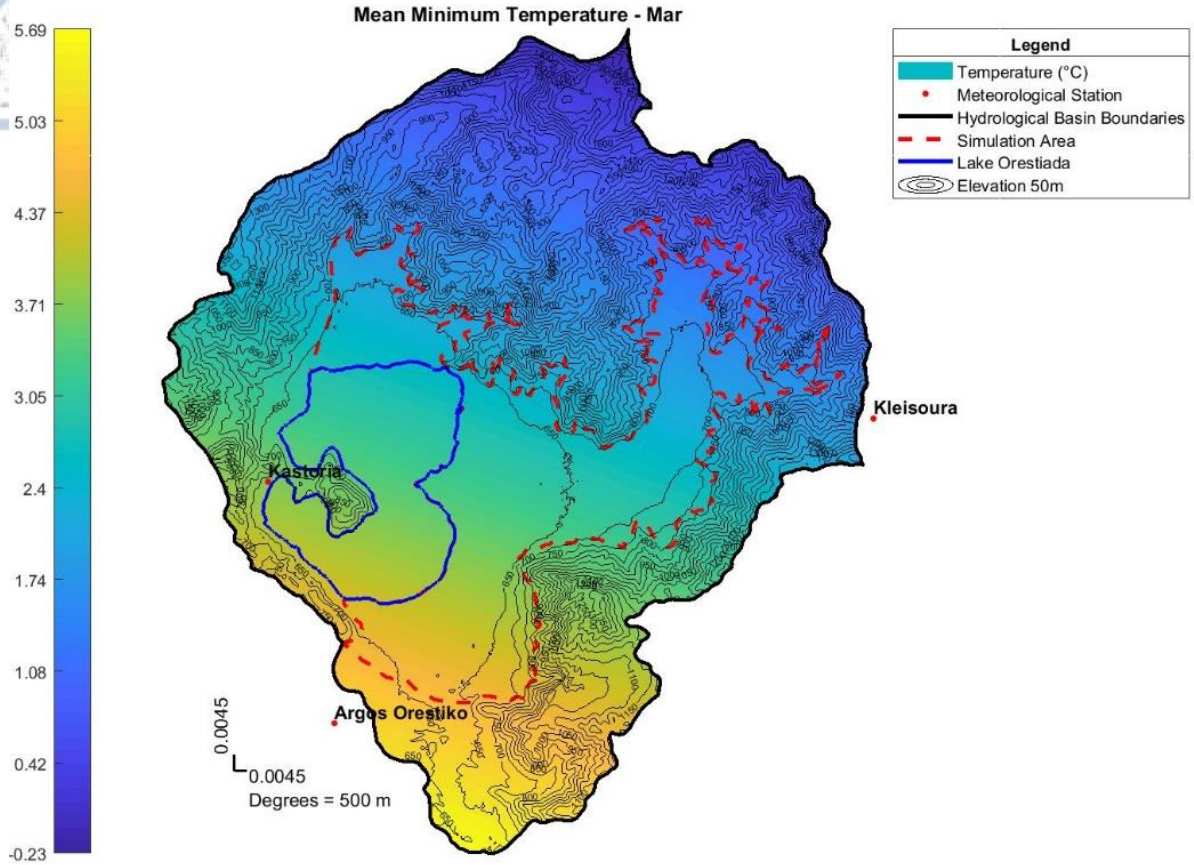

Figure 115 - Mean monthly Minimum Temperature of March at Kastoria basin

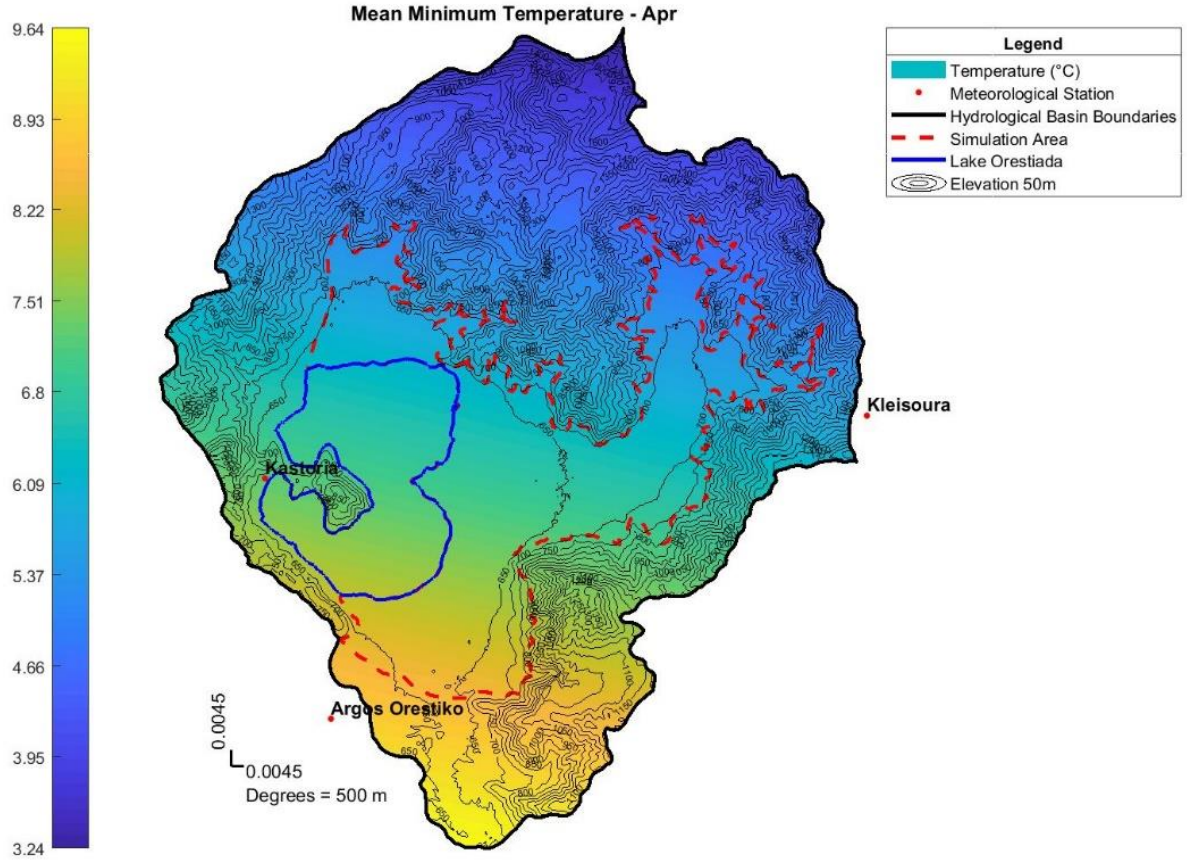

Figure 116 - Mean monthly Minimum Temperature of April at Kastoria basin

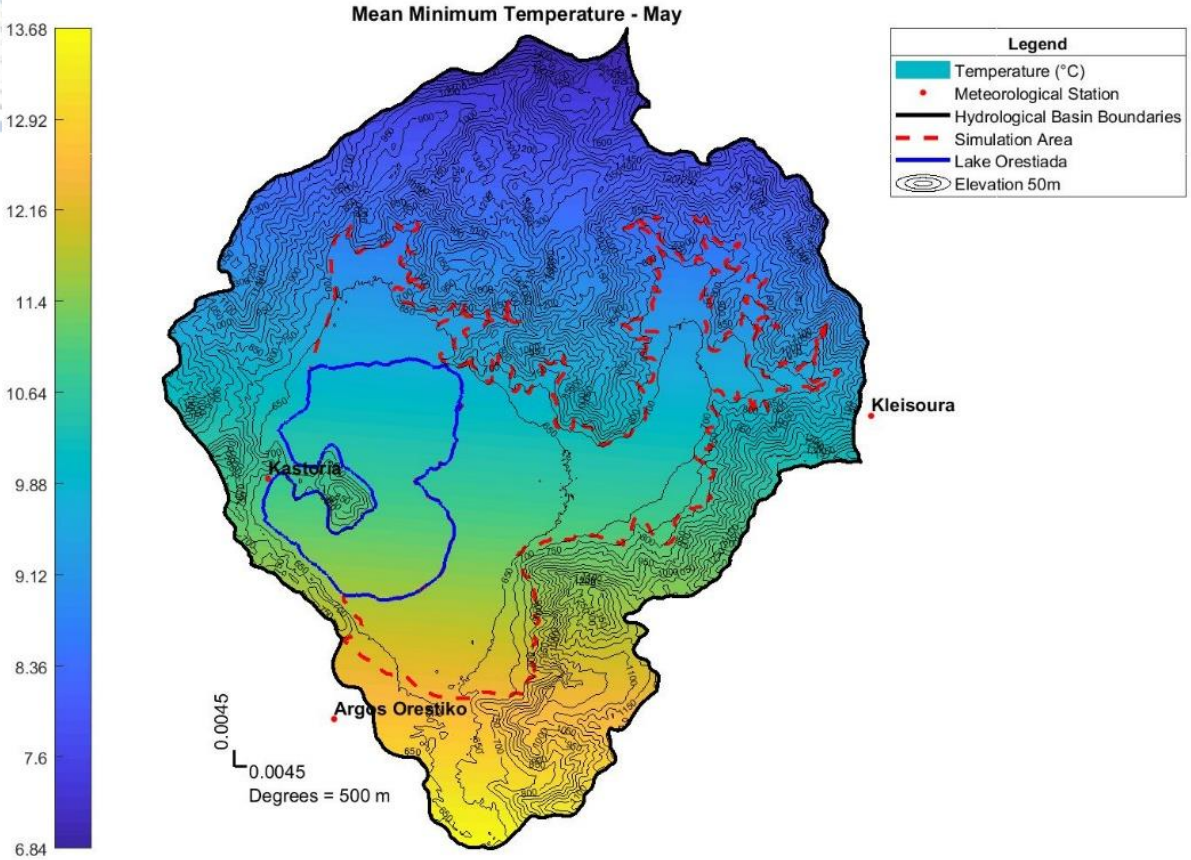

Figure 117 - Mean monthly Minimum Temperature of May at Kastoria basin

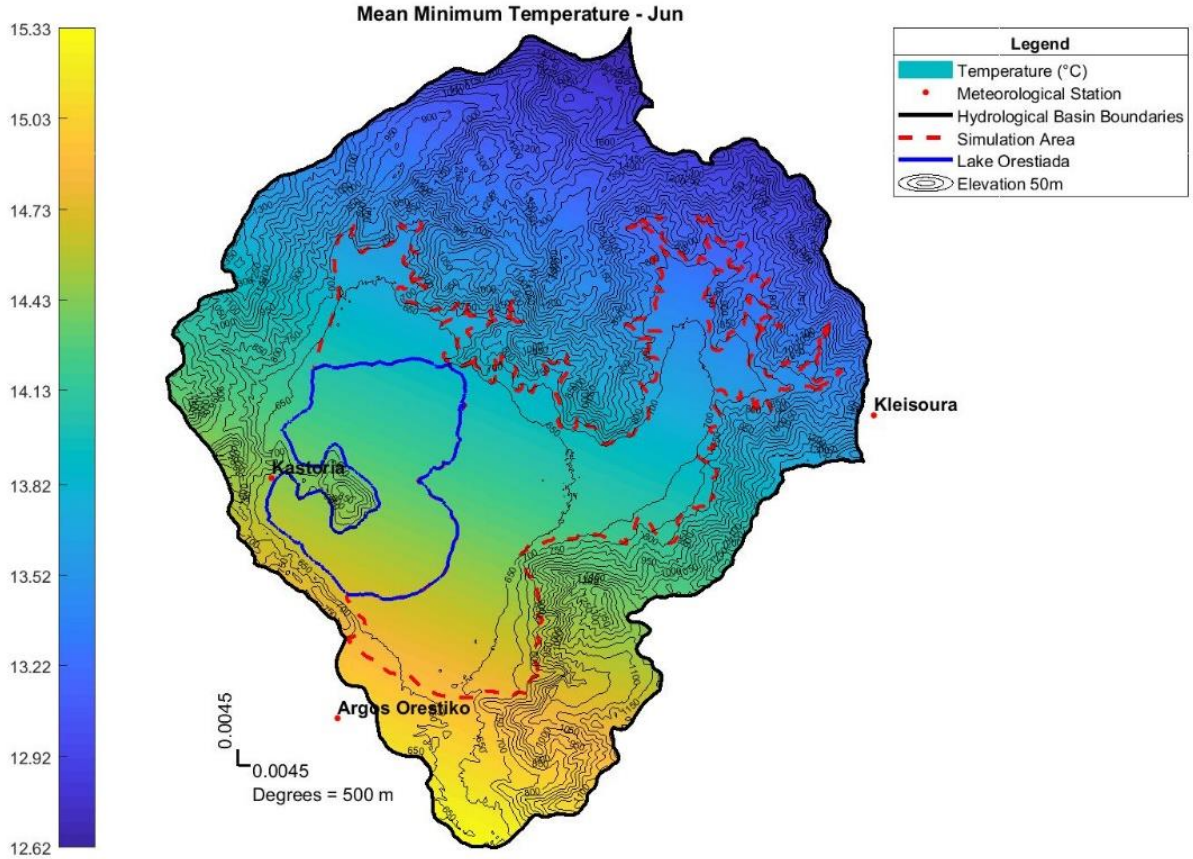

Figure 118 - Mean monthly Minimum Temperature of June at Kastoria basin

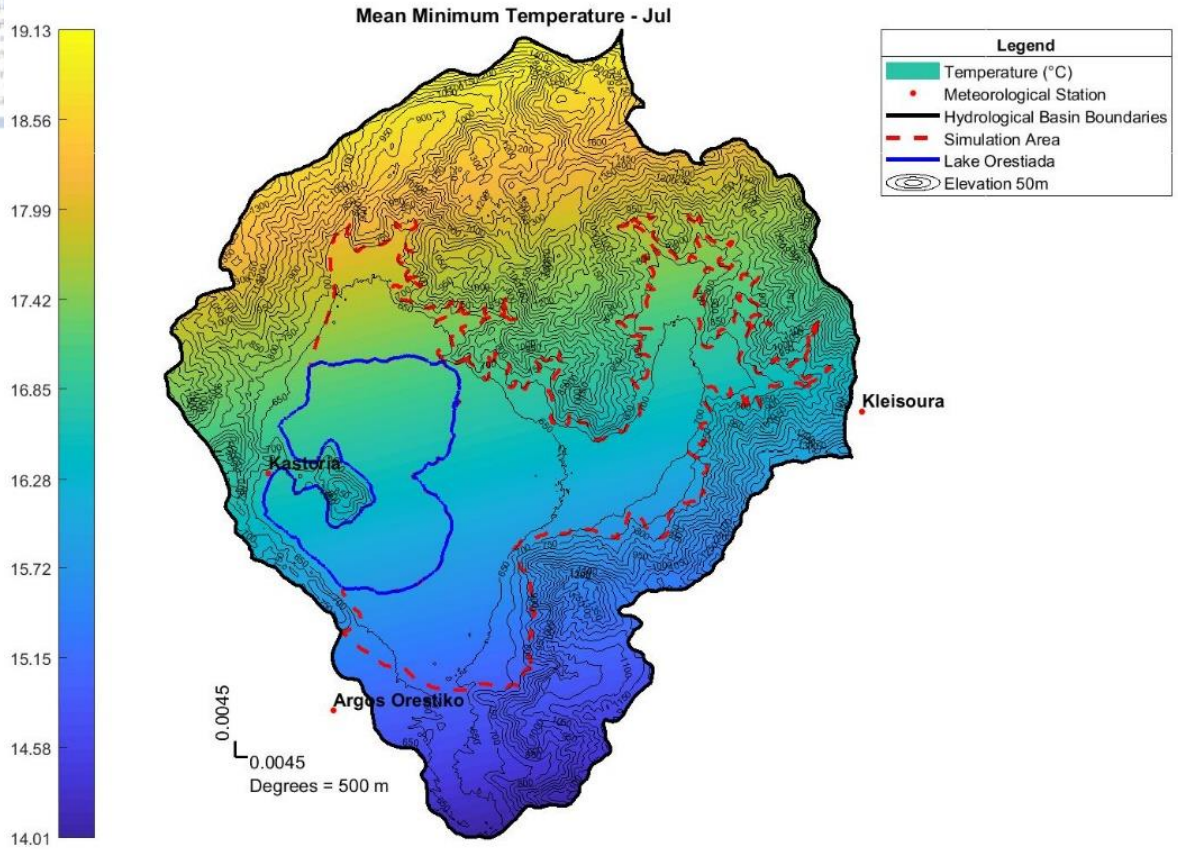

Figure 119 - Mean monthly Minimum Temperature of July at Kastoria basin

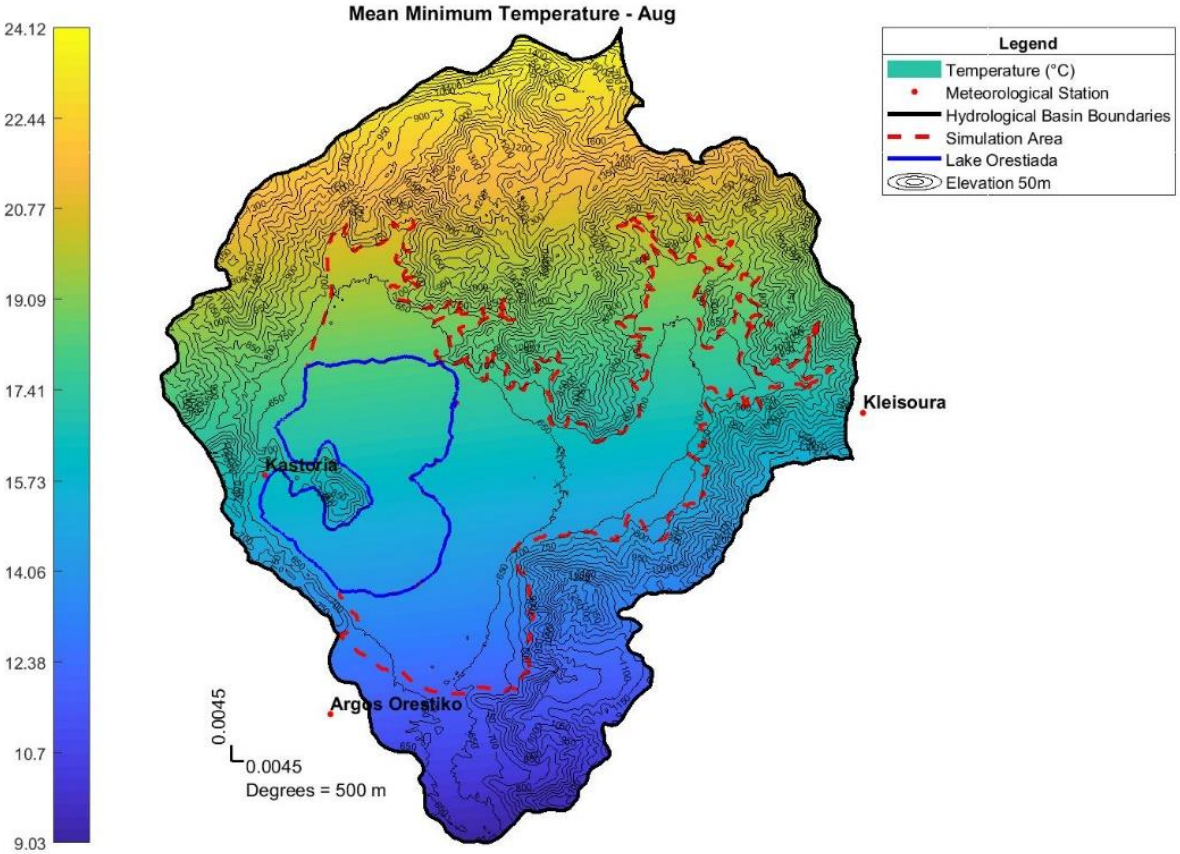

Figure 120 - Mean monthly Minimum Temperature of August at Kastoria basin

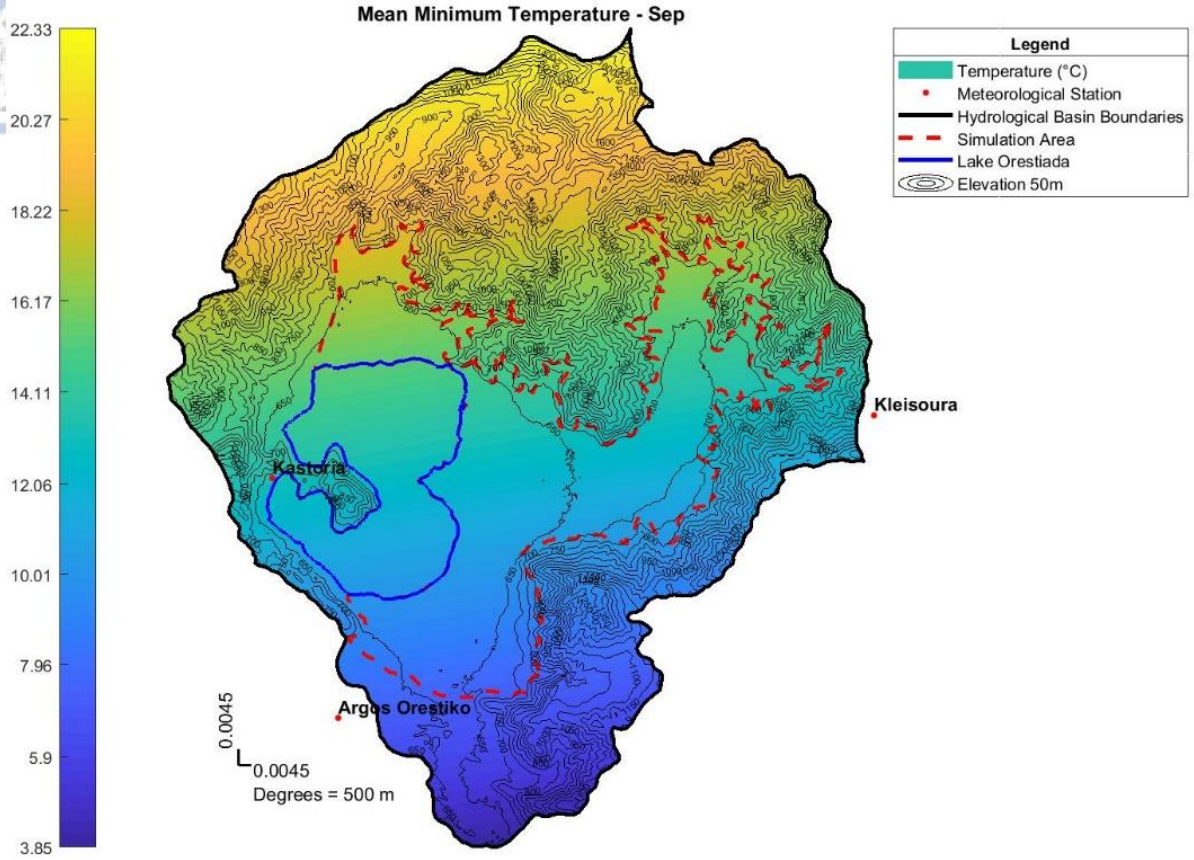

Figure 121 - Mean monthly Minimum Temperature of September at Kastoria basin

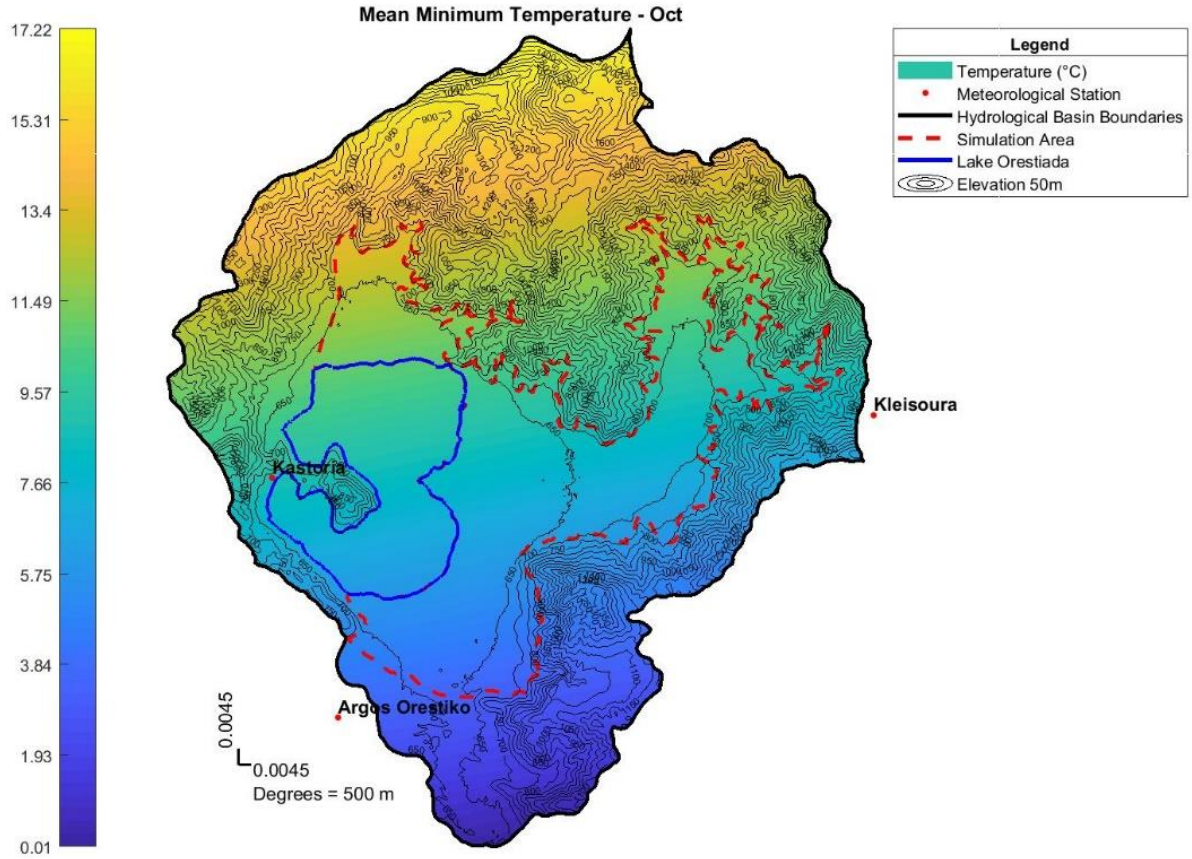

Figure 122 - Mean monthly Minimum Temperature of October at Kastoria basin

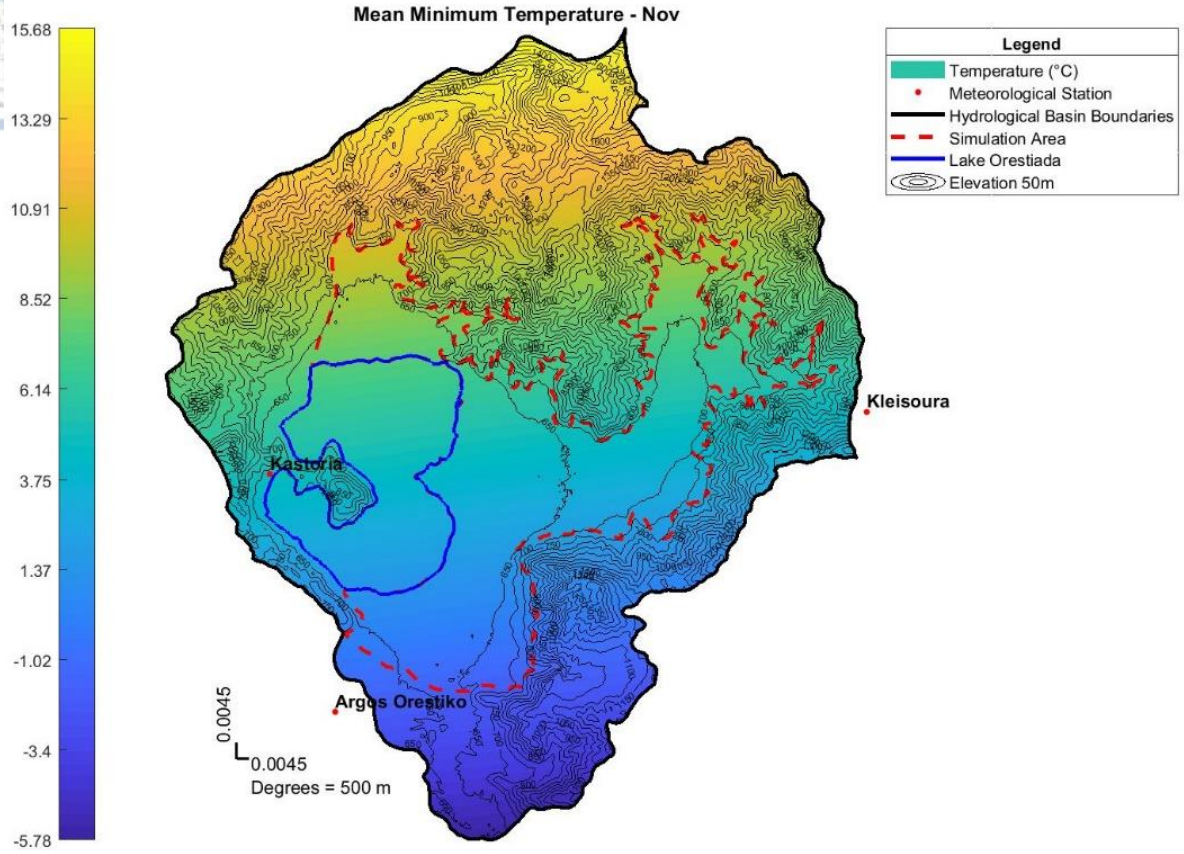

Figure 123 - Mean monthly Minimum Temperature of November at Kastoria basin

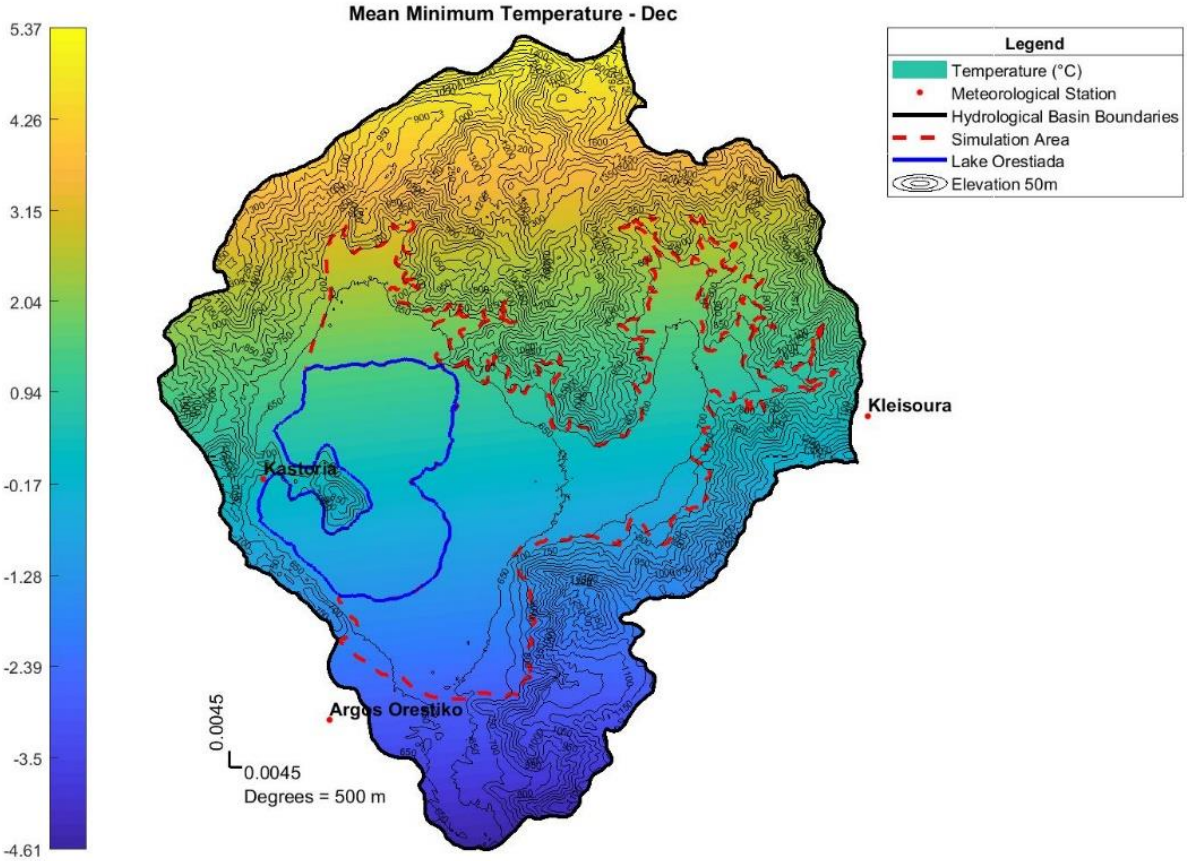

Figure 124 - Mean monthly Minimum Temperature of December at Kastoria basin

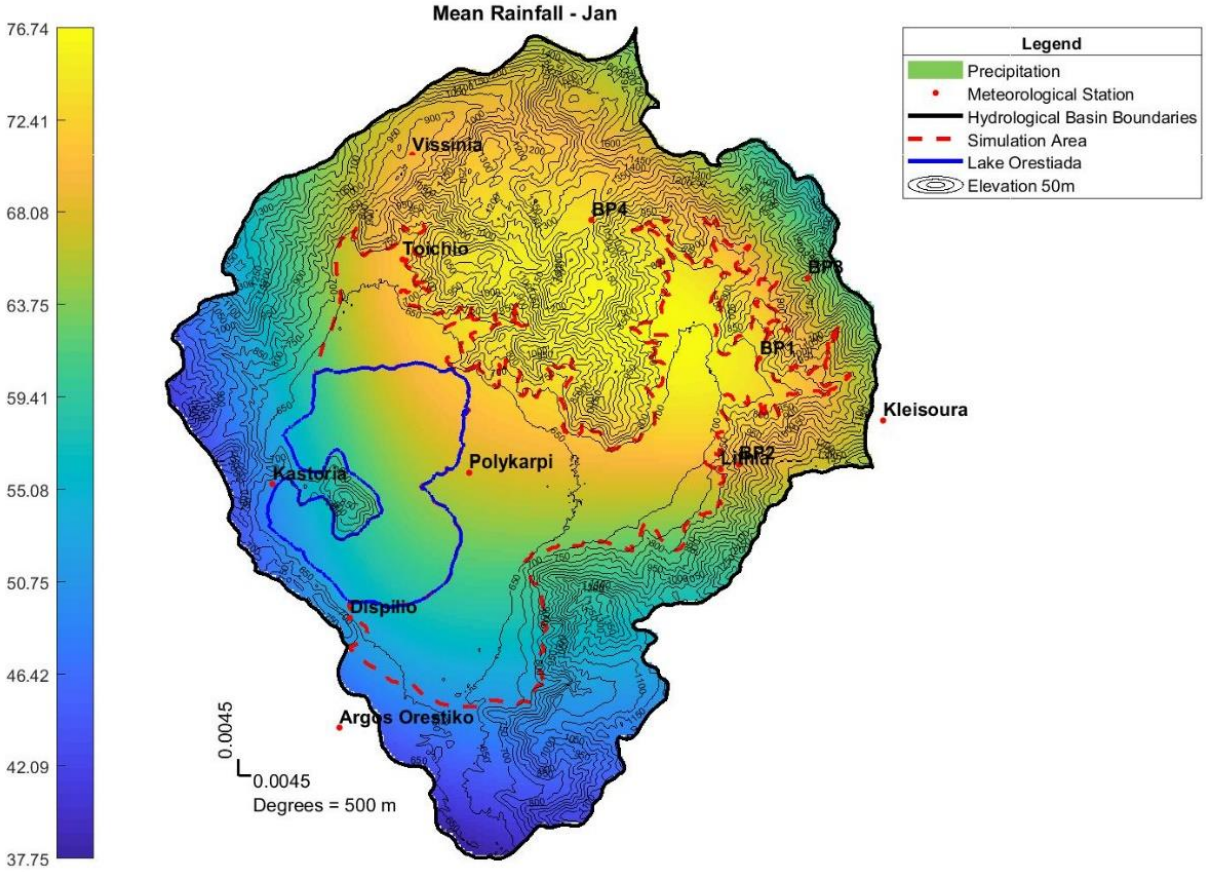

Figure 125 - Mean Monthly Rainfall of January at Kastoria Basin

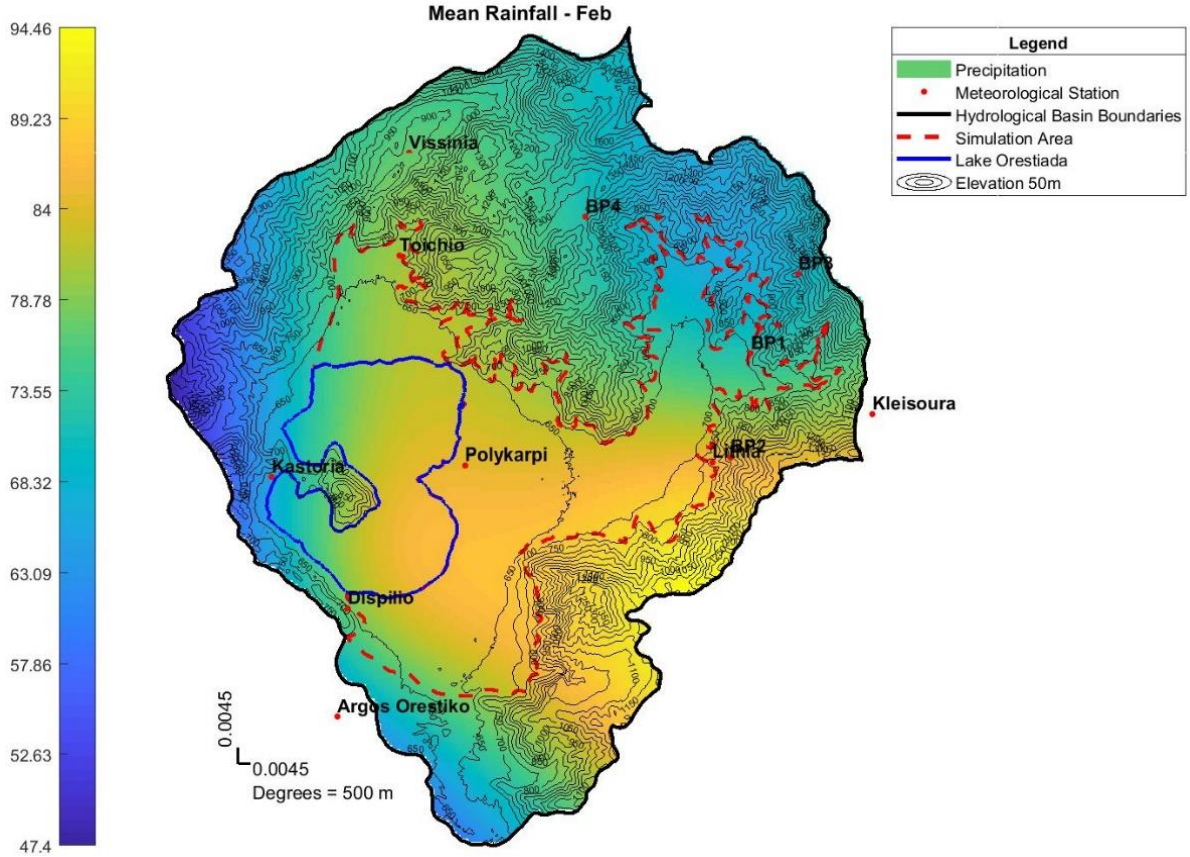

Figure 126 - Mean Monthly Rainfall of February at Kastoria Basin

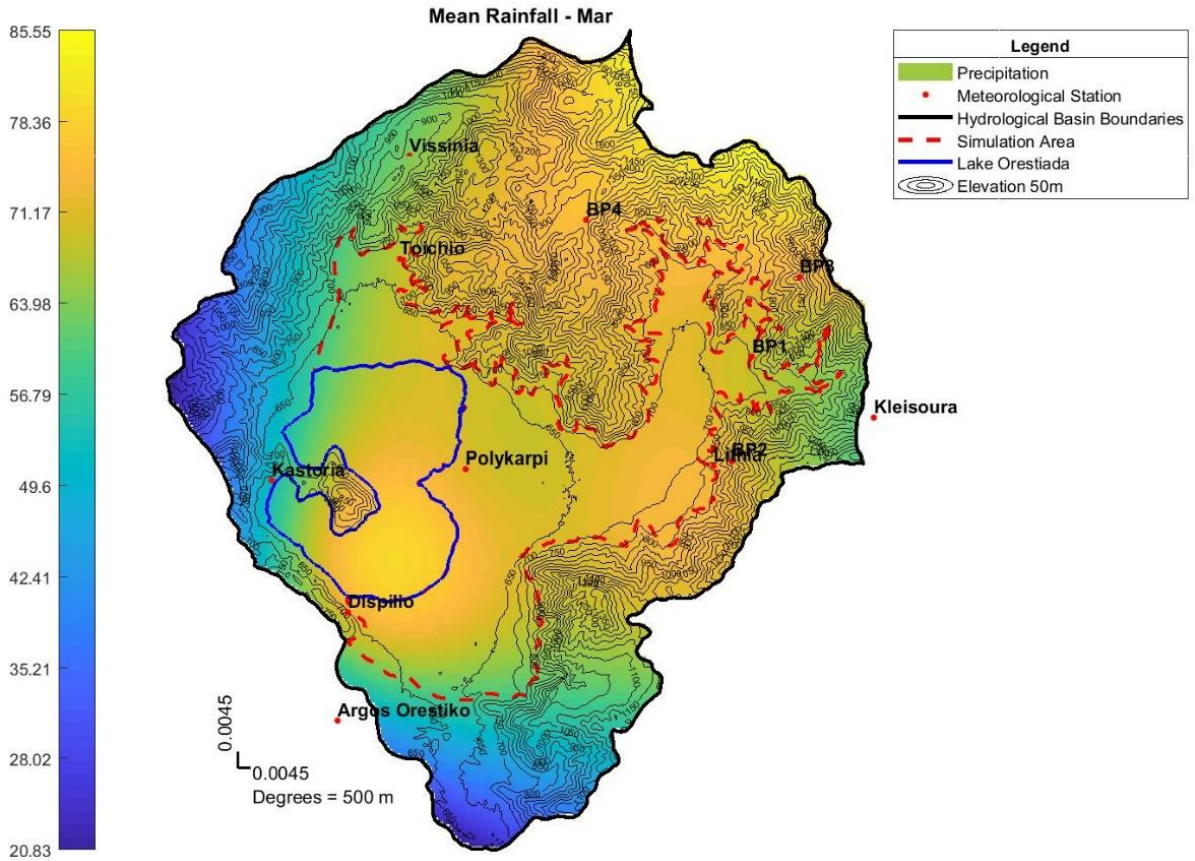

Figure 127 - Mean Monthly Rainfall of March at Kastoria Basin

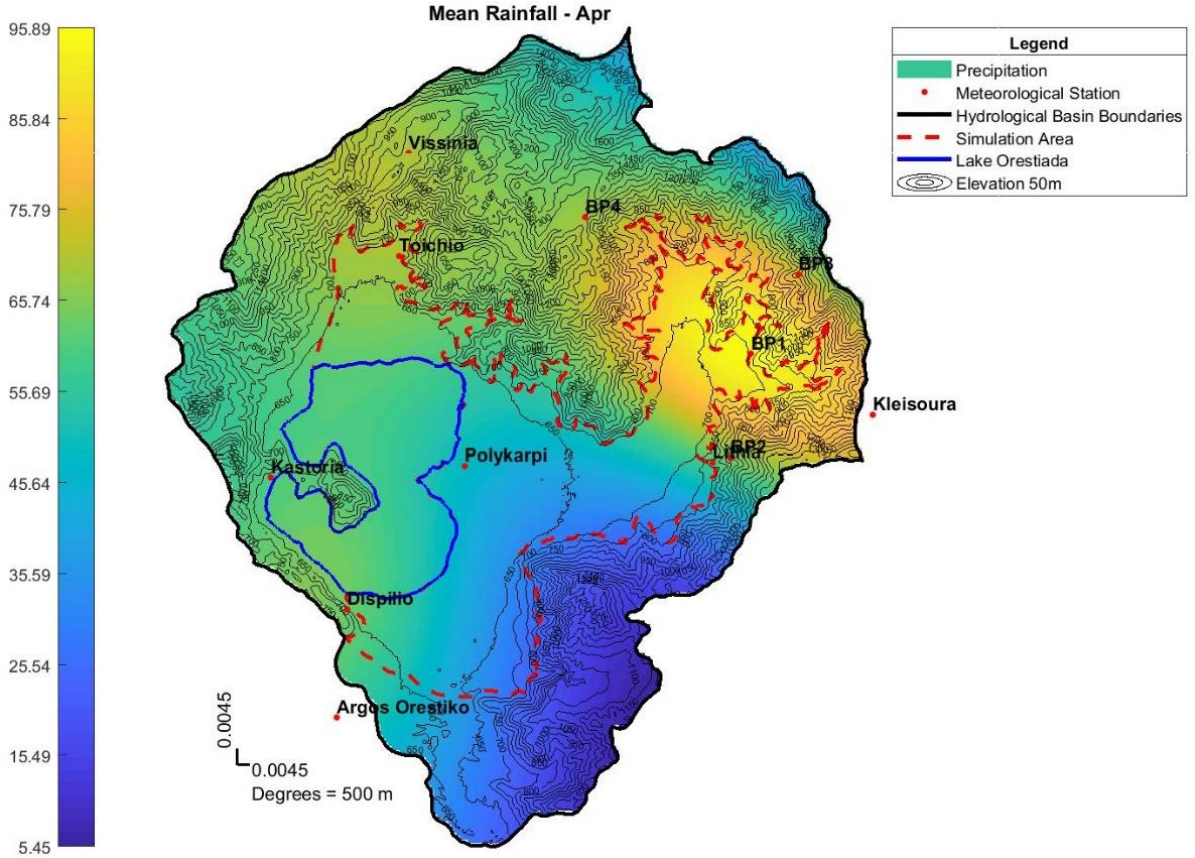

Figure 128 - Mean Monthly Rainfall of April at Kastoria Basin

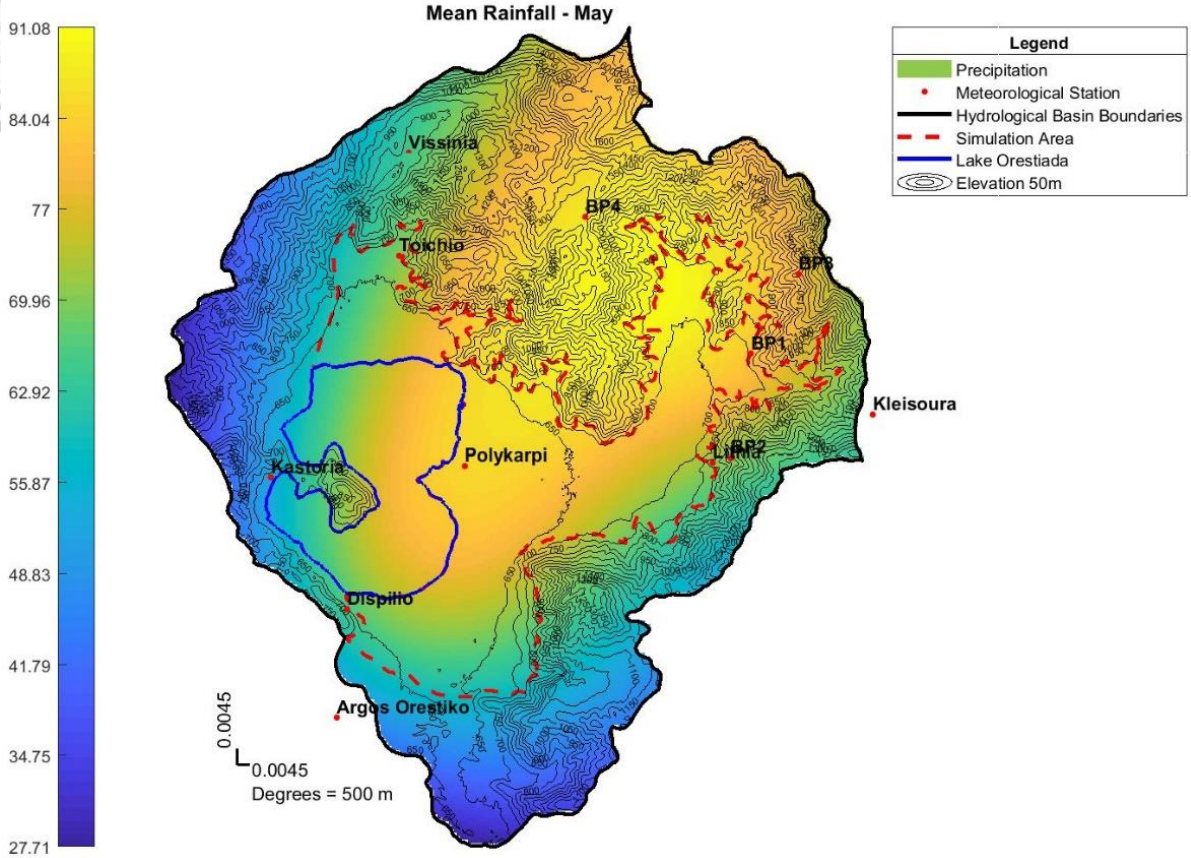

Figure 129 - Mean Monthly Rainfall of May at Kastoria Basin

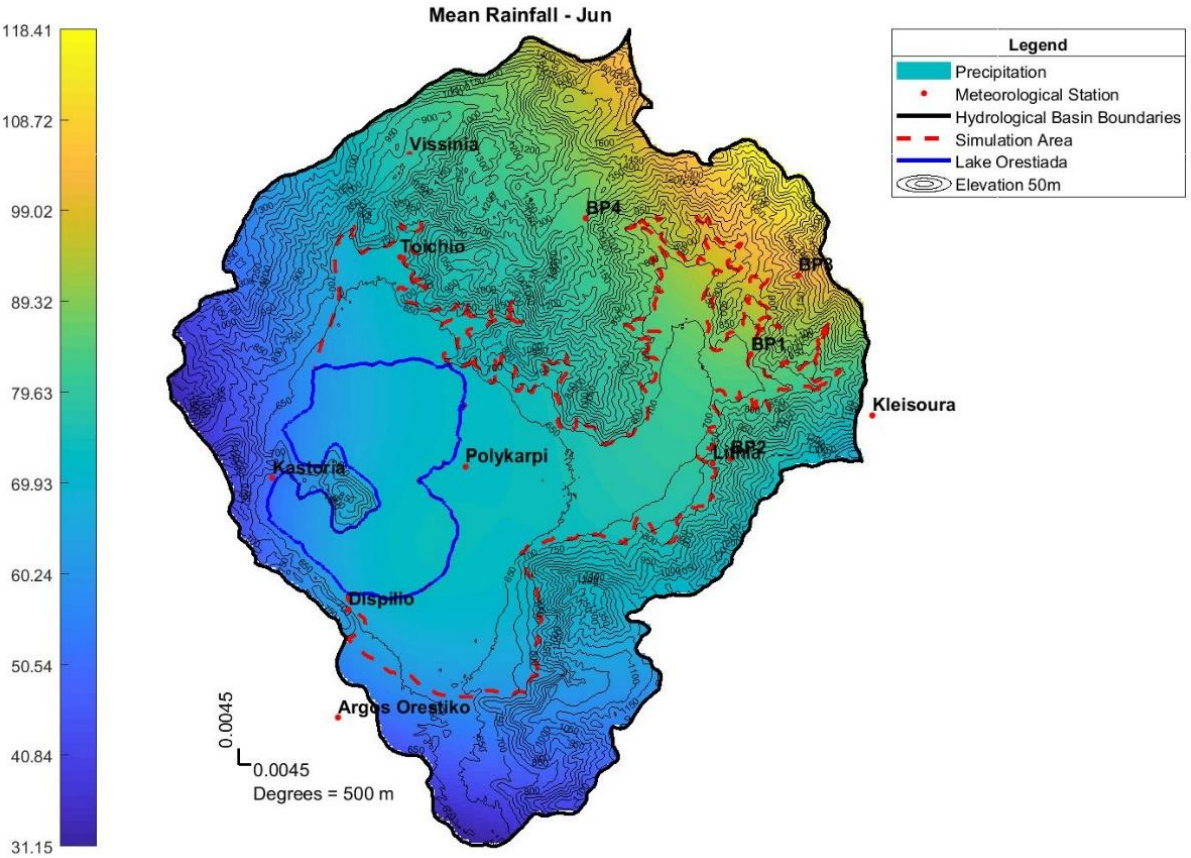

Figure 130 - Mean Monthly Rainfall of June at Kastoria Basin

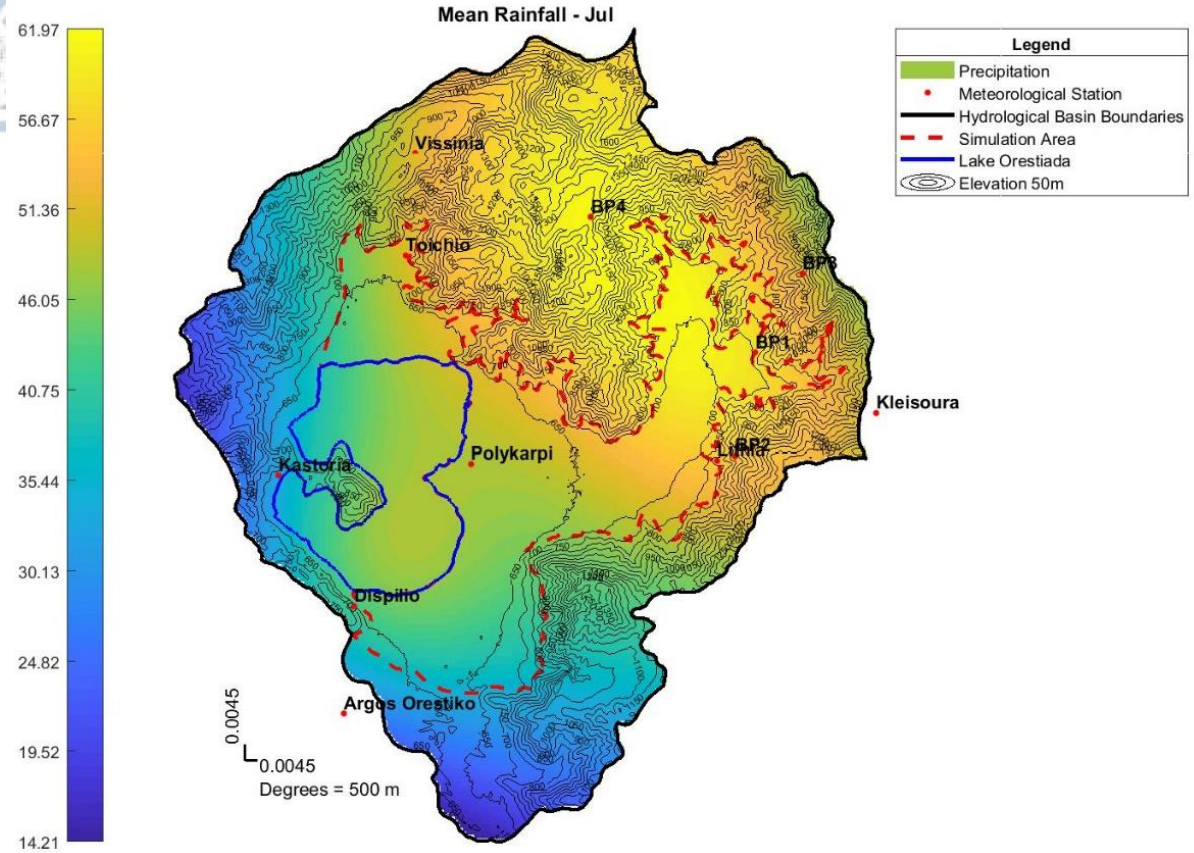

Figure 131 - Mean Monthly Rainfall of July at Kastoria Basin

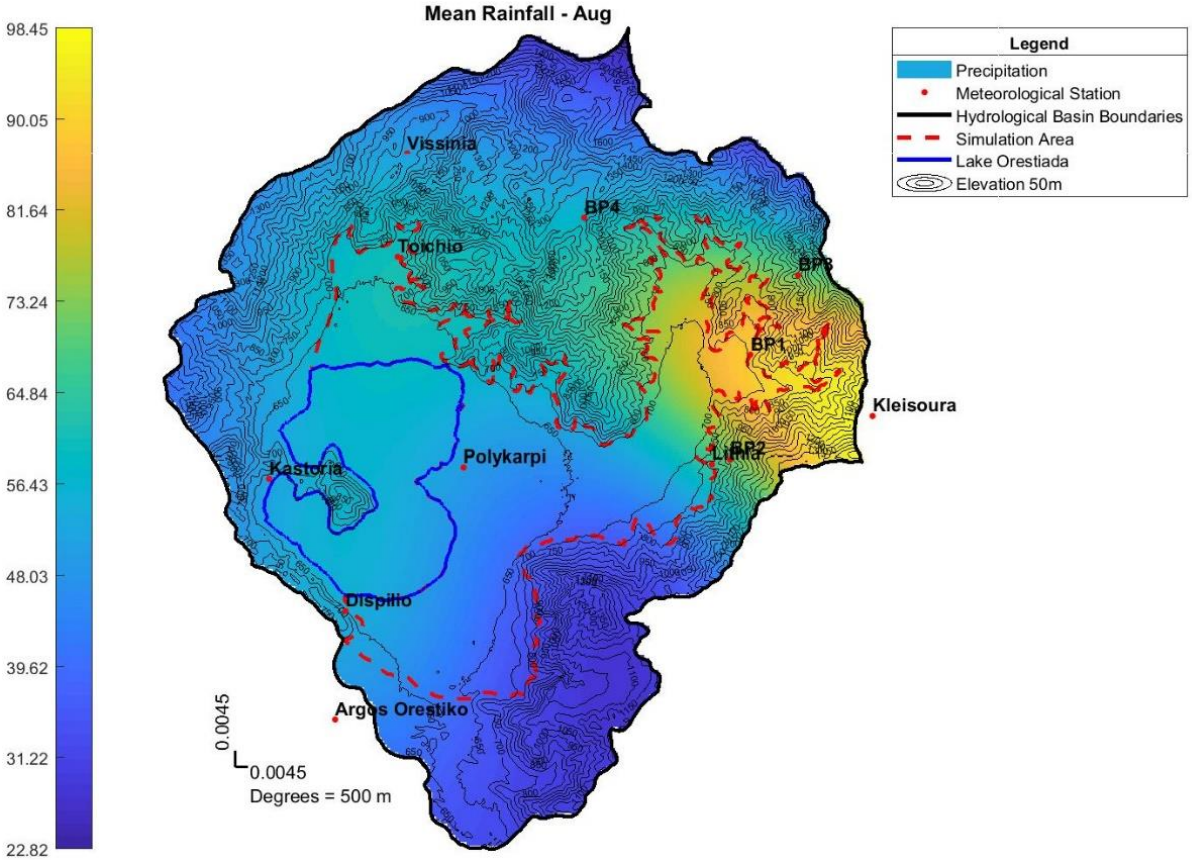

Figure 132 - Mean Monthly Rainfall of August at Kastoria Basin

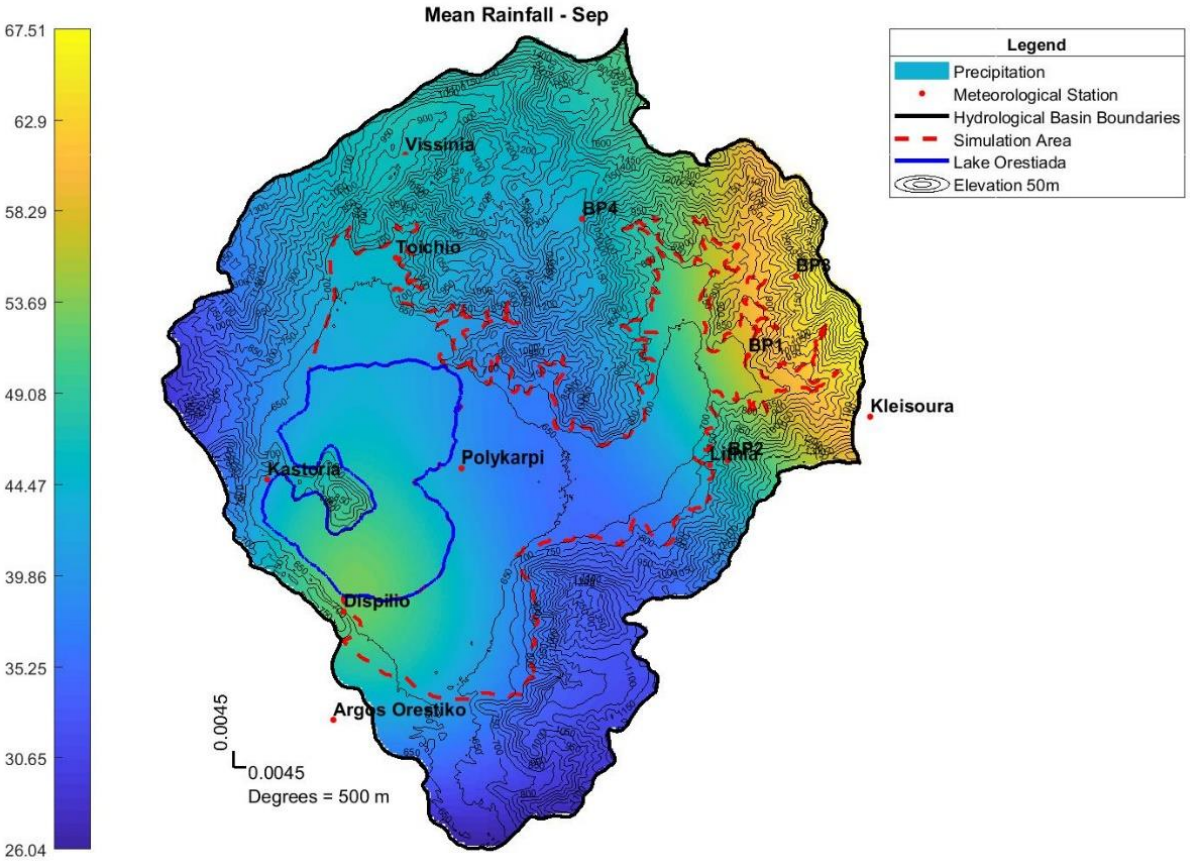

Figure 133 - Mean Monthly Rainfall of September at Kastoria Basin

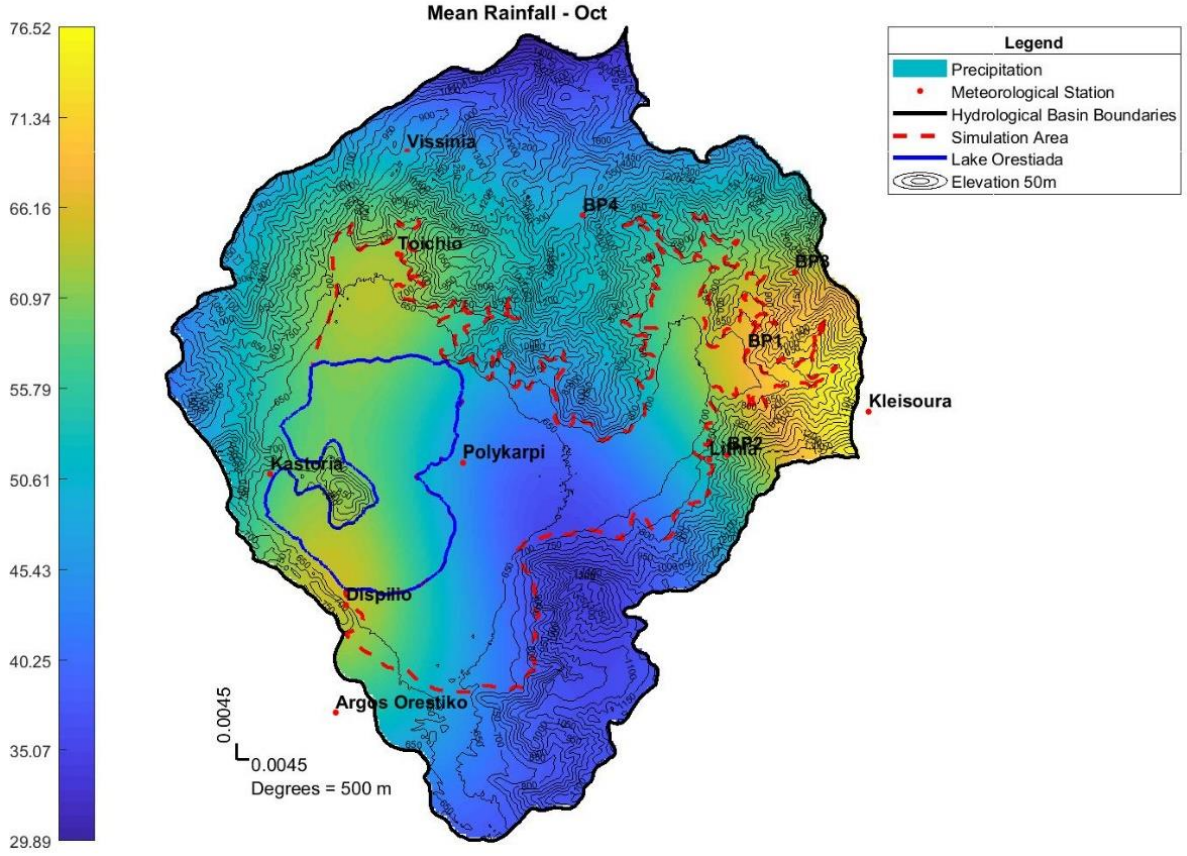

Figure 134 - Mean Monthly Rainfall of October at Kastoria Basin

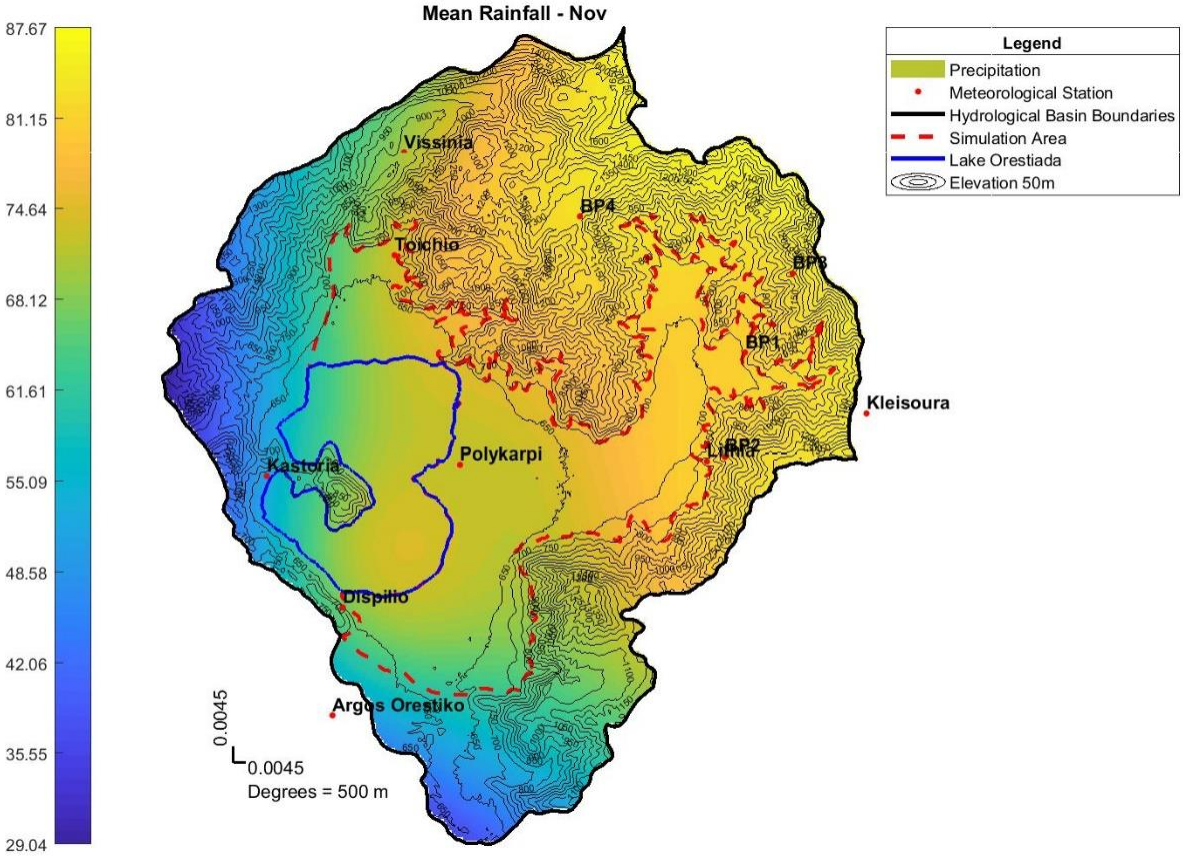

Figure 135 - Mean Monthly Rainfall of November at Kastoria Basin

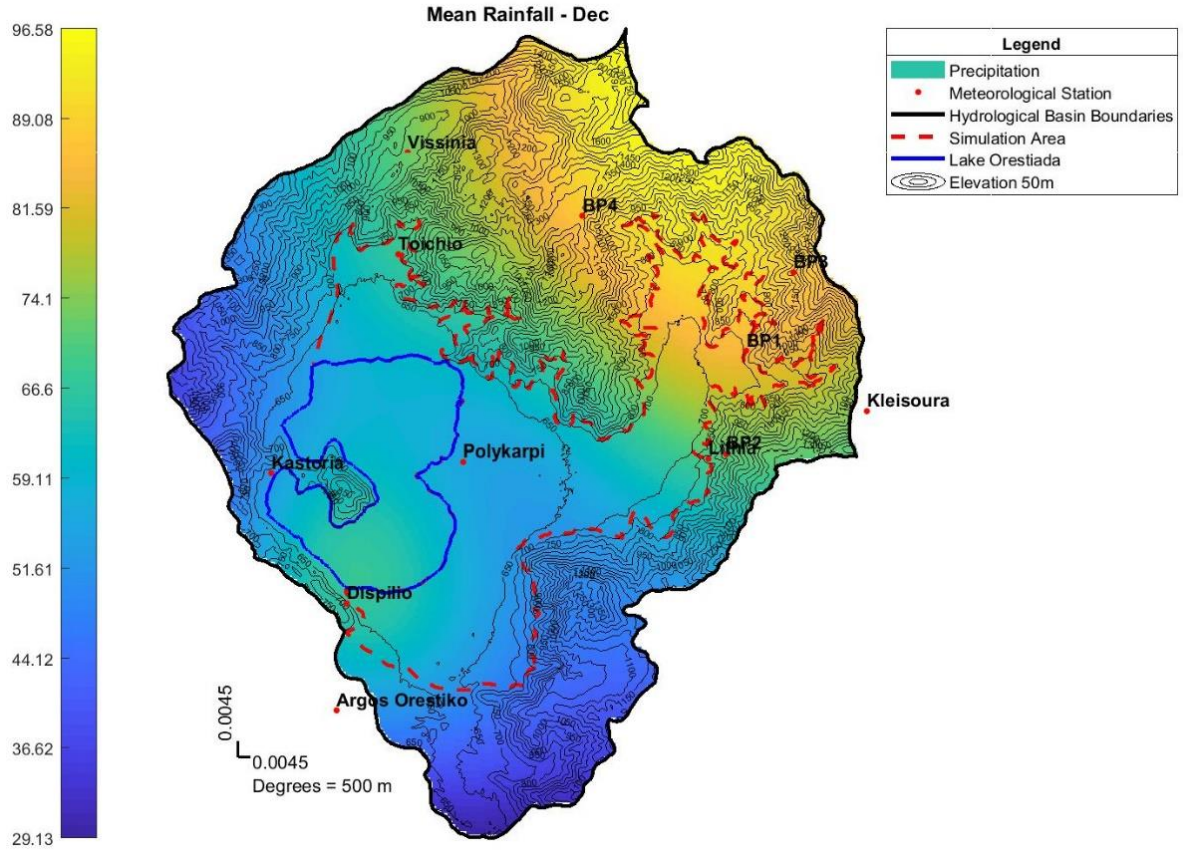

Figure 136 - Mean Monthly Rainfall of December at Kastoria Basin

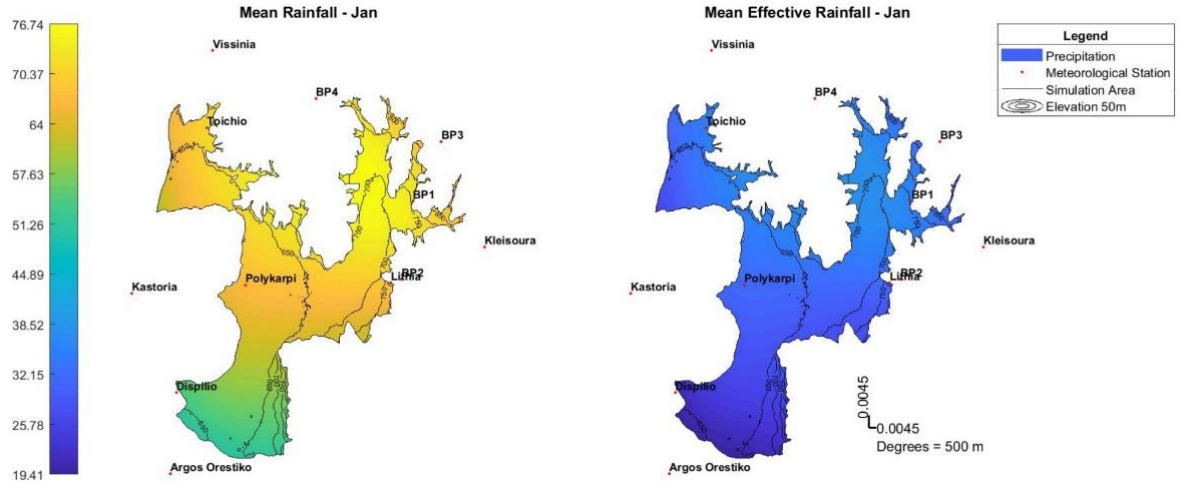

Figure 137 - Mean monthly rainfall and effective rainfall of January at simulation area

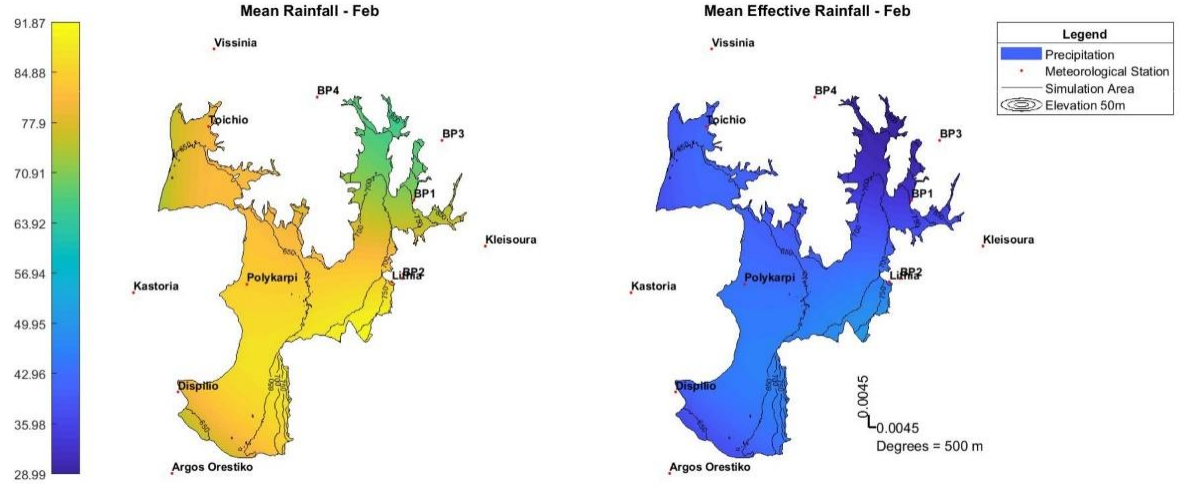

Figure 138 - Mean monthly rainfall and effective rainfall of February at simulation area

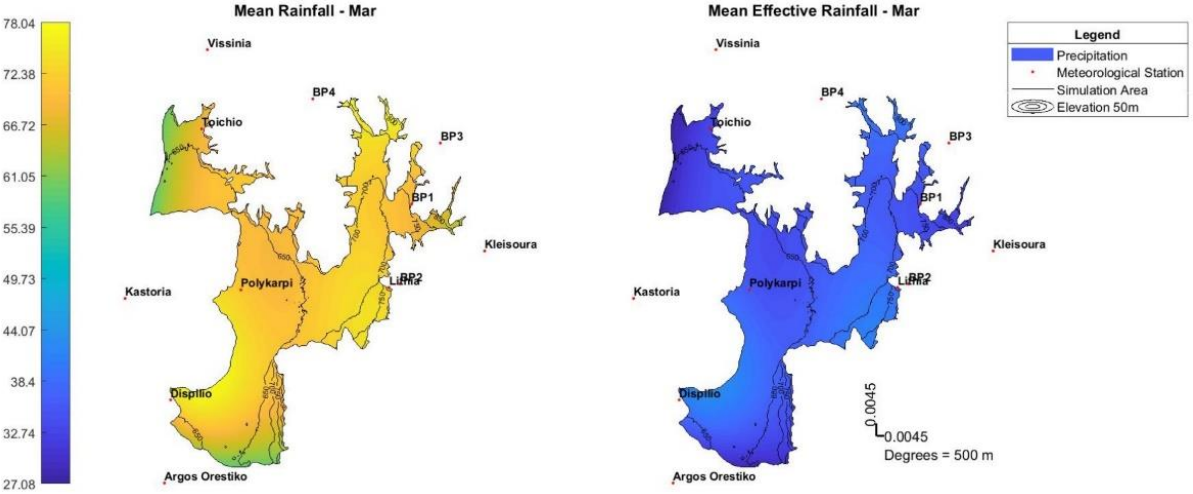

Figure 139 - Mean monthly rainfall and effective rainfall of March at simulation area

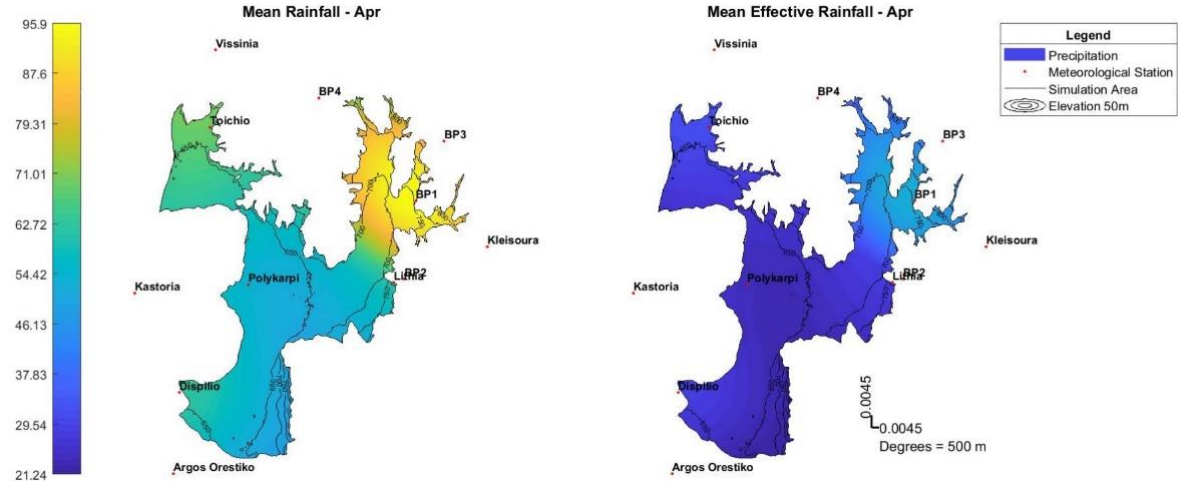

Figure 140 - Mean monthly rainfall and effective rainfall of April at simulation area

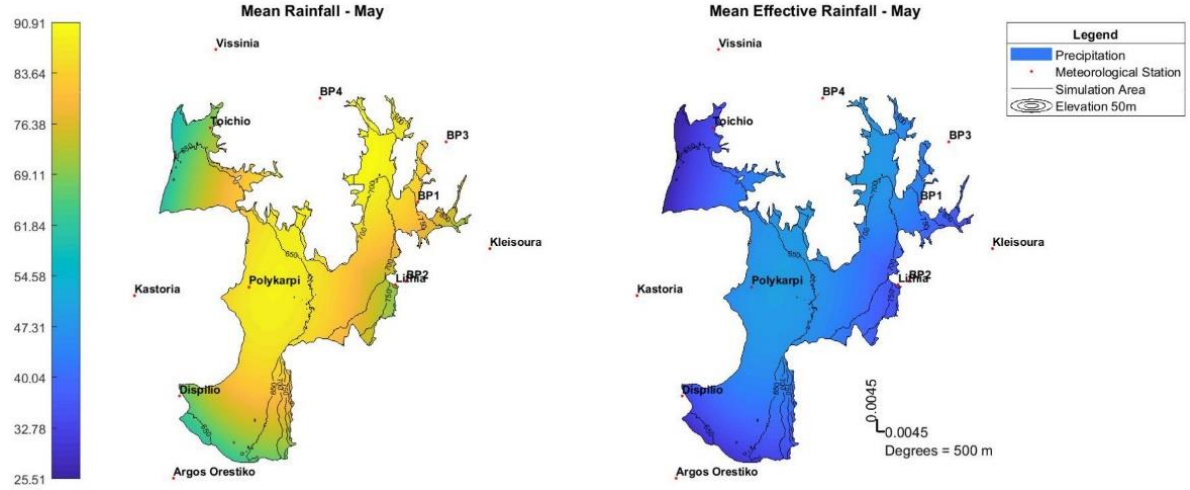

Figure 141 - Mean monthly rainfall and effective rainfall of May at simulation area

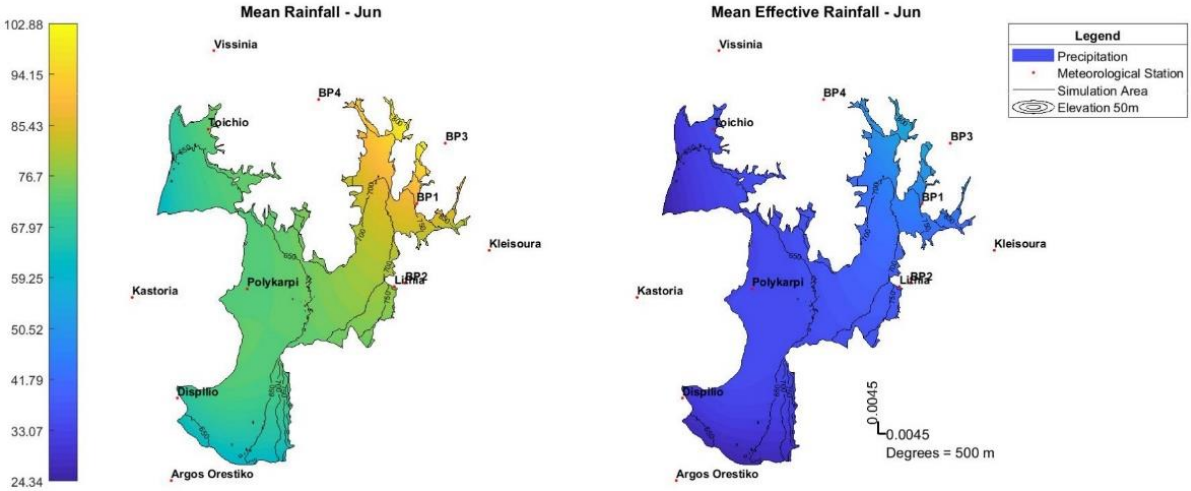

Figure 142 - Mean monthly rainfall and effective rainfall of June at simulation area

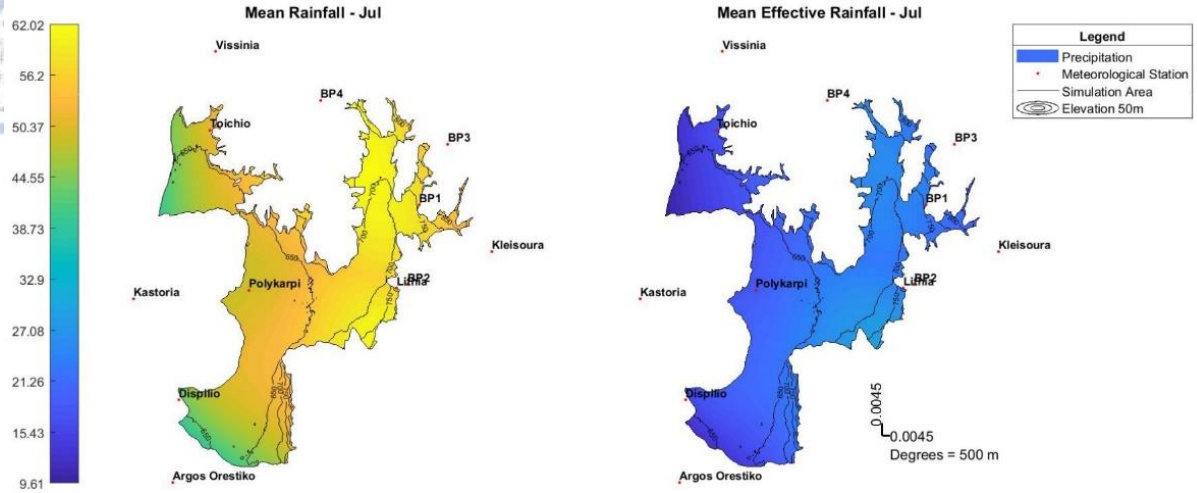

Figure 143 - Mean monthly rainfall and effective rainfall of July at simulation area

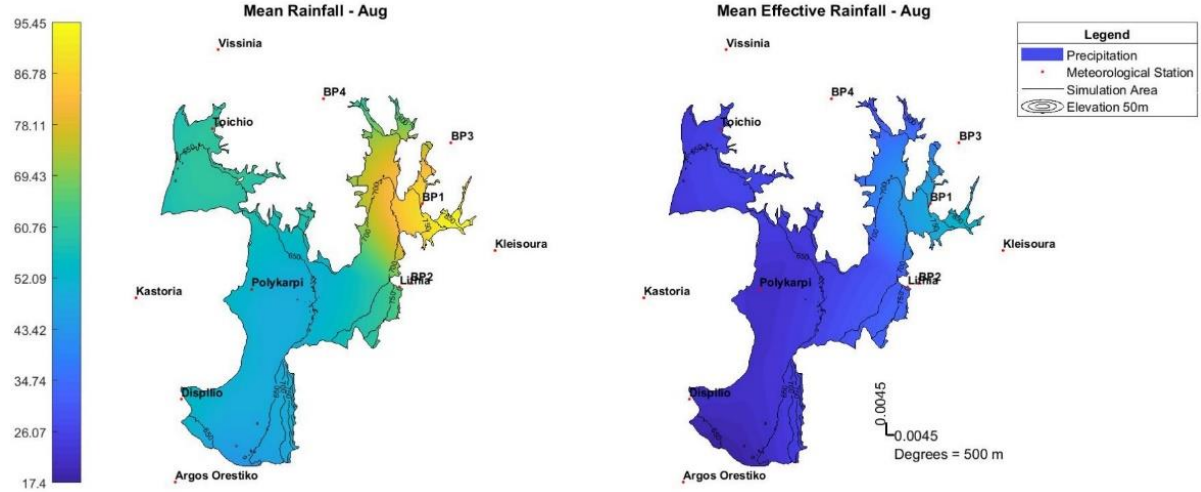

Figure 144 - Mean monthly rainfall and effective rainfall of August at simulation area

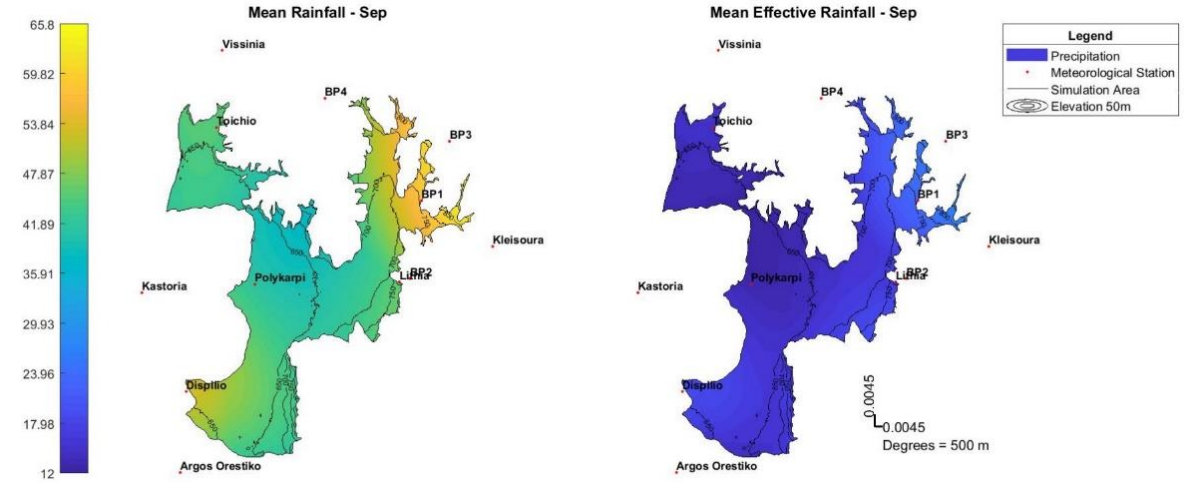

Figure 145 - Mean monthly rainfall and effective rainfall of September at simulation area

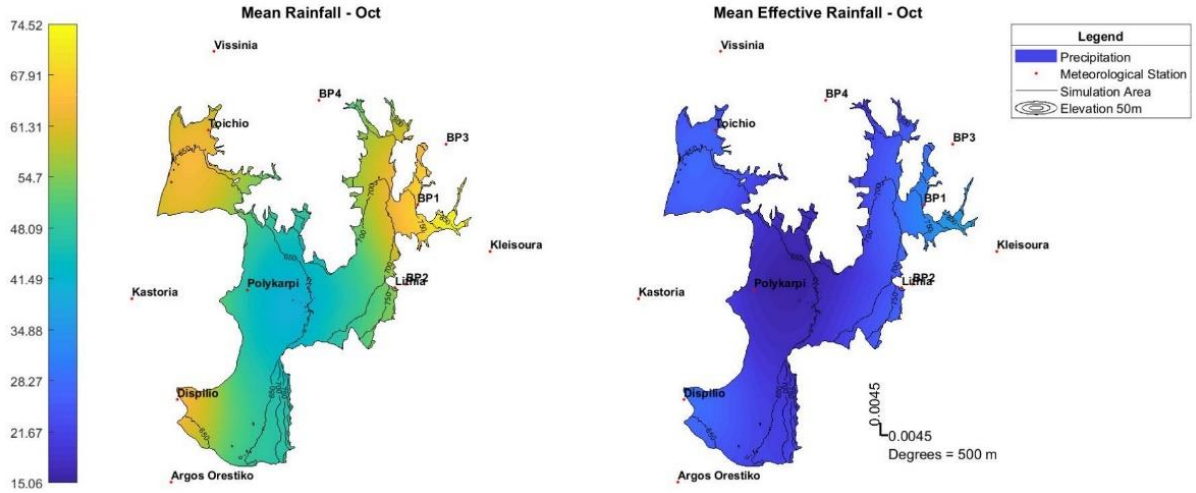

Figure 146 - Mean monthly rainfall and effective rainfall of October at simulation area

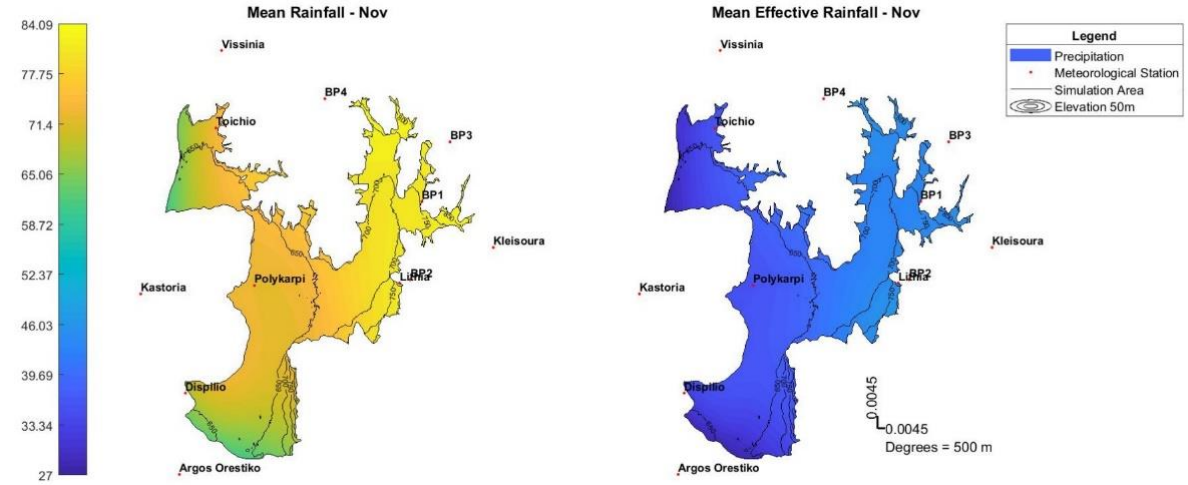

Figure 147 - Mean monthly rainfall and effective rainfall of November at simulation area

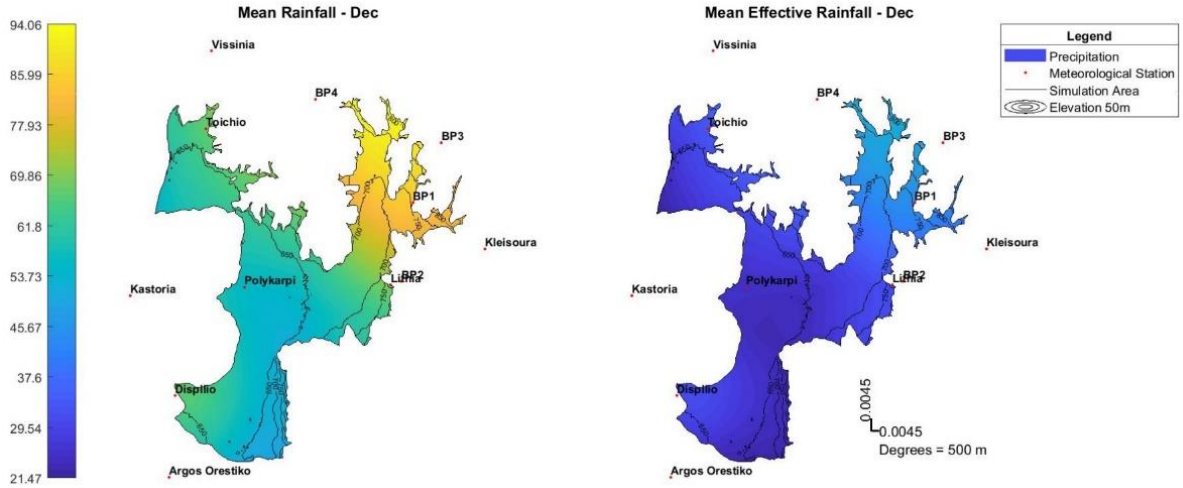

Figure 148 - Mean monthly rainfall and effective rainfall of December at simulation area

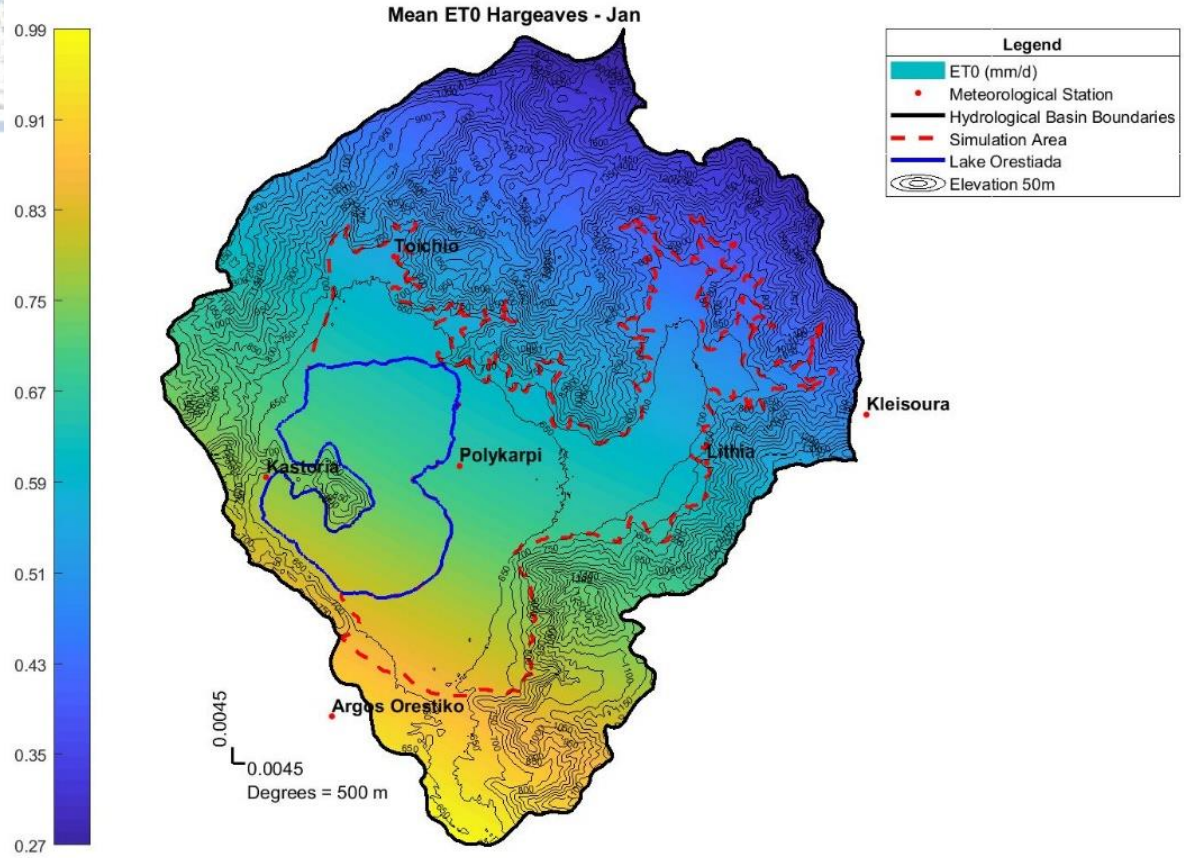

Figure 149 - Mean monthly ET_0 of January at Kastoria basin with the Hargreaves method

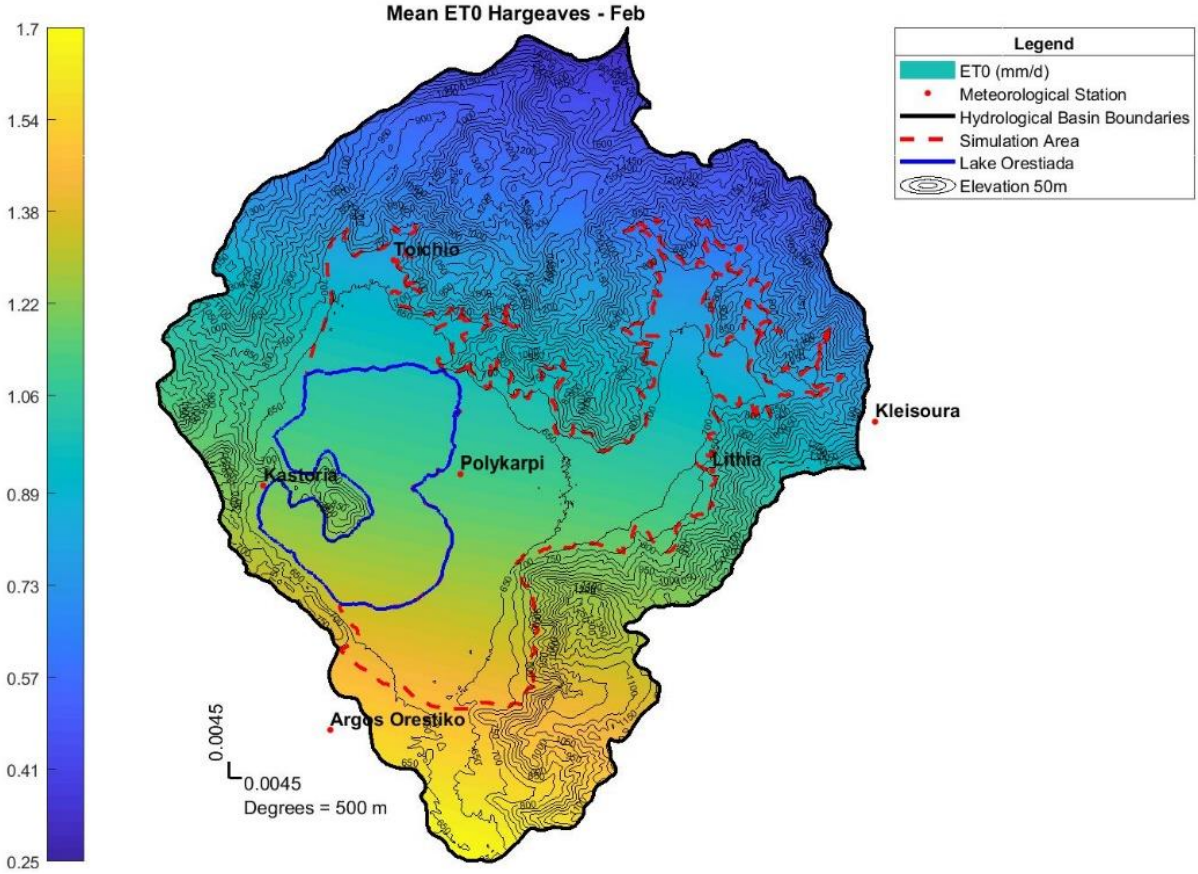

Figure 150 - Mean monthly ET_0 of February at Kastoria basin with the Hargreaves method

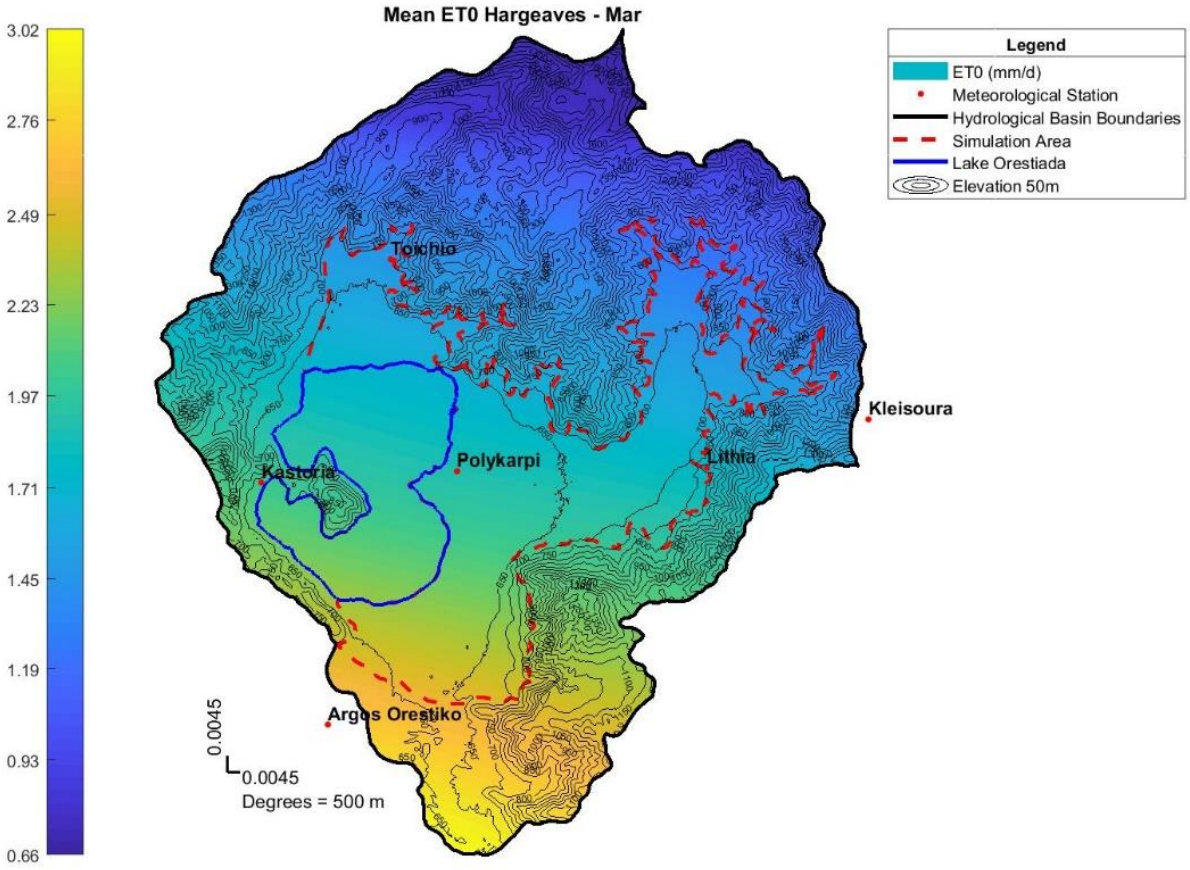

Figure 151 - Mean monthly ET_0 of March at Kastoria basin with the Hargreaves method

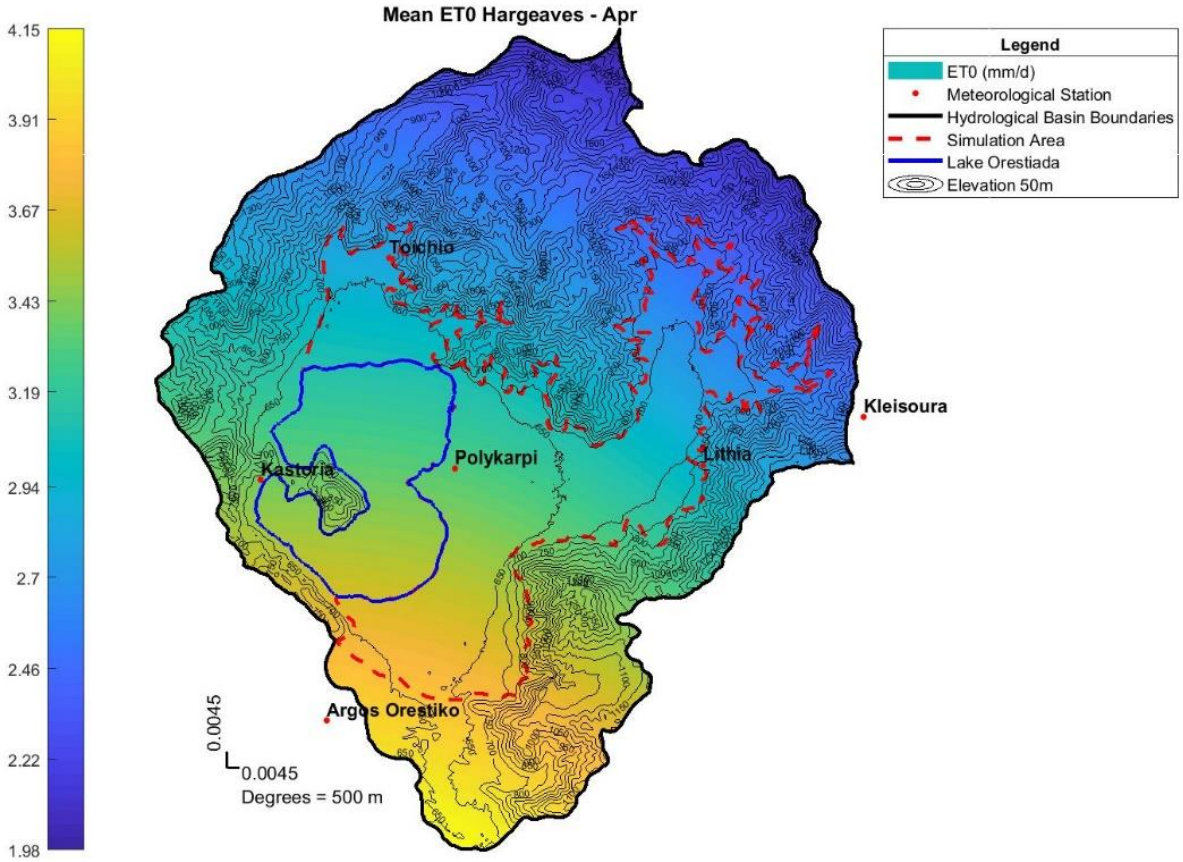

Figure 152 - Mean monthly ET_0 of April at Kastoria basin with the Hargreaves method

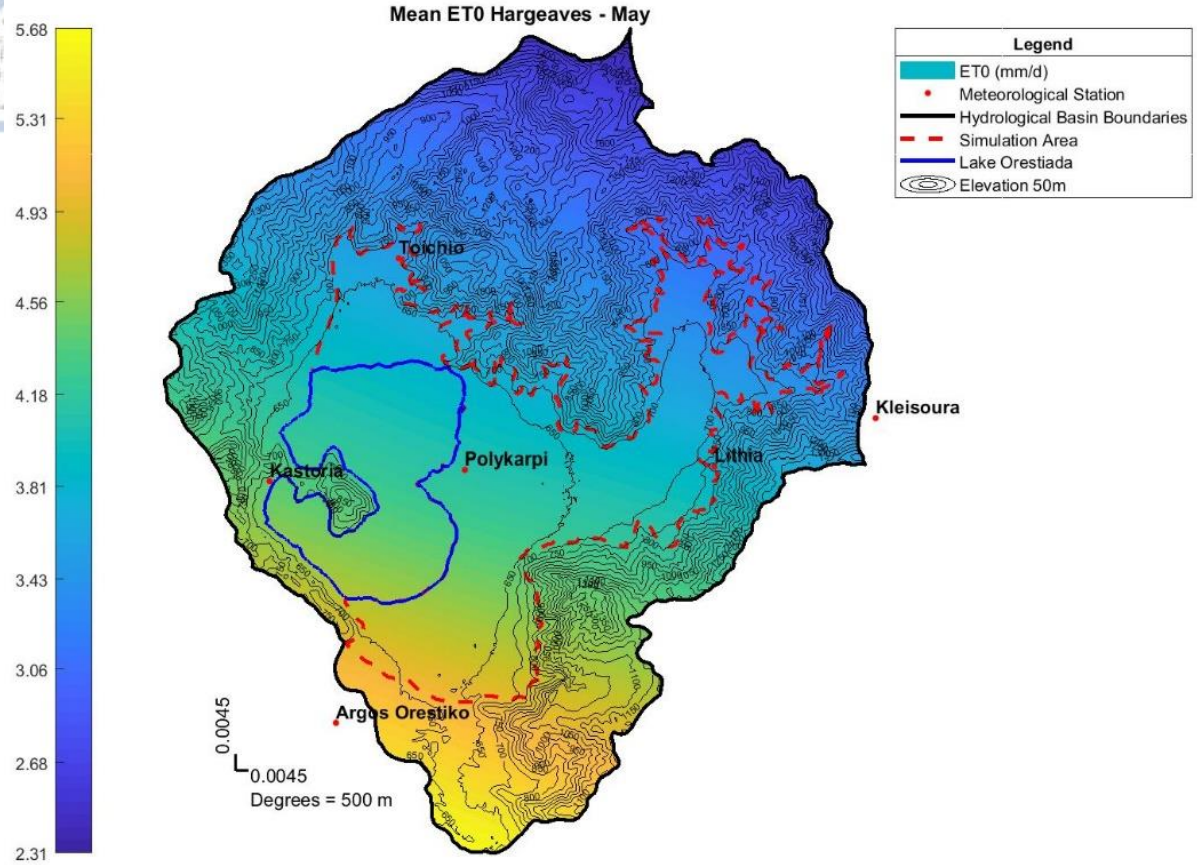

Figure 153 - Mean monthly ET_0 of May at Kastoria basin with the Hargreaves method

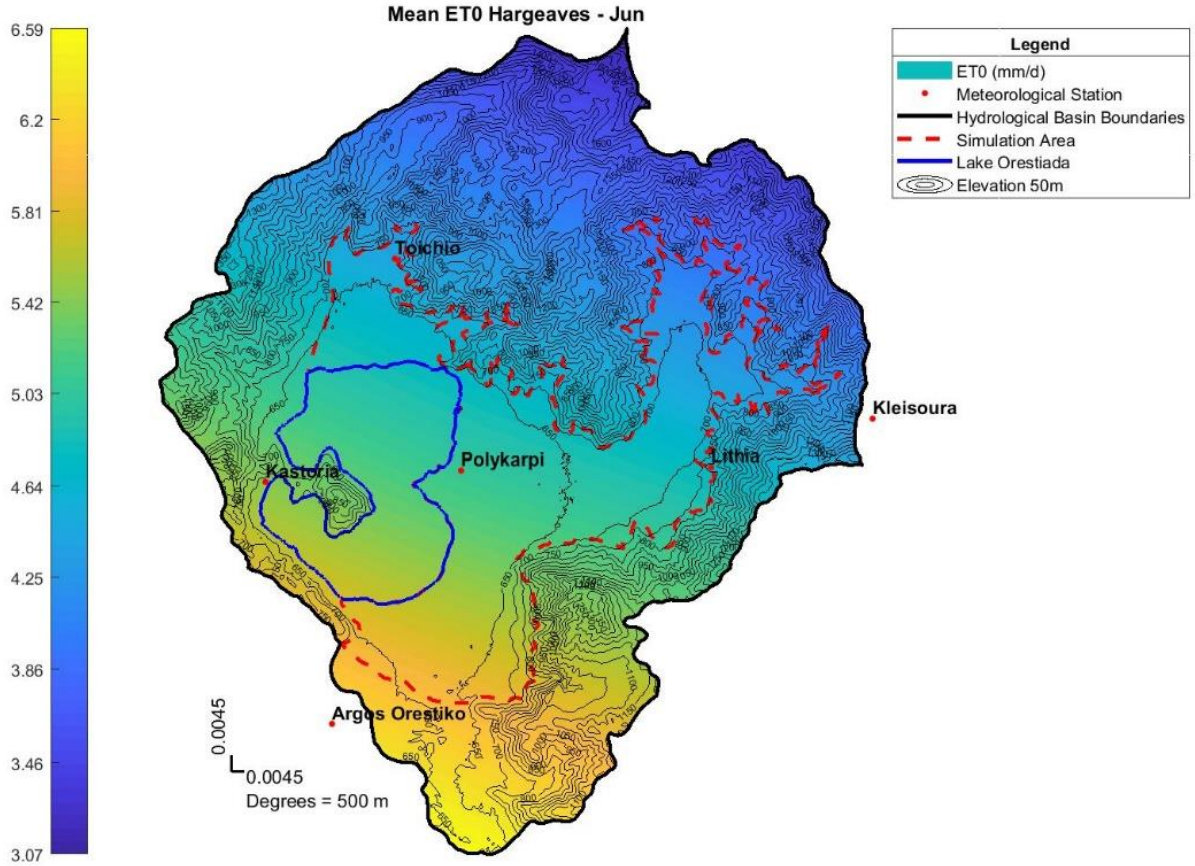

Figure 154 - Mean monthly ET_0 of June at Kastoria basin with the Hargreaves method

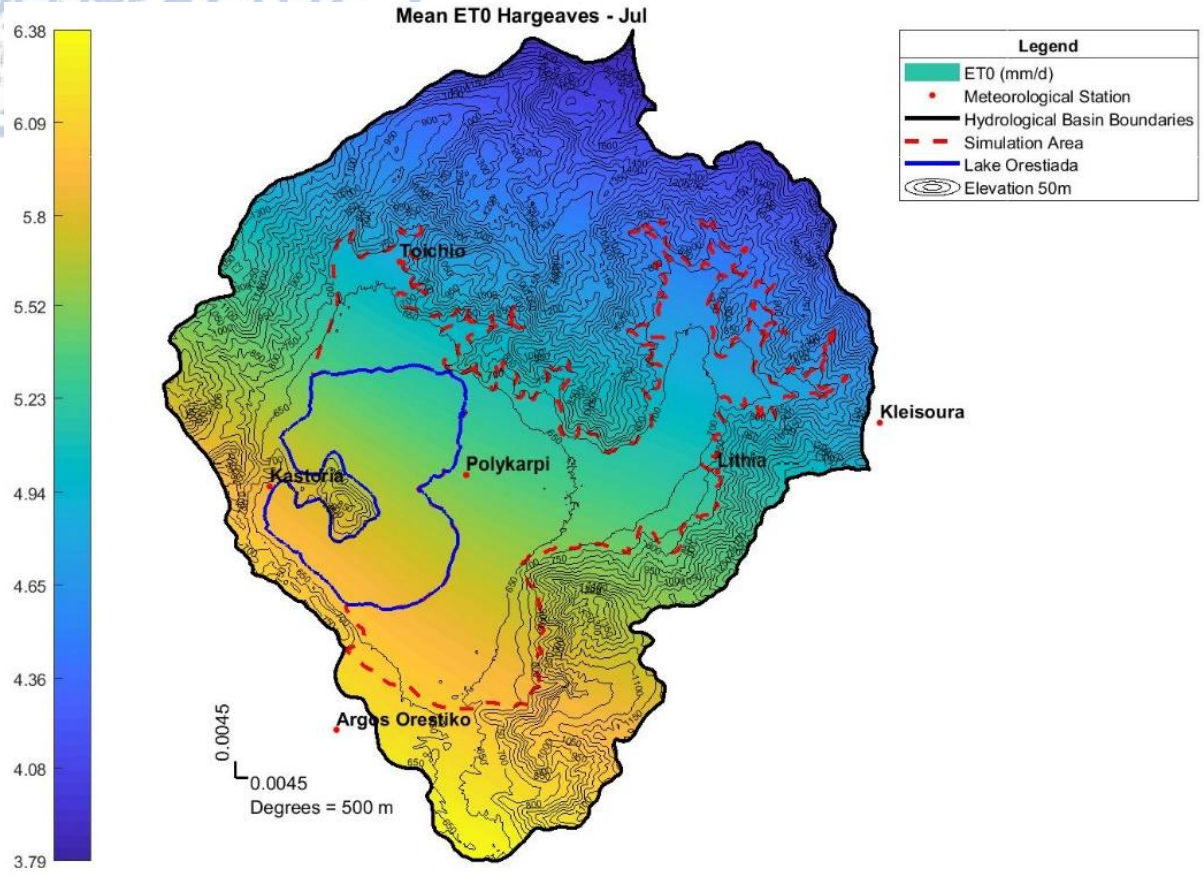

Figure 155 - Mean monthly ET_0 of July at Kastoria basin with the Hargreaves method

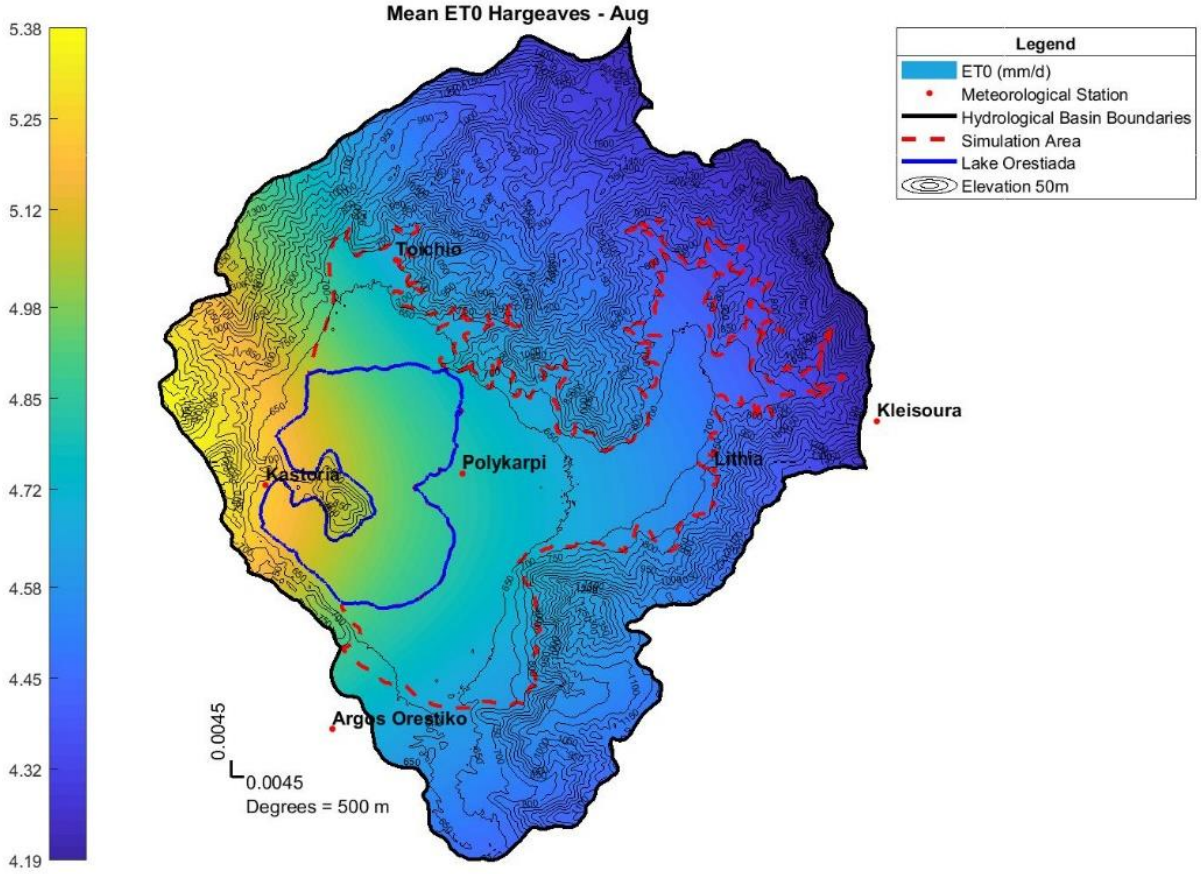

Figure 156 - Mean monthly ET_0 of August at Kastoria basin with the Hargreaves method

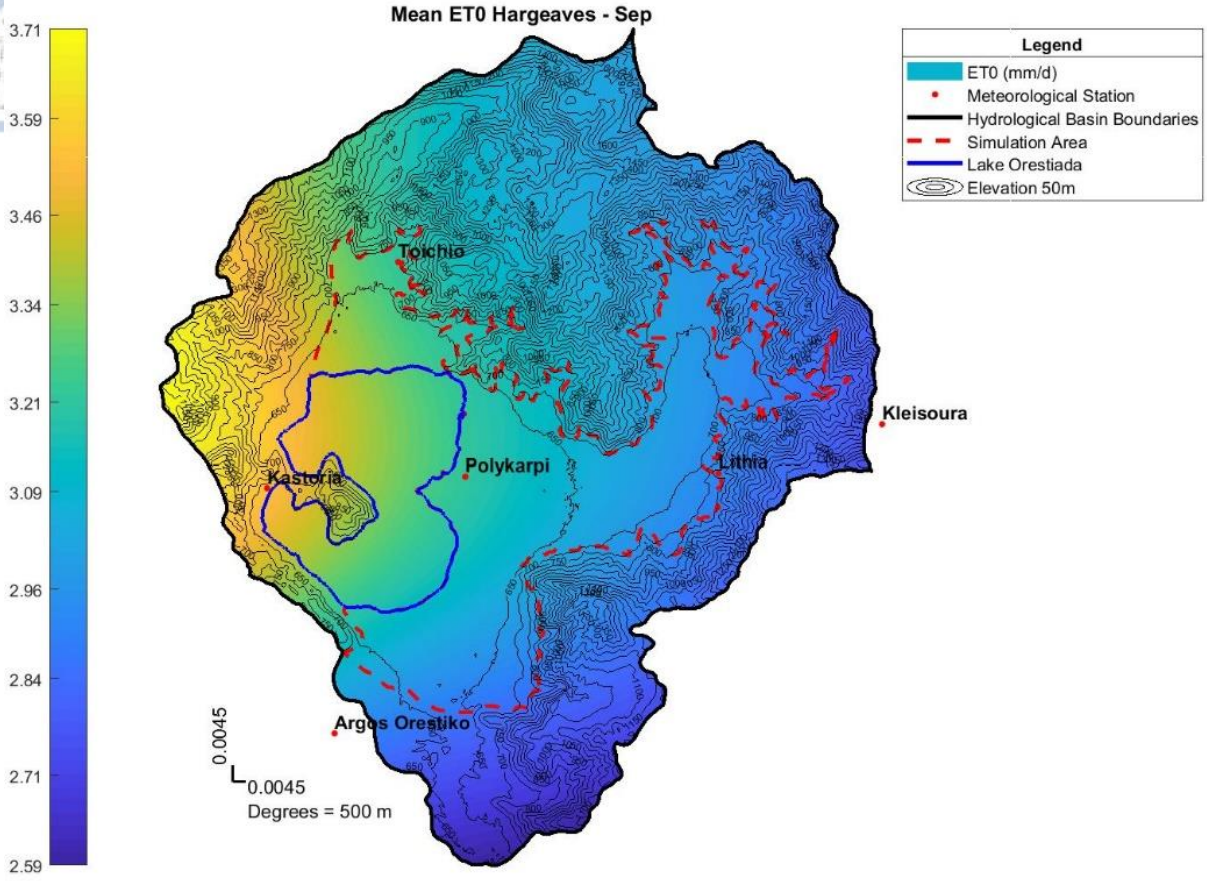

Figure 157 - Mean monthly ET_0 of September at Kastoria basin with the Hargreaves method

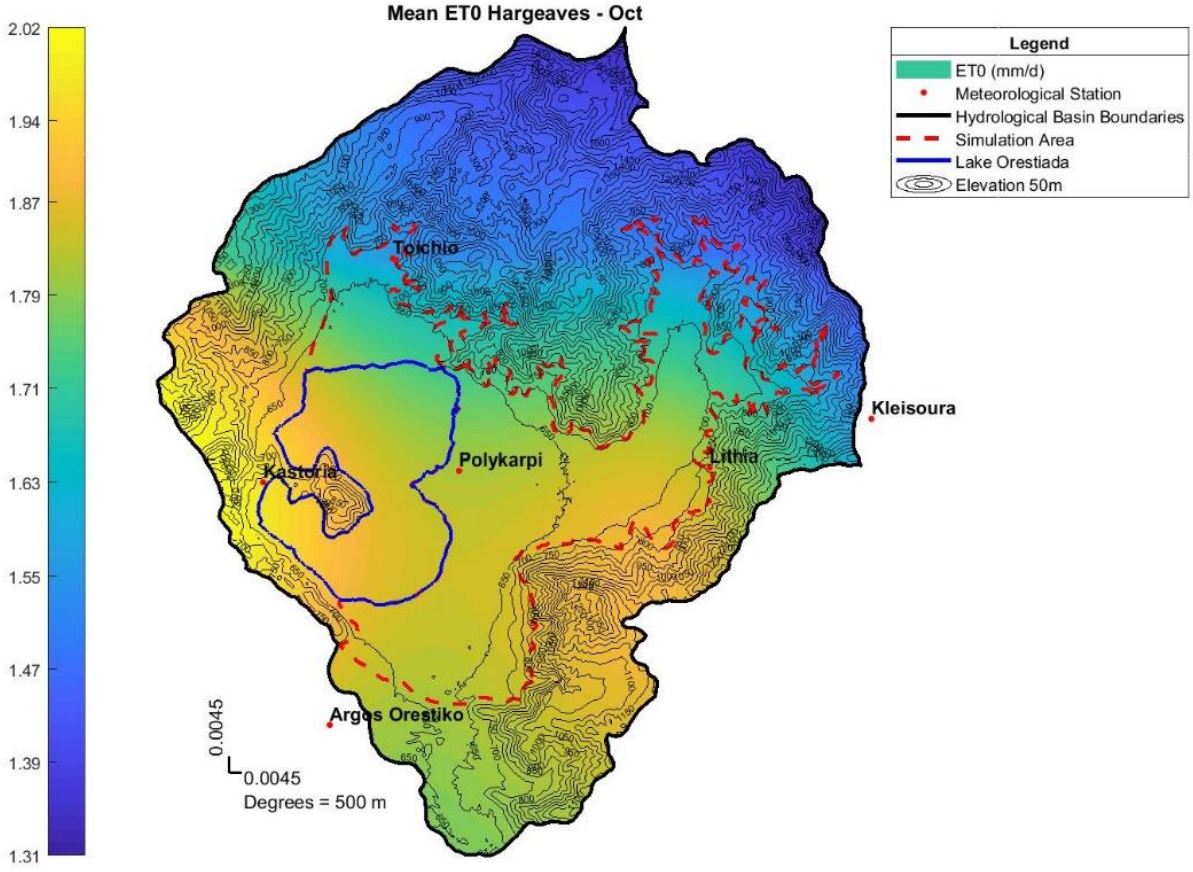

Figure 158 - Mean monthly ET_0 of October at Kastoria basin with the Hargreaves method

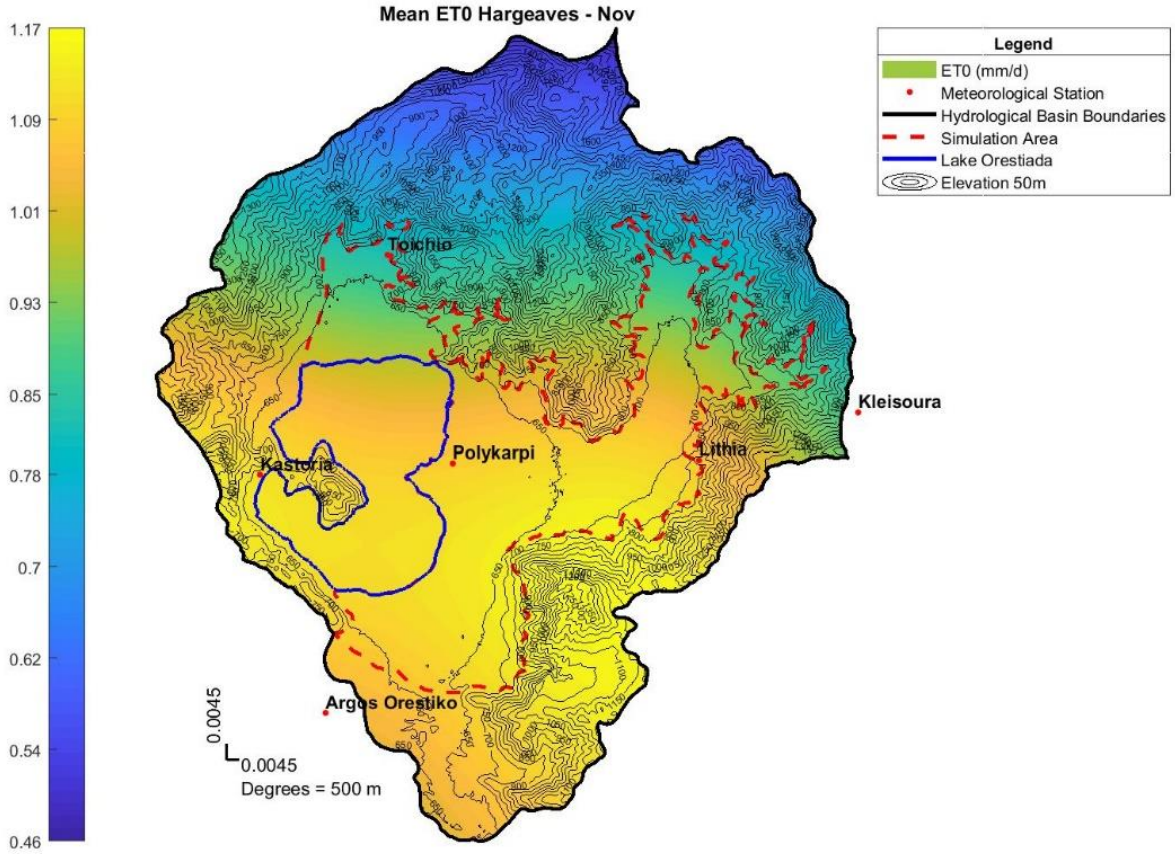

Figure 159 - Mean monthly ET_0 of November at Kastoria basin with the Hargreaves method

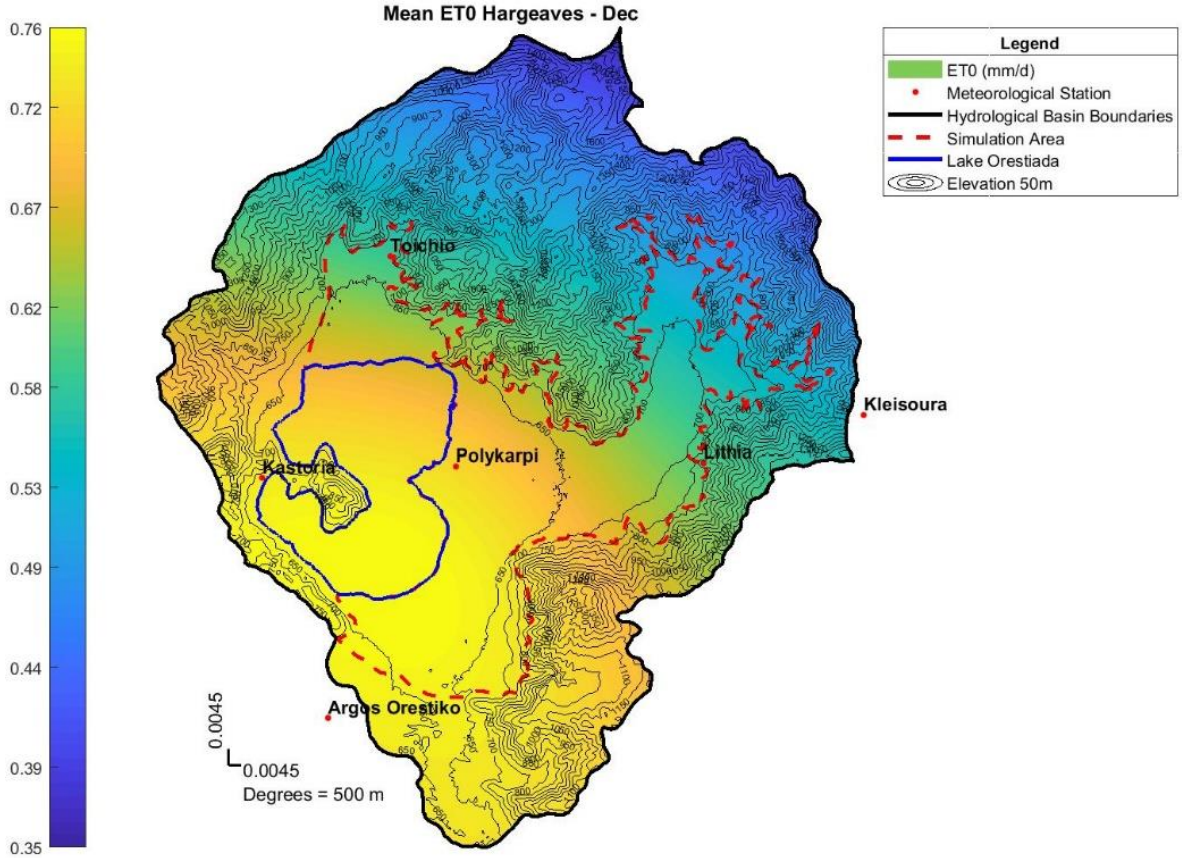

Figure 160 - Mean monthly ET_0 of December at Kastoria basin with the Hargreaves method

APPENDIX D. Supplemental Tables

Table 23 - Taylor statistics for EUR-11 RCMs for the raw and bias-corrected (BC) results of precipitation

Standard Deviation (mm/d)	Reference	Raw	BC	Change
pr EUR-11 ICHEC-EC-EARTH rcp26 r12i1p1 CLMcom-CCLM4-8-17	1.70	1.51	1.66	0.15
pr EUR-11 ICHEC-EC-EARTH rcp26 r12i1p1 KNMI-RACMO22E	1.70	1.17	1.64	0.47
pr EUR-11 ICHEC-EC-EARTH rcp26 r12i1p1 SMHI-RCA4	1.70	1.42	1.66	0.24
pr EUR-11 ICHEC-EC-EARTH rcp26 r3i1p1 DMI-HIRHAM5	1.70	1.12	1.82	0.71
pr EUR-11 IPSL-IPSL-CM5A-LR rcp26 r1i1p1 GERICS-REMO2015	1.70	1.38	1.83	0.45
pr EUR-11 MOHC-HadGEM2-ES rcp26 r1i1p1 KNMI-RACMO22E	1.70	1.45	1.58	0.13
pr EUR-11 MPI-M-MPI-ESM-LR rcp26 r1i1p1 MPI-CSC-REMO2009	1.70	1.21	1.68	0.47
pr EUR-11 MPI-M-MPI-ESM-LR rcp26 r2i1p1 MPI-CSC-REMO2009	1.70	1.22	1.75	0.53
pr EUR-11 NOAA-GFDL-GFDL-ESM2G rcp26 r1i1p1 GER-ICS-REMO2015	1.70	1.56	1.85	0.29
pr EUR-11 CNRM-CERFACS-CNRM-CM5 rcp45 r1i1p1 CLMcom-CCLM4-8-17	1.70	1.32	1.56	0.24
pr EUR-11 CNRM-CERFACS-CNRM-CM5 rcp45 r1i1p1 CNRM-ALADIN53	1.70	1.58	1.54	-0.04
pr EUR-11 CNRM-CERFACS-CNRM-CM5 rcp45 r1i1p1 SMHI-RCA4	1.70	1.32	1.50	0.19
pr EUR-11 ICHEC-EC-EARTH rcp45 r12i1p1 CLMcom-CCLM4-8-17	1.70	1.51	1.66	0.15
pr EUR-11 ICHEC-EC-EARTH rcp45 r12i1p1 KNMI-RACMO22E	1.70	1.17	1.64	0.47
pr EUR-11 ICHEC-EC-EARTH rcp45 r12i1p1 SMHI-RCA4	1.70	1.42	1.66	0.24
pr EUR-11 ICHEC-EC-EARTH rcp45 r1i1p1 KNMI-RACMO22E	1.70	1.12	1.55	0.44
pr EUR-11 ICHEC-EC-EARTH rcp45 r3i1p1 DMI-HIRHAM5	1.70	1.12	1.82	0.71
pr EUR-11 IPSL-IPSL-CM5A-MR rcp45 r1i1p1 IPSL-INERIS-WRF331F	1.70	1.17	1.51	0.34
pr EUR-11 IPSL-IPSL-CM5A-MR rcp45 r1i1p1 SMHI-RCA4	1.70	0.96	1.89	0.93
pr EUR-11 MOHC-HadGEM2-ES rcp45 r1i1p1 CLMcom-CCLM4-8-17	1.70	1.49	1.68	0.20
pr EUR-11 MOHC-HadGEM2-ES rcp45 r1i1p1 KNMI-RACMO22E	1.70	1.45	1.58	0.13
pr EUR-11 MOHC-HadGEM2-ES rcp45 r1i1p1 SMHI-RCA4	1.70	1.47	1.75	0.28
pr EUR-11 MPI-M-MPI-ESM-LR rcp45 r1i1p1 CLMcom-CCLM4-8-17	1.70	1.37	1.55	0.18
pr EUR-11 MPI-M-MPI-ESM-LR rcp45 r1i1p1 MPI-CSC-REMO2009	1.70	1.21	1.68	0.47
pr EUR-11 MPI-M-MPI-ESM-LR rcp45 r1i1p1 SMHI-RCA4	1.70	1.46	1.58	0.12
pr EUR-11 MPI-M-MPI-ESM-LR rcp45 r2i1p1 MPI-CSC-REMO2009	1.70	1.22	1.75	0.53
pr EUR-11 NCC-NorESM1-M rcp45 r1i1p1 DMI-HIRHAM5	1.70	0.99	1.93	0.94
pr EUR-11 CNRM-CERFACS-CNRM-CM5 rcp85 r1i1p1 CLMcom-CCLM4-8-17	1.70	1.32	1.56	0.24
pr EUR-11 CNRM-CERFACS-CNRM-CM5 rcp85 r1i1p1 CNRM-ALADIN53	1.70	1.58	1.54	-0.04
pr EUR-11 CNRM-CERFACS-CNRM-CM5 rcp85 r1i1p1 CNRM-ALADIN63	1.70	1.96	1.43	-0.53
pr EUR-11 CNRM-CERFACS-CNRM-CM5 rcp85 r1i1p1 DMI-HIRHAM5	1.70	1.03	1.88	0.84
pr EUR-11 CNRM-CERFACS-CNRM-CM5 rcp85 r1i1p1 KNMI-RACMO22E	1.70	1.38	1.59	0.21
pr EUR-11 CNRM-CERFACS-CNRM-CM5 rcp85 r1i1p1	1.70	1.32	1.50	0.19

SMHI-RCA4				
pr EUR-11 ICHEC-EC-EARTH rcp85 r12i1p1 CLMcom-CCLM4-8-17	1.70	1.51	1.66	0.15
pr EUR-11 ICHEC-EC-EARTH rcp85 r12i1p1 DMI-HIRHAM5	1.70	1.06	1.94	0.88
pr EUR-11 ICHEC-EC-EARTH rcp85 r12i1p1 KNMI-RACMO22E	1.70	1.17	1.64	0.47
pr EUR-11 ICHEC-EC-EARTH rcp85 r12i1p1 SMHI-RCA4	1.70	1.42	1.66	0.24
pr EUR-11 ICHEC-EC-EARTH rcp85 r1i1p1 DMI-HIRHAM5	1.70	0.88	1.82	0.94
pr EUR-11 ICHEC-EC-EARTH rcp85 r1i1p1 KNMI-RACMO22E	1.70	1.12	1.55	0.44
pr EUR-11 ICHEC-EC-EARTH rcp85 r3i1p1 DMI-HIRHAM5	1.70	1.12	1.82	0.71
pr EUR-11 ICHEC-EC-EARTH rcp85 r3i1p1 KNMI-RACMO22E	1.70	1.30	1.64	0.34
pr EUR-11 IPSL-IPSL-CM5A-MR rcp85 r1i1p1 IPSL-INERIS-WRF331F	1.70	1.17	1.51	0.34
pr EUR-11 IPSL-IPSL-CM5A-MR rcp85 r1i1p1 SMHI-RCA4	1.70	0.96	1.89	0.93
pr EUR-11 MOHC-HadGEM2-ES rcp85 r1i1p1 CLMcom-CCLM4-8-17	1.70	1.49	1.68	0.20
pr EUR-11 MOHC-HadGEM2-ES rcp85 r1i1p1 DMI-HIRHAM5	1.70	1.03	2.05	1.02
pr EUR-11 MOHC-HadGEM2-ES rcp85 r1i1p1 KNMI-RACMO22E	1.70	1.45	1.58	0.13
pr EUR-11 MOHC-HadGEM2-ES rcp85 r1i1p1 SMHI-RCA4	1.70	1.47	1.75	0.28
pr EUR-11 MPI-M-MPI-ESM-LR rcp85 r1i1p1 CLMcom-CCLM4-8-17	1.70	1.37	1.55	0.18
pr EUR-11 MPI-M-MPI-ESM-LR rcp85 r1i1p1 MPI-CSC-REMO2009	1.70	1.21	1.68	0.47
pr EUR-11 MPI-M-MPI-ESM-LR rcp85 r1i1p1 SMHI-RCA4	1.70	1.46	1.58	0.12
pr EUR-11 MPI-M-MPI-ESM-LR rcp85 r2i1p1 MPI-CSC-REMO2009	1.70	1.22	1.75	0.53
pr EUR-11 NCC-NorESM1-M rcp85 r1i1p1 DMI-HIRHAM5	1.70	0.99	1.93	0.94
pr EUR-11 NCC-NorESM1-M rcp85 r1i1p1 GERICS-REMO2015	1.70	1.36	1.73	0.37
RMSD	**Reference**	**Raw**	**BC**	**Percent Change**
pr EUR-11 ICHEC-EC-EARTH rcp26 r12i1p1 CLMcom-CCLM4-8-17	0.00	2.08	2.07	-0.01
pr EUR-11 ICHEC-EC-EARTH rcp26 r12i1p1 KNMI-RACMO22E	0.00	1.88	2.01	0.13
pr EUR-11 ICHEC-EC-EARTH rcp26 r12i1p1 SMHI-RCA4	0.00	2.02	2.04	0.02
pr EUR-11 ICHEC-EC-EARTH rcp26 r3i1p1 DMI-HIRHAM5	0.00	1.87	2.25	0.39
pr EUR-11 IPSL-IPSL-CM5A-LR rcp26 r1i1p1 GERICS-REMO2015	0.00	2.36	2.27	-0.09
pr EUR-11 MOHC-HadGEM2-ES rcp26 r1i1p1 KNMI-RACMO22E	0.00	2.04	2.13	0.09
pr EUR-11 MPI-M-MPI-ESM-LR rcp26 r1i1p1 MPI-CSC-REMO2009	0.00	2.08	2.20	0.12
pr EUR-11 MPI-M-MPI-ESM-LR rcp26 r2i1p1 MPI-CSC-REMO2009	0.00	2.07	2.22	0.16
pr EUR-11 NOAA-GFDL-GFDL-ESM2G rcp26 r1i1p1 GER-ICS-REMO2015	0.00	2.50	2.36	-0.14
pr EUR-11 CNRM-CERFACS-CNRM-CM5 rcp45 r1i1p1 CLMcom-CCLM4-8-17	0.00	2.02	2.00	-0.02
pr EUR-11 CNRM-CERFACS-CNRM-CM5 rcp45 r1i1p1 CNRM-ALADIN53	0.00	2.39	1.99	-0.40
pr EUR-11 CNRM-CERFACS-CNRM-CM5 rcp45 r1i1p1 SMHI-RCA4	0.00	2.14	2.03	-0.11
pr EUR-11 ICHEC-EC-EARTH rcp45 r12i1p1 CLMcom-CCLM4-8-17	0.00	2.08	2.07	-0.01
pr EUR-11 ICHEC-EC-EARTH rcp45 r12i1p1 KNMI-RACMO22E	0.00	1.88	2.01	0.13

pr EUR-11 ICHEC-EC-EARTH rcp45 r12i1p1 SMHI-RCA4	0.00	2.02	2.04	0.02
pr EUR-11 ICHEC-EC-EARTH rcp45 r1i1p1 KNMI-RACMO22E	0.00	1.91	2.02	0.11
pr EUR-11 ICHEC-EC-EARTH rcp45 r3i1p1 DMI-HIRHAM5	0.00	1.87	2.25	0.39
pr EUR-11 IPSL-IPSL-CM5A-MR rcp45 r1i1p1 IPSL-INERIS-WRF331F	0.00	2.13	2.04	-0.08
pr EUR-11 IPSL-IPSL-CM5A-MR rcp45 r1i1p1 SMHI-RCA4	0.00	1.94	2.38	0.44
pr EUR-11 MOHC-HadGEM2-ES rcp45 r1i1p1 CLMcom-CCLM4-8-17	0.00	2.08	2.23	0.15
pr EUR-11 MOHC-HadGEM2-ES rcp45 r1i1p1 KNMI-RACMO22E	0.00	2.04	2.13	0.09
pr EUR-11 MOHC-HadGEM2-ES rcp45 r1i1p1 SMHI-RCA4	0.00	2.15	2.31	0.15
pr EUR-11 MPI-M-MPI-ESM-LR rcp45 r1i1p1 CLMcom-CCLM4-8-17	0.00	2.05	2.07	0.02
pr EUR-11 MPI-M-MPI-ESM-LR rcp45 r1i1p1 MPI-CSC-REMO2009	0.00	2.08	2.20	0.12
pr EUR-11 MPI-M-MPI-ESM-LR rcp45 r1i1p1 SMHI-RCA4	0.00	2.15	2.12	-0.03
pr EUR-11 MPI-M-MPI-ESM-LR rcp45 r2i1p1 MPI-CSC-REMO2009	0.00	2.07	2.22	0.16
pr EUR-11 NCC-NorESM1-M rcp45 r1i1p1 DMI-HIRHAM5	0.00	1.85	2.39	0.54
pr EUR-11 CNRM-CERFACS-CNRM-CM5 rcp85 r1i1p1 CLMcom-CCLM4-8-17	0.00	2.02	2.00	-0.02
pr EUR-11 CNRM-CERFACS-CNRM-CM5 rcp85 r1i1p1 CNRM-ALADIN53	0.00	2.39	1.99	-0.40
pr EUR-11 CNRM-CERFACS-CNRM-CM5 rcp85 r1i1p1 CNRM-ALADIN63	0.00	2.47	1.98	-0.49
pr EUR-11 CNRM-CERFACS-CNRM-CM5 rcp85 r1i1p1 DMI-HIRHAM5	0.00	1.88	2.28	0.41
pr EUR-11 CNRM-CERFACS-CNRM-CM5 rcp85 r1i1p1 KNMI-RACMO22E	0.00	2.20	2.15	-0.06
pr EUR-11 CNRM-CERFACS-CNRM-CM5 rcp85 r1i1p1 SMHI-RCA4	0.00	2.14	2.03	-0.11
pr EUR-11 ICHEC-EC-EARTH rcp85 r12i1p1 CLMcom-CCLM4-8-17	0.00	2.08	2.07	-0.01
pr EUR-11 ICHEC-EC-EARTH rcp85 r12i1p1 DMI-HIRHAM5	0.00	1.76	2.19	0.44
pr EUR-11 ICHEC-EC-EARTH rcp85 r12i1p1 KNMI-RACMO22E	0.00	1.88	2.01	0.13
pr EUR-11 ICHEC-EC-EARTH rcp85 r12i1p1 SMHI-RCA4	0.00	2.02	2.04	0.02
pr EUR-11 ICHEC-EC-EARTH rcp85 r1i1p1 DMI-HIRHAM5	0.00	1.74	2.21	0.47
pr EUR-11 ICHEC-EC-EARTH rcp85 r1i1p1 KNMI-RACMO22E	0.00	1.91	2.02	0.11
pr EUR-11 ICHEC-EC-EARTH rcp85 r3i1p1 DMI-HIRHAM5	0.00	1.87	2.25	0.39
pr EUR-11 ICHEC-EC-EARTH rcp85 r3i1p1 KNMI-RACMO22E	0.00	1.98	2.05	0.06
pr EUR-11 IPSL-IPSL-CM5A-MR rcp85 r1i1p1 IPSL-INERIS-WRF331F	0.00	2.13	2.04	-0.08
pr EUR-11 IPSL-IPSL-CM5A-MR rcp85 r1i1p1 SMHI-RCA4	0.00	1.94	2.38	0.44
pr EUR-11 MOHC-HadGEM2-ES rcp85 r1i1p1 CLMcom-CCLM4-8-17	0.00	2.08	2.23	0.15
pr EUR-11 MOHC-HadGEM2-ES rcp85 r1i1p1 DMI-HIRHAM5	0.00	1.91	2.56	0.66
pr EUR-11 MOHC-HadGEM2-ES rcp85 r1i1p1 KNMI-RACMO22E	0.00	2.04	2.13	0.09
pr EUR-11 MOHC-HadGEM2-ES rcp85 r1i1p1 SMHI-RCA4	0.00	2.15	2.31	0.15
pr EUR-11 MPI-M-MPI-ESM-LR rcp85 r1i1p1 CLMcom-CCLM4-8-17	0.00	2.05	2.07	0.02
pr EUR-11 MPI-M-MPI-ESM-LR rcp85 r1i1p1 MPI-CSC-REMO2009	0.00	2.08	2.20	0.12
pr EUR-11 MPI-M-MPI-ESM-LR rcp85 r1i1p1 SMHI-RCA4	0.00	2.15	2.12	-0.03

pr EUR-11 MPI-M-MPI-ESM-LR rcp85 r2i1p1 MPI-CSC-REMO2009	0.00	2.07	2.22	0.16
pr EUR-11 NCC-NorESM1-M rcp85 r1i1p1 DMI-HIRHAM5	0.00	1.85	2.39	0.54
pr EUR-11 NCC-NorESM1-M rcp85 r1i1p1 GER-ICS-REMO2015	0.00	2.24	2.27	0.03
Pearson's Correlation Coefficient	**Reference**	**Raw**	**BC**	**Percent Change**
pr EUR-11 ICHEC-EC-EARTH rcp26 r12i1p1 CLMcom-CCLM4-8-17	1.00	0.18	0.24	0.07
pr EUR-11 ICHEC-EC-EARTH rcp26 r12i1p1 KNMI-RACMO22E	1.00	0.18	0.27	0.09
pr EUR-11 ICHEC-EC-EARTH rcp26 r12i1p1 SMHI-RCA4	1.00	0.17	0.26	0.09
pr EUR-11 ICHEC-EC-EARTH rcp26 r3i1p1 DMI-HIRHAM5	1.00	0.15	0.17	0.02
pr EUR-11 IPSL-IPSL-CM5A-LR rcp26 r1i1p1 GERICS-REMO2015	1.00	-0.12	0.17	0.29
pr EUR-11 MOHC-HadGEM2-ES rcp26 r1i1p1 KNMI-RACMO22E	1.00	0.18	0.15	-0.02
pr EUR-11 MPI-M-MPI-ESM-LR rcp26 r1i1p1 MPI-CSC-REMO2009	1.00	0.03	0.15	0.12
pr EUR-11 MPI-M-MPI-ESM-LR rcp26 r2i1p1 MPI-CSC-REMO2009	1.00	0.05	0.17	0.11
pr EUR-11 NOAA-GFDL-GFDL-ESM2G rcp26 r1i1p1 GER-ICS-REMO2015	1.00	-0.13	0.10	0.23
pr EUR-11 CNRM-CERFACS-CNRM-CM5 rcp45 r1i1p1 CLMcom-CCLM4-8-17	1.00	0.14	0.25	0.11
pr EUR-11 CNRM-CERFACS-CNRM-CM5 rcp45 r1i1p1 CNRM-ALADIN53	1.00	-0.04	0.24	0.28
pr EUR-11 CNRM-CERFACS-CNRM-CM5 rcp45 r1i1p1 SMHI-RCA4	1.00	0.02	0.20	0.18
pr EUR-11 ICHEC-EC-EARTH rcp45 r12i1p1 CLMcom-CCLM4-8-17	1.00	0.18	0.24	0.07
pr EUR-11 ICHEC-EC-EARTH rcp45 r12i1p1 KNMI-RACMO22E	1.00	0.18	0.27	0.09
pr EUR-11 ICHEC-EC-EARTH rcp45 r12i1p1 SMHI-RCA4	1.00	0.17	0.26	0.09
pr EUR-11 ICHEC-EC-EARTH rcp45 r1i1p1 KNMI-RACMO22E	1.00	0.12	0.22	0.10
pr EUR-11 ICHEC-EC-EARTH rcp45 r3i1p1 DMI-HIRHAM5	1.00	0.15	0.17	0.02
pr EUR-11 IPSL-IPSL-CM5A-MR rcp45 r1i1p1 IPSL-INERIS-WRF331F	1.00	-0.05	0.18	0.23
pr EUR-11 IPSL-IPSL-CM5A-MR rcp45 r1i1p1 SMHI-RCA4	1.00	0.02	0.12	0.10
pr EUR-11 MOHC-HadGEM2-ES rcp45 r1i1p1 CLMcom-CCLM4-8-17	1.00	0.17	0.14	-0.03
pr EUR-11 MOHC-HadGEM2-ES rcp45 r1i1p1 KNMI-RACMO22E	1.00	0.18	0.15	-0.02
pr EUR-11 MOHC-HadGEM2-ES rcp45 r1i1p1 SMHI-RCA4	1.00	0.09	0.11	0.03
pr EUR-11 MPI-M-MPI-ESM-LR rcp45 r1i1p1 CLMcom-CCLM4-8-17	1.00	0.12	0.18	0.06
pr EUR-11 MPI-M-MPI-ESM-LR rcp45 r1i1p1 MPI-CSC-REMO2009	1.00	0.03	0.15	0.12
pr EUR-11 MPI-M-MPI-ESM-LR rcp45 r1i1p1 SMHI-RCA4	1.00	0.08	0.18	0.09
pr EUR-11 MPI-M-MPI-ESM-LR rcp45 r2i1p1 MPI-CSC-REMO2009	1.00	0.05	0.17	0.11
pr EUR-11 NCC-NorESM1-M rcp45 r1i1p1 DMI-HIRHAM5	1.00	0.13	0.14	0.01
pr EUR-11 CNRM-CERFACS-CNRM-CM5 rcp85 r1i1p1 CLMcom-CCLM4-8-17	1.00	0.14	0.25	0.11
pr EUR-11 CNRM-CERFACS-CNRM-CM5 rcp85 r1i1p1 CNRM-ALADIN53	1.00	-0.04	0.24	0.28
pr EUR-11 CNRM-CERFACS-CNRM-CM5 rcp85 r1i1p1 CNRM-ALADIN63	1.00	0.09	0.19	0.10
pr EUR-11 CNRM-CERFACS-CNRM-CM5 rcp85 r1i1p1 DMI-HIRHAM5	1.00	0.10	0.17	0.07

pr EUR-11 CNRM-CERFACS-CNRM-CM5 rcp85 r1i1p1 KNMI-RACMO22E	1.00	-0.01	0.13	0.15
pr EUR-11 CNRM-CERFACS-CNRM-CM5 rcp85 r1i1p1 SMHI-RCA4	1.00	0.02	0.20	0.18
pr EUR-11 ICHEC-EC-EARTH rcp85 r12i1p1 CLMcom-CCLM4-8-17	1.00	0.18	0.24	0.07
pr EUR-11 ICHEC-EC-EARTH rcp85 r12i1p1 DMI-HIRHAM5	1.00	0.24	0.27	0.04
pr EUR-11 ICHEC-EC-EARTH rcp85 r12i1p1 KNMI-RACMO22E	1.00	0.18	0.27	0.09
pr EUR-11 ICHEC-EC-EARTH rcp85 r12i1p1 SMHI-RCA4	1.00	0.17	0.26	0.09
pr EUR-11 ICHEC-EC-EARTH rcp85 r1i1p1 DMI-HIRHAM5	1.00	0.20	0.21	0.01
pr EUR-11 ICHEC-EC-EARTH rcp85 r1i1p1 KNMI-RACMO22E	1.00	0.12	0.22	0.10
pr EUR-11 ICHEC-EC-EARTH rcp85 r3i1p1 DMI-HIRHAM5	1.00	0.15	0.17	0.02
pr EUR-11 ICHEC-EC-EARTH rcp85 r3i1p1 KNMI-RACMO22E	1.00	0.14	0.24	0.09
pr EUR-11 IPSL-IPSL-CM5A-MR rcp85 r1i1p1 IPSL-INERIS-WRF331F	1.00	-0.05	0.18	0.23
pr EUR-11 IPSL-IPSL-CM5A-MR rcp85 r1i1p1 SMHI-RCA4	1.00	0.02	0.12	0.10
pr EUR-11 MOHC-HadGEM2-ES rcp85 r1i1p1 CLMcom-CCLM4-8-17	1.00	0.17	0.14	-0.03
pr EUR-11 MOHC-HadGEM2-ES rcp85 r1i1p1 DMI-HIRHAM5	1.00	0.09	0.07	-0.02
pr EUR-11 MOHC-HadGEM2-ES rcp85 r1i1p1 KNMI-RACMO22E	1.00	0.18	0.15	-0.02
pr EUR-11 MOHC-HadGEM2-ES rcp85 r1i1p1 SMHI-RCA4	1.00	0.09	0.11	0.03
pr EUR-11 MPI-M-MPI-ESM-LR rcp85 r1i1p1 CLMcom-CCLM4-8-17	1.00	0.12	0.18	0.06
pr EUR-11 MPI-M-MPI-ESM-LR rcp85 r1i1p1 MPI-CSC-REMO2009	1.00	0.03	0.15	0.12
pr EUR-11 MPI-M-MPI-ESM-LR rcp85 r1i1p1 SMHI-RCA4	1.00	0.08	0.18	0.09
pr EUR-11 MPI-M-MPI-ESM-LR rcp85 r2i1p1 MPI-CSC-REMO2009	1.00	0.05	0.17	0.11
pr EUR-11 NCC-NorESM1-M rcp85 r1i1p1 DMI-HIRHAM5	1.00	0.13	0.14	0.01
pr EUR-11 NCC-NorESM1-M rcp85 r1i1p1 GERICS-REMO2015	1.00	-0.01	0.13	0.14

Table 24 - Taylor statistics for EUR-11 RCMs for the raw and bias-corrected (BC) results of temperature

Standard Deviation (°C)	**Reference**	**Raw**	**BC**	**Change**
tas EUR-11 ICHEC-EC-EARTH rcp26 r12i1p1 CLMcom-CCLM4-8-17	7.45	8.02	7.48	-0.54
tas EUR-11 ICHEC-EC-EARTH rcp26 r12i1p1 KNMI-RACMO22E	7.45	7.80	7.50	-0.30
tas EUR-11 ICHEC-EC-EARTH rcp26 r12i1p1 SMHI-RCA4	7.45	7.15	7.40	0.25
tas EUR-11 ICHEC-EC-EARTH rcp26 r3i1p1 DMI-HIRHAM5	7.45	6.86	7.36	0.51
tas EUR-11 IPSL-IPSL-CM5A-LR rcp26 r1i1p1 GERICS-REMO2015	7.45	7.04	7.50	0.45
tas EUR-11 MOHC-HadGEM2-ES rcp26 r1i1p1 KNMI-RACMO22E	7.45	8.59	7.58	-1.01
tas EUR-11 MPI-M-MPI-ESM-LR rcp26 r1i1p1 MPI-CSC-REMO2009	7.45	6.71	7.40	0.69
tas EUR-11 MPI-M-MPI-ESM-LR rcp26 r2i1p1 MPI-CSC-REMO2009	7.45	6.87	7.42	0.56
tas EUR-11 NOAA-GFDL-GFDL-ESM2G rcp26 r1i1p1 GERICS-REMO2015	7.45	6.05	7.43	1.38
tas EUR-11 CNRM-CERFACS-CNRM-CM5 rcp45 r1i1p1 CLMcom-CCLM4-8-17	7.45	7.83	7.44	-0.39
tas EUR-11 CNRM-CERFACS-CNRM-CM5 rcp45 r1i1p1 CNRM-ALADIN53	7.45	7.95	7.37	-0.58
tas EUR-11 CNRM-CERFACS-CNRM-CM5 rcp45 r1i1p1 SMHI-RCA4	7.45	7.22	7.37	0.16
tas EUR-11 ICHEC-EC-EARTH rcp45 r12i1p1 CLMcom-CCLM4-8-17	7.45	8.02	7.48	-0.54
tas EUR-11 ICHEC-EC-EARTH rcp45 r12i1p1 KNMI-RACMO22E	7.45	7.80	7.50	-0.30
tas EUR-11 ICHEC-EC-EARTH rcp45 r12i1p1 SMHI-RCA4	7.45	7.15	7.40	0.25

tas EUR-11 ICHEC-EC-EARTH rcp45 r1i1p1 KNMI-RACMO22E	7.45	7.28	7.50	0.21
tas EUR-11 ICHEC-EC-EARTH rcp45 r3i1p1 DMI-HIRHAM5	7.45	6.86	7.36	0.51
tas EUR-11 IPSL-IPSL-CM5A-MR rcp45 r1i1p1 IPSL-INERIS-WRF331F	7.45	7.02	7.44	0.42
tas EUR-11 IPSL-IPSL-CM5A-MR rcp45 r1i1p1 SMHI-RCA4	7.45	7.52	7.45	-0.08
tas EUR-11 MOHC-HadGEM2-ES rcp45 r1i1p1 CLMcom-CCLM4-8-17	7.45	9.05	7.46	-1.59
tas EUR-11 MOHC-HadGEM2-ES rcp45 r1i1p1 KNMI-RACMO22E	7.45	8.59	7.58	-1.01
tas EUR-11 MOHC-HadGEM2-ES rcp45 r1i1p1 SMHI-RCA4	7.45	7.69	7.41	-0.28
tas EUR-11 MPI-M-MPI-ESM-LR rcp45 r1i1p1 CLMcom-CCLM4-8-17	7.45	7.56	7.48	-0.08
tas EUR-11 MPI-M-MPI-ESM-LR rcp45 r1i1p1 MPI-CSC-REMO2009	7.45	6.71	7.40	0.69
tas EUR-11 MPI-M-MPI-ESM-LR rcp45 r1i1p1 SMHI-RCA4	7.45	7.19	7.41	0.22
tas EUR-11 MPI-M-MPI-ESM-LR rcp45 r2i1p1 MPI-CSC-REMO2009	7.45	6.87	7.42	0.56
tas EUR-11 NCC-NorESM1-M rcp45 r1i1p1 DMI-HIRHAM5	7.45	7.03	7.37	0.34
tas EUR-11 CNRM-CERFACS-CNRM-CM5 rcp85 r1i1p1 CLMcom-CCLM4-8-17	7.45	7.83	7.44	-0.39
tas EUR-11 CNRM-CERFACS-CNRM-CM5 rcp85 r1i1p1 CNRM-ALADIN53	7.45	7.95	7.37	-0.58
tas EUR-11 CNRM-CERFACS-CNRM-CM5 rcp85 r1i1p1 CNRM-ALADIN63	7.45	7.11	7.42	0.31
tas EUR-11 CNRM-CERFACS-CNRM-CM5 rcp85 r1i1p1 DMI-HIRHAM5	7.45	7.18	7.38	0.19
tas EUR-11 CNRM-CERFACS-CNRM-CM5 rcp85 r1i1p1 KNMI-RACMO22E	7.45	7.94	7.57	-0.37
tas EUR-11 CNRM-CERFACS-CNRM-CM5 rcp85 r1i1p1 SMHI-RCA4	7.45	7.22	7.37	0.16
tas EUR-11 ICHEC-EC-EARTH rcp85 r12i1p1 CLMcom-CCLM4-8-17	7.45	8.02	7.48	-0.54
tas EUR-11 ICHEC-EC-EARTH rcp85 r12i1p1 DMI-HIRHAM5	7.45	7.13	7.40	0.27
tas EUR-11 ICHEC-EC-EARTH rcp85 r12i1p1 KNMI-RACMO22E	7.45	7.80	7.50	-0.30
tas EUR-11 ICHEC-EC-EARTH rcp85 r12i1p1 SMHI-RCA4	7.45	7.15	7.40	0.25
tas EUR-11 ICHEC-EC-EARTH rcp85 r1i1p1 DMI-HIRHAM5	7.45	6.98	7.38	0.40
tas EUR-11 ICHEC-EC-EARTH rcp85 r1i1p1 KNMI-RACMO22E	7.45	7.28	7.50	0.21
tas EUR-11 ICHEC-EC-EARTH rcp85 r3i1p1 DMI-HIRHAM5	7.45	6.86	7.36	0.51
tas EUR-11 ICHEC-EC-EARTH rcp85 r3i1p1 KNMI-RACMO22E	7.45	7.82	7.56	-0.26
tas EUR-11 IPSL-IPSL-CM5A-MR rcp85 r1i1p1 IPSL-INERIS-WRF331F	7.45	7.02	7.44	0.42
tas EUR-11 IPSL-IPSL-CM5A-MR rcp85 r1i1p1 SMHI-RCA4	7.45	7.52	7.45	-0.08
tas EUR-11 MOHC-HadGEM2-ES rcp85 r1i1p1 CLMcom-CCLM4-8-17	7.45	9.05	7.46	-1.59
tas EUR-11 MOHC-HadGEM2-ES rcp85 r1i1p1 DMI-HIRHAM5	7.45	8.10	7.40	-0.69
tas EUR-11 MOHC-HadGEM2-ES rcp85 r1i1p1 KNMI-RACMO22E	7.45	8.59	7.58	-1.01
tas EUR-11 MOHC-HadGEM2-ES rcp85 r1i1p1 SMHI-RCA4	7.45	7.69	7.41	-0.28
tas EUR-11 MPI-M-MPI-ESM-LR rcp85 r1i1p1 CLMcom-CCLM4-8-17	7.45	7.56	7.48	-0.08
tas EUR-11 MPI-M-MPI-ESM-LR rcp85 r1i1p1 MPI-CSC-REMO2009	7.45	6.71	7.40	0.69
tas EUR-11 MPI-M-MPI-ESM-LR rcp85 r1i1p1 SMHI-RCA4	7.45	7.19	7.41	0.22
tas EUR-11 MPI-M-MPI-ESM-LR rcp85 r2i1p1 MPI-CSC-REMO2009	7.45	6.87	7.42	0.56
tas EUR-11 NCC-NorESM1-M rcp85 r1i1p1 DMI-HIRHAM5	7.45	7.03	7.37	0.34
tas EUR-11 NCC-NorESM1-M rcp85 r1i1p1 GERICS-REMO2015	7.45	6.31	7.38	1.08
RMSD	**Reference**	**Raw**	**BC**	**Change**
tas EUR-11 ICHEC-EC-EARTH rcp26 r12i1p1 CLMcom-CCLM4-8-17	0.00	2.71	2.60	-0.11
tas EUR-11 ICHEC-EC-EARTH rcp26 r12i1p1 KNMI-RACMO22E	0.00	2.70	2.51	-0.19
tas EUR-11 ICHEC-EC-EARTH rcp26 r12i1p1 SMHI-RCA4	0.00	2.57	2.31	-0.26
tas EUR-11 ICHEC-EC-EARTH rcp26 r3i1p1 DMI-HIRHAM5	0.00	2.43	2.27	-0.16

tas EUR-11 IPSL-IPSL-CM5A-LR rcp26 r1i1p1 GERICS-REMO2015	0.00	3.00	2.84	-0.16
tas EUR-11 MOHC-HadGEM2-ES rcp26 r1i1p1 KNMI-RACMO22E	0.00	3.16	2.94	-0.21
tas EUR-11 MPI-M-MPI-ESM-LR rcp26 r1i1p1 MPI-CSC-REMO2009	0.00	2.59	2.40	-0.19
tas EUR-11 MPI-M-MPI-ESM-LR rcp26 r2i1p1 MPI-CSC-REMO2009	0.00	2.70	2.53	-0.17
tas EUR-11 NOAA-GFDL-GFDL-ESM2G rcp26 r1i1p1 GERICS-REMO2015	0.00	2.81	2.37	-0.44
tas EUR-11 CNRM-CERFACS-CNRM-CM5 rcp45 r1i1p1 CLMcom-CCLM4-8-17	0.00	2.52	2.43	-0.10
tas EUR-11 CNRM-CERFACS-CNRM-CM5 rcp45 r1i1p1 CNRM-ALADIN53	0.00	2.44	2.19	-0.26
tas EUR-11 CNRM-CERFACS-CNRM-CM5 rcp45 r1i1p1 SMHI-RCA4	0.00	2.39	2.18	-0.20
tas EUR-11 ICHEC-EC-EARTH rcp45 r12i1p1 CLMcom-CCLM4-8-17	0.00	2.71	2.60	-0.11
tas EUR-11 ICHEC-EC-EARTH rcp45 r12i1p1 KNMI-RACMO22E	0.00	2.70	2.51	-0.19
tas EUR-11 ICHEC-EC-EARTH rcp45 r12i1p1 SMHI-RCA4	0.00	2.57	2.31	-0.26
tas EUR-11 ICHEC-EC-EARTH rcp45 r1i1p1 KNMI-RACMO22E	0.00	2.85	2.70	-0.14
tas EUR-11 ICHEC-EC-EARTH rcp45 r3i1p1 DMI-HIRHAM5	0.00	2.43	2.27	-0.16
tas EUR-11 IPSL-IPSL-CM5A-MR rcp45 r1i1p1 IPSL-INERIS-WRF331F	0.00	2.95	2.54	-0.41
tas EUR-11 IPSL-IPSL-CM5A-MR rcp45 r1i1p1 SMHI-RCA4	0.00	2.80	2.59	-0.22
tas EUR-11 MOHC-HadGEM2-ES rcp45 r1i1p1 CLMcom-CCLM4-8-17	0.00	3.11	2.54	-0.56
tas EUR-11 MOHC-HadGEM2-ES rcp45 r1i1p1 KNMI-RACMO22E	0.00	3.16	2.94	-0.21
tas EUR-11 MOHC-HadGEM2-ES rcp45 r1i1p1 SMHI-RCA4	0.00	2.63	2.44	-0.19
tas EUR-11 MPI-M-MPI-ESM-LR rcp45 r1i1p1 CLMcom-CCLM4-8-17	0.00	2.70	2.67	-0.03
tas EUR-11 MPI-M-MPI-ESM-LR rcp45 r1i1p1 MPI-CSC-REMO2009	0.00	2.59	2.40	-0.19
tas EUR-11 MPI-M-MPI-ESM-LR rcp45 r1i1p1 SMHI-RCA4	0.00	2.58	2.44	-0.15
tas EUR-11 MPI-M-MPI-ESM-LR rcp45 r2i1p1 MPI-CSC-REMO2009	0.00	2.70	2.53	-0.17
tas EUR-11 NCC-NorESM1-M rcp45 r1i1p1 DMI-HIRHAM5	0.00	2.44	2.29	-0.15
tas EUR-11 CNRM-CERFACS-CNRM-CM5 rcp85 r1i1p1 CLMcom-CCLM4-8-17	0.00	2.52	2.43	-0.10
tas EUR-11 CNRM-CERFACS-CNRM-CM5 rcp85 r1i1p1 CNRM-ALADIN53	0.00	2.44	2.19	-0.26
tas EUR-11 CNRM-CERFACS-CNRM-CM5 rcp85 r1i1p1 CNRM-ALADIN63	0.00	2.79	2.48	-0.30
tas EUR-11 CNRM-CERFACS-CNRM-CM5 rcp85 r1i1p1 DMI-HIRHAM5	0.00	2.36	2.28	-0.08
tas EUR-11 CNRM-CERFACS-CNRM-CM5 rcp85 r1i1p1 KNMI-RACMO22E	0.00	2.96	2.77	-0.18
tas EUR-11 CNRM-CERFACS-CNRM-CM5 rcp85 r1i1p1 SMHI-RCA4	0.00	2.39	2.18	-0.20
tas EUR-11 ICHEC-EC-EARTH rcp85 r12i1p1 CLMcom-CCLM4-8-17	0.00	2.71	2.60	-0.11
tas EUR-11 ICHEC-EC-EARTH rcp85 r12i1p1 DMI-HIRHAM5	0.00	2.40	2.35	-0.04
tas EUR-11 ICHEC-EC-EARTH rcp85 r12i1p1 KNMI-RACMO22E	0.00	2.70	2.51	-0.19
tas EUR-11 ICHEC-EC-EARTH rcp85 r12i1p1 SMHI-RCA4	0.00	2.57	2.31	-0.26
tas EUR-11 ICHEC-EC-EARTH rcp85 r1i1p1 DMI-HIRHAM5	0.00	2.37	2.29	-0.08
tas EUR-11 ICHEC-EC-EARTH rcp85 r1i1p1 KNMI-RACMO22E	0.00	2.85	2.70	-0.14
tas EUR-11 ICHEC-EC-EARTH rcp85 r3i1p1 DMI-HIRHAM5	0.00	2.43	2.27	-0.16
tas EUR-11 ICHEC-EC-EARTH rcp85 r3i1p1 KNMI-RACMO22E	0.00	3.02	2.92	-0.09
tas EUR-11 IPSL-IPSL-CM5A-MR rcp85 r1i1p1 IPSL-INERIS-WRF331F	0.00	2.95	2.54	-0.41
tas EUR-11 IPSL-IPSL-CM5A-MR rcp85 r1i1p1 SMHI-RCA4	0.00	2.80	2.59	-0.22
tas EUR-11 MOHC-HadGEM2-ES rcp85 r1i1p1 CLMcom-CCLM4-8-17	0.00	3.11	2.54	-0.56
tas EUR-11 MOHC-HadGEM2-ES rcp85 r1i1p1 DMI-HIRHAM5	0.00	2.58	2.39	-0.18

tas EUR-11 MOHC-HadGEM2-ES rcp85 r1i1p1 KNMI-RACMO22E	0.00	3.16	2.94	-0.21
tas EUR-11 MOHC-HadGEM2-ES rcp85 r1i1p1 SMHI-RCA4	0.00	2.63	2.44	-0.19
tas EUR-11 MPI-M-MPI-ESM-LR rcp85 r1i1p1 CLMcom-CCLM4-8-17	0.00	2.70	2.67	-0.03
tas EUR-11 MPI-M-MPI-ESM-LR rcp85 r1i1p1 MPI-CSC-REMO2009	0.00	2.59	2.40	-0.19
tas EUR-11 MPI-M-MPI-ESM-LR rcp85 r1i1p1 SMHI-RCA4	0.00	2.58	2.44	-0.15
tas EUR-11 MPI-M-MPI-ESM-LR rcp85 r2i1p1 MPI-CSC-REMO2009	0.00	2.70	2.53	-0.17
tas EUR-11 NCC-NorESM1-M rcp85 r1i1p1 DMI-HIRHAM5	0.00	2.44	2.29	-0.15
tas EUR-11 NCC-NorESM1-M rcp85 r1i1p1 GERICS-REMO2015	0.00	2.80	2.45	-0.35
Spearman's Correlation Coefficient	**Reference**	**Raw**	**BC**	**Change**
tas EUR-11 ICHEC-EC-EARTH rcp26 r12i1p1 CLMcom-CCLM4-8-17	1.00	0.94	0.94	0.00
tas EUR-11 ICHEC-EC-EARTH rcp26 r12i1p1 KNMI-RACMO22E	1.00	0.94	0.94	0.01
tas EUR-11 ICHEC-EC-EARTH rcp26 r12i1p1 SMHI-RCA4	1.00	0.94	0.95	0.01
tas EUR-11 ICHEC-EC-EARTH rcp26 r3i1p1 DMI-HIRHAM5	1.00	0.94	0.95	0.01
tas EUR-11 IPSL-IPSL-CM5A-LR rcp26 r1i1p1 GERICS-REMO2015	1.00	0.92	0.93	0.01
tas EUR-11 MOHC-HadGEM2-ES rcp26 r1i1p1 KNMI-RACMO22E	1.00	0.93	0.93	-0.01
tas EUR-11 MPI-M-MPI-ESM-LR rcp26 r1i1p1 MPI-CSC-REMO2009	1.00	0.93	0.94	0.01
tas EUR-11 MPI-M-MPI-ESM-LR rcp26 r2i1p1 MPI-CSC-REMO2009	1.00	0.93	0.93	0.01
tas EUR-11 NOAA-GFDL-GFDL-ESM2G rcp26 r1i1p1 GERICS-REMO2015	1.00	0.93	0.95	0.01
tas EUR-11 CNRM-CERFACS-CNRM-CM5 rcp45 r1i1p1 CLMcom-CCLM4-8-17	1.00	0.94	0.94	0.00
tas EUR-11 CNRM-CERFACS-CNRM-CM5 rcp45 r1i1p1 CNRM-ALADIN53	1.00	0.95	0.95	0.00
tas EUR-11 CNRM-CERFACS-CNRM-CM5 rcp45 r1i1p1 SMHI-RCA4	1.00	0.94	0.95	0.01
tas EUR-11 ICHEC-EC-EARTH rcp45 r12i1p1 CLMcom-CCLM4-8-17	1.00	0.94	0.94	0.00
tas EUR-11 ICHEC-EC-EARTH rcp45 r12i1p1 KNMI-RACMO22E	1.00	0.94	0.94	0.01
tas EUR-11 ICHEC-EC-EARTH rcp45 r12i1p1 SMHI-RCA4	1.00	0.94	0.95	0.01
tas EUR-11 ICHEC-EC-EARTH rcp45 r1i1p1 KNMI-RACMO22E	1.00	0.93	0.94	0.01
tas EUR-11 ICHEC-EC-EARTH rcp45 r3i1p1 DMI-HIRHAM5	1.00	0.94	0.95	0.01
tas EUR-11 IPSL-IPSL-CM5A-MR rcp45 r1i1p1 IPSL-INERIS-WRF331F	1.00	0.92	0.94	0.02
tas EUR-11 IPSL-IPSL-CM5A-MR rcp45 r1i1p1 SMHI-RCA4	1.00	0.93	0.94	0.01
tas EUR-11 MOHC-HadGEM2-ES rcp45 r1i1p1 CLMcom-CCLM4-8-17	1.00	0.95	0.94	-0.01
tas EUR-11 MOHC-HadGEM2-ES rcp45 r1i1p1 KNMI-RACMO22E	1.00	0.93	0.93	-0.01
tas EUR-11 MOHC-HadGEM2-ES rcp45 r1i1p1 SMHI-RCA4	1.00	0.94	0.94	0.00
tas EUR-11 MPI-M-MPI-ESM-LR rcp45 r1i1p1 CLMcom-CCLM4-8-17	1.00	0.93	0.93	0.00
tas EUR-11 MPI-M-MPI-ESM-LR rcp45 r1i1p1 MPI-CSC-REMO2009	1.00	0.93	0.94	0.01
tas EUR-11 MPI-M-MPI-ESM-LR rcp45 r1i1p1 SMHI-RCA4	1.00	0.94	0.94	0.01
tas EUR-11 MPI-M-MPI-ESM-LR rcp45 r2i1p1 MPI-CSC-REMO2009	1.00	0.93	0.93	0.01
tas EUR-11 NCC-NorESM1-M rcp45 r1i1p1 DMI-HIRHAM5	1.00	0.94	0.94	0.00
tas EUR-11 CNRM-CERFACS-CNRM-CM5 rcp85 r1i1p1 CLMcom-CCLM4-8-17	1.00	0.94	0.94	0.00
tas EUR-11 CNRM-CERFACS-CNRM-CM5 rcp85 r1i1p1 CNRM-ALADIN53	1.00	0.95	0.95	0.00
tas EUR-11 CNRM-CERFACS-CNRM-CM5 rcp85 r1i1p1 CNRM-ALADIN63	1.00	0.93	0.94	0.01
tas EUR-11 CNRM-CERFACS-CNRM-CM5 rcp85 r1i1p1 DMI-HIRHAM5	1.00	0.94	0.94	0.00
tas EUR-11 CNRM-CERFACS-CNRM-CM5 rcp85 r1i1p1 KNMI-RACMO22E	1.00	0.93	0.93	0.00
tas EUR-11 CNRM-CERFACS-CNRM-CM5 rcp85 r1i1p1 SMHI-RCA4	1.00	0.94	0.95	0.01

tas EUR-11 ICHEC-EC-EARTH rcp85 r12i1p1 CLMcom-CCLM4-8-17	1.00	0.94	0.94	0.00
tas EUR-11 ICHEC-EC-EARTH rcp85 r12i1p1 DMI-HIRHAM5	1.00	0.94	0.94	0.00
tas EUR-11 ICHEC-EC-EARTH rcp85 r12i1p1 KNMI-RACMO22E	1.00	0.94	0.94	0.01
tas EUR-11 ICHEC-EC-EARTH rcp85 r12i1p1 SMHI-RCA4	1.00	0.94	0.95	0.01
tas EUR-11 ICHEC-EC-EARTH rcp85 r1i1p1 DMI-HIRHAM5	1.00	0.94	0.95	0.00
tas EUR-11 ICHEC-EC-EARTH rcp85 r1i1p1 KNMI-RACMO22E	1.00	0.93	0.94	0.01
tas EUR-11 ICHEC-EC-EARTH rcp85 r3i1p1 DMI-HIRHAM5	1.00	0.94	0.95	0.01
tas EUR-11 ICHEC-EC-EARTH rcp85 r3i1p1 KNMI-RACMO22E	1.00	0.92	0.92	0.00
tas EUR-11 IPSL-IPSL-CM5A-MR rcp85 r1i1p1 IPSL-INERIS-WRF331F	1.00	0.92	0.94	0.02
tas EUR-11 IPSL-IPSL-CM5A-MR rcp85 r1i1p1 SMHI-RCA4	1.00	0.93	0.94	0.01
tas EUR-11 MOHC-HadGEM2-ES rcp85 r1i1p1 CLMcom-CCLM4-8-17	1.00	0.95	0.94	-0.01
tas EUR-11 MOHC-HadGEM2-ES rcp85 r1i1p1 DMI-HIRHAM5	1.00	0.95	0.95	0.00
tas EUR-11 MOHC-HadGEM2-ES rcp85 r1i1p1 KNMI-RACMO22E	1.00	0.93	0.93	-0.01
tas EUR-11 MOHC-HadGEM2-ES rcp85 r1i1p1 SMHI-RCA4	1.00	0.94	0.94	0.00
tas EUR-11 MPI-M-MPI-ESM-LR rcp85 r1i1p1 CLMcom-CCLM4-8-17	1.00	0.93	0.93	0.00
tas EUR-11 MPI-M-MPI-ESM-LR rcp85 r1i1p1 MPI-CSC-REMO2009	1.00	0.93	0.94	0.01
tas EUR-11 MPI-M-MPI-ESM-LR rcp85 r1i1p1 SMHI-RCA4	1.00	0.94	0.94	0.01
tas EUR-11 MPI-M-MPI-ESM-LR rcp85 r2i1p1 MPI-CSC-REMO2009	1.00	0.93	0.93	0.01
tas EUR-11 NCC-NorESM1-M rcp85 r1i1p1 DMI-HIRHAM5	1.00	0.94	0.94	0.00
tas EUR-11 NCC-NorESM1-M rcp85 r1i1p1 GERICS-REMO2015	1.00	0.93	0.94	0.01

Table 25 - Annual projected values and percent change for precipitation yielded from the bias-corrected models that were chosen for the period 2019-2038, 2039-2058 and 2059-2078

Name (2019-2038)	Reference Values	Projected Values	Percent Change
pr EUR-11 IPSL-IPSL-CM5A-LR rcp26 r1i1p1 GER-ICS-REMO2015	799.93	781.64	-2.29
pr EUR-11 MPI-M-MPI-ESM-LR rcp26 r1i1p1 MPI-CSC-REMO2009	799.93	772.25	-3.46
pr EUR-11 IPSL-IPSL-CM5A-MR rcp45 r1i1p1 IPSL-INERIS-WRF331F	799.93	804.51	0.57
pr EUR-11 MOHC-HadGEM2-ES rcp45 r1i1p1 SMHI-RCA4	799.93	798.48	-0.18
pr EUR-11 MPI-M-MPI-ESM-LR rcp45 r1i1p1 MPI-CSC-REMO2009	799.93	765.27	-4.33
pr EUR-11 MPI-M-MPI-ESM-LR rcp45 r1i1p1 SMHI-RCA4	799.93	689.35	-13.82
pr EUR-11 CNRM-CERFACS-CNRM-CM5 rcp85 r1i1p1 CLMcom-CCLM4-8-17	799.93	753.81	-5.77
pr EUR-11 MPI-M-MPI-ESM-LR rcp85 r1i1p1 CLM-com-CCLM4-8-17	799.93	733.89	-8.26
pr EUR-11 MPI-M-MPI-ESM-LR rcp85 r1i1p1 MPI-CSC-REMO2009	799.93	745.05	-6.86
pr EUR-11 MPI-M-MPI-ESM-LR rcp85 r1i1p1 SMHI-RCA4	799.93	713.84	-10.76
Name (2059-2058)	**Reference Values**	**Projected Values**	**Percent Change**
pr EUR-11 IPSL-IPSL-CM5A-LR rcp26 r1i1p1 GER-ICS-REMO2015	799.93	733.49	-8.31
pr EUR-11 MPI-M-MPI-ESM-LR rcp26 r1i1p1 MPI-CSC-REMO2009	799.93	753.26	-5.83
pr EUR-11 IPSL-IPSL-CM5A-MR rcp45 r1i1p1 IPSL-INERIS-WRF331F	799.93	778.90	-2.63
pr EUR-11 MOHC-HadGEM2-ES rcp45 r1i1p1 SMHI-RCA4	799.93	772.26	-3.46

pr EUR-11 MPI-M-MPI-ESM-LR rcp45 r1i1p1 MPI-CSC-REMO2009	799.93	774.04	-3.24
pr EUR-11 MPI-M-MPI-ESM-LR rcp45 r1i1p1 SMHI-RCA4	799.93	752.38	-5.94
pr EUR-11 CNRM-CERFACS-CNRM-CM5 rcp85 r1i1p1 CLMcom-CCLM4-8-17	799.93	797.12	-0.35
pr EUR-11 MPI-M-MPI-ESM-LR rcp85 r1i1p1 CLM-com-CCLM4-8-17	799.93	669.43	-16.31
pr EUR-11 MPI-M-MPI-ESM-LR rcp85 r1i1p1 MPI-CSC-REMO2009	799.93	754.64	-5.66
pr EUR-11 MPI-M-MPI-ESM-LR rcp85 r1i1p1 SMHI-RCA4	799.93	730.27	-8.71
Name (2059-2078)	**Reference Values**	**Projected Values**	**Percent Change**
pr EUR-11 IPSL-IPSL-CM5A-LR rcp26 r1i1p1 GER-ICS-REMO2015	799.93	743.15	-7.10
pr EUR-11 MPI-M-MPI-ESM-LR rcp26 r1i1p1 MPI-CSC-REMO2009	799.93	753.93	-5.75
pr EUR-11 IPSL-IPSL-CM5A-MR rcp45 r1i1p1 IPSL-INERIS-WRF331F	799.93	798.42	-0.19
pr EUR-11 MOHC-HadGEM2-ES rcp45 r1i1p1 SMHI-RCA4	799.93	700.96	-12.37
pr EUR-11 MPI-M-MPI-ESM-LR rcp45 r1i1p1 MPI-CSC-REMO2009	799.93	755.43	-5.56
pr EUR-11 MPI-M-MPI-ESM-LR rcp45 r1i1p1 SMHI-RCA4	799.93	762.10	-4.73
pr EUR-11 CNRM-CERFACS-CNRM-CM5 rcp85 r1i1p1 CLMcom-CCLM4-8-17	799.93	778.83	-2.64
pr EUR-11 MPI-M-MPI-ESM-LR rcp85 r1i1p1 CLM-com-CCLM4-8-17	799.93	735.15	-8.10
pr EUR-11 MPI-M-MPI-ESM-LR rcp85 r1i1p1 MPI-CSC-REMO2009	799.93	729.87	-8.76
pr EUR-11 MPI-M-MPI-ESM-LR rcp85 r1i1p1 SMHI-RCA4	799.93	711.83	-11.01

Table 26 – Seasonal projected values and percent change for precipitation yielded from the bias-corrected models that were chosen for the period 2019-2038, 2039-2058 and 2059-2078

Name (2019-2038)	Season	Reference Values	Projected Values	Percent Change
pr EUR-11 IPSL-IPSL-CM5A-LR rcp26 r1i1p1 GERICS-REMO2015	Winter	236.91	240.92	1.69
pr EUR-11 IPSL-IPSL-CM5A-LR rcp26 r1i1p1 GERICS-REMO2015	Spring	215.98	189.99	-12.03
pr EUR-11 IPSL-IPSL-CM5A-LR rcp26 r1i1p1 GERICS-REMO2015	Summer	131.29	119.74	-8.80
pr EUR-11 IPSL-IPSL-CM5A-LR rcp26 r1i1p1 GERICS-REMO2015	Autumn	215.75	230.99	7.06
pr EUR-11 MPI-M-MPI-ESM-LR rcp26 r1i1p1 MPI-CSC-REMO2009	Winter	236.91	257.85	8.84
pr EUR-11 MPI-M-MPI-ESM-LR rcp26 r1i1p1 MPI-CSC-REMO2009	Spring	215.98	212.70	-1.52
pr EUR-11 MPI-M-MPI-ESM-LR rcp26 r1i1p1 MPI-CSC-REMO2009	Summer	131.29	115.38	-12.12
pr EUR-11 MPI-M-MPI-ESM-LR rcp26 r1i1p1 MPI-CSC-REMO2009	Autumn	215.75	186.32	-13.64
pr EUR-11 IPSL-IPSL-CM5A-MR rcp45 r1i1p1 IPSL-INERIS-WRF331F	Winter	236.91	213.24	-9.99
pr EUR-11 IPSL-IPSL-CM5A-MR rcp45 r1i1p1 IPSL-INERIS-WRF331F	Spring	215.98	241.98	12.03
pr EUR-11 IPSL-IPSL-CM5A-MR rcp45 r1i1p1 IPSL-INERIS-WRF331F	Summer	131.29	143.65	9.41
pr EUR-11 IPSL-IPSL-CM5A-MR rcp45 r1i1p1 IPSL-INERIS-WRF331F	Autumn	215.75	205.64	-4.69

pr EUR-11 MOHC-HadGEM2-ES rcp45 r1i1p1 SMHI-RCA4	Winter	236.91	240.21	1.39
pr EUR-11 MOHC-HadGEM2-ES rcp45 r1i1p1 SMHI-RCA4	Spring	215.98	177.57	-17.79
pr EUR-11 MOHC-HadGEM2-ES rcp45 r1i1p1 SMHI-RCA4	Summer	131.29	112.97	-13.96
pr EUR-11 MOHC-HadGEM2-ES rcp45 r1i1p1 SMHI-RCA4	Autumn	215.75	267.74	24.10
pr EUR-11 MPI-M-MPI-ESM-LR rcp45 r1i1p1 MPI-CSC-REMO2009	Winter	236.91	222.52	-6.07
pr EUR-11 MPI-M-MPI-ESM-LR rcp45 r1i1p1 MPI-CSC-REMO2009	Spring	215.98	217.22	0.57
pr EUR-11 MPI-M-MPI-ESM-LR rcp45 r1i1p1 MPI-CSC-REMO2009	Summer	131.29	103.61	-21.08
pr EUR-11 MPI-M-MPI-ESM-LR rcp45 r1i1p1 MPI-CSC-REMO2009	Autumn	215.75	221.92	2.86
pr EUR-11 MPI-M-MPI-ESM-LR rcp45 r1i1p1 SMHI-RCA4	Winter	236.91	201.45	-14.97
pr EUR-11 MPI-M-MPI-ESM-LR rcp45 r1i1p1 SMHI-RCA4	Spring	215.98	197.58	-8.52
pr EUR-11 MPI-M-MPI-ESM-LR rcp45 r1i1p1 SMHI-RCA4	Summer	131.29	93.39	-28.87
pr EUR-11 MPI-M-MPI-ESM-LR rcp45 r1i1p1 SMHI-RCA4	Autumn	215.75	196.93	-8.72
pr EUR-11 CNRM-CERFACS-CNRM-CM5 rcp85 r1i1p1 CLMcom-CCLM4-8-17	Winter	236.91	215.25	-9.14
pr EUR-11 CNRM-CERFACS-CNRM-CM5 rcp85 r1i1p1 CLMcom-CCLM4-8-17	Spring	215.98	215.22	-0.35
pr EUR-11 CNRM-CERFACS-CNRM-CM5 rcp85 r1i1p1 CLMcom-CCLM4-8-17	Summer	131.29	80.54	-38.66
pr EUR-11 CNRM-CERFACS-CNRM-CM5 rcp85 r1i1p1 CLMcom-CCLM4-8-17	Autumn	215.75	242.79	12.53
pr EUR-11 MPI-M-MPI-ESM-LR rcp85 r1i1p1 CLMcom-CCLM4-8-17	Winter	236.91	210.19	-11.28
pr EUR-11 MPI-M-MPI-ESM-LR rcp85 r1i1p1 CLMcom-CCLM4-8-17	Spring	215.98	210.05	-2.75
pr EUR-11 MPI-M-MPI-ESM-LR rcp85 r1i1p1 CLMcom-CCLM4-8-17	Summer	131.29	102.64	-21.83
pr EUR-11 MPI-M-MPI-ESM-LR rcp85 r1i1p1 CLMcom-CCLM4-8-17	Autumn	215.75	211.01	-2.20
pr EUR-11 MPI-M-MPI-ESM-LR rcp85 r1i1p1 MPI-CSC-REMO2009	Winter	236.91	231.89	-2.12
pr EUR-11 MPI-M-MPI-ESM-LR rcp85 r1i1p1 MPI-CSC-REMO2009	Spring	215.98	208.09	-3.65
pr EUR-11 MPI-M-MPI-ESM-LR rcp85 r1i1p1 MPI-CSC-REMO2009	Summer	131.29	103.77	-20.97
pr EUR-11 MPI-M-MPI-ESM-LR rcp85 r1i1p1 MPI-CSC-REMO2009	Autumn	215.75	201.30	-6.70
pr EUR-11 MPI-M-MPI-ESM-LR rcp85 r1i1p1 SMHI-RCA4	Winter	236.91	217.64	-8.13
pr EUR-11 MPI-M-MPI-ESM-LR rcp85 r1i1p1 SMHI-RCA4	Spring	215.98	187.78	-13.06
pr EUR-11 MPI-M-MPI-ESM-LR rcp85 r1i1p1 SMHI-RCA4	Summer	131.29	127.42	-2.95
pr EUR-11 MPI-M-MPI-ESM-LR rcp85 r1i1p1 SMHI-RCA4	Autumn	215.75	181.01	-16.10
Name (2039-2058)	**Season**	**Reference Values**	**Projected Values**	**Percent Change**

pr EUR-11 IPSL-IPSL-CM5A-LR rcp26 r1i1p1 GERICS-REMO2015	Winter	236.91	195.78	-17.36
pr EUR-11 IPSL-IPSL-CM5A-LR rcp26 r1i1p1 GERICS-REMO2015	Spring	215.98	189.99	-12.03
pr EUR-11 IPSL-IPSL-CM5A-LR rcp26 r1i1p1 GERICS-REMO2015	Summer	131.29	110.33	-15.97
pr EUR-11 IPSL-IPSL-CM5A-LR rcp26 r1i1p1 GERICS-REMO2015	Autumn	215.75	237.39	10.03
pr EUR-11 MPI-M-MPI-ESM-LR rcp26 r1i1p1 MPI-CSC-REMO2009	Winter	236.91	197.89	-16.47
pr EUR-11 MPI-M-MPI-ESM-LR rcp26 r1i1p1 MPI-CSC-REMO2009	Spring	215.98	215.48	-0.24
pr EUR-11 MPI-M-MPI-ESM-LR rcp26 r1i1p1 MPI-CSC-REMO2009	Summer	131.29	110.86	-15.56
pr EUR-11 MPI-M-MPI-ESM-LR rcp26 r1i1p1 MPI-CSC-REMO2009	Autumn	215.75	229.03	6.15
pr EUR-11 IPSL-IPSL-CM5A-MR rcp45 r1i1p1 IPSL-INERIS-WRF331F	Winter	236.91	224.59	-5.20
pr EUR-11 IPSL-IPSL-CM5A-MR rcp45 r1i1p1 IPSL-INERIS-WRF331F	Spring	215.98	199.05	-7.84
pr EUR-11 IPSL-IPSL-CM5A-MR rcp45 r1i1p1 IPSL-INERIS-WRF331F	Summer	131.29	132.44	0.87
pr EUR-11 IPSL-IPSL-CM5A-MR rcp45 r1i1p1 IPSL-INERIS-WRF331F	Autumn	215.75	222.82	3.28
pr EUR-11 MOHC-HadGEM2-ES rcp45 r1i1p1 SMHI-RCA4	Winter	236.91	219.24	-7.46
pr EUR-11 MOHC-HadGEM2-ES rcp45 r1i1p1 SMHI-RCA4	Spring	215.98	137.69	-36.25
pr EUR-11 MOHC-HadGEM2-ES rcp45 r1i1p1 SMHI-RCA4	Summer	131.29	106.59	-18.81
pr EUR-11 MOHC-HadGEM2-ES rcp45 r1i1p1 SMHI-RCA4	Autumn	215.75	308.74	43.10
pr EUR-11 MPI-M-MPI-ESM-LR rcp45 r1i1p1 MPI-CSC-REMO2009	Winter	236.91	224.38	-5.29
pr EUR-11 MPI-M-MPI-ESM-LR rcp45 r1i1p1 MPI-CSC-REMO2009	Spring	215.98	220.17	1.94
pr EUR-11 MPI-M-MPI-ESM-LR rcp45 r1i1p1 MPI-CSC-REMO2009	Summer	131.29	92.29	-29.71
pr EUR-11 MPI-M-MPI-ESM-LR rcp45 r1i1p1 MPI-CSC-REMO2009	Autumn	215.75	237.20	9.94
pr EUR-11 MPI-M-MPI-ESM-LR rcp45 r1i1p1 SMHI-RCA4	Winter	236.91	227.83	-3.83
pr EUR-11 MPI-M-MPI-ESM-LR rcp45 r1i1p1 SMHI-RCA4	Spring	215.98	190.69	-11.71
pr EUR-11 MPI-M-MPI-ESM-LR rcp45 r1i1p1 SMHI-RCA4	Summer	131.29	81.48	-37.94
pr EUR-11 MPI-M-MPI-ESM-LR rcp45 r1i1p1 SMHI-RCA4	Autumn	215.75	252.38	16.98
pr EUR-11 CNRM-CERFACS-CNRM-CM5 rcp85 r1i1p1 CLMcom-CCLM4-8-17	Winter	236.91	226.92	-4.22
pr EUR-11 CNRM-CERFACS-CNRM-CM5 rcp85 r1i1p1 CLMcom-CCLM4-8-17	Spring	215.98	215.79	-0.09
pr EUR-11 CNRM-CERFACS-CNRM-CM5 rcp85 r1i1p1 CLMcom-CCLM4-8-17	Summer	131.29	111.17	-15.33
pr EUR-11 CNRM-CERFACS-CNRM-CM5 rcp85 r1i1p1 CLMcom-CCLM4-8-17	Autumn	215.75	243.25	12.74
pr EUR-11 MPI-M-MPI-ESM-LR rcp85 r1i1p1 CLMcom-CCLM4-8-17	Winter	236.91	223.32	-5.73

pr EUR-11 MPI-M-MPI-ESM-LR rcp85 r1i1p1 CLMcom-CCLM4-8-17	Spring	215.98	187.62	-13.13
pr EUR-11 MPI-M-MPI-ESM-LR rcp85 r1i1p1 CLMcom-CCLM4-8-17	Summer	131.29	69.81	-46.83
pr EUR-11 MPI-M-MPI-ESM-LR rcp85 r1i1p1 CLMcom-CCLM4-8-17	Autumn	215.75	188.67	-12.55
pr EUR-11 MPI-M-MPI-ESM-LR rcp85 r1i1p1 MPI-CSC-REMO2009	Winter	236.91	242.36	2.30
pr EUR-11 MPI-M-MPI-ESM-LR rcp85 r1i1p1 MPI-CSC-REMO2009	Spring	215.98	194.50	-9.95
pr EUR-11 MPI-M-MPI-ESM-LR rcp85 r1i1p1 MPI-CSC-REMO2009	Summer	131.29	99.10	-24.52
pr EUR-11 MPI-M-MPI-ESM-LR rcp85 r1i1p1 MPI-CSC-REMO2009	Autumn	215.75	218.68	1.36
pr EUR-11 MPI-M-MPI-ESM-LR rcp85 r1i1p1 SMHI-RCA4	Winter	236.91	214.15	-9.60
pr EUR-11 MPI-M-MPI-ESM-LR rcp85 r1i1p1 SMHI-RCA4	Spring	215.98	164.16	-24.00
pr EUR-11 MPI-M-MPI-ESM-LR rcp85 r1i1p1 SMHI-RCA4	Summer	131.29	114.35	-12.91
pr EUR-11 MPI-M-MPI-ESM-LR rcp85 r1i1p1 SMHI-RCA4	Autumn	215.75	237.62	10.14
Name (2059-2078)	**Season**	**Reference Values**	**Projected Values**	**Percent Change**
pr EUR-11 IPSL-IPSL-CM5A-LR rcp26 r1i1p1 GERICS-REMO2015	Winter	236.91	190.15	-19.74
pr EUR-11 IPSL-IPSL-CM5A-LR rcp26 r1i1p1 GERICS-REMO2015	Spring	215.98	244.70	13.29
pr EUR-11 IPSL-IPSL-CM5A-LR rcp26 r1i1p1 GERICS-REMO2015	Summer	131.29	109.95	-16.26
pr EUR-11 IPSL-IPSL-CM5A-LR rcp26 r1i1p1 GERICS-REMO2015	Autumn	215.75	198.36	-8.06
pr EUR-11 MPI-M-MPI-ESM-LR rcp26 r1i1p1 MPI-CSC-REMO2009	Winter	236.91	204.09	-13.85
pr EUR-11 MPI-M-MPI-ESM-LR rcp26 r1i1p1 MPI-CSC-REMO2009	Spring	215.98	206.79	-4.26
pr EUR-11 MPI-M-MPI-ESM-LR rcp26 r1i1p1 MPI-CSC-REMO2009	Summer	131.29	130.85	-0.34
pr EUR-11 MPI-M-MPI-ESM-LR rcp26 r1i1p1 MPI-CSC-REMO2009	Autumn	215.75	212.20	-1.65
pr EUR-11 IPSL-IPSL-CM5A-MR rcp45 r1i1p1 IPSL-INERIS-WRF331F	Winter	236.91	227.03	-4.17
pr EUR-11 IPSL-IPSL-CM5A-MR rcp45 r1i1p1 IPSL-INERIS-WRF331F	Spring	215.98	216.99	0.47
pr EUR-11 IPSL-IPSL-CM5A-MR rcp45 r1i1p1 IPSL-INERIS-WRF331F	Summer	131.29	141.44	7.73
pr EUR-11 IPSL-IPSL-CM5A-MR rcp45 r1i1p1 IPSL-INERIS-WRF331F	Autumn	215.75	212.95	-1.30
pr EUR-11 MOHC-HadGEM2-ES rcp45 r1i1p1 SMHI-RCA4	Winter	236.91	209.01	-11.78
pr EUR-11 MOHC-HadGEM2-ES rcp45 r1i1p1 SMHI-RCA4	Spring	215.98	169.67	-21.44
pr EUR-11 MOHC-HadGEM2-ES rcp45 r1i1p1 SMHI-RCA4	Summer	131.29	82.74	-36.98
pr EUR-11 MOHC-HadGEM2-ES rcp45 r1i1p1 SMHI-RCA4	Autumn	215.75	239.55	11.03
pr EUR-11 MPI-M-MPI-ESM-LR rcp45 r1i1p1 MPI-CSC-REMO2009	Winter	236.91	249.62	5.37
pr EUR-11 MPI-M-MPI-ESM-LR rcp45 r1i1p1 MPI-CSC-REMO2009	Spring	215.98	188.08	-12.92
pr EUR-11 MPI-M-MPI-ESM-LR rcp45 r1i1p1 MPI-CSC-REMO2009	Summer	131.29	97.42	-25.80

pr EUR-11 MPI-M-MPI-ESM-LR rcp45 r1i1p1 MPI-CSC-REMO2009	Autumn	215.75	220.30	2.11
pr EUR-11 MPI-M-MPI-ESM-LR rcp45 r1i1p1 SMHI-RCA4	Winter	236.91	223.82	-5.52
pr EUR-11 MPI-M-MPI-ESM-LR rcp45 r1i1p1 SMHI-RCA4	Spring	215.98	185.51	-14.11
pr EUR-11 MPI-M-MPI-ESM-LR rcp45 r1i1p1 SMHI-RCA4	Summer	131.29	106.58	-18.82
pr EUR-11 MPI-M-MPI-ESM-LR rcp45 r1i1p1 SMHI-RCA4	Autumn	215.75	246.19	14.11
pr EUR-11 CNRM-CERFACS-CNRM-CM5 rcp85 r1i1p1 CLMcom-CCLM4-8-17	Winter	236.91	244.92	3.38
pr EUR-11 CNRM-CERFACS-CNRM-CM5 rcp85 r1i1p1 CLMcom-CCLM4-8-17	Spring	215.98	204.63	-5.26
pr EUR-11 CNRM-CERFACS-CNRM-CM5 rcp85 r1i1p1 CLMcom-CCLM4-8-17	Summer	131.29	92.62	-29.46
pr EUR-11 CNRM-CERFACS-CNRM-CM5 rcp85 r1i1p1 CLMcom-CCLM4-8-17	Autumn	215.75	236.66	9.69
pr EUR-11 MPI-M-MPI-ESM-LR rcp85 r1i1p1 CLMcom-CCLM4-8-17	Winter	236.91	224.97	-5.04
pr EUR-11 MPI-M-MPI-ESM-LR rcp85 r1i1p1 CLMcom-CCLM4-8-17	Spring	215.98	222.60	3.06
pr EUR-11 MPI-M-MPI-ESM-LR rcp85 r1i1p1 CLMcom-CCLM4-8-17	Summer	131.29	76.01	-42.10
pr EUR-11 MPI-M-MPI-ESM-LR rcp85 r1i1p1 CLMcom-CCLM4-8-17	Autumn	215.75	211.57	-1.94
pr EUR-11 MPI-M-MPI-ESM-LR rcp85 r1i1p1 MPI-CSC-REMO2009	Winter	236.91	227.96	-3.78
pr EUR-11 MPI-M-MPI-ESM-LR rcp85 r1i1p1 MPI-CSC-REMO2009	Spring	215.98	200.80	-7.03
pr EUR-11 MPI-M-MPI-ESM-LR rcp85 r1i1p1 MPI-CSC-REMO2009	Summer	131.29	94.44	-28.07
pr EUR-11 MPI-M-MPI-ESM-LR rcp85 r1i1p1 MPI-CSC-REMO2009	Autumn	215.75	206.66	-4.21
pr EUR-11 MPI-M-MPI-ESM-LR rcp85 r1i1p1 SMHI-RCA4	Winter	236.91	223.42	-5.69
pr EUR-11 MPI-M-MPI-ESM-LR rcp85 r1i1p1 SMHI-RCA4	Spring	215.98	164.64	-23.77
pr EUR-11 MPI-M-MPI-ESM-LR rcp85 r1i1p1 SMHI-RCA4	Summer	131.29	99.88	-23.93
pr EUR-11 MPI-M-MPI-ESM-LR rcp85 r1i1p1 SMHI-RCA4	Autumn	215.75	223.90	3.78

Table 27 – Annual projected values and percent change for temperature yielded from the bias-corrected models that were chosen for the period 2019-2038, 2039-2058 and 2059-2078

Name (2019-2038)	Reference Values	Projected Values	Change
tas EUR-11 IPSL-IPSL-CM5A-LR rcp26 r1i1p1 GERICS-REMO2015	24.62	27.82	3.19
tas EUR-11 MPI-M-MPI-ESM-LR rcp26 r1i1p1 MPI-CSC-REMO2009	24.62	25.80	1.18
tas EUR-11 IPSL-IPSL-CM5A-MR rcp45 r1i1p1 IPSL-INERIS-WRF331F	24.62	26.71	2.09
tas EUR-11 MOHC-HadGEM2-ES rcp45 r1i1p1 SMHI-RCA4	24.62	26.91	2.29
tas EUR-11 MPI-M-MPI-ESM-LR rcp45 r1i1p1 MPI-CSC-REMO2009	24.62	25.55	0.93
tas EUR-11 MPI-M-MPI-ESM-LR rcp45 r1i1p1 SMHI-RCA4	24.62	25.87	1.24
tas EUR-11 CNRM-CERFACS-CNRM-CM5 rcp85 r1i1p1 CLM-	24.62	24.56	-0.07

com-CCLM4-8-17			
tas EUR-11 MPI-M-MPI-ESM-LR rcp85 r1i1p1 CLMcom-CCLM4-8-17	24.62	23.87	-0.76
tas EUR-11 MPI-M-MPI-ESM-LR rcp85 r1i1p1 MPI-CSC-REMO2009	24.62	25.07	0.45
tas EUR-11 MPI-M-MPI-ESM-LR rcp85 r1i1p1 SMHI-RCA4	24.62	24.85	0.23
Name (2039-2058)	**Reference Values**	**Projected Values**	**Change**
tas EUR-11 IPSL-IPSL-CM5A-LR rcp26 r1i1p1 GERICS-REMO2015	24.62	28.84	4.22
tas EUR-11 MPI-M-MPI-ESM-LR rcp26 r1i1p1 MPI-CSC-REMO2009	24.62	25.71	1.08
tas EUR-11 IPSL-IPSL-CM5A-MR rcp45 r1i1p1 IPSL-INERIS-WRF331F	24.62	28.52	3.89
tas EUR-11 MOHC-HadGEM2-ES rcp45 r1i1p1 SMHI-RCA4	24.62	27.90	3.28
tas EUR-11 MPI-M-MPI-ESM-LR rcp45 r1i1p1 MPI-CSC-REMO2009	24.62	26.49	1.87
tas EUR-11 MPI-M-MPI-ESM-LR rcp45 r1i1p1 SMHI-RCA4	24.62	27.15	2.53
tas EUR-11 CNRM-CERFACS-CNRM-CM5 rcp85 r1i1p1 CLM-com-CCLM4-8-17	24.62	25.64	1.01
tas EUR-11 MPI-M-MPI-ESM-LR rcp85 r1i1p1 CLMcom-CCLM4-8-17	24.62	26.34	1.71
tas EUR-11 MPI-M-MPI-ESM-LR rcp85 r1i1p1 MPI-CSC-REMO2009	24.62	27.73	3.10
tas EUR-11 MPI-M-MPI-ESM-LR rcp85 r1i1p1 SMHI-RCA4	24.62	27.67	3.05
Name (2059-2078)	**Reference Values**	**Projected Values**	**Change**
tas EUR-11 IPSL-IPSL-CM5A-LR rcp26 r1i1p1 GERICS-REMO2015	24.62	29.03	4.41
tas EUR-11 MPI-M-MPI-ESM-LR rcp26 r1i1p1 MPI-CSC-REMO2009	24.62	25.54	0.92
tas EUR-11 IPSL-IPSL-CM5A-MR rcp45 r1i1p1 IPSL-INERIS-WRF331F	24.62	29.23	4.61
tas EUR-11 MOHC-HadGEM2-ES rcp45 r1i1p1 SMHI-RCA4	24.62	29.43	4.81
tas EUR-11 MPI-M-MPI-ESM-LR rcp45 r1i1p1 MPI-CSC-REMO2009	24.62	26.88	2.26
tas EUR-11 MPI-M-MPI-ESM-LR rcp45 r1i1p1 SMHI-RCA4	24.62	27.16	2.54
tas EUR-11 CNRM-CERFACS-CNRM-CM5 rcp85 r1i1p1 CLM-com-CCLM4-8-17	24.62	27.81	3.19
tas EUR-11 MPI-M-MPI-ESM-LR rcp85 r1i1p1 CLMcom-CCLM4-8-17	24.62	28.43	3.80
tas EUR-11 MPI-M-MPI-ESM-LR rcp85 r1i1p1 MPI-CSC-REMO2009	24.62	29.78	5.16
tas EUR-11 MPI-M-MPI-ESM-LR rcp85 r1i1p1 SMHI-RCA4	24.62	30.06	5.44

Table 28 - Seasonal projected values and percent change for temperature yielded from the bias-corrected models that were chosen for the period 2019-2038, 2039-2058 and 2059-2078

Name (2019-2038)	**Season**	**Reference Values**	**Projected Values**	**Change**
tas EUR-11 IPSL-IPSL-CM5A-LR rcp26 r1i1p1 GERICS-REMO2015	Winter	3.12	5.03	1.91
tas EUR-11 IPSL-IPSL-CM5A-LR rcp26 r1i1p1 GERICS-REMO2015	Spring	11.23	12.30	1.07
tas EUR-11 IPSL-IPSL-CM5A-LR rcp26 r1i1p1 GERICS-REMO2015	Summer	21.77	23.45	1.68
tas EUR-11 IPSL-IPSL-CM5A-LR rcp26 r1i1p1 GERICS-REMO2015	Autumn	13.12	14.85	1.73
tas EUR-11 MPI-M-MPI-ESM-LR rcp26 r1i1p1 MPI-CSC-REMO2009	Winter	3.12	3.11	-0.01
tas EUR-11 MPI-M-MPI-ESM-LR rcp26 r1i1p1 MPI-CSC-REMO2009	Spring	11.23	11.93	0.71

tas EUR-11 MPI-M-MPI-ESM-LR rcp26 r1i1p1 MPI-CSC-REMO2009	Summer	21.77	22.75	0.97
tas EUR-11 MPI-M-MPI-ESM-LR rcp26 r1i1p1 MPI-CSC-REMO2009	Autumn	13.12	13.82	0.69
tas EUR-11 IPSL-IPSL-CM5A-MR rcp45 r1i1p1 IPSL-INERIS-WRF331F	Winter	3.12	4.35	1.23
tas EUR-11 IPSL-IPSL-CM5A-MR rcp45 r1i1p1 IPSL-INERIS-WRF331F	Spring	11.23	12.30	1.07
tas EUR-11 IPSL-IPSL-CM5A-MR rcp45 r1i1p1 IPSL-INERIS-WRF331F	Summer	21.77	22.77	1.00
tas EUR-11 IPSL-IPSL-CM5A-MR rcp45 r1i1p1 IPSL-INERIS-WRF331F	Autumn	13.12	14.00	0.88
tas EUR-11 MOHC-HadGEM2-ES rcp45 r1i1p1 SMHI-RCA4	Winter	3.12	4.74	1.62
tas EUR-11 MOHC-HadGEM2-ES rcp45 r1i1p1 SMHI-RCA4	Spring	11.23	15.22	4.00
tas EUR-11 MOHC-HadGEM2-ES rcp45 r1i1p1 SMHI-RCA4	Summer	21.77	22.62	0.85
tas EUR-11 MOHC-HadGEM2-ES rcp45 r1i1p1 SMHI-RCA4	Autumn	13.12	11.24	-1.89
tas EUR-11 MPI-M-MPI-ESM-LR rcp45 r1i1p1 MPI-CSC-REMO2009	Winter	3.12	3.56	0.44
tas EUR-11 MPI-M-MPI-ESM-LR rcp45 r1i1p1 MPI-CSC-REMO2009	Spring	11.23	11.25	0.02
tas EUR-11 MPI-M-MPI-ESM-LR rcp45 r1i1p1 MPI-CSC-REMO2009	Summer	21.77	22.71	0.93
tas EUR-11 MPI-M-MPI-ESM-LR rcp45 r1i1p1 MPI-CSC-REMO2009	Autumn	13.12	13.60	0.48
tas EUR-11 MPI-M-MPI-ESM-LR rcp45 r1i1p1 SMHI-RCA4	Winter	3.12	3.47	0.35
tas EUR-11 MPI-M-MPI-ESM-LR rcp45 r1i1p1 SMHI-RCA4	Spring	11.23	11.73	0.51
tas EUR-11 MPI-M-MPI-ESM-LR rcp45 r1i1p1 SMHI-RCA4	Summer	21.77	22.85	1.07
tas EUR-11 MPI-M-MPI-ESM-LR rcp45 r1i1p1 SMHI-RCA4	Autumn	13.12	13.68	0.56
tas EUR-11 CNRM-CERFACS-CNRM-CM5 rcp85 r1i1p1 CLMcom-CCLM4-8-17	Winter	3.12	2.91	-0.21
tas EUR-11 CNRM-CERFACS-CNRM-CM5 rcp85 r1i1p1 CLMcom-CCLM4-8-17	Spring	11.23	10.85	-0.38
tas EUR-11 CNRM-CERFACS-CNRM-CM5 rcp85 r1i1p1 CLMcom-CCLM4-8-17	Summer	21.77	22.08	0.31
tas EUR-11 CNRM-CERFACS-CNRM-CM5 rcp85 r1i1p1 CLMcom-CCLM4-8-17	Autumn	13.12	13.27	0.15
tas EUR-11 MPI-M-MPI-ESM-LR rcp85 r1i1p1 CLMcom-CCLM4-8-17	Winter	3.12	1.83	-1.29
tas EUR-11 MPI-M-MPI-ESM-LR rcp85 r1i1p1 CLMcom-CCLM4-8-17	Spring	11.23	10.73	-0.49
tas EUR-11 MPI-M-MPI-ESM-LR rcp85 r1i1p1 CLMcom-CCLM4-8-17	Summer	21.77	22.39	0.62
tas EUR-11 MPI-M-MPI-ESM-LR rcp85 r1i1p1 CLMcom-CCLM4-8-17	Autumn	13.12	12.78	-0.35
tas EUR-11 MPI-M-MPI-ESM-LR rcp85 r1i1p1 MPI-CSC-REMO2009	Winter	3.12	2.47	-0.65
tas EUR-11 MPI-M-MPI-ESM-LR rcp85 r1i1p1 MPI-CSC-REMO2009	Spring	11.23	11.29	0.06
tas EUR-11 MPI-M-MPI-ESM-LR rcp85 r1i1p1 MPI-CSC-REMO2009	Summer	21.77	22.94	1.16

tas EUR-11 MPI-M-MPI-ESM-LR rcp85 r1i1p1 MPI-CSC-REMO2009	Autumn	13.12	13.45	0.33
tas EUR-11 MPI-M-MPI-ESM-LR rcp85 r1i1p1 SMHI-RCA4	Winter	3.12	2.25	-0.87
tas EUR-11 MPI-M-MPI-ESM-LR rcp85 r1i1p1 SMHI-RCA4	Spring	11.23	11.22	-0.01
tas EUR-11 MPI-M-MPI-ESM-LR rcp85 r1i1p1 SMHI-RCA4	Summer	21.77	22.86	1.09
tas EUR-11 MPI-M-MPI-ESM-LR rcp85 r1i1p1 SMHI-RCA4	Autumn	13.12	13.37	0.25
Name (2039-2058)	**Season**	**Reference Values**	**Projected Values**	**Change**
tas EUR-11 IPSL-IPSL-CM5A-LR rcp26 r1i1p1 GERICS-REMO2015	Winter	3.12	5.62	2.50
tas EUR-11 IPSL-IPSL-CM5A-LR rcp26 r1i1p1 GERICS-REMO2015	Spring	11.23	12.71	1.48
tas EUR-11 IPSL-IPSL-CM5A-LR rcp26 r1i1p1 GERICS-REMO2015	Summer	21.77	24.12	2.35
tas EUR-11 IPSL-IPSL-CM5A-LR rcp26 r1i1p1 GERICS-REMO2015	Autumn	13.12	15.24	2.11
tas EUR-11 MPI-M-MPI-ESM-LR rcp26 r1i1p1 MPI-CSC-REMO2009	Winter	3.12	3.47	0.35
tas EUR-11 MPI-M-MPI-ESM-LR rcp26 r1i1p1 MPI-CSC-REMO2009	Spring	11.23	11.49	0.27
tas EUR-11 MPI-M-MPI-ESM-LR rcp26 r1i1p1 MPI-CSC-REMO2009	Summer	21.77	22.69	0.92
tas EUR-11 MPI-M-MPI-ESM-LR rcp26 r1i1p1 MPI-CSC-REMO2009	Autumn	13.12	13.76	0.64
tas EUR-11 IPSL-IPSL-CM5A-MR rcp45 r1i1p1 IPSL-INERIS-WRF331F	Winter	3.12	5.38	2.26
tas EUR-11 IPSL-IPSL-CM5A-MR rcp45 r1i1p1 IPSL-INERIS-WRF331F	Spring	11.23	13.38	2.15
tas EUR-11 IPSL-IPSL-CM5A-MR rcp45 r1i1p1 IPSL-INERIS-WRF331F	Summer	21.77	23.76	1.98
tas EUR-11 IPSL-IPSL-CM5A-MR rcp45 r1i1p1 IPSL-INERIS-WRF331F	Autumn	13.12	14.52	1.40
tas EUR-11 MOHC-HadGEM2-ES rcp45 r1i1p1 SMHI-RCA4	Winter	3.12	4.86	1.74
tas EUR-11 MOHC-HadGEM2-ES rcp45 r1i1p1 SMHI-RCA4	Spring	11.23	15.75	4.52
tas EUR-11 MOHC-HadGEM2-ES rcp45 r1i1p1 SMHI-RCA4	Summer	21.77	23.49	1.72
tas EUR-11 MOHC-HadGEM2-ES rcp45 r1i1p1 SMHI-RCA4	Autumn	13.12	11.69	-1.43
tas EUR-11 MPI-M-MPI-ESM-LR rcp45 r1i1p1 MPI-CSC-REMO2009	Winter	3.12	3.76	0.64
tas EUR-11 MPI-M-MPI-ESM-LR rcp45 r1i1p1 MPI-CSC-REMO2009	Spring	11.23	11.70	0.48
tas EUR-11 MPI-M-MPI-ESM-LR rcp45 r1i1p1 MPI-CSC-REMO2009	Summer	21.77	23.55	1.77
tas EUR-11 MPI-M-MPI-ESM-LR rcp45 r1i1p1 MPI-CSC-REMO2009	Autumn	13.12	13.97	0.84
tas EUR-11 MPI-M-MPI-ESM-LR rcp45 r1i1p1 SMHI-RCA4	Winter	3.12	3.94	0.82
tas EUR-11 MPI-M-MPI-ESM-LR rcp45 r1i1p1 SMHI-RCA4	Spring	11.23	12.26	1.03
tas EUR-11 MPI-M-MPI-ESM-LR rcp45 r1i1p1 SMHI-RCA4	Summer	21.77	23.94	2.17
tas EUR-11 MPI-M-MPI-ESM-LR rcp45 r1i1p1 SMHI-RCA4	Autumn	13.12	14.16	1.04
tas EUR-11 CNRM-CERFACS-CNRM-CM5 rcp85 r1i1p1 CLMcom-	Winter	3.12	3.99	0.87

CCLM4-8-17				
tas EUR-11 CNRM-CERFACS-CNRM-CM5 rcp85 r1i1p1 CLMcom-CCLM4-8-17	Spring	11.23	11.52	0.29
tas EUR-11 CNRM-CERFACS-CNRM-CM5 rcp85 r1i1p1 CLMcom-CCLM4-8-17	Summer	21.77	22.36	0.59
tas EUR-11 CNRM-CERFACS-CNRM-CM5 rcp85 r1i1p1 CLMcom-CCLM4-8-17	Autumn	13.12	13.39	0.27
tas EUR-11 MPI-M-MPI-ESM-LR rcp85 r1i1p1 CLMcom-CCLM4-8-17	Winter	3.12	3.07	-0.05
tas EUR-11 MPI-M-MPI-ESM-LR rcp85 r1i1p1 CLMcom-CCLM4-8-17	Spring	11.23	11.90	0.67
tas EUR-11 MPI-M-MPI-ESM-LR rcp85 r1i1p1 CLMcom-CCLM4-8-17	Summer	21.77	23.43	1.66
tas EUR-11 MPI-M-MPI-ESM-LR rcp85 r1i1p1 CLMcom-CCLM4-8-17	Autumn	13.12	14.27	1.14
tas EUR-11 MPI-M-MPI-ESM-LR rcp85 r1i1p1 MPI-CSC-REMO2009	Winter	3.12	3.85	0.73
tas EUR-11 MPI-M-MPI-ESM-LR rcp85 r1i1p1 MPI-CSC-REMO2009	Spring	11.23	12.31	1.08
tas EUR-11 MPI-M-MPI-ESM-LR rcp85 r1i1p1 MPI-CSC-REMO2009	Summer	21.77	24.21	2.44
tas EUR-11 MPI-M-MPI-ESM-LR rcp85 r1i1p1 MPI-CSC-REMO2009	Autumn	13.12	15.07	1.95
tas EUR-11 MPI-M-MPI-ESM-LR rcp85 r1i1p1 SMHI-RCA4	Winter	3.12	3.45	0.33
tas EUR-11 MPI-M-MPI-ESM-LR rcp85 r1i1p1 SMHI-RCA4	Spring	11.23	12.89	1.66
tas EUR-11 MPI-M-MPI-ESM-LR rcp85 r1i1p1 SMHI-RCA4	Summer	21.77	24.15	2.38
tas EUR-11 MPI-M-MPI-ESM-LR rcp85 r1i1p1 SMHI-RCA4	Autumn	13.12	14.85	1.73
Name (2059-2078)	**Season**	**Reference Values**	**Projected Values**	**Change**
tas EUR-11 IPSL-IPSL-CM5A-LR rcp26 r1i1p1 GERICS-REMO2015	Winter	3.12	5.97	2.85
tas EUR-11 IPSL-IPSL-CM5A-LR rcp26 r1i1p1 GERICS-REMO2015	Spring	11.23	12.44	1.22
tas EUR-11 IPSL-IPSL-CM5A-LR rcp26 r1i1p1 GERICS-REMO2015	Summer	21.77	23.89	2.12
tas EUR-11 IPSL-IPSL-CM5A-LR rcp26 r1i1p1 GERICS-REMO2015	Autumn	13.12	15.75	2.63
tas EUR-11 MPI-M-MPI-ESM-LR rcp26 r1i1p1 MPI-CSC-REMO2009	Winter	3.12	3.68	0.56
tas EUR-11 MPI-M-MPI-ESM-LR rcp26 r1i1p1 MPI-CSC-REMO2009	Spring	11.23	11.39	0.16
tas EUR-11 MPI-M-MPI-ESM-LR rcp26 r1i1p1 MPI-CSC-REMO2009	Summer	21.77	22.38	0.60
tas EUR-11 MPI-M-MPI-ESM-LR rcp26 r1i1p1 MPI-CSC-REMO2009	Autumn	13.12	13.64	0.52
tas EUR-11 IPSL-IPSL-CM5A-MR rcp45 r1i1p1 IPSL-INERIS-WRF331F	Winter	3.12	5.87	2.75
tas EUR-11 IPSL-IPSL-CM5A-MR rcp45 r1i1p1 IPSL-INERIS-WRF331F	Spring	11.23	13.55	2.33
tas EUR-11 IPSL-IPSL-CM5A-MR rcp45 r1i1p1 IPSL-INERIS-WRF331F	Summer	21.77	23.95	2.18
tas EUR-11 IPSL-IPSL-CM5A-MR rcp45 r1i1p1 IPSL-INERIS-WRF331F	Autumn	13.12	15.09	1.96
tas EUR-11 MOHC-HadGEM2-ES rcp45 r1i1p1 SMHI-RCA4	Winter	3.12	5.80	2.68

tas EUR-11 MOHC-HadGEM2-ES rcp45 r1i1p1 SMHI-RCA4	Spring	11.23	16.37	5.14
tas EUR-11 MOHC-HadGEM2-ES rcp45 r1i1p1 SMHI-RCA4	Summer	21.77	24.12	2.35
tas EUR-11 MOHC-HadGEM2-ES rcp45 r1i1p1 SMHI-RCA4	Autumn	13.12	12.58	-0.55
tas EUR-11 MPI-M-MPI-ESM-LR rcp45 r1i1p1 MPI-CSC-REMO2009	Winter	3.12	3.63	0.51
tas EUR-11 MPI-M-MPI-ESM-LR rcp45 r1i1p1 MPI-CSC-REMO2009	Spring	11.23	12.02	0.79
tas EUR-11 MPI-M-MPI-ESM-LR rcp45 r1i1p1 MPI-CSC-REMO2009	Summer	21.77	23.91	2.13
tas EUR-11 MPI-M-MPI-ESM-LR rcp45 r1i1p1 MPI-CSC-REMO2009	Autumn	13.12	14.20	1.07
tas EUR-11 MPI-M-MPI-ESM-LR rcp45 r1i1p1 SMHI-RCA4	Winter	3.12	3.91	0.79
tas EUR-11 MPI-M-MPI-ESM-LR rcp45 r1i1p1 SMHI-RCA4	Spring	11.23	12.48	1.25
tas EUR-11 MPI-M-MPI-ESM-LR rcp45 r1i1p1 SMHI-RCA4	Summer	21.77	23.87	2.10
tas EUR-11 MPI-M-MPI-ESM-LR rcp45 r1i1p1 SMHI-RCA4	Autumn	13.12	14.06	0.94
tas EUR-11 CNRM-CERFACS-CNRM-CM5 rcp85 r1i1p1 CLMcom-CCLM4-8-17	Winter	3.12	4.92	1.80
tas EUR-11 CNRM-CERFACS-CNRM-CM5 rcp85 r1i1p1 CLMcom-CCLM4-8-17	Spring	11.23	12.58	1.35
tas EUR-11 CNRM-CERFACS-CNRM-CM5 rcp85 r1i1p1 CLMcom-CCLM4-8-17	Summer	21.77	23.65	1.88
tas EUR-11 CNRM-CERFACS-CNRM-CM5 rcp85 r1i1p1 CLMcom-CCLM4-8-17	Autumn	13.12	14.47	1.34
tas EUR-11 MPI-M-MPI-ESM-LR rcp85 r1i1p1 CLMcom-CCLM4-8-17	Winter	3.12	4.78	1.66
tas EUR-11 MPI-M-MPI-ESM-LR rcp85 r1i1p1 CLMcom-CCLM4-8-17	Spring	11.23	12.39	1.16
tas EUR-11 MPI-M-MPI-ESM-LR rcp85 r1i1p1 CLMcom-CCLM4-8-17	Summer	21.77	24.41	2.63
tas EUR-11 MPI-M-MPI-ESM-LR rcp85 r1i1p1 CLMcom-CCLM4-8-17	Autumn	13.12	15.28	2.16
tas EUR-11 MPI-M-MPI-ESM-LR rcp85 r1i1p1 MPI-CSC-REMO2009	Winter	3.12	5.60	2.48
tas EUR-11 MPI-M-MPI-ESM-LR rcp85 r1i1p1 MPI-CSC-REMO2009	Spring	11.23	13.08	1.86
tas EUR-11 MPI-M-MPI-ESM-LR rcp85 r1i1p1 MPI-CSC-REMO2009	Summer	21.77	25.13	3.36
tas EUR-11 MPI-M-MPI-ESM-LR rcp85 r1i1p1 MPI-CSC-REMO2009	Autumn	13.12	15.74	2.62
tas EUR-11 MPI-M-MPI-ESM-LR rcp85 r1i1p1 SMHI-RCA4	Winter	3.12	5.29	2.17
tas EUR-11 MPI-M-MPI-ESM-LR rcp85 r1i1p1 SMHI-RCA4	Spring	11.23	13.76	2.53
tas EUR-11 MPI-M-MPI-ESM-LR rcp85 r1i1p1 SMHI-RCA4	Summer	21.77	25.44	3.67
tas EUR-11 MPI-M-MPI-ESM-LR rcp85 r1i1p1 SMHI-RCA4	Autumn	13.12	15.63	2.50

References

1. Abdo, K. S., Fiseha, B. M., Rientjes, T. H. M., Gieske, A. S. M., & Haile, A. T., 2009; Assessment of climate change impacts on the hydrology of Gilgel Abay catchment in Lake Tana basin, Ethiopia, 3669(September), pp. 3661–3669

2. Al-jawad, J. Y., Alsa, H. M., Bertram, D., & Kalin, R. M., 2019; A comprehensive optimum integrated water resources management approach for multidisciplinary water resources management problems, 239(February), pp. 211–224

3. Allen, R. G., Pereira, L. S., Raes, D., Smith, M., & Ab, W., 1998; Crop evapotranspiration - Guidelines for computing crop water requirements - FAO Irrigation and drainage paper 56, pp. 1–15

4. Ampas, V., Baltas, E. & Papamichail, D., 2007; Comparison of different methods for the estimation of the reference crop evapotranspiration in the Florina region. WSEAS Journal, 2(12), pp. 1449-1454.

5. Anderson M. & Woessner W., 1991; Applied groundwater modelling. Simulation of flow and advective transport: London, Academic Press

6. Antonopoulos, V. Z., & Antonopoulos, A. V., 2018; Evaluation of different methods to estimate evapotranspiration in a Mediterranean area monthly reference, pp. 61–77

7. Arampatzis, G., Panagopoulos, A., Pisinaras, V., Tziritis, E. & Wendland, F., 2018; Identifying potential effects of climate change on the development of water resources in Pinios River Basin, Central Greece. Applied Water Science, 8(2), pp. 1–17

8. Aubouin, J., 1959; Contribution a l'étude géologique de la Grèce septentrionale: Les confines de l' Epire et de la Thessalie. Ann. Géol. Pays Hell. vol. X., Athènes, pp. 1-484

9. Bergström, S., Carlsson, B., Gardelin, M., Lindström, G., Pettersson, A., & Rummukainen, M, 2001; Climate change impacts on runoff in Sweden – assessments by global climate models, dynamical downscaling and hydrological modelling. Climate Research 16, pp. 101–112

10. Biel, R. E., 1944; Climatology of the Mediterranean area: Chicago, The University of Chicago Press.

11. Blaney, H.F. & Criddle, W.D., 1950; Determining Water Requirements in Irrigated Areas from Climatological and Irrigation Data, USDA (SCS) TP-96

12. Block, P. J., Filhou, F. A. S., Sun, L. & Kwon, H.-H., 2009; A streamflow forecasting framework using multiple climate and hydrological models. Journal of the American Water Resources Association (JAWRA) 45(4), pp. 823–843

13. Blyth, E. M., Harding, R. J., & Essery, R., 1999; A coupled dual source GCM SVAT. Hydrology and Earth System Sciences 3(1), pp. 71–84

14. Booij, M. J., 2005; Impact of climate change on river flooding assessed with different spatial model resolutions. Journal of Hydrology 303, pp. 176–198

15. Bosshard, T., Carambia, M., Goergen, K., Kotlarski, S., Krahe, P., Zappa, M., Schär, C., 2013; Quantifying uncertainty sources in an ensemble of hydrological climate-impact projections. Water Resour Res 49(3), pp. 1523–1536

16. Brunn, J., 1956; Contribution a l'étude géologique du Pinde septentrional et d'une, partie de la Macédoine occidentale. Ann. Geol. des Pays Hell. 7.

17. Brunn, J., 1959; Zone du Vardar et Pélagonienne en Grèce, C. R. Somm. Soc. Geol. France, No 6, pp. 138-139.

18. Brunn, J., 1961; Les sutures ophiolitiques. Contribution à I' étude des relations entre phenomènes magmatiques et orogéniques. Rev. Gé-ogr. Phys. Geol. dyn. IV, fasc. 2, p. 86-96, et fasc. 3, pp. 181-202.

19. Burlando, P., & Rosso, R., 2002; Effects of transient climate change on basin hydrology. 1. Precipitation scenarios for the Arno River, central Italy, 1175(October 2001), pp. 1151–1175

20. Chahine, M. T., 1992. The hydrologic cycle and its influence on climate. Nature, 359, pp. 373-380

21. Chirokov, A., 2016; Scattered Data Interpolation and Approximation using Radial Base Functions (https://www.mathworks.com/matlabcentral/fileexchange/10056-scattered-data-interpolation-and-approximation-using-radial-base-functions?s_tid=prof_contriblnk), MATLAB Central File Exchange. Retrieved June 14, 2018.

22. Christensen, J.H, & Christensen, O.B 2010; A summary of the PRUDENCE model projections of changes in European climate by the end of this century. Clim Change 81, pp. 7–30

23. Cohen, S.J., 1990; Bringing the global warming issue closer to home: the challenge of regional impact studies. Bulletin of the American Meteorological Society, 71, pp. 520-526

24. Council, E.P., 2000; Directive 2000/60/EC of the European Parliament and of the Council of 23 October 2000 establishing a framework for Community action in the field of water policy. Official Journal of the European Parliament, pp. 1–72

25. DEH, 1974; Pournari Hydroelectric Project - Hydrology Report, Public Power Corporation, Athens.

26. Deidda, R., Marrocu, M., Caroletti, G, Pusceddu, G., Langousis, A., Lucarini, V., Puliga, A., Speranza, A., 2013; Regional climate models' performance in representing precipitation and temperature over selected Mediterranean areas. Hydrol Earth Syst Sci 17(12), pp. 5041–5059

27. Déqué, M., Rowell, D. P., Lüthi, D., & Giorgi, F., 2007; An intercomparison of regional climate simulations for Europe: assessing uncertainties in model projections, pp. 53–70

28. D'Errico, J., 2012; fminsearchbnd, fminsearchcon (https://www.mathworks.com/matlabcentral/fileexchange/8277-fminsearchbnd-fminsearchcon?s_tid=FX_rc3_behav), MATLAB Central File Exchange. Retrieved June 14, 2018.

29. Doherty, J., 2015; Calibration and Uncertainty Analysis for Complex Environmental Models. Watermark Numerical Computing, Brisbane, Australia. ISBN: 978-0-9943786-0-6.

30. Doorenbos J. & Pruitt W., 1977; Guidelines for predicting crop water requirements: Rome, Food and Agriculture Organization, Irrigation and drainage paper.

31. Dubrovsky, M., Hayes, M. J., Duce, P., Trnka, M., Svoboda, M., & Zara, P., 2013; Multi-GCM projections of future drought and climate variability indicators for the Mediterranean region. Regional Environmental Change, 14(December), pp. 1907–1919

32. Efthimiou, N., Alexandris, S., Karavitis, C., & Mamassis, N., 2013; Comparative analysis of reference evapotranspiration estimation between various methods and the FAO56 Penman - Monteith procedure, pp. 19–34.

33. ELSTAT, 1991,2001,2011; Population data for Kastoria basin

34. Emberger, L., 1930; Climate on a formula applicable in botanical geography. Comptes Rendus de l'Académie des Sciences, 1991, 389-390.

35. Engwirda, D., 2018; INPOLY: A fast points-in-polygon test (https://www.github.com/dengwirda/inpoly), GitHub. Retrieved July 01, 2018.

36. European Environment Agency, 2009; Water resources across Europe- confronting water scarcity and drought. EEA Report No 2/2009. http://www.eea.europa.eu/publicatio ns/water -resources-across-europe. Accessed 2 Aug 2018

37. FEFLOW 7.2 (Finite Element Subsurface Flow & Transport Simulation System) User's Manual, 2009; WASY Institute for Water Resource Planning and Systems Research Ltd., Berlin.

38. Fetter C., 1989; Applied hydrogeology, USA, Merrill Publishing Company.

39. Fiseha, B.M., Setegn, S.G., Melesse, A.M., Volpi, E., Fiori, A., 2014; Impact of climate change on the hydrology of upper Tiber River Basin using bias corrected regional climate model. Water Resour Manag 28(5), pp. 1327–1343

40. Foughali, A., Tramblay, Y., Bargaoui, Z., Carreau, J., & Ruelland, D., 2015; Hydrological Modeling in Northern Tunisia with Regional Climate Model Outputs: Performance Evaluation and Bias-Correction in Present Climate Conditions, pp. 459–473

41. Fowler, H.J., Blenkinsop, S. & Tebaldi, C., 2007; Review Linking climate change modelling to impacts studies: recent advances in downscaling techniques for hydrological modelling. International journal of climatology, 27: pp. 1547-1578

42. Franke L.O., Reily T.E. & Bennett G.D., 1987; Definition of boundary and initial conditions in the analysis of saturated ground-water flow systems - An introduction, Techniques of water-resources investigations of the United States Geological Survey: Washington, US Government Printing Office Book 3.

43. Freeze AR. & Cherry J.A., 1979; Groundwater: Englewood Cliffs, NJ, Prentice Hall, Inc.

44. García-Ruiz, J.M., López-Moreno, J.I., Vicente-Serrano, S.M., Lasanta– Martínez, S.T. & Begueía, S., 2011; Mediterranean water resources in a global change scenario. Earth Sci Rev 105(3), pp. 121–139

45. Gates, W.L., 1985; The use of general circulation models in the analysis of the ecosystem impacts of climatic change. Climate Change, 7, pp. 267-284

46. Georgiou, PJ, Papamichail, D.M. & Papazifiriou, Z., 2000; Comparative Assessment of Penman and Penman-Monteith Methods with Evidence of Evapotranspiration Reporting in Greece. Proceedings of the 5th Pan-Hellenic Scientific Conference of Meteorology - Climatology and Atmospheric Physics, pp. 395-402. (in Greek)

47. Geraghty & Miller, Inc., 1993; Computer Aided Design Software for groundwater modeling: Virginia.

48. Gianneli E., 2009; Hydrogeology investigation of basins of Greece: example from the basin of Agioi Anargiroi, Kastoria, Aristotle University of Thessaloniki. (in Greek)

49. Giorgi, F. & Lionello, P., 2008; Climate change projections for the Mediterranean region. Global Planet Change 63(2), pp. 90–104

50. Giorgi, F., 2006; Climate change hot-spots, Geophysical Research Letters, 33, L08707.

51. Giorgi, F., Marinucci, M. R., Bates, G. T. & De Canio, G., 1993; Development of a second-generation regional climate model (RegCM2), I. Boundary-layer and radiative transfer, Mon. Weather Rev., 121, pp. 2794–2813

52. Gobiet, A. & D. Jacob, 2011; The EURO-CORDEX-Initiative. WCRP Open Science Conference Denver, 24-28 Oct. 2011. Poster no. W108B

53. Graham, L.P., Andréasson, J., Carlsson, B., 2007; Assessing climate change impacts on hydrology from an ensemble of regional climate models, model scales and linking methods—a case study on the Lule River basin. Climate Change 81(S1), pp. 293–307

54. Greek Ministry of Agriculture, 1989; Determination of minimum and maximum crop water requirements for rational use of irrigation water, F16/6631: Athens, National Publishing Organization of Greece. (in Greek)

55. Hansen V., Israelsen O., & Stringham G., 1980; Irrigation principles and practices: New York, John Wiley and Sons.

56. Hargreaves, G.H., Samani, Z.A., 1982; Estimating potential evapotranspiration. J. Irrig. Drain. Eng. ASCE, 108(3), pp. 225–230

57. Hargreaves, G.H., Samani, Z.A., 1985; Reference crop evapotranspiration from temperature. Trans. ASAE, 1(2), pp. 96-99

58. Haugen, J. & Haakensatd, H., 2005; Validation of HI-AR version 2 with 50km and 25km resolution, Tech. Rep. General Technical report 9, RegClim

59. Haylock, M. R., Cawley, G. C., Harpham, C., Wilby, R. L., & Goodess, C. M., 2006; Downscaling heavy precipitation over the United Kingdom: a comparison of dynamical and statistical methods and their future projections. International Journal of Meteorology, 1415(March), pp. 1397–1415

60. Hellenic Center for Marine Research, 2008; Network Development and Monitoring of the Inland, Transitional and Coastal Waters of the Country - Assessment / Classification of their Ecological Situation: Assessment of Ecological Quality of Water Bodies, defined by the Central Water Service in the 14 Water districts of Greece for the types of water bodies defined in Directive 2000/60/EU (in Greek)

61. Hellenic Ministry for the Environment, Energy and Climate Change- Special Secretariat for Water, 2014; Compilation of management plan for the river basins of Western Macedonia water district (GR09)-management plan. Special Secretariat for Water, Athens

62. Hellstrom, C., Chen, D., Achberger, C. & Raisanen, J., 2001; Comparison of climate change scenarios for Sweden based on statistical and dynamical downscaling of monthly precipitation. Climate Research 19, pp. 45–55

63. Hewitson, B. C., & Crane, R. G., 1996; Climate downscaling: techniques and application, Clim Res, 07(2), pp. 85–95

64. Hrissanthou, V., Mylopoulos, N., Tolikas, D., & Mylopoulos, Y., 2003; Simulation Modeling of Runoff, Groundwater Flow and Sediment Transport into Kastoria Lake, Greece. Water Resources Management, 17(March), pp. 223–242

65. Hydrological and Hydrogeological study of Kastoria lake. Proposals for artificial recharge. IGME, 2005, Kozani (in Greek)

66. IGME, 1990; Kastoria Sheet: Athens, Institute of Geology and Mineral exploration, Geological map of Greece, 1: 50,000.

67. IGME, 1990; Koritsa-Mesopotamia Sheet: Athens, Institute of Geology and Mineral exploration, Geological map of Greece, 1: 50,000.

68. IGME: Savoyat, E., Verdier, A., Monopolis D., 1971; Argos Orestiko Sheet: Athens, Institute of Geology and Mineral exploration, Geological map of Greece, 1: 50,000. (in Greek)

69. Ines, A. V. M. & Hansen, J. W., 2006; Bias correction of daily GCM rainfall for crop simulation studies. Agricultural and Forest Meteorology 138, pp. 44–53

70. Institute of Geology and Mining Research, Department of Water Resources and Environment, 2010; Registration and evaluation of the Hydrogeological characteristics of Groundwater and Aquifers Systems, Subproject 3: Monitoring of water balances of the upper part of Aliakmonas river, Vermio, Ptolemaida (EL 09)

71. IPCC, 1995a.; Climate Change 1995: The Science of Climate Change Contribution of Working Group I to the Second Assessment Report of the Intergovernmental Panel on Climate Change, Houghton JT, Meiro Filho LG, Callander BA, Harris N, Kattenberg A, Maskell K (eds). Cambridge University Press: pp. 572

72. IPCC, 1995b.; Climate Change 1995: Impacts, Adaptations and Mitigation of Climate Change: Scientific–Technical Analyses Contribution ofWorking Group II to the Second Assessment Report of the Intergovernmental Panel on Climate Change, Watson RT, Zinyowera MC, Moss RH (eds). Cambridge University Press: 878

73. IPCC, 1995c.; Climate Change 1995: Economic and Social Dimensions ofClimate Change Contribution ofWorking Group III to the Second Assessment Report of the Intergovernmental Panel on Climate Change, Bruce J, Lee H, Haites E (eds). Cambridge University Press: pp. 448

74. IPCC, 1997.; The regional impacts of climate change: an assessment of vulnerability, Watson RT, Zinyowera MC, Moss RH, Dokken DJ (eds). A special report of IPCC Working Group II

75. IPCC, 2007.; Climate Change 2007. Synthesis Report. Contribution of Working Groups I, II and III to the Fourth Assessment Report of the Intergovernmental Panel on Climate Change. IPCC, Geneva, Switzerland

76. Jacob, D., 2001; A note to the simulation of the annual and inter-annual variability of the water budget over the Baltic Sea drainage basin, Meteorology and Atmospheric Physics, 77(1- 4), pp. 61-73

77. Jacob, D., Bärring, L., Christensen, O.B., Christensen, J.H, de Castro, M., Déqué, M., Giorgi, F., Hagemann, S., Hirschi, M., Jones, R., Kjellström, E., Lenderink, G., Rockel, B., Sánchez, E., Schär, C., Seneviratne, S.I., Somot, S., van Ulden, A., van den Hurk, B., 2007; An inter-comparison of regional climate models for Europe: model performance in in present-day climate. Clim Change 81, pp. 31–52

78. Jacob, D., Elizalde, A., Haensler, A., Hagemann, S., Kumar, P., Podzun, R., Rechid, D., Remedio, A.R., Saeed, F., Sieck, K., Teichmann, C. & Wilhelm, C., 2012; Assessing the transferability of the regional climate model REMO to different coordinated regional climate downscaling experiment (CORDEX) regions. Atmosphere 3, pp. 181–199, doi: 10.3390/atmos3010181

79. Jha, M., Pan, Z., Takle, E. S. & Gu, R., 2004; The impacts of climate change on stream flow in the Upper Mississippi River Basin: a regional climate model perspective. Journal of Geophysical Research 109, pp. 1–12

80. Kalogeropoulos, K. & Chalkias, C., 2013; Modelling the impacts of cli- mate change on surface runoff in small Mediterranean catchments: empirical evidence from Greece. Water Environ J 27(4), pp. 505–513

81. Kilias, A. & Mountrakis, D., 1989; The Pelagonian Nappe, tectonics, metamorphism and magmatism. Bulletin of Geological Society of Greece, 23(1), pp. 29-46.

82. Kilias, A., 1980; Geological and Tectonic investigation of East Varnounta Mount (NW Macedonia), Phd Dissertation, Thessaloniki, pp. 271. (in Greek).

83. Kim, J.W., Chang, J.T., Baker, N.L., Wilks, D.S. & Gates, W.L., 1984; The statistical problem of climate inversion: Determination of the relationship between local and large-scale climate. Monthly Weather Review, 112, pp. 2069–2077

84. Kleinn, J., Frei, C., Gurtz, J., Lu, D., Vidale, P. L., & Scha, C., 2005; Hydrologic simulations in the Rhine basin driven by a regional climate model, 110, pp. 1–18

85. Koster, R. D. & Suarez, M. J., 1994; The components of a SVAT scheme and their effects on a GCMs hydrological cycle. Advances in Water Resources 17(1–2), pp. 61–78

86. Koutroulis, A.G, Grillakis, M.G, Daliakopoulos, I.N, Tsanis, I.K, Jacob, D.,2016; Cross sectoral impacts on water availability at + 2 °C and + 3 °C for east Mediterranean island states: the case of Crete. J Hydrol 532, pp. 16–28

87. Kupiainen, M., Samuelsson, P., Jones, C., Jansson, C., Willén, U., Hansson, U., Ullerstig, A., Wang, S. & Döscher, R., 2011; Rossby Centre regional atmospheric model, RCA4. Rossby Centre Newsletter

88. Lagouvardos, K., Kotroni, V., Bezes, A., Koletsis, I., Kopania, T., Lykoudis, S., & Vougioukas, S., 2017; The automatic weather stations NOANN network of the National Observatory of Athens: operation and database. https://doi.org/10.1002/gdj3.44

89. Leander, R. & Buishand, T.A. 2007; Resampling of regional climate model output for the simulation of extreme river flows. Journal of Hydrology, 332: 487-496

90. Leander, R., Buishand, T. A., van den Hurk, B. J. J. M. & de Wit, M. J. M., 2008; Estimated changes in flood quantiles of the river Meuse from resampling of regional climate model output. Journal of Hydrology 351, pp. 331–343

91. Lee, D.-K., Cha, D.-H. & Kang, H.-S., 2004; Regional climate simulation of the 1998 summer flood over East Asia. Journal of the Meteorological Society of Japan 82, pp. 1735–1753

92. Lerner, D., Issar, A. & Simmers, I., (eds.), 1990; Groundwater recharge. A guide to understanding and estimating natural recharge, 8: Hannover, Verlag Heinz Heise

93. Ludwig, R., Roson, R., Zografos, C. & Kallis, G., 2011; Towards an interdisciplinary research agenda on climate change, water and security in Southern Europe and neighboring countries. Environ Sci Policy 14(7), pp. 794–803

94. Luo, X., Xu, Y., & Xu, J., 2010; Application of Radial Basis Function Network for Spatial Precipitation Interpolation. 18th International Conference on Geoinformatics: GIScience in Change, Geoinformatics 2010, Peking University, Beijing, China, June, 18-20, 2010

95. Maratos, G., 1972; Geology of Greece; Vol. A, Athens, pp. 183

96. Mavrommatis, G., 1980a; The bioclimate of Greece. Climate and natural vegetation relations, bioclimatic maps. I.D.E.A, Athens.

97. Milano, M., Ruelland, D., Fernandez, S., Dezetter, A., Fabre, J., Servat, E., Fritsch, J-M, Ardoin-Bardin, S. & Thivet, G., 2013; Current state of Mediterranean water resources and future trends under climatic and anthropogenic changes. Hydrol Sci J 58(3), pp. 498–518

98. Ministry of Agriculture and Food, 2013; Chemical quality control of water supply (surface and underground) at basin river scale of Macedonia – Thrace and Thessalia (in Greek)

99. Mountrakis D., 1983; Geoogical Structure of Norrthern Pelagonian Zone and the geo-tectonic evolution of Internal Hellinides, Treatise for Geography, Aristotle University of Thessaloniki, pp. 289. (in Greek)

100. Mountrakis D., 2010; Geology of Greece, Thessaloniki, University Studio Press. (in Greek)

101. Mountrakis, D., 1982b; Emplacement of the Kastoria ophiolite on the western edge of the Internal Hellenides (Greece). Ofioliti, 7, N. 2/3, pp. 397-406.

102. Mountrakis., D., 1979; Resultats préliminaires de I' étude stratigraphique de la région de Kastoria (NW Macédoine, Grèce). Sei. Ann. Fac. Phys. Mathem., Univ. Thessaloniki, 19, pp. 163-173.

103. Murphy, J, 2000; Predictions of climate change over Europe using statistical and dynamical downscaling techniques. International Journal of Climatology 20, pp. 489–501

104. Murphy, J., 1998; An evaluation of statistical and dynamical techniques for downscaling local climate. Journal of Climate 12, pp. 2256–2284

105. Navarra, A., & Tubiana, L., 2013; Regional assessment of climate change in the Mediterranean. Springer, Dordrecht

106. OPEKEPE, 2006-2018; Statistical Agricultural Data for Kastoria Basin

107. OPEKEPE, 2006-2018; Statistical Live stock Data for Kastoria Basin

108. Panagopoulos A., 1996; A methodology for groundwater resources management of a typical alluvial aquifer system in Greece, Ph.D. dissertation. The University of Birmingham, Birmingham.

109. Panagopoulos A., Pechlivanidou S., Vrouhakis Y., Karyotis Th., Arampatzis G., Hatzigiannakis E. & Panoras A., 2008; Determining reference conditions for groundwater bodies using simple historical data; the case of eastern Thessaly, Greece. E-Proc. 36th Int. Congress of the International Association of Hydrogeologists, Toyama, pp. 1-7.

110. Panagopoulos, A., Arampatzis, G., Tziritis, E., Pisinaras, V. & Herrmann, F., 2016; Assessment of climate change impact in the hydrological regime of River Pinios Basin, central Greece, Desalination and Water Treatment, 57(March 2014), pp. 2256–2267

111. Pantelis D., Kouskouras A., Chastas G., Chrysoulas Ch., 2015; Management Plan of the Conservation Area of Lake Kastoria, Region of Western Macedonia, Directorate-General for Development Planning, Environment and Infrastructure, Directorate of Technical Works of Kastoria, Greek Republic, pp. 293

112. Papadopoulou-Mourkidou E., Spyridis A. - Koutalou V.E. - YETOS, Perleros V., Lionis M., Levoyannis M., 2013; Chemical control of irrigation waters (surface and underground) on a scale basis river basin of Macedonia-Thrace and Thessaly. (in Greek)

113. Pavlopoulos K., Skendos A. & Kotabassis Ch., 2010; Geomorphological mapping and study of the wider area of Dispilio-Limni Kastoria. (in Greek)

114. Payne, J. T., Wood, A. W., Hamlet, A. F., Palmer, R. N. & Lettenmaier, D. P., 2004; Mitigating the effects of climate change on the water resources of the Columbia river basin. Climatic Change 62, pp. 233–256

115. Piao, S., Ciais, P., Huang, Y., Shen, Z., Peng, S., Li, J., Zhou, L., Liu, H., Ma, Y., Ding, Y., Friedlingstein, P., Liu, C., Tan, K., Yu, Y., Zhang, T. & Fang, J., 2010; Resources and agriculture in China, Nature, *467*(7311), pp. 43–51

116. Pisinaras, V., 2016; Assessment of Future Climate Change Impacts in A Mediterranean Aquifer. Global Nest Journal, 18(1), pp. 119–130

117. Robinson, P.J. & Finkelstein, P.L., 1989; Strategies for Development of Climate Scenarios. Final Report to the U.S. Environmental Protection Agency. Atmosphere Research and Exposure Assessment Laboratory, Office of Research and Development, USEPA, Research Triangle Park, NC, pp. 73

118. Rockel, B., Will, A. & Hense, A. (eds.), 2008; Special issue Regional climate modelling with COSMO-CLM (CCLM). Meteorologische Zeitschrift 17 (4).

119. Rushton K.R. & Wedderburn L.A., 1973; Starting conditions for aquifer simulations: Ground Water, v. 11, no. 1, pp.37-42.

120. Ruti, P., Somot, S., Giorgi, F., Dubois, C. et al., 2016; MED-CORDEX initiative for Mediterranean Climate studies, Bulletin of the American Meteorological Society

121. Sakkas, C., 1985; Engineering Hydrology. Issue 1: Hydrology Surface Water, Xanthi

122. Schmidli, J., Frei, C. & Vidale, P. L., 2006; Downscaling from GCM precipitation: a benchmark for dynamical and statistical downscaling methods. International Journal of Climatology 26, pp. 679–689

123. Schröter, D., Cramer, W., Leemans, R., Prentice, I. C. et al., 2005; Ecosystem service supply and vulnerability to global change in Europe. Science 310(5752), pp. 1333–1337

124. Schwanghart, W., 2010; Ordinary Kriging (https://www.mathworks.com/matlabcentral/fileexchange/29025-ordinary-kriging), MATLAB Central File Exchange. Retrieved June 14, 2018.

125. Schwanghart, W., 2010; variogramfit (https://www.mathworks.com/matlabcentral/fileexchange/25948-variogramfit?s_tid=FX_rc1_behav), MATLAB Central File Exchange. Retrieved June 14, 2018.

126. Shaw E.M., 1994; Hydrology in practice. Third edition: London, Chapman and Hall.

127. Skamarock, W.C., Klemp, J.B., Dudhia, J., Gill, D.O., Duda, D.M.B.M.G., Huang, X.Y., Wang, W. & Powers, J.G., 2008; A description of the advanced research WRF version 3. NCAR Technical note 475

128. Smith, J.B. & Tirpak, D.A. (eds.) 1989; The Potential Effects of Global Climate Change on the United States. Report to Congress, United States Environmental Protection Agency, EPA-230-05-89- 050, Washington, DC, pp. 409

129. Soulios G., 1985; Contribution to the hydrogeological study of the karst aquifer systems of the Greek Domain, Thessaloniki, Aristotle University of Thessaloniki. (in Greek)

130. Stamos, A., Mattheopoulos A., 2002; Hydrogeological recognition of Kastoria basin - Programming Agreement KEDKE-YPEDA-IGME, IGME. (in Greek)

131. Taylor, K.E., 2001; Summarizing multiple aspects of model performance in a single diagram. Journal of Geophysical Research: Atmospheres 106(D7), pp. 7183–7192

132. Teutschbein, C. & Seibert J., 2013; Is bias correction of Regional Climate Model (RCM) simulations possible for non-stationary conditions? Hydrol Earth Syst Sci 17, pp. 5061–5077

133. Teutschbein, C., & Seibert, J., 2010; Regional Climate Models for Hydrological Impact Studies at the Catchment Scale: A Review of Recent Modeling Strategies, 7, pp. 834–860

134. Tolika, K., Anagnostopoulou, C., Maheras, P., & Vafiadis, M., 2008; Simulation of future changes in extreme rainfall and temperature conditions over the Greek area: a comparison of two statistical downscaling approaches. Global Planet Change 63, pp. 132–151

135. Tolika, K., Anagnostopoulou, C., Velikou, K., Vagenas, C., 2016; A comparison of the updated very high-resolution model RegCM3_10km with the previous version RegCM3_25km over the complex terrain of Greece: present and future projections. Theoretical and Applied Climatology, 126 (3-4), pp. 715-726

136. Tolika, K., Zanis, P. & Anagnostopoulou, C., 2012; Regional climate change scenarios for Greece: Future temperature and Precipitation projections from Ensembles of RCMs. Global Nest Journal, 14(4), pp. 407-421

137. Tolikas, D., Mylopoulos, G., 2000; Determination of discharges, sediments and water quality of the torrents of the catchment area of Kastoria lake. Trend investigations and application of alternative load reduction scenarios. Aristotle University of Thessaloniki, Department of Civil Engineering, Department of Hydraulics & Environmental Engineering. Thessaloniki. (in Greek)

138. Tsakiri P. E., 2009; Bryophyte flora of Greece: phytogeographical and ecological study of bryophytes at the aquatic system of the Upper Aliakmonas river (Western Macedonia), Department of Biology, Aristotle University of Thessaloniki.

139. Tsakiris G., 2008; Protection and Management of Water Resources in Greece. (in Greek)

140. Turco M., Quintana-Seguí P., Llasat M.C., Herrera S. & Gutiérrez J.M., 2011; Testing MOS precipitation downscaling for ENSEMBLES regional climate models over Spain, Journal of Geophysical Research, 116, D18109

141. Vafeiadis P., 1983; Hydrogeological investigation of Kastoria basin, Aristotle University of Thessaloniki.

142. Van der Linden, P. & Mitchell, J. F. B., 2009; ENSEMBLES: Climate Change and its Impacts: Summary of research and results from the ENSEMBLES project, Met Office Hadley Centre, FitzRoy Road, Exeter EX1 3PB, UK, available at: http://ensembles-eu.metoffice.com/docs/Ensembles_final_report_Nov09.pdf

143. Van Meijgaard E., van Ulft L., van de Berg W., Bosveld B., van der Hurk B., Lenderik G., & Siebesma A., 2008; The knmi regional atmospheric climate model RA-EC version 2.1., Tech. Rep. 302, KNMI, http, //www.knmi.nl/knmilibrary/knmipubTR/TR302.pdf

144. Ven Te Chow, 1964; Handbook of Applied Hydrology: USA, Mc Graw Hill.

145. Wang H.F., Anderson M.P., 1982; Introduction to groundwater modeling, New York, W.H. Freeman and Company.

146. Wilby, R. L. & Wigley, T. M, 1997; Downscaling general circulation model output: a review of methods and limitations. Progress in Physical Geography 21, pp. 530–548

147. Wilby, R. L., Charles, S. P., Zorita, E., Timbal, B., Whetton, P. & Mearns, L. O., 2004; Guidelines for Use of Climate Scenarios Developed from Statistical Downscaling Methods, Supporting material to the Intergovernmental Panel on Climate Change 27

148. Wilby, R.L., Charles, S.P., Zorita, E., Timbal, B., Whetton, P., Mearns, L.O., 2004; Guidelines for use of climate scenarios developed from statistical downscaling methods. Supporting material of the Intergovernamental Panel on Climate Change

149. Wilby, R.L., Hay, L.E., Gutowski, W.J., Arritt, R.W., Tackle, E.S., Leavesley, G.H. and Clark, M. 2000. Hydrological responses to dynamically and statistically downscaled General Circulation Model output. Geophysical Research Letters, 27, pp. 1199–1202

150. Wilcke, R.A.I., Mendlik, T. & Gobiet, A., 2013; Multi-variable error correction of regional climate models, Climatic Change, 120:871, pp. 871–887

151. Wright E., Benfield A., Edmunds W., Kitching R., 1982; Hydrogeology of the Kufra and Sirte basins, eastern Libya: Quaiierly Journal of Engineering Geology, v. 15, pp. 83-103.

152. Xu, C.-Y. & Singh, V.P., 2002; Cross Comparison of Empirical Equations for Calculating Potential Evapotranspiration with Data from Switzerland. Water Resources Management, 16, pp. 197–219

153. Xu, C.Y., Widen, E., & Halldin S., 2005; Modeling hydrological consequences of climate change - Progress and challenges. Advances in Atmospheric Sciences, 22(6), pp. 789-797

154. Yeh W.G., 1986; Review of parameter identification procedures in groundwater hydrology: The inverse problem: Water Resources Research, v. 22, no. 2, pp. 95-108.

155. Yeh, T. J. I. M., 1992; Stochastic Modelling of Groundwater Flow And Solute Transport In Aquifers, *6* (September 1989), pp. 369–395

156. Zanis, P., Katragkou, E., Ntogras, C., Marougianni, G., Tsikerdekis, A., Feidas, H., Anadranistakis, E. & Melas, D., 2015; A transient high-resolution regional climate simulation for Greece for the period 1960-2100: Evaluation and future projections, Climate Research, 64: pp. 123–140

157. Zhang, X., & Srinivasan, R., 2009; GIS-based Spatial Precipitation Estimation: A Comparison of Geostatistical Approaches. Journal of the American Water Resources Association, 45(4), pp. 894–906

Table of Figures (Figures)

Figure 1 - Elevation along Gkioli stream 15
Figure 2 - Slope map of Kastoria Basin 16
Figure 3 - Geological Map of Kastoria Basin (based on IGME sheets Kastoria, Argos Orestiko, Koristsa-Mesopotamia with modifications) 18
Figure 4 - Synthetic Stratigraphic Column of the main formations of Kastoria basin (adapted from IGME, 1981) 19
Figure 5 - Elevation map and positions of meteorological stations used in this thesis 23
Figure 6 – Mean, Max and Min Monthly Temperature for period 2000-2018 at Kastoria Basin 24
Figure 7 - Monthly Mean Temperature for period 2000-2018 at Kastoria Basin 24
Figure 8 - Mean Monthly Maximum Temperature for period 2010-2018 at Kastoria basin 26
Figure 9 - Mean Monthly Minimum Temperature for period 2010-2018 at Kastoria basin 26
Figure 10 - Mean Monthly Temperature for period 2010-2018 at Kastoria Basin 27
Figure 11 - Mean Monthly Evaporation for period 1999-2010 at Dispilio station 28
Figure 12 - Mean Monthly Rainfall for period 2000-2018 at Kastoria Basin 29
Figure 13 - Mean Annual Precipitation - Elevation Relationship 31
Figure 14 – Mean Monthly Rainfall for years 2000-2018 32
Figure 15 - Mean Annual Rainfall 2000-2018 32
Figure 16 - Annual Rainfall at Kastoria Basin for period 2000-2018 33
Figure 17 - Mean Monthly ET_0 for the period 2010-2018 estimated with the Hargreaves method 37
Figure 18 - Mean Annual ET_0 for period 2010-2018 estimated with the Hargreaves method 37
Figure 19 - Mean Annual ET_0 for Grow Period of 2010-2018 estimated with the Hargreaves method 38
Figure 20 - Stations used to perform bias-correction and the corresponding grid-points extracted from the RCMs 41
Figure 21 - Taylor diagram of Raw and bias-corrected (BC) EUR-11 RCM precipitation data for the control period 1986-2005 43
Figure 22 - Box-plots of total annual precipitation variation according to the results from the ten selected RCMs for the periods 2019-2038, 2039-2058 and 2059-2078 45
Figure 23 - Box-plots of autumn total precipitation variation according to results from the selected models for the periods 2019-2038, 2039-2058 and 2059-2078 47
Figure 24 - Box-plots of winter total precipitation variation according to results from the selected models for the periods 2019-2038, 2039-2058 and 2059-2078 48
Figure 25 - Box-plots of spring total precipitation variation according to results from the selected models for the periods 2019-2038, 2039-2058 and 2059-2078 49
Figure 26 - Box-plots of summer total precipitation variation according to results from the selected models for the periods 2019-2038, 2039-2058 and 2059-2078 50
Figure 27 - Cumulative frequency diagram of monthly precipitation for the control period (1986-2005) and the selected RCMs for the three sub-periods 51
Figure 28 - Taylor diagram of Raw and bias-corrected (BC) RCM temperature data of the selected EUR-11 RCMs for the control period 1986-2005 54
Figure 29 - Box-plots of average annual temperature variation according to results from the selected RCMs for the periods 2019-2038, 2039-2058 and 2059-2078 55
Figure 30 - Box-plots of autumn average temperature variation according to the results of the selected models for the periods 2019-2038, 2039-2058 and 2059-2078 56
Figure 31 - Box-plots of winter average temperature variation according to the results of the selected models for the periods 2019-2038, 2039-2058 and 2059-2078 57
Figure 32 - Box-plots of spring average temperature variation according to the results of the selected models for the periods 2019-2038, 2039-2058 and 2059-2078 58
Figure 33 - Box-plots of summer average temperature variation according to the results of the selected models for the periods 2019-2038, 2039-2058 and 2059-2078 59
Figure 34 - Cumulative frequency diagram of monthly temperature for the control period (1986-2005) and the selected RCMs for the two sub-periods 60
Figure 35 - Nine sub-basins of Kastoria basin (adapted from Tolikas & Mylopoulos, 2000) 64
Figure 36 - Hydrogeological map of Kastoria Basin 68
Figure 37 - Hydrogeological cross-section of Koritsa Heights (IGME, 2005) 70
Figure 38 - Hydrogeological cross-section of Aposkepos and Kefalari springs (IMGE, 2005) 70
Figure 39 - Hydrogeological cross-section of Mpouz-Mpounar Spring (IGME, 2005) 71
Figure 40 - Hydrogeological cross-section of Militsa spring (IGME, 2005) 71

Figure 41 - Typical Stratigraphic Sequence of the Quaternary sediments of the plains area perimetrically of Kastoria Lake (adapted from IGME, 2005) 74
Figure 42 - Location of ERTs, VES and boreholes used for the ERTs (data form IGME, 2010 and Gianneli, 2009) 76
Figure 43 - Legend of ERTs 76
Figure 44 - ERT S 77
Figure 45 - ERT T 78
Figure 46 - ERT Y 78
Figure 47 - ERT F 79
Figure 48 - ERT X 79
Figure 49 - ERT P 80
Figure 50 - Location of 15 Boreholes with the Hydraulic Parameters 81
Figure 51 - Position of the 60 Monitoring Points in the Simulation Area 82
Figure 52 - Piezometric map for May 2004 84
Figure 53 - Piezometric map for May 2012 85
Figure 54 - Piezometric Isolines using Kastoria Lake as a reference 87
Figure 55 - Location of main river flow and stage gauging stations. 90
Figure 56 - Transmission losses between gauging stations P3/P2-P1 91
Figure 57 - Recharge and Discharge areas. Rainfall Infiltration happens to the entire simulation area. 93
Figure 58 - Block diagram of water balance elements in the study area 94
Figure 59 - Box-plots of total annual infiltrated precipitation amount variation for Korissos karst system according to the results from the ten chose RCMs for the periods 2019-2038, 2039-2058 and 2059-2078 99
Figure 60 - Workflow of a Groundwater Flow Model (Panagopoulos, 1996) 101
Figure 61 - 2D horizontal mesh of the modelled area 104
Figure 62 - Assigned Boundary Conditions 106
Figure 63 - Spatial Distribution of the interpolated Hydraulic conductivity 108
Figure 64 - Calibrated hydraulic conductivity as produced by PEST 109
Figure 65 - Stress applied to the modelled system 110
Figure 66 - Distribution of target heads in the modelled domain 115
Figure 67 - Calibrated steady state piezometric map. The green dots are the selected calibration points 118
Figure 68 - Hydraulic head distribution for the last time step of the transient simulation 121
Figure 69 - Absolute critical water levels in the designed model 123
Figure 70 - Hydraulic head distribution at 1 Jan 2079 for RCP 2.6 A 124
Figure 71 - Hydraulic head distribution at 1 Jan 2079 for RCP 2.6 B 125
Figure 72 - Hydraulic head distribution at 1 Jan 2079 for RCP 4.5 A 125
Figure 73 - Hydraulic head distribution at 1 Jan 2079 for RCP 4.5 B 126
Figure 74 - Hydraulic head distribution at 1 Jan 2079 for RCP 4.5 C 126
Figure 75 - Hydraulic head distribution at 1 Jan 2079 for RCP 4.5 D 127
Figure 76 - Hydraulic head distribution at 1 Jan 2079 for RCP 8.5 A 127
Figure 77 - Hydraulic head distribution at 1 Jan 2079 for RCP 8.5 B 128
Figure 78 - Hydraulic head distribution at 1 Jan 2079 for RCP 8.5 C 128
Figure 79 - Hydraulic head distribution at 1 Jan 2079 for RCP 8.5 D 129
Figure 80 - Box-plots of total annual precipitation amount variation received by the surface of the Kastoria lake according to the results from the ten chose RCMs for the periods 2019-2038, 2039-2058 and 2059-2078 132
Figure 81 - Box-plots of total annual evaporation amount variation from the surface of the Kastoria lake according to the results from the ten selected RCMs for the periods 2019-2038, 2039-2058 and 2059-2078 134
Figure 82 - Box-plots of annual surface runoff amount variation at Kastoria basin according to the results from the ten selected RCMs for the periods 2019-2038, 2039-2058 and 2059-2078 136
Figure 83 - Box-plots of annual sub-surface runoff amount variation at Kastoria basin according to the results from the ten selected RCMs for the periods 2019-2038, 2039-2058 and 2059-2078 138
Figure 84 - Box-plots of annual total runoff amount variation at Kastoria basin according to the results from the ten selected RCMs for the periods 2019-2038, 2039-2058 and 2059-2078 140
Figure 85 - Location of West Macedonia in relation with the Tectonic zones of Northern Greece (Gianneli, 2009) 147
Figure 86 - Synthetic Stratigraphic Column of W.D GR 09 147
Figure 87 - Isothermal zone of 15 °C at EL 09 (YPAN, 2008). The red box roughly delineates the basin of Kastoria 165

Figure 88 - Rainfall zone of 800 mm at EL 09 (YPAN, 2008). The red box roughly delineates the basin of Kastoria 165
Figure 89 - Mean monthly Temperature of January at Kastoria basin 166
Figure 90 - Mean monthly Temperature of February at Kastoria basin 166
Figure 91 - Mean monthly Temperature of March at Kastoria basin 167
Figure 92 - Mean monthly Temperature of April at Kastoria basin 167
Figure 93 - Mean monthly Temperature of May at Kastoria basin 168
Figure 94 - Mean monthly Temperature of June at Kastoria basin 168
Figure 95 - Mean monthly Temperature of July at Kastoria basin 169
Figure 96 - Mean monthly Temperature of August at Kastoria basin 169
Figure 97 - Mean monthly Temperature of September at Kastoria basin 170
Figure 98 - Mean monthly Temperature of October at Kastoria basin 170
Figure 99 - Mean monthly Temperature of November at Kastoria basin 171
Figure 100 - Mean monthly Temperature of December at Kastoria basin 171
Figure 101 - Mean monthly Maximum Temperature of January at Kastoria basin 172
Figure 102 - Mean monthly Maximum Temperature of February at Kastoria basin 172
Figure 103 - Mean monthly Maximum Temperature of March at Kastoria basin 173
Figure 104 - Mean monthly Maximum Temperature of April at Kastoria basin 173
Figure 105 - Mean monthly Maximum Temperature of May at Kastoria basin 174
Figure 106 - Mean monthly Maximum Temperature of June at Kastoria basin 174
Figure 107 - Mean monthly Maximum Temperature of July at Kastoria basin 175
Figure 108 - Mean monthly Maximum Temperature of August at Kastoria basin 175
Figure 109 - Mean monthly Maximum Temperature of September at Kastoria basin 176
Figure 110 - Mean monthly Maximum Temperature of October at Kastoria basin 176
Figure 111 - Mean monthly Maximum Temperature of November at Kastoria basin 177
Figure 112- Mean monthly Maximum Temperature of December at Kastoria basin 177
Figure 113 - Mean monthly Minimum Temperature of January at Kastoria basin 178
Figure 114 - Mean monthly Minimum Temperature of February at Kastoria basin 178
Figure 115 - Mean monthly Minimum Temperature of March at Kastoria basin 179
Figure 116 - Mean monthly Minimum Temperature of April at Kastoria basin 179
Figure 117 - Mean monthly Minimum Temperature of May at Kastoria basin 180
Figure 118 - Mean monthly Minimum Temperature of June at Kastoria basin 180
Figure 119 - Mean monthly Minimum Temperature of July at Kastoria basin 181
Figure 120 - Mean monthly Minimum Temperature of August at Kastoria basin 181
Figure 121 - Mean monthly Minimum Temperature of September at Kastoria basin 182
Figure 122 - Mean monthly Minimum Temperature of October at Kastoria basin 182
Figure 123 - Mean monthly Minimum Temperature of November at Kastoria basin 183
Figure 124 - Mean monthly Minimum Temperature of December at Kastoria basin 183
Figure 125 - Mean Monthly Rainfall of January at Kastoria Basin 184
Figure 126 - Mean Monthly Rainfall of February at Kastoria Basin 184
Figure 127 - Mean Monthly Rainfall of March at Kastoria Basin 185
Figure 128 - Mean Monthly Rainfall of April at Kastoria Basin 185
Figure 129 - Mean Monthly Rainfall of May at Kastoria Basin 186
Figure 130 - Mean Monthly Rainfall of June at Kastoria Basin 186
Figure 131 - Mean Monthly Rainfall of July at Kastoria Basin 187
Figure 132 - Mean Monthly Rainfall of August at Kastoria Basin 187
Figure 133 - Mean Monthly Rainfall of September at Kastoria Basin 188
Figure 134 - Mean Monthly Rainfall of October at Kastoria Basin 188
Figure 135 - Mean Monthly Rainfall of November at Kastoria Basin 189
Figure 136 - Mean Monthly Rainfall of December at Kastoria Basin 189
Figure 137 - Mean monthly rainfall and effective rainfall of January at simulation area 190
Figure 138 - Mean monthly rainfall and effective rainfall of February at simulation area 190
Figure 139 - Mean monthly rainfall and effective rainfall of March at simulation area 190
Figure 140 - Mean monthly rainfall and effective rainfall of April at simulation area 191
Figure 141 - Mean monthly rainfall and effective rainfall of May at simulation area 191
Figure 142 - Mean monthly rainfall and effective rainfall of June at simulation area 191
Figure 143 - Mean monthly rainfall and effective rainfall of July at simulation area 192
Figure 144 - Mean monthly rainfall and effective rainfall of August at simulation area 192
Figure 145 - Mean monthly rainfall and effective rainfall of September at simulation area 192
Figure 146 - Mean monthly rainfall and effective rainfall of October at simulation area 193

Figure 147 - Mean monthly rainfall and effective rainfall of November at simulation area 193
Figure 148 - Mean monthly rainfall and effective rainfall of December at simulation area 193
Figure 149 - Mean monthly ET_0 of January at Kastoria basin with the Hargreaves method 194
Figure 150 - Mean monthly ET_0 of February at Kastoria basin with the Hargreaves method 194
Figure 151 - Mean monthly ET_0 of March at Kastoria basin with the Hargreaves method 195
Figure 152 - Mean monthly ET_0 of April at Kastoria basin with the Hargreaves method 195
Figure 153 - Mean monthly ET_0 of May at Kastoria basin with the Hargreaves method 196
Figure 154 - Mean monthly ET_0 of June at Kastoria basin with the Hargreaves method 196
Figure 155 - Mean monthly ET_0 of July at Kastoria basin with the Hargreaves method 197
Figure 156 - Mean monthly ET_0 of August at Kastoria basin with the Hargreaves method 197
Figure 157 - Mean monthly ET_0 of September at Kastoria basin with the Hargreaves method 198
Figure 158 - Mean monthly ET_0 of October at Kastoria basin with the Hargreaves method 198
Figure 159 - Mean monthly ET_0 of November at Kastoria basin with the Hargreaves method 199
Figure 160 - Mean monthly ET_0 of December at Kastoria basin with the Hargreaves method 199

Table of Figures (Tables)

Table 1 - Area and Percentage Share of Area of Elevation Classes 13
Table 2 - Meteorological Station Info used in this thesis 22
Table 3 – Annual Temperature Statistics for period 2000-2018 at Kastoria Basin 25
Table 4 - Monthly Means for 2000-2018 at Kastoria Basin 25
Table 5 - Monthly Evaporation Statistics for period 1999-2010 at Dispilio station 28
Table 6 - Annual Evaporation Statistics for period 1999-2010 at Dispilio station 28
Table 7 - Monthly Rainfall Statistics for period 2000-2018 at Kastoria Basin 30
Table 8 - Annual Rainfall Statistics in mm for period 2000-2018 at Kastoria basin 30
Table 9 - Monthly Means of Percent Change of Hargreaves method of Estimation of Evapotranspiration for five meteorological station at Kastoria basin 34
Table 10 - Monthly Means of Percent Change of Blaney-Criddle method of Estimation of Evapotranspiration for five meteorological station at Kastoria basin 34
Table 11 - Mean Monthly Reference Evapotranspiration Statistics for period 2000-2018 at Kastoria Basin 35
Table 12 - Annual Reference Evapotranspiration Statistics in mm for period 2000-2018 at Kastoria basin 36
Table 13 - Original Names and Hereafter Names of the selected RCMs 41
Table 14 – Projections of Climate Change at the end of the projected period 62
Table 15 - Torrents and sub-basins of Lake Kastoria Watershed (Tolikas & Mylopoulos, 2000) 63
Table 16 - Water Balance of Lake Orestiada 65
Table 17 - Hydraulic Parameters of 15 boreholes at Kastoria basin 80
Table 18 – Seasonal values of inflows/outflows of the aquifer due to the hydraulic interaction with the torrent Xiropotamos (+ denotes influent behavior while - denotes effluent behavior) 92
Table 19 - Water balance of the alluvial aquifer of Kastoria 97
Table 20 - Water balance of the dynamic steady state model 119
Table 21 – Statistical Parameters for the steady state model 119
Table 22 - Statistical parameters of each stress-period for the transient state model 120
Table 23 - Taylor statistics for EUR-11 RCMs for the raw and bias-corrected (BC) results of precipitation 200
Table 24 - Taylor statistics for EUR-11 RCMs for the raw and bias-corrected (BC) results of temperature 204
Table 25 - Annual projected values and percent change for precipitation yielded from the bias-corrected models that were chosen for the period 2019-2038, 2039-2058 and 2059-2078 208
Table 26 – Seasonal projected values and percent change for precipitation yielded from the bias-corrected models that were chosen for the period 2019-2038, 2039-2058 and 2059-2078 209
Table 27 – Annual projected values and percent change for temperature yielded from the bias-corrected models that were chosen for the period 2019-2038, 2039-2058 and 2059-2078 213
Table 28 - Seasonal projected values and percent change for temperature yielded from the bias-corrected models that were chosen for the period 2019-2038, 2039-2058 and 2059-2078 214